

Novel inhibitors of the human Farnesyl Pyrophosphate Synthase

Joris W. De Schutter

Thesis submitted to McGill University in partial fulfillment of the requirements for the
degree of

Doctor of Philosophy

Department of Chemistry
McGill University, Montreal

December 2012

© Joris W. De Schutter

Abstract

Joris W. De Schutter
McGill University

Supervisor: Youla S. Tsantrizos

Farnesyl pyrophosphate synthase (FPPS) occupies the first branching point of the mevalonate pathway, an important biosynthetic route that provides essential lipid molecules, such as steroids and isoprenoids, in mammalian cells. The enzyme catalyzes the sequential condensation of dimethylallyl pyrophosphate (DMAPP) with isopentenyl pyrophosphate (IPP) to produce farnesyl pyrophosphate (FPP). This metabolite is required for the post-translational modification of ~2% of the total mammalian proteome and this modification is critical for proper subcellular localization and function of many proteins including the small GTPases, which are essential for cell signalling and proliferation. Currently, nitrogen containing bisphosphonates (*N*-BPs) are the only class of approved drugs that target the human FPPS. *N*-BPs bind to the allylic sub-pocket of the active site *via* metal-mediated interactions between their bisphosphonate moiety and a highly conserved, aspartate rich motif on the protein surface. Due to their inherent charged nature and strong affinity for hydroxyapatite, the therapeutic applications of *N*-BPs are mainly restricted to the treatment of osteoporosis and bone metastasis. However, recent clinical evidence shows that *N*-BPs improve the survival of multiple myeloma (MM) patients via mechanisms unrelated to their skeletal benefit.

A structure-based approach was pursued in designing new hFPPS inhibitors with improved biopharmaceutical properties compared to the commercial drugs. Biophysical studies, including NMR, ITC and X-ray crystallography, were employed to probe the protein plasticity and show that our novel inhibitors occupy a larger portion of the active site as compared to the current drugs. A differential scanning fluorimetry (DSF) assay was also developed in order to demonstrate a positive correlation between the thermal stabilization properties and the *in vitro* inhibition potency of our inhibitors. Furthermore, this technique allowed us to identify inhibitors that bind to an allosteric pocket of the enzyme. In summary, the synthesis, SAR and inhibitor-induced conformational changes of the hFPPS enzyme, and the potential implications to drug discovery, will be discussed.

Résumé

Joris W. De Schutter
McGill University

Superviseure: Youla S. Tsantrizos

La synthase farnésyl-pyrophosphate (FPPS) est à l'origine du premier point de dérivation de la voie du mévalonate, une route biosynthétique important qui fournit des molécules de lipides essentiels, tel que les stéroïdes et isoprénoïdes, dans les cellules de mammifères. L'enzyme catalyse la condensation séquentielle du diméthylallyl-pyrophosphate (DMAPP) avec l'isopentényl-pyrophosphate (IPP) afin de produire le farnésyl-pyrophosphate (FPP). Ce métabolite est nécessaire dans la modification post-translationnelle de ~2% de tous les protéomes mammifères et cette modification est indispensable pour une localisation subcellulaire saine et la fonction de plusieurs protéines tel que les petites GTPases, protéines essentielles à la signalisation et prolifération cellulaire. Présentement, la seule classe de médicaments approuvée qui vise la FPPS humaine comprend les bisphosphonates contenant un groupe azote (*N*-BP). Les *N*-BPs se lient à la sous-poche allylique du site actif *via* des interactions médiées par des métaux entre leur groupe fonctionnel bisphosphonate et un motif hautement conservé riche en aspartate retrouvé à la surface de la protéine. En raison de leur nature chargée et haute affinité pour l'hydroxyapatite, les applications thérapeutiques des *N*-BPs sont majoritairement restreintes aux traitements de l'ostéoporose et de la métastase osseuse. Par contre, des évidences clinique récente démontrent que les *N*-BPs augmentent la survie de patients atteints de myélome multiple (MM) par des mécanismes non-reliés à leur bénéfice squelettique.

Une approche basée sur la structure a été poursuivie afin de développer des nouveaux inhibiteurs de la hFPPS avec des propriétés biopharmaceutiques améliorées comparativement aux médicaments sur le marché. Des études biophysiques, incluant RMN, titration calorimétrique (ITC) et par cristallographie à rayons X, ont été utilisées afin de sonder la plasticité de la protéine et démontrer que notre inhibiteur original occupe une plus grande proportion du site actif relativement aux médicaments sur le marché. Une analyse de fluorimétrie différentielle à balayage (DSF) a également été développée pour illustrer une corrélation positive entre les propriétés de stabilisation thermique et l'effet d'inhibition *in*

vitro de nos inhibiteurs. Qui plus est, cette technique nous a permis d'identifier les inhibiteurs qui se lient à la poche allostérique de la protéine. En résumé, la synthèse, les relations structure-activité (SAR) et les changements conformationnels de l'enzyme hFPPS causés par les inhibiteurs, ainsi que les applications potentiels reliées à découverte de nouvelle drogue, seront discutés.

Acknowledgements:

First and foremost, I wish to thank Professor Tsantrizos for truly excellent mentorship and support over the course of my graduate studies. The hFPPS project was a fantastic learning experience and gave me the opportunity to perform exciting research and to meaningfully contribute to science. I have acquired many new skills and interdisciplinary techniques that I feel have prepared me well for a successful career. Thank you for always replying to my emails, writing countless reference letters and, of course, swiftly and efficiently editing this dissertation, Spartan-style.

I am thankful to my parents and sisters for supporting me in every way, including crossing the Atlantic Ocean to pursue my scientific ambitions.

I am very fortunate to have many great friends and family members, in Canada and Belgium, who know how to appreciate the best things in life.

Thanks to Janice Lawandi for psychological and physical re-equilibrations.

Thanks to Mitch Huot, I don't think I can share a one-person fumehood with anyone else.

Thanks to Adrienne Langille for being an amazing bad cop.

Thanks to other members of the Tsantrizos group for the positive, professional and supportive atmosphere; Dr. John Mancuso, Serge Zaretsky, Julien Poupart, Joseph Shaw, Zheping Hu, Yih-Shyan Lin, Carlos Leung, Cookie Cho, Cyrus Lacbay, Jinming Guan and Demetrios Gritzalis.

Thanks to Daniel Rivalti for expertise, Tim Hortons and arrow-pushing.

Thanks to Rodrigo Mendoza-Sanchez for words of wisdom and idle chatter.

Thanks to the Gleason group members for chemicals, glassware and beyond.

Thanks to the Auclair group members for the use of instruments, advice and Naruto! Kenward Vong, Amelie Menard, Siqi Zhu and Eric Habib.

Thanks to the Mittermaier group members for helping with all our enzymatic tribulations (Eric Meneses).

Thanks to the Dahma group members for allowing us to crash on your couch and showing me how to tame an NMR machine (Matthew Hassler).

Thanks to the Sleiman group members for maintaining an amazing pH meter and for CD experiments (Katie Castor).

Thanks to the CJ Li group members for always working late (Camille Correia).

Thanks to the CGSS members, it's been a pleasure making grad life nicer for everybody.

Thanks to Chantal Marotte for 6 years of guidance through the labyrinth that is academic bureaucracy.

I wish to thank all the McGill Chemistry Department faculty, administration and support staff.

A special thanks to Robert Godin for translating the abstract of this thesis.

I wish to thank the many funding agencies for generous funding and supporting international students.

Preface

I started my graduate studies at the Chemistry Department of McGill University in September of 2007 in the research group of Professor Nicolas Moitessier. Over the course of two years I contributed to the development of the ACE computational model, which led to a publication in a peer-reviewed journal:

Toward a Computational Tool Predicting the Stereochemical Outcome of Asymmetric Reactions. Development of the Molecular Mechanics-Based Program ACE and Application to Asymmetric Epoxidation Reactions

Weill, N.; Corbeil, C.; De Schutter, J.W.; Moitessier, N.

J. Comp. Chem. **2011**, 32 , 2878-2889

It should be noted that my PhD thesis does not include any of my research contributions to the ACE project.

In September of 2009, I joined the research group of Professor Youla S. Tsantrizos and commenced a new project on the identification of novel hFPPS inhibitors and investigations on the protein plasticity of this enzyme; my PhD thesis focuses on only this project.

For the sake of conciseness, not every detail of my graduate work has been included in the discussions of this dissertation. However, in order to deliver a complete account, the corresponding synthesis protocols are included in the experimental sections. An in-house code has been linked with every reaction to provide each compound with a unique identifier and also as a convenient reference to the corresponding lab notebook entry and raw instrumental data.

Appendix I provides a current list of all hFPPS crystal structures deposited in the PDB database.

Appendix II contains the ^1H -NMR spectra of final compounds, in numerical order by in-house code.

Appendix III contains the HPLC UV traces of final compounds, in numerical order by in-house code.

Table of Contents:

1	Introduction	15
1.1	Druggable vs. undruggable therapeutic targets	15
1.2	The mevalonate pathway and Farnesyl Pyrophosphate Synthase	18
1.2.1	The mevalonate pathway:	18
1.2.2	Commercial drugs targeting the mevalonate pathway:	20
1.2.3	Prenylation:	21
1.3	Implication of the mevalonate pathway in oncogenesis	23
1.3.1	Farnesyl transferase inhibitors:	23
1.3.2	Apppl as a pro-apoptotic factor:	24
1.3.3	hFPPS inhibition and immune response:	24
1.3.4	Multiple Myeloma:	25
1.4	The structure and catalytic function of hFPPS	26
1.5	Bisphosphonates, inhibitors of hFPPS	32
1.6	Inhibitors of the hFPPS, biopharmaceutical properties and clinical implications	38
1.6.1	Active site inhibitors:	38
1.6.2	Allosteric inhibitors of hFPPS	42
1.7	Research goals	45
1.8	References	46
2	First generation bisphosphonate inhibitors: exploring the hFPPS active site	51
2.1	Preface	51
2.2	Inhibitor design	52
2.3	Molecular modeling studies	56
2.4	Synthesis	59
2.5	Characterization of α -fluoro bisphosphonic acids:	63
2.6	Human FPPS inhibition screening and SAR	65
2.7	NMR line broadening studies	69
2.8	Conclusions and Outlook	72

2.9	Acknowledgments.....	73
2.10	References	74
2.11	Experimental.....	76
2.11.1	Docking studies.....	76
2.11.2	Synthesis:	77
2.11.3	hFPPS enzymatic inhibition assay	109
2.11.4	¹ H NMR line broadening experiments.....	111
3	Branched hFPPS active site inhibitors.....	113
3.1	Preface.....	113
3.2	Introduction	113
3.3	Branched Inhibitor design	114
3.4	Synthesis of branched bisphosphonate inhibitors	116
3.4.1	Rearrangement strategy	116
3.4.2	Condensation strategy.....	117
3.4.3	Sequential alkylation strategy	119
3.5	Synthesis of inhibitors with a branched pyridine core and their <i>in vitro</i> activity against hFPPS	122
3.6	Conclusions and outlook.....	130
3.7	References	131
3.8	Experimental	132
3.8.1	Synthesis	132
3.8.2	<i>In vitro</i> Inhibition Assay for hFPPS (M1):.....	151
3.8.3	<i>In vitro</i> Inhibition Assay for hGGPPS:.....	152
4	X-ray crystallography: SAR and revised binding mode	153
4.1	Preface.....	153
4.2	Synthesis and enzymatic activity of bisphosphonic acids with different α -substituents.....	154
4.2.1	2-aminopyridine bisphosphonates	154
4.2.2	Synthesis:	155

4.3	hFPPS/4.5 co-crystal X-ray structure	158
4.4	SAR and cell based anti-proliferation activity	162
4.4.1	SAR:	162
4.4.2	Antiproliferation activity in MM cell lines	165
4.5	Conclusions and outlook	167
4.6	References	168
4.7	Experimental.....	169
4.7.1	Docking studies	169
4.7.2	Synthesis.....	171
4.7.3	Enzymatic inhibition assays	182
5	Exploring the allylic sub-pocket and the importance of π-interactions	183
5.1	Preface	183
5.2	Introduction	184
5.3	Inhibitor design rationale.....	185
5.4	Synthesis.....	187
5.5	<i>In vitro</i> enzymatic activity and SAR	191
5.5.1	Pyridine core – aromatic sidechain connectivity.....	191
5.5.2	π -interactions with Phe112.....	192
5.6	Conclusions and outlook	194
5.7	References	195
5.8	Experimental.....	196
5.8.1	Computational modeling.....	196
5.8.2	Synthesis.....	196
5.8.3	Enzymatic inhibition assays	218
6	Towards non-bisphosphonate active site inhibitors of hFPPS: investigation of bioisosteres	219
6.1	Preface	219
6.2	Introduction	219
6.3	Synthesis of bioisosteric replacements of (bis)phosphonates.....	224

6.4	<i>In vitro</i> enzymatic activity of bioisostere analogs.....	230
6.5	Conclusions and outlook	231
6.6	References	232
6.7	Experimental	234
6.7.1	Synthesis	234
6.7.2	Enzymatic inhibition assays.....	251
7	Modification of the hFPPS enzymatic assay.....	253
7.1	Preface	253
7.2	Introduction	253
7.3	Exploring the effect of assay buffer components.....	256
7.3.1	Magnesium concentration.....	256
7.3.2	Detergent.....	256
7.3.3	hFPPS and substrate concentrations	258
7.4	Sensitized hFPPS enzymatic assay	260
7.5	Conclusions and outlook	262
7.6	References	263
7.7	Experimental	264
7.7.1	Synthesis	264
7.7.2	<i>In vitro</i> Inhibition Assay for hFPPS (M2):.....	265
8	Differential Scanning Fluorimetry and allosteric binding	267
8.1	Preface	267
8.2	Introduction	268
8.2.1	Differential Scanning Fluorimetry (DSF):.....	269
8.2.2	Limitations of DSF:	272
8.3	Development and validation of a DSF protocol for hFPPS	274
8.3.1	Development of a DSF protocol for hFPPS:	274
8.3.2	Validation of hFPPS DSF protocol:.....	275
8.4	Elucidation of ligand binding properties by DSF:	279

8.4.1	The effect of Mg^{2+} :	280
8.4.2	The effect of DMSO, NaCl and detergent on hFPPS stability and ligand binding:	
8.4.3	Elucidation of binding characteristics by DSF	285
8.5	Inhibitor and fragment screening by hFPPS	288
8.5.1	ΔT_m - IC_{50} correlation	288
8.5.2	Fragment-based screening by DSF:	292
8.6	DSF co-incubation studies, elucidation of binding mode	293
8.7	Discovery of the allosteric binding mode of thienopyrimidines	300
8.8	Conclusions and outlook	305
8.9	Acknowledgements	305
8.10	References	306
8.11	Experimental	308
8.11.1	Synthesis	308
8.11.2	Enzymatic inhibition assays:	314
8.11.3	DSF protocol for hFPPS:	314
9	Contributions to knowledge	315
9.1	Summary of accomplishments	319
9.2	Claims to original knowledge	319
9.3	Peer reviewed publications	320
9.4	Patent applications	321
9.5	Conference proceedings	322
10	Appendices	323

List of Tables:

Table 1.1: <i>N</i> -BP inhibition kinetics.	35
Table 1.2: Thermodynamic data for <i>N</i> -BPs.	35
Table 1.3: Zoledronate inhibition data for proteins outside the mevalonate pathway.....	40
Table 2.1: Enzymatic potency and HAP affinity of risedronate analogs.....	53
Table 2.2: hFPPS enzymatic inhibition data.....	66
Table 3.1: Condensation optimization conditions	118
Table 3.2: Conditions for reverse sequential addition	120
Table 3.3: hFPPS and hGGPPS inhibition data for analogs 3.19 and 3.20	125
Table 3.4: Effect of temperature and reaction time on amination yield	126
Table 3.5: Diazotization conditions attempted on 2-amino- <i>n</i> Bu-pyridine scaffold	127
Table 3.6: Diazotization conditions attempted on 2- <i>N,N</i> -dimethyl-pyridine 3.25	128
Table 3.7: hFPPS and hGGPPS inhibition data for inhibitor 3.28	129
Table 4.1: Anti-proliferation activity data in MM cell lines.....	166
Table 5.1: hFPPS and hGGPPS enzymatic inhibition data for inhibitor 5.4 , 5.8 – 5.10 ...	192
Table 5.2: hFPPS and hGGPPS enzymatic inhibition data for cyclopropyl analogs.....	193
Table 6.1: hFPPS enzymatic inhibition data for bioisosteres.	230
Table 7.1: Summary of various hFPPS enzymatic assay conditions	261
Table 7.2: Comparison of <i>in vitro</i> hFPPS M1 and M2 assay conditions.	262
Table 8.1: ITC thermodynamic data for hFPPS/ 4.5 1:3 at 30°C	297
Table 8.2: Human FPPS inhibition data of thienopyrimidine based inhibitors	304
Table 9.1: Enzymatic inhibition and anti-proliferation data.....	30417

List of Schemes:

Scheme 1.1: Enzymatic reaction mechanism of FPPS	30
Scheme 1.2: Mechanism of time-dependent <i>N</i> -BP inhibition	34
Scheme 2.1: Synthesis of 6-substituted-3-amino-bisphosphonates.....	59
Scheme 2.2: Synthetic route towards α -fluoro bisphosphonates.....	61
Scheme 2.3: Example of a successful Suzuki cross coupling with a pyridinyl chloride.....	62
Scheme 2.4: Synthesis of <i>N</i> -THP-protected indazole-5-boronic pinacol ester 2.15	62
Scheme 2.5: hFPPS enzymatic assay protocol	65
Scheme 3.1: Beckmann rearrangement of hydroxylamines	116
Scheme 3.2: Beckmann rearrangement attempt on pyridine scaffold	116
Scheme 3.3: Condensation strategy.....	117
Scheme 3.4: Triethyl orthoacetate condensation test reaction	117
Scheme 3.5: Two step synthesis of branched bisphosphonate	118
Scheme 3.6: General α -fluorination conditions.....	119
Scheme 3.7: Sequential alkylation strategy	119
Scheme 3.8: Second alkylation on pyridine-bisphosphonate precursor	120
Scheme 3.9: Reverse sequential alkylation	120
Scheme 3.10: Synthesis of 3.14	122
Scheme 3.11: Sequential Suzuki cross-couplings	123
Scheme 3.12: Modified reaction sequence to branched pyridine core inhibitors	124
Scheme 3.13: Unsuccessful Buchwald-Hartwig cross-coupling on 3.21	125
Scheme 3.14: Buchwald-Hartwig cross coupling on 3.12	126
Scheme 3.15: Diazotization on 2-amino- <i>n</i> Bu-pyridine scaffold	127
Scheme 3.16: Diazotization on 2- <i>N,N</i> -dimethyl-pyridine 3.25	128
Scheme 3.17: Continuation of 2-amino- <i>n</i> Bu-pyridine 3.23	128
Scheme 3.18: Sonogashira strategy	129
Scheme 4.1: Synthesis issues with 3-bromo-5-(bromomethyl)pyridine	156
Scheme 4.2: 5-Het-pyridine-3-bisphosphonates with varying α -substituents	157
Scheme 5.1: Cross-coupling with benzyl trifluoroborate	187
Scheme 5.2: Synthesis of bisphosphonates with an amide linker	188

Scheme 5.3: Synthesis of (4-cyclopropoxyphenyl)boronic acid 5.13	189
Scheme 5.4: Synthesis of novel cyclopropyl-bearing boron coupling partners.....	190
Scheme 6.1: Synthesis of analog 6.5	225
Scheme 6.2: Side reaction observed with catalytic hydrogenation.....	226
Scheme 6.3: Synthesis of analog 6.6	226
Scheme 6.4: Synthesis of analog 6.8	227
Scheme 6.5: Synthesis of analog 6.9	228
Scheme 6.6: Synthesis of inhibitors 6.10 and 6.11	229
Scheme 6.7: Synthesis of inhibitors 6.12 – 6.14	229
Scheme 7.1: ³ H-IPP dependant hFPPS assay.....	254
Scheme 7.2: Colorimetric hFPPS assay	255
Scheme 8.1: Two state thermodynamic equilibrium model.....	271
Scheme 8.2: Mixed mechanism of DSF equilibria	273

List of Figures:

Figure 1.1: Crystal structure of HIV-1 integrase with raltegravir	17
Figure 1.2: Raltegravir interactions with HIV integrase Mg ²⁺ metals.	17
Figure 1.3: The mevalonate pathway.	20
Figure 1.4: Biosynthesis of farnesyl pyrophosphate	22
Figure 1.5: Tipifarnib	24
Figure 1.6: ApppI	24
Figure 1.7: Crystal structure of apo hFPPS.....	26
Figure 1.8: Overlap of hFPPS in the open conformation.....	27
Figure 1.9: Overlap of hFPPS in the semi-closed conformation	28
Figure 1.10: Pyrophosphate stabilization in the allylic sub-pocket.	29
Figure 1.11: Pyrophosphate stabilization in the IPP sub-pocket	29
Figure 1.12: Charge compensation of the pyrophosphate moieties in hFPPS	30
Figure 1.13: Enzymatic mechanism of FPPS.....	31
Figure 1.14: Common bisphosphonates.....	32
Figure 1.15: a) <i>N</i> -BP –hFPPS bifurcated hydrogen bonds.	33
Figure 1.16: <i>N</i> -BP inhibition mechanism.....	37
Figure 1.17: Risedronate and zoledronate.....	38
Figure 1.18: <i>N</i> -BP enzymatic inhibition data in the mevalonate pathway.....	40
Figure 1.19: hGGPPS inhibitors	41
Figure 1.20: Fragment optimization of allosteric inhibitors	42
Figure 1.21: hFPPS allosteric pocket.	43
Figure 1.22: Allosteric mechanism of inhibition.	44
Figure 2.1: 2 nd pKa of differentially substituted phosphonic acids ⁴	53
Figure 2.2: Inhibitor design approach	54
Figure 2.3: Crystal structure of ternary complex hFPPS/ZOL/IPP (PDB 1ZW5).	55
Figure 2.4: Structural diversity of docking input structures.	57
Figure 2.5: <i>In silico</i> screening results	58
Figure 2.6: Proton-decoupled ¹³ P NMR spectrum of inhibitor 2.25	63
Figure 2.7: ¹⁹ F spectrum of inhibitor 2.25 , splitting due to ¹ H and ³¹ P.....	64

Figure 2.8: { ¹⁹ F, ¹³ C}HMQC NMR spectrum of inhibitor 2.25	64
Figure 2.9: Novel inhibitors, comparison <i>para</i> - vs. <i>meta</i> -substituted inhibitors.....	67
Figure 2.10: Novel inhibitors, comparison of the pyridine substitution pattern.....	68
Figure 2.11: Docking output pose of inhibitor 2.22	70
Figure 2.12: 2.22 and risedronate by ¹ H NMR line broadening experiment.....	71
Figure 2.13: 2.22 and IPP by ¹ H NMR line broadening experiment.....	71
Figure 3.1: Potential inhibitor branching points.....	115
Figure 4.1: Comparison of pyridine scaffolds of novel inhibitors.....	154
Figure 4.2: SAR of 2-aminopyridine bisphosphonates for hFPPS	155
Figure 4.3: Novel pyridine scaffold for bisphosphonate inhibitors.....	155
Figure 4.4: 4.5 binding mode vs. docking output pose.....	159
Figure 4.5: 4.5 induced opening of allylic sub-pocket.	159
Figure 4.6: Comparison of PDB 1ZW5, 1YV5 and 4DEM	160
Figure 4.7: Enzymatic activity comparison of different pyridine cores	162
Figure 4.8: hFPPS activity data for bisphosphonate with varying α -substituents	163
Figure 4.9: Pyridine core – hFPPS potential hydrogen bonds.....	164
Figure 4.10: Side view of hFPPS/ 4.5 , planarity of bio-active conformation	164
Figure 4.11: Output poses of 4.5 docked to the fully closed active site	170
Figure 5.1: Examples of π -interactions.....	184
Figure 5.2: 3-aminopyridine and 2-aminopyridine based bisphosphonic acids	185
Figure 5.3: Predicted CH/ π -interaction with Phe 112 and 5.15.....	186
Figure 5.4: Suzuki cross-coupling synthetic strategy	189
Figure 5.5: Novel inhibitors with extended cyclopropyl moiety.....	190
Figure 5.6: Novel inhibitors with a flexible linker	191
Figure 5.7: Novel cyclopropyl bearing bisphosphonates.....	193
Figure 6.1: Common bioisosteres used to replace amide and ester moieties	220
Figure 6.2: Common bioisostere replacements	221
Figure 6.3: Examples of phosphonate/phosphate bioisosteres	223
Figure 6.4: Bioisosteres successfully for pyrophosphate recognition motifs	223
Figure 6.5: Active site metal configurations for HIV 1 integrase and hFPPS.	223
Figure 6.6: Bioisostere analogues of hFPPS inhibitors	224

Figure 7.1: hFPPS enzymatic data at different Mg^{2+} concentrations.....	257
Figure 7.2: Catalytic turnover over time at 10 nM and 1 nM hFPPS	259
Figure 7.3: Inhibitors tested in M1 and M2 assays.....	262
Figure 8.1: Typical DSF melting curve.....	270
Figure 8.2: Negative first derivative of melting curve	270
Figure 8.3: Increase in T_m due to ligand binding	272
Figure 8.4: Example of DSF titration curve	272
Figure 8.5: Triplicate of hFPPS melting curve,	275
Figure 8.6: Risedronate titration curve in the absence and presence of IPP	276
Figure 8.7: Combined titration curves for risedronate	277
Figure 8.8: Triplicate melting curve for second batch of hFPPS	278
Figure 8.9: Risedronate titrations across batches of purified hFPPS protein	278
Figure 8.10: Inhibitors for DSF experiments	279
Figure 8.11: Stabilizing effect of $MgCl_2$ on hFPPS	281
Figure 8.12: DSF titration curves for allosteric inhibitors 1.5 and 1.6	281
Figure 8.13: Destabilizing effect of DMSO on hFPPS	284
Figure 8.14: Destabilizing effect of NaCl on hFPPS	284
Figure 8.15: Effect of buffer composition on risedronate binding	286
Figure 8.16: Effect of buffer composition on 4.5 binding	286
Figure 8.17: Effect of buffer composition on 1.5 binding	287
Figure 8.18: Overlay of DSF titration curves according to <i>in vitro</i> potency	289
Figure 8.19: Pyridine correlation between stabilization and enzymatic activity.	290
Figure 8.20: General structures 8.1 ; 8.2 and 8.3	290
Figure 8.21: Titration curves for inhibitors differing only in heterocyclic nitrogen.....	291
Figure 8.22: DSF fragment screening	292
Figure 8.23: Titration curves of DMAPP, IPP, GPP and FPP	294
Figure 8.24: DSF parallel titrations of risedronate with GPP and IPP	295
Figure 8.25: DSF parallel titration of 4.5 with IPP	296
Figure 8.26: Titration curves of 4.5 with IPP, PPi and Pi.....	297
Figure 8.27: DSF parallel titration of 2.22 with IPP	298
Figure 8.28: DSF parallel titrations of 1.5 with risedronate and IPP	299

Figure 8.29: Examples of thienopyrimidine bisphosphonates.....	300
Figure 8.30: Thienopyridine correlation stabilization and enzymatic activity	301
Figure 8.31: DSF parallel titration of 8.4 with IPP.....	301
Figure 8.32: hFPPS/ 8.5 protein crystal structure.....	302
Figure 8.33: Expansion of hFPPS/ 8.5 crystal structure.....	302
Figure 8.34: Non-bisphosphonate thienopyrimidine analogs	304
Figure 9.1: Selected inhibitors of hFPPS and hGGPPS	304
Figure 9.2: ¹ H NMR bone affinity assay	304

1 Introduction

1.1 Druggable vs. undruggable therapeutic targets

Living organisms are comprised of molecules that are delicately balanced by chemical reactions, catalyzed by other biomolecules such as proteins, which enable each individual to function properly from birth to death. These biological processes are scrupulously regulated to maintain a healthy equilibrium. When an endogenous or exogenous factor interferes, the balance is disturbed and the organism enters a state of disease; which, when left untreated, can cause serious damage and even death. The disease state is usually characterized by up- or down-regulation of one or more biological pathways, which cause aberrant behaviour of the affected cells and the encompassing tissues and organs. In order to treat the malignancy, the causative factors need to be removed and the deregulated biomolecules and processes need to be restored to the proper balance. This can be achieved at many levels of the living cell: inside the nucleus, by modulating transcription from DNA to RNA; in the cytosol, by affecting the function and metabolism of biomolecules or at the plasma membrane, by influencing signalling networks. These are simply abstract concepts of how to alter the biology and unravelling the intricate workings of illnesses, in order to develop efficacious therapeutic treatments, is one of the most difficult scientific challenges.

The first step in modern drug discovery is the identification and validation of a therapeutic target, the biomolecule that is key for a critical step of the disease state. This can essentially be anything, including DNA, RNA, structural proteins, signaling proteins, enzymes or hormones. The challenge lies in selecting a target that can be reached and affected by small molecules, without disrupting healthy cellular functions and leading to toxic side-effects. In addition, the target must be validated to ensure that no alternative pathways can compensate for the altered function of the target, thus overcoming therapeutic interventions via some biochemical redundancy mechanism. That is to say, there exist many alternate routes that can rescue the viability of the disease pathway, rendering the modulation of the target ineffective.

Most drug discovery efforts target a protein, either endogenous to the human body or from an exogenous organism such as viruses or bacteria. Therapeutic targets are generally classified as either “druggable” or “undruggable” according to their genomic characteristics,¹ biological role,² and the overall structural features of the protein.³

Genetic variability makes all living things unique and this includes proteins. For a protein to be considered druggable, it cannot exhibit large gene sequence variations across individuals, as this will make it unlikely that a single small molecule can be effective as a therapeutic agent for the general public. Furthermore, the target should have few analogous proteins in the human family and be involved in only one or two cellular signaling pathways, to minimize undesirable side-effects. Binding sites on proteins usually exist out of functional necessity, with highly conserved amino acid residues; therefore, most successful drugs achieve their activity by competing for a binding site on a protein with an endogenous biomolecule. For example, target enzymes with a deep ($\sim 250 \text{ \AA}^3$ volume), lipophilic active site are considered highly druggable. High throughput screening (HTS) of such proteins using a functional assay and large compound libraries often leads to the identification of “hits”, molecules that are suitable for further structure-activity relationship (SAR) investigations. In contrast, proteins with shallow, solvent exposed binding sites are classified as undruggable because there is limited surface area to interact with small molecules and they can be easily displaced by surrounding biomolecules. Enzymes with deep, but highly charged pockets are also considered undruggable, as small molecules with complementary shape and electrostatic surface must also be charged in order to tightly bind and will thus have very poor biopharmaceutical properties. A large family of such enzymes are the nucleic acid processing and prenyl synthase enzymes, which interact with a phosphodiester, phosphate or pyrophosphate (also called diphosphate) moiety on their natural substrates via metal-mediated chelation to a cluster of highly conserved acidic residues in their active site.

The problems associated with this class of undruggable targets have been overcome with the development of effective phosphate or pyrophosphate bioisostere moieties. One of the best known examples is the pyrimidinone moiety found in the drug raltegravir (Isentress[®]), an antiviral HIV drug that was marketed in 2007.⁴ Raltegravir is an inhibitor of the HIV-1 integrase enzyme, which is responsible for the introduction of the viral DNA into the host

genome (**Figure 1.1**).⁵ Integrase interacts with the phosphodiester backbone of DNA through two Mg^{2+} ions which are chelated by two structurally conserved Asp residues in the active site of the enzyme. Raltegravir can strongly interact with these Mg^{2+} ions via its pyrimidinone ring, a highly optimized moiety that has good biopharmaceutical properties (**Figure 1.2**). Thus raltegravir serves as an example that, although very challenging, proteins with highly charged pockets can still be druggable at this binding site.

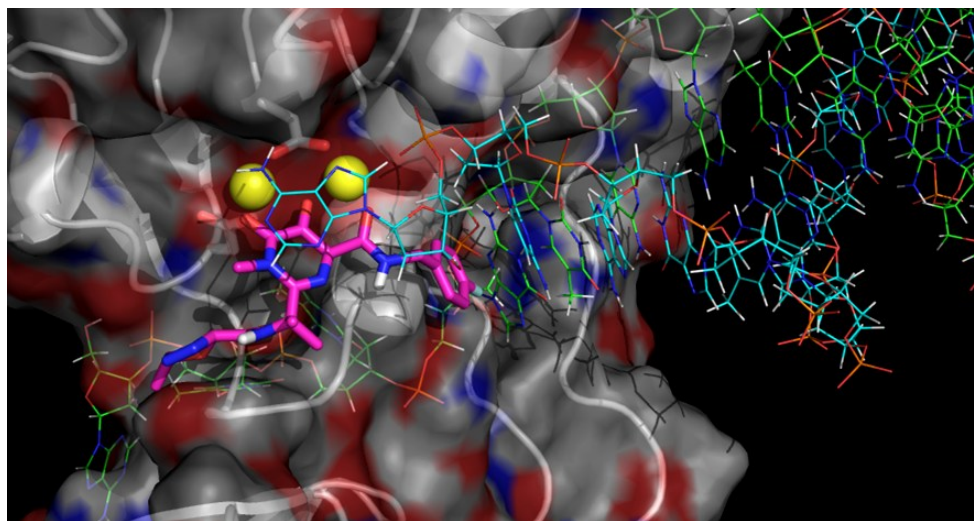


Figure 1.1: Crystal structure of HIV-1 integrase with raltegravir and two DNA strands (PDB 3OYA). The protein surface is shown as a semi-transparent surface, Mg^{2+} ions are shown as yellow spheres. Raltegravir is depicted in stick form (pink) and both DNA strands in line representation (blue and green).

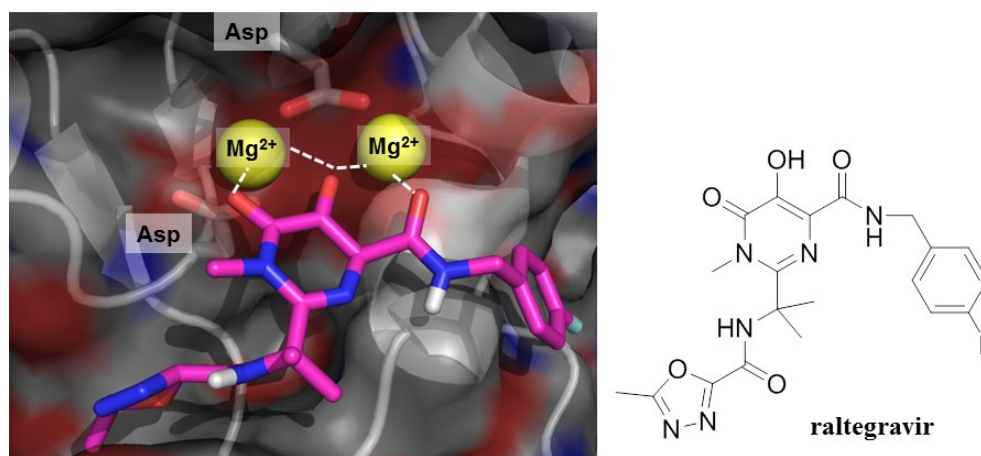


Figure 1.2: Asp residues are shown and raltegravir interactions with Mg^{2+} are indicated with dashed lines.

1.2 The mevalonate pathway and Farnesyl Pyrophosphate Synthase

1.2.1 The mevalonate pathway:

The mevalonate pathway starts with the conversion of acetyl-CoA to 3-hydroxy-3-methylglutaryl-CoA (HMG-CoA) and the thioester bond is subsequently reduced to form mevalonate by HMG-CoA reductase (**Figure 1.3**, **Figure 1.4**). After two sequential phosphorylations, the first alkene bond is introduced with the synthesis of isopentenyl pyrophosphate (IPP) and its isomer dimethylallyl pyrophosphate (DMAPP). These five carbon isoprene units serve as the building blocks for all higher isoprenoids. The pathway continues with the head-to-tail condensation of DMAPP and IPP, catalyzed by farnesyl pyrophosphate synthase (FPPS), to form the intermediate geranyl pyrophosphate (GPP). Next, the FPPS enzyme performs a second condensation with another unit of IPP to form the C₁₅ farnesyl pyrophosphate product (FPP). This is the first branching point in the mevalonate pathway, as FPP can be converted to a myriad of other important biomolecules; for example, two units of FPP can be combined (head-to-head condensation) into squalene, which can be further elaborated into various steroids, such as cholesterol. FPP can also be further elongated with another unit of IPP by geranylgeranyl pyrophosphate synthase (GGPPS) to form the C₂₀ geranylgeranyl pyrophosphate (GGPP), which is the precursor for higher isoprenoids.

Regulation of the mevalonate pathway:

It has long been established that end products (e.g. the steroids, especially cholesterol) produce negative feedback to enzymes at the start of the mevalonate pathway, through mechanisms such as suppressing their gene expression; in order to maintain homeostasis inside the cell.⁶ The molar concentrations of the intermediate metabolites are entirely dependent on the expression levels of the associated proteins, which vary significantly depending on tissue and cell function; and whether in a healthy or disease state. Despite decades of work, the intracellular concentrations of mevalonate pathway intermediates in the human body are not known. This is mainly due to two reasons; the isoprenoids do not contain any chromophores and can thus not be detected by UV analysis. Also, the alkene

bonds and pyrophosphate moieties are both biologically and chemically unstable, resulting in large data variations depending on sample extraction protocols. The amounts measured for different samples are often determined by diverse methods and are difficult to correlate as the concentrations are reported in different units that cannot be easily interconverted. The concentration of circulating FPP in human blood plasma has been measured to be 6.6 ng/mL (~17 nM) by HPLC with Fluorescence Detection (HPLC-FL), and levels were found to remain constant over the course of the day (determined by patient monitoring).⁷ In recently deceased brain tissue of elderly (age 71-80) the endogenous FPP and GGPP levels were found to be 4.5 and 10.6 ng/mg protein, respectively, as determined by UHPLC-MS/MS.^{8,9} Across 4 human multiple myeloma cell (MM) lines (RPMI-8226, U266, H929 and K562) HPLC-FL was also used to measure GPP (0.029 to 0.101 pmol/10⁶ cells), FPP (0.087 to 0.751 pmol/10⁶ cells) and GGPP (0.154 to 0.320 pmol/10⁶ cells).¹⁰ These findings highlight that the involvement of the mevalonate pathway may vary significantly between MM cancer types and that MM is not one single disease, but rather a collection of phenotypically related malignancies.¹¹ In a hepatoma cell line (HepG2), DMAPP/IPP, GPP, FPP and GGPP were found to be under the detection limit of the HPLC-MS/MS methodology utilized (<0.5 μ M) and only the DMAPP and IPP isoprenoids could be measured after the addition of FPPS inhibitors.¹² Finally, although not in human tissue, in an early report from 1988, Rilling and co-workers describe a protocol using isotopically labelled isoprenoids precursors to measure mevalonate pathway intermediates in rats and mice on controlled diets.¹³ They performed their studies on the liver tissue, which is important in the production of cholesterol and thus relies heavily on the mevalonate pathway. IPP and FPP concentrations were measured to be ~0.5 μ M in well fed mice and rats; and in starved animals IPP drops 3-fold, while FPP remains the same. Furthermore, the authors measured the concentrations of the enzymes FPPS and SQS to be 350 ng/mL and 4.2 ng/mL, respectively; underscoring the importance of FPPS at the first branching point of the mevalonate pathway.

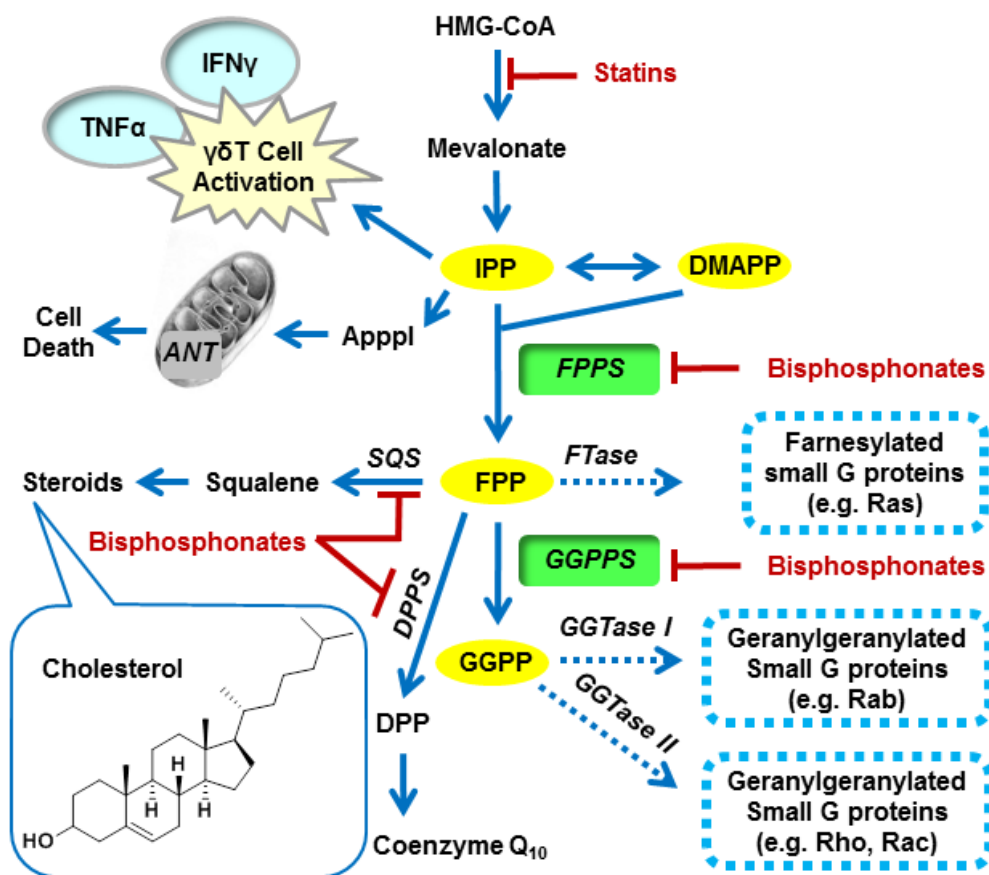


Figure 1.3: The mevalonate pathway. Dashed arrows indicate prenylation-related events. The names of key enzymes are depicted in *italic*, inhibition by drugs is shown in red.

1.2.2 Commercial drugs targeting the mevalonate pathway:

High levels of cholesterol are strongly associated with cardiovascular disease. Consequently key enzymes of the mevalonate pathway have been the focus of extensive medicinal chemistry efforts towards the discovery of cholesterol lowering drugs. This led to the development of the statins, a class of drugs that inhibit HMG-CoA reductase and are therapeutically used for the prevention of cardiovascular disease and strokes (**Figure 1.3**). Atorvastatin (Lipitor[®] by Pfizer) is the most clinically used statin and its sales have surpassed \$100 billion US, making it the best-selling drug to date.¹⁴

The bisphosphonates are a class of drugs that are currently used for bone-related malignancies, which also exert their action through inhibition in the mevalonate pathway. The common bisphosphonate moiety is a non-hydrolysable mimic of the pyrophosphate

found in the natural substrates (**Figure 1.4**). However, the pyrophosphate moiety is common to all isoprenoid substrates and, consequently, the relatively small bisphosphonate drugs are often non-selective in binding to only one prenylase enzyme in the mevalonate pathway (**Figure 1.3**). Nonetheless, bisphosphonate drugs are clinically used to treat osteoporosis and cancer metastasis in bone tissue; this class of compounds will be discussed in more detail in section 1.5.

1.2.3 Prenylation:

FPP and GGPP can also serve as substrates for the posttranslational modification of proteins, a process known as prenylation, in which the lipophilic alkenyl chain is covalently attached to a cysteine residue at (or near) the C terminus of the protein (**Figure 1.3**, dashed arrows). There are two distinct recognition sequences for prenylation;¹⁵ the CaaX motif is recognized by farnesyl- (FTase) and geranylgeranyl transferase I (GGTase I). ‘C’ is a cysteine, ‘a’ an aliphatic amino acid, and ‘X’ a terminal residue specific for either transferase. The second recognition sequence is the CXC or CC motif, for GGTase II. After prenylation, the terminal three amino acids are cleaved off (–aaX) and the terminal carboxylate is subsequently methylated.¹⁶ The prenyl chain can bury deep into the phospholipid bilayer of the cell and its attachment makes a protein also considerably more lipophilic. Prenylation of proteins thus leads to their association with plasma membranes. In total, an estimated 2% of the total mammalian proteome is covalently modified with a farnesyl or geranylgeranyl alkenyl chain.¹⁷

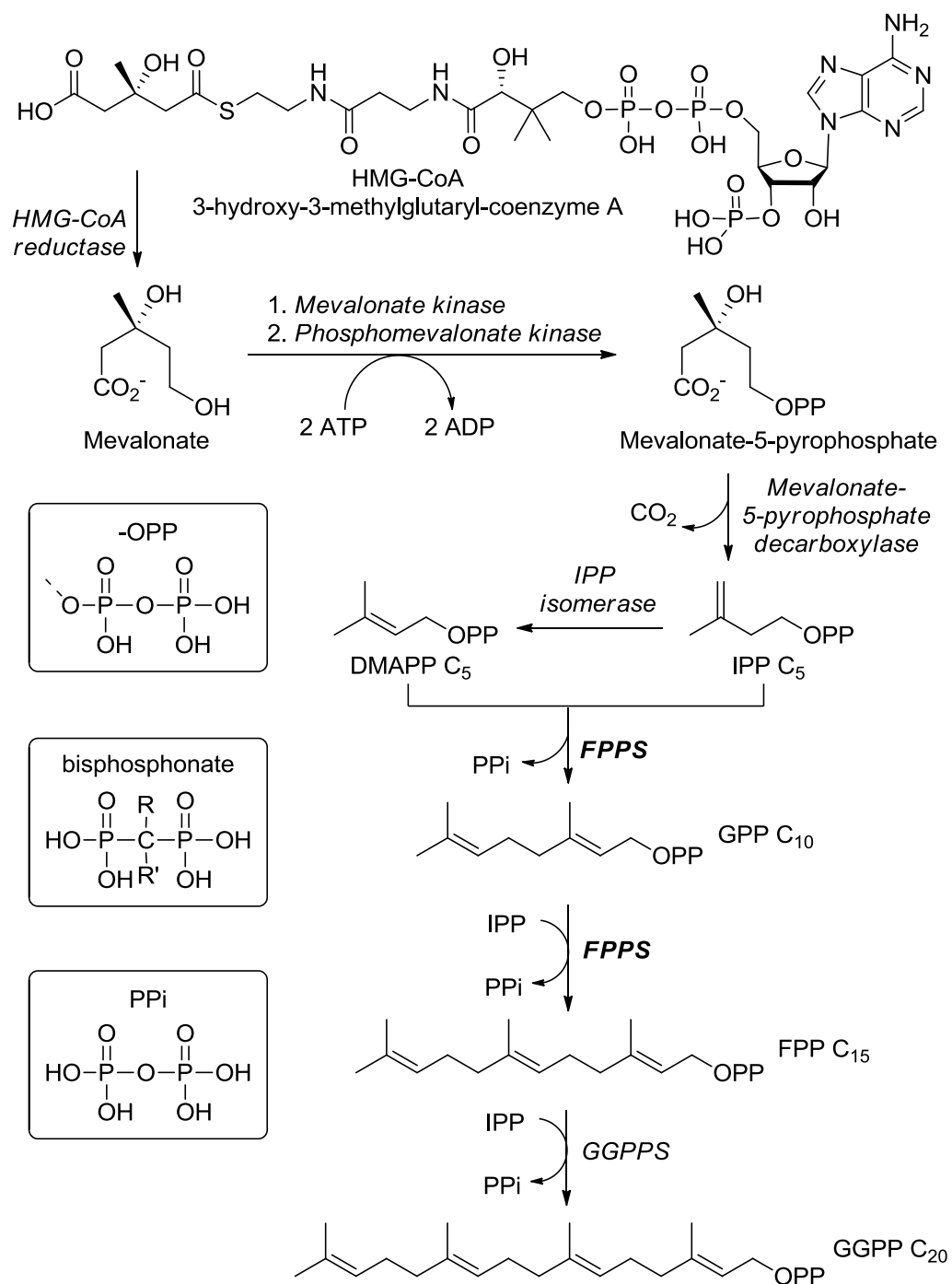


Figure 1.4: Biosynthesis of farnesyl pyrophosphate. The names of key enzymes are written in *italic*.

1.3 Implication of the mevalonate pathway in oncogenesis

Numerous mechanisms leading to anti-cancer activity have been associated with drugs that inhibit the human FPPS; some of the most significant recent findings are summarized below.

1.3.1 Farnesyl transferase inhibitors:

The majority of small GTPases, a large family of signalling proteins that are fundamentally important for cell survival, are prenylated.¹⁷⁻¹⁹ This modification is essential for their intracellular membrane localization and critical for their proper biological function in a multitude of signal transduction pathways. The group of farnesylated proteins includes H-Ras, K-Ras, N-Ras and RhoB GTPases, whereas geranylgeranylated GTPases include RhoA, RhoB, RhoC, Rac1, Cdc42, R-Ras and Rap1a. Many human cancers have been found to harbour activating oncogenic mutations in the RAS genes, between 8% and 93%, depending on the tumor type.¹⁸ The high rate of farnesylated oncogenes, such as for pancreatic (90% K-Ras mutations)^{20,21}, lung, and colon (~30% K-Ras mutations)²² carcinomas, sparked the interest to develop selective FTase inhibitors as novel anti-cancer agents. A large medicinal chemistry effort produced several potent leads, with Tipifarnib (**Figure 1.5**) being the first to enter clinical trials. However, despite promising pre-clinical data, it failed to exhibit significant efficacy in man.²³ Subsequent studies towards understanding this discrepancy between pre-clinical and clinical data revealed that the oncogenic Ras proteins are geranylgeranylated in the presence of FTase inhibitors, thus restoring their biological function.²⁴ Hence it was discovered that substrate specificity of the three prenyl transferase enzymes, is not absolutely stringent and cross-prenylation can occur when necessary; which is likely responsible for the failure of the FTase inhibitors to demonstrate significant clinical efficacy. It is expected that such a biological redundancy mechanism cannot compromise the clinical effects of a drug candidate that *directly* down-regulates the biosynthesis of FPP by inhibiting hFPPS.

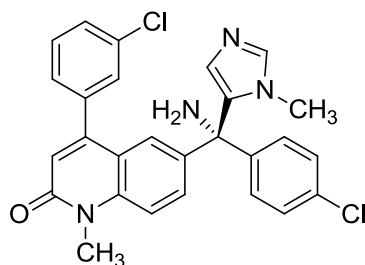


Figure 1.5: Tipifarnib

1.3.2 ApppI as a pro-apoptotic factor:

Recently, the inhibition of hFPPS has been correlated with the detection of pro-apoptotic triphosphoric acid 1-adenosin-50-yl 3-(3-methylbut-3-enyl) ester (ApppI, **Figure 1.6**), an ATP analog that forms as a consequence of intracellular accumulation of IPP.²⁵ ApppI is an inhibitor of mitochondrial adenine nucleotide translocase (ANT) and a direct inducer of apoptosis (**Figure 1.3**).²⁶ This mechanism of cytotoxic effects has been demonstrated *in vitro* in cultured human myeloma cells (RPMI 8226), as well as *in vivo*, in rabbit animal models.^{27,28}

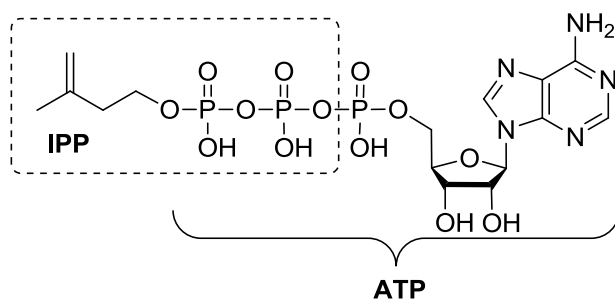


Figure 1.6: ApppI

1.3.3 hFPPS inhibition and immune response:

An additional consequence to intracellular IPP accumulation is the direct stimulation of $\gamma\delta$ T cells (**Figure 1.3**); IPP is a natural antigen that is recognized by human V γ 2V δ 2-bearing T cells.²⁹ Human T cells carrying the $\gamma\delta$ T cell receptors account for 2-5% of CD3+ T cells in the peripheral blood and are strongly implicated in the innate immune response against

tumors and pathogens. During tumor invasion (or infection), the level of $\gamma\delta$ T cells expressing V γ 2V δ 2 T-cell antigen receptors grows such that they can represent the majority of circulating T cells. Short hairpin RNA-mediated knockdown of hFPPS in tumor cell lines have been shown to activate V γ 2V δ 2 T cells and induce IFN- γ secretion.³⁰ Activation of $\gamma\delta$ T cells *in vitro* has been reported with good correlation with respect to the level of hFPPS inhibition.^{30,31} Evidence for the stimulation of V γ 2V δ 2-bearing T cells by bisphosphonates has also been observed in prostate cancer patients; the observed T cell effects coincided with reduction in serum prostate-specific antigen (PSA), providing further evidence of the antitumor immune response *in vivo*.³²

1.3.4 Multiple Myeloma:

Multiple myeloma (MM) is a cancer of the blood plasma cells, in particular B lymphocytes, which are responsible for the production of antibodies. Although it only comprises ~1 % of all human cancers, MM accounts for approximately 2% of all cancer-related deaths because there is no cure, only life-prolonging treatment.³³ With the best therapies available today, the median increase in disease-free survival is only 3-4 years. A recent report of whole genome sequencing of 38 MM patient tumors has demonstrated that exactly 50% of these patients harbor either K-Ras or N-Ras protein coding constitutively activating mutations, underscoring the importance of these oncogenes in this disease.³⁴ There now exists clinical evidence for improved disease-free survival of MM^{35,36}, breast^{37,38} and prostate^{39,40} cancer patients, when treated with standard adjuvant therapy plus a bisphosphonate drug (which are potent inhibitors of the human FPPS), that is independent of the skeletal benefit.

As indicated above, pre-clinical and clinical investigations have provided evidence for multiple mechanisms that mediate the bisphosphonate-induced antitumor effects,⁴¹ including apoptotic cell death,⁴² cell cycle disruption,⁴³ and $\gamma\delta$ T cell activation.⁴⁴ Because of the high level of expression of the hFPPS in MM primary cancer tissues and MM cell lines (personal communication; M. Sebag and co-workers; unpublished data; MUHC and Montreal General Hospital multiple myeloma clinic), the novel hFPPS inhibitors described in this thesis were assayed against several MM cell lines.

1.4 The structure and catalytic function of hFPPS

Human FPPS (hFPPS) exists as a 41 kDa homodimer in solution and is comprised of 10 central α - helices (A to J). In contrast to the smaller microbial FPPS variants, avian and human FPPS possess three short helices (α -1, 2, 3) between helix H and I (**Figure 1.7**).

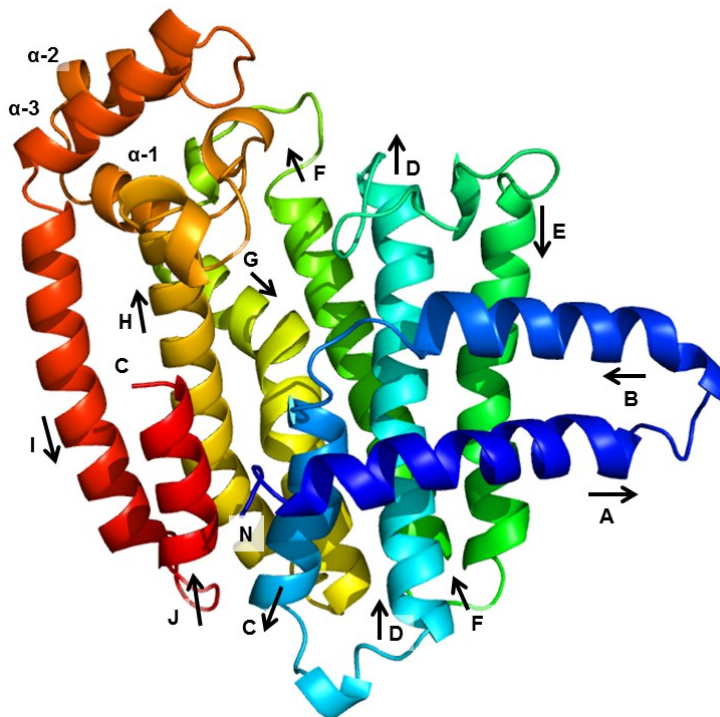


Figure 1.7: Crystal structure of apo hFPPS (PDB 2F7M). Secondary protein structure is shown in rainbow color scheme from the N-terminus (blue) to C-terminus (red); the helix directionality (arrows) and nomenclature (letters) are indicated.

In the unligated, apo state hFPPS adopts an “open conformation” in which the binding pockets for the substrates are relatively disordered. Upon occupation of the allylic sub-pocket by either the DMAPP or GPP substrate (or a bisphosphonate inhibitor) the enzyme undergoes a large structural rearrangement to the “semi-closed conformation” (**Figure 1.8**).⁴⁵ It is believed that the pyrophosphate moiety of the allylic substrate is ligated to metal cations in the cytosol and it brings 3 Mg^{2+} ions into the active site, where they are chelated to three aspartate residues. These critical acidic residues are part of two highly conserved DDXXD motifs (D = aspartate, Asp) found in all FPPS enzymes, ¹¹⁷DDIMD¹²¹ and ²⁵⁷DDYLD²⁶¹ for human FPPS. For this chelation to occur the loops which contain the

DDXXD motifs, D-E and H-I loop, move closer together and form a “gate” which closes access to the allylic sub-pocket.

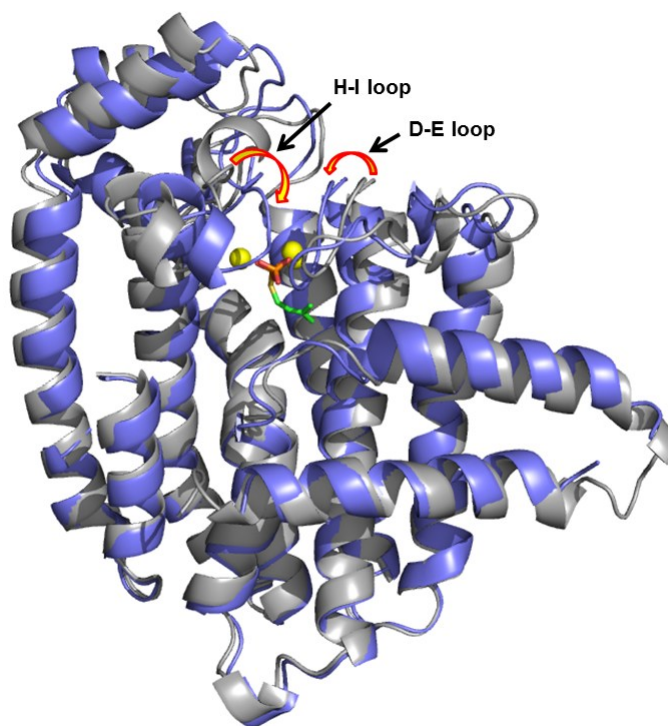


Figure 1.8: Overlap of hFPPS in the open conformation (grey, PDB 2F7M) and semi-closed conformation (blue, PDB 1YV5). Mg^{2+} ions are represented by yellow spheres, the allylic ligand is shown in stick representation with carbon, sulfur, phosphorus and oxygen atoms in green, yellow, orange and red respectively (PDB 1RQI).

In the semi-closed conformation the IPP sub-pocket is partially formed and upon binding of the IPP substrate the enzyme undergoes subtle structural changes to form the final, “fully closed conformation” (**Figure 1.9**). The B-C loop moves in closer to the active site to shield the substrate from bulk solvent, but most importantly the highly basic C-terminal tail swings inward to stabilize the pyrophosphate moiety of the IPP substrate. In fact, if the IPP sub-pocket is unoccupied the final ³⁶⁴KRRK³⁶⁷ residues exist unstructured in the solvent and cannot be resolved by X-ray diffraction; only when IPP binds does the backbone become rigidified and can the C-tail residues be observed. Overall the active site is characterized by two distinct sub-pockets, the allylic sub-pocket for binding the DMAPP

and GPP substrates and the IPP sub-pocket; together forming a deep channel into the center of the enzyme.

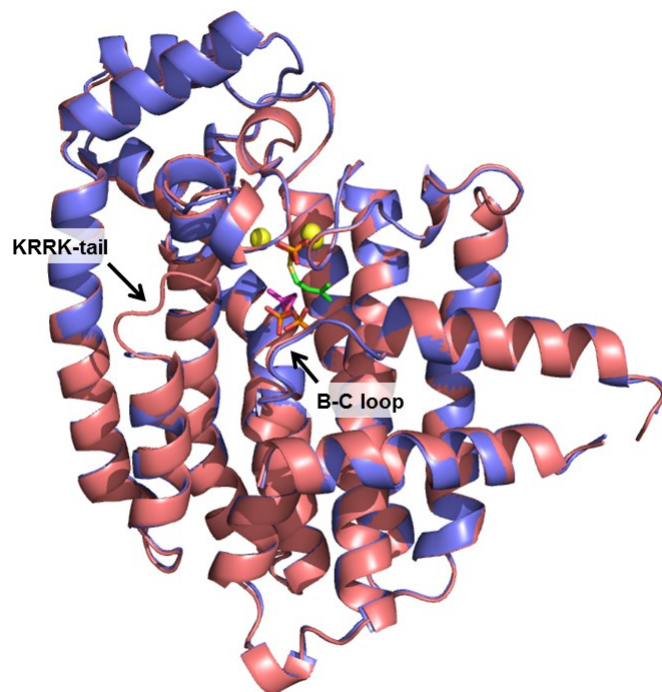


Figure 1.9: Overlap of hFPPS in the semi-closed conformation (blue, PDB 1YV5) and fully closed conformation (maroon, PDB 1ZW5). The allylic ligand and IPP are shown in stick representation, in green and magenta respectively (PDB 1RQI).

Human and other FPPS enzymes form exclusively *E*-double bonds and a C₁₅ final product via exquisite stereo-control during the catalytic condensation of 2 IPP and 1 DMAPP unit. Insight into the mechanism of the catalytic steps has been obtained by Hosfield and co-workers from the ternary structure of *E. coli* FPPS with IPP and DMSPP bound to the active site.⁴⁶ DMSPP is a unreactive thio-analog the DMAPP substrate. These studies suggested that upon binding of an allylic substrate to FPPS, the negative charges of the pyrophosphate moiety are stabilized by the three Mg²⁺ ions that are also coordinated to three aspartic acid residues, Arg 126, Lys 200 and Lys 271 in the active site (e.g. hFPPS, **Figure 1.10**). When IPP co-binds, the pyrophosphate moiety is exclusively stabilized by basic amino acids. The KRRK tail swerves inwards to allow Arg 365 and Lys to make direct salt bridges with IPP (**Figure 1.11a**).⁴⁵ In addition, Arg 127 interacts from the frontal

opening of the binding site and Arg 74 slightly shifts upwards from the bottom of the pocket to make contact (**Figure 1.11b**).

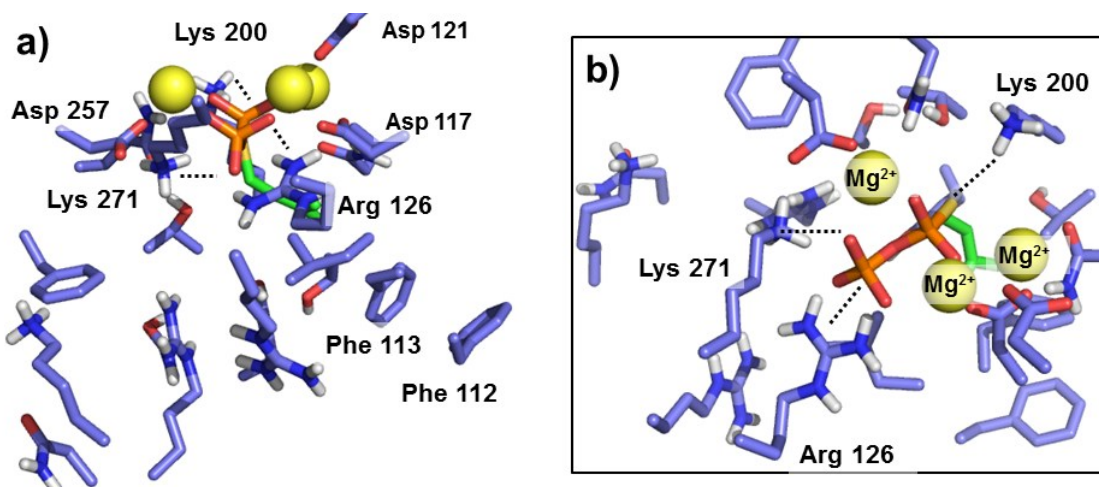


Figure 1.10: Pyrophosphate stabilization in the allylic sub-pocket. Interactions between DMSPP (green backbone, PDB 1RQI) and hFPPS active site residues (blue, PDB 1YV5) are indicated with dashed lines. (a) frontal view of the active site; (b) top view.

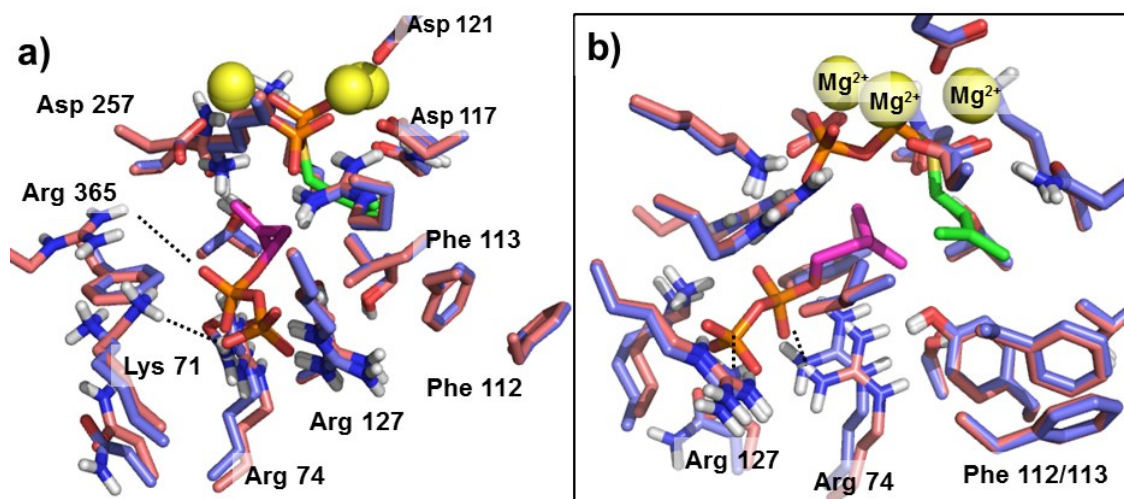


Figure 1.11: Pyrophosphate stabilization in the IPP sub-pocket. Interactions between IPP (magenta backbone PDB 1RQI) and hFPPS active site residues of the fully closed form (maroon, PDB 1ZW5) are indicated with dashed lines. Residues from the semi-closed form are shown for reference (blue, PDB 1YV5). (a) frontal view of the active site; (b) side view

Based on the crystal structure of the *E. coli* FPPS/DMSPP/IPP ternary complex (PDB 1RQI), Hosfield and co-workers proposed a three step enzymatic reaction mechanism: ionization, condensation and elimination.⁴⁶ It is clear that the negative charges on the substrates are not equally stabilized with protein interactions when bound to the active site; the three negative charges (3^-) of the IPP substrate are stabilized by four basic residues, for a balance of a 1^+ charge (**Figure 1.12a**). The 3^- charge of the allylic substrate is matched by 3 basic residues and 3 metals for a total of 3^+ , turning the pyrophosphate group into a good leaving group (**Figure 1.12b**). Upon ionization of the allylic substrate, Lys 200 is perfectly positioned for hydrogen bonding to the oxygen atom that was dissociated from C1 of DMAPP (**Scheme 1.1**). The alkene moiety of IPP then performs a nucleophilic attack on the intermediate carbocation (condensation) and finally the expelled pyrophosphate unit is exquisitely positioned above the IPP unit to stereoselectively deprotonate the pro-R allylic hydrogen atom in order to exclusively form the *E* double bond (**Figure 1.13**).

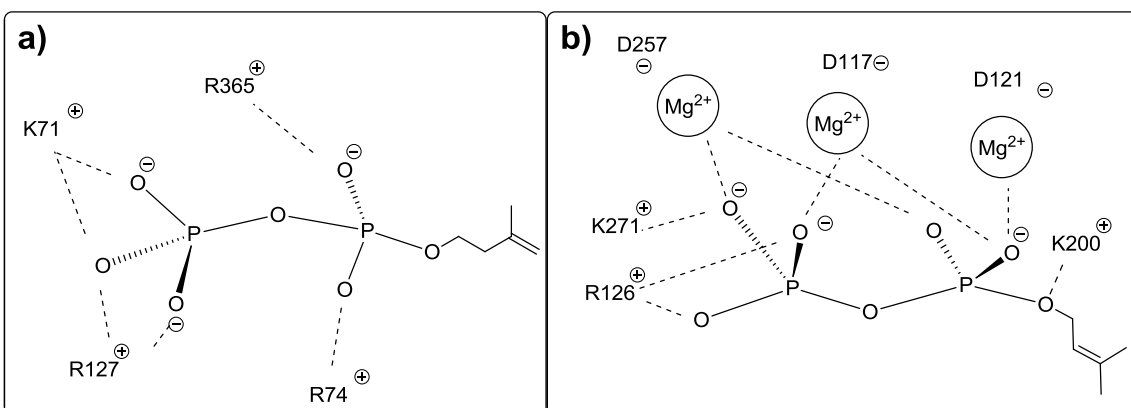
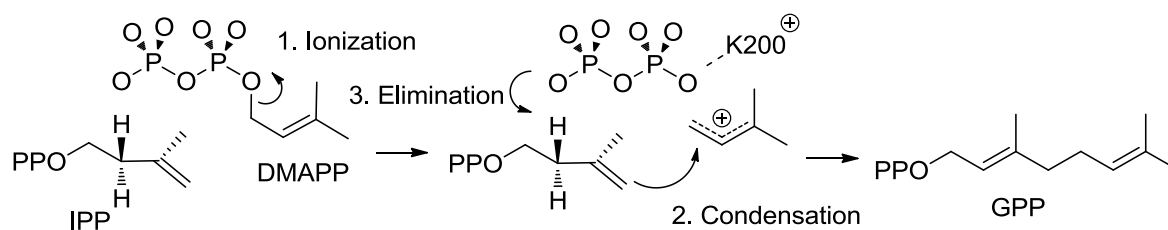


Figure 1.12: Charge compensation of the pyrophosphate moiety of the IPP substrate (a) and allylic substrate (b)



Scheme 1.1: Enzymatic reaction mechanism of FPPS

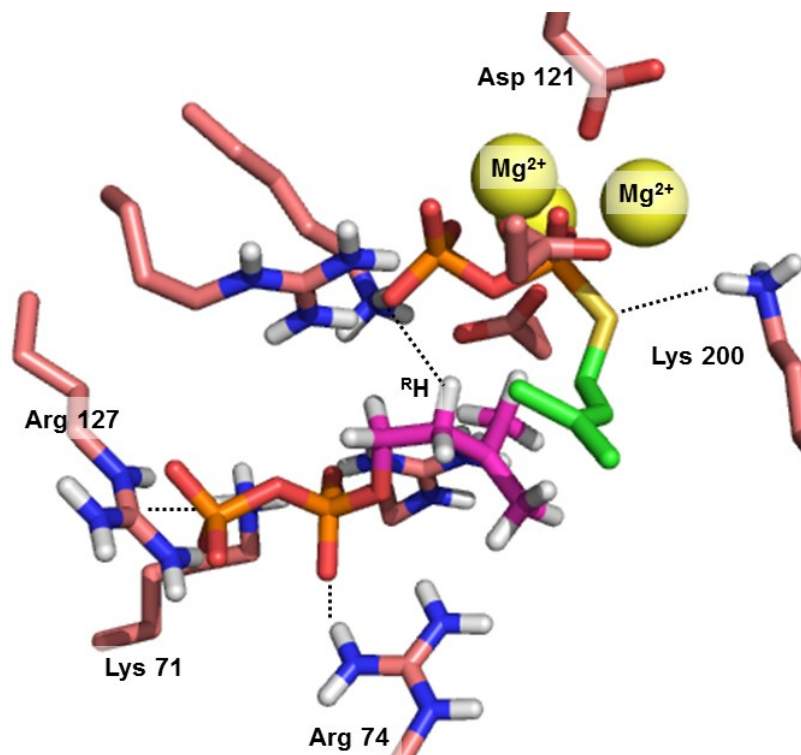


Figure 1.13: Crystal structure of the *E.coli* FPPS/DMSPP/IPP ternary complex (PDB 1RQI). DMSPP (green) and IPP (magenta) are shown in stick representation.

The chain length control of the FPPS condensation reaction is regulated by two phenylalanine residues, Phe 112 and 113, which form the wall of the allylic sub-pocket and are commonly referred to as the “capping phenyls” (**Figure 1.10**). This has been demonstrated by Poulter and co-workers, who used site-directed mutagenesis to change Phe 112 and 113 (F112 and F113) to a smaller serine residue (Ser, S) in avian FPPS.⁴⁷ Indeed, the avian FPPS F112S mutant was capable of producing GGPP (C₂₀) and the corresponding F113S mutant led to the formation of a C₂₅ product. The combined mutant F112S/F113S resulted in even longer chains, as detected by HRMS, and the corresponding crystal structure confirmed that the allylic sub-pocket was approximately 5.8 Å³ larger compared to the wild type avian FPPS.

1.5 Bisphosphonates, inhibitors of hFPPS

In spite of the fact that the active site of hFPPS is, *from a traditional perspective*, an undruggable pocket, a number of drugs are currently in clinical use that bind to this highly charged cavity. As mentioned in section 1.3, the bisphosphonates (BPs) are a class of drugs that inhibit hFPPS. They act as non-hydrolysable substrate mimics of the pyrophosphate moiety found in the natural substrates, where the central oxygen atom has been replaced by a carbon atom (**Figure 1.14**). The first reports of bisphosphonates go back as early as 1865.⁴⁸ These compounds were originally used exclusively for industrial purposes; for example as fertilizers and “water softeners” (due to their ability to chelate Ca^{2+} , preventing CaCO_3 from precipitating). In the 1960s it was discovered that BPs inhibit bone resorption and thus began their use in the treatment of various bone malignancies. During the 1970s BPs were introduced in oncology to reduce the occurrence of skeletal complications as a result of metastasis of the cancer to the bone tissue. Since the 1990s BPs are also commonly used in the prevention and treatment of osteoporosis.⁴⁹

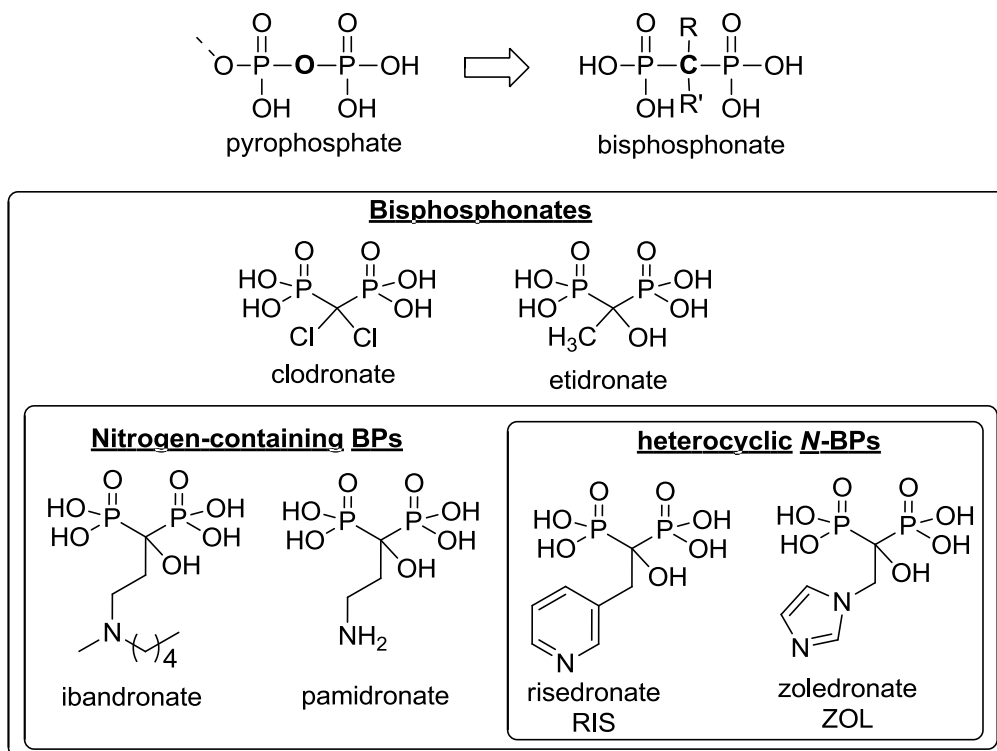


Figure 1.14: Common bisphosphonates

Dozens of bisphosphonates have been evaluated in clinical trials and they can be arbitrarily divided in 3 sub-types: (a) non-nitrogen-containing BPs, (b) nitrogen-containing BPs (*N*-BPs) and (c) nitrogen-containing heterocyclic BPs (**Figure 1.14**). This is also the relative order of increasing enzymatic potency against hFPPS *in vitro*. This trend has been rationalized by the observation that the heterocyclic nitrogen atom is within hydrogen bonding distance of two active site residues, Lys 200 and Thr 201, in hFPPS co-crystal structures with these inhibitors (**Figure 1.15a**); and that a protonated nitrogen heterocycle would mimic the cationic transition state of the allylic substrate in the enzymatic reaction (**Scheme 1.1**).⁵⁰ Indeed the heterocyclic *N*-BPs occupy the allylic sub-pocket exclusively, as has been demonstrated by various co-crystal structures including a ternary complex of hFPPS with zoledronate and the IPP substrate.⁴⁵ The bisphosphonate moiety perfectly mimics the binding mode of the pyrophosphate of the allylic substrates, and binds to the Mg^{2+} triad in the active site.

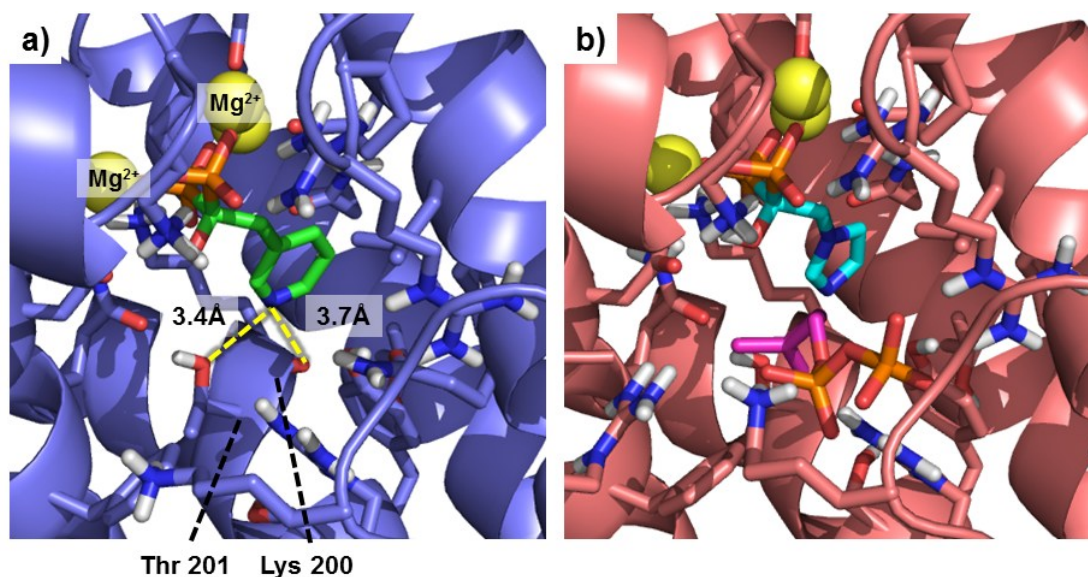
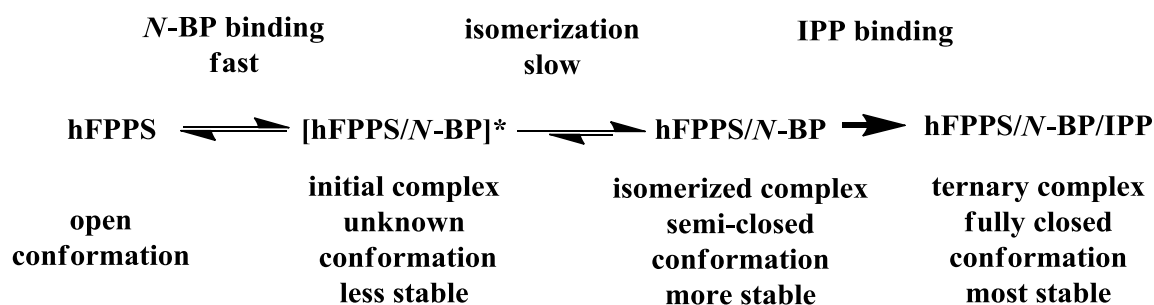


Figure 1.15: a) Crystal structure of hFPPS/RIS (PDB 1YV5). b) hFPPS/ZOL/IPP (PDB 1ZW5) complexes. Ligands are shown in stick representation, risedronate (green), zoledronate (cyan) and IPP (magenta) and the bifurcated hydrogen bond with the backbone carbonyl of Lys 200 and sidechain of Thr 201 is indicated with yellow dashed lines.

The exceptional *in vitro* enzymatic potency of the *N*-BPs is somewhat surprising considering these compounds only occupy approximately two thirds of the allylic sub-pocket, or one third of the entire active site cavity. This observation has been thoroughly investigated and in 2006 Oppermann and co-workers (SGC, UK) published a study comprised of enzyme kinetics and ITC measurements,⁵⁰ immediately followed by a manuscript by Jahnke and co-workers (Novartis) with X-ray crystallography and Differential Scanning Calorimetry (DSC) data.⁴⁵ Taken together, the reported results reveal the mechanistic details of hFPPS inhibition by *N*-BPs.

The inhibition kinetics of *N*-BPs exhibit characteristics corresponding to a slow, tight binding model; where an initial inhibitor/enzyme complex slowly isomerizes to a more stable form, presumably with significant conformational changes of the protein (**Scheme 1.2**). This is reflected in the enzymatic activity of the *N*-BPs, which display a time-dependent inhibition. If the compounds are pre-incubated with the enzyme, before the addition of the substrates, the isomerization has time to occur, forming the more stable semi-closed conformation and the measured half maximal inhibitory concentration (IC₅₀) values are significantly lower compared to the values observed when the assays are run without pre-incubation of the inhibitor with the enzyme (80-fold for risedronate and 115-fold for zoledronate, **Table 1.1**).



Scheme 1.2: Mechanism of time-dependent *N*-BP inhibition

ITC measurements reveal that the binding of *N*-BPs to hFPPS is entropy-driven (**Table 1.2**). The unfavorable enthalpy component is most likely due to disruption of interactions of water molecules with the polar regions of the enzyme and the bisphosphonates. This is reflected by the higher ΔH value for zoledronate, which is slightly more polar than risedronate. The interactions between the inhibitor and enzyme active site are not strong enough to counter the enthalpy loss, but the associated desolvation entropy gain shifts the equilibrium towards the bound complex. In other words, return of structured waters from inside the enzyme active site (and around the *N*-BPs) to the bulk solvent results in an increase in degrees of freedom of the water molecules, a net entropy gain large enough to promote binding. The final, calculated Gibbs free energy also matches the enzymatic potency of the inhibitors.

constant	IPP	GPP	RIS	ZOL
K_m	$1.8 \pm 0.3 \mu\text{M}$	$2.1 \pm 0.2 \mu\text{M}$		
k_{cat}	0.42 s^{-1}			
IC_{50}				
Initial			450 nM	475 nM
Pre-incubated (10 min)			5.7 nM	4.1 nM

Table 1.1: *N*-BP inhibition kinetics.⁵⁰

([hFPPS] ~10 nM; [GPP] and [IPP] 0.2 - 20 μM)

	ΔH kcal/mol	$T\Delta S$ kcal/mol	ΔG kcal/mol
RIS	+ 1.8	+ 10.5	- 8.8
ZOL	+ 2.1	+ 12	- 10

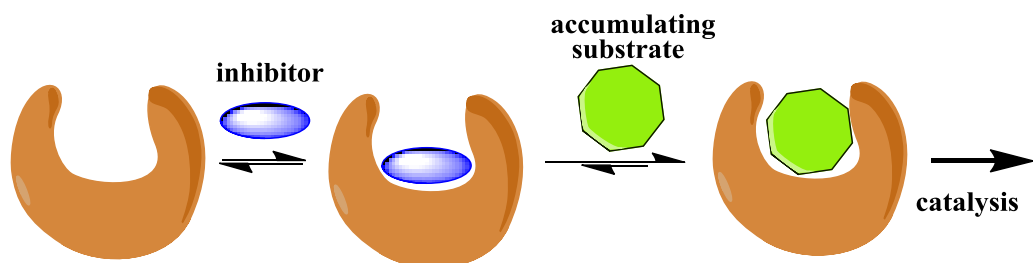
Table 1.2: Thermodynamic data for *N*-BPs.⁵⁰

DSC thermal stability analysis of various *N*-BPs revealed that hFPPS/*N*-BP complexes (semi-closed conformation) melt at a higher temperature than the apo-protein (open conformation) and the increase in melting temperature (ΔT_m) correlates to the enzymatic potency of the *N*-BP in the complex. In other words, stronger active site inhibitors form more stable complexes with the hFPPS protein. The addition of IPP led to a further stabilization of the complexes (fully closed conformation). For example: hFPPS/ZOL melts at 80.6°C ($\Delta T_m = 25.2^\circ\text{C}$) whereas hFPPS/ZOL/IPP melts at 85.6°C ($\Delta T_m = 30.2^\circ\text{C}$), providing an additional 5°C increase in melting temperature. These findings and the discovery of a ternary crystal structure of hFPPS/ZOL/IPP (in which zoledronate occupies the allylic sub-pocket and IPP occupies its respective sub-pocket, PDB 1ZW5), led Jahnke and co-workers to postulate a novel mechanism of inhibition, different from the commonly observed competitive inhibition (**Figure 1.16**). Inhibition of hFPPS leads to the intracellular accumulation of IPP, which in turn will bind to the inhibited hFPPS/*N*-BP complexes, further stabilizing them in the fully closed conformation. This in turn closes the active site off from bulk solvent and prevents the DMAPP and GPP substrates from competing with the *N*-BP inhibitor, which is now locked inside the active site. Thus inhibition of hFPPS by *N*-BPs mimics a non-covalent irreversible inhibition mechanism and the substrate-stabilized hFPPS-inhibitor complex is assumed to be the most representative form of *in vivo* inhibited hFPPS.

In summary, the exceptional *in vitro* enzymatic potency of the *N*-BPs is attributed to the fact that the IPP substrate co-binds to the inhibited hFPPS and together induce the fully closed conformation of the enzyme; which shields both ligands from the bulk solvent and prevents the inhibitor from being displaced by accumulating substrate.

Despite all the structural, kinetic and thermodynamic data available the exact nature of the rate-limiting isomerization step remains unknown. It could be due to desolvation/(de)protonation of the *N*-BP inhibitors⁵¹ or conformational changes of the hFPPS enzyme.⁵² The structure of hFPPS in the presence of Mg^{2+} , but without any bound allylic ligand; remains unknown and could provide insight to better understand the kinetic isomerization step.

a) classical competitive inhibition model



b) hFPPS inhibition by *N*-BPs

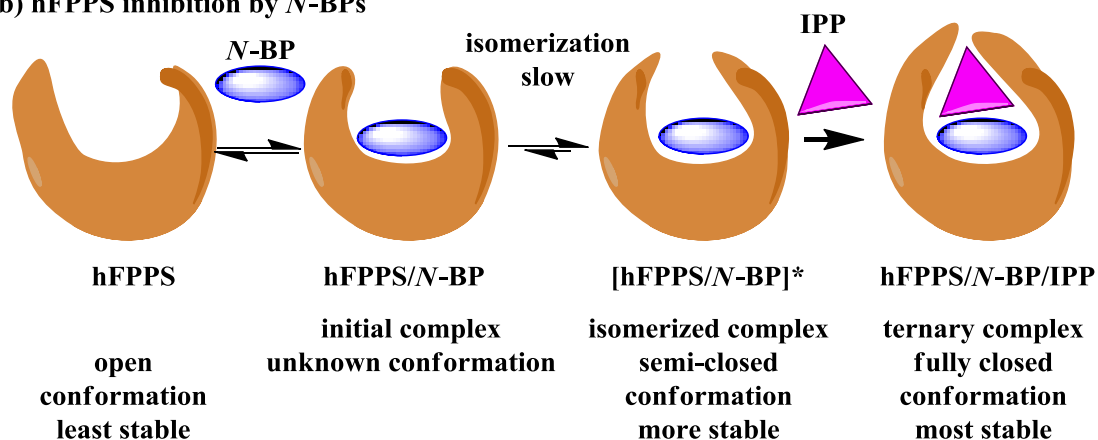


Figure 1.16: a) In a competitive inhibition mechanism, the accumulation of substrate eventually displaces the inhibitor, leading to resumption of catalytic activity. b) With FPPS, the accumulating IPP substrate binds to and further stabilizes the FPPS/*N*-BP complex, thereby blocking the allylic substrates from displacing the *N*-BP inhibitor.

1.6 Inhibitors of the hFPPS, biopharmaceutical properties and clinical implications

1.6.1 Active site inhibitors:

The bisphosphonates owe their therapeutic value to a combination of key biopharmaceutical properties. The α -hydroxy bisphosphonate moiety (**Figure 1.17**, highlighted with dashed ellipsoids), often referred to as the “bone hook”, has great affinity for Ca^{2+} ions and binds avidly to hydroxyapatite. Therefore, upon reaching the systemic blood circulation, ~50% of the *N*-BP drug is excreted directly via the urinary tract and the remainder accumulates almost exclusively in bone tissue. Due to the high polarity of the bisphosphonate moiety, *N*-BPs have extremely poor cell membrane permeability and essentially cannot penetrate into soft tissue or circulating blood cells. Bone homeostasis is maintained by constant turnover and regulated by the anabolic osteoblasts and catabolic osteoclasts. In order to break down bone tissue, osteoclasts dissolve hydroxyapatite by local acidification and absorb the material through fluid-phase endocytosis. Therefore any *N*-BPs that were bound to the bone tissue are transferred directly into the cytosol of the osteoclast, without having to traverse the cell membrane. Finally, by inhibiting the mevalonate pathway, cell death is induced and the bone catabolism is reduced *in vivo*. Due to this unique combination of pharmacokinetic and pharmacodynamic properties *N*-BPs are almost exclusively active against osteoclasts, and it is via this mechanism that the bisphosphonates exert their clinical function as antiresorptive drugs, with minimal side-effects.⁴⁹

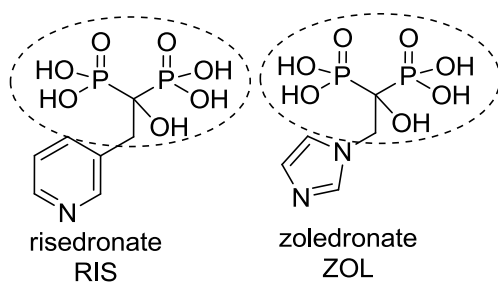


Figure 1.17: Risedronate and zoledronate

Zoledronate (ZOL)) and risedronate (RIS) are the most potent hFPPS inhibitors with reported IC_{50} values of 4.1 nM and 5.7 nM, respectively, and they are also the most clinically relevant. Risedronate (Actonel[®], Sanofi-Aventis) is used to treat osteoporosis in elderly patients and it is typically taken orally: 5mg daily, 35 mg weekly or 150 mg monthly. Due to the poor oral bioavailability (0.63%) and complications with food, risedronate must be taken on an empty stomach and only water may be consumed for the next 2.5 hours. Additionally, irritation of the esophagus is commonly experienced (due to the acidic nature of bisphosphonates), and this leads to poor patient adherence to the dosage regime. In contrast, zoledronate (Zometa[®], Novartis) has no oral bioavailability and must be administered by i.v. For osteoporosis, zoledronate is given once a year in a 5 mg dose (under the tradename Aclasta[®]) as it can suppress bone resorption for such extended periods of time.⁵³ As chemotherapy is already administered via i.v., zoledronate is readily included in order to prevent and treat bone cancer metastasis.

There now exists significant pre-clinical and clinical evidence that modulating the activity of hFPPS can have desirable anti-cancer effects (refer to section 1.3). However, the bisphosphonates are the only currently available drugs that inhibit hFPPS; and these drugs have no distribution into soft tissues due to their inherent polarity. The central bisphosphonate moiety confers high polarity to the hFPPS inhibitors, but is also crucial to their enzymatic potency as it is the main pharmacophore that anchors them to the active site. Furthermore, some bisphosphonates exhibit poor target selectivity, due to their small size and the fact that the bisphosphonate moiety is a substrate mimic for pyrophosphate, a common moiety for all prenylation substrates of numerous enzymes in the mevalonate pathway. Not surprisingly, *N*-BPs have been shown to inhibit a large variety of enzymes including hGGPPS (**Figure 1.18**, inhibitor **1.1**)⁵⁴, squalene synthase (SQS, ibandronate)⁵⁵ and decaprenyl synthase (DPPS, ZOL and **1.1**)^{31,54}. Even outside of the mevalonate pathway they can also inhibit various enzymes (**Table 1.3**); for example zoledronate inhibits acid sphingomyelinase (aSMase)⁵⁶, a membrane-associated signal transduction protein involved in plasma membrane composition, and several matrix metalloproteinases (MMP)⁵⁷, critical for regulation of structural proteins (e.g. collagen). It should be noted that aSMase and MMPs can be found on the outer leaflet of the cell membrane and,

consequently, they are likely inhibited by *N*-BPs in the bone micro-environment *in vivo* and in various cell-based assays *in vitro*. The bisphosphonate moiety can also potentially bind to any phosphate/pyrophosphate recognition element found in the human proteome, and there are many such proteins, including kinases (ATP binding pocket), phosphatases and any number of nucleotide/nucleoside processing enzymes. The target selectivity issue may be exacerbated due to the small size of the current *N*-BP drugs, which can fit in any number of binding pockets. Therefore, in order to improve lipophilicity (an important property for cell-membrane permeability), the bisphosphonate will have to either be replaced by a less polar Mg^{2+} chelator (such as the pyrimidinone in raltegravir, **Figure 1.2**) or inhibitors of hFPPS will have to be identified that do not engage in interactions with the highly conserved aspartic acid motif within the allylic sub-pocket of the active site (*e.g.* allosteric inhibitors). In order to develop hFPPS inhibitors that can serve as useful leads for novel therapeutic agents for non-skeletal cancers, a key focus of this PhD thesis is the discovery of less polar, highly selective inhibitors of the human FPPS.

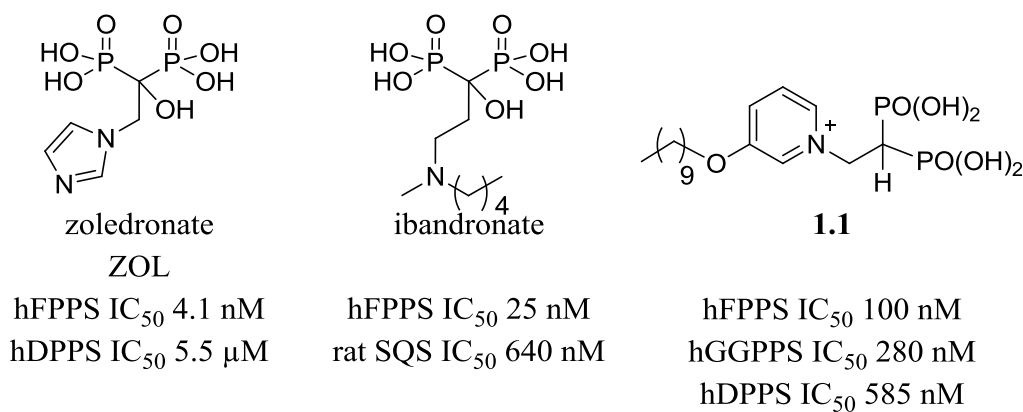


Figure 1.18: *N*-BP enzymatic inhibition data in the mevalonate pathway.^{31,54,55}

		Matrix metalloproteinases			
	aSMAse	MMP-2	MMP-8	MMP-9	MMP-14
zoledronate IC ₅₀	5.1 μM	7.0 μM	18 μM	52 μM	13 μM

Table 1.3: Zoledronate inhibition data for proteins outside the mevalonate pathway.^{56,57}

Some degree of selectivity for bisphosphonates can be achieved with the size of the sidechain, *i.e.* increasing the total volume of the inhibitors. Indeed, enzymes with relatively small and well-defined active sites, such as hFPPS, simply cannot accommodate inhibitors with a very large sidechain. This principle of size exclusion is the main method by which selectivity for hGGPPS over hFPPS has been accomplished thus far. hGGPPS has a significantly larger active site in order to bind the C₁₅ allylic substrate (FPP) and the C₂₀ GGPP product. This enzyme is selectively inhibited by bisphosphonates **1.2**⁵⁴ and **1.3**⁵⁸ (**Figure 1.19**); however, they may still inhibit other enzymes that use FPP as a substrate. For example, compound **1.2** also inhibits *E.coli* Undecaprenyl pyrophosphate synthase (UPPS) with an IC₅₀ value of 1.1 μM.⁵⁹ This underscores the importance of developing inhibitors that engage in specific interactions, unique to the intended binding pocket architecture, in order to achieve selectivity for the target protein; rather than rely on general characteristics.

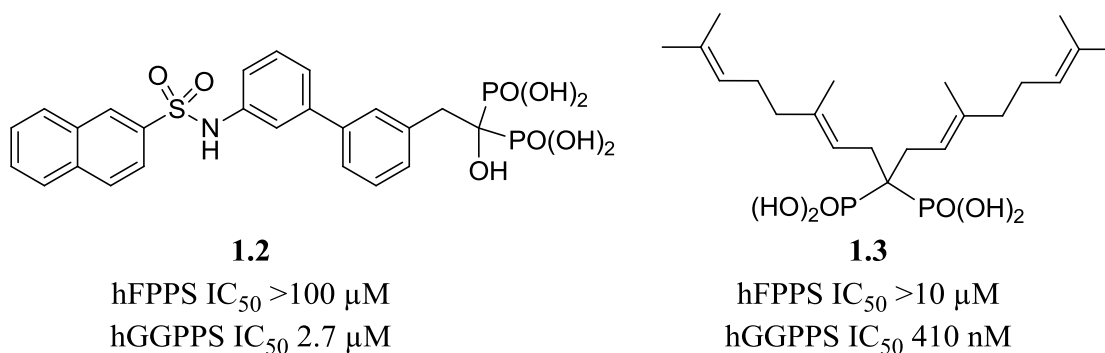


Figure 1.19: hGGPPS inhibitors

1.6.2 Allosteric inhibitors of hFPPS

In 2010 Jahnke and co-workers (Novartis) reported the discovery of an allosteric pocket near the active site of hFPPS and showed that compounds binding to this pocket inhibit the enzyme.⁶⁰ Initially, 400 fragments were screened using NMR spectroscopy, leading to 4 hits (all carboxylic acids *e.g.* **1.4**, **Figure 1.20**) with weak binding affinity. These compounds, having IC₅₀ values over 500 μ M, would have been missed by traditional high throughput screening (HTS) biochemical assays, for which enzymatic activity below 100 μ M is generally required.⁶¹ In contrast, ligand observed NMR is well suited to detect compounds that bind weakly to proteins and this technique will be explained in more detail in section 2.7. X-ray crystallography confirmed that the 4 hits bound to a pocket adjacent to the active site and a ternary crystal structure with inhibitor **1.4** and zoledronate co-bound was also resolved (**Figure 1.21a**). The allosteric binding site is situated right next to the IPP sub-pocket, at the C-terminus of the enzyme, and is composed of a small hydrophobic pocket, next to the basic residues that are responsible for stabilizing the pyrophosphate moiety of the IPP substrate. ITC measurements indicate that the binding is enthalpy driven, as a combination of hydrophobic interactions in the pocket and salt bridges between the carboxylates of the inhibitors and the nearby basic residues. The obtained binary crystal structures showed that the allosteric binders induce the open conformation of hFPPS (**Figure 1.21b**); while the ternary hFPPS/ZOL/**1.4** complex adopts the semi-closed conformation (**Figure 1.21a**).

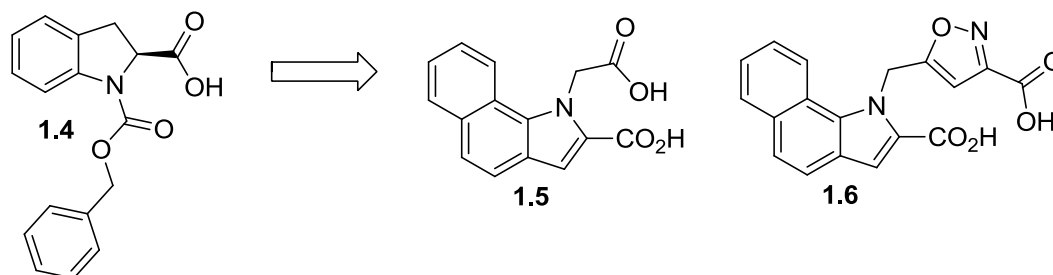


Figure 1.20: Fragment optimization of allosteric inhibitors

Further fragment screenings and hit optimization efforts lead to the development of **1.5** and **1.6**, with IC_{50} values of 200 nM and 80 nM, respectively, against hFPPS (**Figure 1.20**). The mechanism of allosteric inhibition is attributed to two simultaneous effects: occupation of the allosteric pocket blocks the C-terminal KRRK-tail from clamping down on the active site, precluding catalysis (Arg 365, **Figure 1.22**). Also, the proximity of the negatively charged allosteric inhibitors can electrostatically repulse the IPP substrate and prevent it from binding. The inhibition is also time-independent, clearly distinguished from the *N*-BPs. At this time, the biological role of the allosteric pocket is unknown; given the architectural complementarity, as well as the fact that lipophilic carboxylic acid molecules can bind to it, it is reasonable to assume that it may be occupied by phosphate-containing biomolecules in a regulatory role. However, ATP, GTP and analogs were found not to inhibit the hFPPS enzyme.

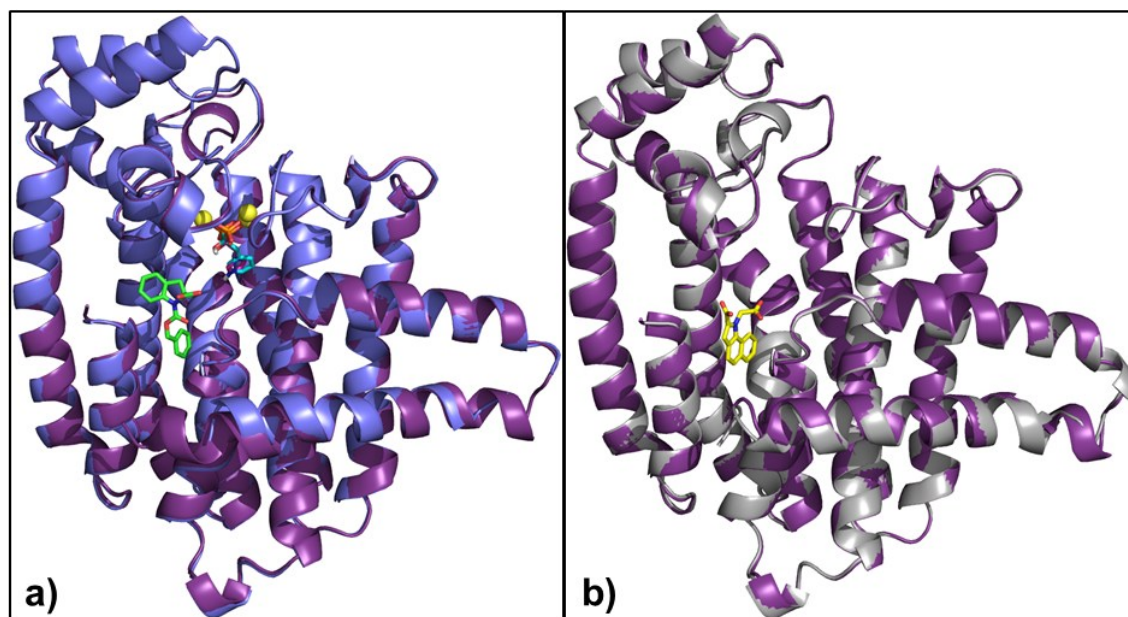


Figure 1.21: a) overlap of hFPPS/RIS complex (blue, PDB 1YV5) and hFPPS/ZOL/**1.4** ternary complex (purple, PDB 3N45), both in the semi-closed conformation. Risedronate, zoledronate and **1.4** are shown in stick representation, cyan, magenta and green respectively. b) Overlap of hFPPS apo structure (grey, PDB 2F7M) and hFPPS/**1.5** complex (purple, PDB 3N6K), both in the open conformation; **1.5** is shown in yellow.

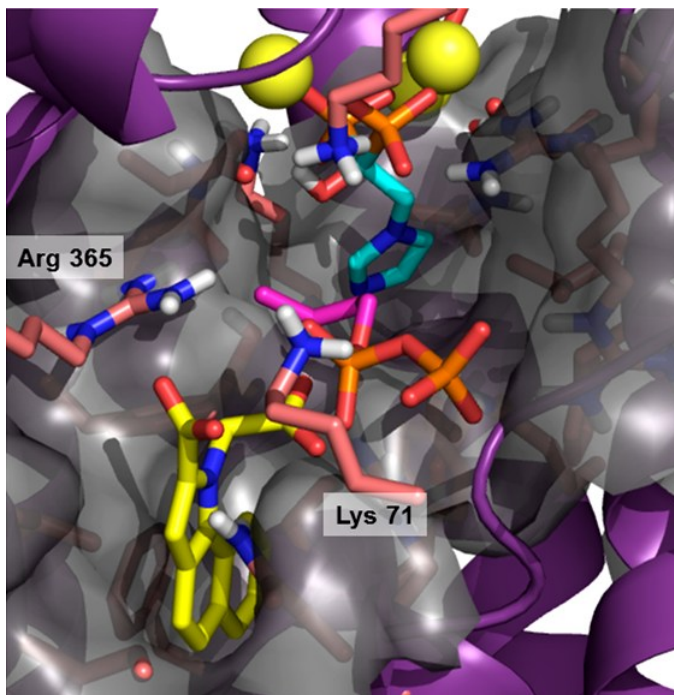


Figure 1.22: Composite picture. hFPPS/**1.5** protein tertiary structure (purple backbone, semi-transparent surface, PDB 3N6K) overlapped with hFPPS/ZOL/IPP residue sidechains (maroon, PDB 1ZW5). Zoledronate, IPP and **1.5** are shown in stick representation, cyan, magenta and yellow respectively.

Finally, pre-clinical profiling of **1.5**, showed that this compound has poor cell-membrane permeability, presumably due to the presence of two carboxylic acid moieties; to date no follow up on these compounds has been reported in either the scientific or patent literature.

1.7 Research goals

Recent clinical investigations have provided strong evidence that nitrogen-containing bisphosphonate (*N*-BPs) inhibitors of hFPPS are disease modifying agents that improve survival in patients with multiple myeloma via mechanisms that are unrelated to their skeletal effects.^{35,36} However, the therapeutic value of currently available drugs that target hFPPS is limited by their poor biopharmaceutical properties and high affinity for bone. Consequently, the development of novel hFPPS inhibitors with improved cell-membrane permeability, good target selectivity and distribution in non-skeletal tissue is of crucial importance. However, due to the charged nature of the active site and the overall plasticity of the protein, hFPPS is considered, *in the traditional sense*, as an “undruggable” target and avoided by most pharmaceutical industries as a high risk therapeutic target. Therefore it is all the more suited for an academic medicinal chemistry research program.

Our goals are to develop novel inhibitors by probing the size, shape and electrostatic surface complementarity between our inhibitors and the active site, or allosteric pocket, of hFPPS. Our SAR studies include the evaluation of both *N*-BP and non-*N*-BP molecules and are guided by structural data (*in silico*, NMR, X-ray crystallography and DSF). Biological evaluations of our compounds include enzyme inhibition assays (using hFPPS and hGGPPS) and cell-based assays using human MM cell lines.

In summary, this thesis describes structural investigations that focus on the plasticity of the hFPPS protein and the mechanism of inhibition of this target. A structure-based approach was also used to design novel inhibitors of this enzyme that exhibit better biopharmaceutical properties as compared to those of the current clinically relevant *N*-BP drugs. Preliminary evaluation in anti-proliferation assays with a panel of multiple myeloma cells is also described, providing evidence of the potential role of hFPPS inhibitors in treating multiple myeloma.

1.8 References

- (1) Hopkins, A. L.; Groom, C. R.; The druggable genome *Nat. Rev. Drug. Discov.* **2002**, *1*, 727.
- (2) Billingsley, M. L.; Druggable Targets and Targeted Drugs: Enhancing the Development of New Therapeutics *Pharmacology* **2008**, *82*, 239.
- (3) Kozakov, D.; Hall, D. R.; Chuang, G.-Y.; Cencic, R.; Brenke, R.; Grove, L. E.; Beglov, D.; Pelletier, J.; Whitty, A.; Vajda, S.; Structural conservation of druggable hot spots in protein–protein interfaces *Proc. Natl. Acad. Sci. U.S.A.* **2011**, *108*, 13528.
- (4) Summa, V.; Petrocchi, A.; Bonelli, F.; Crescenzi, B.; Donghi, M.; Ferrara, M.; Fiore, F.; Gardelli, C.; Gonzalez Paz, O.; Hazuda, D. J.; Jones, P.; Kinzel, O.; Laufer, R.; Monteagudo, E.; Muraglia, E.; Nizi, E.; Orvieto, F.; Pace, P.; Pescatore, G.; Scarpelli, R.; Stillmock, K.; Witmer, M. V.; Rowley, M.; Discovery of Raltegravir, a Potent, Selective Orally Bioavailable HIV-Integrase Inhibitor for the Treatment of HIV-AIDS Infection *J. Med. Chem.* **2008**, *51*, 5843.
- (5) Hazuda, D. J.; Felock, P.; Witmer, M.; Wolfe, A.; Stillmock, K.; Grobler, J. A.; Espeseth, A.; Gabryelski, L.; Schleif, W.; Blau, C.; Miller, M. D.; Inhibitors of Strand Transfer That Prevent Integration and Inhibit HIV-1 Replication in Cells *Science* **2000**, *287*, 646.
- (6) Goldstein, J. L.; Brown, M. S.; Regulation of the mevalonate pathway *Nature* **1990**, *343*, 425.
- (7) Saisho, Y.; Morimoto, A.; Umeda, T.; Determination of Farnesyl Pyrophosphate in Dog and Human Plasma by High-Performance Liquid Chromatography with Fluorescence Detection *Anal. Biochem.* **1997**, *252*, 89.
- (8) Hooff, G. P.; Volmer, D. A.; Wood, W. G.; Müller, W. E.; Eckert, G. P.; Isoprenoid quantitation in human brain tissue: a validated HPLC–fluorescence detection method for endogenous farnesyl- (FPP) and geranylgeranylpyrophosphate (GGPP) *Anal. Bioanal. Chem.* **2008**, *392*, 673.
- (9) Hooff, G. P.; Patel, N.; Wood, W. G.; Müller, W. E.; Eckert, G. P.; Volmer, D. A.; A rapid and sensitive assay for determining human brain levels of farnesyl-(FPP) and geranylgeranylpyrophosphate (GGPP) and transferase activities using UHPLC-MS/MS *Anal. Bioanal. Chem.* **2010**, *398*, 1801.
- (10) Holstein, S.; Tong, H.; Kuder, C.; Hohl, R.; Quantitative Determination of Geranyl Diphosphate Levels in Cultured Human Cells *Lipids* **2009**, *44*, 1055.
- (11) van der Spek, E.; Targeting the mevalonate pathway in multiple myeloma *Leukemia Res.* **2010**, *34*, 267.
- (12) Henneman, L.; van Cruchten, A. G.; Denis, S. W.; Amolins, M. W.; Placzek, A. T.; Gibbs, R. A.; Kulik, W.; Waterham, H. R.; Detection of nonsterol isoprenoids by HPLC–MS/MS *Anal. Biochem.* **2008**, *383*, 18.
- (13) Bruenger, E.; Rilling, H. C.; Determination of isopentenyl diphosphate and farnesyl diphosphate in tissue samples with a comment on secondary regulation of polyisoprenoid biosynthesis *Anal. Biochem.* **1988**, *173*, 321.
- (14) The, L.; Lessons from Lipitor and the broken blockbuster drug model *Lancet* **2011**, *378*, 1976.

- (15) Harris, C. M.; Poulter, C. D.; Recent studies of the mechanism of protein prenylation *Nat. Prod. Rep.* **2000**, *17*, 137.
- (16) Winter-Vann, A. M.; Casey, P. J.; Post-prenylation-processing enzymes as new targets in oncogenesis *Nat. Rev. Cancer* **2005**, *5*, 405.
- (17) Nguyen, U. T. T.; Guo, Z.; Delon, C.; Wu, Y.; Deraeve, C.; Franzel, B.; Bon, R. S.; Blankenfeldt, W.; Goody, R. S.; Waldmann, H.; Wolters, D.; Alexandrov, K.; Analysis of the eukaryotic prenolome by isoprenoid affinity tagging *Nat. Chem. Biol.* **2009**, *5*, 227.
- (18) Berndt, N.; Hamilton, A. D.; Sebt, S. M.; Targeting protein prenylation for cancer therapy *Nat. Rev. Cancer* **2011**, *11*, 775.
- (19) Goldfinger, L. E.; Choose your own path: specificity in Ras GTPase signaling *Mol. Biosys.* **2008**, *4*, 293.
- (20) Deramaut, T.; Rustgi, A. K.; Mutant KRAS in the initiation of pancreatic cancer *Biochim. Biophys. Acta* **2005**, *1756*, 97.
- (21) Slebos, R. J. C.; Hoppin, J. A.; Tolbert, P. E.; Holly, E. A.; Brock, J. W.; Zhang, R. H.; Bracci, P. M.; Foley, J.; Stockton, P.; McGregor, L. M.; Flake, G. P.; Taylor, J. A.; K-ras and p53 in Pancreatic Cancer: Association with Medical History, Histopathology, and Environmental Exposures in a Population-based Study *Cancer Epidemiol. Biomarkers Prev.* **2000**, *9*, 1223.
- (22) Wittinghofer, A.; Waldmann, H.; Ras—A Molecular Switch Involved in Tumor Formation *Angew. Chem. Int. Ed.* **2000**, *39*, 4192.
- (23) Thomas, X.; Elhamri, M.; Tipifarnib in the treatment of acute myeloid leukemia *Biol. Targets Ther.* **2007**, *1*, 415.
- (24) Whyte, D. B.; Kirschmeier, P.; Hockenberry, T. N.; Nunez-Oliva, I.; James, L.; Catino, J. J.; Bishop, W. R.; Pai, J.-K.; K- and N-Ras Are Geranylgeranylated in Cells Treated with Farnesyl Protein Transferase Inhibitors *J. Bio. Chem.* **1997**, *272*, 14459.
- (25) Mönkkönen, H.; Auriola, S.; Lehenkari, P.; Kellinsalmi, M.; Hassinen, I. E.; Vepsäläinen, J.; Mönkkönen, J.; A new endogenous ATP analog (Apppl) inhibits the mitochondrial adenine nucleotide translocase (ANT) and is responsible for the apoptosis induced by nitrogen-containing bisphosphonates *Br. J. Pharmacol.* **2006**, *147*, 437.
- (26) Mönkkönen, H.; Ottewill, P. D.; Kuokkanen, J.; Mönkkönen, J.; Auriola, S.; Holen, I.; Zoledronic acid-induced IPP/Apppl production in vivo *Life Sci.* **2007**, *81*, 1066.
- (27) Mitrofan, L. M.; Pelkonen, J.; Mönkkönen, J.; The level of ATP analog and isopentenyl pyrophosphate correlates with zoledronic acid-induced apoptosis in cancer cells in vitro *Bone* **2009**, *45*, 1153.
- (28) Rääkkönen, J.; Crockett, J. C.; Rogers, M. J.; Mönkkönen, H.; Auriola, S.; Mönkkönen, J.; Zoledronic acid induces formation of a pro-apoptotic ATP analogue and isopentenyl pyrophosphate in osteoclasts in vivo and in MCF-7 cells in vitro *Br. J. Pharmacol.* **2009**, *157*, 427.
- (29) Morita, C. T.; Jin, C.; Sarikonda, G.; Wang, H.; Nonpeptide antigens, presentation mechanisms, and immunological memory of human V γ 2V δ 2 T cells: discriminating friend from foe through the recognition of prenyl pyrophosphate antigens *Immunology Reviews* **2007**, *215*, 59.
- (30) Wang, H.; Sarikonda, G.; Puan, K.-J.; Tanaka, Y.; Feng, J.; Giner, J.-L.; Cao, R.; Mönkkönen, J.; Oldfield, E.; Morita, C. T.; Indirect Stimulation of Human V γ 2V δ 2 T Cells through Alterations in Isoprenoid Metabolism *J. Immunol.* **2011**, *187*, 5099.

- (31) Zhang, Y.; Cao, R.; Yin, F.; Lin, F.-Y.; Wang, H.; Krysiak, K.; No, J.-H.; Mukkamala, D.; Houlihan, K.; Li, J.; Morita, C. T.; Oldfield, E.; Lipophilic Pyridinium Bisphosphonates: Potent $\gamma\delta$ T Cell Stimulators *Angew. Chem. Int. Ed.* **2010**, *49*, 1136.
- (32) Naoe, M.; Ogawa, Y.; Takeshita, K.; Morita, J.; Shichijo, T.; Fuji, K.; Fukagai, T.; Iwamoto, S.; Terao, S.; Zoledronate Stimulates T Cells in Prostate Cancer Patients *Oncology Res.* **2010**, *18*, 493.
- (33) Raab, M. S.; Podar, K.; Breitkreutz, I.; Richardson, P. G.; Anderson, K. C.; Multiple myeloma *Lancet*, 374, 324.
- (34) Chapman, M. A.; Lawrence, M. S.; Keats, J. J.; Cibulskis, K.; Sougnez, C.; Schinzel, A. C.; Harview, C. L.; Brunet, J.-P.; Ahmann, G. J.; Adli, M.; Anderson, K. C.; Ardlie, K. G.; Auclair, D.; Baker, A.; Bergsagel, P. L.; Bernstein, B. E.; Drier, Y.; Fonseca, R.; Gabriel, S. B.; Hofmeister, C. C.; Jagannath, S.; Jakubowiak, A. J.; Krishnan, A.; Levy, J.; Liefeld, T.; Lonial, S.; Mahan, S.; Mfuko, B.; Monti, S.; Perkins, L. M.; Onofrio, R.; Pugh, T. J.; Rajkumar, S. V.; Ramos, A. H.; Siegel, D. S.; Sivachenko, A.; Stewart, A. K.; Trudel, S.; Vij, R.; Voet, D.; Winckler, W.; Zimmerman, T.; Carpten, J.; Trent, J.; Hahn, W. C.; Garraway, L. A.; Meyerson, M.; Lander, E. S.; Getz, G.; Golub, T. R.; Initial genome sequencing and analysis of multiple myeloma *Nature* **2011**, *471*, 467.
- (35) Morgan, G. J.; Davies, F. E.; Gregory, W. M.; Cocks, K.; Bell, S. E.; Szubert, A. J.; Navarro-Coy, N.; Drayson, M. T.; Owen, R. G.; Feyler, S.; Ashcroft, A. J.; Ross, F.; Byrne, J.; Roddie, H.; Rudin, C.; Cook, G.; Jackson, G. H.; Child, J. A.; First-line treatment with zoledronic acid as compared with clodronic acid in multiple myeloma (MRC Myeloma IX): A randomised controlled trial *Lancet* **2010**, *376*, 1989.
- (36) Coleman, R.; Gnant, M.; Morgan, G.; Clezardin, P.; Effects of Bone-Targeted Agents on Cancer Progression and Mortality *J. Natl. Cancer Inst.* **2012**, *104*, 1059.
- (37) Gnant, M.; Dubsy, P.; Fitzal, F.; Bachleitner-Hofmann, T.; Exner, R.; Blaha, P.; Jakesz, R.; Schippinger, W.; Greil, R.; Bisphosphonates as adjuvant therapy for breast cancer *Cur. Breast Cancer. Rep.* **2009**, *1*, 54.
- (38) Almubarak, H.; Jones, A.; Chaisuparat, R.; Zhang, M.; Meiller, T. F.; Scheper, M. A.; Zoledronic acid directly suppresses cell proliferation and induces apoptosis in highly tumorigenic prostate and breast cancers *J. Carcinogenesis* **2011**, *10*.
- (39) Parker, C. C.; The role of bisphosphonates in the treatment of prostate cancer *BJU Int.* **2005**, *95*, 935.
- (40) Dieli, F.; Vermijlen, D.; Fulfarò, F.; Caccamo, N.; Meraviglia, S.; Cicero, G.; Roberts, A.; Buccheri, S.; D'Asaro, M.; Gebbia, N.; Salerno, A.; Eberl, M.; Hayday, A. C.; Targeting Human $\gamma\delta$ T Cells with Zoledronate and Interleukin-2 for Immunotherapy of Hormone-Refractory Prostate Cancer *Cancer Research* **2007**, *67*, 7450.
- (41) Steinbrunn, T.; Stühmer, T.; Gattenlöhner, S.; Rosenwald, A.; Mottok, A.; Unzicker, C.; Einsele, H.; Chatterjee, M.; Bargou, R. C.; Mutated RAS and constitutively activated Akt delineate distinct oncogenic pathways, which independently contribute to multiple myeloma cell survival *Blood* **2011**, *117*, 1998.
- (42) Guenther, A.; Gordon, S.; Tiemann, M.; Burger, R.; Bakker, F.; Green, J. R.; Baum, W.; Roelofs, A. J.; Rogers, M. J.; Gramatzki, M.; The bisphosphonate zoledronic acid has antimyeloma activity in vivo by inhibition of protein prenylation *Int. J. Cancer* **2010**, *126*, 239.

- (43) Wasko, B. M.; Dudakovic, A.; Hohl, R. J.; Bisphosphonates Induce Autophagy by Depleting Geranylgeranyl Diphosphate *J. Pharmacol. Exp. Ther.* **2011**, 337, 540.
- (44) Kunzmann, V.; Bauer, E.; Feurle, J.; Tony, F. W.; Hans-Peter; Wilhelm, M.; Stimulation of $\gamma\delta$ T cells by aminobisphosphonates and induction of antiplasma cell activity in multiple myeloma *Blood* **2000**, 96, 384.
- (45) Rondeau, J.-M.; Bitsch, F.; Bourgier, E.; Geiser, M.; Hemmig, R.; Kroemer, M.; Lehmann, S.; Ramage, P.; Rieffel, S.; Strauss, A.; Green, J. R.; Jahnke, W.; Structural Basis for the Exceptional in vivo Efficacy of Bisphosphonate Drugs *ChemMedChem* **2006**, 1, 267.
- (46) Hosfield, D. J.; Zhang, Y.; Dougan, D. R.; Broun, A.; Tari, L. W.; Swanson, R. V.; Finn, J.; Structural Basis for Bisphosphonate-mediated Inhibition of Isoprenoid Biosynthesis *J. Bio. Chem.* **2004**, 279, 8526.
- (47) Tarshis, L. C.; Proteau, P. J.; Kellogg, B. A.; Sacchettini, J. C.; Poulter, C. D.; Regulation of product chain length by isoprenyl diphosphate synthases *Proc. Natl. Acad. Sci. U.S.A.* **1996**, 93, 15018.
- (48) Menshutkin, N.; Ueber die Einwirkung des chloroacetyls auf phosphorige saure *Ann. Chem. Pharma.* **1865**, 133, 317.
- (49) Russell, R. G. G.; Xia, Z.; Dunford, J. E.; Oppermann, U. D. O.; Kwaasi, A.; Hulley, P. A.; Kavanagh, K. L.; Triffitt, J. T.; Lundy, M. W.; Phipps, R. J.; Barnett, B. L.; Coxon, F. P.; Rogers, M. J.; Watts, N. B.; Ebetino, F. H.; Bisphosphonates *Ann. New York Acad. Sci.* **2007**, 1117, 209.
- (50) Kavanagh, K. L.; Guo, K.; Dunford, J. E.; Wu, X.; Knapp, S.; Ebetino, F. H.; Rogers, M. J.; Russell, R. G. G.; Oppermann, U.; The molecular mechanism of nitrogen-containing bisphosphonates as antiosteoporosis drugs *Proc. Natl. Acad. Sci. U.S.A.* **2006**, 103, 7829.
- (51) Hounslow, A. M.; Carran, J.; Brown, R. J.; Rejman, D.; Blackburn, G. M.; Watts, D. J.; Determination of the Microscopic Equilibrium Dissociation Constants for Risedronate and Its Analogues Reveals Two Distinct Roles for the Nitrogen Atom in Nitrogen-Containing Bisphosphonate Drugs *J. Med. Chem.* **2008**, 51, 4170.
- (52) Ohno, K.; Mori, K.; Orita, M.; Takeuchi, M.; Computational Insights into Binding of Bisphosphates to Farnesyl Pyrophosphate Synthase *Curr. Med. Chem.* **2011**, 18, 220.
- (53) Reid, I. R.; Brown, J. P.; Burckhardt, P.; Horowitz, Z.; Richardson, P.; Trechsel, U.; Widmer, A.; Devogelaer, J.-P.; Kaufman, J.-M.; Jaeger, P.; Body, J.-J.; Brandi, M. L.; Broell, J.; Di Micco, R.; Genazzani, A. R.; Felsenberg, D.; Happ, J.; Hooper, M. J.; Ittner, J.; Leb, G.; Mallmin, H.; Murray, T.; Ortolani, S.; Rubinacci, A.; Sääf, M.; Samsioe, G.; Verbruggen, L.; Meunier, P. J.; Intravenous Zoledronic Acid in Postmenopausal Women with Low Bone Mineral Density *New Eng. J. Med.* **2002**, 346, 653.
- (54) Zhang, Y.; Cao, R.; Yin, F.; Hudock, M. P.; Guo, R.-T.; Krysiak, K.; Mukherjee, S.; Gao, Y.-G.; Robinson, H.; Song, Y.; No, J. H.; Bergan, K.; Leon, A.; Cass, L.; Goddard, A.; Chang, T.-K.; Lin, F.-Y.; Beek, E. V.; Papapoulos, S.; Wang, A. H. J.; Kubo, T.; Ochi, M.; Mukkamala, D.; Oldfield, E.; Lipophilic Bisphosphonates as Dual Farnesyl/Geranylgeranyl Diphosphate Synthase Inhibitors: An X-ray and NMR Investigation *J. Am. Chem. Soc.* **2009**, 131, 5153.

- (55) Lolli, M. L.; Rolando, B.; Tosco, P.; Chaurasia, S.; Stilo, A. D.; Lazzarato, L.; Gorassini, E.; Ferracini, R.; Oliaro-Bosso, S.; Fruttero, R.; Gasco, A.; Synthesis and preliminary pharmacological characterisation of a new class of nitrogen-containing bisphosphonates (N-BPs) *Bioorg. Med. Chem.* **2010**, *18*, 2428.
- (56) Roth, A. G.; Drescher, D.; Yang, Y.; Redmer, S.; Uhlig, S.; Arenz, C.; Potent and Selective Inhibition of Acid Sphingomyelinase by Bisphosphonates *Angew. Chem. Int. Ed.* **2009**, *48*, 7560.
- (57) Rubino, M. T.; Agamennone, M.; Campestre, C.; Campiglia, P.; Cremasco, V.; Faccio, R.; Laghezza, A.; Loiodice, F.; Maggi, D.; Panza, E.; Rossello, A.; Tortorella, P.; Biphenyl Sulfonylamino Methyl Bisphosphonic Acids as Inhibitors of Matrix Metalloproteinases and Bone Resorption *ChemMedChem* **2011**, *6*, 1258.
- (58) Wiemer, A. J.; Yu, J. S.; Lamb, K. M.; Hohl, R. J.; Wiemer, D. F.; Mono- and dialkyl isoprenoid bisphosphonates as geranylgeranyl diphosphate synthase inhibitors *Bioorg. Med. Chem.* **2008**, *16*, 390.
- (59) Sinko, W.; de Oliveira, C.; Williams, S.; Van Wynsberghe, A.; Durrant, J. D.; Cao, R.; Oldfield, E.; McCammon, J. A.; Applying Molecular Dynamics Simulations to Identify Rarely Sampled Ligand-bound Conformational States of Undecaprenyl Pyrophosphate Synthase, an Antibacterial Target *Chem. Bio. Drug Des.* **2011**, *77*, 412.
- (60) Jahnke, W.; Rondeau, J.-M.; Cotesta, S.; Marzinzik, A.; Pellé, X.; Geiser, M.; Strauss, A.; Götte, M.; Bitsch, F.; Hemmig, R.; Henry, C.; Lehmann, S.; Glickman, J. F.; Roddy, T. P.; Stout, S. J.; Green, J. R.; Allosteric non-bisphosphonate FPPS inhibitors identified by fragment-based discovery *Nat. Chem. Biol.* **2010**, *6*, 660.
- (61) Hubbard, R. E.; Murray, J. B. Experiences in fragment-based lead discovery Elsevier **2011**; Vol. 493, p 509.

2 First generation bisphosphonate inhibitors: exploring the hFPPS active site

2.1 Preface

Most of the work presented in this chapter has been published in the following manuscript and patent application:

“Novel bisphosphonate inhibitors of the human farnesyl pyrophosphate synthase”
De Schutter, J.W.; Zaretsky, S.; Welbourn, S.; Pause, A.; Tsantrizos Y.S., *Bioorg. Med. Chem. Lett.* **2010**, *20*, 5781-5786

“Heterocycl-yl-pyridinyl-based Bisphosphonic Acid, Pharmaceutically Acceptable Salt Thereof, Composition Thereof and Method of Use Thereof”
Tsantrizos, Y.S.*; De Schutter, J.W.; Lin, Y.-S.
PCT/CA2001/050322; filed May 18, **2011**

I performed all computational work, ~95% of the synthesis of compounds described in this chapter, all the enzymatic assays and also ran the NMR line broadening studies with the assistance of Dr. Tara Sprules (QANUC). Serge Zaretsky was a summer undergraduate student in the Tsantrizos research group (2009), he contributed to the synthesis of four inhibitors and also expressed the hFPPS protein. Sarah Welbourn (a PhD student in the Pause research group) purified the hFPPS protein and helped with the initial enzymatic assay protocols.

2.2 Inhibitor design

As described in the introduction (Chapter 1), the major shortcomings of current commercial hFPPS inhibitors (such as risedronate and zoledronate) are the high polarity, poor cell membrane permeability, oral bioavailability and poor selectivity.^{1,2} The central α -hydroxy bisphosphonate moiety is the main pharmacophore anchoring these inhibitors to the enzyme through three Mg^{2+} -mediated interactions with three highly conserved Asp residues in the active site. This bisphosphonic acid moiety is highly charged (up to tetra-anionic state) and it is highly desirable to replace it with a more lipophilic bioisostere. Replacement of this moiety with a more lipophilic bioisostere is expected to dramatically improve the biopharmaceutical properties of hFPPS inhibitors. However, finding a suitable bioisostere is a significant challenge. Previously, the simple replacement of one phosphonic acid with a carboxylic acid moiety was found to reduce the potency of risedronate by more than 40,000-fold (**Table 2.1**).³ Consequently, for our initial investigations, we decided to retain the bisphosphonate moiety and reduce the overall polarity of our compounds by replacing the $\text{C}\alpha$ -hydroxyl and increasing the lipophilicity of the heterocyclic side chain. The α -hydroxy bisphosphonate moiety has high affinity for hydroxyapatite (HAP) due to its ability to form chelates with Ca^{2+} ions, thus localizing the drugs to bone tissue. Replacing the central hydroxyl moiety with hydrogen significantly reduces the affinity for hydroxyapatite, as determined by the retention times of the corresponding analogs on a hydroxyapatite-loaded HPLC column (**Table 2.1**).³ However, the enzymatic potency of the H-analog for hFPPS is also reduced by 7-fold. In a series of α -halogenated risedronate analogs, the HAP affinity is equivalent to the H-analog, and enzymatic potency correlates to the electronegativity of the halogen, i.e. lowering the second pKa of the bisphosphonic acid more closely to that of the natural pyrophosphate substrate (**Figure 2.1**).⁴ Since the bisphosphonate binds in its tetra-anionic form to the Mg^{2+} triad, increasing the acidity facilitates binding and increases the enzymatic potency. However, the steric bulk and lipophilicity of a Br atom in close proximity to three charged metal ions is not favourable. Thus, the α -fluoro bisphosphonates are the most attractive replacement of the α -hydroxy bisphosphonate moiety due to both decreased HAP-affinity and only a modest 3-fold decrease in enzymatic potency.

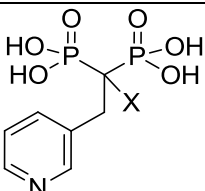
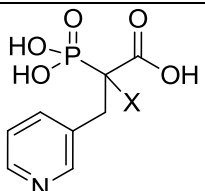
			
-X	HAP affinity (retention time), min	hFPPS inhibition IC ₅₀ (nM)	hFPPS inhibition IC ₅₀ (μM)
-OH	9.97	5.7	253
-H	5.83	34.2	<i>nd</i>
-F	5.93	16.4	> 600
-Cl	6.03	94.6	> 600
-Br	5.73	340.4	> 600

Table 2.1: Enzymatic potency and HAP affinity of risedronate analogs. (reproduced from Marma *et. al.*)³ (*nd* = not determined)

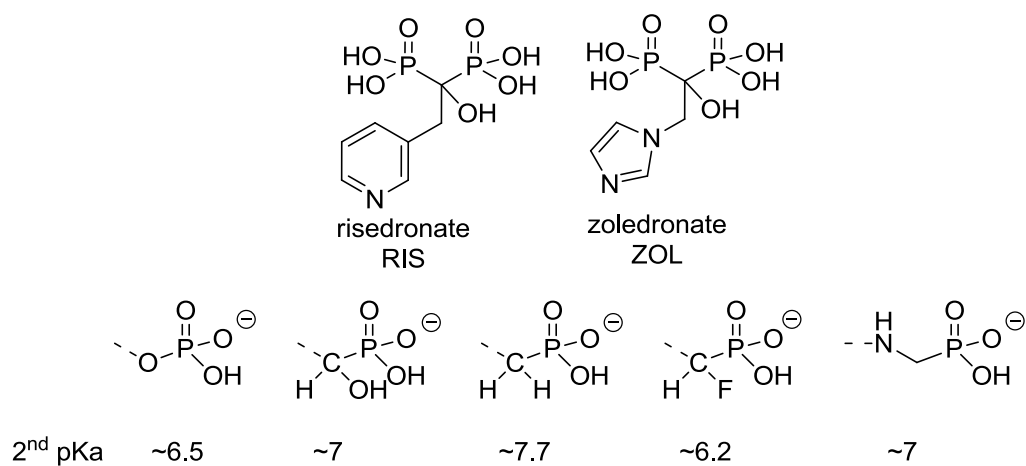


Figure 2.1: 2nd pKa of differentially substituted phosphonic acids⁴

We decided to employ a pyridine scaffold for the core of our inhibitors, as it has more sites for substitution compared to an imidazole core, and risedronate has some (*albeit very poor*) oral bioavailability (0.63%), whereas zoledronate exhibits no bioavailability and has to be administered by i.v. (**Figure 2.1**).²

Since our goal is to develop new inhibitors that occupy a larger portion of the active site as compared to the current drugs (e.g. risedronate), we initially set out to design inhibitors that could occupy both the allylic (GPP) and IPP sub-pockets simultaneously. If successful, such compounds should form more stable inhibitor-hFPPS complexes (fully closed conformation)⁵ in one single binding event, which may prove beneficial and eliminate the time-dependent nature of inhibition observed with the current *N*-BP's.⁶ The crystal structure of the ternary complex of FPPS/ZOL/IPP (PDB 1ZW5) reveals that zoledronate and IPP are in very close proximity to each other and form a Van der Waals contact (**Figure 2.3**). Therefore, we envisioned that appropriately designed substituent(s) attached to the pyridine core (i.e. R substituents to the general structure shown in **Figure 2.2**) could occupy the IPP sub-pocket and engage in favourable interactions with the protein.

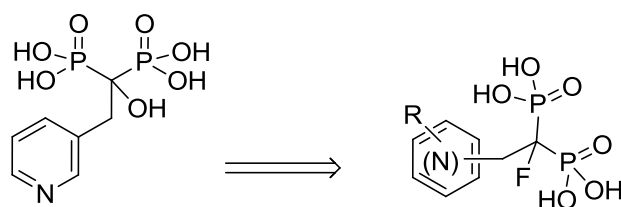


Figure 2.2: Inhibitor design approach

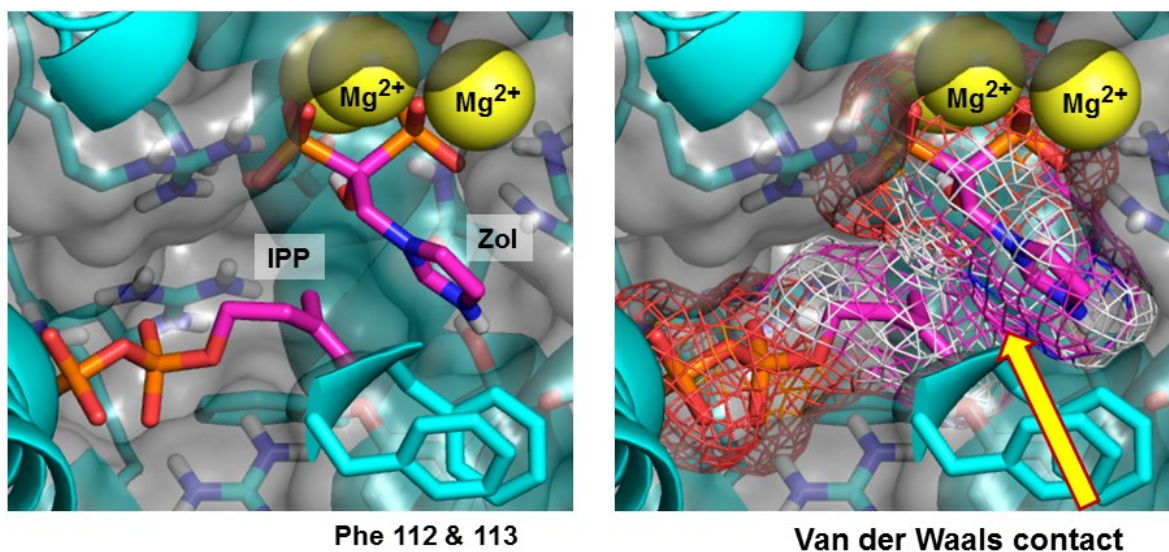


Figure 2.3: Crystal structure of ternary complex hFPPS/ZOL/IPP (PDB 1ZW5). Semi-transparent protein surface of the active site (protein residues covering the active site were removed for clarity). The IPP substrate and the bound inhibitors are shown in stick form. The carbon backbone of IPP and zoledronate are highlighted in magenta, protein residues in cyan. Oxygen, nitrogen and phosphorus atoms are coloured in red, blue and orange, respectively. The yellow spheres represent the Mg²⁺ ions. Key residues are indicated. Van der Waals radii of the IPP substrate and zoledronate inhibitor shown as a mesh.

2.3 Molecular modeling studies

At the time the hFPPS project was initiated, 22 crystal structures of human FPPS were available in the PDB database (please refer to Appendix I). To take advantage of this wealth of structural information we performed a molecular docking study to guide the design of our novel inhibitors that would satisfy the criteria laid out in the previous section. Given the large conformational changes of hFPPS (open, semi-closed, fully closed)^{5,6} it is crucial to select the appropriate crystal structure for the coordinates of the docking model, as this will entirely determine the outcome of the study. Since our goal was to develop inhibitors that occupy both sub-pockets of the active site simultaneously, we decided to employ the hFPPS/ZOL/IPP ternary complex. In this structure the active site is fully closed and represents the most stable conformation of the enzyme. Of the two ternary crystal structures available 1ZW5 was selected as it has a better resolution (2.30 Å) than 2F8Z (2.60 Å). The X-ray coordinates were then converted into a molecular docking grid with the Glide program (version 5.5, Schrödinger, LLC, New York, NY 2009).⁷ It should be noted that in this computational model the residues are rigid, but some protein flexibility is mimicked by scaling down the Van der Waals radii of nonpolar atoms on the protein surface.⁸ The compounds were docked into the computational model with Glide using standard parameters of XP-mode,⁹ and the bisphosphonate was considered fully deprotonated in all cases.

Based on the results from an initial *in silico* screening we concluded that an *ortho*-substitution pattern between the R-substituent on the pyridine side chain and the bisphosphonate moiety does not appear to be able to fit in the active site, therefore only *meta*- and *para*-substitution patterns were investigated (**Figure 2.4**). The heterocyclic nitrogen was positioned at every available position of the pyridine core and (for the purpose of the *in silico* studies) considered in both the unprotonated and protonated states in order to ascertain potential interactions with Lys 200 and Thr 201. A diverse set of small heterocycles (Het) was selected for the R-substituents, based on commercially available boronic acid fragments that could be readily attached to the pyridine core through a Suzuki cross-coupling reaction (a sub-set of these heterocycles is shown in **Figure 2.4**). After considering all possible permutations, the input set of compounds for the next round of *in silico* screening consisted of more than 200 molecules.

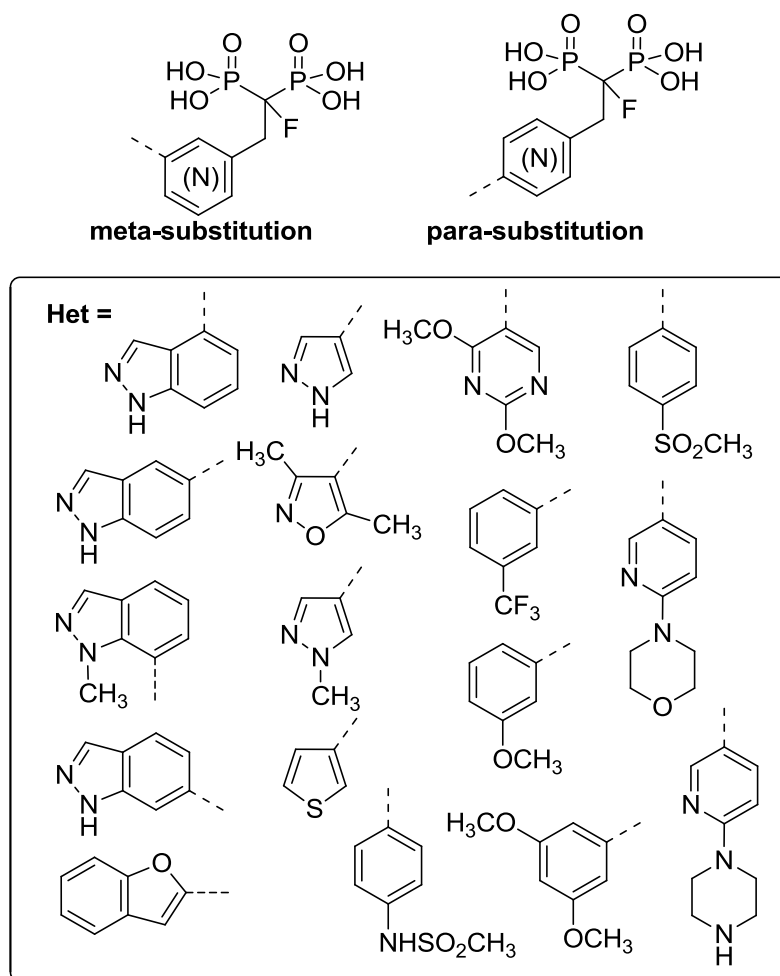


Figure 2.4: Structural diversity of docking input structures.

The docking score assigned by Glide (gscore) was used only as a qualitative measure and assessment was based mostly on visual inspection of the output poses. Proper alignment between the bisphosphonate moiety (BP) and the Mg^{2+} ions was checked first, output poses that did not closely resemble the BP- Mg^{2+} interactions observed in the hFPPS crystal structures were rejected. In general, compounds with *para*-substitution between the bisphosphonate moiety and the R-substituent appeared to not fit well in the hFPPS active site, as many of them did not generate valid output poses.

As expected, larger R-substituents (e.g. 1*H*-indazole substituents) were unable to fit in the small allylic sub-pocket and instead the output pose for such analogs had the entire pyridinyl sidechain into the IPP sub-pocket (**Figure 2.5b**). Consequently, the pyridine

nitrogen of these compounds presumably could not engage in interactions with Lys 200 and Thr 201. Of all the derivatives docked with unprotonated pyridine cores more than 80 could bind into the IPP sub-pocket, placing the pyridine moiety approximately 90° from that of the enzyme-bound side chain of zoledronate (**Figure 2.5**, panel **a** vs. **b**).

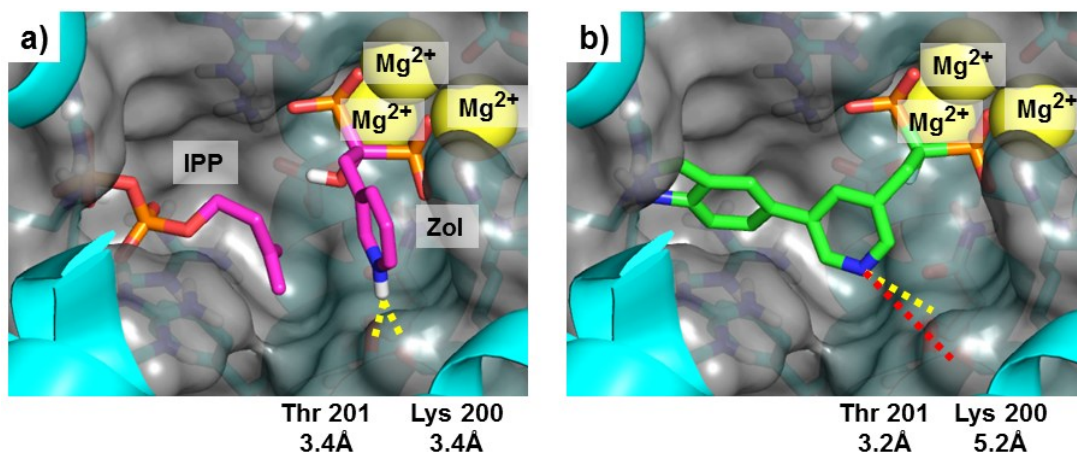
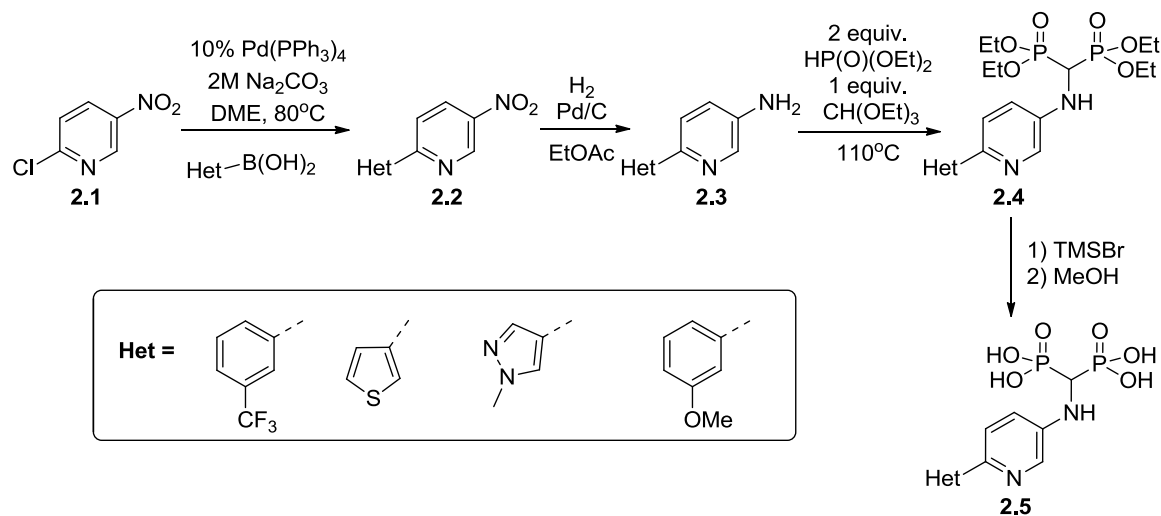


Figure 2.5: (a) crystal structure of ternary complex hFPPS/ZOL/IPP (PDB 1ZW5) the distances between the pyridine heterocyclic nitrogen are shown as dashed lines and indicated; (b) example of an output pose with the R-substituent occupying the IPP sub-pocket

2.4 Synthesis

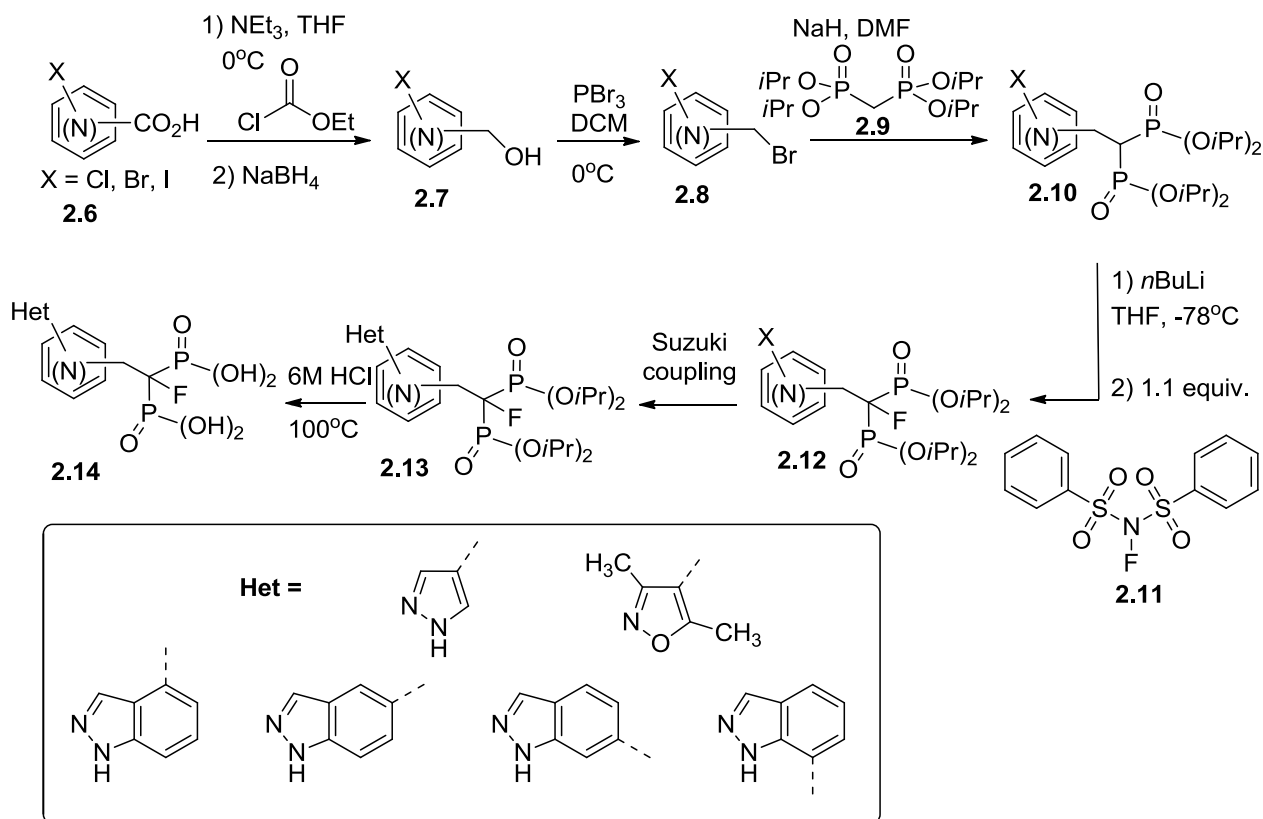
Serge Zaretsky had initiated the synthesis of 6-substituted-3-amino-bisphosphonates **2.5** from 6-chloro-3-nitropyridine **2.1** (Scheme 2.1) and performed the initial Suzuki cross-coupling with several heterocyclic (Het) boronic acids. Although these analogs were unable to fit in our computational model (in many cases the program couldn't generate an output pose), it was decided to finish these compounds to test the validity of the docking results. From the Suzuki-coupled products **2.2**, compounds of which sufficient material was obtained, the synthesis was continued. Following catalytic hydrogenation of the nitro groups (30-80% yield), the corresponding anilines **2.3** were converted to tetra-ethyl bisphosphonate esters **2.4** by condensation with diethyl phosphite and triethyl orthoformate at high temperature (40-100%). Deprotection of the ethyl esters was performed by transesterification with bromotrimethylsilane, followed by methanolysis of the silyl esters. Although this reaction proceeds very slowly (incomplete conversion even after 48 h at RT), it allowed for isolation of the pure final products **2.5** by simple trituration (25-65% isolated yield).



Scheme 2.1: Synthesis of 6-substituted-3-amino-bisphosphonates

The synthesis of α -fluoro bisphosphonates was initiated with the appropriately substituted halo- benzoic, picolinic, nicotinic or isonicotinic acid **2.6**, which was first converted to the corresponding mixed anhydride with ethyl chloroformate, reduced with NaBH₄ to produce the alcohols **2.7** and then treated with PBr₃ to obtain the intermediate bromides **2.8**; yields for both the reduction and bromination ranged from 50% to 90% (**Scheme 2.2**). Deprotonation of tetraisopropyl methylenebis(phosphonate) **2.9** with sodium hydride, followed by nucleophilic substitution on the bromides **2.8** produced the aromatic bisphosphonates **2.10** in yields of 30-60%. Purification of these products proved to be difficult and they were always contaminated with 5-30% of the tetraisopropyl methylenebis(phosphonate) starting material **2.9** as determined by ³¹P NMR. Fortunately, this impurity could be eliminated in the next step. Fluorination at C α using the conditions previously reported by McKenna and co-workers (1.2 equiv. NaH, THF followed by 1.5 equiv Selectfluor[®] in DMF)³ failed for these compounds. In particular the poor solubility of Selectfluor[®] proved to be problematic, therefore the more soluble *N*-fluoro-*N*-(phenylsulfonyl)benzenesulfonamide (NFSI, **2.11**) was explored as the fluorinating agent. This resulted in moderate yields which could be improved by changing the base to *n*BuLi to furnish the key α -fluoro bisphosphonate intermediates **2.12** in yields of 30-90%.

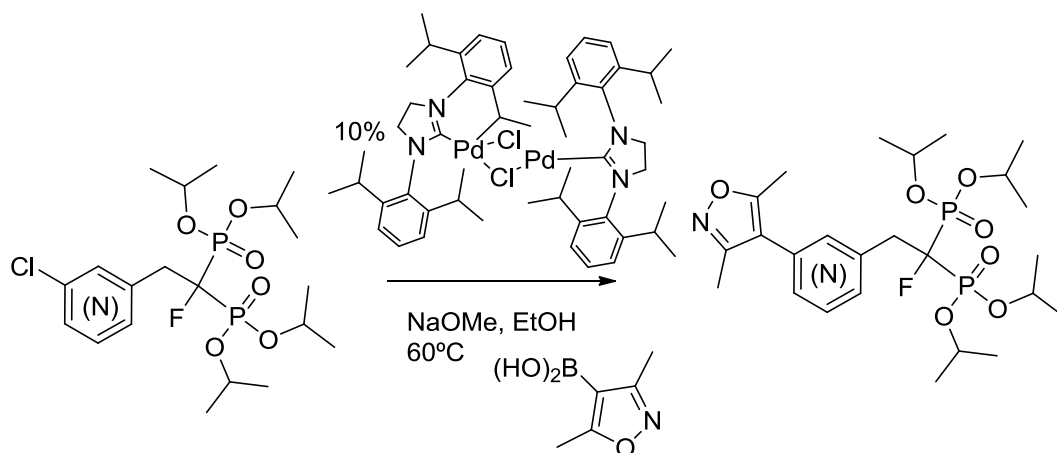
Subsequently, the Suzuki cross-coupling reactions were performed on the aromatic halide precursors **2.12** under standard conditions (1.2 equiv. Het-B(OH)₂, 10% Pd(PPh₃)₄, 2M Na₂CO₃, DME, 80°C) to furnish biaryls **2.13**. Although these conditions were satisfactory for intermediates containing an iodo-phenyl (50-65%) and 3-bromo-pyridine moiety (30-70%), they failed on the less reactive 2-chloro-pyridine precursors. Therefore alternative conditions were screened for solvent (DME, 1,4-dioxane, DMF, Toluene, Toluene/EtOH 1:1); temperature (up to 110°C thermally and up to 150°C with microwave radiation); palladium source (Pd(PPh₃)₄, Pd(P[*t*-Bu]₃)₂, Pd(OAc)₂, Pd₂(dba)₃); ligand (S-Phos, RuPhos, PdCl₂(dppf).CH₂Cl₂) and base (aqueous and anhydrous K₂CO₃ and Cs₂CO₃). Although some desired products could be isolated under several of these conditions, yields were generally poor (30-35%) and unreliable. The final deprotection of the bisphosphonate tetra-isopropyl esters **2.13** was achieved in 6N HCl at 100°C followed by C₁₈ reversed phase chromatography purification to provide the bisphosphonic acids **2.14** in 50-75% yield.



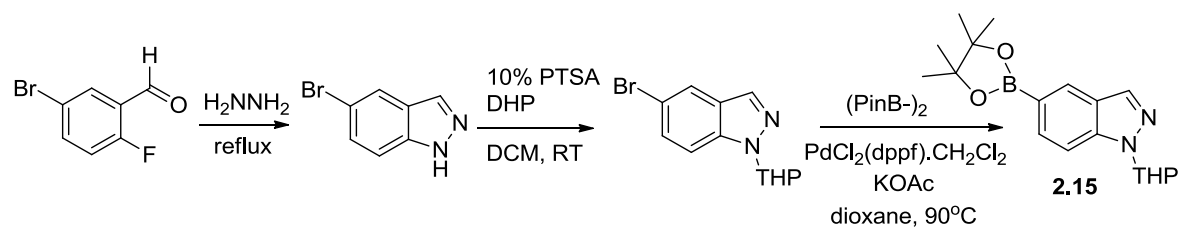
Scheme 2.2: Synthetic route towards α -fluoro bisphosphonates

Cross-couplings with chloro substrates are notoriously difficult and it is known that strongly coordinating heterocycles (such as pyridines) can displace the ligand(s) from Pd catalytic center, as those substrates are strong σ -donors and are present in larger quantities than the ligands (e.g. 10-20 mol%).^{10,11} Not surprisingly there are relatively few reports in the scientific literature in which 2-chloropyridines are used successfully. However the methodology by Cazin and co-workers caught our attention and was successfully employed with (3,5-dimethylisoxazol-4-yl)boronic acid (**Scheme 2.3**, 30-50%).¹² Unfortunately these harsh conditions did not work for the other boronate coupling partners of interest, presumably due to the presence of a free NH. In order to resolve this potential source of these reactivity issues, a protecting group strategy was explored. The commonly employed carbamate-type protecting groups for NH-moieties have been reported to degrade on indazole and pyrazole scaffolds under Pd catalysis conditions. However, Watson and co-workers found that ether-type protecting groups worked well for Buchwald-Hartwig type cross-couplings, in particular the THP-group (tetrahydro-2H-pyran).¹³ Therefore the *N*-

THP-protected indazole-5-boronic pinacol ester **2.15** was synthesized in an effort overcome the difficulties with the Suzuki cross couplings (**Scheme 2.4**, full details in experimental section). Unfortunately this protecting group strategy did not significantly ameliorate the synthetic problems and only a limited number of analogs were obtained. Nonetheless, we were successful in synthesizing 15 final compounds and we decided to first obtain some preliminary biological data before investing more effort on the synthesis of new analogs.



Scheme 2.3: Example of a successful Suzuki cross coupling with a pyridinyl chloride



Scheme 2.4: Synthesis of *N*-THP-protected indazole-5-boronic pinacol ester **2.15**

2.5 Characterization of α -fluoro bisphosphonic acids:

It worth noting that the incorporation of two phosphorus atoms and a fluorine atom leads to fairly complex NMR spectra for our novel inhibitors as both ^{13}P and ^{19}F couple not only with each other (**Figure 2.6**, **Figure 2.7**) and ^1H , but also cause splitting in the ^{13}C spectrum. For the intermediate tetra esters the isopropyl or ethyl ^{13}C signals are commonly split into doublets due to the proximity of one phosphorus atom. For all fluorinated compounds the benzylic carbon is a doublet or doublet of triplets due to coupling with fluorine and sometimes also phosphorus. In some cases long-range coupling is also observed with some aromatic carbons. The $\text{C}\alpha$ can be particularly difficult to characterize as it is a quaternary carbon atom and is always split into a doublet of triplets, by ^{19}F and ^{31}P , respectively. This signal is most difficult to fully resolve for the final compounds as they are insoluble in MeOD or DMSO- d_6 and have only limited solubility in D_2O . Consequently, insufficient signal-to-noise ratio made the clear identification of the $\text{C}\alpha$ carbon atom difficult to see on a routine ^{13}C NMR spectrum. In order to circumvent this issue $\{^{19}\text{F}, ^{13}\text{C}\}$ HMQC NMR spectra were acquired to unequivocally assign the $\text{C}\alpha$ (**Figure 2.8**).

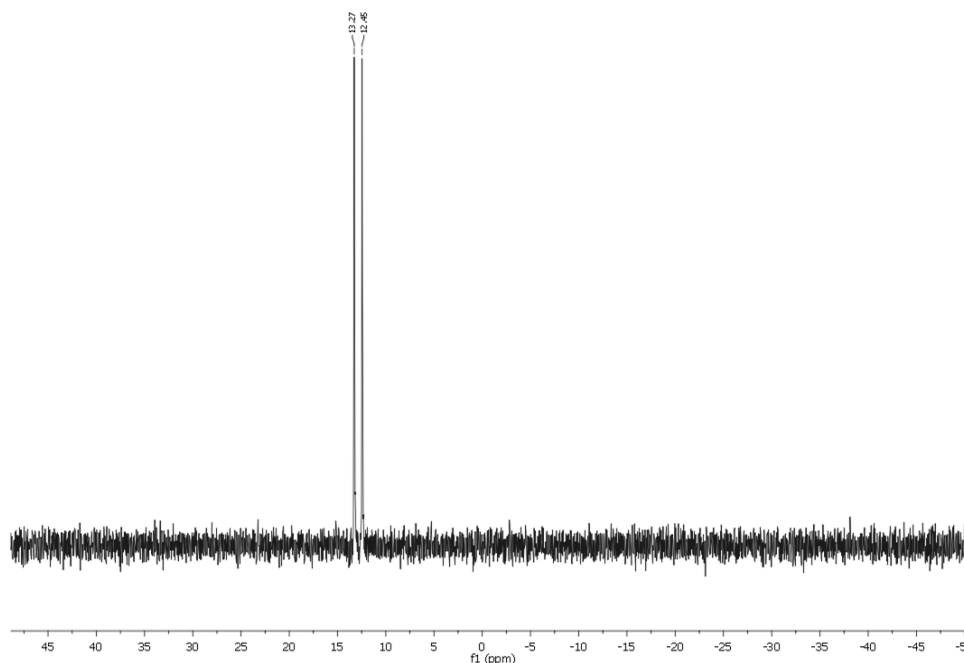


Figure 2.6: Proton-decoupled ^{13}P NMR spectrum of inhibitor **2.25**, doublet due to coupling with ^{19}F

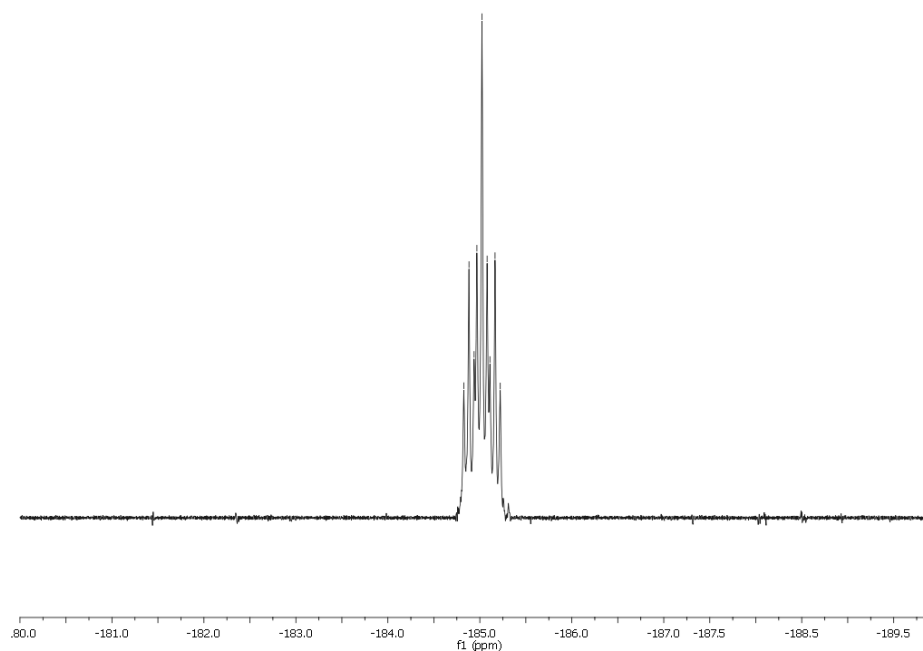


Figure 2.7: ^{19}F spectrum of inhibitor **2.25**, splitting due to ^1H and ^{31}P

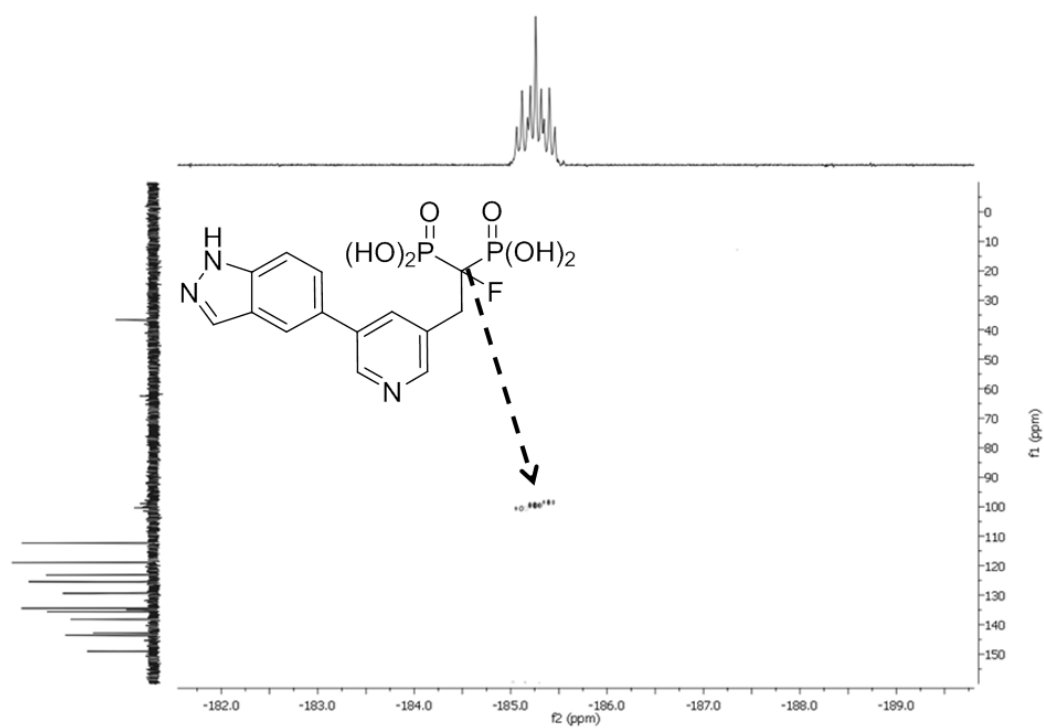
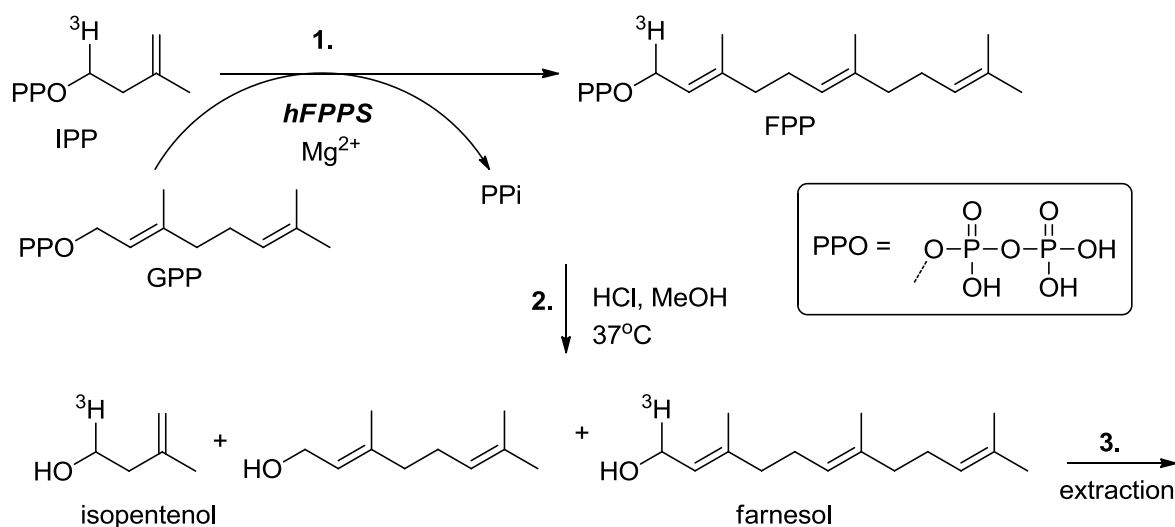


Figure 2.8: $\{^{19}\text{F}, ^{13}\text{C}\}$ HMQC NMR spectrum of inhibitor **2.25**

2.6 Human FPPS inhibition screening and SAR

A clone encoding the human recombinant FPPS enzyme with an *N*-terminal His₆-tag (vector p11; SGC Oxford) was expressed in *E. coli* and purified as previously described.^{1,6} For this preliminary evaluation of our compounds, the enzyme was only partly purified (the final gel filtration on a Superdex 200 column was not performed). The hFPPS activity was measured using similar assay conditions as those reported by Dunford and coworkers,¹⁴ except the pre-incubation period was reduced to 5 min in the presence of the GPP substrate instead of 10 min in the absence of the GPP substrate. In short, the inhibitors are pre-incubated with the hFPPS enzyme and GPP substrate for 5 min at 37°C. Then, the tritium-labelled IPP substrate is added and the enzymatic reaction is allowed to proceed for 10 min at 37°C; next, the reaction is quenched by the addition of MeOH/HCl and all the organic pyrophosphates are hydrolyzed to the corresponding alcohols and inorganic pyrophosphate (10 min at 37°C incubation). Finally, the tritium-labelled farnesol is extracted out of the aqueous mixture with ligroin (³H-labelled isopentenol remains in the aqueous phase) and a precise aliquot is counted to determine enzymatic turnover (**Scheme 2.5**).



Scheme 2.5: hFPPS enzymatic assay protocol

Initially, the potential of all compounds to inhibit hFPPS was evaluated at the concentrations of 100, 10 and 1 μ M (**Table 2.2**). The *para*-substituted compounds (e.g. analogs **2.16**, **2.17**, **2.18** and **2.19**, **Figure 2.9**), which were predicted to be inactive, were found to be the least active, in agreement with our computational model. Furthermore, inhibitors with the same heterocycle *meta* to the bisphosphonate moiety are significantly more potent compared to the *para*-analogs (**2.20** vs. **2.24**; **2.21** vs. **2.25**; **2.22** and **2.23** vs. **2.26**).

	1 μ M	10 μ M	100 μ M
RIS	83%	98%	100%
2.16	<i>nd</i>	0%	13%
2.17	<i>nd</i>	0%	29%
2.18	<i>nd</i>	0%	10%
2.19	<i>nd</i>	0%	11%
2.20	0%	46%	87%
2.21	0%	57%	92%
2.22	0%	22%	74%
2.23	18%	57%	<i>nd</i>
2.24	10%	81%	97%
2.25	57%	95%	100%
2.26	65%	95%	100%
2.27	1%	41%	91%
2.28	0%	34%	92%
2.29	11%	86%	97%
2.30	0%	33%	82%
2.31	0%	9%	56%

Table 2.2: hFPPS enzymatic inhibition. The values of % inhibition shown are the average of three determinations. (<10% standard deviation)
(*nd* = not determined)

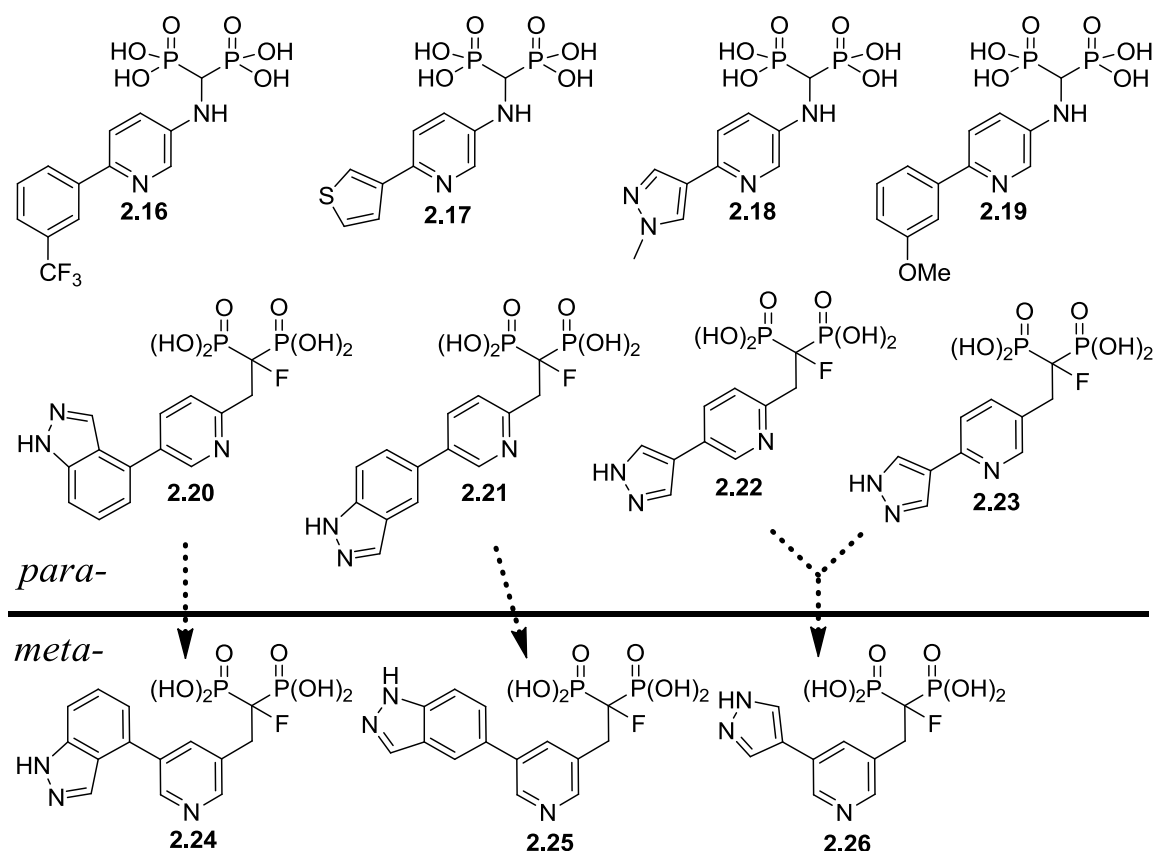


Figure 2.9: Novel inhibitors, comparison *para*- vs. *meta*-substituted inhibitors

The phenyl analog **2.27** was significantly less active against hFFPS compared to the corresponding pyridine based inhibitor **2.25**, indicating that the heterocyclic nitrogen forms an important interaction with the enzyme (**Figure 2.10**). This is supported by the observation that the position of the pyridine has a large effect on enzymatic inhibition (**2.24** vs. **2.28**) and is preferred *meta* to the bisphosphonate moiety (**2.29** vs. **2.30** and **2.31**). Taken together, the SAR suggest an all *meta* substitution pattern between bisphosphonate moiety, heterocyclic sidechain and pyridine nitrogen is best suited to complement the hFFPS active site. Finally, the full dose response assay was run for compounds exhibiting >50% inhibition at 1 μ M and the corresponding IC_{50} values were calculated to be: 270 nM (risedronate), 710 nM (**2.25**) and 640 nM (**2.26**). Such a 2-3 fold decrease in enzymatic *in vitro* potency is expected for compounds missing the $C\alpha$ -OH moiety and **2.25** and **2.26** represent promising new leads for further optimization.

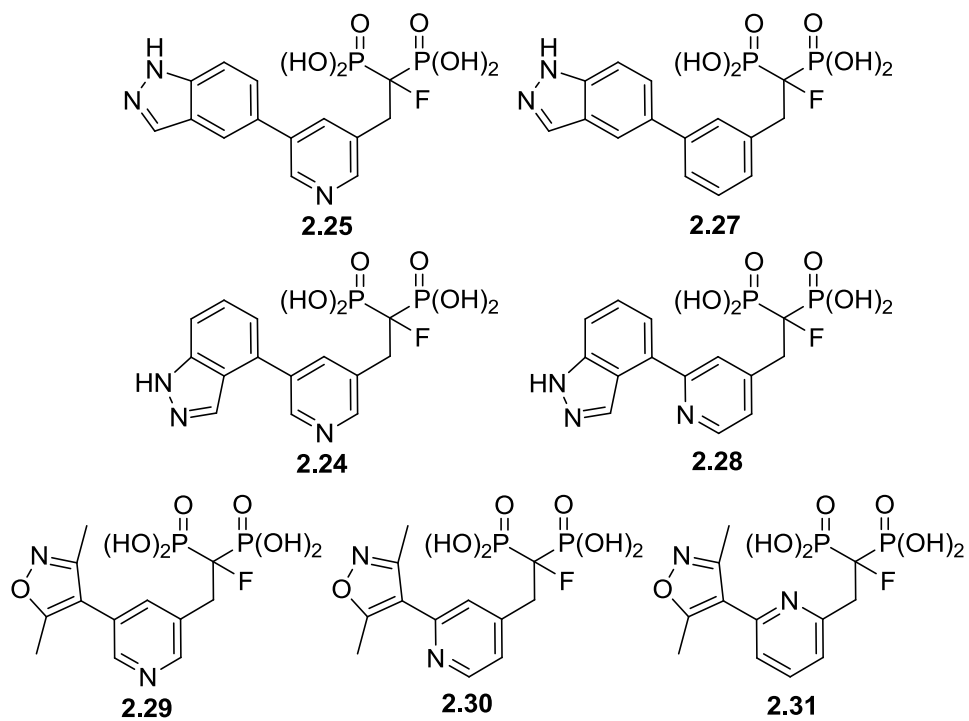


Figure 2.10: Novel inhibitors, comparison of the pyridine substitution pattern

2.7 NMR line broadening studies

Based on the available structural data and our *in silico* model, it seemed reasonable to assume that the potency of **2.25** and **2.26** originates from interactions with the hFPPS active site that are different from those observed with risedronate. In order to probe the binding mode of our inhibitors, competition experiments were conducted using ligand-detected ^1H NMR line broadening techniques.^{15,16} When a ligand binds to a protein it adopts the characteristics of a macromolecule and the magnetic spins of the nuclei require more time to relax from their excited state. Under the parameters of the experiment, the relaxation time is too short to observe the associated resonance and the signals of the protein-bound ligand do not appear in the ^1H NMR spectrum. The magnetic spins of the fraction of ligand that exists in the free, solvated state can rapidly relax and the signals appear as sharp peaks in the Fourier transformed spectrum. Since weak inhibitors quickly equilibrate between both distinct states, the averaged effect is observed as line broadening in the NMR spectrum and indicates binding of a ligand to a protein.

Line broadening of the ^1H resonances of inhibitor **2.22** was observed by the addition of hFPPS to the NMR sample, in a dose dependant manner, confirming the binding of **2.22** to the enzyme. Addition of risedronate or IPP to the hFPPS/**2.22** NMR sample restored the ^1H resonances of **2.22** almost completely (**Figure 2.12** and **Figure 2.13**). These results demonstrate that **2.22** competes for binding with risedronate and IPP as both can restore the signal strength and sharpness in the ^1H spectrum and this is to be expected if **2.22** is displaced from the enzyme cavity and into solution. This data suggests **2.22** binds simultaneously into both the allylic and IPP sub-pocket, consistent with the model developed from our docking studies (**Figure 2.11**). However the possibility exists that binding of either species to the protein can induce a conformational change, prohibiting binding of **2.22**, and such events were not accounted for in our computational model (hFPPS was considered rigid). Furthermore, titration of IPP into hFPPS has been reported to exhibit dual binding characteristics by ITC.¹ This data strongly suggests that a second unit of IPP can bind to hFPPS, presumably in the allylic sub-pocket. Therefore it is possible that, at high molar excess, IPP displaces the weakly bound **2.22**. A control competition experiment between risedronate and IPP cannot be performed, due to the high affinity of

risedronate for the enzyme (it does not equilibrate quickly enough). Later in our studies we acquired crystallographic evidence (Chapter 4) that demonstrates that an analogous inhibitor binds exclusively in the allylic sub-pocket and a conclusive DSF parallel titration experiment (Chapter 8) has confirmed that **2.22** does not occupy the IPP sub-pocket.

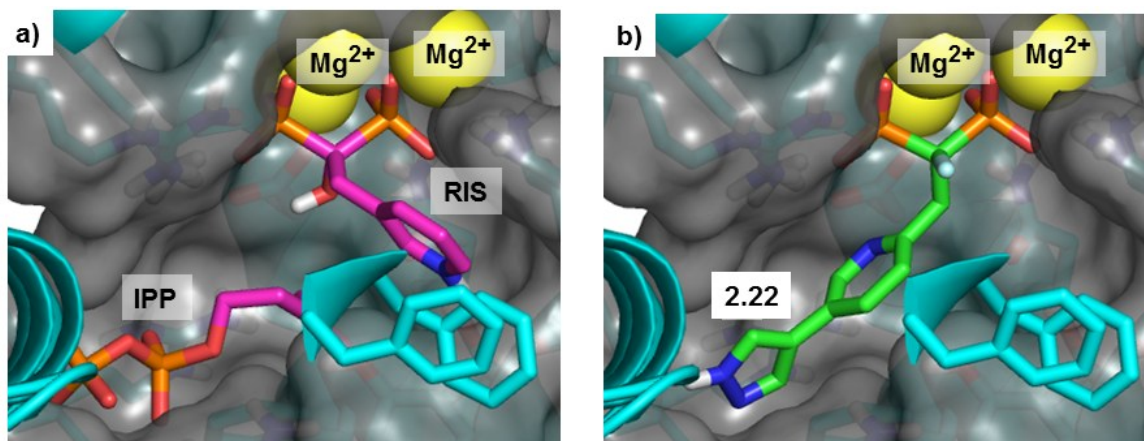


Figure 2.11: (a) composite picture of IPP occupying the IPP sub-pocket (PDB 1ZW5) and risedronate occupying the allylic sub-pocket (PDB 1YV5); (b) Glide docking output pose of inhibitor **2.22**, occupying both sub-pockets simultaneously

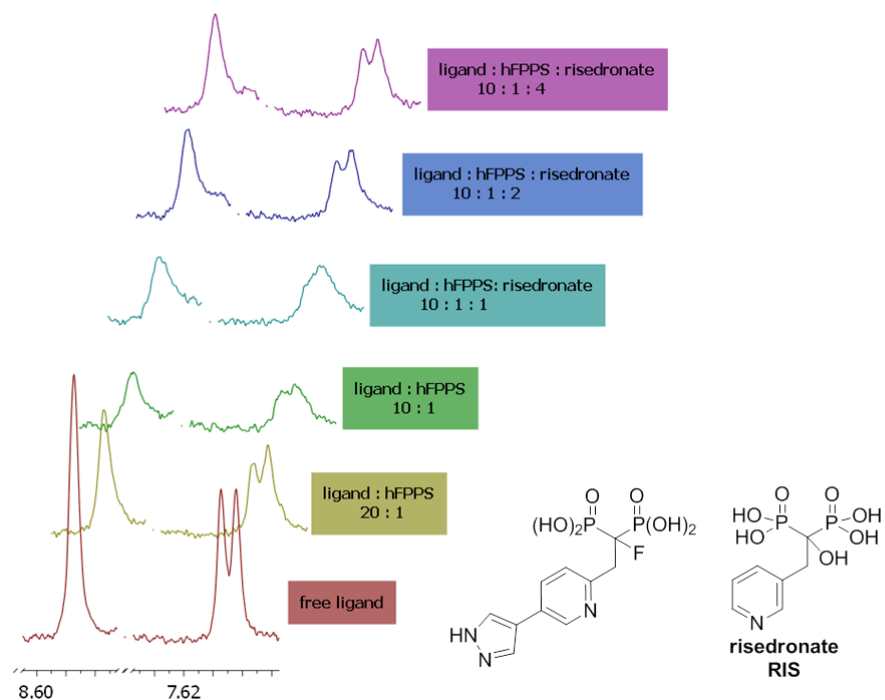


Figure 2.12: Competition study between inhibitor **2.22** and risedronate by ^1H NMR line broadening.

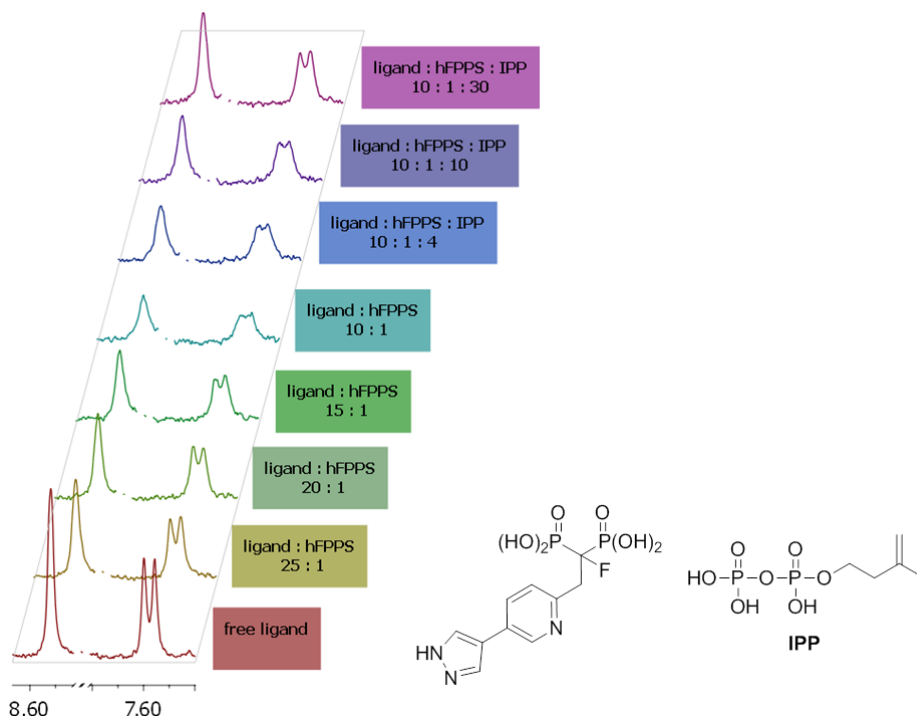


Figure 2.13: Competition study between inhibitor **2.22** and IPP by ^1H NMR line broadening.

2.8 Conclusions and Outlook

In summary, a small library of substituted pyridine bisphosphonates was docked into hFPPS using a computational model based on the protein structure of the hFPPS/ZOL/IPP ternary complex (PDB 1ZW5). The *in silico* screening results suggested large heterocycles cannot fit into the allylic pocket and that *meta*-substitution between the substituent and bisphosphonate moiety best complements active site, with the heterocycle in the IPP sub-pocket. The computational data was further analyzed to select derivatives that were synthesized and tested for enzymatic inhibition against hFPPS. The obtained SAR confirmed the preference for *meta*-substitution and suggested that the pyridine nitrogen forms an important interaction with protein. The combined data showed that an all *meta* substitution pattern between bisphosphonate moiety, heterocyclic sidechain and pyridine nitrogen is best suited to complement the hFPPS active site.

Docking and ^1H line broadening NMR data suggest that the binding mode of these inhibitors is distinctly different from risedronate. However, as will be discussed in Chapters 4 and 8, these compounds do not occupy the IPP sub-pocket.

2.9 Acknowledgments

We wish to thank Professor Nicolas Moitessier and Dr. Eric Therrien for their contributions to the computational studies (Chemistry Department, McGill University).

We would like to thank Frederik Morin (Chemistry Department, McGill University) for helping with the acquisition of { ^{19}F , ^{13}C } HMQC spectra for all final compounds. We are grateful to Dr. James Dunford (The Botnar Research Centre, The Institute of Musculoskeletal Sciences University of Oxford Nuffield Orthopaedic Centre) for his valuable advice on the set-up of the hFPPS assay. We also wish to thank Dr. Tara Sprules for assistance with the set-up of the ^1H Line broadening NMR experiments, which were acquired on a 500 MHz NMR instrument at the Québec/Eastern Canada High Field NMR Facility, supported by the Natural Sciences and Engineering Research Council of Canada, the Canada Foundation for Innovation, the Québec ministère de la recherche en science et technologie, and McGill University. We gratefully acknowledge the financial support of McGill University and the Natural Sciences and Engineering Research Council of Canada (NSERC), the Canadian Institute of Health Research (CIHR) and the Groupe de Recherche Axé sur la Structure des Protéines (GRASP).

2.10 References

- (1) Kavanagh, K. L.; Guo, K.; Dunford, J. E.; Wu, X.; Knapp, S.; Ebetino, F. H.; Rogers, M. J.; Russell, R. G. G.; Oppermann, U.; The molecular mechanism of nitrogen-containing bisphosphonates as antiosteoporosis drugs *Proc. Natl. Acad. Sci. U.S.A.* **2006**, *103*, 7829.
- (2) Russell, R. G. G.; Xia, Z.; Dunford, J. E.; Oppermann, U. D. O.; Kwaasi, A.; Hulley, P. A.; Kavanagh, K. L.; Triffitt, J. T.; Lundy, M. W.; Phipps, R. J.; Barnett, B. L.; Coxon, F. P.; Rogers, M. J.; Watts, N. B.; Ebetino, F. H.; Bisphosphonates *Ann. New York Acad. Sci.* **2007**, *1117*, 209.
- (3) Marma, M. S.; Xia, Z.; Stewart, C.; Coxon, F.; Dunford, J. E.; Baron, R.; Kashemirov, B. A.; Ebetino, F. H.; Triffitt, J. T.; Russell, R. G. G.; McKenna, C. E.; Synthesis and Biological Evaluation of α -Halogenated Bisphosphonate and Phosphonocarboxylate Analogues of Risedronate *J. Med. Chem.* **2007**, *50*, 5967.
- (4) Romanenko, V. D.; Kukhar, V. P.; Fluorinated Phosphonates: Synthesis and Biomedical Application *Chem. Rev.* **2006**, *106*, 3868.
- (5) Rondeau, J.-M.; Bitsch, F.; Bourgier, E.; Geiser, M.; Hemmig, R.; Kroemer, M.; Lehmann, S.; Ramage, P.; Rieffel, S.; Strauss, A.; Green, J. R.; Jahnke, W.; Structural Basis for the Exceptional in vivo Efficacy of Bisphosphonate Drugs *ChemMedChem* **2006**, *1*, 267.
- (6) Dunford, J. E.; Kwaasi, A. A.; Rogers, M. J.; Barnett, B. L.; Ebetino, F. H.; Russell, R. G. G.; Oppermann, U.; Kavanagh, K. L.; Structure–Activity Relationships Among the Nitrogen Containing Bisphosphonates in Clinical Use and Other Analogues: Time-Dependent Inhibition of Human Farnesyl Pyrophosphate Synthase *J. Med. Chem.* **2008**, *51*, 2187.
- (7) Friesner, R. A.; Banks, J. L.; Murphy, R. B.; Halgren, T. A.; Klicic, J. J.; Mainz, D. T.; Repasky, M. P.; Knoll, E. H.; Shelley, M.; Perry, J. K.; Shaw, D. E.; Francis, P.; Shenkin, P. S.; Glide: A New Approach for Rapid, Accurate Docking and Scoring. 1. Method and Assessment of Docking Accuracy *J. Med. Chem.* **2004**, *47*, 1739.
- (8) Halgren, T. A.; Murphy, R. B.; Friesner, R. A.; Beard, H. S.; Frye, L. L.; Pollard, W. T.; Banks, J. L.; Glide: A New Approach for Rapid, Accurate Docking and Scoring. 2. Enrichment Factors in Database Screening *J. Med. Chem.* **2004**, *47*, 1750.
- (9) Friesner, R. A.; Murphy, R. B.; Repasky, M. P.; Frye, L. L.; Greenwood, J. R.; Halgren, T. A.; Sanschagrin, P. C.; Mainz, D. T.; Extra Precision Glide: Docking and Scoring Incorporating a Model of Hydrophobic Enclosure for Protein–Ligand Complexes *J. Med. Chem.* **2006**, *49*, 6177.
- (10) Tang, Y.-Q.; Lu, J.-M.; Shao, L.-X.; NHC–Pd(II)–Im (NHC = N-heterocyclic carbene; Im = 1-methylimidazole) complexes as efficient catalysts for Suzuki–Miyaura coupling reactions of aryl chlorides *J. Organomet. Chem.* **2011**, *696*, 3741.
- (11) Prieto, M.; Zurita, E.; Rosa, E.; Muñoz, L.; Lloyd-Williams, P.; Giralt, E.; Arylboronic Acids and Arylpinacolboronate Esters in Suzuki Coupling Reactions Involving Indoles. Partner Role Swapping and Heterocycle Protection *J. Org. Chem.* **2004**, *69*, 6812.
- (12) Diebolt, O.; Braunstein, P.; Nolan, S. P.; Cazin, C. S. J.; Room-temperature activation of aryl chlorides in Suzuki–Miyaura coupling using a $[\text{Pd}(\mu\text{-Cl})\text{Cl}(\text{NHC})_2]$ complex (NHC = N-heterocyclic carbene) *Chem. Comm.* **2008**, 3190.

- (13) Slade, D. J.; Pelz, N. F.; Bodnar, W.; Lampe, J. W.; Watson, P. S.; Indazoles: Regioselective Protection and Subsequent Amine Coupling Reactions *J. Org. Chem.* **2009**, *74*, 6331.
- (14) Dunford, J. E.; Thompson, K.; Coxon, F. P.; Luckman, S. P.; Hahn, F. M.; Poulter, C. D.; Ebetino, F. H.; Rogers, M. J.; Structure-Activity Relationships for Inhibition of Farnesyl Diphosphate Synthase in Vitro and Inhibition of Bone Resorption in Vivo by Nitrogen-Containing Bisphosphonates *J. Pharmacol. Exper. Ther.* **2001**, *296*, 235.
- (15) Ni, F. *Recent Developments in Transferred NOE Methods*; Pergamon, **1994**.
- (16) Tsantrizos, Y. S.; Bolger, G.; Bonneau, P.; Cameron, D. R.; Goudreau, N.; Kukolj, G.; LaPlante, S. R.; Llinàs-Brunet, M.; Nar, H.; Lamarre, D.; Macrocyclic Inhibitors of the NS3 Protease as Potential Therapeutic Agents of Hepatitis C Virus Infection *Angew. Chem. Int. Ed.* **2003**, *42*, 1356.

2.11 Experimental

2.11.1 Docking studies

Computational studies: All calculations were performed using the Schrödinger suite: Maestro (version 9.0), Glide (version 5.5), ConfGen, (version 2.1), LigPrep, (version 2.3, Schrödinger, LLC, New York, NY, 2009.

All images were generated using PyMol (www.pymol.org)

Docking :

Protein Preparation: All crystal structures were downloaded directly from the PDB database and prepared using the Protein Preparation Wizard feature using standard parameters. The proteins were overlapped with the secondary structure alignment tool, using the hinge-region between Helix I and II as reference.

Docking Grid Generation: Three grids were generated using standard parameters, encompassing the two active site sub-pockets (*i.e.* binding sites of IPP and ZOL) from the hFPPS/IPP/ZOL ternary complex (PDB: 1ZW5).

Docking:

All bisphosphonates were docked in their fully ionized (tetra-anion) forms, conformation libraries were generated using ConfGen (using the parameters: “standard” and “intermediate”; only input minimization) followed by LigPrep (retain original ionization state; output tautomers). Docking was performed with Glide (5.5), flexible docking, extra precision (XP-mode), standard parameters.

Analysis: All output structures were visually inspected and poses that did not have the bisphosphonate moiety properly aligned to the Mg^{2+} -triad (as compared to the crystal structures of 1ZW5) were rejected. In general, high conformational consistency of the output poses was observed.

2.11.2 Synthesis:

General. All intermediate compounds were purified by normal phase flash column chromatography on silica gel using a CombiFlash instrument and the solvent gradient indicated. Library analogs were also purified at the bisphosphonate tetra ester stage by normal-phase chromatography on silica gel (using a CombiFlash instrument). The purified tetra esters were fully characterized by ^1H , ^{13}C and ^{31}P NMR, and MS. Only compounds isolated in >90% purity and sufficient quantities were processed further to the ester hydrolysis step. The final bisphosphonic acid products were characterized by ^1H , ^{13}C , ^{31}P NMR and HRMS data before they were used in our *structure-activity-relationship* (SAR) studies. Chemical shifts (δ) are reported in ppm relative to the internal deuterated solvent (^1H , ^{13}C) or external H_3PO_4 . (δ 0.00 ^{31}P), unless indicated otherwise. Low- and High-Resolution MS spectra were recorded at the McGill University, MS facilities using electrospray ionization ($\text{ESI}^{+/-}$).

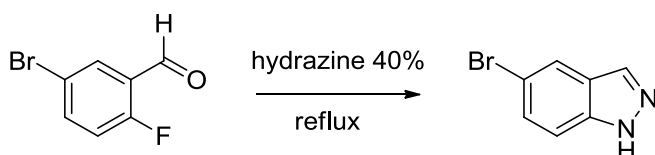
Synthesis of THP protected indazole-5-boronic pinacol ester **2.15**:

This boron reagent was synthesized according to literature procedure:

Slade, D.J. *et. al.*, *J. Org. Chem.* **2009**, 6331

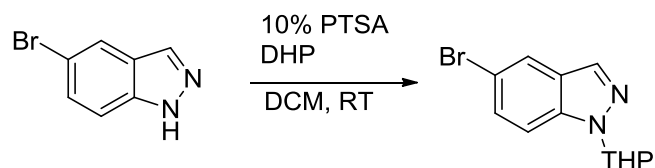
Furuya, T. *et. al.*, *Org. Lett.* **2009**, 2860

JDS-02-122: 5-bromo-1H-indazole



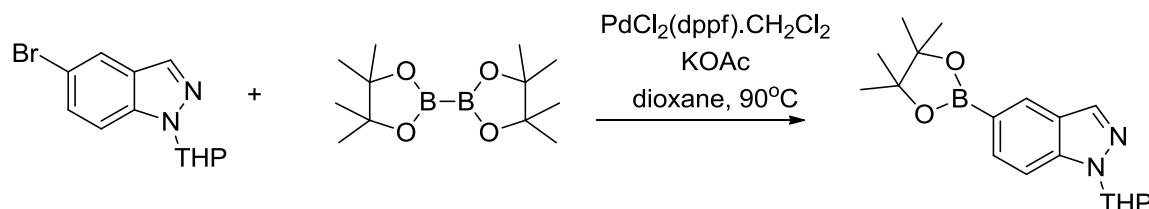
Isolated 1050 mg as a white powder (43%). ^1H NMR (300 MHz, CDCl_3) δ 8.03 (s, 1H), 7.92 (dd, $J = 1.7, 0.7$ Hz, 1H), 7.48 (dd, $J = 8.8, 1.8$ Hz, 1H), 7.39 (d, $J = 8.8$ Hz, 1H).

JDS-02-123: 5-bromo-1-(tetrahydro-2H-pyran-2-yl)-1H-indazole



Isolated 1500 mg as a pale yellow oil (100%). ¹H NMR (300 MHz, CDCl₃) δ 7.96 (s, 1H), 7.86 (d, *J* = 0.8 Hz, 1H), 7.53 – 7.42 (m, 2H), 5.70 (dd, *J* = 9.2, 2.7 Hz, 1H), 4.00 (d, *J* = 11.5 Hz, 1H), 3.74 (d, *J* = 1.8 Hz, 1H), 2.51 (dd, *J* = 13.2, 9.3 Hz, 1H), 2.09 (dd, *J* = 21.8, 9.3 Hz, 3H), 1.87 – 1.61 (m, 4H).

JDS-02-125: 1-(tetrahydro-2H-pyran-2-yl)-5-(4,4,5,5-tetramethyl-1,3,2-dioxaborolan-2-yl)-1H-indazole

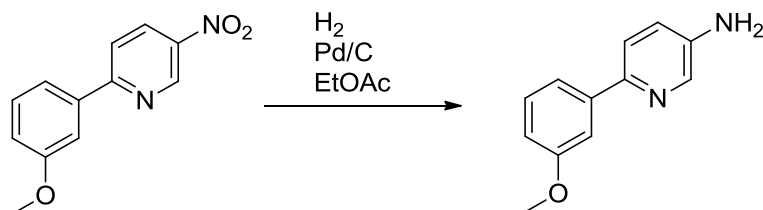


Isolated 1357 mg as a yellow oil (77%). ¹H NMR (400 MHz, CDCl₃) δ 8.25 (s, 1H), 8.03 (s, 1H), 7.79 (dd, *J* = 8.5, 1.0 Hz, 1H), 7.56 (d, *J* = 8.5 Hz, 1H), 5.73 (dd, *J* = 9.4, 2.7 Hz, 1H), 4.03 (d, *J* = 11.6 Hz, 1H), 3.75 (td, *J* = 11.4, 2.8 Hz, 1H), 2.58 (d, *J* = 11.4 Hz, 1H), 2.16 (d, *J* = 7.6 Hz, 1H), 1.76 (t, *J* = 9.3 Hz, 2H), 1.66 (s, 1H), 1.36 (s, 12H).

Synthesis of 2.3, general procedure for the catalytic hydrogenation:

A solution of aryl nitrate (1 equivalent) in EtOAc was evacuated and refilled with Argon. Palladium on charcoal (0.1 equivalent) was added, the reaction vessel was flushed with hydrogen gas, equipped with an hydrogen filled balloon and stirred at RT overnight. The RBF was flushed with Argon and the reaction mixture was filtered over a plug of Celite and rinsed 3 times with EtOAc. The filtrate was concentrated in vacuo and purified by normal phase column chromatography on silica gel (silica gel was pre-treated with 1% NEt₃ in hexanes/EtOAc in a 3:1 ratio) using a gradient from 100% hexanes to 100% EtOAc and then to 25% MeOH.

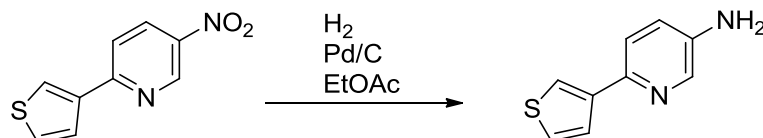
JDS01-14: 6-(3-methoxyphenyl)pyridin-3-amine



Isolated 60 mg as a bright yellow solid (31%).

¹H NMR (300 MHz, CDCl₃) δ 8.18 (d, *J* = 2.9 Hz, 1H), 7.53 (d, *J* = 8.5 Hz, 1H), 7.51 – 7.48 (m, 1H), 7.48 – 7.43 (m, 1H), 7.33 (t, *J* = 7.9 Hz, 1H), 7.04 (dd, *J* = 8.5, 2.9 Hz, 1H), 6.89 (dd, *J* = 8.1, 2.6 Hz, 1H), 3.88 (s, 3H). MS (ESI): calcd 201.10, found 201.3 [M+H]⁺

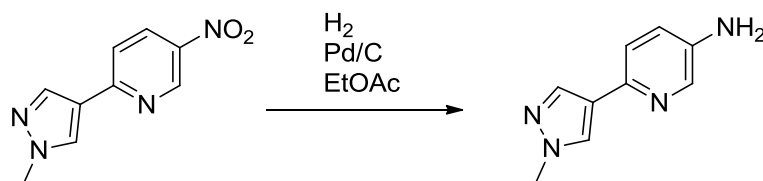
JDS01-15: 6-(thiophen-3-yl)pyridin-3-amine



Isolated 62 mg as a bright yellow solid (38%).

¹H NMR (300 MHz, CDCl₃) δ 8.34 (d, *J* = 2.7 Hz, 1H), 7.78 (dd, *J* = 2.7, 1.5 Hz, 1H), 7.61 (d, *J* = 5.1 Hz, 1H), 7.56 (d, *J* = 8.5 Hz, 1H), 7.43 – 7.35 (m, 2H). MS (ESI): calcd 177.05, found 176.1 [M+H]⁺

JDS01-16: 6-(1-methyl-1H-pyrazol-4-yl)pyridin-3-amine



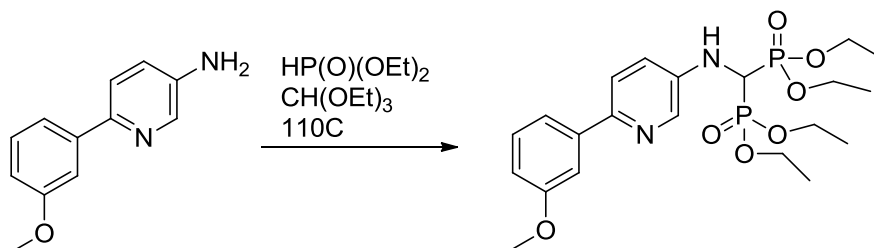
Isolated 217 mg as a yellow powder (84%)

¹H NMR (300 MHz, CDCl₃) δ 8.06 (d, *J* = 2.8 Hz, 1H), 7.81 (d, *J* = 13.8 Hz, 2H), 7.30 – 7.24 (m, 1H), 6.99 (dd, *J* = 8.4, 2.9 Hz, 1H), 3.92 (s, 3H), 3.65 (s, 2H). MS (ESI): calcd 175.10, found 175.2 [M+H]⁺

Synthesis of 2.5, general procedure for the bisphosphonate condensation reactions:

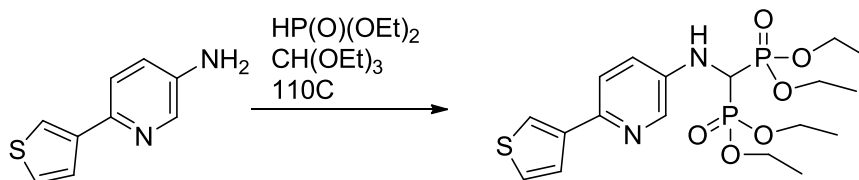
To a 15 mL pressure vessel was added in sequence aniline substrate (1 equivalent), diethyl phosphite (2 equivalents) and triethyl orthoformate (1 equivalent). The vessel was tightly sealed and the reaction mixture was stirred overnight at 110°C. The reaction mixture was allowed to cool to room temperature and concentrated in vacuo. The residue purified by normal phase column chromatography on silica gel (silica gel was pre-treated with 1% NEt₃ in hexanes/EtOAc in a 3:1 ratio) using a gradient from 100% hexanes to 100% EtOAc and then to 25% MeOH.

JDS01-27: tetraethyl (((6-(3-methoxyphenyl)pyridin-3-yl)amino)methylene)bis(phosphonate)



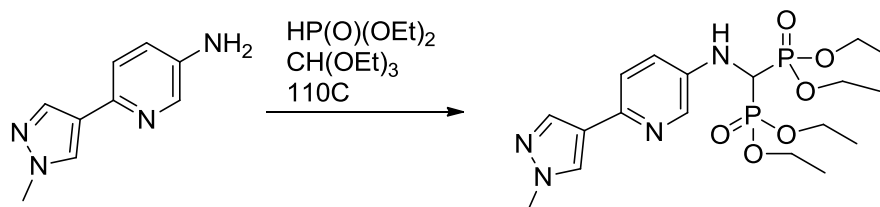
Isolated 146 mg of product (64%). ¹H NMR (300 MHz, CDCl₃) δ 8.20 (d, *J* = 2.8, 1H), 7.58 (d, *J* = 8.7, 1H), 7.53 – 7.43 (m, 2H), 7.33 (t, *J* = 7.9, 1H), 7.07 (dd, *J* = 2.9, 8.6, 1H), 6.89 (dd, *J* = 2.6, 8.1, 1H), 4.32 – 4.11 (m, 9H), 3.88 (s, 3H), 1.29 (dt, *J* = 7.1, 12.5, 12H). ³¹P NMR (81 MHz, CDCl₃) δ 14.76. MS (ESI): calcd 509.16, found 509.2 [M+Na]⁺

JDS01-19: tetraethyl (((6-(thiophen-3-yl)pyridin-3-yl)amino)methylene)bis(phosphonate)



Isolated 50 mg of product (36%). ¹H NMR (300 MHz, CDCl₃) δ 8.13 (d, *J* = 3.0 Hz, 1H), 7.72 – 7.68 (m, 1H), 7.59 – 7.55 (m, 1H), 7.47 (d, *J* = 8.5 Hz, 1H), 7.36 (dd, *J* = 5.1, 3.0 Hz, 1H), 7.25 (s, 1H), 7.04 (dd, *J* = 8.8, 3.0 Hz, 1H), 4.21 (m, 9H), 1.28 (m, 12H). ³¹P NMR (81 MHz, CDCl₃) δ 14.73. MS (ESI): calcd 485.10, found 485.2 [M+Na]⁺

JDS01-20: tetraethyl (((6-(1-methyl-1H-pyrazol-4-yl)pyridin-3-yl)amino)methylene)bis(phosphonate)



Isolated 359 mg of product (100%). ^1H NMR (300 MHz, CDCl_3) δ 8.08 (d, $J = 3.0$ Hz, 1H), 7.81 (d, $J = 13.0$ Hz, 2H), 7.30 (d, $J = 8.5$ Hz, 1H), 7.01 (dd, $J = 8.5, 2.8$ Hz, 1H), 4.20 (m, 9H), 3.93 (s, 3H), 1.29 (m, 12H). ^{31}P NMR (81 MHz, CDCl_3) δ 14.85. MS (ESI): calcd 483.15, found 483.2 $[\text{M}+\text{Na}]^+$

Synthesis of 2.7, general procedure for the reduction of aromatic carboxylic acids:

Method A:

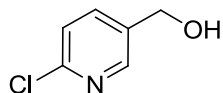
To a solution of carboxylic acid (1 equivalent) and triethylamine (1.1 equivalent) in 30 mL anhydrous THF at 0°C was added ethylchloroformate (1 equivalent) dropwise via syringe under an Argon atmosphere and the reaction was stirred at RT for 1 h. The suspension was filtered over a glass frit filter and the residue was washed twice with 5 mL THF. The filtrate was transferred to a 100 mL RBF and cooled to 0°C . Sodium borohydride (3 equivalents) was added in portions followed by 5 mL H_2O , dropwise via syringe. The reaction was stirred at RT overnight and then concentrated in vacuo. The residue was transferred to a separatory funnel, diluted with 30 mL water and extracted 6 times with 30 mL EtOAc, the combined organic layers were dried over sodium sulfate and concentrated in vacuo and purified by normal phase column chromatography on silica gel (silica gel was pre-treated with 1% NEt_3 in hexanes/EtOAc in a 3:1 ratio) using a gradient from 100% hexanes to 100% EtOAc and then to 25% MeOH.

Method B:

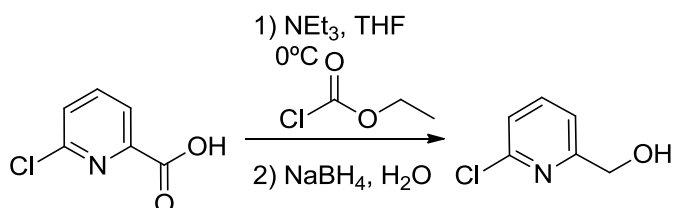
To a solution of carboxylic acid (1 equivalent) in 25 mL anhydrous THF was added borane (1.0M in THF; 2 equivalents) dropwise via syringe under an Argon atmosphere. The reaction was stirred at 50°C overnight. The reaction mixture was cooled down and slowly quenched with 5 mL MeOH. The crude was concentrated in vacuo and purified by normal

phase column chromatography on silica gel (silica gel was pre-treated with 1% NEt_3 in hexanes/EtOAc in a 3:1 ratio) using a gradient from 100% hexanes to 100% EtOAc.

(6-chloropyridin-3-yl)methanol is commercially available



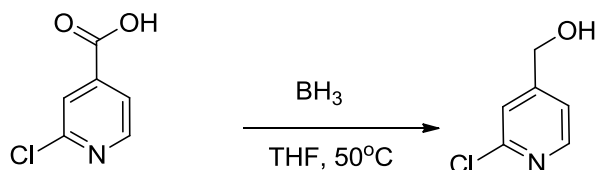
JDS-02-044: (6-chloropyridin-2-yl)methanol



Method A; isolated as a clear, colorless oil (790 mg, 87%). ^1H NMR (400 MHz, CDCl_3) δ 7.66 (t, $J = 7.7$ Hz, 1H), 7.25 (m, 2H), 4.75 (d, $J = 5.6$ Hz, 2H), 2.99 (t, $J = 5.6$ Hz, 1H).

Matches literature data: Lee, K. C.; Chi, D. Y., *J. Org. Chem.* **1999**, 64, 8576

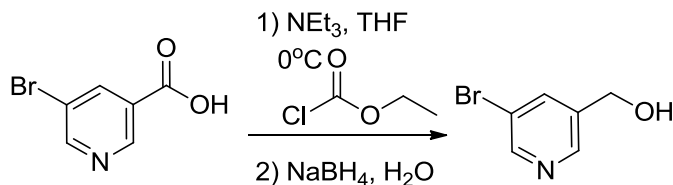
JDS-02-019: (2-chloropyridin-4-yl)methanol



Method B; isolated as a white powder (1100 mg, 60%). ^1H NMR (300 MHz, CDCl_3) δ 8.34 (d, $J = 5.1$ Hz, 1H), 7.37 (s, 1H), 7.21 (d, $J = 5.1$ Hz, 1H), 4.76 (s, 2H).

Matches literature data: Van Eis, M. *et. al.*, PCT Int. Appl., 2008074752, 26 Jun 2008

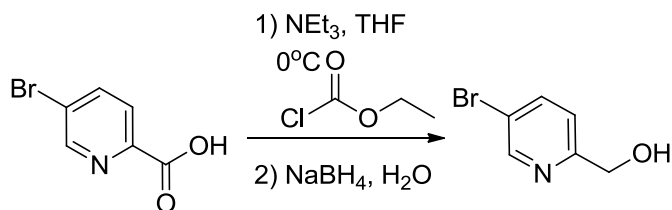
JDS-02-027, JDS08-029: (5-bromopyridin-3-yl)methanol



Method A; Isolated 426 mg (46%) of a clear, colorless oil. ^1H NMR (300 MHz, CDCl_3) δ 8.60 (d, $J = 2.2$ Hz, 1H), 8.50 (s, 1H), 7.89 (s, 1H), 4.74 (d, $J = 5.8$ Hz, 2H), 1.96 (t, $J = 5.7$

Hz, 1H). ^{13}C NMR (75 MHz, CDCl_3) δ 149.40, 145.95, 138.67, 137.58, 120.96, 61.39. MS (ESI): calcd 187.971 and 189.969, found 187.97 and 189.96 $[\text{M}+\text{H}]^+$

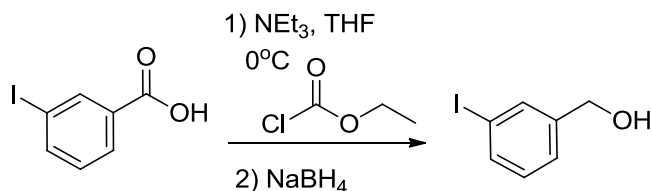
JDS-02-030: (5-bromopyridin-2-yl)methanol



Method A; isolated 772 mg (55%) of a clear, colorless oil. ^1H NMR (400 MHz, CDCl_3) δ 8.63 (d, J = 2.0 Hz, 1H), 7.82 (dd, J = 8.3, 2.3 Hz, 1H), 7.19 (d, J = 8.2 Hz, 1H), 4.73 (d, J = 5.2 Hz, 2H), 3.30 (t, J = 5.3 Hz, 1H).

Matches literature data: Roelfes, G. *et. al.*, *Inorg. Chem.* **2003**, 42, 2639

JDS-04-137: (3-iodophenyl)methanol



Method A; isolated 1830mg (97%) of product as a pale yellow oil. ^1H NMR (400 MHz, CDCl_3) δ 7.74 (s, 1H), 7.63 (d, J = 7.9 Hz, 1H), 7.32 (d, J = 7.7 Hz, 1H), 7.10 (t, J = 7.7 Hz, 1H), 4.66 (d, J = 5.3 Hz, 2H), 1.67 (t, J = 5.8 Hz, 1H). ^{13}C NMR (75 MHz, CDCl_3) δ 143.10, 136.58, 135.82, 130.27, 126.01, 94.49, 64.30.

Synthesis of **2.8**, general procedure for bromination of benzylic alcohols:

To a solution of benzylic alcohol (1 equivalent) 20 mL anhydrous DCM at 0°C was added phosphorus tribromide (1.2 equivalent) dropwise via syringe (solution turns cloudy) under Argon atmosphere and the reaction was stirred at RT for 2 h. The mixture was cooled 0°C and carefully quenched with 5 mL water followed by 2M K_2CO_3 until neutral on pH-paper. The mixture was transferred to a separatory funnel, separated and the aqueous phase was extracted 3 times with 30 mL EtOAc. The combined organic layers were dried over sodium sulfate and concentrated in vacuo and purified by normal phase column

chromatography on silica gel (silica gel was pre-treated with 1% NEt₃ in hexanes/EtOAc in a 3:1 ratio) using a gradient from 100% hexanes to 50% EtOAc.

JDS-02-040: 2-(bromomethyl)-6-chloropyridine



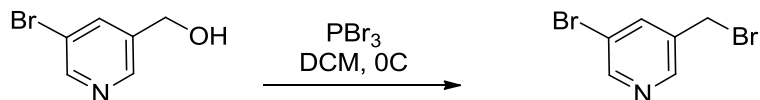
Isolated as a white solid (314 mg, 46%, based on recovered starting material). ¹H NMR (400 MHz, CDCl₃) δ 7.67 (t, *J* = 7.8 Hz, 1H), 7.39 (d, *J* = 7.6 Hz, 1H), 7.27 (d, *J* = 5.3 Hz, 1H), 4.50 (s, 2H).

JDS-02-033: 4-(bromomethyl)-2-chloropyridine



Isolated as a pale pink crystals (700 mg, 50%, pas on recovered starting material). ¹H NMR (300 MHz, CDCl₃) δ 8.37 (d, *J* = 5.1 Hz, 1H), 7.35 (s, 1H), 7.27 – 7.20 (m, 1H), 4.35 (s, 2H). ¹³C NMR (75 MHz, CDCl₃) δ 150.15, 149.22, 124.14, 122.35, 29.27.

JDS-01-048: 3-bromo-5-(bromomethyl)pyridine



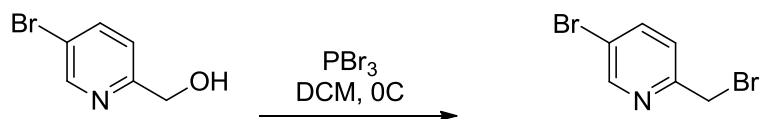
Isolated 1293 mg as white crystals (69%). ¹H NMR (300 MHz, CDCl₃) δ 8.61 (d, *J* = 2.2 Hz, 1H), 8.54 (d, *J* = 2.0 Hz, 1H), 7.89 (t, *J* = 2.1 Hz, 1H), 4.42 (s, 2H).

JDS-02-026: 5-(bromomethyl)-2-chloropyridine



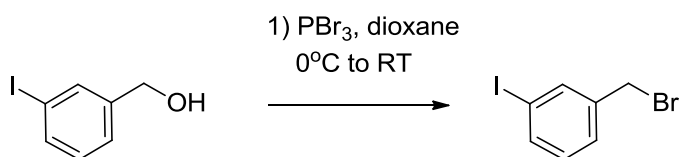
Isolated 1253 mg (87%) of a clear colorless oil. ¹H NMR (300 MHz, CDCl₃) δ 8.40 (d, *J* = 2.5 Hz, 1H), 7.70 (dd, *J* = 8.2, 2.6 Hz, 1H), 7.33 (dd, *J* = 8.1, 0.5 Hz, 1H), 4.52 – 4.40 (m, 2H).

JDS-02-035: 5-bromo-2-(bromomethyl)pyridine



Isolated 1124 mg of dark pink crystals (68% based on recovered starting material). ^1H NMR (300 MHz, CDCl_3) δ 8.63 (d, $J = 2.3$ Hz, 1H), 7.82 (dd, $J = 8.3, 2.4$ Hz, 1H), 7.34 (d, $J = 8.2$ Hz, 1H), 4.50 (s, 2H).

JP01-048: 1-(bromomethyl)-3-iodobenzene

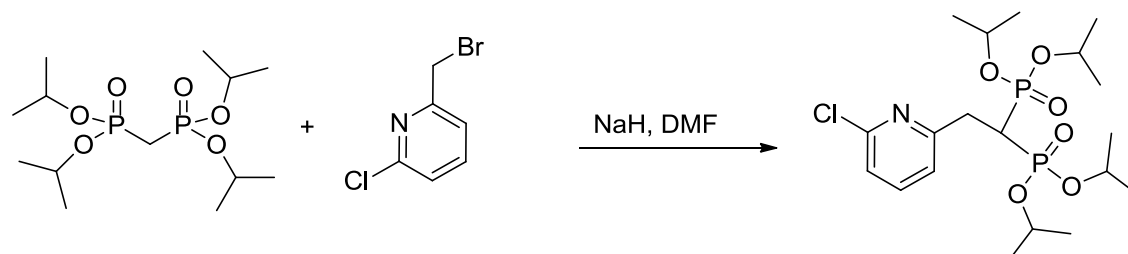


Isolated 2523mg (72%) of product as white crystals. ^1H NMR (400 MHz, CDCl_3) δ 7.75 (t, $J = 1.7$ Hz, 1H), 7.63 (d, $J = 7.9$ Hz, 1H), 7.36 (d, $J = 7.7$ Hz, 1H), 7.08 (t, $J = 7.8$ Hz, 1H), 4.40 (s, 2H). ^{13}C NMR (75 MHz, CDCl_3) δ 139.90, 137.88, 137.42, 130.43, 128.27, 94.26, 31.90.

Synthesis of **2.10**, general procedure for bisphosphonate alkylations:

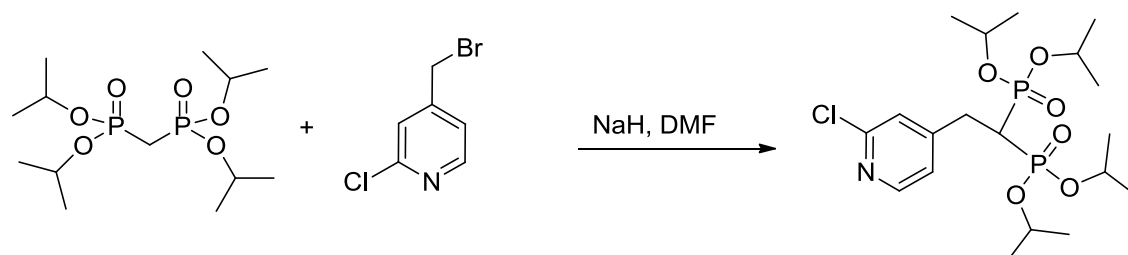
To a solution of tetra-isopropyl methylenebis(phosphonate) ester or tetra-ethyl methylenebis(phosphonate) ester (1 equivalent) in 20 mL anhydrous DMF at 0°C was added NaH (1.1 equivalent) in one portion and the suspension was stirred at RT for 1 h. The reaction was cooled to 0°C and the benzylic bromide (1 equivalent) was transferred with syringe as a solution in 10 mL DMF. The reaction was stirred overnight and quenched by dropwise addition of MeOH. The crude concentrated in vacuo and redissolved in 60 mL EtOAc, washed 3 times with 10 mL water and once with brine. The combined organic layers were dried over sodium sulfate, concentrated in vacuo and purified by normal phase column chromatography on silica gel (silica gel was pre-treated with 1% NEt_3 in hexanes/EtOAc in a 3:1 ratio) using a gradient from 100% hexanes to 100% EtOAc and then to 50% MeOH.

JDS-02-46: tetraisopropyl (2-(6-chloropyridin-2-yl)ethane-1,1-diyl)bis(phosphonate)



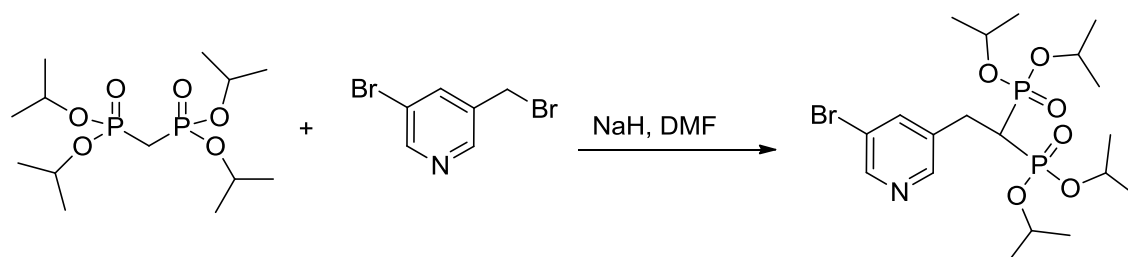
Isolated as a clear, colorless oil (1037 mg, 57%) contaminated with ~3% tetra-*i*Pr-methylene bisphosphonate ester as determined by ^{31}P -NMR. ^1H NMR (300 MHz, CDCl_3) δ 7.58 – 7.45 (m, 1H), 7.13 (dd, $J = 7.7, 4.4$ Hz, 2H), 4.83 – 4.66 (m, 4H), 3.29 (m, 3H), 1.38 – 1.18 (m, 24H). ^{31}P NMR (81 MHz, CDCl_3) δ 18.88.

JDS-02-36: tetraisopropyl (2-(2-chloropyridin-4-yl)ethane-1,1-diyl)bis(phosphonate)



Isolated as a pale, yellow oil contaminated with 6.5% tetra-*i*Pr-methylene bisphosphonate ester as determined by ^{31}P -NMR (979 mg, 57%). ^1H NMR (300 MHz, CDCl_3) δ 8.27 (d, $J = 5.1$ Hz, 1H), 7.26 (m, 1H), 7.15 (d, $J = 5.1$ Hz, 1H), 4.77 (m, 4H), 3.17 (td, $J = 16.3, 6.4$ Hz, 2H), 2.46 (tt, $J = 23.9, 6.4$ Hz, 1H), 1.41 – 1.20 (m, 24H). ^{31}P NMR (81 MHz, CDCl_3) δ 17.77.

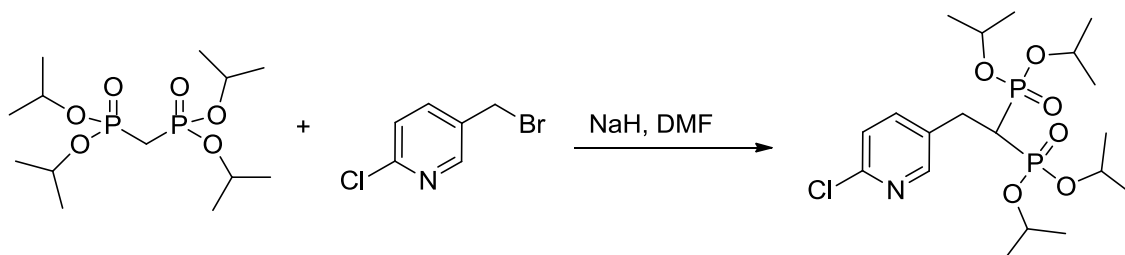
JDS-01-045: tetraisopropyl (2-(5-bromopyridin-3-yl)ethane-1,1-diyl)bis(phosphonate)



Isolated 776 mg (47%) of colorless oil contaminated with 6% tetra-*i*Pr-methylene bisphosphonate ester as determined by ^{31}P -NMR. ^1H NMR (300 MHz, CDCl_3) δ 8.52 (d, J

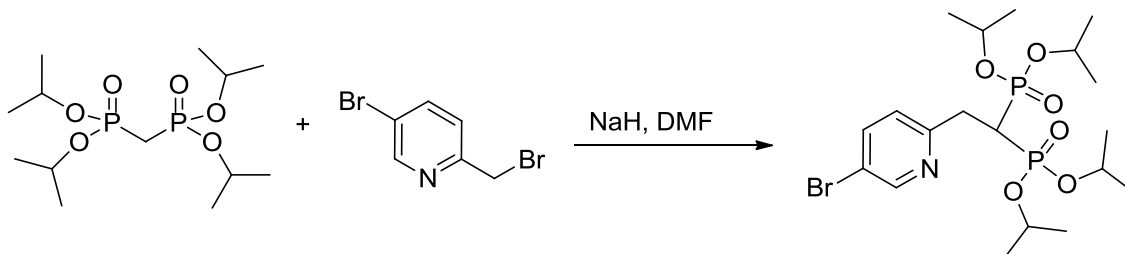
= 2.0 Hz, 1H), 8.43 (s, 1H), 7.79 (t, $J = 2.0$ Hz, 1H), 4.77 (m, 4H), 3.19 (td, $J = 16.1$, 6.4 Hz, 2H), 2.43 (ddd, $J = 23.9$, 20.7, 5.8 Hz, 1H), 1.42 – 1.18 (m, 24H). ^{31}P NMR (81 MHz, CDCl_3) δ 17.57.

JDS-02-29: tetraisopropyl (2-(6-chloropyridin-3-yl)ethane-1,1-diyl)bis(phosphonate)



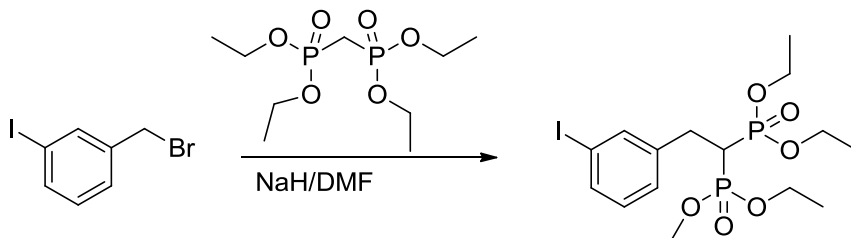
Isolated as a clear oil (919mg, 32%), contaminated with 29 % tetra-*i*Pr-methylene bisphosphonate ester as determined by ^{31}P -NMR. ^1H NMR (300 MHz, CDCl_3) δ 8.29 (d, $J = 2.2$ Hz, 1H), 7.61 (dd, $J = 8.3$, 2.5 Hz, 1H), 7.24 (m, 1H), 4.76 (m, 4H), 3.19 (td, $J = 16.2$, 6.3 Hz, 2H), 2.39 (m, 1H), 1.29 (m, 24H). ^{31}P NMR (81 MHz, CDCl_3) δ 18.01.

JDS-02-38: tetraisopropyl (2-(5-bromopyridin-2-yl)ethane-1,1-diyl)bis(phosphonate)



Product isolated as a pale brown oil (1244 mg, 54%). ^1H NMR (300 MHz, CDCl_3) δ 8.56 (d, $J = 2.3$ Hz, 1H), 7.68 (dd, $J = 8.3$, 2.4 Hz, 1H), 7.11 (d, $J = 8.3$ Hz, 1H), 4.74 (m, 4H), 3.46 – 3.10 (m, 3H), 1.27 (m, 24H). ^{31}P NMR (81 MHz, CDCl_3) δ 19.03.

JP-01-49: tetraethyl (2-(3-iodophenyl)ethane-1,1-diyl)bis(phosphonate)

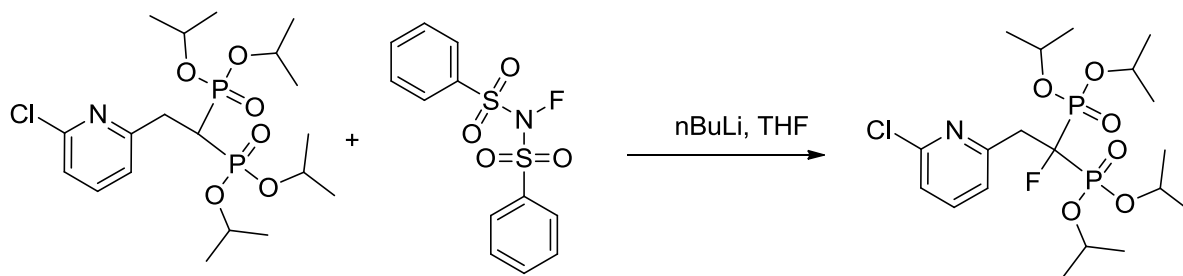


Isolated 1329mg (52%) of product as a pale yellow oil. ^1H NMR (400 MHz, CDCl_3) δ 7.63 (s, 1H), 7.54 (d, J = 7.9 Hz, 1H), 7.24 (d, J = 7.0 Hz, 1H), 7.01 (t, J = 7.8 Hz, 1H), 4.23 – 4.02 (m, 10H), 3.18 (td, J = 16.4, 6.2 Hz, 2H), 2.58 (tt, J = 23.8, 6.3 Hz, 1H), 1.41 – 1.22 (m, 15H). ^{13}C NMR (75 MHz, CDCl_3) δ 142.06, 138.01, 135.50, 129.95, 128.24, 93.99, δ 62.61 (dd, J = 17.1, 6.5 Hz), 39.00 (t, J = 132.9 Hz), 30.76 (d, J = 4.8 Hz), 16.31 (d, J = 6.7 Hz). ^{31}P NMR (81 MHz, CDCl_3) δ 20.05. MS (ESI): calcd 527.02, found 527.04 $[\text{M}+\text{Na}]^+$

Synthesis of **2.12**, general procedure for fluorination at bisphosphonate α -methylene:

To a solution of tetra-isopropyl bisphosphonate (1equiv) in 50 mL anhydrous THF at -78°C was added $n\text{-BuLi}$ (1.6 M in hexanes, 1.2 equiv) dropwise via syringe under an Argon atmosphere and the solution was stirred for 60 min at -78°C . N -fluorobenzenesulfonimide (1.1 equiv) was added via syringe as solution in 5 mL THF. The reaction was stirred at -78°C for 10 min and slowly warmed to RT over 6 h. The reaction was quenched with 1 mL MeOH, concentrated in vacuo, redissolved in 100 mL EtOAc and washed three times with 10 mL water and once with brine. The organic layer was dried over sodium sulfate, concentrated in vacuo and purified by normal phase column chromatography on silica gel (silica gel was pre-treated with 1% NEt_3 in hexanes/EtOAc in a 3:1 ratio) using a gradient from 100% hexanes to 100% EtOAc and then to 10-50% MeOH.

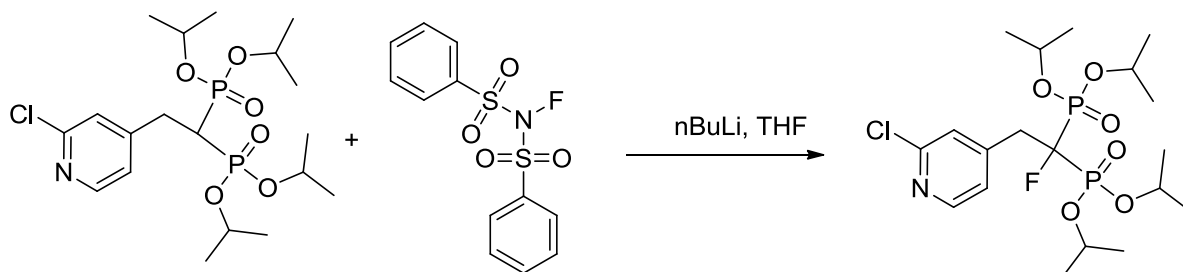
JDS-02-47: tetraisopropyl (2-(6-chloropyridin-2-yl)-1-fluoroethane-1,1-diyl)bis(phosphonate)



Isolated as a pale brown oil (805 mg, 87%, based on recovered starting material). ^1H NMR (300 MHz, CDCl_3) δ 7.54 (t, J = 7.8 Hz, 1H), 7.31 (dd, J = 6.7, 1.1 Hz, 1H), 7.20 (dd, J = 7.8, 0.8 Hz, 1H), 4.92 – 4.73 (m, 4H), 3.74 – 3.49 (m, 2H), 1.31 (m, 24H). ^{13}C NMR (126 MHz, CDCl_3) δ 153.75 (t, J = 9.8 Hz), 147.38, 135.53, 121.77 (d, J = 3.0 Hz), 119.75, 91.83 (dt, J = 191.7, 158.8 Hz), 70.28 (dt, J = 29.7, 3.5 Hz), 38.27 (d, J = 18.5 Hz), 21.39

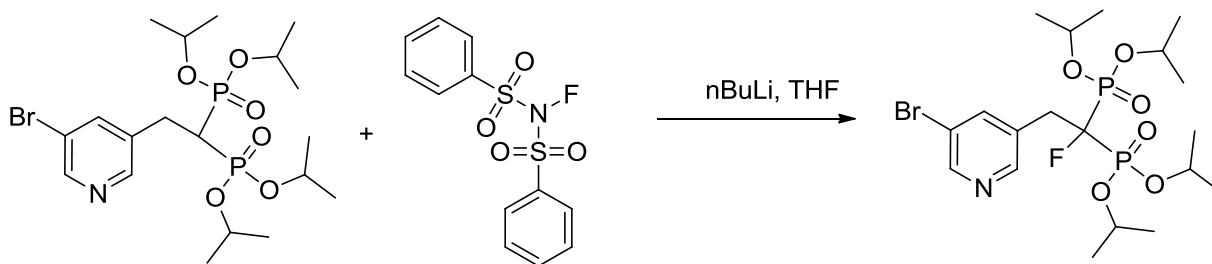
(dd, $J = 67.4, 28.8$ Hz). ^{19}F NMR (470 MHz, CDCl_3) δ -193.41 (tt, $J = 77.0, 27.5$ Hz). ^{31}P NMR (81 MHz, CDCl_3) δ 9.40 (d, $J = 76.9$ Hz). MS (ESI): calcd 510.86, found 510.2 $[\text{M}+\text{Na}]^+$

JDS-02-42: tetraisopropyl (2-(2-chloropyridin-4-yl)-1-fluoroethane-1,1-diyl)bis(phosphonate)



Isolated 746 mg (79%) of a brown oil. ^1H NMR (300 MHz, CDCl_3) δ 8.27 (dd, $J = 5.1, 0.5$ Hz, 1H), 7.31 (s, 1H), 7.18 (dt, $J = 5.1, 1.2$ Hz, 1H), 4.92 – 4.73 (m, 4H), 3.52 – 3.28 (m, 2H), 1.41 – 1.18 (m, 24H). ^{13}C NMR (75 MHz, CDCl_3) δ 150.75, 148.66, 146.99 (td, $J = 8.5, 1.2$ Hz), 126.98 (d, $J = 1.5$ Hz), 125.35 (d, $J = 1.3$ Hz), 94.00 (dt, $J = 194.2, 157.8$ Hz), 73.12 (dt, $J = 40.1, 3.4$ Hz), 37.76 (d, $J = 18.9$ Hz), 24.19 (d, $J = 20.3$ Hz), 23.57 (dt, $J = 28.1, 3.0$ Hz). ^{19}F NMR (470 MHz, CDCl_3) δ -192.79 (tt, $J = 74.0, 26.2$ Hz). ^{31}P NMR (81 MHz, CDCl_3) δ 9.09 (d, $J = 74.2$ Hz). MS (ESI): calcd 510.86, found 510.2 $[\text{M}+\text{Na}]^+$

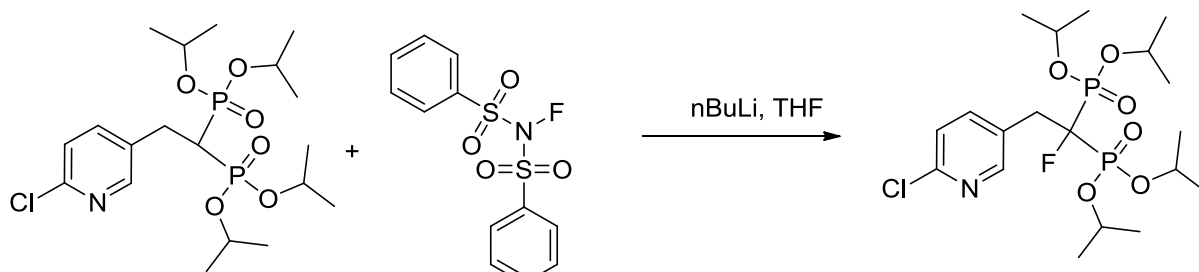
JDS-01-055: tetraisopropyl (2-(5-bromopyridin-3-yl)-1-fluoroethane-1,1-diyl)bis(phosphonate)



Isolated 790 mg (73% based on recovered starting material) as a pale brown oil. ^1H NMR (300 MHz, CDCl_3) δ 8.55 (d, $J = 2.1$ Hz, 1H), 8.43 (s, 1H), 7.81 (s, 1H), 4.82 (m, 4H), 3.57 – 3.27 (m, 2H), 1.29 (m, 24H). ^{13}C NMR (126 MHz, CDCl_3) δ 150.13, 148.96, 141.23, 132.21 (t, $J = 8.1$ Hz), 119.74, 94.21 (dt, $J = 192.9, 157.7$ Hz), 73.06 (dt, $J = 61.8, 3.4$ Hz), 35.70 (d, $J = 19.4$ Hz), 24.24 (d, $J = 31.7$ Hz), 23.63 (dt, $J = 45.3, 3.0$ Hz). ^{19}F NMR (470

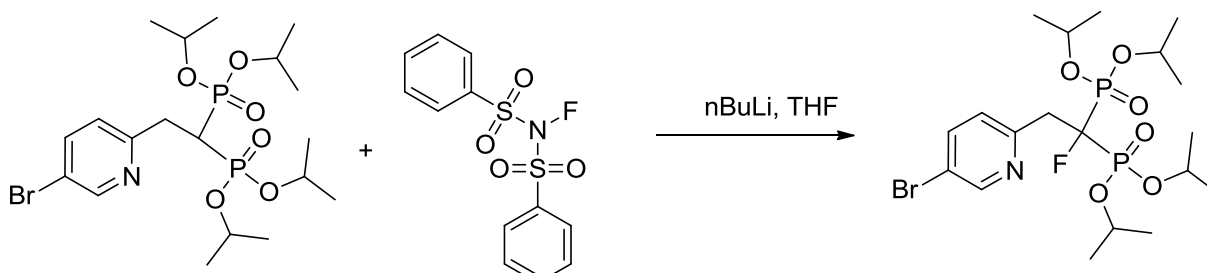
MHz, CDCl₃) δ -192.85 (tt, J = 74.5, 26.7 Hz). ³¹P NMR (81 MHz, CDCl₃) δ 9.25 (d, J = 74.6 Hz). MS (ESI): calcd 554.08, found 554.3 [M+Na]⁺

JDS-02-041: tetraisopropyl (2-(6-chloropyridin-3-yl)-1-fluoroethane-1,1-diyl)bis(phosphonate)



Isolated 283 mg (30%) as a brown oil. ¹H NMR (300 MHz, CDCl₃) δ 8.29 (d, J = 2.2 Hz, 1H), 7.61 (d, J = 8.1 Hz, 1H), 7.30 – 7.17 (m, 1H), 4.82 (m, 4H), 3.42 (dd, J = 14.4, 12.2 Hz, 2H), 1.45 – 1.13 (m, 24H). ¹³C NMR (75 MHz, CDCl₃) δ 151.75 (d, J = 1.3 Hz), 149.85, 141.51 (d, J = 1.6 Hz), 129.29 (t, J = 9.1 Hz), 123.09, 94.22 (dt, J = 192.5, 157.6 Hz), 73.06 (dt, J = 30.7, 3.5 Hz), 35.30 (d, J = 19.4 Hz), 24.22 (d, J = 17.4 Hz), 23.60 (dt, J = 26.0, 3.0 Hz). ¹⁹F NMR (470 MHz, cdcl₃) δ -193.21 (tt, J = 74.7, 26.5 Hz). ³¹P NMR (81 MHz, CDCl₃) δ 9.35 (d, J = 74.7 Hz). MS (ESI): calcd 487.15, found 510.0 [M+Na]⁺

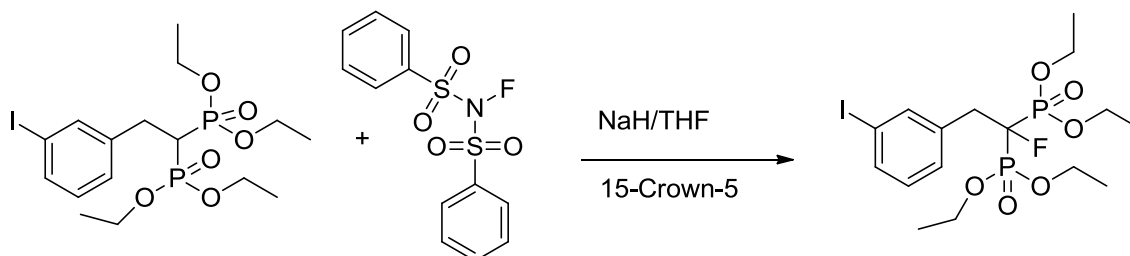
JDS-02-43: tetraisopropyl (2-(5-bromopyridin-2-yl)-1-fluoroethane-1,1-diyl)bis(phosphonate)



Isolated 483 mg (38 %) of a brown oil. ¹H NMR (300 MHz, CDCl₃) δ 8.59 (d, J = 2.3 Hz, 1H), 7.70 (dd, J = 8.4, 2.4 Hz, 1H), 7.30 (d, J = 8.4 Hz, 1H), 4.82 (m, 4H), 3.72 – 3.46 (m, 2H), 1.43 – 1.17 (m, 24H). ¹³C NMR (126 MHz, CDCl₃) δ 154.08 (t, J = 9.6 Hz), 149.62, 138.03, 127.17 (d, J = 2.6 Hz), 119.08, 94.45 (dt, J = 192.7, 158.1 Hz), 73.47 – 71.99 (m), 40.56 (d, J = 18.4 Hz), 24.23 (d, J = 28.9 Hz), 23.65 (dt, J = 30.5, 2.9 Hz). ¹⁹F NMR (470

MHz, CDCl₃) δ -193.81 (tt, J = 76.0, 27.1 Hz). ³¹P NMR (81 MHz, CDCl₃) δ 9.44 (d, J = 75.9 Hz). MS (ESI): calcd 554.08, found 554.4 [M+Na]⁺

JP-01-50: tetraethyl (1-fluoro-2-(3-iodophenyl)ethane-1,1-diyl)bis(phosphonate)



Isolated 431mg (59%) of product as a clear oil. ¹H NMR (400 MHz, CDCl₃) δ 7.70 (s, 1H), 7.57 (t, J = 16.5 Hz, 1H), 7.30 (d, J = 7.6 Hz, 1H), 7.02 (t, J = 7.8 Hz, 1H), 4.31 – 4.05 (m, 8H), 3.54 – 3.33 (m, 2H), 1.27 (dd, J = 15.4, 7.2 Hz, 12H). ¹³C NMR (75 MHz, CDCl₃) δ 139.94 (d, J = 1.4 Hz), 136.56 (t, J = 8.5 Hz), 135.98, 130.50 (d, J = 1.2 Hz), 129.47, 95.40 (dt, J = 193.7, 155.5 Hz), 93.47, 63.97 (d, J = 31.8 Hz), 37.98 (d, J = 19.0 Hz), 16.32 (t, J = 2.9 Hz). ³¹P NMR (81 MHz, CDCl₃) δ 10.50 (d, J = 72.6 Hz). MS (ESI): calcd 545.01, found 545.01 [M+Na]⁺

Synthesis of 2.13, general procedures for Suzuki cross-couplings:

Method A:

A 5 mL vial was charged with the aryl halide (1 equiv), Pd(PPh₃)₄ or Pd(P[*t*-Bu]₃)₂ (0.1 to 0.2 equiv), a stir bar and the boron-coupling partner (1.2 equivalents) if a solid. The vial was capped with a rubber septum, evacuated and back-filled with Argon; anhydrous DME was added via syringe to bring the final concentration of aryl halide to 0.1M and the solution was flushed with Argon. At this point the boron-coupling partner, if not at solid, was added as a solution in DME. 2M Na₂CO₃ or K₂CO₃ solution (2.5 equivalents) was added and the vial was flushed again with Argon. The reaction vessel was equipped with an Argon-filled balloon and stirred at 80°C until complete consumption of starting material. The reaction mixture was cooled down, diluted with EtOAc and filtered through a plug of Celite, rinsed three times with EtOAc/MeOH 1:1. The filtrate concentrated in vacuo and purified by normal phase column chromatography on silica gel (silica gel was pre-treated

with 1% NEt₃ in hexanes/EtOAc in a 3:1 ratio) using a gradient from 100% hexanes to 100% EtOAc and then to 25% MeOH.

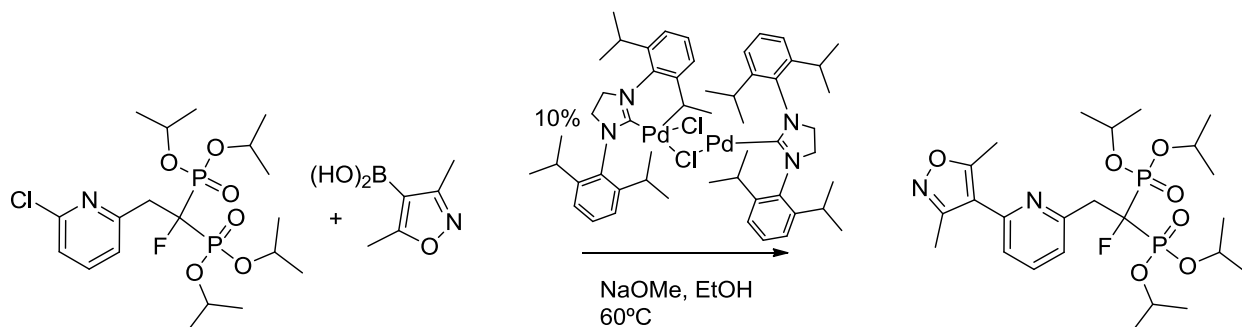
Method B:

A 2-5 mL microwave vial was charged with the aryl halide (1 equivalent), Pd(PPh₃)₄ or Pd(P[*t*-Bu]₃)₂ (0.1 to 0.2 equivalent), a stir bar and the boron-coupling partner (1.5 to 2 equivalents) if a solid. The vial was capped with a rubber septum, evacuated and back-filled with Argon; anhydrous Tol/EtOH 1:1 was added via syringe to bring the final concentration of aryl halide to 0.1M and the solution was flushed with Argon. At this point the boron-coupling partner, if not at solid, was added as a solution in EtOH. 2M Na₂CO₃ or K₂CO₃ solution (2.5 equivalents) was added and the vial was flushed again with Argon. The reaction vessel was sealed with a Teflon lined cap and irradiated to 110°C until complete consumption of starting material. The reaction mixture was cooled down, diluted with EtOAc and filtered through a plug of Celite, rinsed three times with EtOAc/MeOH 1:1. The filtrate concentrated in vacuo and purified by normal phase column chromatography on silica gel (silica gel was pre-treated with 1% NEt₃ in hexanes/EtOAc in a 3:1 ratio) using a gradient from 100% hexanes to 100% EtOAc and then to 25% MeOH.

Method C (Reference: S. J. Cazin, Chem. Comm, **2008**, 3190):

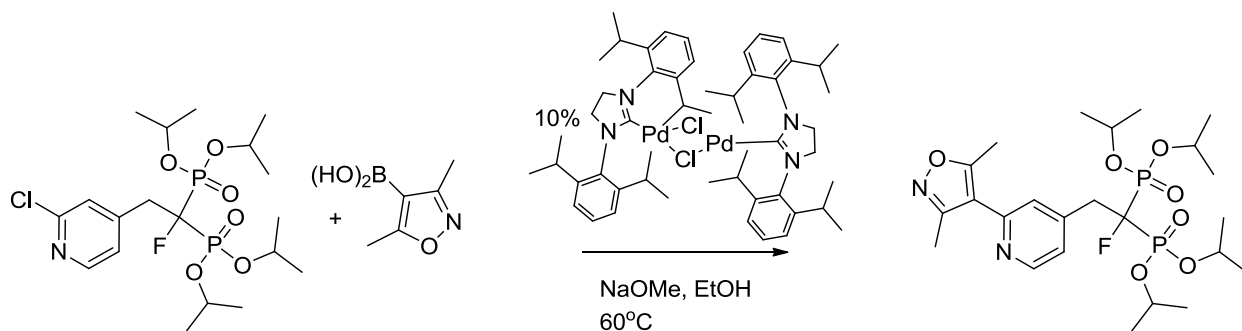
A 5 mL vial was charged [Pd(μ-Cl)Cl(IPr)]₂ (Dichloro(di-μ-chloro)bis[1,3-bis(2,6-di-*i*-propylphenyl)imidazol-2-ylidene]dipalladium(II), CAS#444910-17-2) (0.1 equivalent), a stir bar, sodium methoxide (1.5 equivalents) and the boron-coupling partner (1.2 equivalents). The vial was capped with a rubber septum, evacuated and back-filled with Argon; The aryl halide was added as a solution in anhydrous EtOH via syringe to bring the final concentration of aryl halide to 0.1M and the solution was flushed with Argon.. The reaction vessel was equipped with an Argon-filled balloon and stirred at 60°C until complete consumption of starting material. The reaction mixture was cooled down, diluted with EtOAc and filtered through a plug of Celite, rinsed three times with EtOAc/MeOH 1:1. The filtrate concentrated in vacuo and purified by normal phase column chromatography on silica gel (silica gel was pre-treated with 1% NEt₃ in hexanes/EtOAc in a 3:1 ratio) using a gradient from 100% hexanes to 100% EtOAc and then to 25% MeOH.

JDS02-094: tetraisopropyl (2-(6-(3,5-dimethylisoxazol-4-yl)pyridin-2-yl)-1-fluoroethane-1,1-diyl)bis(phosphonate)



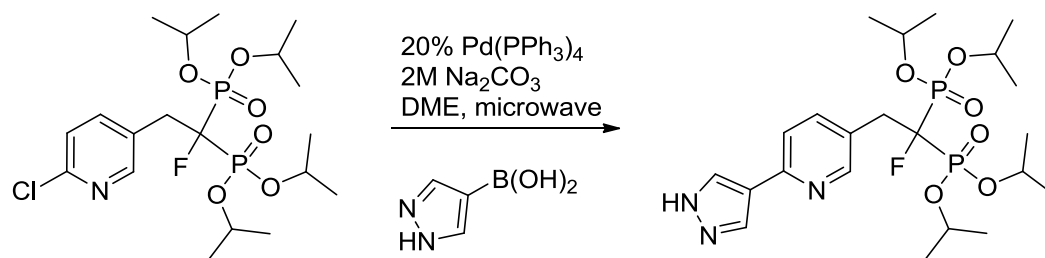
Method C; Pale orange oil (36 mg, 53%) ^1H NMR (300 MHz, CDCl_3) δ 7.64 (t, $J = 7.8$ Hz, 1H), 7.32 (d, $J = 7.8$ Hz, 1H), 7.21 (d, $J = 7.7$ Hz, 1H), 4.92 – 4.77 (m, 4H), 3.79 – 3.58 (m, 2H), 2.61 (s, 3H), 2.46 (s, 3H), 1.28 (m, 24H). MS (ESI): calcd 571.21; found 571.2 $[\text{M}+\text{Na}]^+$

JDS02-106: tetraisopropyl (2-(2-(3,5-dimethylisoxazol-4-yl)pyridin-4-yl)-1-fluoroethane-1,1-diyl)bis(phosphonate)



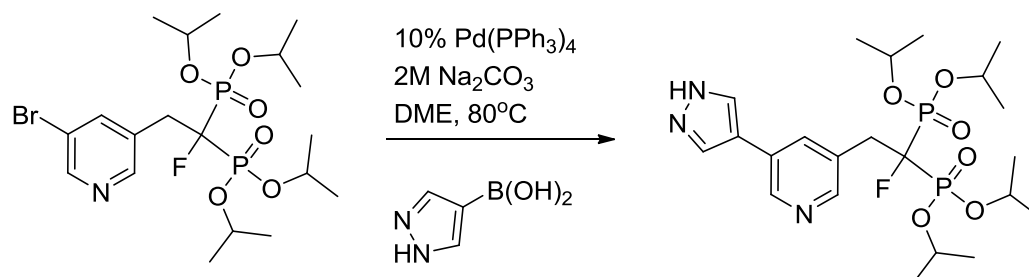
Method C; Pale orange oil (27 mg, 33%). ^1H NMR (300 MHz, CDCl_3) δ 8.56 (d, $J = 5.1$ Hz, 1H), 7.31 (s, 1H), 7.20 (d, $J = 5.1$ Hz, 1H), 4.84 (m, 4H), 3.58 – 3.36 (m, 2H), 2.57 (s, 3H), 2.43 (s, 3H), 1.37 – 1.18 (m, 24H). MS (ESI): calcd 571.21; found 571.2 $[\text{M}+\text{Na}]^+$

JDS-02-049: tetraisopropyl (2-(6-(1H-pyrazol-4-yl)pyridin-3-yl)-1-fluoroethane-1,1-diyl)bis(phosphonate)



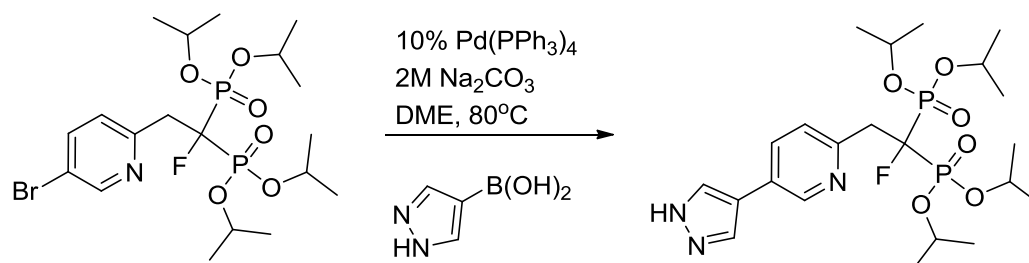
Method A; Isolated 29 mg (35%) as a yellow oil. ^1H NMR (500 MHz, CDCl_3) δ 8.48 (s, 1H), 8.09 (s, 2H), 7.65 (d, J = 8.0 Hz, 1H), 7.41 (d, J = 7.9 Hz, 1H), 4.91 – 4.71 (m, 4H), 3.44 (m, 2H), 1.43 – 1.17 (m, 24H). ^{31}P NMR (81 MHz, CDCl_3) δ 9.58 (d, J = 75.3 Hz). MS (ESI): calcd 542.20, found 542.1 $[\text{M}+\text{Na}]^+$

JDS-02-051: tetraisopropyl (2-(5-(1H-pyrazol-4-yl)pyridin-3-yl)-1-fluoroethane-1,1-diyl)bis(phosphonate)



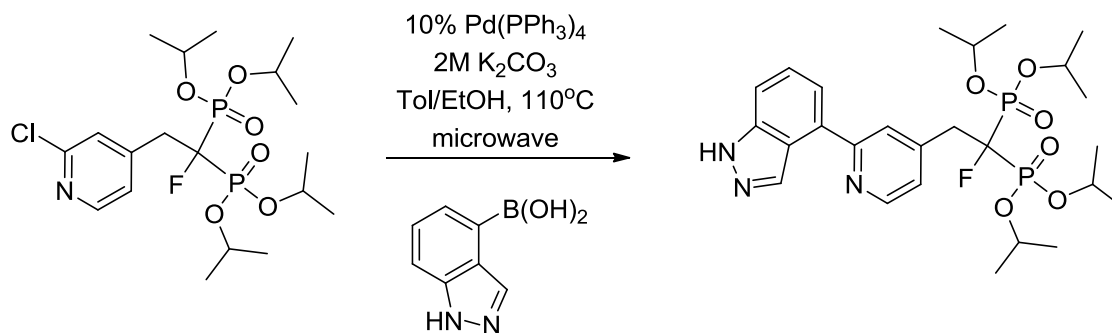
Method A; Isolated 56 mg (68%) as a brown oil. ^1H NMR (500 MHz, CDCl_3) δ 8.67 (d, J = 2.1 Hz, 1H), 8.41 (s, 1H), 7.89 (s, 2H), 7.77 (s, 1H), 4.90 – 4.74 (m, 4H), 3.56 – 3.42 (m, 2H), 1.29 (m, 24H). ^{31}P NMR (81 MHz, CDCl_3) δ 9.52 (d, J = 74.7 Hz). MS (ESI): calcd 542.20, found 520.3 $[\text{M}+\text{H}]^+$, 542.3 $[\text{M}+\text{Na}]^+$

JDS-02-052: tetraisopropyl (2-(5-(1H-pyrazol-4-yl)pyridin-2-yl)-1-fluoroethane-1,1-diyl)bis(phosphonate)



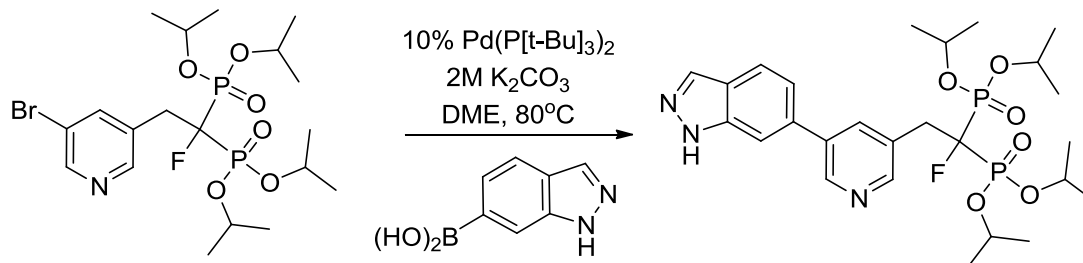
Method A; Isolated 30 mg (36%) as a brown oil. ^1H NMR (500 MHz, CDCl_3) δ 8.70 (d, J = 1.9 Hz, 1H), 7.85 (s, 2H), 7.67 (dd, J = 8.1, 2.3 Hz, 1H), 7.42 (d, J = 8.0 Hz, 1H), 4.85 (m, 4H), 3.76 – 3.61 (m, 2H), 1.38 – 1.18 (m, 24H). ^{31}P NMR (81 MHz, CDCl_3) δ 9.62 (d, J = 76.7 Hz). MS (ESI): calcd 542.20, found 542.1 $[\text{M}+\text{Na}]^+$

JDS-02-056: tetraisopropyl (2-(2-(1H-indazol-4-yl)pyridin-4-yl)-1-fluoroethane-1,1-diyl)bis(phosphonate)



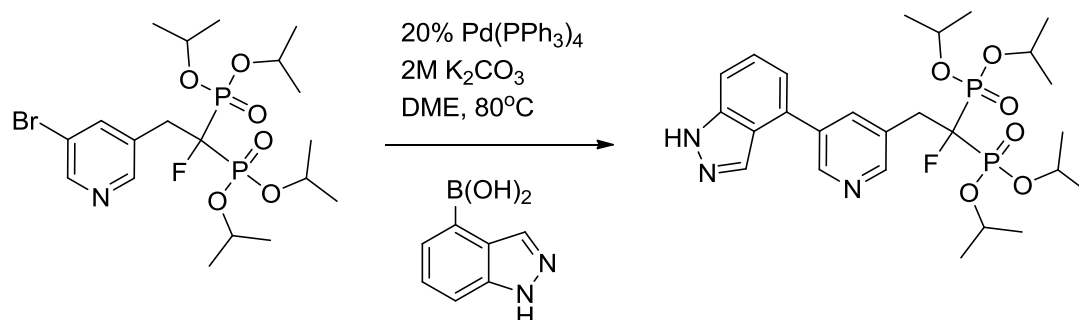
Method B; Isolated 28 mg (31%) as a yellow oil. ^1H NMR (400 MHz, CDCl_3) δ 8.70 – 8.64 (m, 2H), 7.85 (s, 1H), 7.61 (d, J = 7.1 Hz, 1H), 7.55 (d, J = 8.0 Hz, 1H), 7.51 – 7.43 (m, 1H), 7.28 (d, J = 5.0 Hz, 1H), 4.93 – 4.71 (m, 4H), 3.64 – 3.44 (m, 2H), 1.46 – 1.15 (m, 24H). ^{31}P NMR (81 MHz, CDCl_3) δ 9.30 (d, J = 73.3 Hz). MS (ESI): calcd 592.21, found 592.1 $[\text{M}+\text{Na}]^+$

JDS-02-064: tetraisopropyl (2-(5-(1H-indazol-6-yl)pyridin-3-yl)-1-fluoroethane-1,1-diyl)bis(phosphonate)



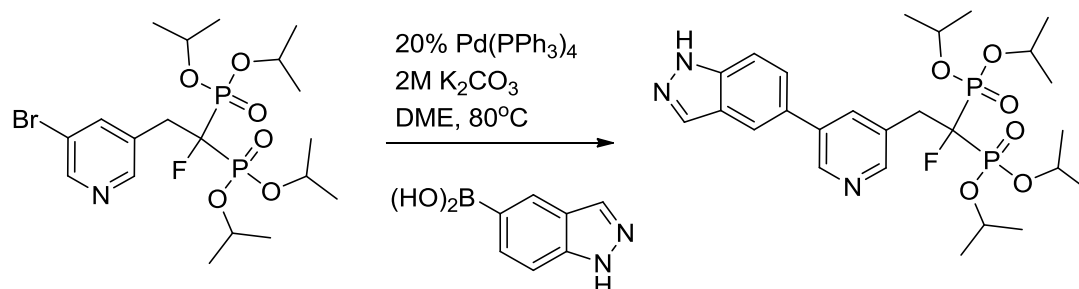
Method A; Isolated 29 mg (32%) as a brown oil. ^1H NMR (300 MHz, CDCl_3) δ 8.79 (d, J = 2.2 Hz, 1H), 8.53 (s, 1H), 8.11 (s, 1H), 7.94 (s, 1H), 7.85 (d, J = 8.0 Hz, 1H), 7.70 (s, 1H), 7.39 (d, J = 9.7 Hz, 1H), 4.91 – 4.74 (m, 4H), 3.66 – 3.43 (m, 2H), 1.46 – 1.16 (m, 24H). ^{31}P NMR (81 MHz, CDCl_3) δ 9.45 (d, J = 74.4 Hz). MS (ESI): calcd 592.21, found 592.2 $[\text{M}+\text{Na}]^+$

JDS-02-065: tetraisopropyl (2-(5-(1H-indazol-4-yl)pyridin-3-yl)-1-fluoroethane-1,1-diyl)bis(phosphonate)



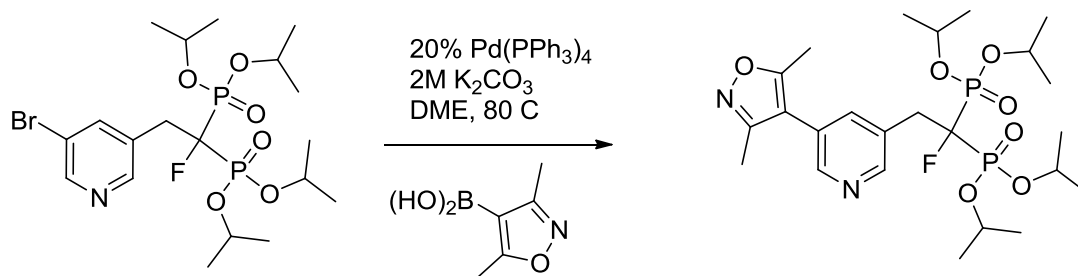
Method A; Isolated 48 mg (53%) as a brown oil. ¹H NMR (300 MHz, cdcl₃) δ 8.84 (d, *J* = 2.1 Hz, 1H), 8.58 (s, 1H), 8.32 (s, 1H), 7.58 – 7.45 (m, 2H), 7.28 (d, *J* = 1.0 Hz, 1H), 4.85 (m, 4H), 3.68 – 3.47 (m, 2H), 1.41 – 1.14 (m, 24H). ³¹P NMR (81 MHz, CDCl₃) δ 9.50 (d, *J* = 74.1 Hz). MS (ESI): calcd 592.21, found 592.1 [M+Na]⁺

JDS-02-066: tetraisopropyl (2-(5-(1H-indazol-5-yl)pyridin-3-yl)-1-fluoroethane-1,1-diyl)bis(phosphonate)



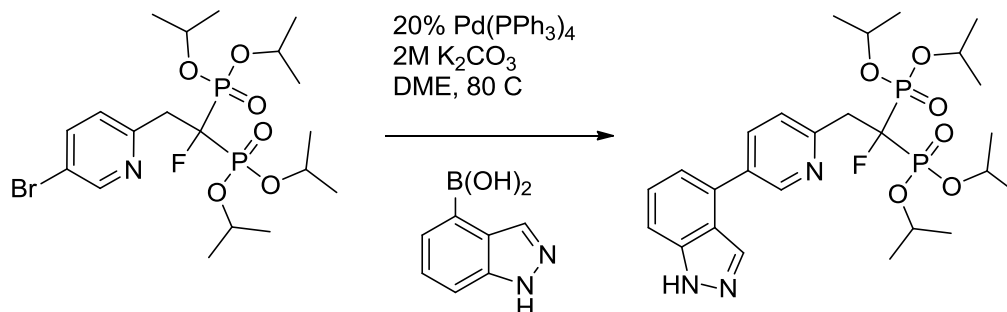
Method A; Isolated 41 mg (45%) as a brown oil. ¹H NMR (300 MHz, cdcl₃) δ 8.77 (d, *J* = 2.2 Hz, 1H), 8.50 (s, 1H), 8.15 (s, 1H), 7.95 (s, 1H), 7.92 (s, 1H), 7.61 (s, 2H), 4.84 (m, 4H), 3.69 – 3.44 (m, 2H), 1.43 – 1.13 (m, 24H). ³¹P NMR (81 MHz, CDCl₃) δ 9.54 (d, *J* = 74.8 Hz). MS (ESI): calcd 592.21, found 592.1 [M+Na]⁺

JDS-02-067: tetraisopropyl (2-(5-(3,5-dimethylisoxazol-4-yl)pyridin-3-yl)-1-fluoroethane-1,1-diyl)bis(phosphonate)



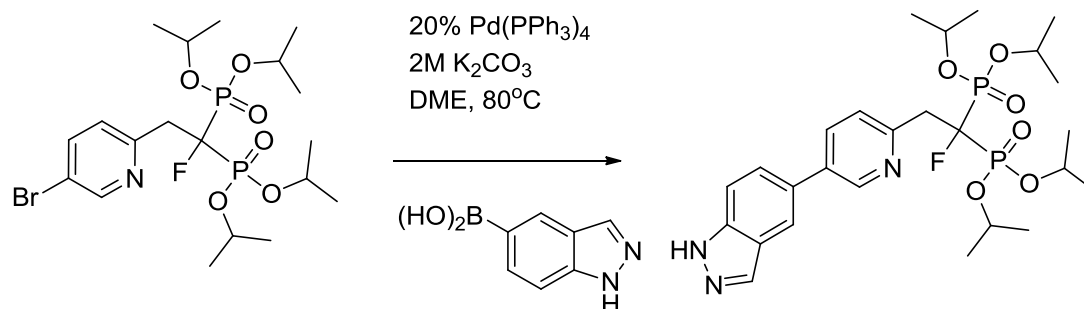
Method A; Isolated 41 mg (47%) as a brown oil. ^1H NMR (300 MHz, CDCl_3) δ 8.53 (s, 1H), 8.42 (d, $J = 2.2$ Hz, 1H), 7.57 (s, 1H), 4.95 – 4.73 (m, 4H), 3.61 – 3.35 (m, 2H), 2.44 (s, 3H), 2.30 (s, 3H), 1.42 – 1.10 (m, 24H). ^{31}P NMR (81 MHz, CDCl_3) δ 9.46 (d, $J = 74.2$ Hz). MS (ESI): calcd 571.21, found 571.1 $[\text{M}+\text{Na}]^+$

JDS-02-068: tetraisopropyl (2-(5-(1H-indazol-4-yl)pyridin-2-yl)-1-fluoroethane-1,1-diyl)bis(phosphonate)



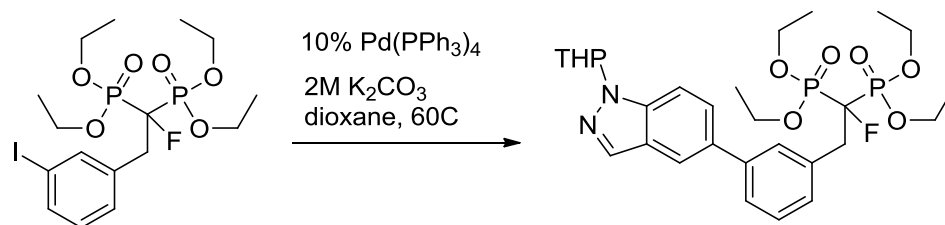
Method A; Isolated 39 mg (43%) as a brown oil. ^1H NMR (300 MHz, CDCl_3) δ 8.90 (d, $J = 2.1$ Hz, 1H), 8.17 (s, 1H), 7.91 (dd, $J = 8.1, 2.3$ Hz, 1H), 7.60 – 7.43 (m, 3H), 7.23 (d, $J = 7.0$ Hz, 1H), 4.94 – 4.78 (m, 4H), 3.86 – 3.64 (m, 2H), 1.39 – 1.22 (m, 24H). ^{31}P NMR (81 MHz, CDCl_3) δ 9.58 (d, $J = 75.7$ Hz). MS (ESI): calcd 592.21, found 592.2 $[\text{M}+\text{Na}]^+$

JDS-02-069: tetraisopropyl (2-(5-(1H-indazol-5-yl)pyridin-2-yl)-1-fluoroethane-1,1-diyl)bis(phosphonate)



Method A; Isolated 32 mg (35%) as a brown oil. ¹H NMR (300 MHz, CDCl₃) δ 8.82 (d, *J* = 2.1 Hz, 1H), 8.14 (s, 1H), 7.92 (s, 1H), 7.82 (dd, *J* = 8.1, 2.5 Hz, 1H), 7.60 (s, 2H), 7.50 (d, *J* = 8.3 Hz, 1H), 4.92 – 4.69 (m, 4H), 3.82 – 3.58 (m, 2H), 1.44 – 1.16 (m, 24H). ³¹P NMR (81 MHz, CDCl₃) δ 9.61 (d, *J* = 76.0 Hz). MS (ESI): calcd 592.21, found 592.2 [M+Na]⁺

JDS-04-141: tetraethyl (1-fluoro-2-(3-(1-(tetrahydro-2H-pyran-2-yl)-1H-indazol-5-yl)phenyl)ethane-1,1-diyl)bis(phosphonate)

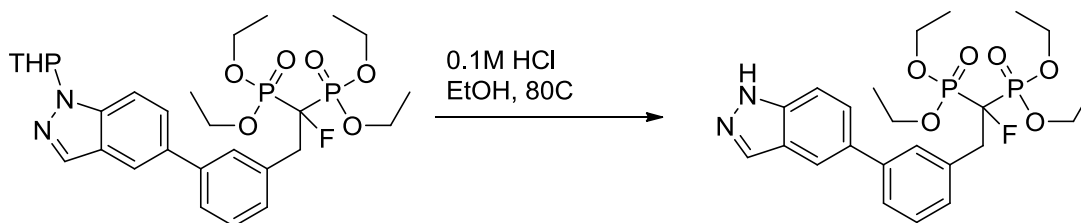


Method A; Isolated 115mg (51%) of product as a clear oil. ¹H NMR (400 MHz, CDCl₃) δ 8.07 (s, 1H), 7.90 (s, 1H), 7.67 – 7.62 (m, *J* = 4.5 Hz, 3H), 7.54 – 7.49 (m, 1H), 7.39 – 7.30 (m, *J* = 13.9, 7.0 Hz, 2H), 5.75 (dd, *J* = 9.4, 2.7 Hz, 1H), 4.29 – 4.01 (m, 8H), 3.81 – 3.73 (m, 1H), 3.69 – 3.51 (m, 2H), 2.58 (s, 1H), 2.23 – 2.06 (m, 3H), 1.84 – 1.62 (m, 3H), 1.29 – 1.20 (m, 12H). ¹³C NMR (75 MHz, CDCl₃) δ 140.79, 138.94, 134.68, 134.77 – 134.44 (m), 134.28, 130.28, 129.78, 128.23, 126.56, 125.90, 125.34, 118.97, 110.33, 95.87 (dt, *J* = 193.0, 155.3 Hz), 85.39, 67.48, 63.89 (d, *J* = 28.1 Hz), 38.56 (d, *J* = 18.9 Hz), 29.41, 25.11, 22.59, 16.28. ³¹P NMR (81 MHz, CDCl₃) δ 10.74 (d, *J* = 72.4 Hz). MS (ESI): calcd 619.21, found 619.27 [M+Na]⁺

General procedure for THP-deprotection:

To a solution of THP protected compound (1 equivalent) in anhydrous EtOH was added ethanolic HCl (1.0M, 2.5 equivalents) via syringe for a final concentration of 0.1M HCl. The reaction was stirred at 80°C for 12h. The reaction mixture was concentrated in vacuo (NaHCO₃ in receiving flask), the crude was dissolved in 100 mL EtOAc and washed with 10mL satd. NaHCO₃, water and brine. The organic layer was dried over sodium sulfate, concentrated in vacuo and purified by normal phase column chromatography on silica gel (silica gel was pre-treated with 1% NEt₃ in hexanes/EtOAc in a 3:1 ratio) using a gradient from 100% hexanes to 100% EtOAc and then to 10-50% MeOH.

JDS-04-143: tetraethyl (2-(3-(1H-indazol-5-yl)phenyl)-1-fluoroethane-1,1-diyl)bis(phosphonate)



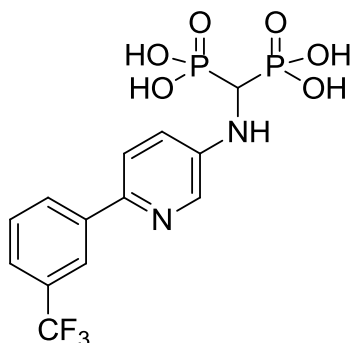
Isolated 54mg (63%), as a clear oil. ¹H NMR (400 MHz, CD₃OD) δ 8.10 (s, 1H), 8.01 – 7.96 (m, 1H), 7.73 – 7.56 (m, 4H), 7.42 – 7.36 (m, 1H), 7.31 – 7.26 (m, 1H), 4.29 – 4.01 (m, 8H), 3.55 (ddd, *J* = 35.5, 24.0, 11.3 Hz, 2H), 1.26 (td, *J* = 7.1, 4.6 Hz, 12H). ¹³C NMR (75 MHz, CD₃OD) δ 141.06, 139.63, 134.07, 134.01, 133.95, 129.90, 129.39, 128.07, 126.38, 125.75, 123.57, 118.27, 110.09, 95.60 (dt, *J* = 191.8, 157.7 Hz), 64.18 (d, *J* = 17.6 Hz), 38.19 (d, *J* = 19.0 Hz), 15.25. ³¹P NMR (81 MHz, CD₃OD) δ 12.91 (d, *J* = 74.2 Hz). MS (ESI): calcd 535.15, found 535.16 [M+Na]⁺

Synthesis of 2.5, general procedure of deprotection of tetra-ethyl bisphosphonate esters:

A 12 mL Teflon lined screw cap vial was charged with the tetra-ethyl bisphosphonate compound, dissolved in 5 mL distilled DCM and cooled in an ice bath. Bromotrimethyl silane (15 equivalents) was added via syringe and the reaction mixture was stirred at RT for 5-7 days. The reaction mixture was transferred to a 10 mL recovery flask and concentrated in vacuo (satd. NaHCO₃ in receiving flask). To the resulting oil was added 2 mL of HPLC-grade MeOH and concentrated in vacuo, this was repeated a total of five times. The crude

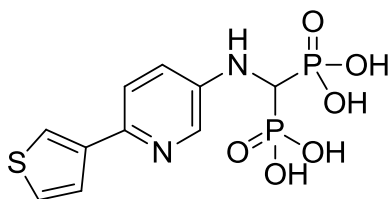
thus obtained was suspended in a minimum amount of HPLC-grade MeOH, the mixture was sonicated and the desired compound was precipitated out of solution by the addition of Milli-Q water. The slurry was filtered and the cake washed twice with Milli-Q water, twice with HPLC-grade CH₃CN and twice with distilled Et₂O. The residue was then dried under high vacuum to obtain the desired product.

Inhibitor 2.16 (JDS01-11): (((6-(3-(trifluoromethyl)phenyl)pyridin-3-yl)amino)methylene)diphosphonic acid



Isolated 20 mg of pale yellow powder (25%). ¹H NMR (500 MHz, D₂O) δ 8.03 (s, 1H), 7.99 (d, *J* = 2.6 Hz, 1H), 7.94 (d, *J* = 7.5 Hz, 1H), 7.64 – 7.53 (m, 3H), 7.14 (d, *J* = 8.6 Hz, 1H), 3.54 (t, *J* = 19.1 Hz, 1H). ¹³C NMR (126 MHz, d₂o) δ 145.22, 141.75, 139.84, 134.76, 130.36, 130.11, 129.42, 129.04, 125.31, 123.67, 123.14, 122.24, 122.20, 122.10, 119.55, 104.99 δ 53.24 (t, *J* = 128.3 Hz). ³¹P NMR (81 MHz, D₂O) δ 16.03. MS (ESI): calcd 411.01, found 411.1 [M-H][−]

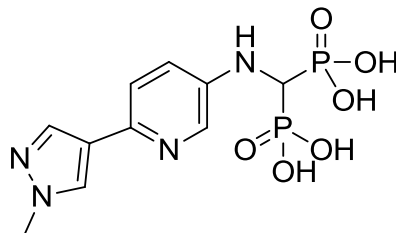
Inhibitor 2.17 (JDS01-023): (((6-(thiophen-3-yl)pyridin-3-yl)amino)methylene)diphosphonic acid



Isolated 10 mg of pale yellow powder (25%). ¹H NMR (500 MHz, D₂O) δ 7.82 (d, *J* = 2.6, 1H), 7.54 (dd, *J* = 1.4, 2.9, 1H), 7.44 (d, *J* = 8.4, 1H), 7.40 (m, 2H), 7.03 (dd, *J* = 2.9, 8.7, 1H), 3.45 (t, *J* = 19.5, 1H). ¹³C NMR (126 MHz, d₂o) δ 144.58, 141.40, 140.06, 134.23, 126.87, 125.64, 121.80, 120.07, 119.96, δ 53.10 (t, *J* = 127.3 Hz). ³¹P NMR (81 MHz,

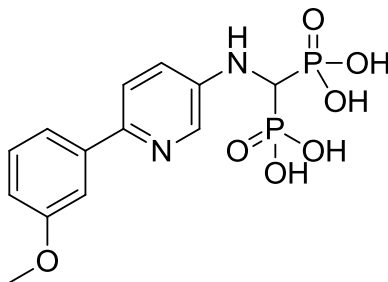
D₂O) δ 15.88. HRMS (ESI): calcd 348.98130 (C₁₀H₁₁N₂O₆P₂S), found (m/z) 348.98149 [M-H]⁻

Inhibitor 2.18 (JDS01-24): (((6-(1-methyl-1H-pyrazol-4-yl)pyridin-3-yl)amino)methylene)diphosphonic acid



Isolated 188 mg of pale yellow powder (69%). ¹H NMR (500 MHz, D₂O) δ 7.73 – 7.64 (m, 3H), 7.20 (d, J = 8.5, 1H), 6.93 (dd, J = 3.2, 8.7, 1H), 3.69 (s, 3H), 3.33 (t, J = 19.2, 1H), ¹³C NMR (75 MHz, D₂O) δ 144.23, 137.39, 136.14, 133.90, 128.46, 122.65, 120.97, 120.38, δ 53.31 (t, J = 128.3 Hz) 38.15. ³¹P NMR (81 MHz, D₂O) δ 16.28. HRMS (ESI): calcd 347.03103 (C₁₀H₁₃N₄O₆P₂), found (m/z) 347.03134 [M-H]⁻

Inhibitor 2.19 (JDS01-28): (((6-(3-methoxyphenyl)pyridin-3-yl)amino)methylene)diphosphonic acid

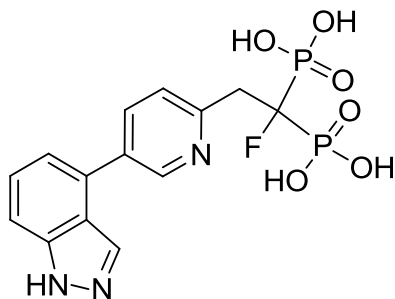


Isolated 44 mg of pale yellow powder (63%). ¹H NMR (500 MHz, D₂O) δ 7.89 (d, J = 2.9, 1H), 7.50 (d, J = 8.4, 1H), 7.32 – 7.26 (m, 3H), 7.05 (dd, J = 2.8, 9.0, 1H), 6.87 – 6.83 (m, 1H), 3.76 (s, 3H), 3.47 (t, J = 19.3, 1H). ¹³C NMR (126 MHz, d₂o) δ 167.16, 159.25, 144.99, 142.91, 140.90, 134.58, 130.16, 122.12, 119.74, 118.63, 113.29, 110.89, 55.32, δ 53.11 (t, J = 127.8 Hz). ³¹P NMR (81 MHz, D₂O) δ 15.85. HRMS (ESI): calcd 373.03545 (C₁₃H₁₅N₂O₇P₂), found (m/z) 373.03593 [M-H]⁻

Synthesis of **2.14**, general procedure for the deprotection of tetra-isopropyl bisphosponate esters:

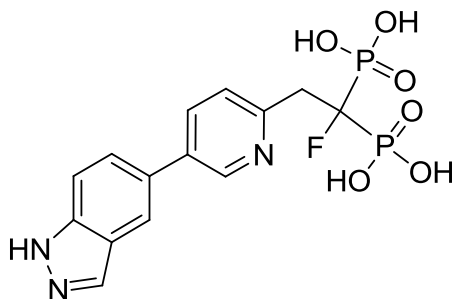
The bisphosphonate ester was transferred to a pressure vessel, dissolved in 6M HCl, the vessel was tightly sealed and the mixture was stirred at 100°C for 12 h. The reaction was cooled down, , filtered through a small cotton plug, transferred to recovery flask and concentrated to remove excess water and HCl (with satd. NaHCO₃ in receiving flask). The residue was lyophilized to dryness and weighed. The crude was suspended in 500 µL milliQ water and 1 to 3 equivalents of sodium hydroxide (1.030 M) solution was added via micropipette to dissolve the bisphosphonic acid. The solution was purified by reverse phase column chromatography on 10 cm of spherical C18 silica (45-75 µm, 70Å, Supelco) using a gradient from water to acetonitrile.

Inhibitor 2.20 (JDS-02-073): (2-(5-(1H-indazol-4-yl)pyridin-2-yl)-1-fluoroethane-1,1-diyl)diphosphonic acid, monosodium salt



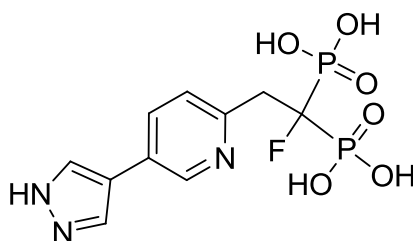
Isolated 23.7mg (64%) as a pale, yellow powder. ¹H NMR (500 MHz, D₂O) δ 8.46 (s, 1H), 8.04 (s, 1H), 7.91 (d, *J* = 7.9 Hz, 1H), 7.53 (d, *J* = 8.2 Hz, 1H), 7.46 (d, *J* = 8.6 Hz, 1H), 7.37 – 7.31 (m, 1H), 7.12 (d, *J* = 7.1 Hz, 1H), 3.58 – 3.47 (m, 2H). ¹³C NMR (75 MHz, D₂O) δ 158.21 – 157.87 (m), 145.89 (s), 143.50 (s), 135.71 (s), 132.86 (s), 132.64 (s), 130.72 (s), 126.72 (s), 126.17 (s), 120.62 (s), 119.27 (s), 111.40 (s), 41.03 (d, *J* = 18.1 Hz). {¹⁹F, ¹³C}HMQC NMR (470 MHz, D₂O) δ – 186 (¹⁹F) correlates with 100 (¹³C). ¹⁹F NMR (470 MHz, D₂O) δ -185.97 (tt, *J* = 65.7, 25.7 Hz). ³¹P NMR (81 MHz, D₂O) δ 13.70 (d, *J* = 65.7 Hz). HRMS (ESI): calcd 400.02691 (C₁₄H₁₃O₆N₃FP₂), found (*m/z*) 400.02654 [M-H][–]

Inhibitor 2.21 (JDS-02-074): (2-(5-(1H-indazol-5-yl)pyridin-2-yl)-1-fluoroethane-1,1-diyl)diphosphonic acid, monosodium salt



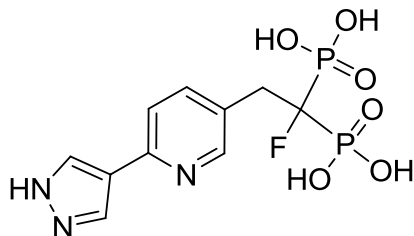
Isolated 14.4mg (47%) as a pale, yellow powder. ^1H NMR (500 MHz, D_2O) δ 8.46 (d, J = 2.4 Hz, 1H), 8.00 (s, 1H), 7.89 (s, 1H), 7.81 (dd, J = 8.2, 2.4 Hz, 1H), 7.54 (dd, J = 24.0, 9.2 Hz, 2H), 7.46 (d, J = 8.3 Hz, 1H), 3.51 – 3.39 (m, 2H). ^{13}C NMR (126 MHz, D_2O) δ 157.25 – 156.88 (m), 144.97 (s), 143.55 (s), 134.61 (s), 134.39 (s), 134.15 (s), 129.19 (s), 126.71 (s), 125.01 (s), 123.28 (s), 118.63 (s), 112.70 (s), 40.89 (d, J = 17.5 Hz). $\{^{19}\text{F}, ^{13}\text{C}\}$ HMQC NMR (470 MHz, D_2O) δ – 186 (^{19}F) correlates with 100 (^{13}C). ^{19}F NMR (470 MHz, D_2O) δ -185.96 (tt, J = 66.6, 26.2 Hz). ^{31}P NMR (81 MHz, D_2O) δ 13.69 (d, J = 65.8 Hz). HRMS (ESI): calcd 400.02691 ($\text{C}_{14}\text{H}_{13}\text{O}_6\text{N}_3\text{FP}_2$), found (m/z) 400.02683 [$\text{M}-\text{H}$] $^-$

Inhibitor 2.22 (JDS-02-077): (2-(5-(1H-pyrazol-4-yl)pyridin-2-yl)-1-fluoroethane-1,1-diyl)diphosphonic acid, monosodium salt



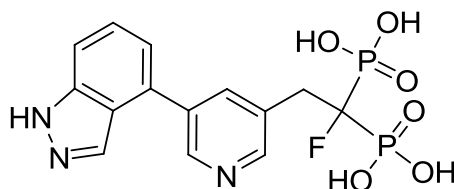
Isolated 15.1mg (53%) as a pale brown powder. ^1H NMR (500 MHz, D_2O) δ 8.36 (d, J = 1.8 Hz, 1H), 8.19 (s, 1H), 7.88 (s, 2H), 7.83 (s, 1H), 3.29 (dt, J = 23.5, 11.5 Hz, 2H). ^{13}C NMR (75 MHz, D_2O) δ 143.57 (s), 133.14 (s), 133.01 (s), 126.88 (s), 126.41 (s), 117.95 (s), 40.84 (d, J = 17.2 Hz). $\{^{19}\text{F}, ^{13}\text{C}\}$ HMQC NMR (470 MHz, D_2O) δ – 186 (^{19}F) correlates with 99 (^{13}C). ^{19}F NMR (470 MHz, D_2O) δ -185.79 – -186.24 (m). ^{31}P NMR (81 MHz, D_2O) δ 13.65 (d, J = 65.9 Hz). HRMS (ESI): calcd 350.01126 ($\text{C}_{10}\text{H}_{11}\text{O}_6\text{N}_3\text{FP}_2$), found (m/z) 350.01147 [$\text{M}-\text{H}$] $^-$

Inhibitor 2.23 (JDS-02-075): (2-(6-(1H-pyrazol-4-yl)pyridin-3-yl)-1-fluoroethane-1,1-diyl)diphosphonic acid, monosodium salt



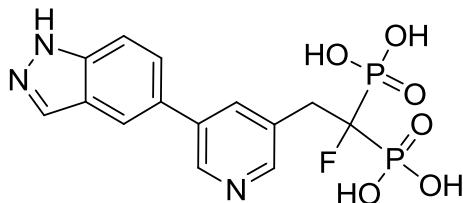
Isolated 17.8mg (65%) as a yellow powder. ^1H NMR (500 MHz, D_2O) δ 8.25 (s, 1H), 7.96 (s, 2H), 7.71 (d, $J = 7.9$ Hz, 1H), 7.42 (d, $J = 8.2$ Hz, 1H), 3.48 (s, 1H), 3.33 – 3.17 (m, 2H). ^{13}C NMR (126 MHz, D_2O) δ 168.26 (s), 150.46 (s), 149.09 (s), 141.02 (s), 135.00 (s), 120.93 (s), 119.16 (s), 36.33 (d, $J = 15.6$ Hz). $\{^{19}\text{F}, ^{13}\text{C}\}$ HMQC NMR (470 MHz, D_2O) δ – 185 (^{19}F) correlates with 99 (^{13}C). ^{19}F NMR (470 MHz, D_2O) δ -184.91 – -185.35 (m). ^{31}P NMR (81 MHz, D_2O) δ 14.08 (d, $J = 67.4$ Hz). HRMS (ESI): calcd 400.02691 ($\text{C}_{14}\text{H}_{13}\text{O}_6\text{N}_3\text{FP}_2$), found (m/z) 400.02683 $[\text{M}-\text{H}]^-$

Inhibitor 2.24 (JDS-02-070): (2-(5-(1H-indazol-4-yl)pyridin-3-yl)-1-fluoroethane-1,1-diyl)diphosphonic acid, monosodium salt



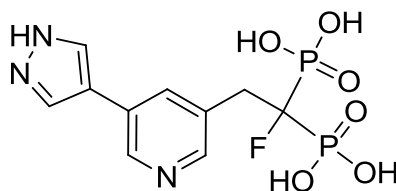
Isolated 32.2mg (71%) as a white powder. ^1H NMR (500 MHz, D_2O) δ 8.43 (s, 1H), 8.39 (s, 1H), 8.12 (s, 1H), 8.09 (s, 1H), 7.44 (d, $J = 8.6$ Hz, 1H), 7.32 (t, $J = 7.8$ Hz, 1H), 7.13 (d, $J = 6.7$ Hz, 1H), 3.47 – 3.35 (m, 2H). ^{13}C NMR (75 MHz, D_2O) δ 150.08 (s), 144.59 (s), 141.53 (s), 139.33 (s), 135.19 (m), 134.03 (s), 133.14 (s), 130.99 (s), 126.88 (s), 120.55 (s), 120.07 (s), 110.63 (s), 99.50 (dt, $J = 178.6, 136.1$ Hz), 36.61 (d, $J = 18.5$ Hz). $\{^{19}\text{F}, ^{13}\text{C}\}$ HMQC NMR (470 MHz, D_2O) δ – 185 ppm (^{19}F) correlates with 99 ppm (^{13}C). ^{19}F NMR (470 MHz, D_2O) δ -184.92 – -185.37 (m). ^{31}P NMR (81 MHz, D_2O) δ 12.47 (d, $J = 66.9$ Hz). HRMS (ESI): calcd 400.02691 ($\text{C}_{14}\text{H}_{13}\text{O}_6\text{N}_3\text{FP}_2$), found (m/z) 400.02650 $[\text{M}-\text{H}]^-$

Inhibitor 2.25 (JDS-02-071): (2-(5-(1H-indazol-5-yl)pyridin-3-yl)-1-fluoroethane-1,1-diyl)diphosphonic acid, monosodium salt



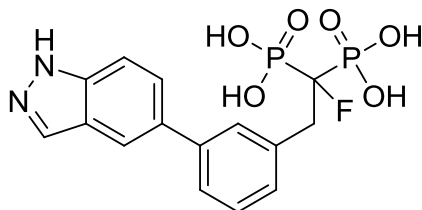
Isolated 23.4mg (60%) as a white powder. ^1H NMR (500 MHz, D_2O) δ 8.34 (s, 1H), 8.24 (s, 1H), 7.95 (s, 1H), 7.94 (s, 1H), 7.81 (s, 1H), 7.47 (dd, $J = 26.9, 8.7$ Hz, 2H), 3.41 – 3.28 (m, 2H). ^{13}C NMR (126 MHz, D_2O) δ 149.01 (s), 143.57 (s), 142.80 (s), 138.17 (s), 135.60 (s), 135.02 – 134.83 (m), 134.42 (s), 129.36 (s), 125.40 (s), 123.16 (s), 118.91 (s), 112.30 (s), 99.63 (dt, $J = 177.2, 136.0$ Hz), 36.64 (d, $J = 18.1$ Hz). $\{^{19}\text{F}, ^{13}\text{C}\}$ HMQC NMR (470 MHz, D_2O) δ – 185 (^{19}F) correlates with 99 (^{13}C). ^{19}F NMR (470 MHz, D_2O) δ -184.77 – -185.26 (m). ^{31}P NMR (81 MHz, D_2O) δ 12.86 (d, $J = 66.7$ Hz). HRMS (ESI): calcd 400.02691 ($\text{C}_{14}\text{H}_{13}\text{O}_6\text{N}_3\text{FP}_2$), found (m/z) 400.02648 [$\text{M}-\text{H}$] $^-$

Inhibitor 2.26 (JDS-02-076): (2-(5-(1H-pyrazol-4-yl)pyridin-3-yl)-1-fluoroethane-1,1-diyl)diphosphonic acid, monosodium salt



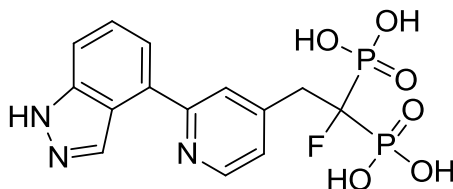
Isolated 36.3mg (69%) as a white powder. ^1H NMR (500 MHz, D_2O) δ 8.35 (d, $J = 1.7$ Hz, 1H), 8.22 (s, 1H), 7.92 (s, 2H), 7.91 (s, 1H), 3.33 (dt, $J = 23.5, 11.8$ Hz, 2H). ^{13}C NMR (126 MHz, D_2O) δ 148.64 (s), 142.23 (s), 136.58 (s), 135.22 – 135.02 (m, $J = 6.5, 3.4$ Hz), 132.24 (s), 127.50 (s), 118.30 (s), 99.56 (dt, $J = 177.8, 136.1$ Hz), 36.55 (d, $J = 18.2$ Hz). $\{^{19}\text{F}, ^{13}\text{C}\}$ HMQC NMR (470 MHz, D_2O) δ – 185 (^{19}F) correlates with 99 (^{13}C). ^{19}F NMR (470 MHz, D_2O) δ -185.11 (tt, $J = 66.6, 26.2$ Hz). ^{31}P NMR (81 MHz, D_2O) δ 14.02 (d, $J = 66.3$ Hz). HRMS (ESI): calcd 350.01126 ($\text{C}_{10}\text{H}_{11}\text{O}_6\text{N}_3\text{FP}_2$), found (m/z) 350.01134 [$\text{M}-\text{H}$] $^-$

Inhibitor 2.27 (JDS-04-145): (2-(3-(1H-indazol-5-yl)phenyl)-1-fluoroethane-1,1-diyl)diphosphonic acid



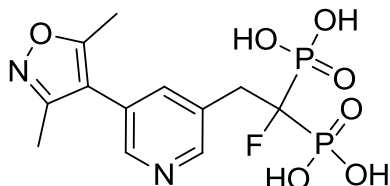
Isolated 11mg (31%) as a white powder ^1H NMR (300 MHz, D_2O) δ 8.03 (s, 1H), 7.97 (s, 1H), 7.71 – 7.58 (m, 2H), 7.55 (d, J = 8.8 Hz, 1H), 7.42 (d, J = 7.6 Hz, 1H), 7.36 – 7.21 (m, 2H), 3.50 – 3.23 (m, 2H). ^{13}C NMR (75 MHz, D_2O) δ 139.99, 139.46, 138.15, 134.62, 133.91, 129.99, 129.88, 128.39, 127.20, 124.84, 123.05, 118.85, 110.83, 104.98, 37.23 $\{^{19}\text{F}$, $^{13}\text{C}\}$ HMQC NMR (470 MHz, D_2O) δ – 185 ppm (^{19}F) correlates with 101 ppm (^{13}C). ^{19}F NMR (470 MHz, D_2O) δ -185.24 (tt, J = 66.7, 26.3 Hz). ^{31}P NMR (D_2O) δ 14.04 (d, J = 67.6 Hz). HRMS (ESI): calcd 399.0317 ($\text{C}_{15}\text{H}_{14}\text{FN}_2\text{O}_6\text{P}_2$), found (m/z) 399.0304 [M-H^-]

Inhibitor 2.28 (JDS-02-078): (2-(2-(1H-indazol-4-yl)pyridin-4-yl)-1-fluoroethane-1,1-diyl)diphosphonic acid, monosodium salt



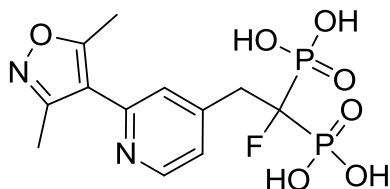
Isolated 29mg (76%) as a white powder. ^1H NMR (500 MHz, D_2O) δ 8.32 (d, J = 5.3 Hz, 1H), 8.13 (s, 1H), 7.70 (s, 1H), 7.48 (d, J = 8.3 Hz, 1H), 7.40 (d, J = 5.5 Hz, 1H), 7.36 – 7.25 (m, 2H), 3.46 – 3.31 (m, 2H). ^{13}C NMR (75 MHz, D_2O) δ 155.12 (s), 150.67 (td, J = 6.7, 3.7 Hz), 147.34 (s), 141.87 (s), 133.92 (s), 132.70 (s), 126.59 (s), 126.42 (s), 126.28 (s), 120.41 (s), 120.19 (s), 111.54 (s), 99.71 (dt, J = 179.5, 135.9 Hz), 39.08 (d, J = 18.8 Hz). $\{^{19}\text{F}$, $^{13}\text{C}\}$ HMQC NMR (470 MHz, D_2O) δ – 185 (^{19}F) correlates with 99 (^{13}C). ^{19}F NMR (470 MHz, D_2O) δ -185.08 (tt, J = 66.1, 23.9 Hz). ^{31}P NMR (81 MHz, D_2O) δ 13.92 (d, J = 66.0 Hz). HRMS (ESI): calcd 400.02691 ($\text{C}_{14}\text{H}_{13}\text{O}_6\text{N}_3\text{FP}_2$), found (m/z) 400.02672 [M-H^-]

Inhibitor 2.29 (JDS-02-072): (2-(5-(3,5-dimethylisoxazol-4-yl)pyridin-3-yl)-1-fluoroethane-1,1-diyl)diphosphonic acid, monosodium salt



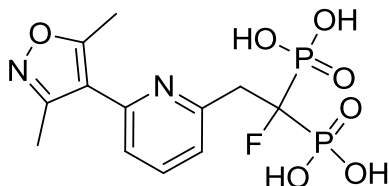
Isolated 25.5mg (74%) as a white powder. ^1H NMR (500 MHz, D_2O) δ 8.39 (s, 1H), 8.24 (d, $J = 1.9$ Hz, 1H), 7.85 (s, 1H), 3.38 (dt, $J = 16.1, 11.7$ Hz, 2H), 2.27 (s, 3H), 2.11 (s, 3H). ^{13}C NMR (75 MHz, D_2O) δ 167.30 (s), 160.15 (s), 150.12 (s), 145.34 (s), 140.45 (s), 135.21 – 134.94 (m), 125.03 (s), 113.49 (s), 36.40 (d, $J = 18.2$ Hz), 10.66 (s), 9.69 (s). $\{^{19}\text{F}, ^{13}\text{C}\}$ HMQC NMR (470 MHz, D_2O) δ – 185 (^{19}F) correlates with 99 (^{13}C). ^{19}F NMR (470 MHz, D_2O) δ -184.88 – -185.55 (m). ^{31}P NMR (81 MHz, D_2O) δ 14.02 (d, $J = 66.3$ Hz). HRMS (ESI): calcd 379.02658 ($\text{C}_{14}\text{H}_{13}\text{O}_6\text{N}_3\text{FP}_2$), found (m/z) 379.02674 $[\text{M}-\text{H}]^-$

Inhibitor 2.30 (JDS02-108) : (2-(2-(3,5-dimethylisoxazol-4-yl)pyridin-4-yl)-1-fluoroethane-1,1-diyl)diphosphonic acid, monosodium salt



Isolated 20.3mg (90%) as a white powder. ^1H NMR (500 MHz, D_2O) δ 8.46 (d, $J = 4.7$ Hz, 1H), 7.53 (s, 1H), 7.50 (d, $J = 4.5$ Hz, 1H), 3.58 – 3.42 (m, 3H), 2.48 (s, 3H), 2.32 (s, 3H). ^{13}C NMR (126 MHz, D_2O) δ 168.53, 160.11, 148.91, 147.88, 147.81, 127.49, 125.72, 115.81, δ 37.03 (d, $J = 18.0$ Hz), 10.93, 9.79. ^{19}F NMR (470 MHz, D_2O) δ -182.13 – -182.51 (m). $\{^{19}\text{F}, ^{13}\text{C}\}$ HMQC NMR (470 MHz, D_2O) δ – 182 ppm (^{19}F) correlates with 96 ppm (^{13}C). ^{31}P NMR (81 MHz, D_2O) δ 14.82 (d, $J = 66.0$ Hz). HRMS (ESI): calcd 379.02603 ($\text{C}_{12}\text{H}_{14}\text{FN}_2\text{O}_7\text{P}_2$), found (m/z) 379.02648 $[\text{M}-\text{H}]^-$

Inhibitor 2.31 (JDS02-107): (2-(6-(3,5-dimethylisoxazol-4-yl)pyridin-2-yl)-1-fluoroethane-1,1-diyl)diphosphonic acid, monosodium salt



Isolated 25 mg (83%) as a white powder. ^1H NMR (500 MHz, D_2O) δ 7.83 (t, $J = 7.8$ Hz, 1H), 7.62 (d, $J = 7.8$ Hz, 1H), 7.33 (d, $J = 7.6$ Hz, 1H), 3.72 – 3.58 (m, 2H), 2.48 (s, 3H), 2.32 (s, 3H). ^{13}C NMR (126 MHz, D_2O) δ 169.48, 159.79, 155.12, 145.93, 140.80, 126.14, 124.07, 113.68, δ 37.98 (d, $J = 21.4$ Hz), 10.98, 9.68. ^{19}F NMR (470 MHz, D_2O) δ -182.58 – -183.03 (m). $\{^{19}\text{F}, ^{13}\text{C}\}$ HMQC NMR (470 MHz, D_2O) δ – 183 ppm (^{19}F) correlates with 95 ppm (^{13}C). ^{31}P NMR (81 MHz, D_2O) δ 12.80 (d, $J = 65.9$ Hz). HRMS (ESI): calcd 379.02603 ($\text{C}_{12}\text{H}_{14}\text{FN}_2\text{O}_7\text{P}_2$), found (m/z) 379.02745 [$\text{M}-\text{H}$] $^-$

2.11.3 hFPPS enzymatic inhibition assay

Expression and purification of recombinant hFPPS:

A plasmid encoding N-terminally His₆-tagged human FPPS was transformed into *E. coli* BL21(DE3) cells. The cells were induced overnight for hFPPS expression in the presence of 1mM IPTG at 18°C and lysed in a buffer containing 50 mM HEPES (pH 7.5), 500 mM NaCl, 10 mM β-mercaptoethanol, 5 mM imidazole, and 5% (v/v) glycerol. The lysate was cleared by centrifugation and passed through a Ni-NTA agarose column. Elution was carried out in an increasing imidazole gradient. The hFPPS containing fractions were pooled and applied to a Superdex 200 column, and the protein was eluted in high purity in a buffer containing 10 mM HEPES (pH 7.5), 500 mM NaCl, 10 mM β-mercaptoethanol, and 5% glycerol. The protein sample was concentrated to 12.5 mg/ml with a spin column concentrator.

In vitro Inhibition Assay for hFPPS:

All assays were run in triplicate using 40 ng of the human recombinant FPPS and 10 μM of each substrates, GPP and IPP (³H-IPP, 3.33 mCi/ mmol) in a final volume of 100 μL buffer containing 50 mM Tris pH 7.7, 2 mM MgCl₂, 0.5 mM TCEP, and 20 μg/mL BSA. Assays were run with a 5 min pre-incubation period: the enzyme, inhibitor and GPP substrate were incubated in the assay buffer in a volume of 90 μL at 37 °C for 10 min. After 10 min, the ³H-IPP substrate was added to start the reaction and also bring the inhibitor and substrates to the desired final concentrations. After addition of all substrates, all assays were incubated at 37°C for 10 min. Assays were terminated by the addition of 200 μL of HCl/methanol (1:4) and incubated for 10 min at 37°C. The assay mixture was then extracted with 700 μL of ligroin (dried through a magnesium sulfate plug) and 300 μL of the ligroin phase was combined with 8 mL of scintillation cocktail. The radioactivity was then counted using a Beckman Coulter LS6500 liquid scintillation counter.

Reagents for Enzymatic assay: Ligroin was purchased from Sigma Aldrich, liquid scintillation cocktail was purchased from MP Biomedicals: Ecolite (#882475), ³H-IPP was purchased from American Radiolabeled Chemicals (ART 0377A: 1mCi/mL, 60Ci/mmol in

0.1M Tris pH7.5), unlabeled IPP and GPP were purchased from Isoprenoids, Lc. as their ammonium salts.

hFPPS solution: The hFPPS enzyme was stored at -80°C as a 2 µg/µL solution in the eluent buffer (50 mM HEPES pH 7.5, 500 mM NaCl, 250 mM imidazole, 5% glycerol, 0.5 mM TCEP).

IPP-solution: ³H-IPP was diluted with IPP to a specific activity of 33 mCi/ mmol and 100µM concentration in 10mM Tris pH 7.7. It was stored at -10°C, warmed to 0°C and kept on ice during assay setup.

GPP-solution: GPP was dissolved and diluted to a 100µM concentration in 10mM Tris pH 7.7. It was stored at -10°C, warmed to 0°C and kept on ice during assay setup.

2.11.4 ^1H NMR line broadening experiments

Spectra were acquired on a 500 MHz Varian INOVA instrument, with a HCN cold probe and z-axis pulsed-field gradients, at the Quebec/Eastern Canada High Field NMR Facility.

Reagents: IPP was purchased from Isoprenoids, Lc. as its ammonium salt. A 40 mM solution was prepared in 0.5 mM Tris buffer at pH 7.7. Risedronate was purchased from Toronto Research Chemicals Inc. as its sodium salt; a 60 mM solution was prepared.

Protein Preparation: hFPPS in buffer (50 mM HEPES pH 7.5, 500 mM NaCl, 250 mM imidazole, 5% glycerol, 0.5 mM TCEP) was concentrated using a centrifugal filter unit (Amicon Ultra-4, 3kDa, cat# UFC800324) as per the manufacturer's directions (4,000 x g), replenishing every 15 min with buffer containing 50 mM Tris pH 7.7, 500 mM NaCl, 5% glycerol and 0.5 mM TCEP. After 5 extractions the hFPPS concentration was determined to be 9.31 $\mu\text{g}/\mu\text{L}$.

Buffer solution: was prepared containing 500 mM Tris pH 7.7, 20 mM MgCl_2 , 5 mM TCEP, and 200 $\mu\text{g}/\text{mL}$ BSA.

NMR Experiment: ^1H -NMR spectra were acquired with a 1D presaturation sequence, with a sweep width of 8000 Hz and an acquisition time of 1s. A low power saturation pulse was applied at the HOD frequency during the 3s relaxation delay. A 5 mm NMR-tube was charged with 540 μL D_2O and 6 μL of an inhibitor (*e.g.* compound **8**, 10 mM stock solution) and the tube was briefly mixed using a vortex. The ^1H NMR spectrum was acquired and the water-suppression parameters were determined (pre-saturation). Buffer solution (60 μL) was added to the NMR tube and briefly mixed for a final inhibitor concentration of 100 μM in buffer containing 50 mM Tris buffer at pH 7.7, 2 mM MgCl_2 , 0.5 mM TCEP, and 20 $\mu\text{g}/\text{mL}$ BSA. The ^1H NMR spectrum was acquired of the free inhibitor. Aliquots of the hFPPS-solution were added, followed by brief mixing, to bring the inhibitor to hFPPS ratio as indicated on the Figures (**Figure 2.12**, **Figure 2.13**). Finally, appropriate volumes of either IPP or risedronate solution was added (in increasing concentrations) to obtain the indicated ratios.

3 Branched hFPPS active site inhibitors

3.1 Preface

I performed all the synthesis and enzymatic work described in this chapter. The inhibitor design rationale and general decisions are based on the (incorrect) premise that inhibitors **2.25** and **2.26** bind with the heterocyclic sidechain occupying the IPP sub-pocket. As will be explained in the next and following chapters, this is not the case; i.e. our novel inhibitors occupy the allylic sub-pocket exclusively, but at the time this work was performed the correct binding mode had not yet been established.

3.2 Introduction

In Chapter 2, we described the identification of two novel inhibitors, analogs **2.25** and **2.26**, which exhibit nanomolar potency ($IC_{50} \sim 500$ nM) in inhibiting hFPPS. Although these compounds occupy a larger portion of the hFPPS active site cavity compared to risedronate, their potency for the desired target was far from our objectives ($IC_{50} < 100$ nM). Therefore, to further improve the biopharmaceutical properties of our hFPPS inhibitors we set out to develop branched derivatives of **2.25** and **2.26** that would have better shape and electrostatic complementarity to the enzyme and completely fill the active site. To achieve these goals, the size of our inhibitors would further increase and, as was touched upon in Chapter 1, this could lead to propensity to inhibit hGGPPS more so than hFPPS. Therefore we kept in mind that structural rigidity and careful size-restrictions would be crucial for this aspect of the hFPPS project. To properly assess our progress, an hGGPPS enzymatic assay protocol was set up based on literature precedence and the most selective hGGPPS inhibitor reported to date was synthesized (by Adrienne Langille) and included in every assay as an inhibitor control.^{1,2} Furthermore, our hFPPS assay was adapted to more closely resemble literature conditions and risedronate was included in every assay as an inhibitor control.³ It is worth mentioning that the inhibitors described in chapter 2 were tested for their activity against hGGPPS and no significant inhibition was observed at a concentration of 10 μ M.

3.3 Branched Inhibitor design

One of our objectives in the design of the new inhibitors was to regain the hydrogen bonding interactions between the pyridine nitrogen and Lys 200 and Thr 201 (dashed lines, **Figure 3.1a**), which are known to have a large impact on enzymatic potency (~300-fold loss of potency if removed)⁴ and assumed to have been lost in the binding of inhibitors **2.25** and **2.26** to hFPPS. In addition, we assumed that lipophilic interactions in the allylic sub-pocket, potentially through π -interactions with the capping phenyls, may be possible.³⁻⁵ Based on the binding mode predicted by our computational model (**Figure 3.1a**), analogs branching at either the bisphosphonate C α or the C-2-position of the pyridine core could provide compounds with the desired geometry.

Adding a substituent at C α would generate a quaternary carbon, a “branched bisphosphonate”, which is conformationally very rigid and based on our computational results would point the new substituent directly into the allylic pocket. This would essentially enforce the $\sim 90^\circ$ angle required between the new substituent and the pyridine core. However these branched bisphosphonates may be difficult to synthesize, as both phosphonate moieties are very bulky which may limit the reactivity at the C α due to steric hindrance (**Figure 3.1b**). In contrast, the synthesis of 2,3,5-trisubstituted pyridines is much more established in the scientific literature and standard synthetic procedures could be used to make the corresponding bisphosphonates. Due to the close proximity of the pyridine C-2-position to Lys 200 and Thr 201 (**Figure 3.1a**), it seemed very attractive to install a NH moiety directly at this position in order to form the desired hydrogen bonds. However, the $\sim 90^\circ$ angle between the pyridine core and C-2-substituent would have to be enforced through some conformational rigidity element (to be determined after the synthetic route had been established).

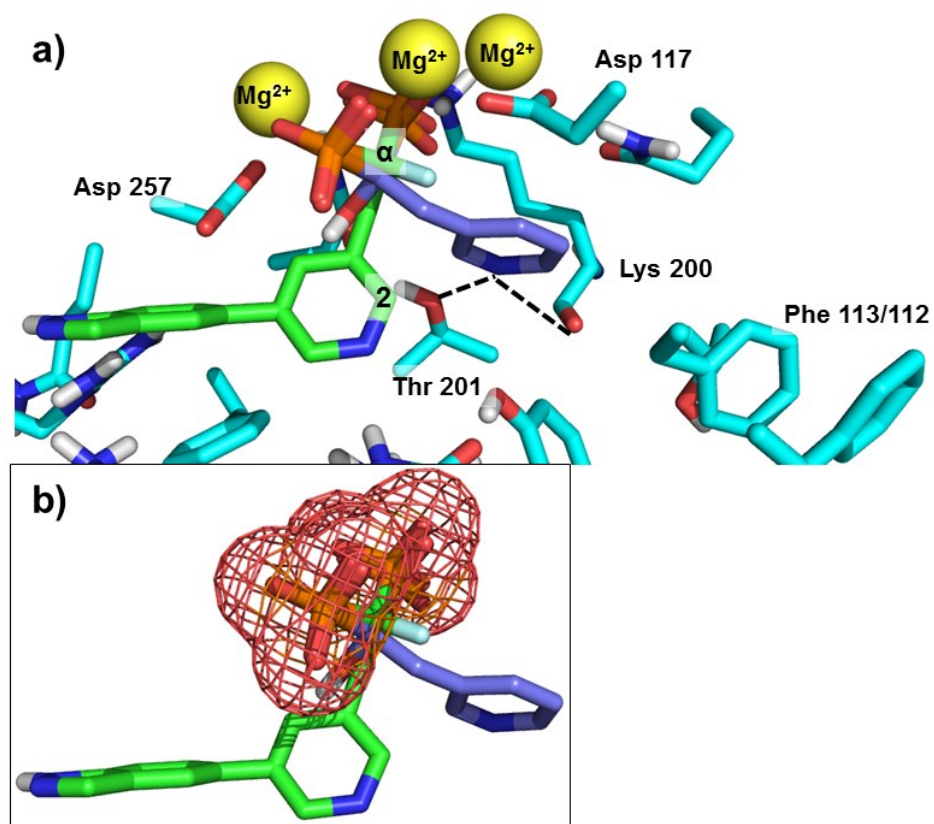
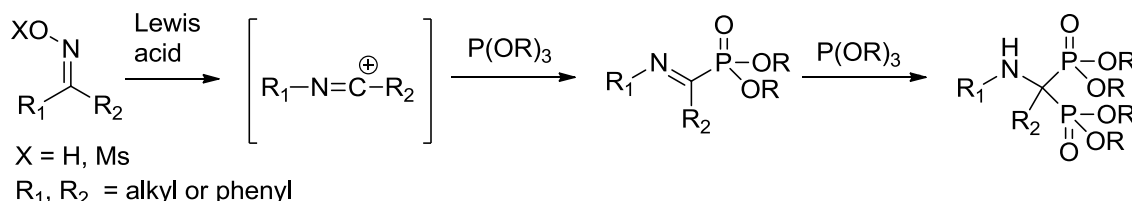


Figure 3.1: (a) Superposition of inhibitor **2.25** (green) Glide docking output pose and risedronate (blue, PDB 1YV5) in the computational model (based on PDB 1ZW5), select active site residues are shown (cyan). (b) Van der Waals radii of both phosphonate moieties shown as a mesh.

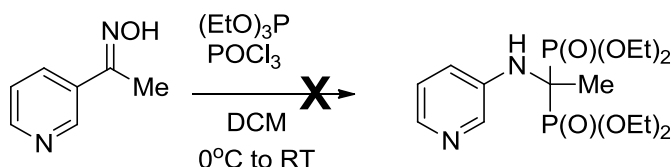
3.4 Synthesis of branched bisphosphonate inhibitors

3.4.1 Rearrangement strategy

One potential strategy utilizes disubstituted hydroxylamines as a precursor and directly converts these intermediates into a tetra-protected bisphosphonates (**Scheme 3.1**). This is an attractive option as it would postpone the incorporation of the bisphosphonate moiety towards the end of the synthesis and would allow for excellent control for installing the -R₁ and -R₂ substituents, each aimed at occupying a different sub-pocket of the hFPPS active site cavity. Shibuya and co-workers reported a concise synthetic study on the conditions for this type of reaction and found that phosphorus oxychloride worked well to initiate the Beckmann rearrangement; and both alkyl and aromatic substituents were well tolerated.⁶ Unfortunately, when these reaction conditions were attempted on a pyridine scaffold, formation of the desired product was not observed (**Scheme 3.2**). Since the heterocyclic nitrogen can coordinate with the Lewis acid and interfere with the reaction, we screened several alternatives (Et₂AlCl, BF₃-OEt₂) and also attempted the reaction with diethyl phosphite instead of triethylphosphite, without success. The pyridine ring is integral to our inhibitor design, and consequently, we shifted focus to other synthetic approaches.



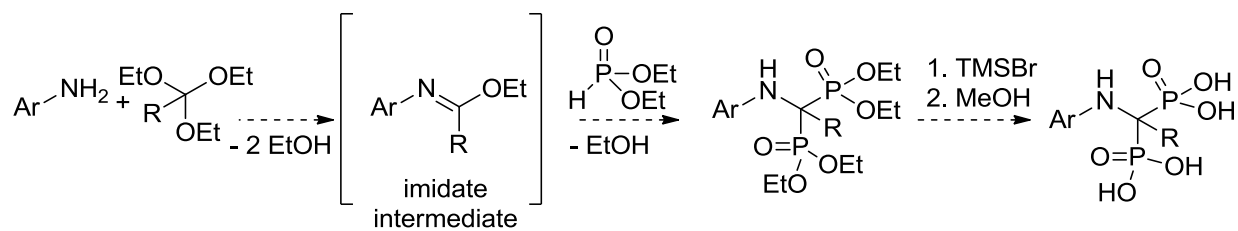
Scheme 3.1: Beckmann rearrangement of hydroxylamines



Scheme 3.2: Beckmann rearrangement attempt on pyridine scaffold

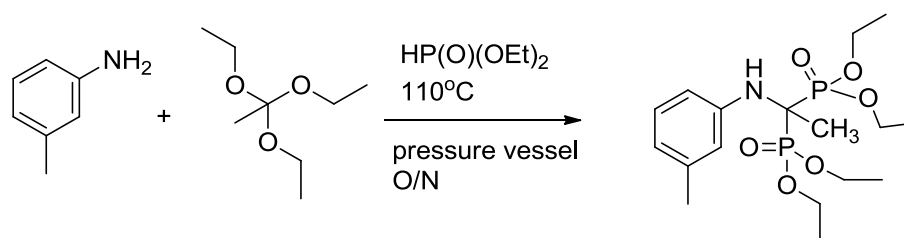
3.4.2 Condensation strategy

Starting from easily accessible anilines and ortho-esters, a condensation-deprotection sequence could allow fast access to a small library of compounds (**Scheme 3.3**).



Scheme 3.3: Condensation strategy

Although this methodology was already successfully applied (with triethyl orthoformate, R = H) in Chapter 2, in a model reaction with *m*-toluidine and triethylorthoacetate (R = CH₃) under the same conditions the desired product was isolated in only ~1% yield (**Scheme 3.4**). We assumed that the steric hindrance of the methyl group, prevented the second diethyl phosphite unit from adding to the intermediate acetimidate (R = CH₃). Since our objective was to attach even larger substituents, optimization of this reaction was undertaken (**Table 3.1**).

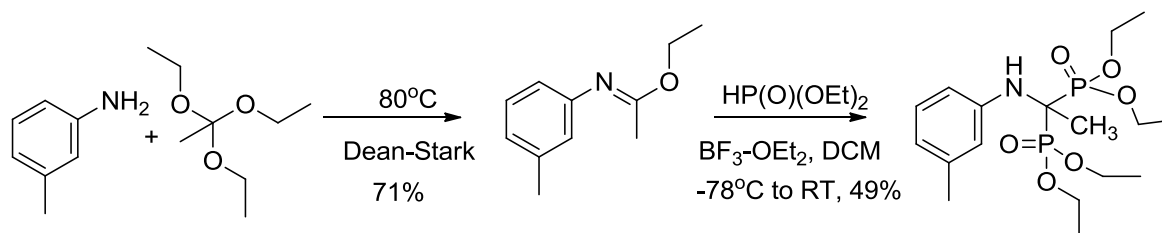


Scheme 3.4: Triethyl orthoacetate condensation test reaction

Entry	Equiv. aniline	Equiv. orthoacetate	Reaction flask	Temp.	Time	Solvent	Yield
1	1	2	Pressure vessel	110 °C	18 h	Neat	1%
2	1	2	Pressure vessel	130 °C	48 h	Neat	15%
3	1.2	6	Pressure vessel	130 °C	48 h	xylene	3%
4	1	2	Dean-Stark	80 °C	18 h	Neat	1%
5	1.1	2.2	Dean-Stark	150 °C	6 h	Neat	43%

Table 3.1: Condensation optimization conditions

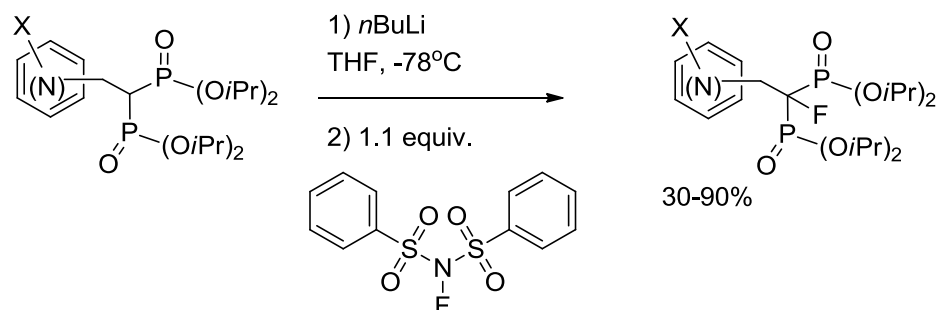
Although the yield could be improved to 43%, the high temperature required (150 °C; **Table 3.1**, entry 5) did not bode well for the substrate scope of the reaction. TLC analysis of the reaction mixture indicated that after one hour at 80 °C all starting aniline had been converted into a less polar intermediate, presumably the acetimidate. Isolation and characterization of the material confirmed it was indeed the acetimidate (**Scheme 3.5**). Addition of a Lewis acid to activate the imidate and subsequent treatment with diethylphosphite furnished the desired branched bisphosphonate in 35% yield over two steps under mild conditions. Unfortunately this methodology failed on pyridine substrates and was therefore also abandoned.



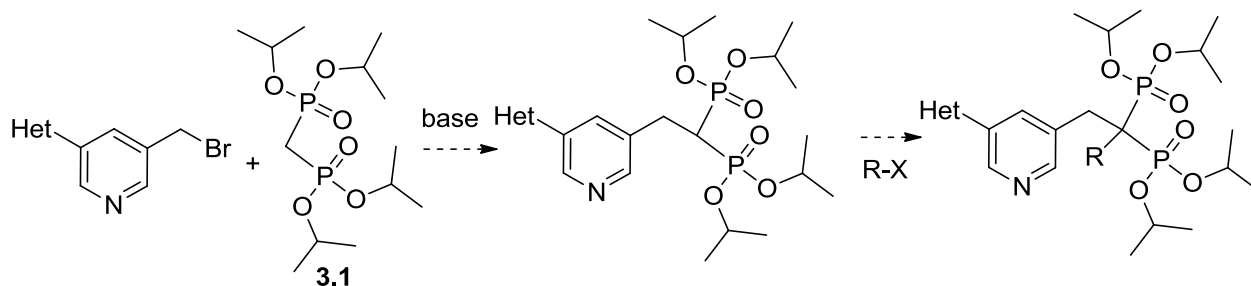
Scheme 3.5: Two step synthesis of branched bisphosphonate

3.4.3 Sequential alkylation strategy

Based on the synthetic methodology used previously to install the C α -fluorine on the inhibitors described in Chapter 2 (**Scheme 3.6**), it was envisioned that branching bisphosphonates could be made by sequential alkylation (**Scheme 3.7**).



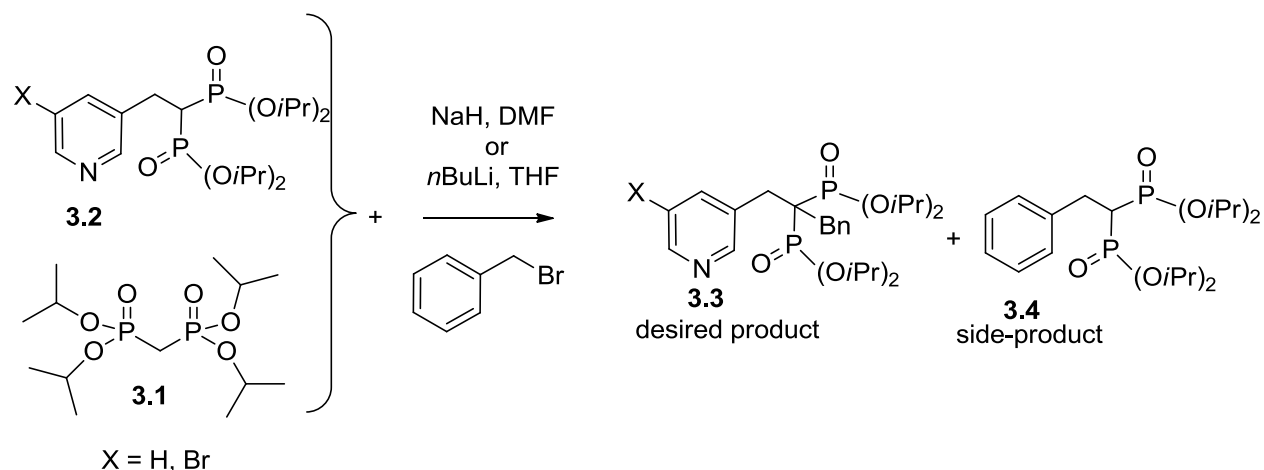
Scheme 3.6: General α -fluorination conditions



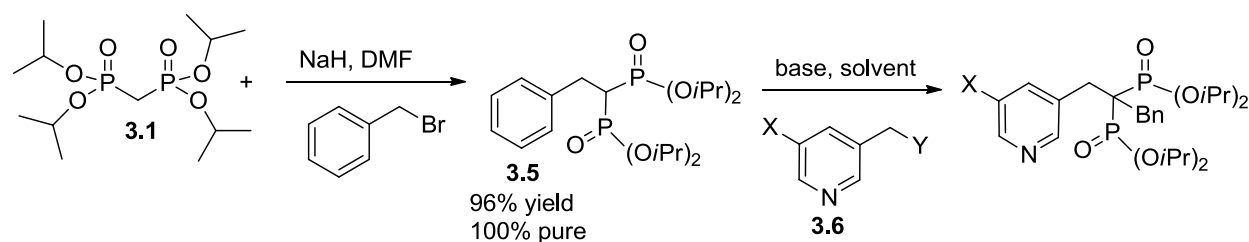
Scheme 3.7: Sequential alkylation strategy

As was mentioned in Chapter 2, the purification of the mono-substituted bisphosphonates can be troublesome and they usually contain 5-30% of the tetra-isopropyl methylenebis(phosphonate) starting material **3.1**, but this impurity could be eliminated after the fluorination. The products of the second alkylation (**Scheme 3.8**, 10-15% yield) proved just as difficult to separate as the starting materials and the bis-alkylated bisphosphonate **3.3** was contaminated with ~15% of benzyl bisphosphonate **3.4**, as determined by ^{31}P NMR. The low yield is most likely due to the larger size of benzyl bromide compared to the F^+ electrophile, but as competitive deprotonation of the tetra-isopropyl methylenebis(phosphonate) **3.1** impurity could also contribute to the low yield, several

attempts were made to obtain 100% pure starting material **3.2**, including various aqueous acidic extractions, column chromatography conditions and HCl-salt formation. Unfortunately none of them proved successful. Therefore the alkylations were performed in reverse order in order to circumvent the purification issues (**Scheme 3.9**).



Scheme 3.8: Second alkylation on pyridine-bisphosphonate precursor



Scheme 3.9: Reverse sequential alkylation

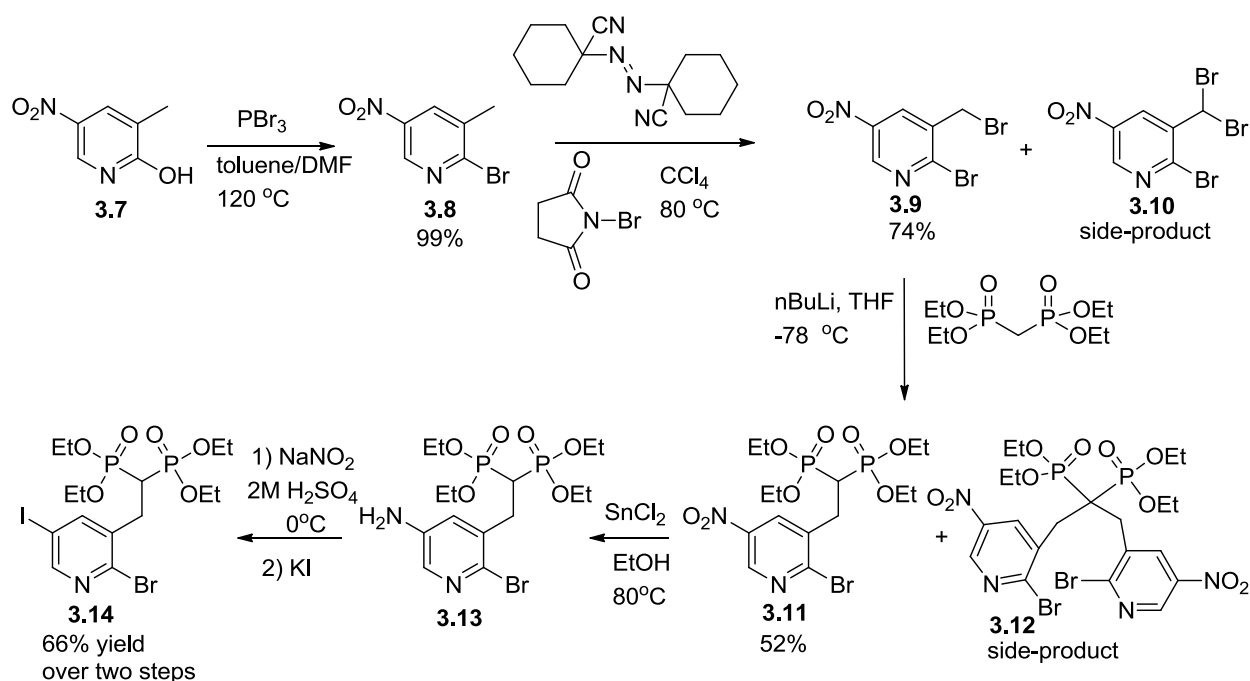
Entry	X	Y	Base	Yield
1	Br	Br	NaH, DMF	0%
2	H	Cl	NaH, DMF	0%
3	Br	Br	<i>n</i> BuLi, THF	0%

Table 3.2: Conditions for reverse sequential addition

The tetraisopropyl (benzyl)-methylenebis(phosphonate) intermediate **3.5** could be isolated in excellent yield and purity (as determined by ^{31}P NMR). Unfortunately, the second alkylation did not proceed (**Table 3.2**) and it was discovered that the pyridine benzylic bromides **3.6**, as well as the corresponding mesylates and tosylates, can be relatively unstable (most likely due to self-polymerization). At this point in time it was decided to focus on the inhibitors with a branching pyridine core (next section), as their synthesis was proceeding much better and advanced intermediates had already been obtained. The purification and stability issues mentioned in this section will be further elaborated upon in the next chapter.

3.5 Synthesis of inhibitors with a branched pyridine core and their *in vitro* activity against hFPPS

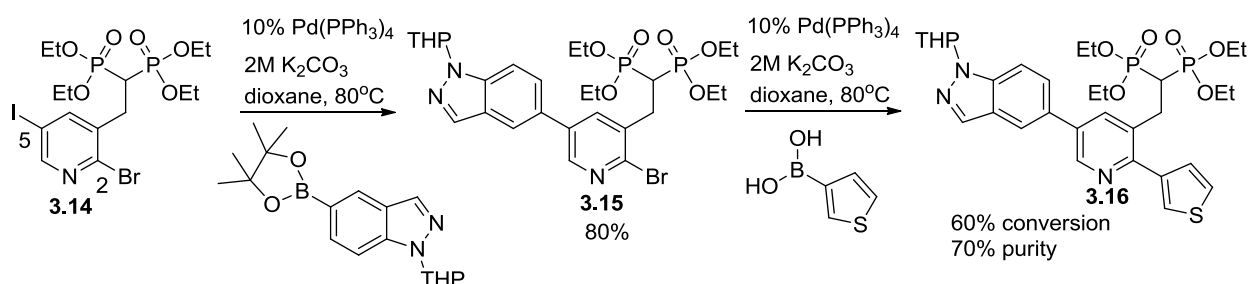
As an alternative strategy, we decided to focus on the design and synthesis of hFPPS inhibitors having a C-2 and C-5 substituted pyridine core, in addition to a bisphosphonate moiety attached at C-3. The synthesis of these compounds was initiated from intermediate 2-bromo-5-iodo-pyridine-3-bisphosphonate tetra-ester (**3.14**), which was synthesized in 6 steps from commercially available pyridinone **3.7** (Scheme 3.10).



Scheme 3.10: Synthesis of tetra-ethyl 2-bromo-5-iodo-pyridine-3-bisphosphonate ester **3.14**

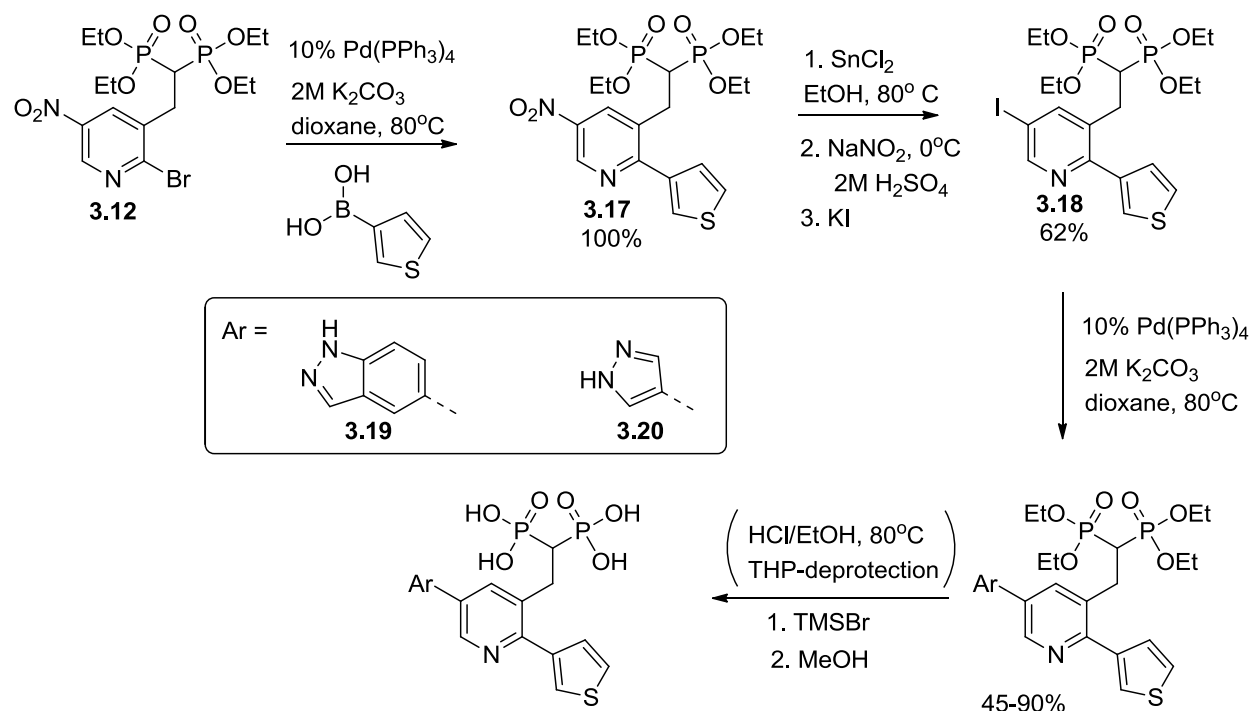
Bromination of the 2-pyridinone **3.7** proceeded with complete conversion, and the corresponding 2-bromo-pyridine **3.8** was isolated in high purity after a simple extraction with toluene. The benzylic bromide could be installed through radical bromination with *N*-bromo-succinimide (NBS) and 10 mol% of radical initiator at 80°C; although complete conversion of starting materials to products proved to be difficult even after 5 days and a small amount of di-brominated side-product **3.10** was also formed. Increasing the

temperature or amount of NBS only increased the amount of di-brominated side-product and did not improve the yield. The addition of more radical initiator over the course of the reaction had minimal effect and therefore the starting material was simply recovered and recycled (74% of isolated yield, based on recovered starting material). To our surprise, the conversion of intermediate **3.9** to the tetraethyl bisphosphonate, under previously established reaction conditions, led to the formation of ~20% dialkylated side-product **3.12**, along with the desired mono-alkylated product **3.11**. This is in sharp contrast to the disappointing results we obtained in our previous synthesis efforts towards branching bisphosphonates through sequential alkylation (section 3.4.3). We speculate that the reduced steric bulk of the tetra-ethyl bisphosphonate moiety and/or the increased acidity of the C α -H through the electron-withdrawing effect of the nitro-substituted pyridine may be the reason for this side-reaction. However, since the desired 2-bromo-5-iodo-pyridine-3-bisphosphonate tetra-ester **3.14** could be quickly acquired in two easy steps, for the purpose of this thesis, it was decided to not revisit the sequential alkylation strategy towards branching inhibitors. The aromatic nitro-group was reduced with stannous chloride and the corresponding aniline **3.13** isolated through extraction with EtOAc in sufficient purity for the following diazotization. Iodination was accomplished through treatment with sodium nitrite followed by potassium iodide to furnish the versatile tetra-ethyl 2-bromo-5-iodo-pyridine-3-bisphosphonate ester building block **3.14**. With this key intermediate in hand, we envisioned that we could install both substituents sequentially via palladium catalyzed cross-coupling reactions; as an initial test the familiar Suzuki reaction was applied (**Scheme 3.11**).



Scheme 3.11: Sequential Suzuki cross-couplings

The first Suzuki reaction proceeded in good yield, with no coupling observed at the C-2 bromide. As expected, the second cross-coupling reaction was more sluggish, leading to only ~60% conversion after 48h (as determined by HPLC analysis). However, even after purification of the reaction mixture, the desired bis-coupled product **3.16** was contaminated with ~20% starting material. This prompted us to examine the reactions in a different order (**Scheme 3.12**). Gratifyingly, the Suzuki reaction proceeded cleanly at the C-2 position of pyridine **3.12**, with quantitative yield.



Scheme 3.12: Modified reaction sequence to branched pyridine core inhibitors

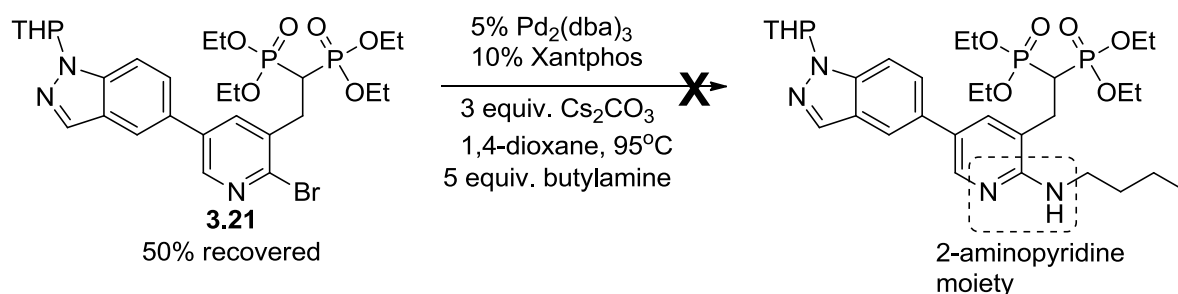
The following reduction and diazotization proceeded in similar yield as before to furnish **3.18** and the second Suzuki cross coupling at the C-5 position of the pyridine core also proceeded smoothly if the boron coupling partner was protected with a THP group (90%), unprotected pyrazole-4-boronic acid gave 45% yield (based on recovered starting material). Based on the SAR established in Chapter 2, the two best heterocyclic substituents (5-indazole and 4-pyrazole) were installed to produce reference compounds. The THP group was removed under acidic conditions and the free bisphosphonic acid was generated as

before, by transesterification with trimethylbromosilane followed by methanolysis. Thus we successfully obtained the first branching bisphosphonates following this modified reaction sequence. However, these two novel compounds (**3.19** and **3.20**) have a very planar overall structure and were not expected to fit well into the hFPPS enzyme site, in the absence of any dramatic conformational changes to the protein. Our expectations were confirmed by evaluating *in vitro* the ability of these compounds in inhibiting hFPPS (**Table 3.3**). Despite their larger size they also did not exhibit significant activity against hGGPPS.

	hFPPS		hGGPPS
concentration	1 μ M	10 μ M	10 μ M
3.19	9%	45%	36%
3.20	0%	41%	37%

Table 3.3: hFPPS and hGGPPS inhibition data for analogs **3.19** and **3.20**

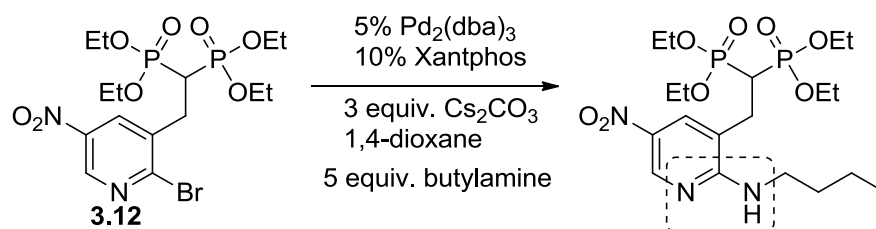
In order to break the planarity and recapture the hydrogen bonding interactions with Lys 200 and Thr 201 we set out to install a NH-moiety at the C-2-position of the pyridine core. The Buchwald-Hartwig cross-coupling did not proceed readily on **3.21**, even after 3 days at 95°C only a trace amount of product could be detected by HPLC analysis (**Scheme 3.13**).⁷ Despite the lack of product formation, or the formation of any discernible side-product, only 50% of starting material could be recovered, which suggested that the 2-amino-3-bisphosphonate-pyridine moiety may be chemically unstable.



Scheme 3.13: Unsuccessful Buchwald-Hartwig cross-coupling on **3.21**

The Buchwald-Hartwig amination was attempted on the 2-bromo-5-nitro-pyridine precursor **3.12** and similarly to the Suzuki cross-coupling, the reaction proceeded smoothly

on this scaffold (**Scheme 3.14**). It was noted that higher temperatures and increased reaction times, decreased the yield; again suggesting that the 2-amino-pyridine moiety may be a source of chemical instability and the desired product may decompose upon formation (**Table 3.4**).



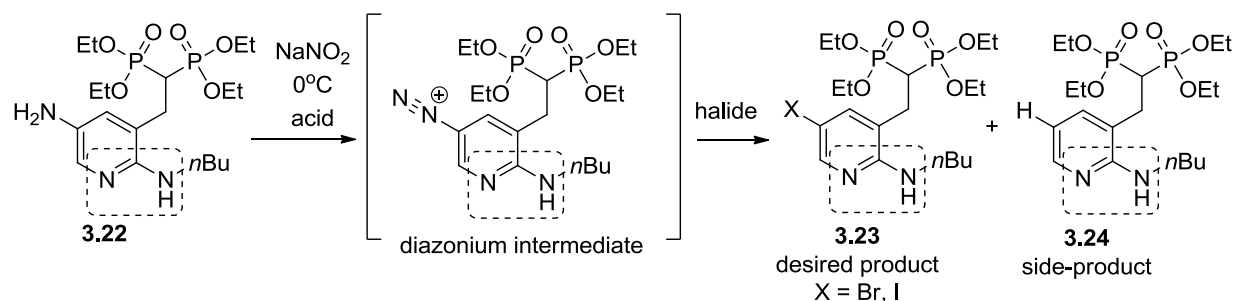
Scheme 3.14: Buchwald-Hartwig cross coupling on **3.12**

Entry	Temperature	Reaction time	Yield
1	95°C	16 h	69%
2	95°C	19 h	29%
3	80°C	8 h	71%

Table 3.4: Effect of temperature and reaction time on amination yield

Reduction of the nitro moiety to the corresponding aniline **3.22** went without any problems, however, diazotization of the 2-aminopyridine scaffold proved to be difficult (**Scheme 3.15**). The previously optimized reaction conditions (entry 1, **Table 3.5**) failed to produce the desired halide **3.23** and a significant amount of reduced side-product **3.24** was observed; various other conditions were also explored (entries 2 to 7), with no significant improvement to yield. Since the NH-moiety could be interfering with the reaction, the corresponding *N,N*-dimethyl derivative **3.25** was synthesized (**Scheme 3.16**). Unfortunately the diazotization also failed on this scaffold, ruling out the NH-moiety as the source the problem (**Table 3.6**, entry 1). Since significant amounts of the reduced side-product **3.24** were observed, aprotic reaction conditions were also explored, but were unsuccessful in improving the outcome of the reaction (entries 2 and 3).⁸ At this point, we concluded that the diazonium ion intermediate may be too unstable. Nonetheless, we were able to obtain sufficient amounts of aryl halide to continue with a Suzuki cross-coupling reaction on the

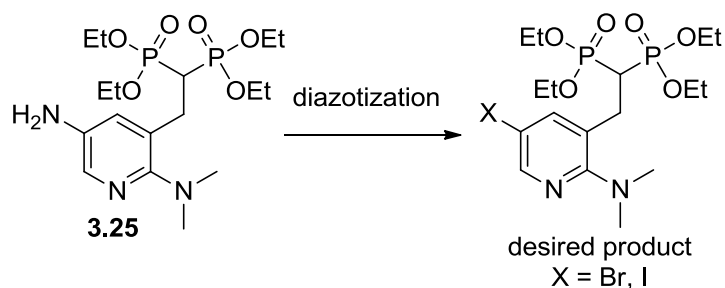
on 2-amino-*n*Bu-pyridine scaffold **3.23**. This reaction proceeded in very low yield (**Scheme 3.17**), providing additional evidence that this scaffold was chemically unstable. Finally, when the tetra-ethyl precursor was exposed to our standard deprotection conditions, decomposition was observed (i.e. black precipitate was formed and multiple signals were observed by ^{31}P NMR). All of our above observations suggest that the 2-aminopyridine moiety may be very unstable next to a bisphosphonate group.



Scheme 3.15: Diazotization on 2-amino-*n*Bu-pyridine scaffold

Entry	Equiv. NaNO ₂	Acid	Halide source	% product	% side-product
1	1.1	H ₂ SO ₄	1.5 equiv. KI	15	40
2	1.1	H ₂ SO ₄	1.5 equiv. KI	10	20
3	2.2	H ₂ SO ₄	3.0 equiv. KI	10	20
4	1.1	H ₂ SO ₄	1.5 equiv. CuBr	20	0
5	2.2	H ₂ SO ₄	3.0 equiv. CuBr	15	35
6	1.1	HBr	1.5 equiv. CuBr	15	0
7	2.2	HBr	3.0 equiv. CuBr	15	0

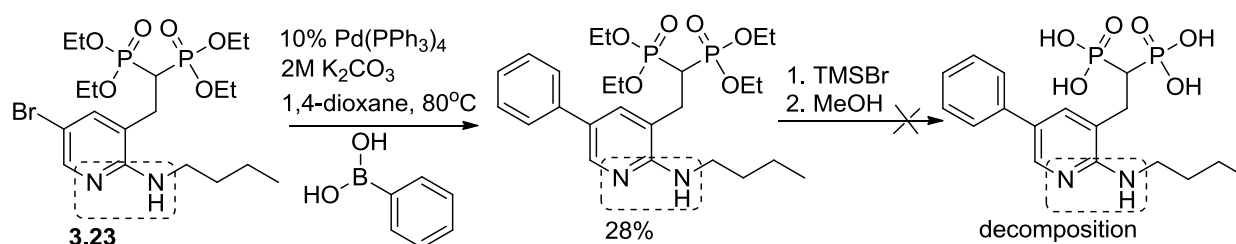
Table 3.5: Diazotization conditions attempted on 2-amino-*n*Bu-pyridine scaffold



Scheme 3.16: Diazotization on 2-*N,N*-dimethyl-pyridine **3.25**

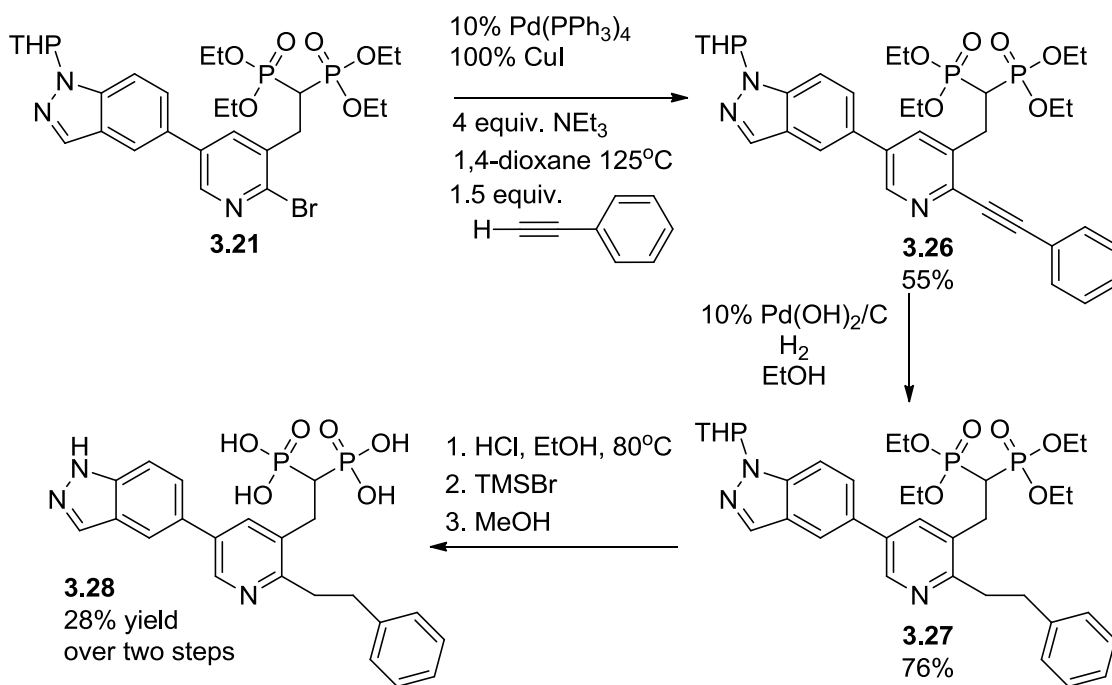
Entry	Nitrite source	Halide source	Acid	Solvent	Temp.	% product
1	1.1 equiv. NaNO ₂	1.5 equiv. CuBr	HBr	H ₂ O	0°C	0
2	1.3 equiv isoamylnitrite	1.5 equiv. CuBr	BF ₃	THF	-10°C	0
3	1.3 equiv isoamylnitrite	2.0 equiv. NaI	BF ₃	THF	-10°C	0

Table 3.6: Diazotization conditions attempted on 2-*N,N*-dimethyl-pyridine **3.25**



Scheme 3.17: Continuation of 2-amino-*n*Bu-pyridine **3.23**

Direct C-C bond formation via Sonogashira cross-coupling of the 2-bromo-pyridine scaffold **3.21** was also explored and found to afford the desired alkyne **3.26** in good yield (**Scheme 3.18**). This alkyne intermediate was easily reduced to the corresponding alkane **3.27** and fully deprotected to furnish bisphosphonic acid **3.28**. However, inhibitor **3.28** did not exhibit any promising activity against either hFPPS or hGGPPS (**Table 3.7**); this is likely due to the rotational freedom around the alkane bond, thus incurring a significant entropy penalty to adopt the required bioactive conformation.



Scheme 3.18: Sonogashira strategy

	hFPPS		hGGPPS
Concentration:	1 μ M	10 μ M	10 μ M
3.28	2%	53%	25%

Table 3.7 hFPPS and hGGPPS inhibition data for inhibitor **3.28**

During the course of these studies, we were successful in obtaining an hFPPS co-crystal structure of one of our pyridine-based inhibitors which revealed it bound exclusively into the allylic sub-pocket (refer to Chapter 4). Given the synthetic challenges of the branched bisphosphonate compounds and the new structural information, the synthetic efforts described in this chapter were suspended in order to pursue more promising directions.

3.6 Conclusions and outlook

In summary, several synthetic routes were explored in making branched, pyridine-based bisphosphonate inhibitors. The 2,5-disubstituted pyridine-3-bisphosphonate derivatives were the only analogs that could be successfully completed and the synthesis was plagued by several limitations, including the instability of the desired 2-aminopyridine scaffold and inherent lack of appropriate conformational rigidity element at the C-2-position. The few model compounds that were synthesized exhibited very weak activity in inhibiting either hFPPS or hGGPPS. Currently another member of the Tsantrizos research group is pursuing the synthesis of a modified branched/spiral scaffold, along the same inhibitor-design principals, that already shows promising activity.

3.7 References

- (1) Wiemer, A. J.; Yu, J. S.; Lamb, K. M.; Hohl, R. J.; Wiemer, D. F.; Mono- and dialkyl isoprenoid bisphosphonates as geranylgeranyl diphosphate synthase inhibitors *Bioorg. Med. Chem.* **2008**, *16*, 390.
- (2) Kavanagh, K. L.; Dunford, J. E.; Bunkoczi, G.; Russell, R. G. G.; Oppermann, U.; The Crystal Structure of Human Geranylgeranyl Pyrophosphate Synthase Reveals a Novel Hexameric Arrangement and Inhibitory Product Binding *J. Bio. Chem.* **2006**, *281*, 22004.
- (3) Dunford, J. E.; Kwaasi, A. A.; Rogers, M. J.; Barnett, B. L.; Ebetino, F. H.; Russell, R. G. G.; Oppermann, U.; Kavanagh, K. L.; Structure–Activity Relationships Among the Nitrogen Containing Bisphosphonates in Clinical Use and Other Analogues: Time-Dependent Inhibition of Human Farnesyl Pyrophosphate Synthase *J. Med. Chem.* **2008**, *51*, 2187.
- (4) Dunford, J. E.; Thompson, K.; Coxon, F. P.; Luckman, S. P.; Hahn, F. M.; Poulter, C. D.; Ebetino, F. H.; Rogers, M. J.; Structure-Activity Relationships for Inhibition of Farnesyl Diphosphate Synthase in Vitro and Inhibition of Bone Resorption in Vivo by Nitrogen-Containing Bisphosphonates *J. Pharmacol. Exper. Ther.* **2001**, *296*, 235.
- (5) Kavanagh, K. L.; Guo, K.; Dunford, J. E.; Wu, X.; Knapp, S.; Ebetino, F. H.; Rogers, M. J.; Russell, R. G. G.; Oppermann, U.; The molecular mechanism of nitrogen-containing bisphosphonates as antiosteoporosis drugs *Proc. Natl. Acad. Sci. U.S.A.* **2006**, *103*, 7829.
- (6) Yokomatsu, T.; Yoshida, Y.; Nakabayashi, N.; Shibuya, S.; Simple and Efficient Method for Preparation of Conformationally Constrained Aminomethylene gem-Diphosphonate Derivatives via Beckmann Rearrangement *J. Org. Chem.* **1994**, *59*, 7562.
- (7) Li, J. J.; Wang, Z.; Mitchell, L. H.; A Practical Buchwald–Hartwig Amination of 2-Bromopyridines with Volatile Amines *J. Org. Chem.* **2007**, *72*, 3606.
- (8) Manka, J. T.; Guo, F.; Huang, J.; Yin, H.; Farrar, J. M.; Sienkowska, M.; Benin, V.; Kaszynski, P.; Synthesis of Polyfunctionalized Biphenyls as Intermediates for a New Class of Liquid Crystals *J. Org. Chem.* **2003**, *68*, 9574.

3.8 Experimental

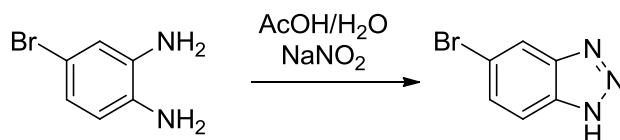
3.8.1 Synthesis

General. All intermediate compounds were purified by normal phase flash column chromatography on silica gel using a CombiFlash instrument and the solvent gradient indicated. Library analogs were also purified at the bisphosphonate tetra ester stage by normal-phase chromatography on silica gel (using a CombiFlash instrument). The purified tetra esters were fully characterized by ^1H , ^{13}C and ^{31}P NMR, and MS. Only compounds isolated in >90% purity and sufficient quantities were processed further to the ester hydrolysis step. The final bisphosphonic acid products were characterized by ^1H , ^{13}C , ^{31}P NMR and MS before they were used in our SAR studies. Chemical shifts (δ) are reported in ppm relative to the internal deuterated solvent (^1H , ^{13}C) or external H_3PO_4 . (δ 0.00 ^{31}P), unless indicated otherwise.

Synthesis of novel boron coupling reagents:

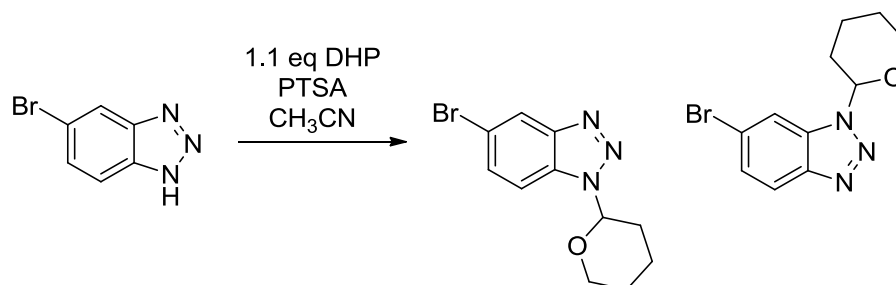
JDS03-030: 5-bromo-1H-benzo[d][1,2,3]triazole

Synthesized according to literature procedure: Han X. J. *et. al. J. Org. Chem.* **2008**, 8502



Isolated 984 mg (98%) as a pale brown powder. ^1H NMR (400 MHz, CDCl_3) δ 8.06 (s, 1H), 7.81 (d, $J = 8.8$ Hz, 1H), 7.56 (dd, $J = 8.8, 1.6$ Hz, 1H).

JDS03-032: 5 and 6-bromo-1-(tetrahydro-2H-pyran-2-yl)-1H-benzo[d][1,2,3]triazole

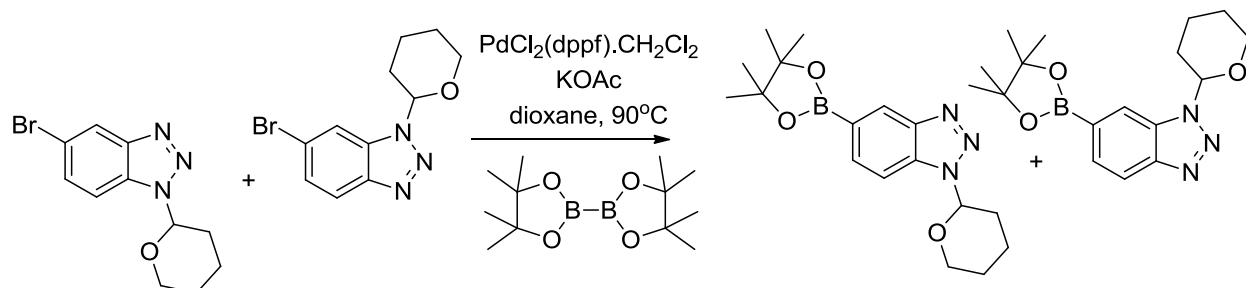


To a solution of 5-bromo-1H-benzo[d][1,2,3]triazole (500 mg, 2.52 mmol) in 15 mL anhydrous acetonitrile was added 3,4-dihydro-2H-pyran (0.25 mL, 2.8 mmol) and paratoluenesulfonic acid monohydrate (48m, 0.25 mmol) and the reaction was stirred at RT for 1h. The crude mixture was concentrated in vacuo and redissolved 100 mL EtOAc, washed with 10 mL satd. NaHCO₃, water and brine. The extract was dried over anhydrous Na₂SO₄, filtered and concentrated in vacuo. The residue was purified by silica gel chromatography on a CombiFlash instrument, using a solvent gradient from 1:10 EtOAc/Hexanes to 50% to give the desired product as a yellow oil (571 mg, 80%). ¹H NMR (400 MHz, CDCl₃) δ 8.23 – 8.21 (m, 1H), 7.95 – 7.91 (m, 2H), 7.64 (m, 1H), 7.57 (m, 1H), 7.49 – 7.46 (m, 1H), 6.01 (m, 2H), 3.98 – 3.85 (m, 2H), 3.83 – 3.73 (m, 2H), 2.62 – 2.49 (m, 2H), 2.27 – 2.11 (m, 4H), 1.88 – 1.72 (m, 6H).

General procedure for the synthesis of boron pinacol esters:

An 8 dram screp caw vial was charged with aryl bromide (1 equivalent), bis(pinacolato)diboron (1.1 equivalents), potassium acetate (2 equivalents) and PdCl₂(dppf).CH₂Cl₂ (0.1 equivalent); the vial was capped with a rubber septum, evacuated and back-filled with Argon. Anhydrous 1,4-dioxane was added via syringe to bring the concentration of aryl bromide to 0.1 M and the mixture was flushed again with Argon. The reaction was stirred at 90°C for 11 h. The reaction mixture was cooled down, diluted with Ethyl acetate, filtered through a Celite and concentrated in vacuo. The residue was purified by silica gel chromatography using a CombiFlash instrument and a solvent gradient from 1% to 100% EtOAc in hexanes.

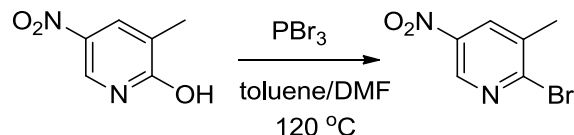
JDS03-033: 1-(tetrahydro-2H-pyran-2-yl)-5 or 6-(4,4,5,5-tetramethyl-1,3,2-dioxaborolan-2-yl)-1H-benzo[d][1,2,3]triazole



Isolated 621 mg (93%) as a yellow oil. ^1H NMR (400 MHz, CDCl_3) δ 8.55 (s, 1H), 8.17 (s, 1H), 8.04 (d, $J = 8.0$ Hz, 1H), 7.88 (d, $J = 8.5$ Hz, 1H), 7.78 (d, $J = 8.7$ Hz, 1H), 7.69 (d, $J = 8.7$ Hz, 1H), 6.04 (d, $J = 8.3$ Hz, 2H), 3.93 (d, $J = 19.0$ Hz, 2H), 3.80 (dd, $J = 11.0, 3.4$ Hz, 2H), 2.71 – 2.56 (m, 2H), 2.21 (d, $J = 9.5$ Hz, 4H), 1.77 (dd, $J = 16.1, 9.3$ Hz, 6H), 1.38 (s, 12H), 1.37 (s, 12H).

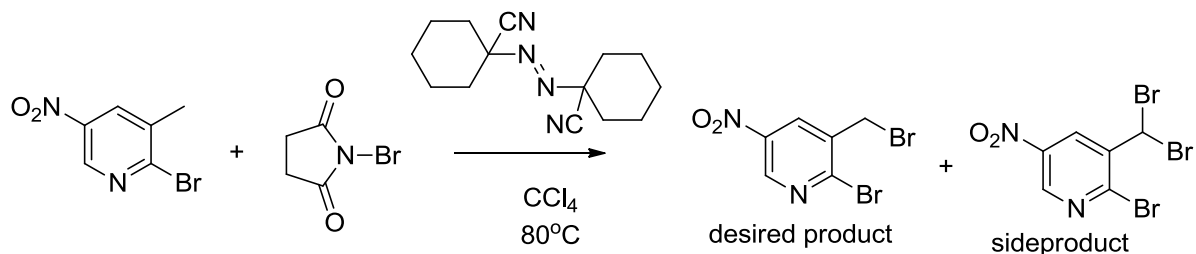
Synthesis of **3.11**

3.8 (JDS-03-050): 2-bromo-3-methyl-5-nitropyridine



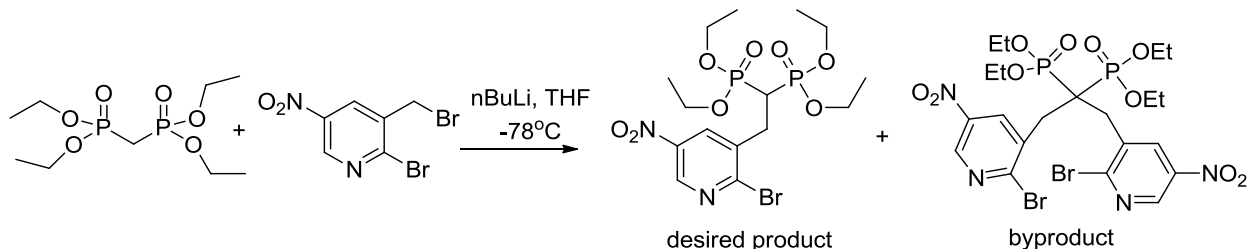
A sample of 3-methyl-5-nitropyridin-2-ol (1.44 g, 9.34 mmol) was placed in 35 mL pressure vessel and dissolved in a mixture of toluene/DMF (10:1 ratio; 15 mL). The vessel was capped with a septum, flushed with Argon and phosphorous tribromide (1.32 mL, 14.0mmol) was added by syringe. The septum cap was replaced by a Teflon cap and the mixture was stirred for 20 min at 120 °C. The mixture was cooled to room temperature, neutralized with a 3M NaOH solution and extracted with toluene (3x100 mL). The combined organic phases were dried over anhydrous MgSO_4 and concentrated under vacuum to give 2.00 g of the desired 2-bromo-3-methyl-5-nitropyridine product as an orange solid (99%). ^1H NMR (400 MHz, CDCl_3) δ 9.04 (d, $J = 2.7$ Hz, 1H), 8.29 (d, $J = 2.5$ Hz, 1H), 2.54 (s, 3H). ^{13}C NMR (126 MHz, CDCl_3) δ 150.65, 142.47, 136.76, 132.75, 22.20.

3.9 (JDS-03-043): 2-bromo-3-(bromomethyl)-5-nitropyridine



A 75 mL pressure vessel was charged with 2-bromo-3-methyl-5-nitropyridine (540 mg, 2.49 mmol), N-bromo-succinimide (452 mg, 2.54 mmol), 1,1'-azobis(cyclohexanecarbonitrile) (61 mg, 0.25 mmol) and 25 mL CCl₄. The vessel was closed with a rubber septum and thoroughly purged with Argon. The rubber septum was switched to a Teflon cap and the reaction mixture was stirred at 100 °C for 42 h. The mixture was cooled to RT, filtered to remove the succinimide byproduct, washed with CCl₄ and concentrated under vacuum. The crude residue was purified by chromatography on silica gel (using a solvent gradient from 1% to 20% EtOAc in hexanes) in order to isolate the desired product as a yellow oil (316 mg; 74% yield based on the amount of recovered starting material), along with some dibrominated byproduct (142 mg) and unreacted starting material (228 mg). ¹H NMR (300 MHz, CDCl₃) δ 9.12 (d, *J* = 2.7 Hz, 1H), 8.55 (d, *J* = 2.6 Hz, 1H), 4.61 (s, 2H). ¹³C NMR (126 MHz, CDCl₃) δ 149.26, 144.42, 136.00, 133.46, 29.75.

3.11 (JDS-03-060): tetraethyl (2-(2-bromo-5-nitropyridin-3-yl)ethane-1,1-diyl)bis(phosphonate)



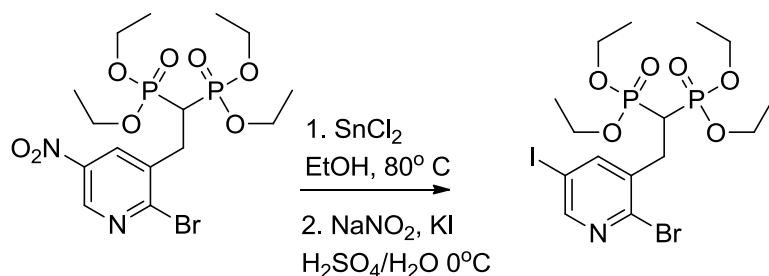
A solution of tetra-ethyl-methylene bisphosphonate ester (3.09 g, 10.73 mmol) in anhydrous THF was placed in a 250 mL RBF, under an atmosphere of argon. The solution was cooled to -78 °C and *n*BuLi (1.6 M in Hexanes, 7.0 mL) was added drop wise by syringe. The mixture was stirred at 0 °C for 5 min and re-cooled to -78°C. A solution of 2-

bromo-3-(bromomethyl)-5-nitropyridine (3.18 g, 10.73 mmol) in 10 mL anhydrous THF was added drop wise by syringe and the reaction was stirred at -78 °C for an additional 4 h. The reaction was quenched with MeOH, concentrated under vacuum and purified by chromatography on silica gel (using a solvent gradient of 1% EtOAc in hexanes to 100% EtOAc and then to 10% MeOH in EtOAc) to isolate the desired bisphosphonate intermediate as a brown oil (2.3 g; 52% yield based on recovered starting material) along with 586 of starting material and 995 mg of bis-alkylated byproduct. ¹H NMR (300 MHz, CDCl₃) δ 9.05 (d, *J* = 2.7 Hz, 1H), 8.45 (d, *J* = 2.7 Hz, 1H), 4.22 – 4.06 (m, 8H), 3.43 (m, 2H), 3.02 (tt, *J* = 22.9, 7.6 Hz, 1H), 1.38 – 1.17 (m, 12H). ¹³C NMR (126 MHz, CDCl₃) δ 149.62 (s), 143.28 (s), 143.13 (s), 137.15 (t, *J* = 9.2 Hz), 134.94 (s), 62.93 (dd, *J* = 41.9, 6.7 Hz), 35.91 (t, *J* = 133.2 Hz), 31.84 (s), 16.30 (d, *J* = 6.2 Hz). ³¹P NMR (81 MHz, CDCl₃) δ 18.99. MS (ESI): calcd 503.0348 and 505.0327, found 503.0 and 505.0 [M+H]⁺; calcd 525.0167 and 527.0147 found 525.0 and 527.0[M+Na]⁺

General procedure for sequential reduction and diazotation:

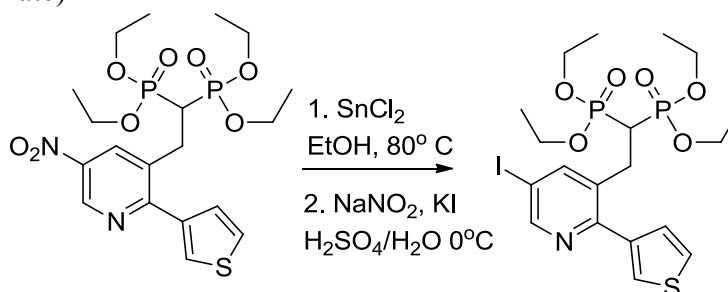
To a solution of 5-nitro-pyridine (1 equivalent) in EtOH (30 mL) in a pressure vessel was added stannous chloride dihydrate (5 equivalents). The vessel was sealed tight with a Teflon cap and the reaction was stirred at 80 °C for 2 h, then cooled to RT and the mixture was slowly added to a cooled solution of saturated aqueous NaHCO₃ (20 mL). The mixture was concentrated under vacuum to remove the EtOH and then extracted with EtOAc (4x 80 mL). The EtOAc layers were combined, dried over anhydrous Na₂SO₄ and concentrated to give the amine intermediate. This material was dissolved in 2M sulfuric acid and cooled in an ice bath. NaNO₂ (1.1 equivalents) was slowly added drop wise as a solution in 1-3 mL water and the mixture was stirred for 15 min. An aqueous solution of KI (1.5 equivalents) in 1-3 mL of water was added drop wise and the mixture was stirred for 40 min at RT. The reaction was quenched with the addition of 0.3 M sodium thiosulfate (3 equivalents), followed by the addition of EtOAc and the pH was carefully adjusted to 8 with 1M NaOH. The mixture was extracted EtOAc (3x 100 mL), dried over anhydrous Na₂SO₄, concentrated under vacuum and purified by column chromatography on silica gel (pre-washed with a dilute solution of NEt₃ in hexanes/EtOAc 9:1) and using a solvent gradient from 10% EtOAc in hexanes to 100% EtOAc and then to 10% MeOH in EtOAc.

3.14 (JDS-03-142): tetraethyl (2-(2-bromo-5-iodopyridin-3-yl)ethane-1,1-diyl)bis(phosphonate)



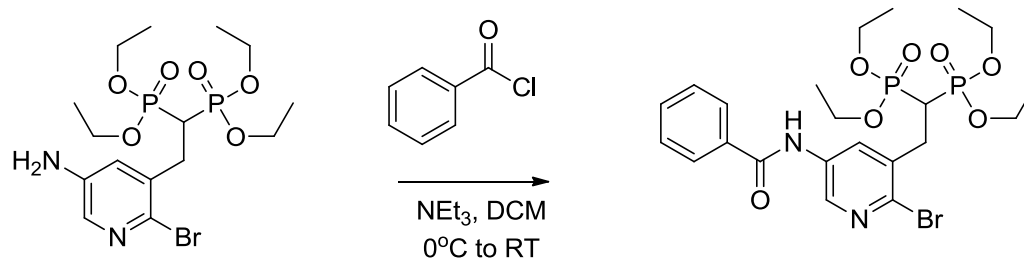
The desired tetraethyl (2-(2-bromo-5-iodopyridin-3-yl)ethane-1,1-diyl)bis(phosphonate) product was isolated as a yellow oil (544 mg, 60% over the two steps). ^1H NMR (400 MHz, CDCl_3) δ 8.43 (d, $J = 2.3$ Hz, 1H), 7.97 (d, $J = 2.2$ Hz, 1H), 4.19 – 4.04 (m, 8H), 3.31 – 3.18 (m, 2H), 3.09 – 2.89 (m, 1H), 1.25 (tt, $J = 10.6, 5.3$ Hz, 12H). ^{13}C NMR (75 MHz, CDCl_3) δ 153.84, 148.42, 143.11, 137.44 (t, $J = 9.1$ Hz), 127.97, 91.17, 62.67 (dd, $J = 38.8, 6.8$ Hz), 35.71 (t, $J = 133.0$ Hz), 16.24 (d, $J = 6.6$ Hz). ^{31}P NMR (81 MHz, CDCl_3) δ 19.17 (s). MS (ESI): calcd 605.93 and 607.93, found 605.9 and 607.9 $[\text{M}+\text{Na}]^+$

3.18 (JDS-03-065): tetraethyl (2-(5-iodo-2-(thiophen-3-yl)pyridin-3-yl)ethane-1,1-diyl)bis(phosphonate)



Isolated 394 mg (62% over two steps) as a yellow oil. ^1H NMR (400 MHz, CDCl_3) δ 8.72 (d, $J = 2.0$ Hz, 1H), 8.01 (d, $J = 1.9$ Hz, 1H), 7.60 (dd, $J = 2.8, 1.2$ Hz, 1H), 7.42 – 7.34 (m, 2H), 4.07 – 3.95 (m, 8H), 3.47 – 3.33 (m, 2H), 2.46 (tt, $J = 23.3, 7.7$ Hz, 1H), 1.22 (td, $J = 7.1, 4.3$ Hz, 12H). ^{13}C NMR (126 MHz, CDCl_3) δ 150.77 (s), 150.29 (s), 144.31 (s), 137.38 (s), 131.65 (s), 125.64 (s), 123.39 (s), 122.44 (s), 88.35 (s), 59.95 (dd, $J = 46.3, 6.8$ Hz), 33.53 (t, $J = 132.9$ Hz), 26.78 (s), 13.66 (d, $J = 4.1$ Hz). ^{31}P NMR (81 MHz, CDCl_3) δ 19.79. MS (ESI): calcd 610.01, found 610.0 $[\text{M}+\text{Na}]^+$

JDS04-126: tetraethyl (2-(5-benzamido-2-bromopyridin-3-yl)ethane-1,1-diyl)bis(phosphonate)

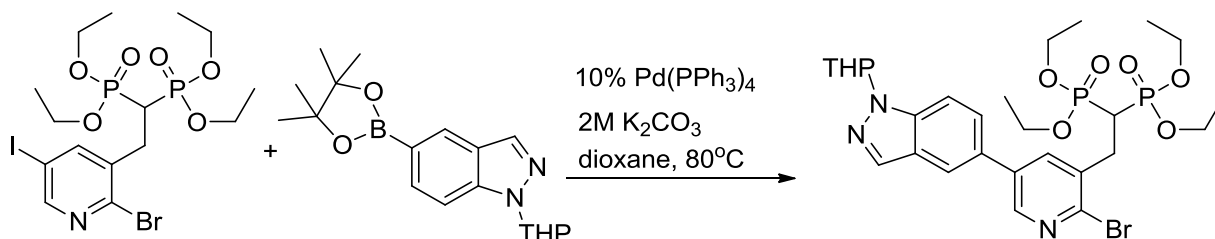


To an ice cooled solution of tetraethyl (2-(5-amino-2-bromopyridin-3-yl)ethane-1,1-diyl)bis(phosphonate) (130 mg, 0.275 mmol) and triethylamine (0.04 mL, 0.3 mmol) in 10 mL anhydrous DCM was added benzoyl chloride (0.04 mL, 0.03 mmol) and the reaction was stirred at RT for 4 h. The reaction was quenched with MeOH, concentrated in vacuo and the residue was purified by silica gel (silica was pre-washed with 0.1% NEt₃ in hexanes/EtOAc 3:1) chromatography on a CombiFlash instrument, using a solvent gradient from 1:10 EtOAc/Hexanes to 100% EtOAc and then to 10% MeOH in EtOAc to give the desired product as a colorless oil (131 mg, 83%). ¹H NMR (400 MHz, CDCl₃) δ 8.65 (d, *J* = 2.6 Hz, 1H), 8.20 (bs, NH), 8.17 (d, *J* = 2.6 Hz, 1H), 7.91 – 7.85 (m, 2H), 7.58 (t, *J* = 7.3 Hz, 1H), 7.50 (t, *J* = 7.4 Hz, 2H), 4.23 – 4.05 (m, 8H), 3.39 – 3.27 (m, 2H), 3.11 (tt, *J* = 22.8, 7.6 Hz, 1H), 1.33 – 1.19 (m, 12H). ¹³C NMR (75 MHz, CDCl₃) δ 165.91, 140.05, 137.42, 135.18, 134.66, 133.99, 132.24, 131.95, 128.77, 127.34, δ 62.78 (dd, *J* = 32.2, 6.8 Hz), 35.77 (t, *J* = 132.7 Hz), 31.70, 16.30 (dd, *J* = 6.1, 4.5 Hz). ³¹P NMR (81 MHz, CDCl₃) δ 21.43 (s). MS (ESI): calcd 577.087 and 579.085, found 577.26 and 579.25 [M+H]⁺

General procedure for Suzuki cross coupling:

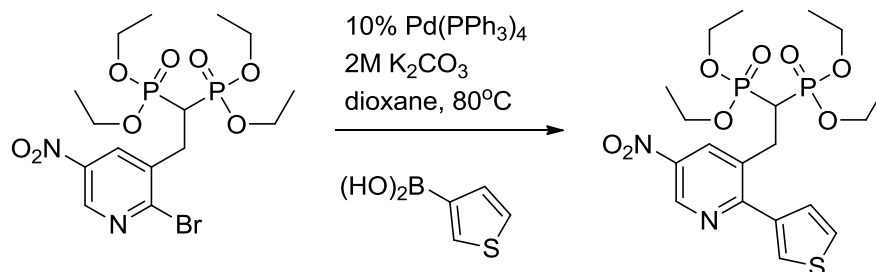
A 5 mL vial was charged with the aryl halide (1 equivalent), Pd(PPh₃)₄ or Pd(P[*t*-Bu]₃)₂ (0.1 equivalent), a stir bar and the boron-coupling partner (1.2 equivalents) if a solid. The vial was capped with a rubber septum, evacuated and back-filled with Argon; anhydrous DME or 1,4-dioxane was added via syringe to bring the final concentration of aryl halide to 0.1M and the solution was flushed with Argon. At this point the boron-coupling partner, if not at solid, was added as a solution in DME or 1,4-dioxane. 2M Na₂CO₃ or K₂CO₃ solution (2.5 equivalents) was added and the vial was flushed again with Argon. The reaction vessel was equipped with an Argon-filled balloon and stirred at 80°C until complete consumption of starting material. The reaction mixture was cooled down, diluted with EtOAc and filtered through a plug of Celite, rinsed three times with EtOAc/MeOH 1:1. The filtrate concentrated in vacuo and purified by normal phase column chromatography on silica gel (silica gel was pre-treated with 1% NEt₃ in hexanes/EtOAc in a 3:1 ratio) using a gradient from 100% hexanes to 100% EtOAc and then to 25% MeOH.

3.15 (JDS-03-080): tetraethyl (2-(2-bromo-5-(1-(tetrahydro-2H-pyran-2-yl)-1H-indazol-5-yl)pyridin-3-yl)ethane-1,1-diyl)bis(phosphonate)



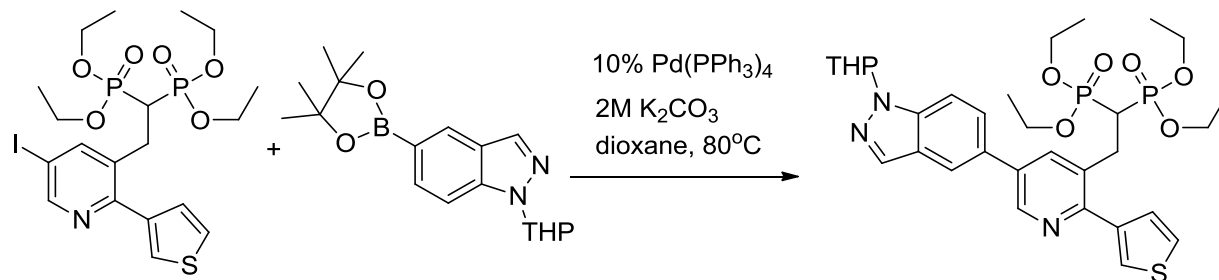
Isolated 30mg (89% based on recovered starting material) as a yellow oil. ¹H NMR (400 MHz, CDCl₃) δ 8.50 (d, *J* = 2.5 Hz, 1H), 8.10 (s, 1H), 7.98 (d, *J* = 2.5 Hz, 1H), 7.91 (s, 1H), 7.70 (d, *J* = 8.7 Hz, 1H), 7.59 (dd, *J* = 8.7, 1.6 Hz, 1H), 5.76 (dd, *J* = 9.3, 2.6 Hz, 1H), 4.22 – 4.00 (m, 8H), 3.77 (s, 1H), 3.47 – 3.34 (m, 2H), 3.24 – 3.07 (m, 1H), 2.15 (d, *J* = 15.1 Hz, 3H), 1.73 (d, *J* = 29.6 Hz, 4H), 1.25 (dt, *J* = 16.2, 7.1 Hz, 12H). ¹³C NMR (75 MHz, CDCl₃) δ 146.37, 142.06, 139.53, 139.27, 136.00, 135.07, 134.32, 129.61, 125.81, 125.41, 119.42, 111.13, 85.49, 69.59, 67.49, 62.68 (dd, *J* = 49.0, 7.0 Hz), 35.96 (t, *J* = 132.7 Hz), 29.38, 25.07, 22.49, 16.68 – 15.87 (m). MS (ESI): calcd 658.14 and 660.14, found: 658.1 and 660.0 [M+H]⁺; calcd 680.13 and 682.12, found 680.1 and 682.1 [M+Na]⁺

3.17 (JDS-03-062): tetraethyl (2-(5-nitro-2-(thiophen-3-yl)pyridin-3-yl)ethane-1,1-diyl)bis(phosphonate)



Isolated 558 mg (100%) as a brown oil. ^1H NMR (400 MHz, CDCl_3) δ 9.33 (d, $J = 2.4$ Hz, 1H), 8.48 (d, $J = 2.4$ Hz, 1H), 7.81 (dd, $J = 2.7, 1.2$ Hz, 1H), 7.53 – 7.44 (m, 2H), 4.09 – 3.99 (m, 8H), 3.68 – 3.54 (m, 2H), 2.56 (tt, $J = 23.2, 7.5$ Hz, 1H), 1.22 (dt, $J = 13.8, 7.1$ Hz, 12H). ^{13}C NMR (126 MHz, CDCl_3) δ 159.00 (s), 142.59 (s), 142.26 (s), 139.38 (s), 133.90 (s), 133.01 (s), 128.37 (s), 127.05 (s), 126.41 (s), 62.71 (dd, $J = 30.9, 6.7$ Hz), 36.18 (t, $J = 133.1$ Hz), 29.66 (s), 16.24 (d, $J = 6.2$ Hz). ^{31}P NMR (81 MHz, CDCl_3) δ 19.42. MS (ESI): calcd 529.09, found 529.2 $[\text{M}+\text{Na}]^+$;

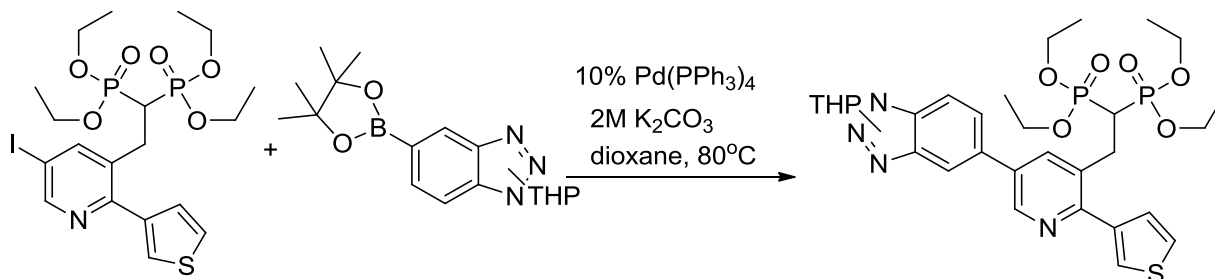
JDS-03-066: tetraethyl (2-(5-(1-(tetrahydro-2H-pyran-2-yl)-1H-indazol-5-yl)-2-(thiophen-3-yl)pyridin-3-yl)ethane-1,1-diyl)bis(phosphonate)



Isolated 82mg (73%) as a yellow oil. ^1H NMR (400 MHz, CDCl_3) δ 8.80 (d, $J = 2.1$ Hz, 1H), 8.11 (s, 1H), 7.98 – 7.93 (m, 2H), 7.74 – 7.62 (m, 3H), 7.43 (d, $J = 2.5$ Hz, 2H), 5.77 (dd, $J = 9.2, 2.5$ Hz, 1H), 4.10 – 3.92 (m, 10H), 3.83 – 3.73 (m, 1H), 3.62 – 3.50 (m, 2H), 2.67 – 2.49 (m, 2H), 2.22 – 2.08 (m, 2H), 1.75 (d, $J = 38.6$ Hz, 4H), 1.20 (m, 12H). ^{13}C NMR (75 MHz, CDCl_3) δ 152.44 (s), 145.93 (s), 140.79 (s), 139.19 (s), 137.70 (s), 134.90 (s), 134.33 (s), 132.30 – 131.38 (m), 130.79 (s), 128.47 (s), 126.03 (s), 125.77 (s), 125.44 (s), 124.63 (s), 119.26 (s), 110.95 (s), 85.46 (s), 67.49 (s), 62.45 (dd, $J = 35.2, 6.7$ Hz), 36.22 (t, $J = 132.8$ Hz), 29.80 (t, $J = 4.2$ Hz), 29.40 (s), 25.09 (s), 22.53 (s), 16.23 (dd, $J =$

6.7, 3.3 Hz). ^{31}P NMR (81 MHz, CDCl_3) δ 20.16 (s). MS (ESI): calcd 662.22, found 662.3 $[\text{M}+\text{H}]^+$; calcd 684.20 found 684.3 $[\text{M}+\text{Na}]^+$

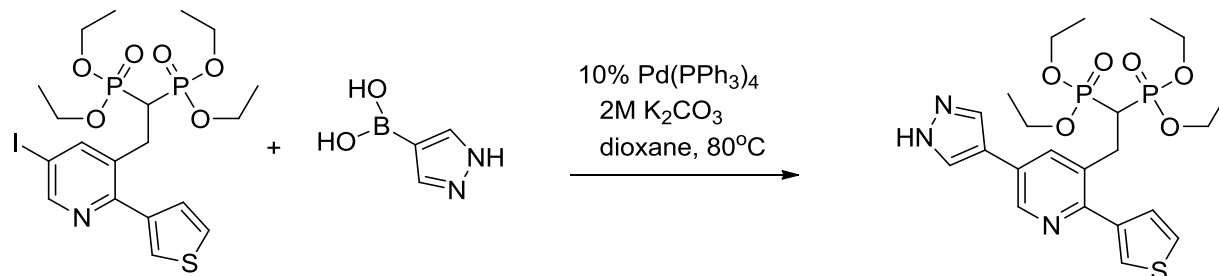
JDS-03-067: tetraethyl (2-(5-(1-(tetrahydro-2H-pyran-2-yl)-1H-benzo[d][1,2,3]triazol-5-yl)-2-(thiophen-3-yl)pyridin-3-yl)ethane-1,1-diyl)bis(phosphonate) & tetraethyl (2-(5-(1-(tetrahydro-2H-pyran-2-yl)-1H-benzo[d][1,2,3]triazol-6-yl)-2-(thiophen-3-yl)pyridin-3-yl)ethane-1,1-diyl)bis(phosphonate)



Isolated 101mg (90%) as an orange oil. ^1H NMR (400 MHz, CDCl_3) δ 8.83 (dd, $J = 2.2, 1.2$ Hz, 2H), 8.29 (s, 1H), 8.16 (dd, $J = 8.6, 0.7$ Hz, 1H), 7.99 (dd, $J = 7.7, 2.3$ Hz, 2H), 7.93 (s, 1H), 7.86 (dd, $J = 8.6, 0.8$ Hz, 1H), 7.76 (dd, $J = 8.6, 1.5$ Hz, 1H), 7.70 – 7.61 (m, 3H), 7.49 – 7.41 (m, 4H), 6.10 (td, $J = 8.1, 3.0$ Hz, 2H), 4.10 – 3.91 (m, 16H), 3.87 – 3.78 (m, 2H), 3.74 (s, 4H), 3.57 (dd, $J = 24.1, 9.9$ Hz, 4H), 2.62 (dd, $J = 17.6, 5.6$ Hz, 4H), 2.32 – 2.15 (m, 4H), 1.82 (dd, $J = 34.7, 16.6$ Hz, 4H), 1.25 – 1.14 (m, 24H). ^{13}C NMR (75 MHz, CDCl_3) δ 153.33, 153.01, 147.05, 146.19, 146.00, 140.55, 140.50, 138.23, 137.96, 137.14, 134.27, 134.20, 133.93, 133.16, 132.25, 132.04, 128.41, 127.13, 125.92, 125.88, 124.94, 124.85, 124.01, 120.57, 117.79, 112.04, 109.21, 85.81, 85.61, 66.77, 63.76, 62.82, 62.74, 62.34, 62.25, 37.90, 36.15, 34.39, 29.69, 29.28, 29.23, 24.85, 24.78, 21.46, 16.25, 16.16.

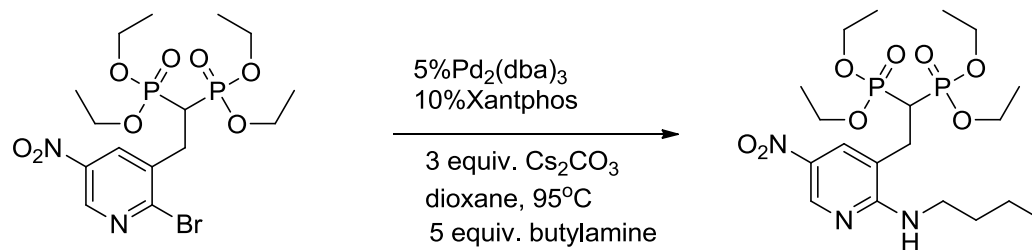
^{31}P NMR (81 MHz, CDCl_3) δ 20.28 (s). MS (ESI $^+$): calcd 663.22, found 663.2 $[\text{M}+\text{H}]^+$; calcd 685.20 found 685.2 $[\text{M}+\text{Na}]^+$

JDS-03-068: tetraethyl (2-(5-(1H-pyrazol-4-yl)-2-(thiophen-3-yl)pyridin-3-yl)ethane-1,1-diyl)bis(phosphonate)



Isolated 28mg (45% based on recovered starting material) as a yellow oil. ^1H NMR (300 MHz, DMSO- d_6) δ 13.05 (s, 1H), 8.73 (s, 1H), 8.34 (bs, 1H), 8.06 (s, 1H), 8.03 (s, 1H), 7.75 (s, 1H), 7.61 (dd, $J = 4.9, 3.2$ Hz, 1H), 7.36 (d, $J = 5.3$ Hz, 1H), 3.95 – 3.76 (m, 8H), 3.37 (m, 2H), 2.98 (m, 1H), 1.06 (q, $J = 7.3$ Hz, 12H). ^{13}C NMR (75 MHz, DMSO- d_6) δ 151.11 (s), 144.08 (s), 141.55 (s), 134.57 (s), 132.10 (t, $J = 8.8$ Hz), 129.46 (s), 127.34 (s), 126.05 (s), 125.09 (s), 118.12 (s), 62.18 (dd, $J = 25.1, 6.7$ Hz), 46.17 (s), 16.41 (t, $J = 5.8$ Hz), 9.09 (s). ^{31}P NMR (81 MHz, DMSO- d_6) δ 20.64 (s). MS (ESI): calcd 528.15, found 528.2 $[\text{M}+\text{H}]^+$; calcd 550.13 found 550.2 $[\text{M}+\text{Na}]^+$

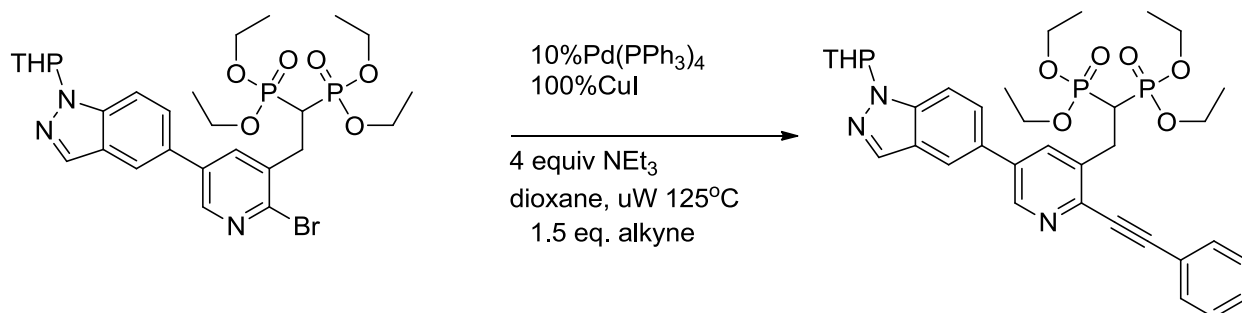
JDS-04-093: tetraethyl (2-(2-(butylamino)-5-nitropyridin-3-yl)ethane-1,1-diyl)bis(phosphonate)



Tetraethyl (2-(2-bromo-5-nitropyridin-3-yl)ethane-1,1-diyl)bis(phosphonate) (77 mg, 0.153 mmol, 1 equivalents) was transferred to a 12 mL Teflon lined screw cap vial and charged with Cs_2CO_3 (150 mg, 0.46 mmol, 3 equivalents), Xantphos (10 mg, 0.017 mmol, 0.11 equivalent) and $\text{Pd}_2(\text{dba})_3$ (7 mg, 0.008 mmol, 0.05 equivalents), capped with a rubber septum and flushed with Argon. 1,4-Dioxane was added to bring the concentration of aryl bromide to 0.05M (2.9 mL), the vial was flushed again with Argon and the mixture was stirred for 1 min before butylamine (0.08 mL, 0.76 mmol, 5 eq) was added, and mixture flushed again. The reaction mixture was sealed with a Teflon cap and stirred at 95 °C for 16

h. The crude was cooled to room temperature, passed through a celite plug, washed with EtOAc/Acetone 1:1 and purified by column chromatography (using a solvent gradient from 5% EtOAc in hexanes to 100% EtOAc and then to 10% MeOH in EtOAc. The desired product was isolated as a yellow solid (52 mg, 69% yield). ^1H NMR (400 MHz, CDCl_3) δ 8.98 (d, $J = 2.7$ Hz, 1H), 8.06 (d, $J = 2.7$ Hz, 1H), 7.10 (t, $J = 5.1$ Hz, 1H), 4.26 – 4.11 (m, 8H), 3.61 – 3.51 (m, 2H), 3.18 – 3.04 (m, 2H), 2.26 (tt, $J = 24.5, 4.5$ Hz, 1H), 1.72 – 1.59 (m, 2H), 1.43 (dt, $J = 14.9, 7.4$ Hz, 2H), 1.39 – 1.30 (m, 12H), 0.95 (t, $J = 7.4$ Hz, 3H). ^{13}C NMR (75 MHz, CDCl_3) δ 159.04, 145.60, 134.37, 132.76, 117.14, 117.07, 63.18, 41.96, 35.06 (t, $J = 132.4$ Hz), 31.19, 26.70, 20.28, 16.34, 16.30, 16.26, 13.82. ^{31}P NMR (81 MHz, CDCl_3) δ 21.27. MS (ESI): calcd 518.18, found 518.15 $[\text{M}+\text{Na}]^+$

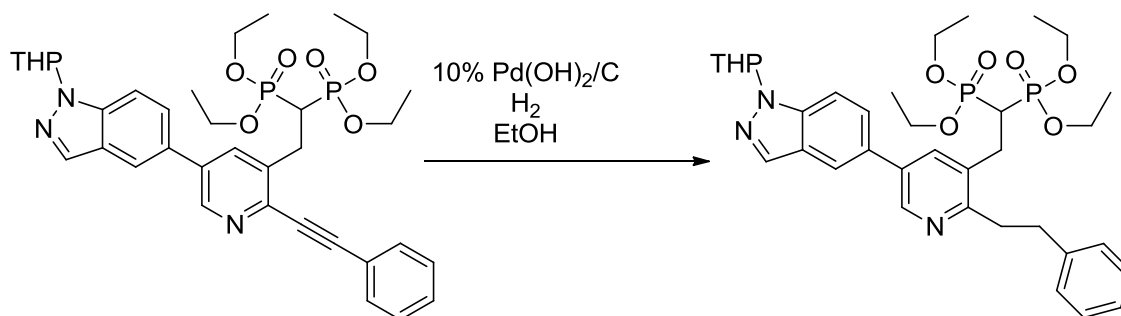
3.26 (JDS07-055): tetraethyl (2-(2-(phenylethynyl)-5-(1-(tetrahydro-2H-pyran-2-yl)-1H-indazol-5-yl)pyridin-3-yl)ethane-1,1-diyl)bis(phosphonate)



A 0.5-2 mL microwave reaction vessel was charged with a magnetic stir bar, tetraethyl (2-(2-bromo-5-(1-(tetrahydro-2H-pyran-2-yl)-1H-indazol-5-yl)pyridin-3-yl)ethane-1,1-diyl)bis(phosphonate) (100.0 mg, 0.152 mmol), $\text{Pd}(\text{PPh}_3)_4$ (17.6 mg, 0.015 mmol) and copper(I) iodide (29.0mg, 0.152 mmol); capped with a septum, degassed and flushed with Argon. A volume of 1.50 mL 1,4-dioxane was added to bring the concentration of the aryl bromide to 0.05M, and the mixture was again degassed and flushed with Argon. Triethylamine (0.08 mL, 0.6 mmol) was added and the mixture was again degassed and flushed with Argon. Phenylacetylene (0.03 mL, 0.23 mmol) was added and the rubber septum was replaced by a Teflon lined seal, under Argon flow. The reaction was irradiated to 125°C for 30min (~60W), reaction progress was monitored HPLC. After 30min, HPLC analysis showed starting material remained, the same amounts of Pd and Cu catalyst base and were added to the reaction vessel and irradiation was continued. After another 30min

HPLC analysis showed starting material remained present, the same amounts of Pd and Cu catalyst, base and were added to the reaction vessel and irradiation was continued. After an additional 60 min, HPLC analysis showed complete conversion. The crude was filtered through a plug of Celite, rinsed with 10 mL 1:1 EtOAc/Acetone and concentrated in vacuo. The residue was purified by silica gel (silica was pre-washed with 0.1% NEt₃ in hexanes:EtOAc 3:1) chromatography using a CombiFlash instrument and a solvent gradient from 1:1 EtOAc/Hexanes to 100% EtOAc and then to 10% MeOH in EtOAc. The product was isolated as a colorless oil (57 mg, 55%). ¹H NMR (400 MHz, CD₃OD) δ 8.84 (s, 1H), 8.20 (s, 1H), 8.17 – 8.14 (m, 2H), 7.85 (d, *J* = 8.8 Hz, 1H), 7.81 (dd, *J* = 8.8, 1.6 Hz, 1H), 7.75 – 7.70 (m, 2H), 7.48 – 7.43 (m, 2H), 5.87 (dd, *J* = 9.8, 2.6 Hz, 1H), 4.17 – 4.03 (m, 8H), 3.84 (td, *J* = 11.1, 3.1 Hz, 1H), 3.64 – 3.53 (m, 2H), 3.49 – 3.37 (m, 1H), 2.52 (dt, *J* = 13.8, 6.7 Hz, 1H), 2.13 (s, 1H), 2.07 (d, *J* = 13.0 Hz, 1H), 1.92 – 1.64 (m, 3H), 1.27 – 1.16 (m, 12H). ¹³C NMR (75 MHz, CD₃OD) δ 139.92, 139.40, 136.88, 134.27, 131.72, 129.64, 129.40, 128.35, 125.71, 125.18, 121.60, 119.31, 111.14, 86.05, 85.19, 78.12, 67.31, δ 62.93 (dd, *J* = 16.8, 6.8 Hz), 35.98 (t, *J* = 134.6 Hz), 29.27, 24.92, 22.31, 15.25 (d, *J* = 6.3 Hz). ³¹P NMR (81 MHz, CD₃OD) δ 24.16 (s). MS (ESI): calcd 680.26, found 680.49 [M+H]⁺

3.27 (JDS07-059): tetraethyl (2-(2-phenethyl-5-(1-(tetrahydro-2H-pyran-2-yl)-1H-indazol-5-yl)pyridin-3-yl)ethane-1,1-diyl)bis(phosphonate)



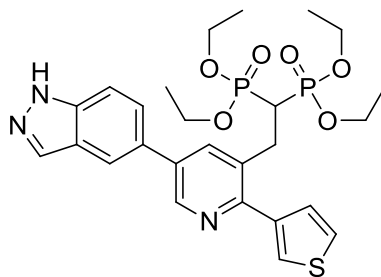
To a solution tetraethyl (2-(2-(phenylethynyl)-5-(1-(tetrahydro-2H-pyran-2-yl)-1H-indazol-5-yl)pyridin-3-yl)ethane-1,1-diyl)bis(phosphonate) (55 mg, 0.081 mmol) in ethanol under an Argon atmosphere was added Pearlman's catalyst (10% Pd(OH)₂/C, 11.4 mg, 0.081 mmol) and the reaction vessel was flushed with hydrogen gas and equipped with a hydrogen-filled balloon. The reaction was stirred 2 h at RT, after which the reaction mixture was flushed with Argon. The suspension was filtered through a plug of Celite and

concentrated in vacuo to yield a yellow foam which was used as such in the next reaction (42 mg, 76%). ^1H NMR (400 MHz, CD_3OD) δ 8.73 (d, $J = 2.2$ Hz, 1H), 8.14 (s, 1H), 8.09 (d, $J = 0.8$ Hz, 1H), 8.02 (d, $J = 2.2$ Hz, 1H), 7.83 (d, $J = 8.8$ Hz, 1H), 7.77 (dd, $J = 8.8, 1.7$ Hz, 1H), 7.29 – 7.23 (m, 2H), 7.23 – 7.15 (m, 3H), 5.86 (dd, $J = 9.8, 2.6$ Hz, 1H), 4.15 – 4.00 (m, 8H), 3.88 – 3.80 (m, 1H), 3.47 (dd, $J = 3.3, 1.7$ Hz, 1H), 3.00 – 2.83 (m, 1H), 2.60 – 2.47 (m, 1H), 2.18 – 2.10 (m, 1H), 2.10 – 2.00 (m, 1H), 1.95 – 1.80 (m, 1H), 1.78 – 1.63 (m, 1H), 1.27 – 1.18 (m, 12H). ^{13}C NMR (75 MHz, CD_3OD) δ 157.40, 145.00, 141.15, 139.28, 137.51, 134.11, 130.55, 128.21, 128.11, 125.85, 125.21, 118.91, 110.84, 85.08, 67.28, δ 62.94 (d, $J = 23.5$ Hz), 35.83, 35.49, 29.25, 24.91, 22.32, 15.19 (d, $J = 6.4$ Hz). ^{31}P NMR (81 MHz, CD_3OD) δ 22.76 (s). MS (ESI): calcd 684.30, found 684.53 $[\text{M}+\text{H}]^+$

General procedure fo THP-deprotection:

To a solution of THP protected compound (1 equivalent) in anhydrous EtOH was added ethanolic HCl (1.0M, 2.5 equivalents) via syringe for a final concentration of 0.1M HCl. The reaction was stirred at 80°C for 12h. The reaction mixture was concentrated in vacuo (NaHCO_3 in receiving flask), the crude was dissolved in 100 mL EtOAc and washed with 10mL satd. NaHCO_3 , water and brine. The organic layer was dried over sodium sulfate, concentrated in vacuo and purified by normal phase column chromatography on silica gel (silica gel was pre-treated with 1% NEt_3 in hexanes/EtOAc in a 3:1 ratio) using a gradient from 100% hexanes to 100% EtOAc and then to 10-25% MeOH.

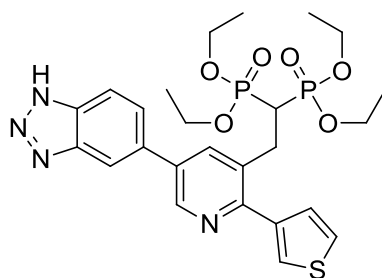
JDS-03-048: tetraethyl (2-(5-(1H-indazol-5-yl)-2-(thiophen-3-yl)pyridin-3-yl)ethane-1,1-diyl)bis(phosphonate)



Isolated 40 mg (76%) as a white foam. ^1H NMR (400 MHz, CDCl_3) δ 8.81 (d, $J = 2.0$ Hz, 1H), 8.15 (s, 1H), 8.01 – 7.94 (m, 2H), 7.65 (dd, $J = 2.5, 1.6$ Hz, 1H), 7.59 (dt, $J = 18.6, 5.0$ Hz, 2H), 7.48 – 7.41 (m, 2H), 4.12 – 3.90 (m, 8H), 3.65 – 3.53 (m, 2H), 2.61 (tt, $J = 23.1,$

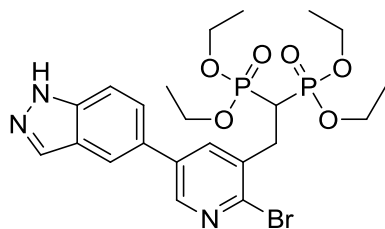
7.6 Hz, 1H), 1.20 (dt, $J = 19.5, 7.1$ Hz, 12H). ^{13}C NMR (75 MHz, CDCl_3) δ 152.36 (s), 145.90 (s), 140.76 (s), 137.83 (s), 135.22 (s), 131.86 (t, $J = 9.0$ Hz), 130.04 (s), 128.45 (s), 125.87 (s), 124.68 (s), 118.96 (s), 110.76 (s), 62.61 (dd, $J = 50.4, 6.7$ Hz), 36.06 (t, $J = 132.8$ Hz), 29.87 (t, $J = 4.5$ Hz), 16.24 (dd, $J = 8.0, 6.6$ Hz). ^{31}P NMR (81 MHz, CDCl_3) δ 20.19 (s). MS (ESI): calcd 600.15, found 600.2 $[\text{M}+\text{Na}]^+$; calcd 1177.30, found 1176.9 $[2\text{M}+\text{Na}]^+$

JDS-03-074: tetraethyl (2-(5-(1H-benzo[d][1,2,3]triazol-5-yl)-2-(thiophen-3-yl)pyridin-3-yl)ethane-1,1-diyl)bis(phosphonate)



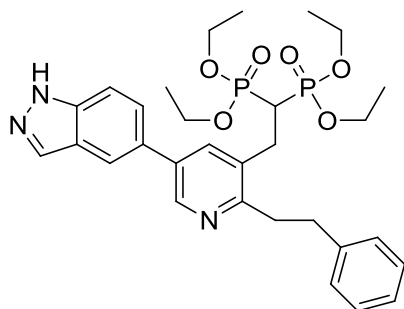
Isolated 55 mg (63%) as a white foam. ^1H NMR (500 MHz, CD_3OD) δ 8.82 (d, $J = 2.2$ Hz, 1H), 8.23 (d, $J = 2.2$ Hz, 1H), 8.21 (s, 1H), 8.03 (d, $J = 8.5$ Hz, 1H), 7.86 (dd, $J = 8.7, 1.4$ Hz, 1H), 7.76 (dd, $J = 2.9, 1.3$ Hz, 1H), 7.64 (dd, $J = 5.0, 2.9$ Hz, 1H), 7.42 (dd, $J = 5.0, 1.3$ Hz, 1H), 4.07 – 3.92 (m, 8H), 3.57 (m, 2H), 2.70 (tt, $J = 23.3, 7.7$ Hz, 1H), 1.20 (td, $J = 7.1, 1.8$ Hz, 12H). ^{13}C NMR (126 MHz, CD_3OD) δ 157.18 (s), 143.80 (s), 143.80 (s), 142.36 (s), 142.34 (s), 138.98 (bs), 138.78 (s), 136.58 (t, $J = 9.1$ Hz), 132.06 (s), 130.00 (s), 129.22 (bs), 129.14 (s), 119.25 (bs), 116.38 (bs), 66.72 (dd, $J = 41.7, 6.9$ Hz), 39.26 (t, $J = 134.2$ Hz), 33.00 (t, $J = 4.4$ Hz), 19.10 (d, $J = 6.4$ Hz). ^{31}P NMR (81 MHz, CD_3OD) δ 23.81 (s). MS (ESI $^+$): calcd 577.14, found 577.2 $[\text{M}-\text{H}]^-$; calcd 601.14, found 601.2 $[\text{M}+\text{Na}]^+$

JDS-04-067: tetraethyl (2-(2-bromo-5-(1H-indazol-5-yl)pyridin-3-yl)ethane-1,1-diyl)bis(phosphonate)



Isolated 81 mg (92%) as a colorless oil. ^1H NMR (400 MHz, CDCl_3) δ 8.51 (s, 1H), 8.14 (s, 1H), 8.00 (s, 1H), 7.94 (s, 1H), 7.57 (s, 2H), 4.26 – 4.00 (m, 8H), 3.50 – 3.35 (m, 2H), 3.17 (m, 1H), 1.26 (dt, $J = 25.5, 7.0$ Hz, 12H). ^{13}C NMR (75 MHz, CD_3OD) δ 146.00, 141.15, 139.79, 139.42, 136.57, 134.93 (t, $J = 9.2$ Hz), 134.16, 128.66, 125.65, 123.63, 119.07, 110.75, 62.99 (dd, $J = 29.9, 6.9$ Hz), 35.28 (t, $J = 134.3$ Hz), 31.17 (t, $J = 4.5$ Hz), 15.22 (d, $J = 6.3$ Hz). ^{31}P NMR (81 MHz, CDCl_3) δ 21.74. MS (ESI): calcd 596.0691 and 598.0670, found: 596.0 and 598.0 $[\text{M}+\text{Na}]^+$

JDS07-064: tetraethyl (2-(5-(1H-indazol-5-yl)-2-phenethylpyridin-3-yl)ethane-1,1-diyl)bis(phosphonate)



Isolated 15.6 mg (44%) as white solid. ^1H NMR (400 MHz, CD_3OD) δ 8.72 (d, $J = 2.1$ Hz, 1H), 8.14 (s, 1H), 8.09 (d, $J = 0.6$ Hz, 1H), 8.01 (d, $J = 2.2$ Hz, 1H), 7.73 (dd, $J = 8.7, 1.6$ Hz, 1H), 7.67 (d, $J = 8.7$ Hz, 1H), 7.26 (m, 2H), 7.23 – 7.16 (m, 3H), 4.16 – 3.98 (m, 8H), 3.26 – 3.14 (m, 4H), 3.06 (m, 2H), 2.91 (tt, $J = 23.6, 7.0$ Hz, 1H), 1.22 (t, $J = 7.1$ Hz, 12H). ^{13}C NMR (75 MHz, CD_3OD) δ 157.26, 144.98, 141.14, 137.53, 134.83, 134.04, 132.83, 129.90, 128.20, 128.09, 125.85, 123.62, 118.72, 110.62, δ 62.89 (dd, $J = 24.7, 6.8$ Hz), 36.90 (t, $J = 134.1$ Hz), 35.81, 35.51, 27.38 15.15 (d, $J = 6.5$ Hz). ^{31}P NMR (81 MHz, CD_3OD) δ 24.32 (s). MS (ESI): calcd 600.24, found: 600.42 $[\text{M}+\text{H}]^+$

General procedure A for final deprotection:

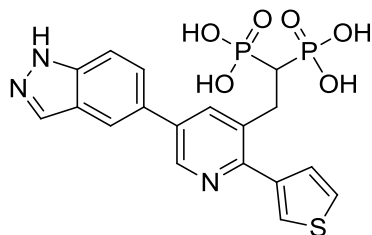
A 12 mL Teflon lined screw cap vial was charged with the tetra-ethyl bisphosphonate compound, dissolved in 5 mL distilled DCM and cooled in an ice bath. Bromotrimethyl silane (15 equivalents) was added via syringe and the reaction mixture was stirred at RT for 5-7 days. The reaction mixture was transferred to a 10 mL recovery flask and concentrated in vacuo (satd. NaHCO_3 in receiving flask). To the resulting oil was added 2 mL of HPLC-grade MeOH and concentrated in vacuo, this was repeated a total of five times. The crude

thus obtained was suspended in a minimum amount of HPLC-grade MeOH, the mixture was sonicated and the desired compound was precipitated out of solution by the addition of Milli-Q water. The slurry was filtered and the cake washed twice with Milli-Q water, twice with HPLC-grade CH₃CN and twice with distilled Et₂O. The residue was then dried under high vacuum to obtain the desired product.

General procedure B for final deprotection:

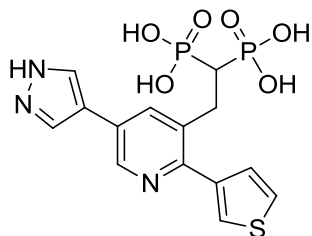
The bisphosphonate ester was transferred to a pressure vessel, dissolved in 6M HCl, the vessel was tightly sealed and the mixture was stirred at 100°C for 12 h. The reaction was cooled down, transferred to recovery flask and concentrated to dryness (with satd. NaHCO₃ in receiving flask). The residue was purified by reverse phase column chromatography on a Teledyne Isco 4.7 g diol-functionalized C18 silica gel column (loaded with dilute NH₄OH in a solid load cartridge containing 2cm of wetted C18 silica and 2cm of sand) using a gradient from 1% formic acid to 1% ammonium formate pH=8. The fractions containing desired product were pooled and lyophilized to obtain bisphosphonic acids as the corresponding tetra-ammonium salt.

Inhibitor 3.19 (JDS-03-069): (2-(5-(1H-indazol-5-yl)-2-(thiophen-3-yl)pyridin-3-yl)ethane-1,1-diyl)diphosphonic acid, tetra-ammonium salt



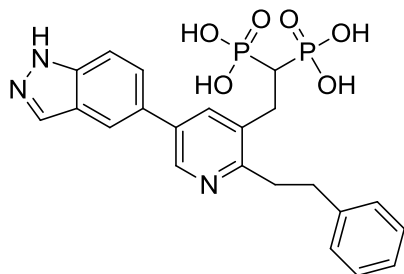
General method B; Isolated 17 mg (27%) as a white powder. ¹H NMR (500 MHz, D₂O) δ 8.55 (d, *J* = 2.1 Hz, 1H), 8.29 (m, 1H), 8.15 – 8.10 (m, 1H), 7.78 (dd, *J* = 8.8, 1.6 Hz, 1H), 7.73 – 7.70 (m, 1H), 7.65 (d, *J* = 8.7 Hz, 1H), 7.44 (dd, *J* = 4.9, 2.9 Hz, 1H), 7.37 (d, *J* = 5.0 Hz, 1H), 3.28 – 3.17 (m, 2H), 2.32 – 2.18 (m, 1H). ¹³C NMR (126 MHz, D₂O) δ 170.94, 151.16, 143.43, 139.62, 139.51, 137.11, 135.39, 134.59, 129.76, 128.98, 126.63, 125.76, 125.48, 122.95, 119.08, 110.92, 28.57. ³¹P NMR (81 MHz, D₂O) δ 18.96. MS (ESI): calcd 464.02, found 464.1 [M-H][−]

Inhibitor 3.20 (JDS-03-082): (2-(5-(1H-pyrazol-4-yl)-2-(thiophen-3-yl)pyridin-3-yl)ethane-1,1-diyl)diphosphonic acid



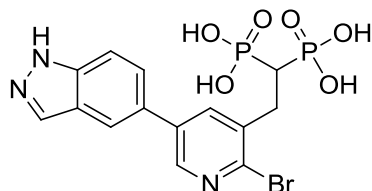
General method A; Isolated 12.3 mg (45%) as a yellow powder. ^1H NMR (500 MHz, D_2O) δ 8.40 (s, 1H), 8.12 (s, 1H), 8.02 (s, 2H), 7.63 (s, 1H), 7.37 (dd, $J = 4.9, 2.9$ Hz, 1H), 7.29 (d, $J = 4.0$ Hz, 1H), 3.14 (d, $J = 16.7$ Hz, 2H), 2.19 – 2.12 (m, 1H). ^{13}C NMR (126 MHz, D_2O) δ 151.15, 142.08, 139.87, 135.17, 132.13, 131.79, 129.03, 128.86, 127.00, 125.80, 125.52, 118.33, 45.29, 29.52, 29.04, 28.47, 29.01 (t, $J = 65.8$ Hz ^{31}P NMR (81 MHz, D_2O) δ 19.12. MS (ESI): calcd 414.0079, found 414.0 $[\text{M}-\text{H}]^-$

Inhibitor 3.28 (JDS07-067): (2-(5-(1H-indazol-5-yl)-2-phenethylpyridin-3-yl)ethane-1,1-diyl)diphosphonic acid



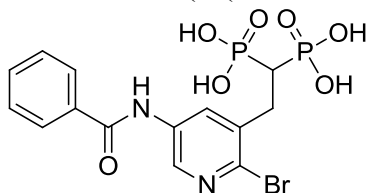
Method A; Isolated 7.7 mg (63%) as a pale yellow powder. ^1H NMR (500 MHz, d_2o) δ 8.46 (s, 1H), 8.19 (s, 1H), 8.16 (s, 1H), 8.10 (s, 1H), 7.78 (d, $J = 8.4$ Hz, 1H), 7.71 (d, $J = 8.6$ Hz, 1H), 7.39 – 7.30 (m, 4H), 7.27 (t, $J = 6.6$ Hz, 1H), 3.36 – 3.21 (m, 4H), 3.08 (t, $J = 7.3$ Hz, 2H), 2.30 (t, $J = 20.4$ Hz, 1H). ^{13}C NMR (75 MHz, D_2O) δ 157.10, 143.21, 141.81, 139.54, 136.97, 136.41, 134.59, 134.03, 130.30, 128.77, 128.39, 126.73, 125.92, 122.99, 118.97, 110.96, 35.29, 34.78, 27.90. HSQC ^1H - ^{13}C : ^1H δ 2.30 correlates with ^{13}C δ 40.58 ^{31}P NMR (81 MHz, d_2o) δ 17.75 (s).

JDS-04-072: (2-(2-bromo-5-(1H-indazol-5-yl)pyridin-3-yl)ethane-1,1-diyl)diphosphonic acid



General method A; Isolated 22 mg (34%) as a white powder. ^1H NMR (500 MHz, D_2O) δ 8.33 (d, $J = 2.4$ Hz, 1H), 8.20 – 8.14 (m, 2H), 8.08 (s, 1H), 7.74 (dd, $J = 8.7, 1.6$ Hz, 1H), 7.69 (d, $J = 8.8$ Hz, 1H), 3.25 (td, $J = 13.8, 6.8$ Hz, 2H), 2.52 – 2.40 (m, 1H). ^{13}C NMR (126 MHz, D_2O) δ 144.72, 140.96, 139.59, 139.52, 139.10, 135.83, 134.66, 129.09, 126.67, 122.92, 119.46, 111.03, 38.62 (t, $J = 111.0$ Hz), 31.63. ^{31}P NMR (81 MHz, D_2O) δ 18.21. MS (ESI): calcd 459.95 and 461.94, found 460.1 and 462.0 $[\text{M}-\text{H}]^-$

JDS04-0131: (2-(5-benzamido-2-bromopyridin-3-yl)ethane-1,1-diyl)diphosphonic acid



Method A; Isolated 36 mg (89%) as a white powder. ^1H NMR (500 MHz, D_2O) δ 8.67 (d, $J = 2.4$ Hz, 1H), 7.96 (d, $J = 2.6$ Hz, 1H), 7.94 (d, $J = 7.3$ Hz, 1H), 7.69 (d, $J = 7.5$ Hz, 1H), 7.61 (t, $J = 7.7$ Hz, 2H), 3.26 (td, $J = 14.5, 7.6$ Hz, 2H), 2.44 (tt, $J = 20.9, 7.5$ Hz, 1H). ^{31}P NMR (81 MHz, D_2O) δ 18.08 (s).

3.8.2 *In vitro* Inhibition Assay for hFPPS:

Standard (M1) hFPPS enzymatic inhibition assay. All assays were run in triplicate using 40 ng of the human recombinant FPPS and 10 μ M of each substrate, GPP and IPP (3 H-IPP, 3.33 mCi/ mmol) in a final volume of 100 μ L buffer containing 50 mM Tris pH 7.7, 2 mM MgCl_2 , 0.5 mM TCEP, and 20 μ g/mL BSA. Assays run with a 10 min pre-incubation period, the enzyme and inhibitor were incubated in the assay buffer in a volume of 80 μ L at 37 °C for 10 min. After 10 min, the substrates were added to start the reaction and also bring the inhibitor and substrate to the desired final concentrations. For assays run without pre-incubation, the reaction was started with the addition of enzyme to the mixture of inhibitor and the two substrates. After addition of all substrates, all assays were incubated at 37°C for 20 min. Assays were terminated by the addition of 200 μ L of HCl/methanol (1:4) and incubated for 10 min at 37 °C. The assay mixture was then extracted with 700 μ L of ligroin (in order to separate reaction products from unused substrate), dried through a plug of anhydrous Mg_2SO_4 and 300 μ L of the dried ligroin phase was combined with 8 mL of scintillation cocktail. The radioactivity was then counted using a Beckman Coulter LS6500 liquid scintillation counter.

Reagents for Enzymatic assay:

Ligroin was purchased from Sigma Aldrich, liquid scintillation cocktail was purchased from MP Biomedicals: Ecolite (#882475), 3 H-IPP was purchased from American Radiolabeled Chemicals (ART 0377A: 1mCi/mL, 60Ci/mmol in 0.1M Tris pH7.5), unlabeled IPP and GPP were purchased from Isoprenoids, Lc. as their ammonium salts.

hFPPS solution: The hFPPS enzyme was stored at -80°C as a 2 μ g/ μ L solution in the eluent buffer (50 mM HEPES pH 7.5, 500 mM NaCl, 250 mM imidazole, 5% glycerol, 0.5 mM TCEP).

IPP-solution: 3 H-IPP was diluted with IPP to a specific activity of 33 mCi/ mmol and 100 μ M concentration in 1 mM Tris pH 7.7. It was stored at -10°C, warmed to 0°C and kept on ice during assay setup.

GPP-solution: GPP was dissolved and diluted to a 100 μ M concentration in 1 mM Tris pH 7.7. It was stored at -10°C, warmed to 0°C and kept on ice during assay setup.

3.8.3 *In vitro* Inhibition Assay for hGGPPS:

The assay was based on literature procedure (see below). All assays were run in triplicate using 80 ng of the human recombinant GGPPS and 10 μ M of each substrate, FPP and IPP (3 H-IPP, 3.33 mCi/ mmol) in a final volume of 100 μ L buffer containing 50 mM Tris pH 7.7, 2 mM $MgCl_2$, 1 mM TCEP, 5 μ g/mL BSA and 0.2% Tween 20. Assays run with a 10 min pre-incubation period, the enzyme and inhibitor were incubated in the assay buffer in a volume of 80 μ L at 37°C for 10 min. After 10 min, the substrates were added to start the reaction and also bring the inhibitor and substrate to the desired final concentrations. For assays run without pre-incubation, the reaction was started with the addition of enzyme to the mixture of inhibitor and the two substrates. After addition of all substrates, all assays were incubated at 37°C for 40 min. Assays were terminated by the addition of 200 μ L of HCl/methanol (1:4) and incubated for 10 min at 37°C. The assay mixture was then extracted with 700 μ L of ligroin (in order to separate reaction products from unused substrate), dried through a plug of anhydrous Mg_2SO_4 and 300 μ L of the dried ligroin phase was combined with 8 mL of scintillation cocktail. The radioactivity was then counted using a Beckman Coulter LS6500 liquid scintillation counter.

hGGPPS solution: The hGGPPS enzyme was stored at -80°C as a 8 μ g/ μ L solution in the eluent buffer (50 mM HEPES pH 7.5, 500 mM NaCl, 250 mM imidazole, 5% glycerol, 0.5 mM TCEP).

IPP-solution: 3 H-IPP was diluted with IPP to a specific activity of 33 mCi/ mmol and 100 μ M concentration in 10 mM Tris pH 7.7. It was stored at -10°C, warmed to 0°C and kept on ice during assay setup.

FPP-solution: FPP was dissolved and diluted to a 100 μ M concentration in 10 mM Tris pH 7.7. It was stored at -10°C, warmed to 0°C and kept on ice during assay setup.

Literature reference:

The Crystal Structure of Human Geranylgeranyl Pyrophosphate Synthase Reveals a Novel Hexameric Arrangement and Inhibitory Product Binding

Kavanagh, K. L.; Dunford, J. E.; Bunkoczi, G.; Russell, R. G. G.; Oppermann, U. *J. Bio. Chem.* **2006**, 281, 22004.

4 X-ray crystallography: SAR and revised binding mode

4.1 Preface

All the work presented in this chapter has been published in the following manuscript:

“Design and Synthesis of Active Site Inhibitors of the Human Farnesyl Pyrophosphate Synthase: Apoptosis and Inhibition of ERK Phosphorylation in Multiple Myeloma Cells”

Lin, Y.-S.; Park, J.; De Schutter, J.W.; Huang, X.-F.; Berghuis, A.; Sebag, M.; Tسانtrizos, Y.S., *J. Med. Chem.* **2012**, *55*, 3201-3215

All 2-aminopyridine based inhibitors (i.e. scaffold **4.2**, **Figure 4.1**) were synthesized and tested for their *in vitro* activity by Yih-Shyan Lin (a PhD student in Prof. Tسانtrizos’ research group). Yih-Shyan Lin and Dr. Jaeok Park (a post-doctoral fellow in Prof. Berghuis’ research group) together expressed and purified all the protein used for enzymatic assay and crystallography studies. Dr. Jaeok Park performed all the X-ray diffraction acquisition and analysis work. Ms. Xian Fang Huang (a research assistant in Dr. Sebag’s laboratory) performed all the anti-proliferation assays on multiple myeloma cells. I performed the computational work and the synthesis and enzymatic evaluation of new pyridine-3-bisphosphonate based inhibitors.

4.2 Synthesis and enzymatic activity of bisphosphonic acids with different α -substituents

4.2.1 2-aminopyridine bisphosphonates

In parallel to our work on α -fluoro bisphosphonates **4.1**, a library of ~30 analogs of 2-aminopyridine based bisphosphonates **4.2** were synthesized (**Figure 4.1**). Similar to the SAR established in chapter 2, it was found that *meta*-substitution between the bisphosphonate moiety and R-group on the pyridine core was preferred. Furthermore, substitution at the C-4 position of the pyridine ring was found to be more favourable than at the C-6 position of the 2-aminopyridine core.

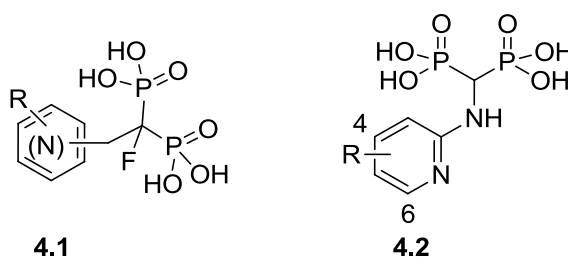


Figure 4.1: Comparison of pyridine scaffolds of novel inhibitors

The 5-indazole analog **4.3** was found to exhibit an IC_{50} of 430 nM against hFPPS (**Figure 4.2**). Surprisingly, truncation to corresponding phenyl analog led to a 3-fold increase in potency (**4.3** vs. **4.4**). Exploration of different substituents on the phenyl ring led to the discovery that ether moieties at the *para*-position significantly increased potency, with the isopropoxyl-derivative **4.5** being ~5-fold more potent than the parent phenyl inhibitor **4.4**. Although attachments of larger carbocycles on the ether oxygen (e.g. analogs **4.6** and **4.7**) did not improve the *in vitro* potency of the compounds, we assumed that the increased lipophilicity may have a positive effect on cell membrane permeability and improve the cell-based potency of these inhibitors.

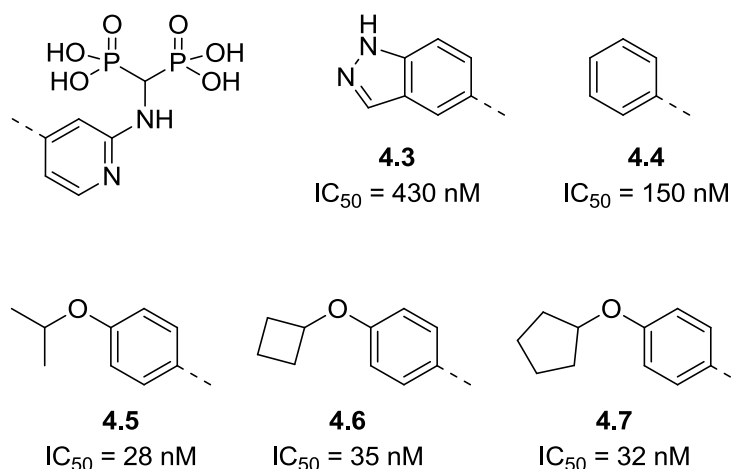


Figure 4.2: SAR of 2-aminopyridine bisphosphonates for hFPPS

4.2.2 Synthesis:

Based on the data obtained from the first generation α -fluoro-5-Het-pyridine-3-bisphosphonates (described in Chapter 2; **4.8**, **Figure 4.3**) and our subsequent SAR studies on the 2-aminopyridine based inhibitors **4.9**, we set out to compare the two pyridine scaffolds and explore the effect of C α -substituents. Previously, the removal of the C α -hydroxyl group from risedronate (to the corresponding C α -H) was found to result in approximately an 8-fold loss in potency.¹ We postulated that the larger heterocyclic sidechains of our inhibitors (as compared to the unsubstituted pyridine ring of risedronate) may contribute sufficiently to the overall binding affinity to compensate for loss of the C α -hydroxyl moiety.

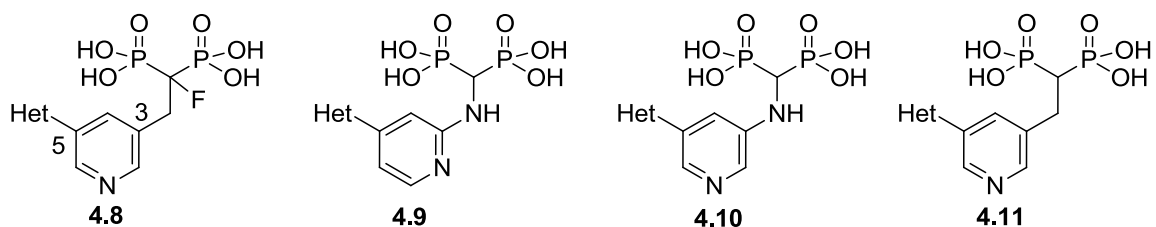
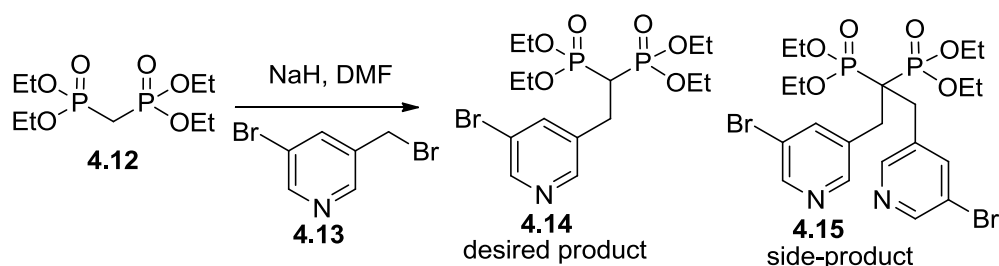


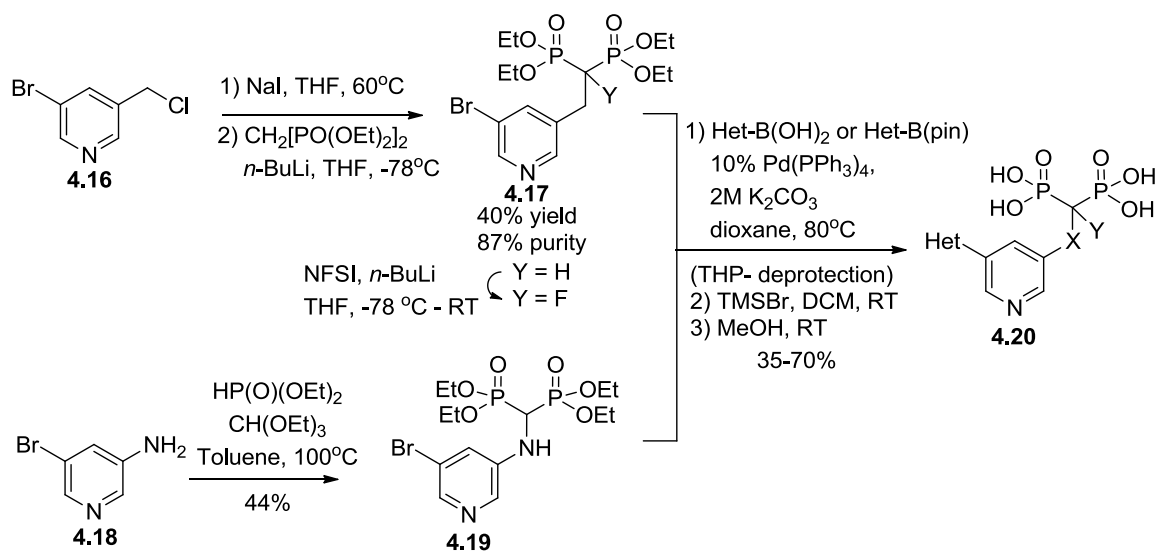
Figure 4.3: Novel pyridine scaffold for bisphosphonate inhibitors

The synthesis of the desired analogs was slightly modified from protocols described in Chapters 2 and 3 (**Scheme 4.1**). The bisphosphonate moiety was introduced as the tetraethyl protected ester, allowing the final deprotection under milder conditions using TMSBr/MeOH at room temperature (as opposed to 6M HCl at 100°C). As previously mentioned, bis-alkylation at C α and chemical instability of the benzylic bromide **4.13** were found to hinder synthetic efforts and result in poor reproducibility. The latter issue could be avoided by making the corresponding benzylic chloride **4.16** and converting it to the iodide *in situ*, immediately prior to the alkylation (**Scheme 4.2**). However, bis-alkylation was also observed under these reaction conditions. In cases where the desired product **4.17** was contaminated with both the tetraethyl methylenebis(phosphonate) starting material **4.12** and the bis-alkylated side product **4.15**, the mixture was dissolved in toluene and washed repeatedly with water to eliminate **4.12** and furnish the desired product in ~90% purity as determined by ^{31}P -NMR. The remaining bis-alkylated side-product was later eliminated in the subsequent Suzuki cross-coupling reactions.

Precursor **4.19** could readily be accessed through standard condensation with triethyl orthoformate and diethylphosphite with the commercial 5-bromopyridin-3-amine **4.18**, although it was found necessary to lower the temperature to 100°C as significant decomposition was observed at 120°C. Next, the desired heterocyclic substituents were attached via Suzuki cross-coupling in moderate yields and, for THP-protected boronate coupling partners, the protecting group was removed under acidic conditions (0.1 M HCl, EtOH, 80°C). Finally, the desired bisphosphonic acids were obtained under standard deprotection conditions with TMSBr, followed by MeOH.



Scheme 4.1: Synthesis issues with tetraethyl methylenebis(phosphonate) and 3-bromo-5-(bromomethyl)pyridine



Scheme 4.2: Improved synthetic route towards 5-Het-pyridine-3-bisphosphonates with varying α -substituents

4.3 hFPPS/4.5 co-crystal X-ray structure

Previous crystallographic studies have shown a three stage conformational change to the hFPPS active site: (1) the “open” unoccupied conformation, (2) the “semi-closed” state formed upon binding of 3 Mg^{2+} ions and an *N*-BP inhibitor in the allylic (DMAPP/GPP) sub-pocket and (3) the “fully closed” active site observed upon additional co-binding of IPP (*e.g.* ternary complex of hFPPS/IPP/ZOL; PDB 1ZW5).^{2,3} The fully closed form involves substantial movement and folding of the C-terminal tail of the protein over the enzyme-bound IPP substrate. The C-terminal basic residues ³⁶⁴KRRK³⁶⁷ are known to be essential for catalysis and play an important role in the conformational changes of the enzyme.⁴ During the catalytic cycle, the fully closed form may be required to shield the intermediate carbocation from bulk water, whereas the open or half-closed forms may facilitate substrate binding and product release.⁵

Our original *in silico* docking results, performed in the fully closed hFPPS conformation (PDB 1ZW5), predicted that the pyridine core of **4.5** would bind in a $\sim 90^\circ$ angle relative to the enzyme-bound zoledronate, placing the 4-isopropoxyphenyl moiety into the IPP sub-pocket (**Figure 4.4**, compare panels **a** and **b**). Similar results were also obtained from docking studies using the “half closed” active site (PDB 1YV5), suggesting that the larger side chain of **4.5** would forbid binding in the allylic sub-pocket alone, without imposing a significant conformational rearrangement to the protein structure. Inhibitor **4.5** was selected for crystallization efforts and a co-crystal structure with hFPPS was obtained at a resolution of 1.85 Å (PDB 4DEM). In contrast to the docking results, the X-ray diffraction data revealed that the inhibitor binds far deeper into the allylic sub-pocket than either zoledronate or risedronate (**Figure 4.6**). Instead of a bifurcated hydrogen bond with Lys 200 and Thr 201, **4.5** forms a water mediated H-bond between the pyridine nitrogen and Gln 254 (**Figure 4.6b**, **Figure 4.9a**). Most interestingly, binding of **4.5** causes a displacement of the capping phenyl 113 and Gln 185, by 1.2 Å and 2.2 Å, respectively (**Figure 4.5b**). This conformational change of the protein allows the 4-isopropoxyphenyl moiety of **4.5** to insert between Phe 113 and the side-chain amide of Gln 185 and to engage in π -stacking interactions with these residues.⁶ This movement opens the allylic sub-pocket to bulk solvent (**Figure 4.5a**).

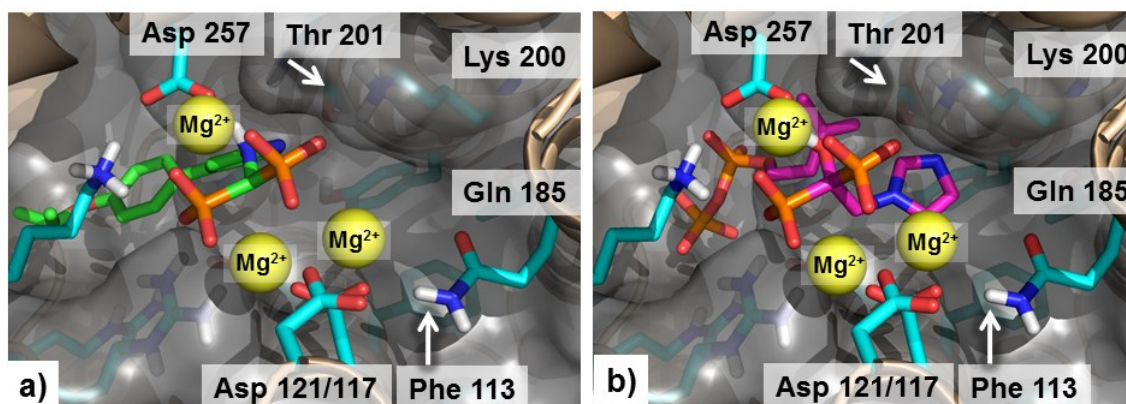


Figure 4.4: (a) Docking output pose for **4.5** in computational model of hFPPS/ZOL/IPP complex (panel b, PDB 1ZW5). Protein secondary structure is depicted in beige, protein surface is rendered semitransparent with residues covering the active site removed for clarity. Key active site residues are shown in stick form (cyan backbone) as well as ligands: IPP (magenta), zoledronate (magenta), **4.5** (green)

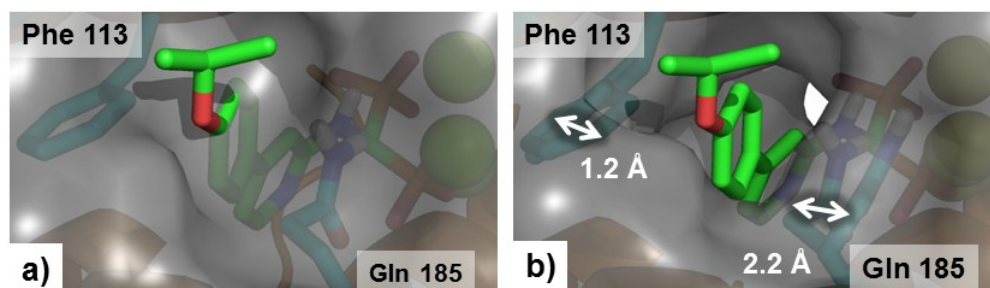


Figure 4.5: (a) Superposition of inhibitor **4.5** binding mode (PDB 4DEM) in the computational model of hFPPS/ZOL/IPP complex (PDB 1ZW5); (b) Superposition of hFPPS/**4.5** crystal structure with Phe 113 and Gln 185 from hFPPS/Zol/IPP complex (PDB 1ZW5); the corresponding shifts are indicated in white arrows with distances in Å.

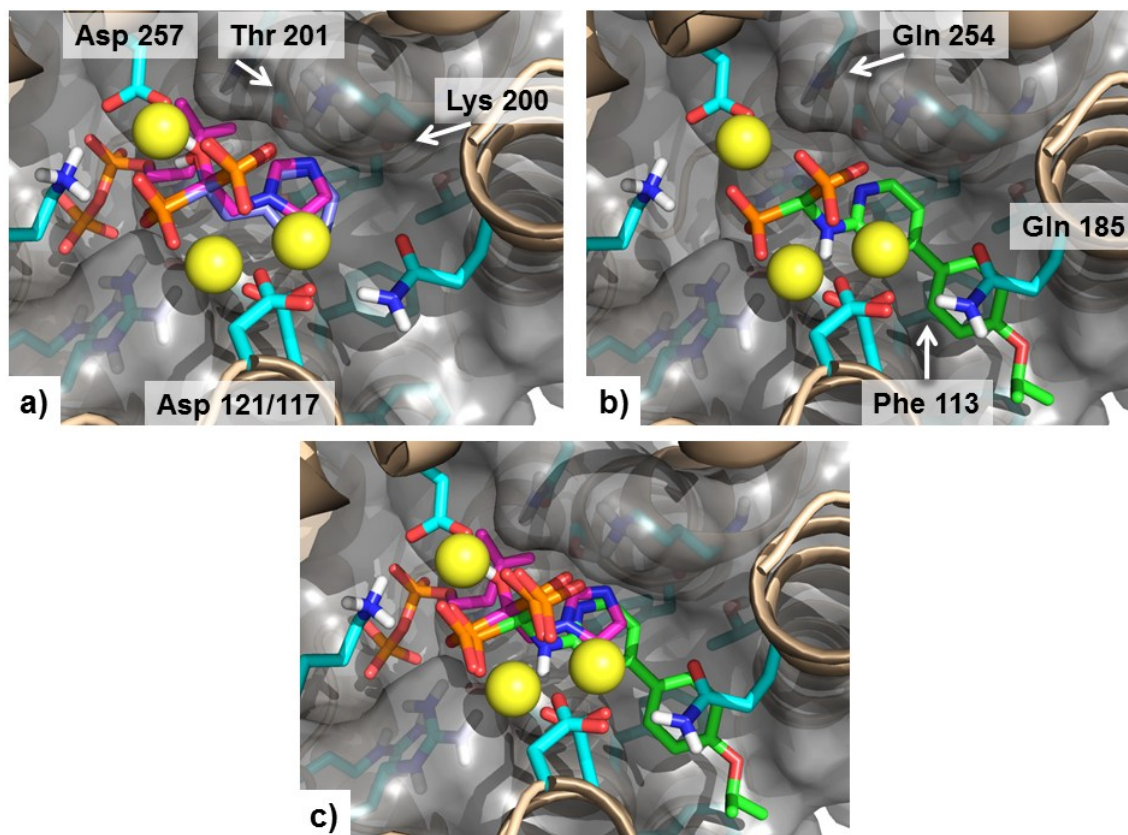


Figure 4.6: (a) Superimposed structures of hFPPS/ZOL/IPP (PDB 1ZW5) and hFPPS/RIS (PDB 1YV5) (b) hFPPS/4.5 (PDB 4DEM) (c) superposition of PDB 1ZW5, 1YV5 and 4DEM. Protein secondary structure is depicted in beige, protein surface is rendered semitransparent with residues covering the active site removed for clarity. Key active site residues are shown in stick form (cyan backbone) as well as ligands: IPP (magenta), zoledronate (magenta), risedronate (blue) and 4.5 (green)

Our previous ^1H NMR line broadening studies indicated that inhibitor **2.22** competes for binding with both IPP and risedronate (Chapter 2), a likely explanation for this apparent conflict with the crystallography data may be that, at high molar excess, the weak affinity of IPP substrate for the allylic sub-pocket⁷ is sufficient to displace protein-bound **2.22**. A complementary DSF experiment will be described in chapter 8. It should be noted that docking of inhibitor **4.5** into a computational model based on its corresponding crystal structure (PDB 4DEM, so-called “self-docking”) generated the correct binding mode, as observed by X-ray diffraction. This demonstrates that although the docking itself is a valid

methodology, the output is inherently biased towards the structural information used for the computational model. As a result, *in silico* predictions are not reliable if significant modifications are made to the ligands as this can cause large protein conformational changes which were not accounted for in our docking studies.⁸ In hindsight, careful analysis of published hFPPS X-ray data revealed similar solvent-exposed allylic pocket conformations (i.e shifted Phe 113 and Gln 185) are adopted in four other hFPPS co-crystal complexes with *N*-BP inhibitors (PDB 3OPM, 3OPN, 2F94 and 3RYE; see Appendix I for a detailed list). Since our *original* design concept was to extend the inhibitors to occupy the IPP-sub-pocket, these four crystal structures were not considered.

4.4 SAR and cell based anti-proliferation activity

4.4.1 SAR:

The *in vitro* potency of inhibitors having the same Het-substituent and either the pyridine-3-bisphosphonate (**4.8**) or the 2-aminopyridine (**4.9**) core was essentially the same in inhibiting hFPPS (**Figure 4.7**). This may be due to the fact that the pyridine nitrogen can form a hydrogen bond with active residues of hFPPS, regardless of its relative position to the bisphosphonate moiety. As mentioned earlier, 2-aminopyridine based analog **4.5** forms a water mediated hydrogen bond with the sidechain carbonyl Gln 254 (**Figure 4.9a**), whereas pyridine-3-bisphosphonate analogs can most likely make a bifurcated hydrogen bond with Lys 200 and Thr 201, similar to risedronate and zoledronate (**Figure 4.9b**).

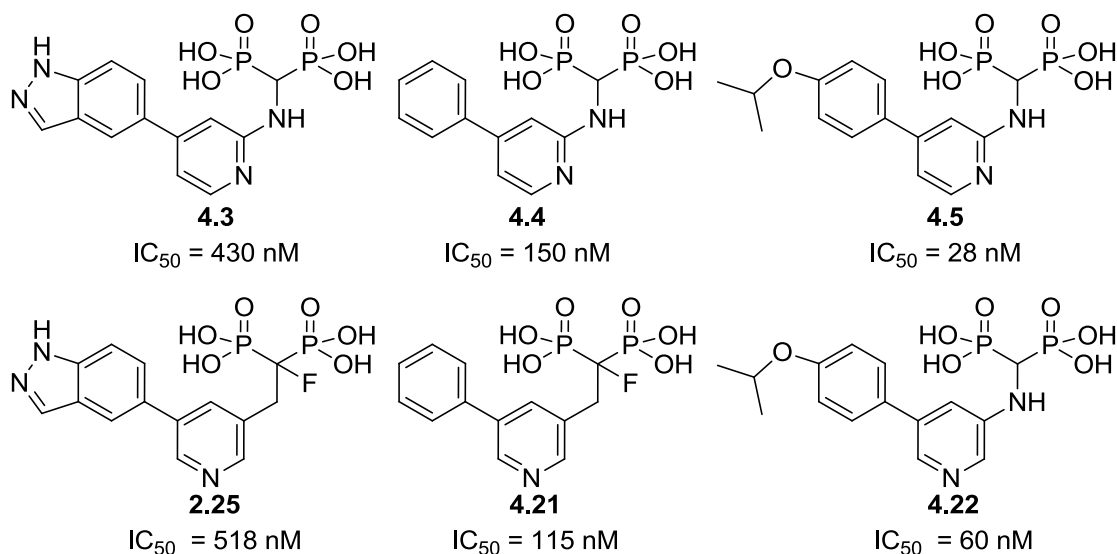


Figure 4.7: Enzymatic activity comparison of different pyridine cores

Removing the α -fluorine results in only a minimal loss (~30%) in enzymatic activity against hFPPS (**4.21** vs. **4.23**, **Figure 4.8**), an improvement over the 3-fold loss potency observed for the unsubstituted risedronate scaffold (**Table 2.1**, Chapter 2). This suggests that even a simple phenyl substituent significantly contributes to the binding affinity and reduces the dependence on the bisphosphonate moiety. Surprisingly, introducing an amine-linker between the pyridine core and the bisphosphonate resulted in a 3-fold increase in

enzymatic potency (**4.23** vs **4.24**). This observation may be attributed to the rigidification of the molecule: the exocyclic nitrogen can delocalize its free electron pair into the pyridine aromatic system and adopt an sp^2 hybridization in this resonance form. This enforces a more planar conformation, which closely resembles the bio-active conformation, in which the bisphosphonate C α is almost co-planar with the pyridine core (**Figure 4.10**). Thus a smaller entropy penalty is incurred to bind appropriately in the hFPPS active site and the enzymatic potency is increased.

It should be noted that none of the inhibitors presented in this chapter showed any significant activity against hGGPPS at 10 μ M (data not shown).

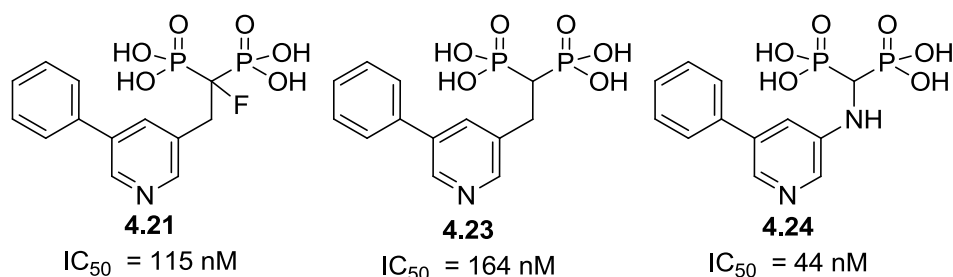


Figure 4.8: hFPPS activity data for bisphosphonate with varying α -substituents

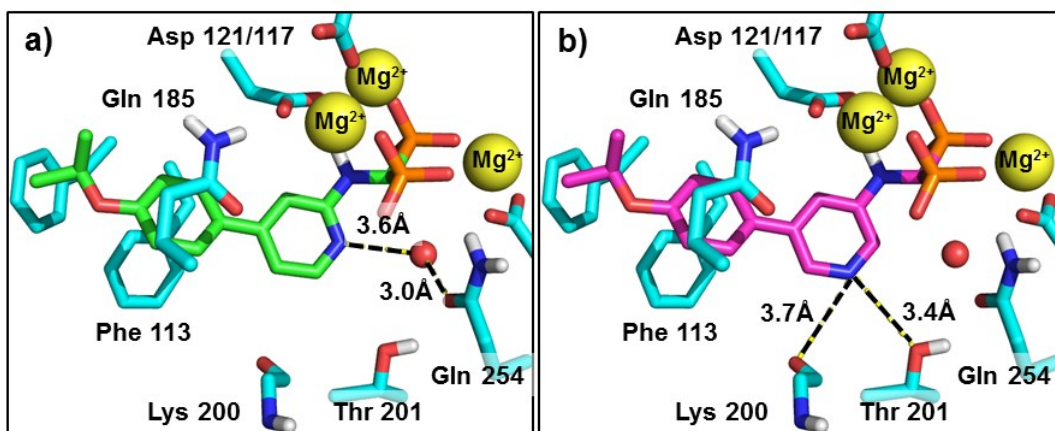


Figure 4.9: (a) water mediated hydrogen bond (dashed lines) between inhibitor **4.5** (green) and Gln 254 (PDB 4DEM); (b) docking output pose of **4.22** (magenta) in the computation model of hFPPS/**4.5** coordinates

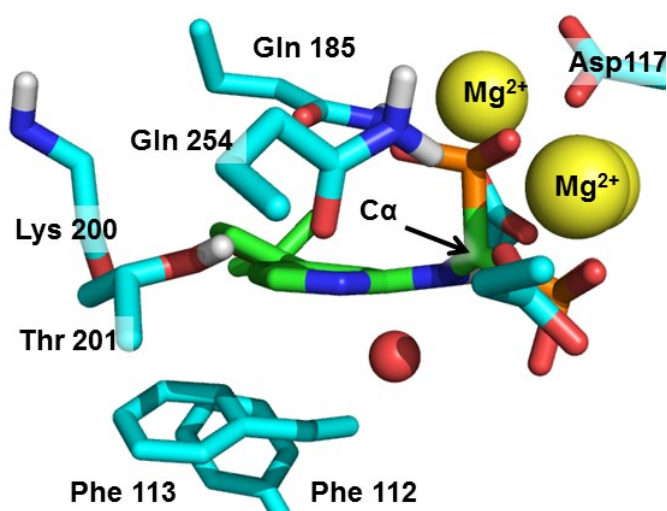


Figure 4.10: Side view of hFPPS/**4.5**, demonstrating the planarity of bio-active conformation (PDB 4DEM)

4.4.2 Antiproliferation activity in MM cell lines

We hypothesized that the increased lipophilicity of **4.5** and analogs with larger carbocycles **4.6** and **4.7** would help cell membrane permeability and improve cell-based potency. Commonly, the calculated logP (clogP) is used as a parameter to estimate the ability of compounds to penetrate cell membranes; statistical analysis of commercial drugs shows that the clogP generally lies between -0.4 to 5.6, with an average of 2.5.⁹ Standard computational methods calculate the clogP of molecules as a weighted average of fragments with experimentally determined logP's. However, phosphonates are not included in the database of programs we have access to,¹⁰ consequently, clogP calculation for this class of bisphosphonic acids are unreliable. Therefore it was decided to use the summed surface area of polar (i.e. O, N) *versus* non-polar (C, CH, CH₂, ...) atom types in our molecules as a comparative measure of lipophilicity. QikProp (a program included in the commercial Maestro computational suite)¹¹ automatically segregates these surface areas by atom type and the SASA (Solvent Accessible Surface Area) and FOSA (Hydrophobic component of SASA) were selected for the purpose of estimating the relative lipophilicity of our compounds (**Table 4.1**, values are given in Å² and calculated using a 1.4 Å radius probe).

Compared to the commercial drugs zoledronate and risedronate, inhibitors **4.5-4.7** have ~3- to ~8-fold reduced enzymatic potency but a significantly increased lipophilic surface area (FOSA/SASA: 6% for risedronate vs. 32% for **4.7**). Therefore, inhibitor **4.7** was selected for further biological evaluation and its anti-proliferation effects were assessed in three multiple myeloma cell lines. Despite the lower enzymatic potency, **4.5** showed consistent improved cell-based potency (albeit modest), suggesting that the higher lipophilicity may be helping cell membrane permeability, thus increasing the intracellular concentration of the compound.

Compound	hFPPS IC ₅₀ (nM)	Predicted Physicochemical Properties		Multiple Myeloma cells EC ₅₀ (μM)		
		SASA	FOSA	JJN3	RPMI- 8226	KMS 28PE
ZOL	4.1	400	23	9.4	10.5	6.4
RIS	11	410	24	10.0		10.6
4.5	28	580	110			
4.6	35	630	180			
4.7	32	680	220	8.6	3.6	3.2

Table 4.1: Enzymatic inhibition data, predicted physiochemical parameters and anti-proliferation activity data and of key analogs from our library of novel hFPPS inhibitors

4.5 Conclusions and outlook

In summary, a library of ~40 compounds was synthesized and tested for their *in vitro* activity in inhibiting hFPPS selectively over hGGPPS. This led to the identification of inhibitors with significantly improved potency (IC_{50} ~30 nM) including **4.7**. This compound was also found to inhibit the proliferation of three multiple myeloma cell lines with equivalent or better potency than the drug zoledronate, in spite its ~8-fold lower *in vitro* activity. Furthermore, a co-crystal structure of inhibitor **4.5** bound to the active site of hFPPS was obtained at a resolution of 1.85 Å (PDB 4DEM). This structural data was a breakthrough for our research, as it showed occupation exclusively in the allylic sub-pocket. The larger sidechains of our novel inhibitors were accommodated by a conformational shift of the Phe 113 and Gln 185 residues, which was not accounted for in our previous, rigid computational model. SAR data of the key analogs revealed that an amine moiety between the pyridine core and the bisphosphonate is strongly preferred, most likely due to rotational constraint resulting in a favored planar conformation similar to the bio-active conformation. Furthermore, the pyridine nitrogen can be positioned either *ortho* or *meta* to the bisphosphonate moiety without affecting enzymatic potency, as hydrogen bonding opportunities are available at both sites.

4.6 References

- (1) Marma, M. S.; Xia, Z.; Stewart, C.; Coxon, F.; Dunford, J. E.; Baron, R.; Kashemirov, B. A.; Ebetino, F. H.; Triffitt, J. T.; Russell, R. G. G.; McKenna, C. E.; Synthesis and Biological Evaluation of α -Halogenated Bisphosphonate and Phosphonocarboxylate Analogues of Risedronate *J. Med. Chem.* **2007**, *50*, 5967.
- (2) Rondeau, J.-M.; Bitsch, F.; Bourgier, E.; Geiser, M.; Hemmig, R.; Kroemer, M.; Lehmann, S.; Ramage, P.; Rieffel, S.; Strauss, A.; Green, J. R.; Jahnke, W.; Structural Basis for the Exceptional in vivo Efficacy of Bisphosphonate Drugs *ChemMedChem* **2006**, *1*, 267.
- (3) Dunford, J. E.; Kwaasi, A. A.; Rogers, M. J.; Barnett, B. L.; Ebetino, F. H.; Russell, R. G. G.; Oppermann, U.; Kavanagh, K. L.; Structure–Activity Relationships Among the Nitrogen Containing Bisphosphonates in Clinical Use and Other Analogues: Time-Dependent Inhibition of Human Farnesyl Pyrophosphate Synthase *J. Med. Chem.* **2008**, *51*, 2187.
- (4) Song, L.; Poulter, C. D.; Yeast farnesyl-diphosphate synthase: site-directed mutagenesis of residues in highly conserved prenyltransferase domains I and II *Proc. Natl. Acad. Sci. U.S.A.* **1994**, *91*, 3044.
- (5) Hosfield, D. J.; Zhang, Y.; Dougan, D. R.; Broun, A.; Tari, L. W.; Swanson, R. V.; Finn, J.; Structural Basis for Bisphosphonate-mediated Inhibition of Isoprenoid Biosynthesis *J. Bio. Chem.* **2004**, *279*, 8526.
- (6) Salonen, L. M.; Ellermann, M.; Diederich, F.; Aromatic Rings in Chemical and Biological Recognition: Energetics and Structures *Angew. Chem. Int. Ed.* **2011**, *50*, 4808.
- (7) Kavanagh, K. L.; Guo, K.; Dunford, J. E.; Wu, X.; Knapp, S.; Ebetino, F. H.; Rogers, M. J.; Russell, R. G. G.; Oppermann, U.; The molecular mechanism of nitrogen-containing bisphosphonates as antiosteoporosis drugs *Proc. Natl. Acad. Sci. U.S.A.* **2006**, *103*, 7829.
- (8) Halgren, T. A.; Murphy, R. B.; Friesner, R. A.; Beard, H. S.; Frye, L. L.; Pollard, W. T.; Banks, J. L.; Glide: A New Approach for Rapid, Accurate Docking and Scoring. 2. Enrichment Factors in Database Screening *J. Med. Chem.* **2004**, *47*, 1750.
- (9) Ghose, A. K.; Viswanadhan, V. N.; Wendoloski, J. J.; A Knowledge-Based Approach in Designing Combinatorial or Medicinal Chemistry Libraries for Drug Discovery. 1. A Qualitative and Quantitative Characterization of Known Drug Databases *J. Comb. Chem.* **1998**, *1*, 55.
- (10) Hirabayashi, H.; Sawamoto, T.; Fujisaki, J.; Tokunaga, Y.; Kimura, S.; Hata, T.; Relationship Between Physicochemical and Osteotropic Properties of Bisphosphonic Derivatives: Rational Design for Osteotropic Drug Delivery System (ODDS) *Pharma Res.* **2001**, *18*, 646.
- (11) Ioakimidis, L.; Thoukydidis, L.; Mirza, A.; Naeem, S.; Reynisson, J.; Benchmarking the Reliability of QikProp. Correlation between Experimental and Predicted Values *QSAR & Comb. Sci.* **2008**, *27*, 445.

4.7 Experimental

4.7.1 Docking studies

Computational studies: All calculations were performed using the Schrödinger suite: Maestro (version 9.0), Glide (version 5.5), ConfGen, (version 2.1), LigPrep, (version 2.3), QikProp (version 3.2), Schrödinger, LLC, New York, NY, 2009.

All images were generated using PyMol (www.pymol.org)

Docking :

Protein Preparation: All crystal structures were downloaded directly from the PDB database and prepared using the Protein Preparation Wizard feature using standard parameters. The proteins were overlapped with the secondary structure alignment tool, using the hinge-region between Helix I and II as reference.

Docking Grid Generation: Three grids were generated using standard parameters, encompassing the two active site sub-pockets (*i.e.* binding sites of IPP and RIS or ZOL) from the hFPPS/RIS binary complex (PDB: 1YV5) and the hFPPS/IPP/ZOL ternary complex (PDB: 1ZW5), as well as the allosteric site from the hFPPS/IPP/FBS-04 ternary complex (PDB: 3N45).

For all protein structures the “rotatable OH-bonds” feature was enabled for the residues listed below:

1YV5 (hFPPS/RIS): Thr 77, Thr 215, Tyr 218, Ser 219

1ZW5 (hFPPS/IPP/ZOL): Thr 215, Tyr 218, Ser 219

3N45 (hFPPS/ZOL/FBS-04): Thr 63, Thr 201, Tyr 204, Ser 205

4DEM (hFPPS/YS04-70): Thr 77, Thr 215, Tyr 218, Ser 219

Docking:

All bisphosphonates were docked in their fully ionized (tetra-anion) forms, conformation libraries were generated using ConfGen (using the parameters: “standard” and “intermediate”; only input minimization) followed by LigPrep (retain original ionization

state; output tautomers). Docking was performed with Glide (5.5), flexible docking, extra precision (XP-mode), standard parameters.

Analysis: All output structures were visually inspected and poses that did not have the bisphosphonate moiety properly aligned to the Mg^{2+} -triad (as compared to the crystal structures of 1YV5 and 1ZW5) were rejected. In general, high conformational consistency of the output poses was observed. For example, for twenty docked poses of inhibitor **4.5** shown below (**Figure 4.11**), bound *in silico* to the fully closed active site (PDB 1ZW5), very high consistency was observed for the binding of the bisphosphonate moiety and the 2-aminopyridine core. The highest variability observed was in the binding orientations of the isopropyl side chain with a maximum range of 1.7 Å

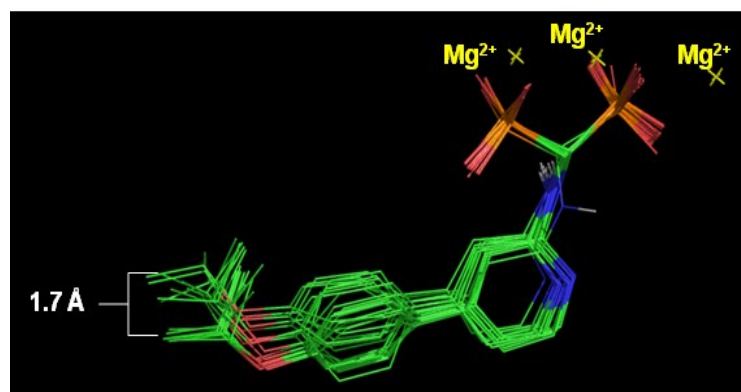


Figure 4.11: Example of output poses of inhibitor **4.5** docked to the fully closed active site (PDB 1ZW5)

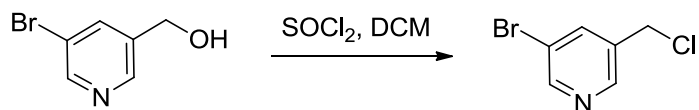
4.7.2 Synthesis

General: All intermediate compounds were purified by normal phase flash column chromatography on silica gel using a CombiFlash instrument and the solvent gradient indicated. The purified bisphosphonate tetra ester precursors of all final inhibitors were analyzed by reverse-phase HPLC and fully characterized by ^1H , ^{13}C and ^{31}P NMR, and MS. The homogeneity of the bisphosphonate tetra esters (>90%) was confirmed by C18 reversed phase HPLC. Quantitative conversion of each tetra ester to the corresponding bisphosphonic acid was confirmed by ^{31}P NMR. All final products were characterized by ^1H , ^{13}C , ^{31}P and ^{19}F NMR and HR-MS. Chemical shifts (δ) are reported in ppm relative to the internal deuterated solvent (^1H , ^{13}C) or external H_3PO_4 (δ 0.00 ^{31}P), unless indicated otherwise. High-Resolution MS spectra were recorded at the McGill University, MS facilities using electrospray ionization ($\text{ESI}^{+/-}$). The homogeneity of the final inhibitors was confirmed by HPLC, only samples with >95% homogeneity were tested in the enzymatic assays for the determination of IC_{50} values. HPLC Analysis was performed using a Waters ALLIANCE[®] instrument (e2695 with 2489 UV detector and 3100 mass spectrometer) and the corresponding traces can be found in Appendix III.

Synthesis of 4.20

(5-bromopyridin-3-yl)methanol: See Chapter 2

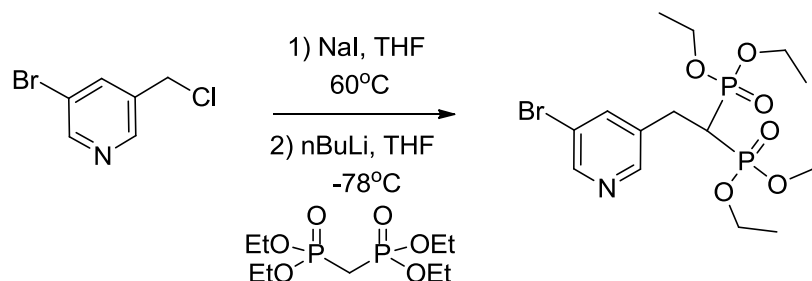
4.16: 3-Bromo-5-(chloromethyl)pyridine:



To an ice cold solution of (5-bromopyridin-3-yl)methanol (1.00 g, 5.35mmol) in an anhydrous DCM thionyl chloride (0.43 mL, 5.88 mmol, 1.1eq) was added via syringe and the mixture was stirred at RT for 3 h. The reaction was quenched with saturated aqueous NaHCO_3 (~10 mL), the product was extracted into DCM (3x25 mL), dried over anhydrous Na_2SO_4 and concentrated to dryness under vacuum to give the desired product as a pale yellow solid (1.09 g) in nearly quantitative yield and sufficiently pure to be used directly in

the next step without purification. ^1H NMR (400 MHz, CDCl_3) δ 8.64 (s, 1H), 8.54 (s, 1H), 7.90 (t, J = 2.1 Hz, 1H), 4.56 (s, 2H).

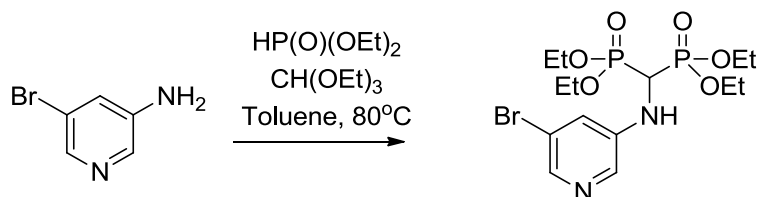
4.17 (JDS-04-025): tetraethyl (2-(5-bromopyridin-3-yl)ethane-1,1-diyl)bis(phosphonate)



To a solution of 3-bromo-5-(chloromethyl)pyridine (1 equivalent) in anhydrous THF, NaI (1.1 equivalent) was added and the suspension was stirred at 60 °C for 1.5 h to form the benzylic iodide. In a separate flask, a cooled solution (-78 °C) of tetraethyl methylenebis(phosphonate) (1equivalent) in anhydrous THF, *n*-BuLi (1.1 eq.) was added drop-wise under Argon. The mixture was stirred at 0 °C for 5 min and re-cooled to -78 °C. The benzylic iodide was then transferred to the solution of the tetraethyl methylenebis(phosphonate) anion via cannula. The reaction mixture was stirred at -78 °C for 1 h, and at RT for 6-12 h. Quenched with a drop of MeOH and concentrated under vacuum. The residue was dissolved in EtOAc and washed with H_2O , 0.3M aqueous $\text{Na}_2\text{S}_2\text{O}_3$ and brine. The EtOAc solution was dried over anhydrous Na_2SO_4 and purified by normal phase flash column chromatography on silica gel (silica was pre-washed with 0.1% NEt_3 in hexanes:EtOAc 3:1) using a CombiFlash instrument and a solvent gradient from 1% EtOAc in hexanes to 100% EtOAc and then to 10%MeOH in EtOAc. The isolated product was contaminated with some of the tetraethyl methylenebis(phosphonate) reagent. This mixture was re-dissolved in 100 mL toluene, washed with H_2O (5x10 mL) and brine, dried over anhydrous Na_2SO_4 and concentrated under vacuum to give the desired compound 37 as a clear oil, in 40% yield and 87% purity (estimated by ^{31}P -NMR). The impurity was determined to be the dialkylated byproduct, which was eliminated after the next step in the synthesis (Suzuki coupling). ^1H NMR (400 MHz, CDCl_3) δ 8.54 (s, 1H), 8.44 (s, 1H), 7.79 (s, 1H), 4.25 – 4.01 (m, 8H), 3.23 (td, J = 16.2, 6.4 Hz, 2H), 2.55 (tt, J = 23.7, 6.4 Hz, 1H), 1.39 – 1.24 (m, 12H). ^{13}C NMR (75 MHz, CDCl_3) δ 150.36, 148.93, 148.57, 141.53, 139.22, 62.79 (dd, J = 17.7, 6.9 Hz), 38.78 (t, J = 133.5 Hz), 28.40 (t, J =

4.8 Hz), 17.09 – 14.20 (m). ^{31}P NMR (81 MHz, CDCl_3) δ 23.05. MS (ESI): calcd 480.03 and 482.03, found 480.0 and 482.0 $[\text{M}+\text{Na}]^+$

4.19 (JDS05-102): tetraethyl (((5-bromopyridin-3-yl)amino)methylene)bis(phosphonate)



A 15 mL pressure vessel was charged with the 5-bromopyridin-3-amine (250 mg, 1.44mmol), diethyl phosphite (1.12 mL, 8.67 mmol), triethyl orthoformate (0.29 mL, 1.73 mmol) and dissolved in 3mL toluene. The reaction was stirred at 80°C for 18h, ^{31}P NMR showed only 10% conversion. The reaction was stirred another 14h at 100°C, Cooled down and concentrated in vacuo. The residue was purified by silica gel (silica was pre-washed with 0.1% NEt_3 in hexanes/EtOAc 3:1) chromatography on a CombiFlash instrument, using a solvent gradient from 1:3 EtOAc/Hexanes to 100% EtOAc and then to 25%MeOH in EtOAc. The product thus obtained was contaminated with ~10% of the mono-phosphonate analog, the mixture was purified by reverse phase chromatography on a CombiFlash instrument using a solvent gradient from 10% CH_3CN /water to 100% CH_3CN . Isolated the desired compound as an off-white powder (290 mg, 44%). ^1H NMR (400 MHz, DMSO-d_6) δ 8.26 (s, 1H), 7.85 (s, 1H), 7.59 (s, 1H), 6.44 (d, J = 10.8 Hz, 1H), 4.84 (td, J = 22.8, 10.7 Hz, 1H), 4.16 – 3.93 (m, 8H), 1.15 (dt, J = 20.7, 7.0 Hz, 12H). ^{13}C NMR (126 MHz, DMSO-d_6) δ 145.31 (t, J = 4.2 Hz), 138.10, 135.62, 121.06, 120.55, 63.08 (dt, J = 17.4, 3.1 Hz), 47.86 (t, J = 144.7 Hz), 16.66 (dt, J = 5.7, 2.8 Hz) ^{31}P NMR (81 MHz, DMSO-d_6) δ 17.22 (s). MS (ESI): calcd 459.04 and 461.04; found 459.2 and 461.2 $[\text{M}+\text{H}]^+$

General Suzuki coupling conditions:

Method A:

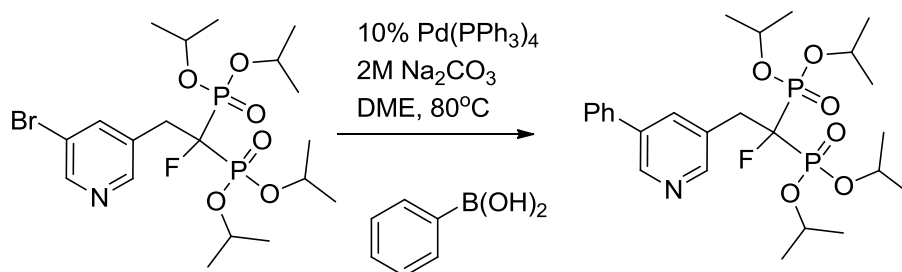
A 5 mL vial was charged with the aryl halide (1 equivalent), Pd(PPh₃)₄ or Pd(P[*t*-Bu]₃)₂ (0.1 equivalent), a stir bar and the boron-coupling partner (1.2 equivalents) if a solid. The vial was capped with a rubber septum, evacuated and back-filled with Argon; anhydrous DME or 1,4-dioxane was added via syringe to bring the final concentration of aryl halide to 0.1M and the solution was flushed with Argon. At this point the boron-coupling partner, if not at solid, was added as a solution in DME or 1,4-dioxane. 2M Na₂CO₃ or K₂CO₃ solution (2.5 equivalents) was added and the vial was flushed again with Argon. The reaction vessel was equipped with an Argon-filled balloon and stirred at 80°C until complete consumption of starting material. The reaction mixture was cooled down, diluted with EtOAc and filtered through a plug of Celite, rinsed three times with EtOAc/MeOH 1:1. The filtrate concentrated in vacuo and purified by normal phase column chromatography on silica gel (silica gel was pre-treated with 1% NEt₃ in hexanes/EtOAc in a 3:1 ratio) using a gradient from 100% hexanes to 100% EtOAc and then to 25% MeOH.

Method B:

A 0.5-2 mL microwave reaction vessel was charged with a magnetic stir bar, boronic acid (1.5 equivalents) and Pd(PPh₃)₄ (0.1 equivalent); capped with a septum, degassed and flushed with Argon. The aryl bromide was added as a solution in dioxane *via* syringe and the vessel again degassed and flushed with Argon. A solution of 2M K₂CO₃ (2.5 equivalents) was added and the mixture was again degassed and flushed with Argon. The rubber septum was replaced by a Teflon lined seal, under Argon flow. The reaction was irradiated to 125°C for 10 to 30min (~40W), reaction progress was followed by TLC and/or HPLC. The crude was filtered through a plug of Celite, rinsed with 10ml 1:1 EtOAc/Acetone and concentrated in vacuo. The residue was purified by silica gel (silica was pre-washed with 0.1% NEt₃ in hexanes:EtOAc 3:1) chromatography using a CombiFlash instrument and a solvent gradient from 1:1 EtOAc/Hexanes to 100% EtOAc and then to 10% MeOH in EtOAc

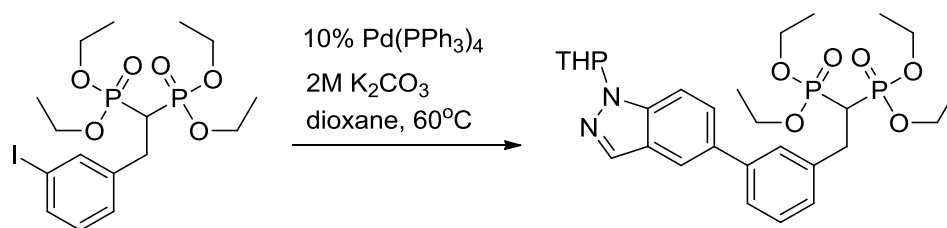
JDS01-149: tetraisopropyl (1-fluoro-2-(5-phenylpyridin-3-yl)ethane-1,1-diyl)bis(phosphonate)

Synthesis of the bromide coupling partner is described in experimental of Chapter 2.



Method A; Isolated 41 mg (69%) as a brown oil. ^1H NMR (300 MHz, CDCl_3) δ 8.72 (d, J = 2.2 Hz, 1H), 8.50 (s, 1H), 7.86 (s, 1H), 7.62 – 7.35 (m, 5H), 4.91 – 4.70 (m, 4H), 3.52 (m, 2H), 1.28 (m, 24H). ^{13}C NMR (75 MHz, CDCl_3) δ 150.66, 146.39, 137.83, δ 137.38 (d, J = 1.3 Hz), 135.65, 130.26 (t, J = 8.0 Hz), 129.03, 127.95, 127.05, 94.58 (dt, J = 192.7, 157.5 Hz), 72.97 (dt, J = 31.5, 3.4 Hz), 36.00 (d, J = 19.3 Hz), 23.79 (ddd, J = 29.5, 23.0, 10.4 Hz). ^{19}F NMR (470 MHz, CDCl_3) δ -193.20 (tt, J = 74.5, 26.8 Hz). ^{31}P NMR (81 MHz, CDCl_3) δ 9.47 (d, J = 74.6 Hz). MS (ESI): calcd 552.20; found 552.1 $[\text{M}+\text{Na}]^+$

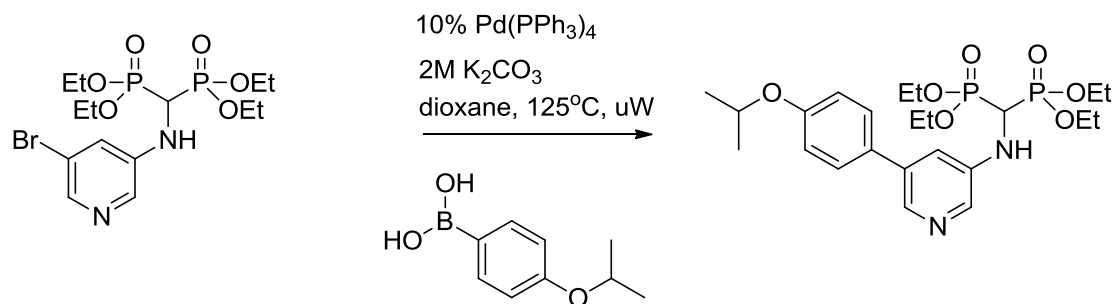
JDS-04-140: tetraethyl (2-(3-(1-(tetrahydro-2H-pyran-2-yl)-1H-indazol-5-yl)phenyl)ethane-1,1-diyl)bis(phosphonate)



Method A; Isolated 115mg (66% based on recovered starting material) of product as a clear oil. ^1H NMR (400 MHz, CDCl_3) δ 8.07 (s, 1H), 7.89 (s, 1H), 7.64 (s, 2H), 7.53 (d, J = 12.2 Hz, 1H), 7.47 (d, J = 7.8 Hz, 1H), 7.36 (t, J = 7.6 Hz, 1H), 5.75 (dd, J = 9.4, 2.7 Hz, 1H), 4.23 – 3.99 (m, 8H), 3.84 – 3.67 (m, 2H), 3.56 – 3.45 (m, 1H), 3.33 (td, J = 16.6, 6.5 Hz, 2H), 2.72 (tt, J = 23.9, 6.4 Hz, 1H), 2.23 – 2.05 (m, 2H), 1.74 (m, 3H), 1.30 – 1.20 (m, 12H). ^{13}C NMR (75 MHz, CDCl_3) δ 141.27, 140.06 (t, J = 7.4 Hz), 138.94, 134.63, 134.24, 128.69, 128.02, 127.41, 126.51, 125.42, 125.31, 118.97, 110.34, 85.38, 67.46,

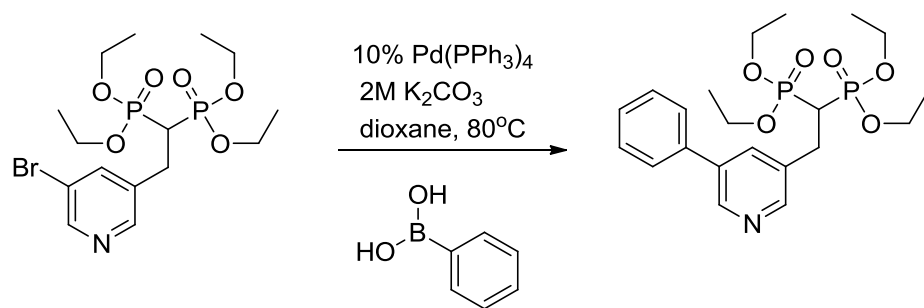
62.52 (dd, $J = 17.1, 6.8$ Hz), 39.07 (t, $J = 132.7$ Hz), 29.39, 25.09, 22.57, 16.26 (d, $J = 6.7$ Hz). ^{31}P NMR (81 MHz, CDCl_3) δ 20.40. MS (ESI): calcd 601.22, found 601.26 $[\text{M}+\text{Na}]^+$

JDS05-116: tetraethyl (((5-(4-isopropoxyphenyl)pyridin-3-yl)amino)methylene)bis(phosphonate)



Method B; Isolated 47 mg (70%) as a pale yellow syrup. ^1H NMR (500 MHz, CDCl_3) δ 8.25 (s, 1H), 8.05 (d, $J = 2.4$ Hz, 1H), 7.49 – 7.44 (m, 2H), 7.13 (s, 1H), 7.00 – 6.94 (m, 2H), 4.65 – 4.55 (m, 1H), 4.33 – 4.10 (m, 9H), 1.37 (d, $J = 6.1$ Hz, 6H), 1.29 (dt, $J = 19.0, 7.1$ Hz, 12H). ^{13}C NMR (126 MHz, CDCl_3) δ 158.08, 142.30, 138.56, 136.51, 134.75, 129.92, 128.15, 117.77, 116.22, 69.94, δ 63.58 (dd, $J = 21.7, 18.6$ Hz), 49.88 (t, $J = 147.7$ Hz), 22.00, 16.39 (dd, $J = 6.0, 2.8$ Hz). ^{31}P NMR (81 MHz, CDCl_3) δ 14.73 (s). MS (ESI): calcd 515.208; found 515.22 $[\text{M}+\text{Na}]^+$

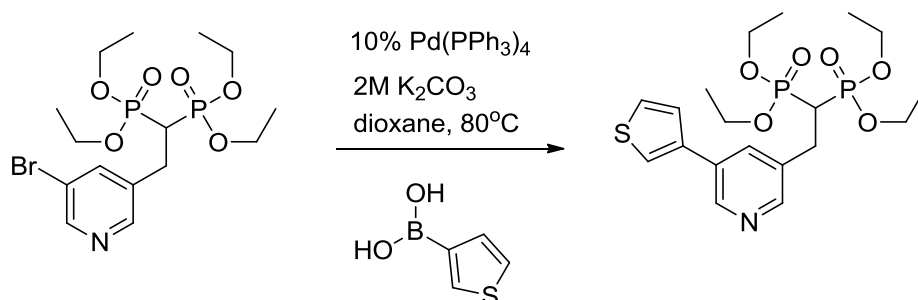
JDS-04-031: tetraethyl (2-(5-phenylpyridin-3-yl)ethane-1,1-diyl)bis(phosphonate)



Method A; Isolated 96 mg (48%) as a pale brown oil. ^1H NMR (400 MHz, CDCl_3) δ 8.72 (d, $J = 1.9$ Hz, 1H), 8.51 (d, $J = 1.7$ Hz, 1H), 7.84 (s, 1H), 7.60 – 7.54 (m, 2H), 7.48 (s, 2H), 7.40 (s, 1H), 4.19 – 4.03 (m, 8H), 3.33 (td, $J = 16.2, 6.6$ Hz, 2H), 2.66 (tt, $J = 23.7, 6.6$ Hz, 1H), 1.26 (q, $J = 7.2$ Hz, 12H). ^{13}C NMR (75 MHz, CDCl_3) δ 148.84, 146.14, 137.53, 136.15, 135.10, 133.52, 129.06, 128.11, 127.04, 62.67 (dd, $J = 17.2, 6.7$ Hz), 38.87 (t, J

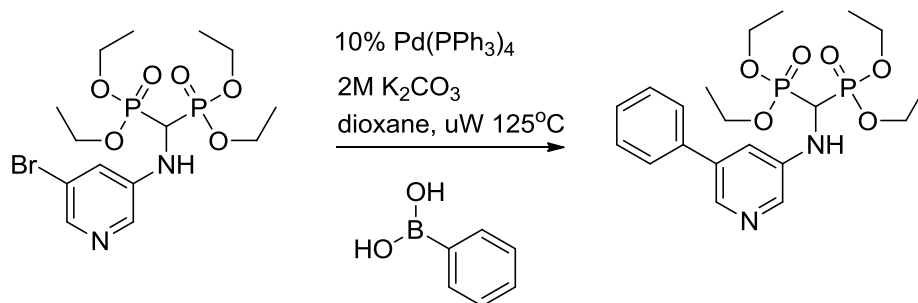
= 133.1 Hz), 28.71 (d, $J = 4.9$ Hz), 17.35 – 15.02 (m). ^{31}P NMR (81 MHz, CDCl_3) δ 19.99. MS (ESI): calcd 478.15; found 478.0 $[\text{M}+\text{Na}]^+$

JDS-04-035: tetraethyl (2-(5-(thiophen-3-yl)pyridin-3-yl)ethane-1,1-diyl)bis(phosphonate)



Method A; Obtained 125mg (56%) as brown oil. ^1H NMR (300 MHz, CDCl_3) δ 8.73 (s, 1H), 8.44 (s, 1H), 7.84 (s, 1H), 7.53 (dd, $J = 2.9, 1.3$ Hz, 1H), 7.47 – 7.42 (m, 1H), 7.39 (dd, $J = 5.0, 1.4$ Hz, 1H), 4.25 – 4.05 (m, 8H), 3.31 (td, $J = 16.2, 6.5$ Hz, 2H), 2.64 (tt, $J = 23.9, 6.4$ Hz, 1H), 1.27 (m, 12H). ^{13}C NMR (75 MHz, CDCl_3) δ 148.72, 145.63, 138.51, 134.07, 126.95, 125.76, 121.36, 62.62 (dd, $J = 18.3, 6.7$ Hz), 38.78 (t, $J = 133.1$ Hz), 16.23 (d, $J = 6.6$ Hz). ^{31}P NMR (81 MHz, CDCl_3) δ 19.91. MS (ESI): calcd 484.11; found 484.0 $[\text{M}+\text{Na}]^+$

JDS05-015: tetraethyl (((5-phenylpyridin-3-yl)amino)methylene)bis(phosphonate)

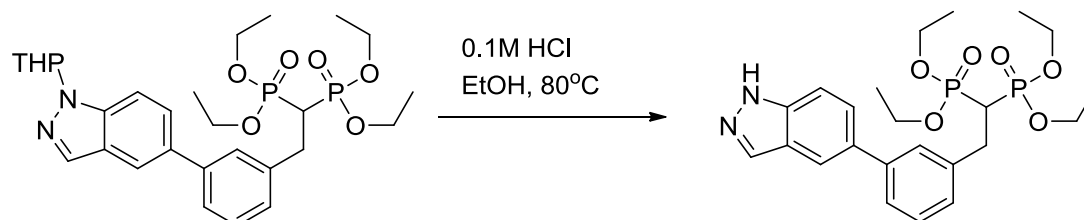


Method B; 34%, isolated as clear, colorless syrup ^1H NMR (400 MHz, $\text{DMSO}-d_6$) δ 8.26 (s, 1H), 8.11 (s, 1H), 7.68 (d, $J = 7.1$ Hz, 2H), 7.57 (s, 1H), 7.46 (t, $J = 7.5$ Hz, 2H), 7.38 (d, $J = 7.2$ Hz, 1H), 6.13 (d, $J = 11.0$ Hz, 1H), 4.95 (td, $J = 22.9, 10.9$ Hz, 1H), 4.07 (d, $J = 7.0$ Hz, 8H), 1.14 (dt, $J = 19.3, 7.0$ Hz, 12H). ^{13}C NMR (126 MHz, CD_3OD) δ 136.33, 134.20, 128.69, 127.91, 126.70, 118.29, δ 63.61 (d, $J = 33.2$ Hz), δ 15.29 (d, $J = 5.2$ Hz). ^{31}P NMR (81 MHz, CD_3OD) δ 20.32 (s). MS (ESI): calcd 479.15; found 479.1 $[\text{M}+\text{Na}]^+$

General procedure fo THP-deprotection:

To a solution of THP protected compound (1 equivalent) in anhydrous EtOH was added ethanolic HCl (1.0M, 2.5 equivalents) via syringe for a final concentration of 0.1M HCl. The reaction was stirred at 80°C for 12h. The reaction mixture was concentrated in vacuo (NaHCO₃ in receiving flask), the crude was dissolved in 100 mL EtOAc and washed with 10mL satd. NaHCO₃, water and brine. The organic layer was dried over sodium sulfate, concentrated in vacuo and purified by normal phase column chromatography on silica gel (silica gel was pre-treated with 1% NEt₃ in hexanes/EtOAc in a 3:1 ratio) using a gradient from 100% hexanes to 100% EtOAc and then to 10-25% MeOH.

JDS-04-142: tetraethyl (2-(3-(1H-indazol-5-yl)phenyl)ethane-1,1-diyl)bis(phosphonate)



Isolated 49mg (57%), as a clear oil. ¹H NMR (400 MHz, CD₃OD) δ 8.10 (s, 1H), 8.00 (s, 1H), 7.70 (dd, *J* = 8.7, 1.6 Hz, 1H), 7.65 – 7.56 (m, *J* = 8.8 Hz, 2H), 7.54 (d, *J* = 7.9 Hz, 1H), 7.39 (t, *J* = 7.7 Hz, 1H), 7.28 (d, *J* = 7.5 Hz, 1H), 4.19 – 4.01 (m, 8H), 3.38 – 3.21 (m, 37H), 3.03 (tt, *J* = 23.9, 6.6 Hz, 1H), 1.26 (td, *J* = 7.1, 0.7 Hz, 12H). ¹³C NMR (75 MHz, CD₃OD) δ 141.48, 139.29 (t, *J* = 7.9 Hz), 134.03, 133.93, 128.51, 127.79, 127.15, 126.42, 125.20, 123.57, 118.32, 110.05, 62.77 (dd, *J* = 14.9, 6.9 Hz), 37.88 (t, *J* = 133.5 Hz), 31.00 (t, *J* = 4.8 Hz), 15.16 (d, *J* = 6.4 Hz).

³¹P NMR (81 MHz, CD₃OD) δ 24.50. MS (ESI⁺): calcd 517.16, found 517.20 [M+Na⁺]⁺

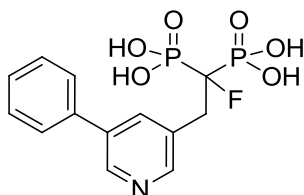
General procedure for the deprotection of tetra-isopropyl bisphosponate esters:

The bisphosphonate ester was transferred to a pressure vessel, dissolved in 6M HCl, the vessel was tightly sealed and the mixture was stirred at 100°C for 12 h. The reaction was cooled down, , filtered through a small cotton plug, transferred to recovery flask and concentrated to remove excess water and HCl (with satd. NaHCO₃ in receiving flask). The residue was lyophilized to dryness and weighed. The crude was suspended in 500 µL milliQ water and 1 to 3 equivalents of sodium hydroxide (1.030 M) solution was added via micropipette to dissolve the bisphosphonic acid. The solution was purified by reverse phase column chromatography on 10 cm of spherical C18 silica (45-75 µm, 70Å, Supelco) using a gradient from water to acetonitrile.

General procedure of deprotection of tetra-ethyl bisphosponate esters:

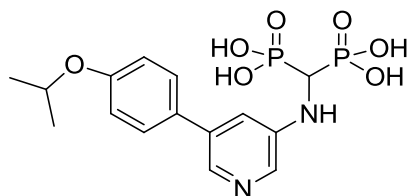
A 12 mL Teflon lined screw cap vial was charged with the tetra-ethyl bisphosphonate compound, dissolved in 5 mL distilled DCM and cooled in an ice bath. Bromotrimethyl silane (15 equivalents) was added via syringe and the reaction mixture was stirred at RT for 5-7 days. The reaction mixture was transferred to a 10 mL recovery flask and concentrated in vacuo (satd. NaHCO₃ in receiving flask). To the resulting oil was added 2 mL of HPLC-grade MeOH and concentrated in vacuo, this was repeated a total of five times. The crude thus obtained was suspended in a minimum amount of HPLC-grade MeOH, the mixture was sonicated and the desired compound was precipitated out of solution by the addition of Milli-Q water. The slurry was filtered and the cake washed twice with Milli-Q water, twice with HPLC-grade CH₃CN and twice with distilled Et₂O. The residue was then dried under high vacuum to obtain the desired product.

Inhibitor 4.21 (JDS-02-055): (1-fluoro-2-(5-phenylpyridin-3-yl)ethane-1,1-diyl)diphosphonic acid, disodium salt



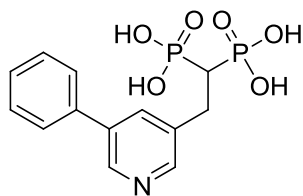
Isolated 24.5mg (80%) as a white powder. ^1H NMR (500 MHz, D_2O) δ 8.51 (d, J = 2.2 Hz, 1H), 8.41 (s, 1H), 8.06 (s, 1H), 7.66 (d, J = 7.2 Hz, 1H), 7.45 (t, J = 7.6 Hz, 2H), 7.36 (t, J = 7.4 Hz, 1H), 3.51 – 3.33 (m, 2H). ^{13}C NMR (75 MHz, D_2O) δ 149.46, 144.16, 138.18, 137.45, 135.40, 129.10, 128.09, 127.10, 35.40. ^{19}F NMR (470 MHz, D_2O) δ -185.66 to -186.35 (m). $\{^{19}\text{F}, ^{13}\text{C}\}$ HMQC NMR (470 MHz, D_2O) δ -186 (^{19}F) correlates with 100 (^{13}C). ^{31}P NMR (81 MHz, D_2O) δ 13.01 (d, J = 66.2 Hz). HRMS (ESI): calcd 360.0208 ($\text{C}_{13}\text{H}_{13}\text{FNO}_6\text{P}_2$), found (m/z) 360.0219 $[\text{M}-\text{H}]^-$

Inhibitor 4.22 (JDS05-119): (((5-(4-isopropoxyphenyl)pyridin-3-yl)amino)methylene)diphosphonic acid



Isolated 23.7 mg (71%) as a white powder ^1H NMR (500 MHz, D_2O) δ 7.97 (d, J = 2.7 Hz, 1H), 7.96 (d, J = 1.8 Hz, 1H), 7.71 – 7.66 (m, 2H), 7.38 – 7.35 (m, 1H), 7.15 – 7.10 (m, 2H), 4.75 (m, obscured by solvent signal, 1H), 3.74 (t, J = 19.1 Hz, 1H), 1.35 (d, J = 6.1 Hz, 6H). ^{13}C NMR (126 MHz, D_2O) δ 156.77, 145.36, 136.20, 133.72, 133.32, 131.07, 128.40, 117.19, 116.80, 71.67, 52.49, 20.99. HSQC ^1H - ^{13}C : ^1H δ 3.74 correlates with ^{13}C δ 52.49. ^{31}P NMR (81 MHz, D_2O) δ 15.05 (s). HRMS m/z : calcd 401.0667 for ($\text{C}_{15}\text{H}_{19}\text{N}_2\text{O}_7\text{P}_2$), found m/z 401.06784 $[\text{M}-\text{H}]^+$

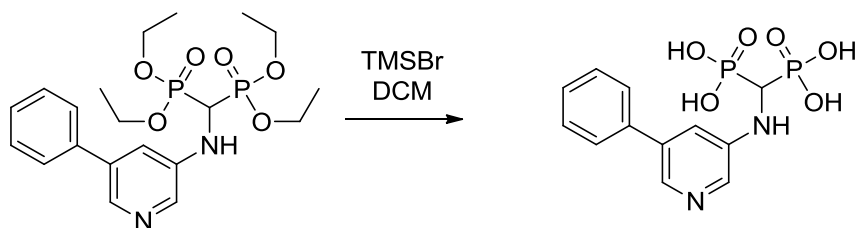
Inhibitor 4.23 (JDS-04-085): (2-(5-phenylpyridin-3-yl)ethane-1,1-diyl)diphosphonic acid



Isolated 30 mg (66%) as a white solid. ^1H NMR (500 MHz, D_2O) δ 8.47 (d, J = 2.1 Hz, 1H), 8.37 (d, J = 1.9 Hz, 1H), 8.02 (s, 1H), 7.63 (d, J = 7.2 Hz, 2H), 7.42 (t, J = 7.6 Hz, 2H), 7.34 (t, J = 7.4 Hz, 1H), 3.08 (td, J = 15.3, 7.0 Hz, 2H), 2.09 (tt, J = 21.0, 6.9 Hz, 1H). ^{13}C NMR (126 MHz, D_2O) δ 147.81, 144.19, 138.38, 137.34, 136.06, 135.99, 129.08,

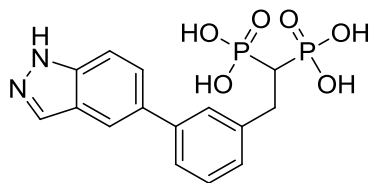
128.14, 127.07, 41.23 (t, $J = 110.6$ Hz), 28.88. ^{31}P NMR (81 MHz, D_2O) δ 19.83 (s). HRMS (ESI): calcd 342.0302 ($\text{C}_{13}\text{H}_{14}\text{NO}_6\text{P}_2$), found (m/z) 342.0301 $[\text{M-H}]^-$

Inhibitor 4.24 (JDS05-020): (((5-phenylpyridin-3-yl)amino)methylene)diphosphonic acid



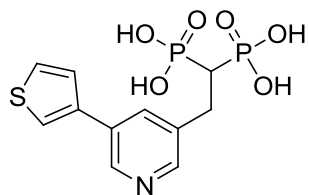
Isolated 16.9 mg (64%) as a white powder. ^1H NMR (500 MHz, D_2O) δ 8.05 (dd, $J = 6.0$, 2.2 Hz, 2H), 7.80 – 7.75 (m, 2H), 7.57 (t, $J = 7.6$ Hz, 2H), 7.52 – 7.47 (m, 1H), 7.46 (s, 1H), 3.80 (t, $J = 19.0$ Hz, 1H). ^{13}C NMR (75 MHz, D_2O) δ 137.83, 136.75, 134.14, 133.73, 133.53, 128.98, 128.06, 127.04, 117.68. (C- α triplet of the bisphosphonate moiety is not clearly visible; however, by HSQC ^1H – ^{13}C correlation it was observed for ^1H at 3.80 ppm to ^{13}C at 52.25 ppm). ^{31}P NMR (81 MHz, D_2O) δ 14.97 (s). HRMS (ESI): calcd 343.0249 ($\text{C}_{12}\text{H}_{13}\text{N}_2\text{O}_6\text{P}_2$), found (m/z) 343.0251 $[\text{M-H}]^-$

JDS-04-144: (2-(3-(1H-indazol-5-yl)phenyl)ethane-1,1-diyl)diphosphonic acid



Isolated 14.2 mg (41%) as beige solid. ^1H NMR (500 MHz, D_2O) δ 8.06 (s, 1H), 7.98 (s, 1H), 7.68 (d, $J = 8.7$ Hz, 1H), 7.64 (s, 1H), 7.57 (d, $J = 8.8$ Hz, 1H), 7.41 (m, 1H), 7.32 (m, 2H), 3.09 (td, $J = 15.6$, 6.5 Hz, 3H). ^{13}C NMR (125 MHz, D_2O) δ 143.43, 140.55, 139.45, 134.64, 133.90, 128.87, 127.88, 127.71, 127.17, 124.40, 123.07, 118.84, 110.84, 41.53 (CH, t, $J = 111.6$ Hz), 31.69. ^{31}P NMR (D_2O) δ 20.40. HRMS (ESI): calcd 381.0411 ($\text{C}_{15}\text{H}_{15}\text{N}_2\text{O}_6\text{P}_2$), found (m/z) 381.0411 $[\text{M-H}]^-$

JDS-04-071: (2-(5-(thiophen-3-yl)pyridin-3-yl)ethane-1,1-diyl)diphosphonic acid:



Isolated 35 mg (35%) as beige powder. ^1H NMR (500 MHz, D_2O) δ 8.50 (d, $J = 2.1$ Hz, 1H), 8.28 (d, $J = 2.0$ Hz, 1H), 8.02 (t, $J = 2.1$ Hz, 1H), 7.71 – 7.65 (m, 1H), 7.44 (s, 1H), 7.44 (d, $J = 0.6$ Hz, 1H), 3.03 (td, $J = 15.2, 6.8$ Hz, 2H), 2.05 (tt, $J = 21.1, 6.8$ Hz, 1H). ^{13}C NMR (126 MHz, D_2O) δ 147.49, 143.57, 138.53, 138.17, 135.16, 131.03, 127.31, 125.89, 122.04, 41.24 (t, $J = 110.9$ Hz), 28.86. ^{31}P NMR (81 MHz, D_2O) δ 18.66 (s). HRMS (ESI): calcd 347.9866 ($\text{C}_{11}\text{H}_{12}\text{NO}_6\text{P}_2\text{S}$), found (m/z) 347.9859 $[\text{M}-\text{H}]^-$

4.7.3 Enzymatic inhibition assays

The *in vitro* inhibition assay for hFPPS (**M1**) and hGGPPS were performed as described in Chapter 3.

5 Exploring the allylic sub-pocket and the importance of π -interactions

5.1 Preface

Most of the work presented in this chapter has been published in the following manuscript:

Design of Potent Bisphosphonate Inhibitors of the Human Farnesyl Pyrophosphate Synthase *via* Targeted Interactions with the Active Site “Capping” Phenyls

De Schutter, J.W.; Shaw, J.; Lin, Y.-S.; Tsantrizos Y.S., *Bioorg. Med. Chem.* **2012**, *20*, 5583-5591

Joseph Shaw was an undergraduate student from the Biochemistry department who performed his Honors' project in Prof. Tsantrizos' research group. He completed the synthesis of inhibitors with an amide linker between the pyridine core and side chain (inhibitors **5.8**, **5.9** and **5.10**), under my supervision. Yih-Shyan Lin synthesized and tested inhibitor **5.14**. I performed the computational docking and the synthesis of all other compounds, as well as performed the enzymatic assays

5.2 Introduction

Non-covalent inter- and intra-molecular interactions involving aromatic systems are ubiquitous in chemical and biological processes and commonly referred to as π -interactions. These attractive forces can be quite strong and determine molecular architecture and assembly.¹ Therefore π -interactions are purposefully designed into novel compounds in both materials chemistry and medicinal chemistry efforts. Many types of π -interactions are known: including the π - π interactions, either face-to-face (“stacked”) (**Figure 5.1a**) or edge-to-face (“T-shaped”) (**b**) between two aromatic systems. In addition, π -cation interactions (**Figure 5.1c**) are important in protein folding (e.g. interactions between an arginine side chain and the aromatic ring of phenylalanine).² Other important interactions include halogen bonding interactions (**Figure 5.1d** and **e**) and π -interactions between an amide moiety and an aromatic ring (**f**).³ The cyclopropyl group is a favored moiety in medicinal chemistry, mainly because of its metabolic stability and its steric, electronic and conformational properties.⁴ It is often incorporated to reduce the rotational freedom of an inhibitor and lock it in the bio-active conformation, resulting in improved enzymatic potency. In addition, the large conformational strain of the cyclopropane unit contorts the molecular orbitals of the ring and as a result the C-C bonds have inherent π -character.⁵ This allows the cyclopropyl moiety to engage in CH/ π -interactions with aromatic systems (**Figure 5.1g**).^{6,7}

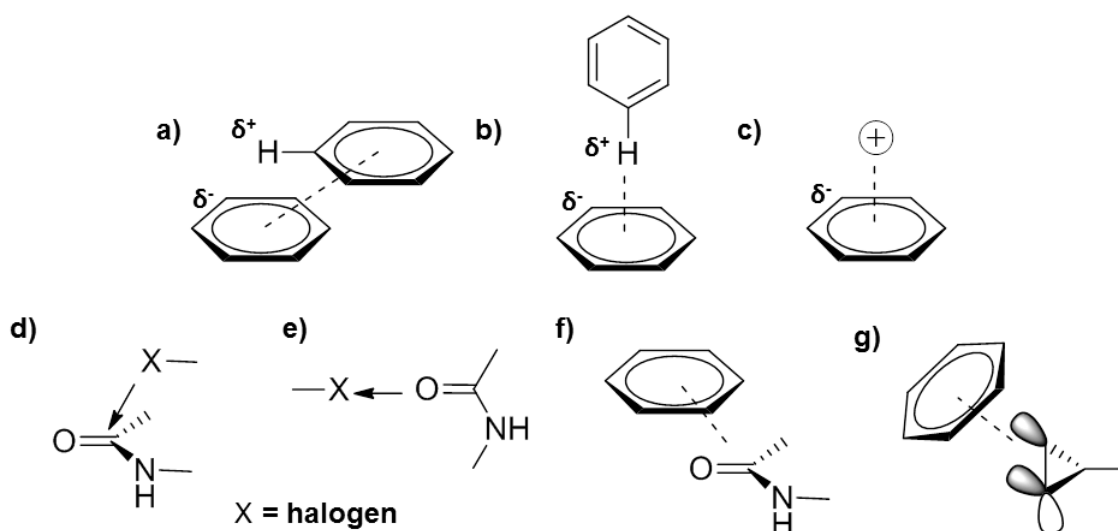


Figure 5.1: Examples of π -interactions

5.3 Inhibitor design rationale

Based on our co-crystal structure of the hFPPS/inhibitor **4.5** complex (PDB 4DEM), we generated a new computational model for molecular docking studies. In the enzyme-bound structure, the isopropoxyphenyl substituent of inhibitor **4.5** displaces the capping phenyl Phe 113 and the side chain of Gln 185, and engages in π -stacking interactions with both of these residues (**Figure 5.3a**). This conformational movement generates a larger binding site, and we reasoned that we could potentially improve ligand-protein interactions by introducing a more flexible linker between pyridine core and phenyl substituents (**Figure 5.2**). Based on our previous SAR data, the core scaffolds **5.1** and **5.2** were selected in order to explore the effects of different linker moieties on the binding affinity of our compounds. We assumed that replacing the direct C-C bond between the pyridine core and 4-isopropoxyphenyl substituent with a more flexible moiety (X) may allow the inhibitor to adopt a “bent” conformation and improve the π -stacking interactions.

Furthermore, the isopropoxy moiety of **4.5** is positioned in close proximity of the second capping phenyl Phe 112 and we wanted to explore if we could establish a second π -interaction in the allylic sub-pocket by installing appropriate moieties at this position. We envisioned that the corresponding cyclopropyl analog could establish a π -interaction with the phenyl sidechain. Indeed, docking said analog into the crystal structure coordinates of the hFPPS/**4.5** complex (PDB 4DEM) predicted a distance of 3.4Å between the two moieties, well suited for a CH/ π -interaction (**Figure 5.3b**).^{6,7}

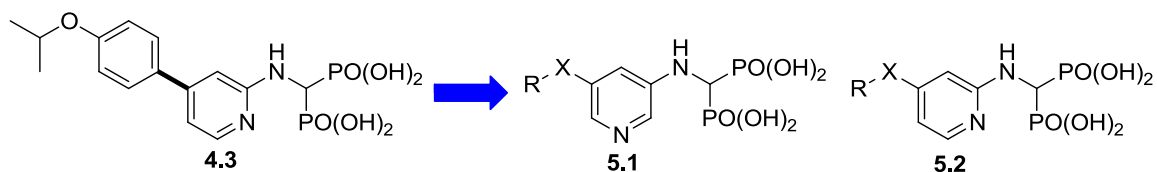


Figure 5.2: 3-aminopyridine and 2-aminopyridine based bisphosphonic acids

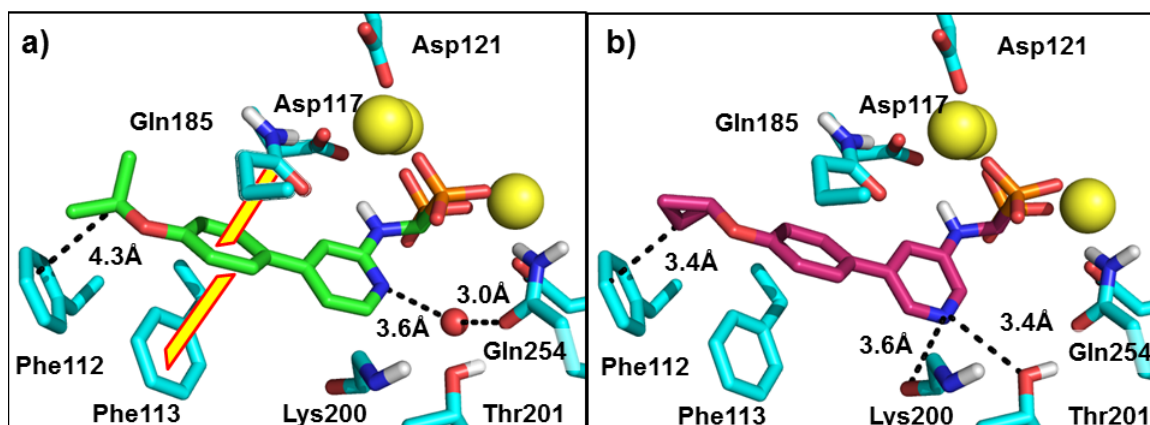
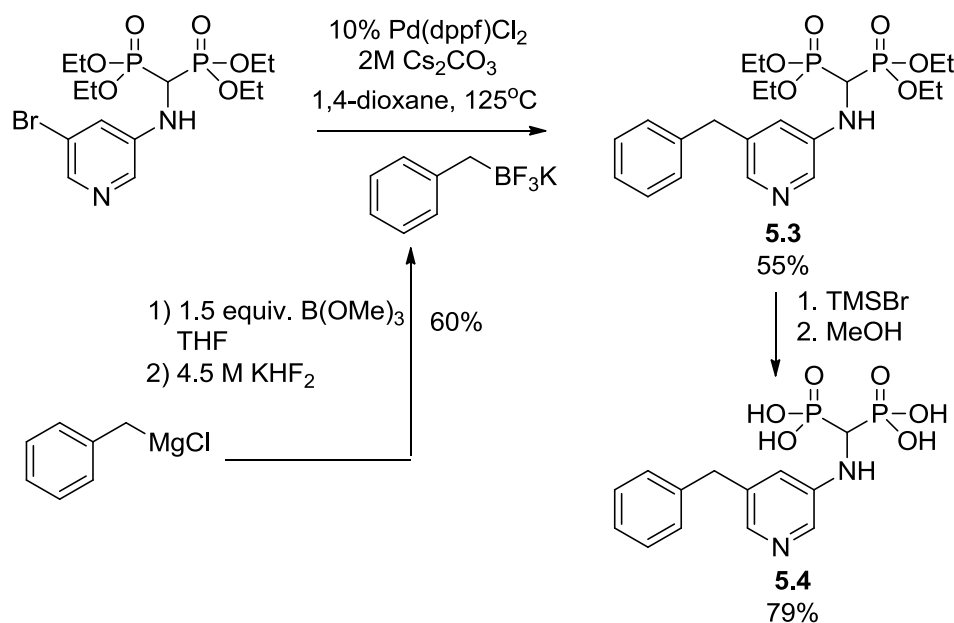


Figure 5.3: (a) Expansion of the allylic sub-pocket in the hFPPS/**4.5** co-crystal structure (PDB 4DEM). (b) Docking output pose of cyclopropyl analog **5.15** in computational model based on hFPPS/**4.5**. Critical active site residues, **4.5** and **5.15** are shown in stick representation in cyan, green and magenta respectively. Distances are indicated as dashed lines, the water molecule mediating the hydrogen bond is shown as a red sphere. The π -stacking interactions between **4.5** and Phe 113 and Gln 185 are highlighted in yellow.

5.4 Synthesis

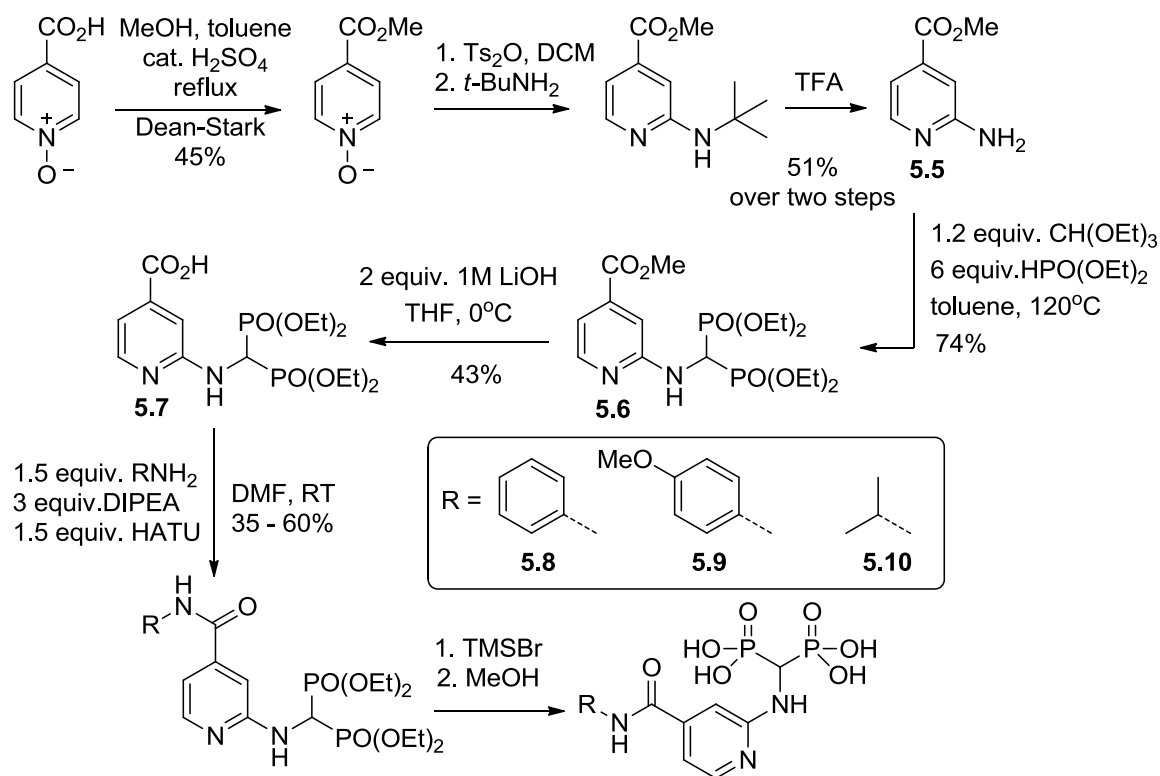
A free methylene unit ($X = \text{CH}_2$, **Figure 5.2**) would allow the most rotational freedom, but this type of bond formation cannot be accomplished with standard Suzuki cross-coupling conditions utilizing non-aromatic boronic acids (i.e. $\text{R-CH}_2\text{B(OH)}_2$). Therefore the trifluoroborate cross-coupling chemistry developed by Molander and co-workers was applied and the benzyl coupling partner was made according to their standard procedure (**Scheme 5.1**).⁸ Thus analog **5.4** could be synthesized using published conditions, although the cross-coupling was found to be sluggish and fresh reagents had to be added twice to the reaction to achieve complete conversion.



Scheme 5.1: Cross-coupling with benzyl trifluoroborate

An amide linker ($X = \text{C(O)NH}$, **Figure 5.2**) between the pyridine core and substituent can act as flexible linker with less rotational freedom compared to the free methylene. The intermediate **5.5** was synthesized according to literature procedure as outlined in **Scheme 5.2**.⁹ Briefly, after forming the methyl ester, the pyridine N-oxide was activated with tosyl anhydride to promote an $\text{S}_{\text{N}}\text{Ar}$ reaction with *tert*-butyl amine at the C-2-position and the *t*Bu group was removed with TFA. The tetra-ethyl bisphosphonate moiety was

subsequently installed using our standard condensation conditions with triethylorthoformate and diethylphosphite to give **5.6**. Following saponification of the methyl ester (performed at 0°C in order to prevent partial deprotection of the phosphonate esters), the free acid **5.7** was amenable to standard amide bond formation conditions with HATU to furnish the desired amides. After hydrolysis of the tetraethyl bisphosphonate esters, the novel inhibitors **5.8** – **5.10** were obtained as yellow solids.



Scheme 5.2: Synthesis of bisphosphonates with an amide linker

In order to form new π -interactions with Phe 112, we envisioned attaching novel aromatic sidechains with a cyclopropyl moiety through the familiar Suzuki cross-coupling (**Figure 5.4**). The required (4-cyclopropoxyphenyl)boronic acid fragment **5.13** has been reported and was synthesized according to literature procedure, as outlined in **Scheme 5.3**.¹⁰ The alkylation of 4-bromophenol and subsequent elimination to produce vinyl ether **5.11** proceeded smoothly, however the reported cyclopropanation conditions (CH₂I₂ followed by ZnEt₂ at 0°C in Et₂O) resulted in only 40% conversion. Therefore a more efficient methodology, developed by Yian and co-workers,¹¹ was employed for this and later

cyclopropanations. This procedure involved the pre-formation of the zinc reagent with TFA prior to the addition of diiodomethane. Finally, following lithium-halogen exchange with *n*BuLi and treatment the trimethylborate, the boronic acid **5.13** was liberated under acidic hydrolysis conditions and isolated by trituration.

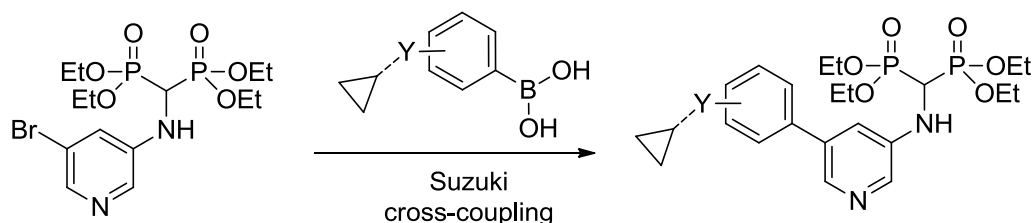
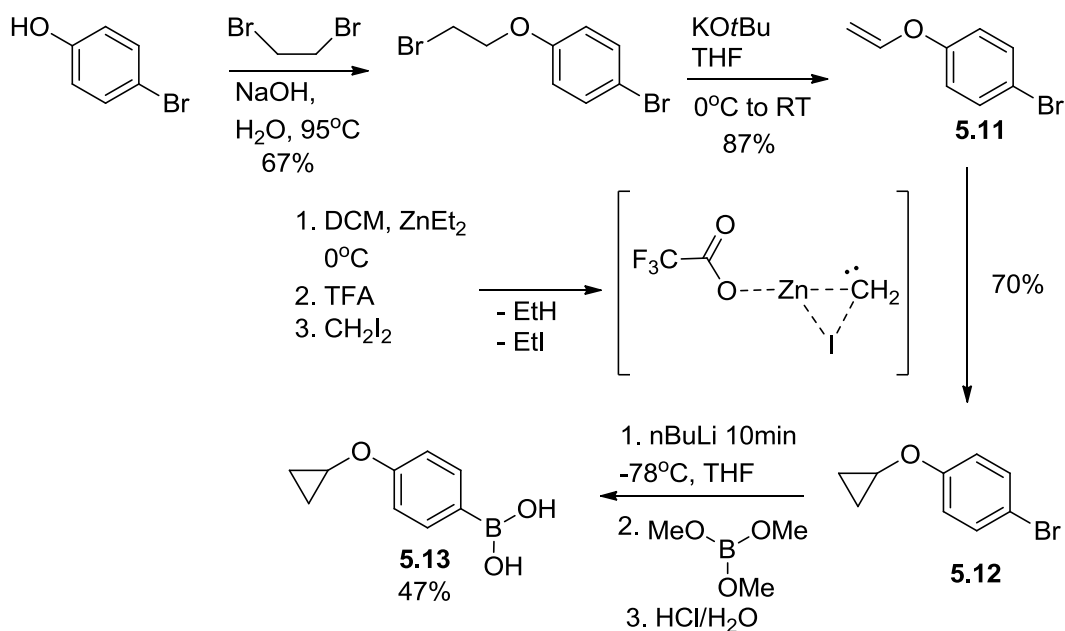


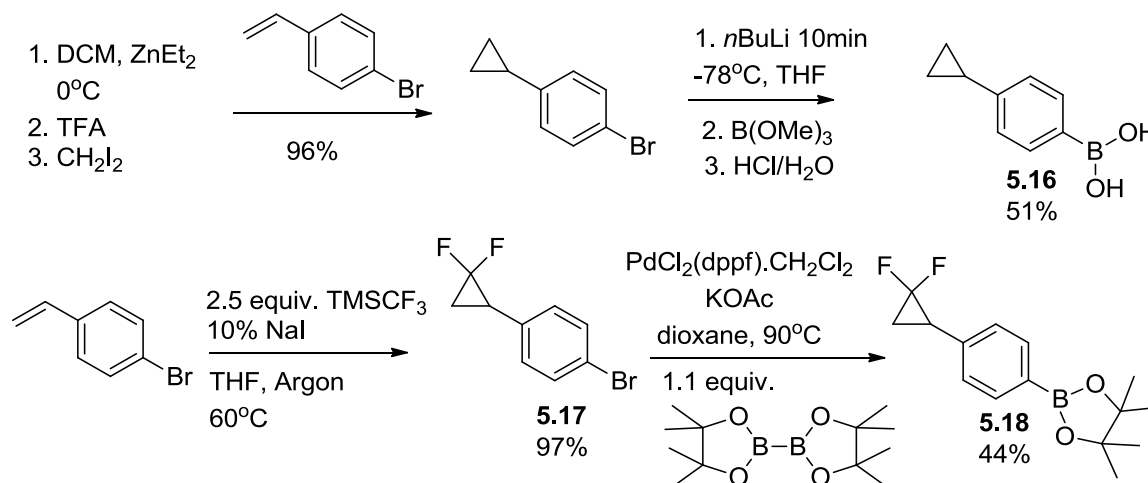
Figure 5.4: Suzuki cross-coupling synthetic strategy



Scheme 5.3: Synthesis of (4-cyclopropoxyphenyl)boronic acid **5.13**

Utilizing the same reaction conditions, (4-cyclopropylphenyl)boronic acid **5.16** was readily synthesized (**Scheme 5.4**). The desired gem-difluoro-cyclopropyl analog **5.17** was installed with cyclopropanation protocol developed by Olah and co-workers.¹² However, subsequent treatment with *n*BuLi led to significant side-product formation, presumably due to the increased acidity of the benzylic hydrogen. Therefore, the corresponding pinacol boron ester was installed via palladium catalysis to furnish the 4-(2,2-difluorocyclopropyl)phenyl

boron coupling partner **5.18**. Lastly we synthesized analogs with a polar linker between the cyclopropyl moiety and the phenyl substituent; including an amide, reverse amide and sulfonamide connection (**Figure 5.5**). The required coupling partners were synthesized using common reaction protocols and full details are provided in the experimental section.



Scheme 5.4: Synthesis of novel cyclopropyl-bearing boron coupling partners

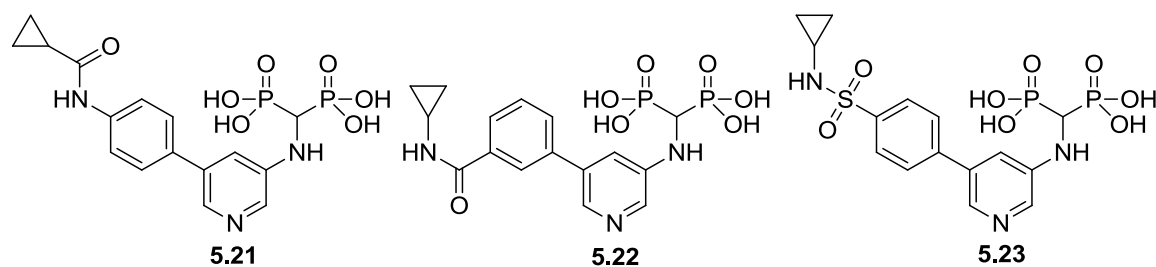


Figure 5.5: Novel inhibitors with extended cyclopropyl moiety

5.5 In vitro enzymatic activity and SAR

5.5.1 Pyridine core – aromatic sidechain connectivity

Disruption of the co-planarity between the pyridine core and the –R substituent by the introduction of a simple methylene linker resulted in greater than 20-fold loss in potency (**5.4** vs. **4.24**; **Figure 5.6**, **Table 5.1**). Most likely, the rotational freedom of the methylene unit is too large, incurring a significant entropy penalty to adopt the bio-active conformation. We expected that an amide bond would maintain the overall co-planarity of the side chain and engage in favorable π -stacking interactions with Phe 113. However, the amide linker proved to be equally detrimental to enzymatic potency and phenyl analog **5.8** exhibited only 65% inhibition at 10 μ M against hFPPS. Incorporation of a *p*-methoxy moiety on the phenyl ring further decreased potency (**5.8** vs. **5.9**); contrary to the SAR observed for inhibitors with a C-C bond between the pyridine core and aromatic sidechain (Chapter 4), where a modest improvement was observed. Replacing the aromatic substituent with a smaller alkyl group (**5.10**) did not provide any improvement, indicating that the amide linker itself does not engage in favorable π -interactions. It was therefore concluded that a direct aryl-aryl bond between the pyridine core and aromatic sidechain is best suited to occupy the extended allylic sub-pocket.

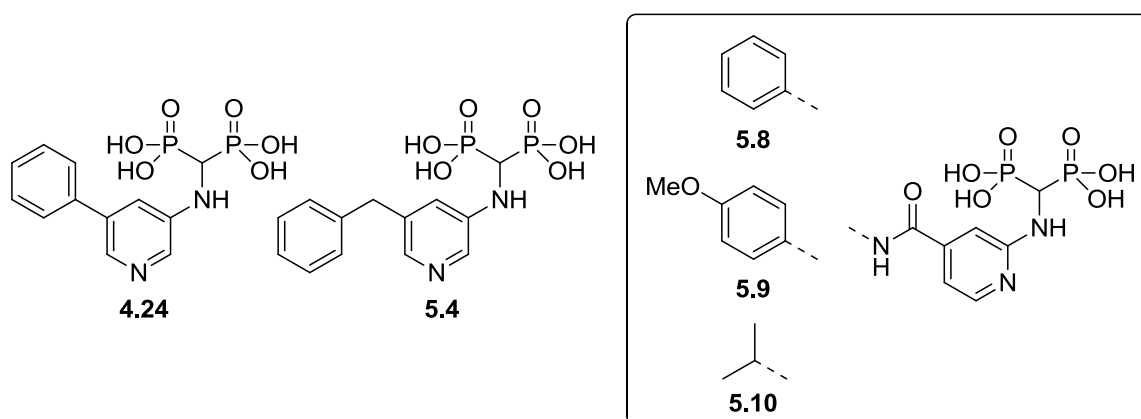


Figure 5.6: Novel inhibitors with a flexible linker

	hFPPS			hGGPPS
Concentration:	0.1 μ M	1 μ M	10 μ M	10 μ M
5.4	16%	55%	89%	5%
5.8	<i>nd</i>	<i>nd</i>	65%	11%
5.9	<i>nd</i>	<i>nd</i>	28%	0%
5.10	<i>nd</i>	<i>nd</i>	41%	0%

Table 5.1: hFPPS and hGGPPS enzymatic inhibition data for inhibitor **5.4**, **5.8** – **5.10**. The values of % inhibition shown are the average of three determinations (<10% standard deviation). (*nd* = not determined)

5.5.2 π -interactions with Phe112

Satisfyingly, cyclopropyl-bearing bisphosphonates **5.14** and **5.15** exhibited a 3-4-fold increase in enzymatic activity against hFPPS compared to the corresponding isopropoxy analogs **4.5** and **4.22**, respectively (**Figure 5.7**). Although this is not a very large improvement, it is significant for such structurally similar compounds (only 2 H atoms differentiate isopropoxy from cyclopropyl) and underscores the importance of π -interactions. It is worth noting that these novel inhibitors are essentially equipotent to risedronate (**Table 5.2**) despite lacking the C α -hydroxy moiety. Furthermore, in spite of their larger size, **5.14** and **5.15** exhibit no appreciable activity against hGGPPS.

Deletion of the ether oxygen (**5.19**, **Table 5.2**) or addition of the gem-difluoro moiety (**5.20**) did not greatly affect the affinity for hFPPS and the corresponding analogs are essentially equipotent. Surprisingly however, these two analogs exhibited significant inhibition activity against hGGPPS and this finding exemplifies the serendipity that is associated with medicinal chemistry research. Small structural modifications can have a large impact on diverse properties of compounds, including binding mode, cell membrane permeability, metabolism or in this case, target selectivity. Presumably, the cyclopropyl moiety is now properly positioned to engage in π -interactions with the hGGPPS active site and **5.19** and **5.20** are new hits against this enzyme.

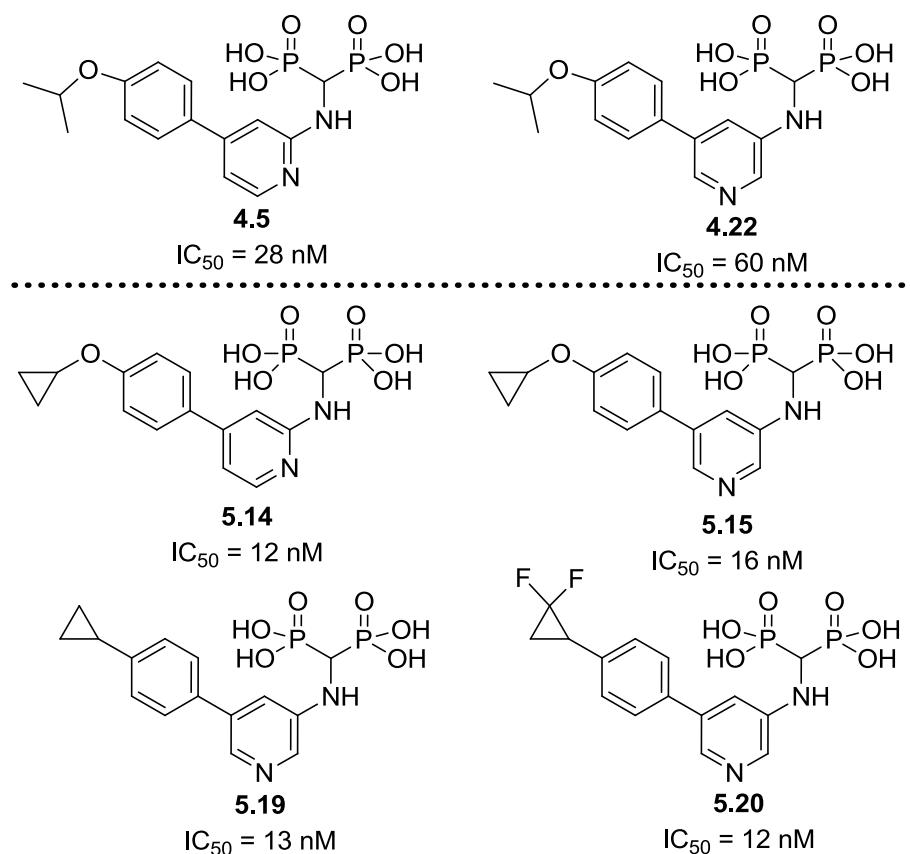


Figure 5.7: Novel cyclopropyl bearing bisphosphosphonates

inhibitor	hFPPS		hGGPPS	
	IC ₅₀	1 μ M	IC ₅₀	10 μ M
RIS	11 nM	100%	<i>nd</i>	0%
5.14	12 nM	100%	<i>nd</i>	26%
5.15	16 nM	99%	<i>nd</i>	10%
5.19	13 nM	99%	4.7 μ M	72%
5.20	24 nM	98%	~5 μ M	57%
5.21	<i>nd</i>	41%	<i>nd</i>	0%
5.22	<i>nd</i>	0%	<i>nd</i>	0%
5.23	<i>nd</i>	5%	<i>nd</i>	11%

Table 5.2: Enzymatic inhibition data for cyclopropyl-bearing compounds. The values of % inhibition shown are the average of three determinations (<10% standard deviation).

(*nd* = not determined)

The binding of **4.5** in the hFPPS active site displaces Phe 113 and Gln 113 and opens the allylic sub-pocket to bulk solvent. Therefore we reasoned that a polar linker between the phenyl sidechain and cyclopropyl moiety may improve binding to the enzyme. Unfortunately, all the linkers explored (**Figure 5.5**, amide **5.21**, reverse amide **5.22** and sulfonamide **5.23**) proved to be detrimental for the enzymatic potency against hFPPS (**Table 5.2**). Presumably, the linkers move the cyclopropyl ring too far away to interact with Phe 112 and no favorable polar interactions are formed in the allylic sub-pocket.

5.6 Conclusions and outlook

In summary, we have demonstrated that the direct aryl-aryl connection between the pyridine core and aromatic substituent is best suited for the expanded allylic sub-pocket. Furthermore, the *in vitro* enzymatic potency was improved to $IC_{50} \sim 15$ nM and is now on par with the drug risedronate, despite lacking a hydroxyl moiety at the bisphosphonate Ca. Computational docking results strongly suggest that the improved potency is due to a novel CH/ π -interaction with capping phenyl Phe 112. Also, the selectivity for hFPPS is retained, in spite of the increased size of the novel inhibitors, which often leads to undesired inhibition of hGGPPS.¹³ However, analogs **5.19** and **5.20** were identified to be active against hGGPPS and exemplify the care that must be taken to properly screen all compounds, as even minor structural modifications can greatly affect inhibitor properties.

5.7 References

- (1) Salonen, L. M.; Ellermann, M.; Diederich, F.; Aromatic Rings in Chemical and Biological Recognition: Energetics and Structures *Angew. Chem. Int. Ed.* **2011**, *50*, 4808.
- (2) Salonen, L. M.; Holland, M. C.; Kaib, P. S. J.; Haap, W.; Benz, J.; Mary, J.-L.; Kuster, O.; Schweizer, W. B.; Banner, D. W.; Diederich, F.; Molecular Recognition at the Active Site of Factor Xa: Cation- π Interactions, Stacking on Planar Peptide Surfaces, and Replacement of Structural Water *Chem. Eur. J.* **2012**, *18*, 213.
- (3) Hardegger, L. A.; Kuhn, B.; Spinnler, B.; Anselm, L.; Ecabert, R.; Stihle, M.; Gsell, B.; Thoma, R.; Diez, J.; Benz, J.; Plancher, J.-M.; Hartmann, G.; Banner, D. W.; Haap, W.; Diederich, F.; Systematic Investigation of Halogen Bonding in Protein-Ligand Interactions *Angew. Chem. Int. Ed.* **2011**, *50*, 314.
- (4) Gagnon, A.; Duplessis, M.; Fader, L.; Arylcyclopropanes: Properties, Synthesis and Use in Medicinal Chemistry *Org. Prep. Proc. Int.* **2010**, *42*, 1.
- (5) Rappoport, Z. *The chemistry of the cyclopropyl group*; Wiley: Chichester; New York, 1987; Vol. 2.
- (6) Ran, J.; Wong, M. W.; Saturated Hydrocarbon-Benzene Complexes: Theoretical Study of Cooperative CH/ π Interactions *J. Phys. Chem. A* **2006**, *110*, 9702.
- (7) Tsuzuki, S.; Honda, K.; Uchimaru, T.; Mikami, M.; Fujii, A.; Magnitude and Directionality of the Interaction Energy of the Aliphatic CH/ π Interaction: Significant Difference from Hydrogen Bond *J. Phys. Chem. A* **2006**, *110*, 10163.
- (8) Molander, G. A.; Ito, T.; Cross-Coupling Reactions of Potassium Alkyltrifluoroborates with Aryl and 1-Alkenyl Trifluoromethanesulfonates *Org. Lett.* **2001**, *3*, 393.
- (9) Yin, J.; Xiang, B.; Huffman, M. A.; Raab, C. E.; Davies, I. W.; A General and Efficient 2-Amination of Pyridines and Quinolines *J. Org. Chem.* **2007**, *72*, 4554.
- (10) Olofsson, K.; PCT Int. Appl.: 2005; Vol. 2005123673.
- (11) Lorenz, J. C.; Long, J.; Yang, Z.; Xue, S.; Xie, Y.; Shi, Y.; A Novel Class of Tunable Zinc Reagents (RXZnCH₂Y) for Efficient Cyclopropanation of Olefins *J. Org. Chem.* **2003**, *69*, 327.
- (12) Wang, F.; Luo, T.; Hu, J.; Wang, Y.; Krishnan, H. S.; Jog, P. V.; Ganesh, S. K.; Prakash, G. K. S.; Olah, G. A.; Synthesis of gem-Difluorinated Cyclopropanes and Cyclopropenes: Trifluoromethyltrimethylsilane as a Difluorocarbene Source *Angew. Chem. Int. Ed.* **2011**, *50*, 7153.
- (13) Zhang, Y.; Cao, R.; Yin, F.; Hudock, M. P.; Guo, R.-T.; Krysiak, K.; Mukherjee, S.; Gao, Y.-G.; Robinson, H.; Song, Y.; No, J. H.; Bergan, K.; Leon, A.; Cass, L.; Goddard, A.; Chang, T.-K.; Lin, F.-Y.; Beek, E. V.; Papapoulos, S.; Wang, A. H. J.; Kubo, T.; Ochi, M.; Mukkamala, D.; Oldfield, E.; Lipophilic Bisphosphonates as Dual Farnesyl/Geranylgeranyl Diphosphate Synthase Inhibitors: An X-ray and NMR Investigation *J. Am. Chem. Soc.* **2009**, *131*, 5153.

5.8 Experimental

5.8.1 Computational modeling

Docking studies were performed as described in Chapter 4.

5.8.2 Synthesis

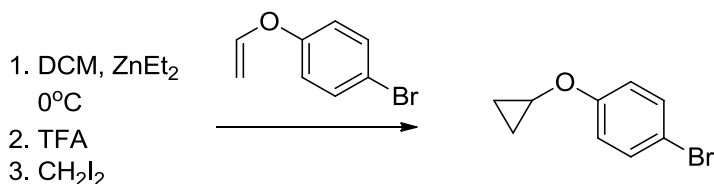
General Procedures for Characterization of Compounds

All intermediate compounds were purified by normal phase flash column chromatography on silica gel using a CombiFlash instrument and the solvent gradient indicated. The purified bisphosphonate tetra ester precursors of all final inhibitors were analyzed by reverse-phase HPLC and fully characterized by ^1H , ^{13}C and ^{31}P NMR, and MS. The homogeneity of the bisphosphonate tetra esters (>90%) was confirmed by C18 reversed phase HPLC. After ester hydrolysis, the final bisphosphonic acid products were precipitated and washed with deionized H_2O , HPLC grade acetonitrile and distilled Et_2O to obtain the inhibitors as white solids; quantitative conversion of each tetra ester to the corresponding bisphosphonic acid was confirmed by ^{31}P NMR. All final products were characterized by ^1H , ^{13}C , ^{31}P and ^{19}F NMR and HR-MS. Chemical shifts (δ) are reported in ppm relative to the internal deuterated solvent (^1H , ^{13}C) or external H_3PO_4 (δ 0.00 ^{31}P), unless indicated otherwise. High-Resolution MS spectra were recorded at the McGill University, MS facilities using electrospray ionization ($\text{ESI}^{+/-}$). The homogeneity of the final inhibitors was confirmed by HPLC. Only samples with >95% homogeneity were tested in the enzymatic assays for the determination of IC_{50} values. HPLC Analysis was performed using a Waters ALLIANCE[®] instrument. See Appendix III for HPLC traces of the final compounds.

Synthesis of novel boron coupling reagents:

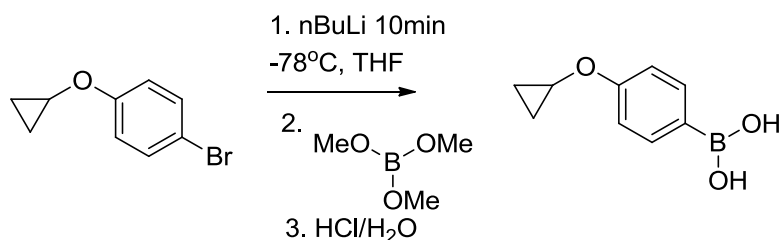
(4-cyclopropoxyphenyl)boronic acid was prepared as previously described (Olofsson, Kristofer *et.al.* PCT Int. Appl 2005123673, 19 Dec **2005**), but with a modified cyclopropanation procedure:

5.12 1-bromo-4-cyclopropoxybenzene

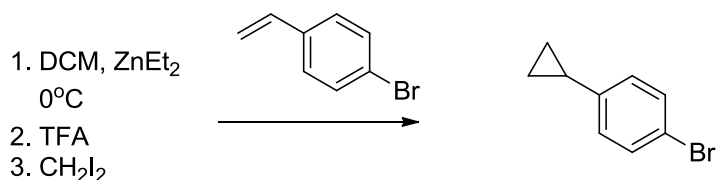


To freshly distilled DCM (40 mL) in a 250 mL RBF was added diethylzinc (18.8 mL 1.1 M in toluene, 20.6 mmol) under an Argon atmosphere and the flask was cooled to 0°C. A solution of TFA (1.58 mL, 20.6 mmol) in 10 mL DCM was added very slowly *via* syringe (careful, strongly exothermic) and the mixture was stirred for 10 min. A solution of CH₂I₂ (1.66 mL, 20.6 mmol) in 10 mL DCM was added *via* syringe and the mixture was stirred 10 min. A solution of alkene (1100 mg, 5.16 mmol) in 10 mL DCM was added *via* syringe and the reaction mixture was stirred at RT for 4h. The reaction was quenched with satd. NH₄Cl (20 mL), diluted with 150 mL toluene, separated and the organic phase was washed with 25 mL satd. NH₄Cl, 25 mL water and brine, dried over Na₂SO₄, filtered and concentrated in vacuo. . The residue was purified by silica gel chromatography using a CombiFlash instrument and hexanes as the eluent. Unreacted starting material and CH₂I₂ elute first followed by the desired product as a pale yellow oil (771 mg, 70%).

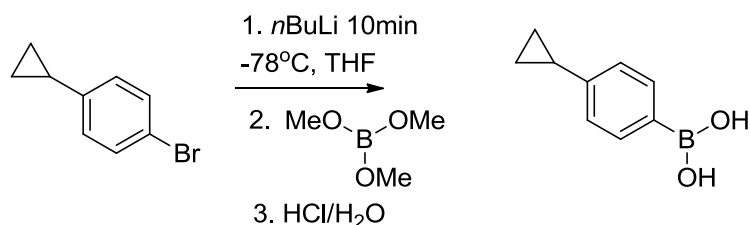
¹H NMR (300 MHz, CDCl₃) δ 7.42 – 7.31 (m, 2H), 6.99 – 6.85 (m, 2H), 3.77 – 3.62 (m, 1H), 0.83 – 0.69 (m, 4H). ¹³C NMR (75 MHz, CDCl₃) δ 158.02, 132.12, 116.75, 113.12, 50.99, 6.19.

5.13 (JDS05-149): (4-cyclopropoxyphenyl)boronic acid

To a solution of aryl bromide (725 mg, 3.40 mmol) in 20 mL anhydrous THF at -78°C was added *n*BuLi (1.6 M in Hex; 2.6 mL, 4.1 mmol) dropwise via under an Argon atmosphere and the mixture is stirred at -78°C for 30min. Trimethylborate (0.57 mL, 5.1 mmol) is added via syringe and the reaction is allowed to warm to RT overnight. The reaction mixture is cooled in an ice bath and quenched with 1M HCl (20.4 mL, 20.4 mmol) and stirred for 3h at RT. The mixture is diluted with 25 mL water, extracted 4 times with 25 mL DCM, the combined organic phases are dried over Na₂SO₄, filtered and concentrated in vacuo. The residue is suspended in petroleum ether, filtered and washed with a minimum of petroleum ether. Isolated 285 mg (47%) as a tan solid in ~90% purity. ¹H NMR (300 MHz, CDCl₃) δ 8.17 (d, *J* = 8.2 Hz, 2H), 7.16 (d, *J* = 8.2 Hz, 2H), 3.90 – 3.78 (m, 1H), 0.89 – 0.73 (m, 4H).

JDS05-132: 1-bromo-4-cyclopropylbenzene

Isolated 621 mg (96%) as a colorless oil. ¹H NMR (400 MHz, CDCl₃) δ 7.35 (d, *J* = 8.4 Hz, 2H), 6.94 (d, *J* = 8.2 Hz, 2H), 1.91 – 1.77 (m, 1H), 0.97 (q, *J* = 6.2 Hz, 2H), 0.66 (d, *J* = 5.9 Hz, 2H). ¹³C NMR (75 MHz, CDCl₃) δ 143.03, 131.19, 127.40, 118.77, 14.98, 9.32.

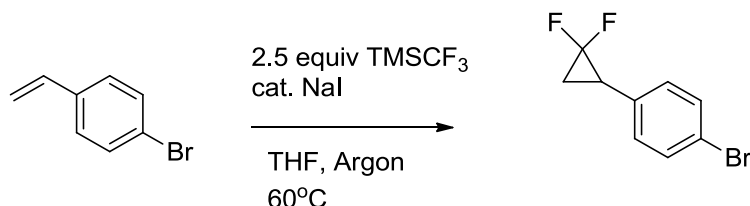
5.16 (JDS05-132): (4-cyclopropylphenyl)boronic acid

Isolated 1100 mg (51%) as a white solid in 100% purity by HPLC. ¹H NMR (400 MHz, CDCl₃) δ 8.10 (d, *J* = 8.0 Hz, 2H), 7.18 (d, *J* = 8.0 Hz, 1H), 1.97 (m, 1H), 1.10 – 0.99 (m, 2H), 0.80 (m, 2H). ¹³C NMR (75 MHz, CDCl₃) δ 149.18, 135.72, 135.64, 125.04, 15.91, 10.12, 3.33.

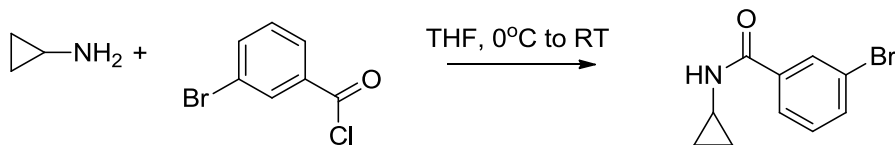
5.17 (JDS09-065): 1-bromo-4-(2,2-difluorocyclopropyl)benzene

This compound was synthesized according to literature procedure:

Wang, F.; Luo, T.; Hu, J.; Wang, Y.; Krishnan, H. S.; Jog, P. V.; Ganesh, S. K.; Prakash, G. K. S.; Olah, G. A. *Angew. Chem. Int. Ed.* **2011**, 50, 7153.



Isolated 310 mg (97%) as a colorless oil. ¹H NMR (300 MHz, CDCl₃) δ 7.45 (d, *J* = 8.5 Hz, 2H), 7.10 (d, *J* = 8.4 Hz, 2H), 2.70 (td, *J* = 12.4, 8.2 Hz, 1H), 1.92 – 1.76 (m, 1H), 1.65 – 1.51 (m, 1H).

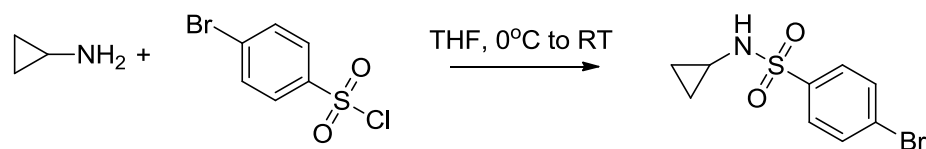
JDS07-011: 3-bromo-*N*-cyclopropylbenzamide

To an ice-cooled solution of 3-bromobenzoyl chloride (900 mg, 0.54 mL, 4.10 mmol) in 30 mL anhydrous THF was added cyclopropylamine (492 mg, 0.60 mL, 8.61 mmol) *via* syringe and the mixture was stirred at RT for 12 h. The volatiles were removed in vacuo and the residue was taken up in 100 mL EtOAc, washed 10 mL water, 10 mL 1 M HCl, 10

mL satd. NaHCO₃ and 10 mL brine. The organic phase was dried over Na₂SO₄ and concentrated in vacuo. The residue was purified by silica gel chromatography using a CombiFlash instrument and a solvent gradient from 1% to 40% EtOAc in hexanes. The desired compound elutes at 35% EtOAc and was collected as a white powder (1002 mg, 100%).

¹H NMR (300 MHz, CDCl₃) δ 7.87 (t, *J* = 1.8 Hz, 1H), 7.65 (m, 1H), 7.58 (ddd, *J* = 8.0, 1.9, 1.0 Hz, 1H), 7.25 (m, overlaps with solvent signal, 1H), 6.55 (bs, 1H), 2.94 – 2.77 (m, 1H), 0.84 (dd, *J* = 7.1, 1.8 Hz, 2H), 0.66 – 0.54 (m, 2H). ¹³C NMR (75 MHz, CDCl₃) δ 167.52, 136.36, 134.36, 130.10, 130.06, 125.51, 122.64, 69.59, 23.24, 6.72, 3.33. MS (ESI): calcd 240.00; found 240.06 [M+H]⁺

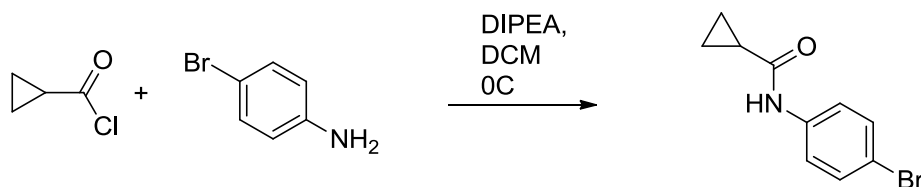
JDS07-010: 4-bromo-*N*-cyclopropylbenzenesulfonamide



To an ice-cooled solution of 4-bromobenzenesulfonyl chloride (495 mg, 1.94 mmol) in 30 mL anhydrous THF was added cyclopropylamine (232 mg, 0.28 mL, 4.07 mmol) *via* syringe and the mixture was stirred at RT for 12h. The volatiles were removed in vacuo and the residue was taken up in 100 mL EtOAc, washed 10 mL water, 10 mL 1 M HCl, 10 mL satd. NaHCO₃ and 10 mL brine. The organic phase was dried over Na₂SO₄ and concentrated in vacuo. The residue was purified by silica gel chromatography using a CombiFlash instrument and a solvent gradient from 1% to 25% EtOAc in hexanes. The desired compound elutes at 25% EtOAc and was collected as a white powder (429 mg, 80%).

¹H NMR (300 MHz, CDCl₃) δ 7.82 – 7.70 (m, 2H), 7.70 – 7.54 (m, 2H), 5.05 (bs, 1H), 2.31 – 2.14 (m, 1H), 0.63 – 0.50 (m, 4H). ¹³C NMR (75 MHz, CDCl₃) δ 138.63, 132.32, 128.97, 127.79, 24.25, 6.19, 3.33. MS (ESI): calcd 276.00; found 276.06 [M+H]⁺

JDS07-009: *N*-(4-bromophenyl)cyclopropanecarboxamide



To an ice-cooled solution of 4-bromoaniline (704 mg, 4.09 mmol) in 30 mL DCM was added *N,N*-diisopropylethylamine (1.50 mL, 8.16 mmol) followed by cyclopropanecarbonyl chloride (0.39 mL, 4.30 mmol) *via* syringe and the mixture was stirred at 0°C for 30 min. The reaction was quenched with methanol and the volatiles were removed in vacuo. The residue was purified by silica gel chromatography using a CombiFlash instrument and a solvent gradient from 2% to 50% EtOAc in hexanes. The desired compound elutes at 40% EtOAc and was collected as a white powder (860 mg, 83%). ¹H NMR (400 MHz, CDCl₃) δ 7.42 (s, 4H), 1.48 (m, 1H), 1.09 (m, 2H), 0.93 – 0.80 (m, 2H). ¹³C NMR (75 MHz, CDCl₃) δ 171.91, 137.14, 131.91, 121.18, 15.79, 8.16, 3.33. MS (ESI): calcd 240.00; found 240.09 [M+H]⁺

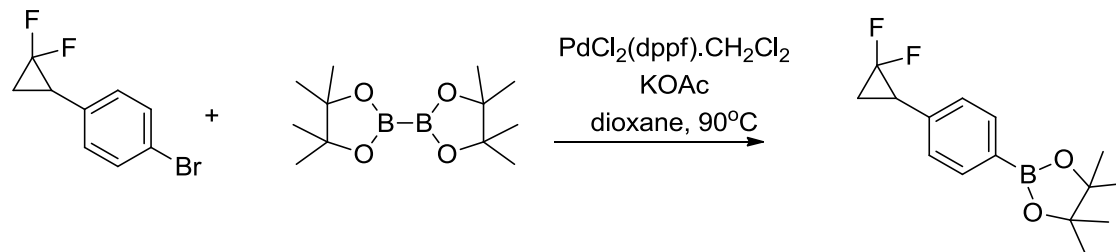
Matches literature spectral data:

Preparation of benzimidazolylpyrrolidinecarboxylates and related compounds as antivirals, Leivers, M.R. *et. al.*; PCT Int. Appl., 2008070447, 12 Jun 2008

General procedure for the synthesis of boron pinacol esters:

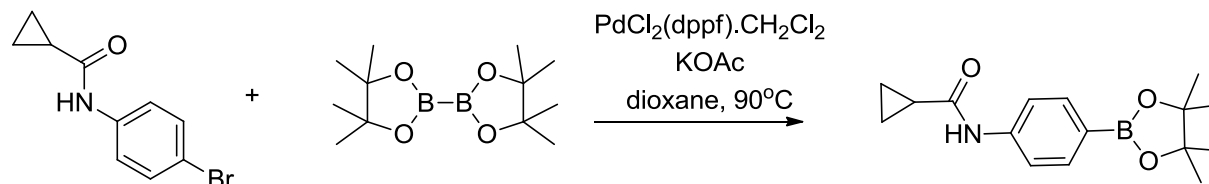
An 8 dram screp caw vial was charged with aryl bromide (1 equivalent), bis(pinacolato)diboron (1.1 equivalents), potassium acetate (2 equivalents) and PdCl₂(dppf).CH₂Cl₂ (0.1 equivalent); the vial was capped with a rubber septum, evacuated and back-filled with Argon. Anhydrous 1,4-dioxane was added via syringe to bring the concentration of aryl bromide to 0.1 M and the mixture was flushed again with Argon. The reaction was stirred at 90°C for 11 h. The reaction mixture was cooled down, diluted with Ethyl acetate, filtered through a Celite and concentrated in vacuo. The residue was purified by silica gel chromatography using a CombiFlash instrument and a solvent gradient from 1% to 100% EtOAc in hexanes.

JDS09-075: 2-(4-(2,2-difluorocyclopropyl)phenyl)-4,4,5,5-tetramethyl-1,3,2-dioxaborolane



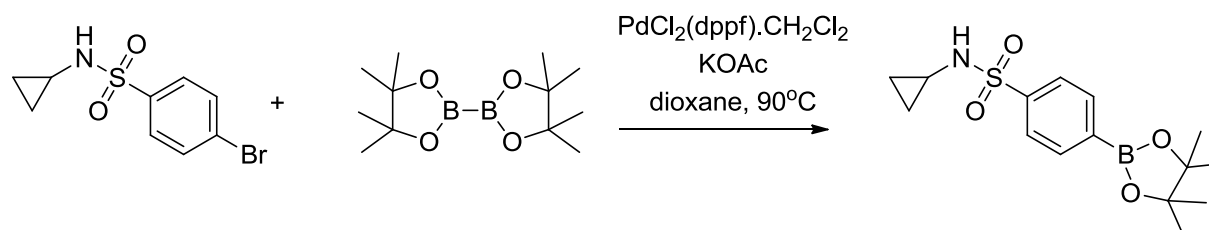
Isolated 90 mg (44%) as a colorless oil. ^1H NMR (400 MHz, CDCl_3) δ 7.77 (d, J = 8.1 Hz, 2H), 7.24 – 7.20 (m, 2H), 2.81 – 2.69 (m, 1H), 1.83 (m, 1H), 1.66 (m, 1H), 1.37 – 1.31 (m, 12H).

JDS07-017: *N*-(4-(4,4,5,5-tetramethyl-1,3,2-dioxaborolan-2-yl)phenyl)cyclopropanecarboxamide



54% yield based on recovered starting material, isolated as a white powder in ~90% purity as determined by ^1H NMR. ^1H NMR (300 MHz, CDCl_3) δ 7.76 (d, J = 8.4 Hz, 2H), 7.52 (d, J = 8.0 Hz, 2H), 1.53 (d, J = 24.2 Hz, 1H), 1.33 (s, 12H), 1.14 – 1.05 (m, 2H), 0.90 – 0.81 (m, 2H). ^{13}C NMR (75 MHz, CDCl_3) δ 172.01, 140.77, 135.77, 118.40, 83.70, 24.85, 15.85, 8.11.

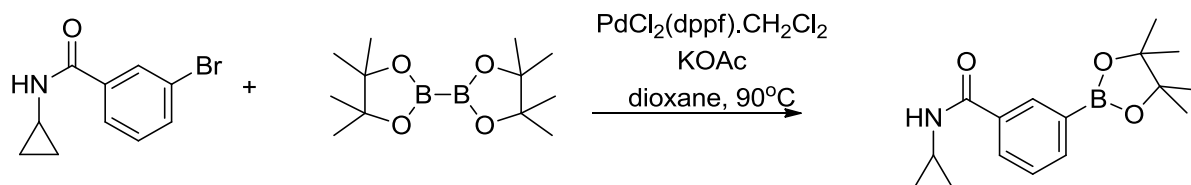
JDS07-013: *N*-cyclopropyl-4-(4,4,5,5-tetramethyl-1,3,2-dioxaborolan-2-yl)benzenesulfonamide



85%, isolated as a pale yellow syrup in ~90% purity as determined by ^1H NMR. ^1H NMR (400 MHz, CDCl_3) δ 7.95 (d, J = 8.3 Hz, 2H), 7.88 (d, J = 8.3 Hz, 2H), 4.84 (s, 1H), 2.28 –

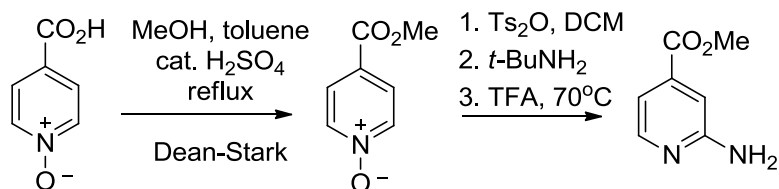
2.18 (m, 1H), 1.36 (s, 12H), 1.29 – 1.22 (m, 1H), 0.61 – 0.55 (m, 4H). ^{13}C NMR (75 MHz, CDCl_3) δ 141.75, 135.22, 126.33, 84.40, 24.83, 24.21, 6.01.

JDS07-014: *N*-cyclopropyl-3-(4,4,5,5-tetramethyl-1,3,2-dioxaborolan-2-yl)benzamide



83%, isolated as white powder in ~90% purity as determined by ^1H NMR. ^1H NMR (300 MHz, CDCl_3) δ 8.02 – 7.95 (m, 2H), 7.92 (d, J = 7.4 Hz, 1H), 7.45 (t, J = 7.9 Hz, 1H), 6.31 (s, 1H), 2.90 (d, J = 3.1 Hz, 1H), 1.35 (s, 12H), 0.87 (m, 2H), 0.63 (m, 2H). ^{13}C NMR (75 MHz, CDCl_3) δ 168.77, 137.81, 133.70, 131.89, 130.62, 128.17, 84.12, 24.85, 23.08, 6.71, 3.33.

5.5 methyl 2-aminoisonicotinate:



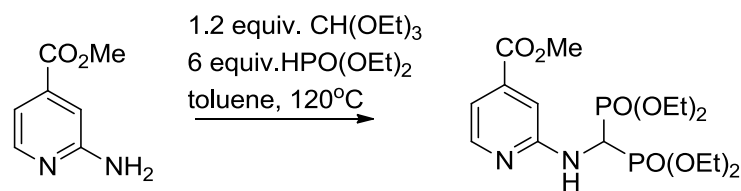
Isonicotinic acid *N*-oxide (3.00 g, 21.6 mmol) was dissolved in 20 mL 1:1 methanol/toluene, a catalytic amount H_2SO_4 was added and the flask was equipped with a Dean Stark trap filled with toluene. The mixture was refluxed overnight. The reaction was terminated by cooling in an ice bath, and neutralized with satd. sodium carbonate. The solution was extracted using (5 x 20 mL) DCM; the organic phases were combined, washed with brine, dried with MgSO_4 , filtered and concentrated in vacuo. The residue was purified by silica gel chromatography using a CombiFlash instrument and a solvent gradient from 100% hexanes to 100% EtOAc to give 4-(methoxycarbonyl)pyridine 1-oxide as a white powder (1.46 mg, 45%). ^1H NMR (300 MHz, CDCl_3) δ 8.24 – 8.16 (m, 2H), 7.93 – 7.79 (m, 2H), 3.94 (s, 3H).

To an ice-cooled solution of the above product (4-(methoxycarbonyl)pyridine 1-oxide, 300 mg, 1.96 mmol) in CHCl_3 was added tosyl anhydride (2877 mg, 8.82 mmol) and the mixture was stirred for 5 min. Next, *t*- BuNH_2 (1.24 mL, 11.8 mmol) was added dropwise

via syringe to the activated N-oxide while maintaining the reaction temperature below 5°C. The reaction was monitored by TLC and until complete consumption of starting material (~30 min) was observed. TFA (10.0 mL, 131 mmol) was added to the reaction mixture and the reaction was stirred at 70°C overnight. The mixture was diluted with water (5 mL) and DCM (10 mL) and carefully neutralized with saturated NaHCO₃. The aqueous layer was extracted using DCM (4 x 10 mL). The combined organic layers were washed once with brine, dried over MgSO₄, filtered and concentrated in vacuo. The residue was purified by silica gel chromatography using a CombiFlash instrument and a solvent gradient from 100% hexanes to 100% EtOAc and then to 25% MeOH in EtOAc (all eluents contained 0.1% triethylamine) to yield the desired methyl 2-aminoisonicotinate product as reddish/brown crystals (153.3 mg, 51%). ¹H NMR (400 MHz, CDCl₃) δ 8.19 (d, J = 5.2 Hz, 1H), 7.16 (dd, J = 5.3, 1.3 Hz, 1H), 7.07 (s, 1H), 4.59 (s, 2H), 3.94 – 3.89 (m, 3H).

Consistent with literature: Yin, J.; Xiang, B.; Huffman, M.A.; Raab, C.E.; David, I.W.; A general and efficient 2-amination of pyridines and quinolines, *J. Org. Chem.* **2007**, *12*, 4554-4557

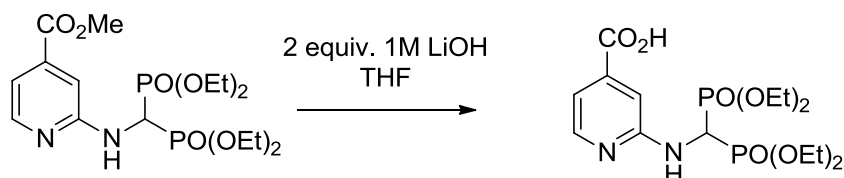
5.6 methyl 2-((bis(diethoxyphosphoryl)methyl)amino)isonicotinate:



A 15 mL pressure vessel was charged with the methyl 2-aminoisonicotinate (50 mg, 0.33 mmol), diethyl phosphite (0.25 mL, 2.0 mmol), triethyl orthoformate (0.07 mL, 0.4 mmol) and dissolved in 1 mL toluene. The mixture was stirred at 120°C overnight. The solution was cooled to room temperature, diluted with ethyl acetate, washed with saturated NaHCO₃, brine, dried over MgSO₄, filtered and concentrated in vacuo. The residue was purified by silica gel (silica was pre-washed with 0.1% NEt₃ in hexanes/EtOAc 3:1) chromatography on a CombiFlash instrument, using a solvent gradient from 1:3 EtOAc/Hexanes to 100% EtOAc and then to 25% MeOH in EtOAc to give the title compound as a pale yellow powder (106.4 mg, 74%). ¹H NMR (400 MHz, CDCl₃) δ 8.21 (d, J = 5.2 Hz, 1H), 7.16 (d, J = 5.3 Hz, 1H), 7.10 (s, 1H), 5.51 (td, J = 22.1, 10.1 Hz, 1H),

5.00 (d, $J = 10.1$ Hz, 1H), 4.26 – 4.07 (m, 8H), 3.92 (s, 3H), 1.25 (td, $J = 7.1, 5.1$ Hz, 12H). ^{13}C NMR (75 MHz, CD_3OD) δ 165.58, 130.92, 122.52, 113.55, 110.87, 107.87, δ 63.47 (d, $J = 17.7$ Hz), 54.46, 44.49 (t, $J = 149.9$ Hz), 15.90 – 14.76 (m). ^{31}P NMR (81 MHz, CD_3OD) δ 18.16 (s). MS (ESI): calcd 461.12; found 461.0 $[\text{M}+\text{Na}]^+$

5.7 2-((bis(diethoxyphosphoryl)methyl)amino)isonicotinic acid:

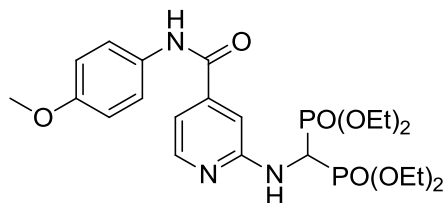


To an ice-cooled solution of methyl 2-((bis(diethoxyphosphoryl)methyl)amino)isonicotinate (50.0 mg, 0.114 mmol) in 5 mL of THF was added 1.0 M LiOH (0.28 mL, 0.285 mmol) and stirred at 0°C for 1h. The reaction mixture was then acidified with 1M HCl and evaporated to dryness under reduced pressure to obtain the free acid. The residue was re-dissolved in EtOAc and washed with water. The aqueous layer was back-extracted with 4 x 10 mL EtOAc. The organic layers were combined, washed with brine, dried over MgSO_4 , filtered and concentrated in vacuo to give the title compound as a yellow solid (20.6 mg, 43 %). ^1H NMR (400 MHz, CD_3OD) δ 8.13 (d, $J = 3.6$ Hz, 1H), 7.27 (s, 1H), 7.11 (d, $J = 4.4$ Hz, 1H), 5.67 (t, $J = 23.5$ Hz, 1H), 4.17 (m, 8H), 1.26 (dd, $J = 14.7, 7.6$ Hz, 12H). ^{31}P NMR (81 MHz, CD_3OD) δ 19.84 (s). MS (ESI): calcd 447.11, found 447.0 $[\text{M}+\text{Na}]^+$

General procedure for amide coupling:

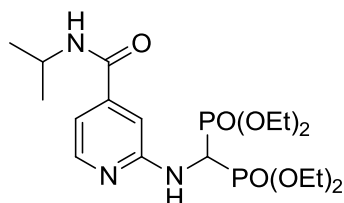
To a mixture of 2-((bis(diethoxyphosphoryl)methyl)amino)isonicotinic acid (1 equivalent) and amine (1.50 equivalents) in a minimal amount of anhydrous DMF was added in sequence: DIPEA (3 equivalents) and HATU (1.50 equivalents). The reaction was stirred at RT overnight. The reaction mixture was diluted with 100 mL EtOAc, washed with 10 mL saturated NaHCO_3 and 5 times 10 mL water and washed with brine, dried over anhydrous MgSO_4 , filtered and concentrated in vacuo. The residue was purified by silica gel (silica was pre-washed with 0.1% NEt_3 in hexanes/EtOAc 3:1) chromatography on a CombiFlash instrument, using a solvent gradient from 1:10 EtOAc/Hexanes to 100% EtOAc and then to 20% MeOH in EtOAc to give the desired amides.

JS: Tetraethyl (((4-((4-methoxyphenyl)carbamoyl)pyridin-2-yl)amino)methylene) bis(phosphonate)



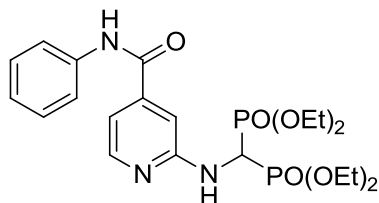
Isolated 145 mg (58%) as a pale yellow solid. ^1H NMR (400 MHz, CD_3OD) δ 8.19 (d, J = 5.3 Hz, 1H), 7.56 (d, J = 9.0 Hz, 2H), 7.16 (s, 1H), 7.05 (d, J = 5.1 Hz, 1H), 6.92 (d, J = 9.0 Hz, 2H), 5.70 (t, J = 23.5 Hz, 1H), 4.27 – 4.07 (m, 8H), 3.79 (s, 3H), 1.35 – 1.17 (m, 12H). ^{13}C NMR (75 MHz, CD_3OD) δ 165.58, 157.14, 156.98, 147.50, 144.16, 130.92, 122.52, 113.55, 110.87, 107.87, δ 63.47 (d, J = 17.6 Hz), 54.46, 44.50 (t, J = 150.2 Hz), 15.24 (dd, J = 6.2, 3.1 Hz). ^{31}P NMR (81 MHz, CD_3OD) δ 19.34 (s). MS (ESI): calcd 530.182, found 530.36 $[\text{M}+\text{H}]^+$

JS: Tetraethyl (((4-(isopropylcarbamoyl)pyridin-2-yl)amino)methylene) bis(phosphonate)



Isolated 118 mg (54%) as a beige solid. ^1H NMR (300 MHz, CD_3OD) δ 8.13 (d, J = 5.3 Hz, 1H), 7.05 (s, 1H), 6.94 (d, J = 5.2 Hz, 1H), 5.67 (t, J = 23.5 Hz, 1H), 4.27 – 4.06 (m, 8H), 3.30 (m, 7H), 1.32 – 1.17 (m, 12H). ^{13}C NMR (75 MHz, CD_3OD) δ 166.51, 157.07, 147.33, 143.93, 110.76, 107.73, δ 63.45 (d, J = 18.2 Hz), 44.47 (t, J = 150.1 Hz), 41.80, 20.99, 15.25 (dd, J = 6.0, 3.0 Hz). ^{31}P NMR (81 MHz, CD_3OD) δ 19.73 (s). MS (ESI): calcd 466.1872, found 466.34 $[\text{M}+\text{H}]^+$

JS: Tetraethyl (((4-(phenylcarbamoyl)pyridin-2-yl)amino)methylene) bis(phosphonate)



Isolated 82 mg (35%) as a pale brown oil. ^1H NMR (400 MHz, CD_3OD) δ 8.19 (t, $J = 5.0$ Hz, 1H), 7.66 (t, $J = 8.3$ Hz, 2H), 7.40 – 7.32 (m, 2H), 7.19 – 7.13 (m, 2H), 7.07 (d, $J = 5.3$ Hz, 1H), 5.71 (t, $J = 23.5$ Hz, 1H), 4.25 – 4.13 (m, 8H), 1.27 (t, $J = 7.1$ Hz, 12H). ^{13}C NMR (75 MHz, CD_3OD) δ 165.44, 157.01, 147.36, 144.02, 130.78, 122.39, 113.41, 110.73, 107.73, δ 63.33 (d, $J = 17.7$ Hz), 44.36 (t, $J = 149.9$ Hz), 16.89 – 13.49 (m). ^{31}P NMR (81 MHz, CD_3OD) δ 19.74 (s). MS (ESI): calcd 500.17), found 500.35 $[\text{M}+\text{H}]^+$

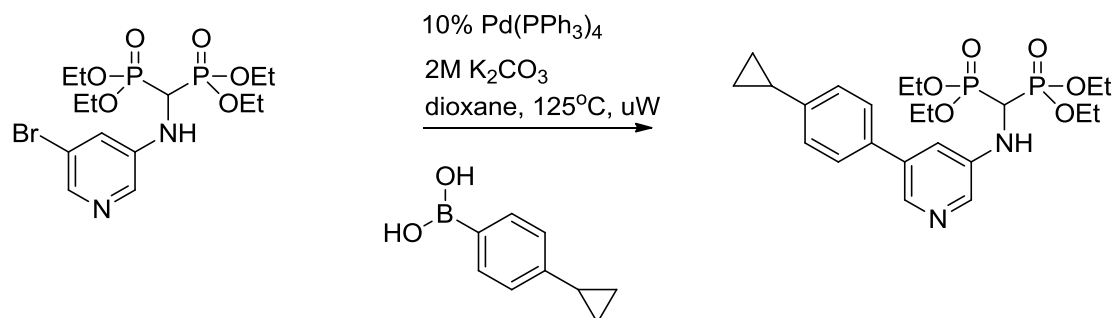
4.19 tetraethyl (((5-bromopyridin-3-yl)amino)methylene)bis (phosphonate)

See Chapter 4

General procedure of Suzuki cross coupling

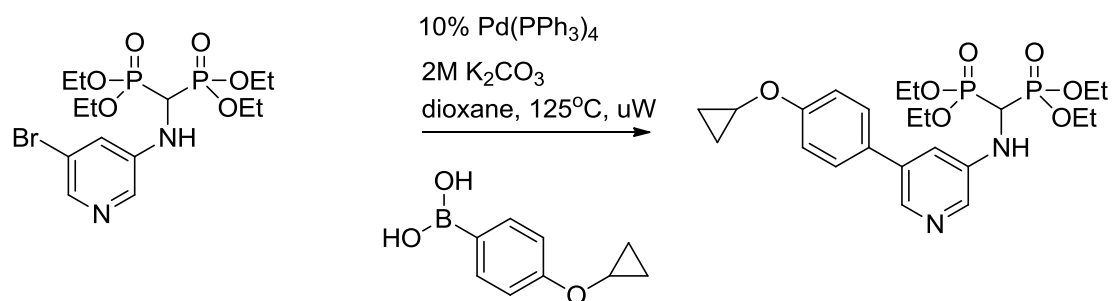
A 2 mL microwave reaction vessel was charged with a magnetic stir bar, boronic acid or boronate ester (1.5 equivalent), $\text{Pd}(\text{PPh}_3)_4$ (0.1 equivalent) and aryl halide (if a solid, 1 equivalent); if the aryl halide is an oil, it was added as a solution in 1,4-dioxane *via* syringe. The reaction vessel was capped with a septum, degassed and flushed with Argon. 1,4-Dioxane was added to bring the concentration of aryl halide to 0.1 M and the mixture was again degassed and flushed with Argon. A solution of 2M K_2CO_3 (2.5 equivalents) was added and the mixture was again degassed and flushed with Argon. The rubber septum was replaced by a Teflon lined seal, under a flow of Argon. The reaction was irradiated to 125 $^\circ\text{C}$ for 10 to 30min ($\sim 40\text{W}$), reaction progress was followed by TLC and/or HPLC. The crude was filtered through a plug of Celite, rinsed with 10 mL 1:1 EtOAc/Acetone and concentrated under vacuum. The residue was purified by silica gel chromatography (silica was pre-washed with 0.1% Et_3N in hexanes/EtOAc, 3:1 ratio) using a CombiFlash instrument and a solvent gradient from 1:1 EtOAc/Hexanes to 100% EtOAc and then to 25% MeOH in EtOAc.

JDS05-136: tetraethyl (((5-(4-cyclopropylphenyl)pyridin-3-yl)amino)methylene)bis(phosphonate)



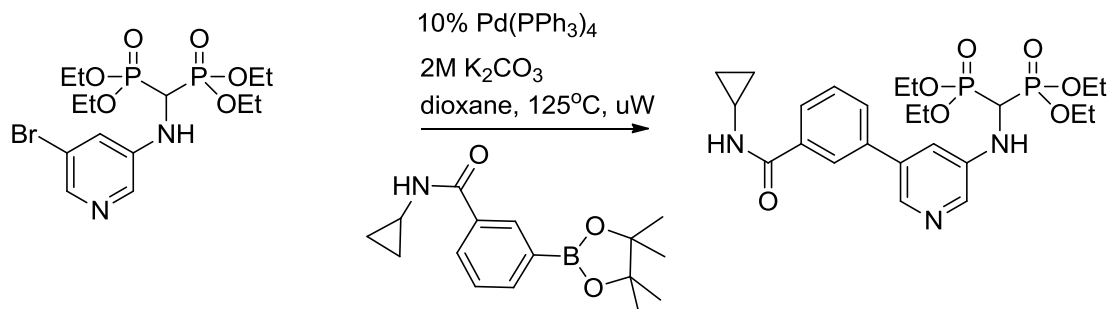
Isolated 53mg (98%) as a colorless oil. ^1H NMR (300 MHz, CDCl_3) δ 8.26 (s, 1H), 8.07 (s, 1H), 7.44 (d, $J = 8.3$ Hz, 2H), 7.16 (m, 3H), 4.39 – 4.02 (m, 8H), 1.94 (ddd, $J = 13.5, 8.5, 5.0$ Hz, 1H), 1.28 (dt, $J = 12.5, 7.1$ Hz, 12H), 1.06 – 0.94 (m, 2H), 0.74 (dt, $J = 6.6, 4.7$ Hz, 2H). ^{13}C NMR (75 MHz, CDCl_3) δ 144.34, 138.66, 135.07, 134.84, 126.92, 126.20, 117.98, δ 63.68 (dt, $J = 23.1, 3.3$ Hz), 49.84 (t, $J = 147.7$ Hz), 16.77 – 15.72 (m), 15.15, 9.53. ^{31}P NMR (81 MHz, CDCl_3) δ 14.73 (s). MS (ESI): calcd 497.20; found 497.37 $[\text{M}+\text{H}]^+$

JDS05-117: Tetraethyl (((5-(4-cyclopropoxyphenyl)pyridin-3-yl)amino)methylene)bis(phosphonate)



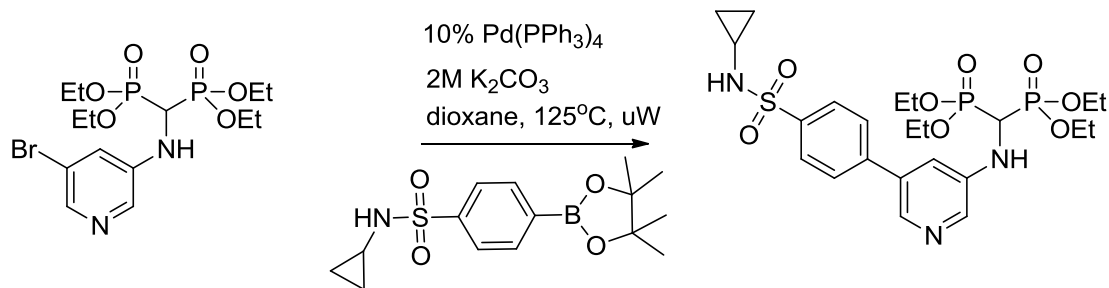
Isolated 66 mg (99%) as a pale yellow oil. ^1H NMR (500 MHz, CDCl_3) δ 8.25 (s, 1H), 8.06 (d, $J = 2.4$ Hz, 1H), 7.51 – 7.45 (m, 2H), 7.16 – 7.11 (m, 3H), 4.30 – 4.10 (m, 8H), 3.81 – 3.75 (m, 1H), 1.29 (dt, $J = 19.1, 7.1$ Hz, 12H), 0.84 – 0.79 (m, 4H). ^{13}C NMR (126 MHz, CDCl_3) δ 159.11, 142.30, 138.63, 136.46, 134.90, 130.55, 128.05, 117.80, 115.49, δ 63.63 (d, $J = 36.9$ Hz), 50.91, 49.89 (t, $J = 147.6$ Hz), 16.85 – 15.63 (m), 6.22. ^{31}P NMR (81 MHz, CDCl_3) δ 14.73 (s). MS (ESI): calcd 513.19; found : 513.20 $[\text{M}+\text{H}]^+$

JDS-07-018: Tetraethyl (((5-(3-(cyclopropylcarbamoyl)phenyl)pyridin-3-yl)amino)methylene)bis(phosphonate)



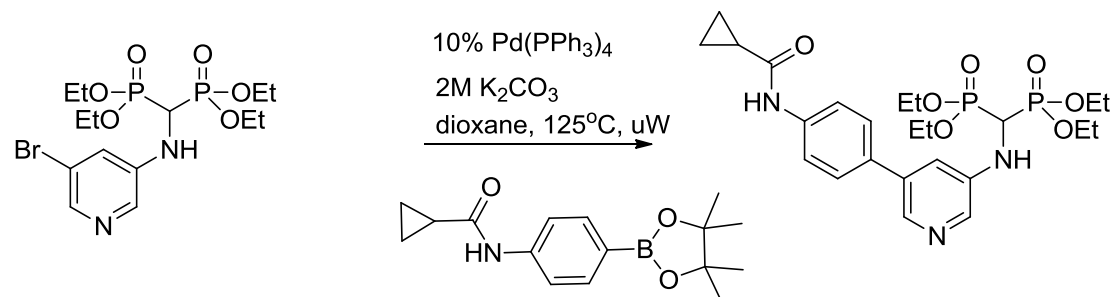
Isolated 28 mg (48%) as colorless oil. ^1H NMR (400 MHz, acetone- d_6) δ 8.34 (s, 1H), 8.23 (s, 1H), 8.13 (s, 1H), 7.90 – 7.80 (m, 3H), 7.62 (s, 1H), 7.54 (t, J = 7.7 Hz, 1H), 5.39 (d, J = 10.8 Hz, 1H), 4.67 (td, J = 22.2, 10.4 Hz, 1H), 4.23 – 4.07 (m, 8H), 2.95 (td, J = 7.3, 3.8 Hz, 1H), 1.23 (dt, J = 18.1, 7.1 Hz, 12H), 0.76 (m, 2H), 0.66 – 0.60 (m, 2H). ^{13}C NMR (75 MHz, acetone- d_6) δ 167.41, 138.47, 137.24, 136.10, 135.71, 129.49, 128.89, 126.62, 125.68, 117.18, δ 62.89 (d, J = 12.8 Hz), 48.80 (t, J = 145.5 Hz), 23.02, 15.85 (d, J = 2.0 Hz), 5.56. ^{31}P NMR (81 MHz, acetone- d_6) δ 20.62 (s). MS (ESI): calcd 540.51, found 540.3 $[\text{M}+\text{H}]^+$

JDS-07-019: Tetraethyl (((5-(4-(N-cyclopropylsulfamoyl)phenyl)pyridin-3-yl)amino)methylene)bis(phosphonate)



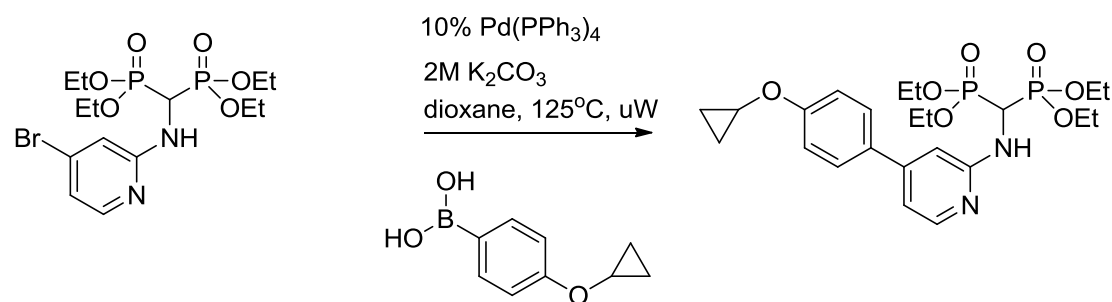
Isolated 22 mg (35%) as a colorless oil. ^1H NMR (400 MHz, acetone- d_6) δ 8.39 (d, J = 2.7 Hz, 1H), 8.28 (d, J = 1.9 Hz, 1H), 7.96 (d, J = 8.7 Hz, 4H), 7.68 (t, J = 2.3 Hz, 1H), 5.44 (d, J = 9.5 Hz, 1H), 4.69 (td, J = 22.1, 10.4 Hz, 1H), 4.23 – 4.08 (m, 8H), 2.25 (m, 1H), 1.23 (dt, J = 17.4, 7.1 Hz, 12H), 0.56 (m, 4H). ^{13}C NMR (75 MHz, acetone- d_6) δ 143.62, 142.39, 139.99, 137.23, 137.01, 134.60, 127.82, 127.53, 117.07, δ 62.86 (d, J = 11.1 Hz), 48.78 (t, J = 146.0 Hz), 24.19, 15.85 (d, J = 1.8 Hz), 5.17. ^{31}P NMR (81 MHz, acetone- d_6) δ 20.56 (s). MS (ESI): calcd 576.56, found 576.3 $[\text{M}+\text{H}]^+$

JDS-07-020: Tetraethyl (((5-(4-(cyclopropanecarboxamido)phenyl)pyridin-3-yl)amino)methylene)bis(phosphonate)



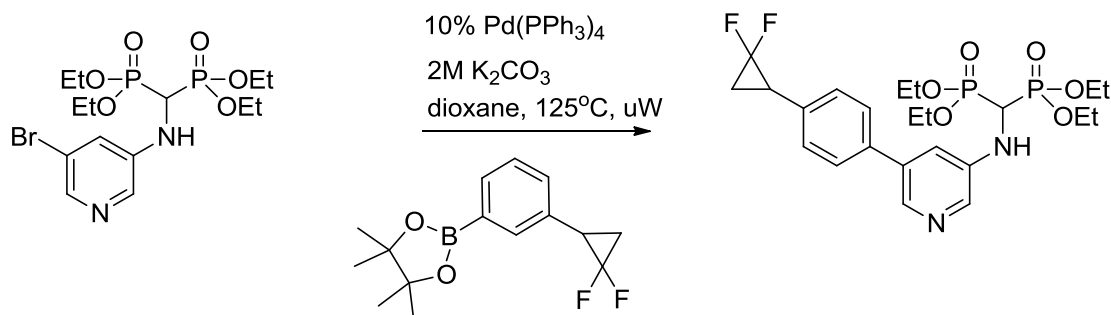
Isolated 28 mg (48%) as colorless oil. ^1H NMR (400 MHz, acetone- d_6) δ 9.52 (s, 1H), 8.27 (d, J = 2.6 Hz, 1H), 8.20 (d, J = 1.8 Hz, 1H), 7.77 (d, J = 8.7 Hz, 2H), 7.64 (d, J = 8.7 Hz, 2H), 7.55 (s, 1H), 5.27 (d, J = 10.4 Hz, 1H), 4.64 (td, J = 22.1, 10.3 Hz, 1H), 4.22 – 4.06 (m, 8H), 1.83 – 1.73 (m, 1H), 1.22 (dt, J = 17.9, 7.1 Hz, 12H), 0.95 – 0.87 (m, 2H), 0.83 – 0.75 (m, 2H). ^{13}C NMR (75 MHz, acetone- d_6) δ 171.65, 139.61, 137.04, 135.61, 132.83, 127.19, 119.34, 119.25, 116.53, δ 62.78 (d, J = 12.9 Hz), 48.89 (t, J = 145.0 Hz), 15.83 (d, J = 1.7 Hz), 14.62, 6.80. ^{31}P NMR (81 MHz, acetone- d_6) δ 20.60 (s). MS (ESI): calcd 540.51, found 540.3 $[\text{M}+\text{H}]^+$

YS05-029: Tetraethyl (((4-(4-cyclopropoxyphenyl)pyridin-2-yl)amino)methylene)bis(phosphonate)



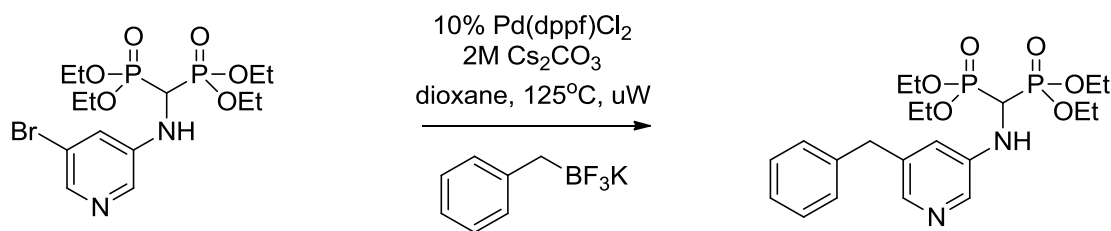
Isolated 49 mg (73%) as a white solid. ^1H NMR (300 MHz, CDCl_3) δ 8.09 (d, J = 5.2 Hz, 1H), 7.52 (d, J = 8.6 Hz, 2H), 7.10 (d, J = 8.6 Hz, 2H), 6.83 (d, J = 5.2 Hz, 1H), 6.70 (s, 1H), 5.58 (td, J = 22.2, 9.5 Hz, 1H), 5.01 (d, J = 9.5 Hz, 1H), 4.14-4.21 (m, 8H), 3.90 – 3.57 (m, 1H), 1.20-1.28 (m, 12H), 0.79 (m, 4H). ^{13}C NMR (75 Hz, CDCl_3) δ 159.71, 156.54, 149.33, 147.73, 131.05, 127.86, 115.39, 112.57, 106.33, 63.26-63.48 (m, CH_2), 50.95, 45.09 (t, J = 146.2 Hz, CH), 16.22-16.36 (m, CH_3), 6.24. ^{31}P NMR (CDCl_3) δ 18.99 ppm. MS (ESI): calcd 513.19, found 513.21 $[\text{M}+\text{H}]^+$

JDS09-082: tetraethyl (((5-(4-(2,2-difluorocyclopropyl)phenyl)pyridin-3-yl)amino)methylene)bis(phosphonate)



Isolated 44.2 mg (76%) as a pale yellow oil. ^1H NMR (400 MHz, CDCl_3) δ 8.27 (s, 1H), 8.10 (d, $J = 2.5$ Hz, 1H), 7.52 (d, $J = 7.9$ Hz, 2H), 7.33 (d, $J = 8.1$ Hz, 2H), 7.15 (s, 1H), 4.32 – 4.12 (m, 9H), 2.80 (m, 1H), 1.94 – 1.81 (m, 1H), 1.67 (m, 1H), 1.36 – 1.21 (m, 12H). ^{13}C NMR (75 MHz, CDCl_3) δ 142.34, 138.79, 136.80, 136.25, 135.61, 133.73, 128.62, 127.14, 118.01, 63.77, 63.51, δ 112.44 (dd, $J = 287.3, 283.9$ Hz), 63.64 (d, $J = 20.1$ Hz), 49.88 (t, $J = 147.7$ Hz), 26.89 (t, $J = 11.5$ Hz), 17.16 (t, $J = 10.5$ Hz), 16.64 – 15.79 (m). ^{31}P NMR (CDCl_3) δ 18.99 ppm. MS (ESI): calcd 533.18, found 533.31 $[\text{M}+\text{H}]^+$

JDS05-124: (((5-benzylpyridin-3-yl)amino)methylene)bis(phosphonate):



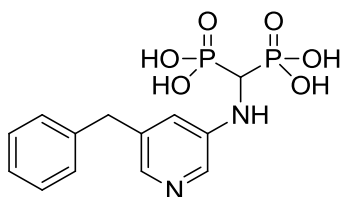
A 0.5-2 mL microwave reaction vessel was charged with a magnetic stir bar, tetraethyl (((5-bromopyridin-3-yl)amino)methylene)bis(phosphonate) (50.0 mg, 0.11 mmol), potassium benzyltrifluoroborate (53.9 mg, 0.27 mmol, 2.5 equivalents) and $\text{Pd}(\text{dppf})\text{Cl}_2 \cdot \text{CH}_2\text{Cl}_2$ (8.0 mg, 0.01 mmol, 0.1 equivalent); capped with a septum, degassed and flushed with Argon. A volume of 1.09 mL 1,4-dioxane was added to bring the concentration of the aryl bromide to 0.1M, and the mixture was again degassed and flushed with Argon. A solution of 2M Cs_2CO_3 (0.16 mL, 2.5 equivalents) was added and the mixture was again degassed and flushed with Argon. The rubber septum was replaced by a Teflon lined seal, under Argon flow. The reaction was irradiated to 125°C for 30min (~40W), reaction progress was monitored HPLC. After 30min, HPLC analysis showed ~30% conversion, the same

amounts of boron reagent, catalyst and base were added to the reaction vessel and irradiation was continued. After another 30min HPLC analysis showed ~66% conversion, the same amounts boron reagent, catalyst and base were added to the reaction vessel and irradiation was continued. After an additional 30 min, HPLC analysis showed complete conversion. The crude was filtered through a plug of Celite, rinsed with 10 mL 1:1 EtOAc/Acetone and concentrated in vacuo. The residue was purified by silica gel (silica was pre-washed with 0.1% NEt₃ in hexanes:EtOAc 3:1) chromatography using a CombiFlash instrument and a solvent gradient from 1:1 EtOAc/Hexanes to 100% EtOAc and then to 25% MeOH in EtOAc. The product was isolated as a purple oil in ~75% purity (40 mg). The mixture was purified by preparative HPLC on a Waters Atlantis C18 column using a gradient from 5% CH₃CN/H₂O to 95% with 0.1% formic acid. Fractions of sufficient purity were pooled and lyophilized to dryness. Isolated 28 mg (55%) as a white, waxy solid. ¹H NMR (400 MHz, DMSO-d₆) δ 8.08 (s, 1H), 7.72 (s, 1H), 7.30 – 7.09 (m, 6H), 5.99 (d, *J* = 10.6 Hz, 1H), 4.63 (td, *J* = 22.9, 10.8 Hz, 1H), 4.13 – 3.86 (m, 8H), 3.79 (s, 2H), 1.09 (dt, *J* = 23.7, 7.0 Hz, 12H). ¹³C NMR (126 MHz, DMSO-d₆) δ 143.65, 141.34, 138.65, 136.65, 135.05, 128.99, 128.79, 126.44, 119.18, δ 62.98 (d, *J* = 21.6 Hz), 48.10 (t, *J* = 144.6 Hz), 38.74, 16.62, 16.60. ³¹P NMR (81 MHz, DMSO-d₆) δ 20.180 (s). MS (ESI): calcd 471.181, found 471.33 [M+H]⁺

General procedure of deprotection of tetra-ethyl bisphosphonate esters:

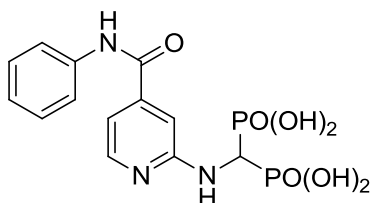
A 12 mL Teflon lined screw cap vial was charged with the tetra-ethyl bisphosphonate compound, dissolved in 5 mL distilled DCM and cooled in an ice bath. Bromotrimethyl silane (15 equivalents) was added via syringe and the reaction mixture was stirred at RT for 5-7 days. The reaction mixture was transferred to a 10 mL recovery flask and concentrated in vacuo (satd. NaHCO₃ in receiving flask). To the resulting oil was added 2 mL of HPLC-grade MeOH and concentrated in vacuo, this was repeated a total of five times. The crude thus obtained was suspended in a minimum amount of HPLC-grade MeOH, the mixture was sonicated and the desired compound was precipitated out of solution by the addition of Milli-Q water. The slurry was filtered and the cake washed twice with Milli-Q water, twice with HPLC-grade CH₃CN and twice with distilled Et₂O. The residue was then dried under high vacuum to obtain the desired product.

Inhibitor 5.4 (JDS05-126): (((5-benzylpyridin-3-yl)amino)methylene)diphosphonic acid



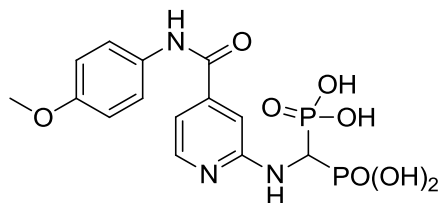
Isolated 15.0 mg (79%) as a white powder. ^1H NMR (500 MHz, D_2O) δ 7.86 (d, $J = 2.5$ Hz, 1H), 7.65 (s, 1H), 7.39 – 7.30 (m, 4H), 7.26 (t, $J = 6.7$ Hz, 1H), 7.07 (s, 1H), 3.92 (s, 2H), 3.65 (t, $J = 19.0$ Hz, 1H). ^{13}C NMR (126 MHz, D_2O) δ 145.17, 140.97, 137.71, 136.16, 132.55, 128.74, 128.69, 126.34, 120.10, δ 52.10 (t, $J = 123.5$ Hz), 38.23. HSQC ^1H - ^{13}C : δ ^1H 3.65 correlates with ^{13}C δ 52.10. ^{31}P NMR (81 MHz, D_2O) δ 15.06 (s). HRMS: calcd 357.0405 for $(\text{C}_{13}\text{H}_{15}\text{N}_2\text{O}_6\text{P}_2)$, found m/z 357.04149 $[\text{M}-\text{H}]^-$

Inhibitor 5.8 (JS02-003): (((4-(Phenylcarbamoyl)pyridin-2-yl)amino)methylene)diphosphonic acid



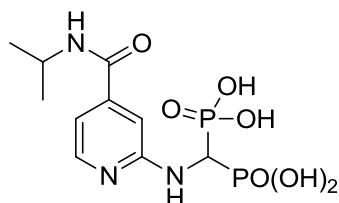
Isolated 19 mg (49%) as fine yellow crystals. ^1H NMR (400 MHz, D_2O) δ 7.93 (d, $J = 5.4$ Hz, 1H), 7.46 (dd, $J = 8.5, 1.1$ Hz, 2H), 7.38 (dd, $J = 10.7, 5.2$ Hz, 2H), 7.21 (t, $J = 7.4$ Hz, 1H), 6.91 (s, 1H), 6.75 (d, $J = 5.4$ Hz, 1H); central methylene obscured by solvent signal. ^{13}C NMR (75 MHz, D_2O) δ 183.70, 168.57, 158.69, 147.68, 143.62, 136.47, 129.10, 125.97, 122.65, 109.11. ^{31}P NMR (81 MHz, D_2O) δ 14.91. HRMS: calcd 386.0307 for $(\text{C}_{13}\text{H}_{14}\text{N}_3\text{O}_7\text{P}_2)$, found (m/z) 386.03035 $[\text{M}-\text{H}]^-$

Inhibitor 5.9 (JS02-018): (((4-((4-Methoxyphenyl)carbamoyl)pyridin-2-yl)amino)methylene) diphosphonic acid



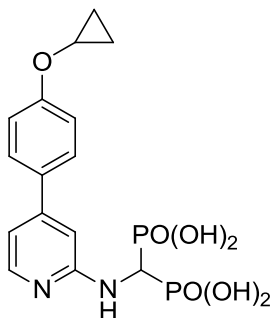
Isolated 33.6 mg (86%) as a fine yellow solid. ^1H NMR (400 MHz, D_2O) δ 7.91 (d, $J = 5.2$ Hz, 1H), 7.35 (d, $J = 9.0$ Hz, 2H), 6.93 (d, $J = 9.0$ Hz, 2H), 6.88 (s, 1H), 6.73 (d, $J = 5.3$ Hz, 1H), 3.73 (s, 3H); central methylene obscured by solvent. ^{13}C NMR (75 MHz, D_2O) δ 183.70, 168.59, 158.83, 156.72, 147.70, 143.48, 129.73, 124.57, 114.34, 108.87, 55.41. ^{31}P NMR (81 MHz, D_2O) δ 14.92. HRMS: calcd 416.0413 for $(\text{C}_{14}\text{H}_{16}\text{N}_3\text{O}_8\text{P}_2)$, found m/z 416.04136 $[\text{M}-\text{H}]^-$

Inhibitor 5.10 (JS02-005): (((4-(Isopropylcarbamoyl)pyridin-2-yl)amino)methylene)diphosphonic acid



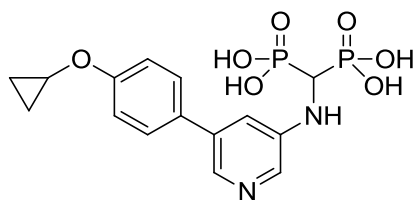
Isolated 14 mg (50%) as a pale yellow solid. ^1H NMR (400 MHz, D_2O) δ 7.90 (d, $J = 5.2$ Hz, 1H), 6.74 (s, 1H), 6.65 (d, $J = 5.1$ Hz, 1H), 4.03 (dt, $J = 13.3, 6.6$ Hz, 1H), 1.16 (d, $J = 6.6$ Hz, 6H); central methylene obscured by solvent signal. ^{13}C NMR (75 MHz, D_2O) δ 183.70, 168.91, 158.64, 147.43, 143.80, 108.90, 42.34, 21.09. ^{31}P NMR (81 MHz, D_2O) δ 14.93. HRMS: calcd 352.0463 for $(\text{C}_{10}\text{H}_{16}\text{N}_3\text{O}_7\text{P}_2)$, found (m/z) 352.04775 $[\text{M}-\text{H}]^-$

Inhibitor 5.14 (YS05-035): (((4-(4-Cyclopropoxyphenyl)pyridin-2-yl)amino)methylene)diphosphonic acid



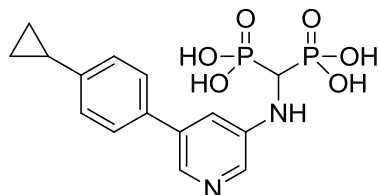
Isolated 27.7 mg (93%) as a white solid. ^1H NMR (500 MHz, D_2O) δ 7.75 (dd, $J = 5.8, 0.6$ Hz, 1H), 7.63 – 7.54 (m, 2H), 7.09 – 7.01 (m, 2H), 6.82 (d, $J = 1.0$ Hz, 1H), 6.74 (dd, $J = 5.8, 1.6$ Hz, 1H), 3.87 (t, $J = 19.2$ Hz, 1H), 3.77 (m, 1H), 0.67-0.71 (m, 2H), 0.58-0.61 (m, 2H). ^{13}C NMR (125 Hz, D_2O) δ 159.16, 157.84, 149.99, 144.55, 130.81, 128.26, 115.46, 110.28, 105.75, 51.77 (t, $J = 122.5$ Hz), 51.30, 5.42. ^{31}P NMR (81 MHz, D_2O) δ 14.04. HRMS: calcd 399.05110 for $(\text{C}_{15}\text{H}_{17}\text{N}_2\text{O}_7\text{P}_2)$, found (m/z) 399.05093 $[\text{M}-\text{H}]^-$

Inhibitor 5.15 (JDS05-120): (((5-(4-cyclopropoxyphenyl)pyridin-3-yl)amino)methylene)diphosphonic acid



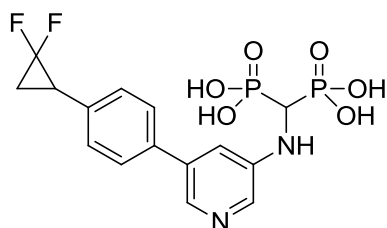
Isolated 27.9 mg (63%) as a pale yellow powder. ^1H NMR (500 MHz, D_2O) δ 7.83 (d, $J = 3.2$ Hz, 2H), 7.56 (d, $J = 8.8$ Hz, 2H), 7.23 (s, 1H), 7.12 (d, $J = 8.8$ Hz, 2H), 3.87 – 3.73 (m, 1H), 3.60 (t, $J = 19.1$ Hz, 1H), 0.77 – 0.57 (m, 4H). ^{13}C NMR (126 MHz, D_2O) δ 158.13, 145.34, 136.24, 133.79, 133.31, 131.12, 128.26, 117.24, 115.51, δ 52.47 (t, $J = 125.3$ Hz), 51.26, 5.43. ^{31}P NMR (81 MHz, D_2O) δ 15.06 (s). HRMS: calcd 399.0511 for $(\text{C}_{15}\text{H}_{17}\text{N}_2\text{O}_7\text{P}_2)$, found m/z 399.05192 $[\text{M}-\text{H}]^-$

Inhibitor 5.19 (JDS05-137): (((5-(4-cyclopropylphenyl)pyridin-3-yl)amino)methylene)diphosphonic acid



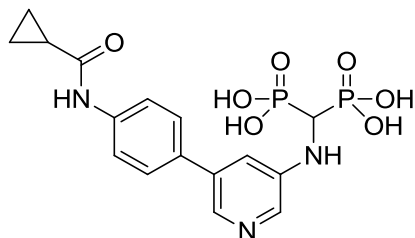
Isolated 25.1 mg (65%) as a white powder. ^1H NMR (500 MHz, D_2O) δ 8.03 (d, J = 2.6 Hz, 2H), 7.67 (d, J = 8.3 Hz, 2H), 7.43 (s, 1H), 7.29 (d, J = 8.3 Hz, 2H), 3.81 (t, J = 18.9 Hz, 1H), 2.06 – 1.98 (m, 1H), 1.10 – 1.02 (m, 2H), 0.82 – 0.74 (m, 2H). ^{13}C NMR (126 MHz, D_2O) δ 144.65, 136.52, 134.85, 134.18, 133.60, 127.09, 125.92, 117.53, 104.99, δ 52.25 (t, J = 122.8 Hz), 14.31, 9.11. ^{31}P NMR (81 MHz, D_2O) δ 15.09 (s). HRMS: calcd 383.0562 for ($\text{C}_{15}\text{H}_{17}\text{N}_2\text{O}_6\text{P}_2$), found m/z 383.05714 [$\text{M}-\text{H}$] $^-$

Inhibitor 5.20 (JDS09-083): (((5-(4-(2,2-difluorocyclopropyl)phenyl)pyridin-3-yl)amino)methylene)diphosphonic acid



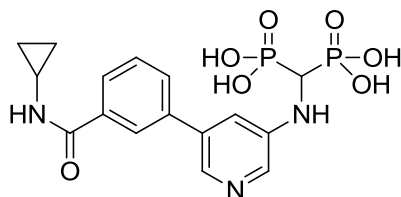
Isolated 24.4 mg (79%) as a white powder. ^1H NMR (500 MHz, D_2O) δ 7.99 (dd, J = 5.0, 2.2 Hz, 2H), 7.71 (d, J = 8.4 Hz, 2H), 7.44 (s, 1H), 7.42 (s, 1H), 7.40 – 7.38 (m, 1H), 3.74 (t, J = 19.0 Hz, 1H), 3.01 – 2.93 (m, 1H), 1.94 (m, 1H), 1.87 – 1.79 (m, 1H). ^{13}C NMR (126 MHz, D_2O) δ 145.31, 136.67, 136.23, 134.05, 133.77, 128.99, 128.53, 127.12, 117.53, 115.59, 113.35, 111.07, 104.99, δ 52.41 (t, J = 124.9 Hz), 26.32 (t, J = 11.2 Hz), 15.98 (t, J = 10.3 Hz). ^{19}F NMR (470 MHz, D_2O) δ -126.29 – -126.72 (m), -142.62 (ddd, J = 19.7, 13.8, 5.5 Hz). ^{31}P NMR (81 MHz, D_2O) δ 14.87 (s). HRMS: calcd 419.03734 for ($\text{C}_{15}\text{H}_{15}\text{F}_2\text{N}_2\text{O}_6\text{P}_2$), found m/z 419.03908 [$\text{M}-\text{H}$] $^-$

Inhibitor 5.21 (JDS-07-024): (((5-(4-(Cyclopropanecarboxamido)phenyl)pyridin-3-yl)amino)methylene) diphosphonic acid



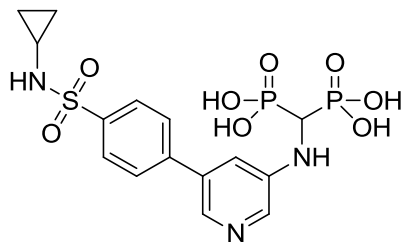
Isolated 20 mg (94%) as a white powder. ^1H NMR (400 MHz, D_2O) δ 7.87 (s, 2H), 7.61 (d, $J = 8.6$ Hz, 2H), 7.45 (d, $J = 8.5$ Hz, 2H), 7.28 (s, 1H), 3.63 (t, $J = 19.1$ Hz, 1H), 1.73 – 1.64 (m, 1H), 0.89 – 0.80 (m, 4H). ^{13}C NMR (75 MHz, D_2O) δ 175.95, 145.24, 137.14, 136.05, 134.12, 134.05, 133.56, 127.55, 121.51, 117.43, δ 52.30 (t, $J = 124.2$ Hz), 14.67, 7.32. ^{31}P NMR (81 MHz, D_2O) δ 15.39 (s). HRMS: calcd 426.0620 for ($\text{C}_{16}\text{H}_{18}\text{N}_3\text{O}_7\text{P}_2$), found m/z 426.06265 [$\text{M}-\text{H}$] $^-$

Inhibitor 5.22 (JDS-07-022): (((5-(3-(Cyclopropylcarbamoyl)phenyl)pyridin-3-yl)amino)methylene) diphosphonic acid



Isolated 20.8 mg (97%) as a white powder. ^1H NMR (400 MHz, D_2O) δ 8.02 (m, 3H), 7.91 (d, $J = 8.1$ Hz, 1H), 7.77 (d, $J = 7.8$ Hz, 1H), 7.62 (t, $J = 7.8$ Hz, 1H), 7.42 (s, 1H), 3.76 (t, $J = 19.0$ Hz, 1H), 2.84 – 2.76 (m, 1H), 0.90 – 0.83 (m, 2H), 0.73 – 0.67 (m, 2H). ^{13}C NMR (75 MHz, D_2O) δ 172.49, 145.34, 138.29, 136.00, 134.24, 134.10, 134.07, 130.60, 129.29, 126.59, 125.48, 117.54, 22.54, 5.44. HSQC $^1\text{H}-^{13}\text{C}$: ^1H δ 3.76 correlates with ^{13}C δ 52.73. ^{31}P NMR (81 MHz, D_2O) δ 15.36 (s). HRMS: calcd 426.0620 for ($\text{C}_{16}\text{H}_{18}\text{N}_3\text{O}_7\text{P}_2$), found m/z 426.06280 [$\text{M}-\text{H}$] $^-$

Inhibitor 5.23 (JDS-07-023): (((5-(4-(*N*-Cyclopropylsulfamoyl)phenyl)pyridin-3-yl)amino)methylene) diphosphonic acid



Isolated 15 mg (85%) as a pale yellow powder. ^1H NMR (400 MHz, D_2O) δ 7.97 – 7.89 (m, 2H), 7.82 (q, J = 8.5 Hz, 4H), 7.32 (s, 1H), 3.62 (t, J = 19.0 Hz, 1H), 2.21 – 2.12 (m, 1H), 0.45 – 0.38 (m, 2H), 0.32 – 0.25 (m, 2H). ^{13}C NMR (75 MHz, D_2O) δ 145.36, 142.82, 137.57, 135.31, 134.66, 134.09, 127.94, 127.44, 117.69, 52.52, 24.23, 4.72. HSQC ^1H - ^{13}C : ^1H δ 3.62 correlates with ^{13}C δ 52.52. ^{31}P NMR (81 MHz, D_2O) δ 15.38 (s). HRMS: calcd 462.0290 for ($\text{C}_{15}\text{H}_{18}\text{N}_3\text{O}_8\text{P}_2\text{S}$), found m/z 462.03099 [$\text{M}-\text{H}$] $^-$

5.8.3 Enzymatic inhibition assays

The *in vitro* inhibition assays for hFPPS (**M1**) and hGGPPS were performed as described in Chapter 3.

6 Towards non-bisphosphonate active site inhibitors of hFPPS: investigation of bioisosteres

6.1 Preface

None of the work presented in this chapter has yet been published. I performed all biological assays and synthesis work except for analog **6.7** (synthesized by Cyrus Lacbay, a PhD candidate in the Tsantrizos research group).

6.2 Introduction

Bioisosteres are structural replacements that mimic the properties of chemical moieties often found in biomolecules and are indistinguishable to the biological target.¹ The incorporation of bioisosteres is common in drug discovery, in order to replace parts of a molecule that are important for enzymatic potency, but have undesirable biopharmaceutical properties. For example, a short peptide may inhibit a protease enzyme of therapeutic interest; however, it would be a poor lead structure due to its rapid metabolic breakdown *in vivo* by various host proteases. The peptide bonds can be replaced by a bioisostere with better metabolic stability (**Figure 6.1**). Such substitutions must conserve the planarity of the amide bond and have a heteroatom (nitrogen and/or oxygen atom) at approximately the same relative position to allow key hydrogen-bond interaction with the biological target. Thus, successful bioisosteres of amide bonds have a similar overall electrostatic shape and size and can bind to the intended target, but are not substrates for various host protease enzymes.

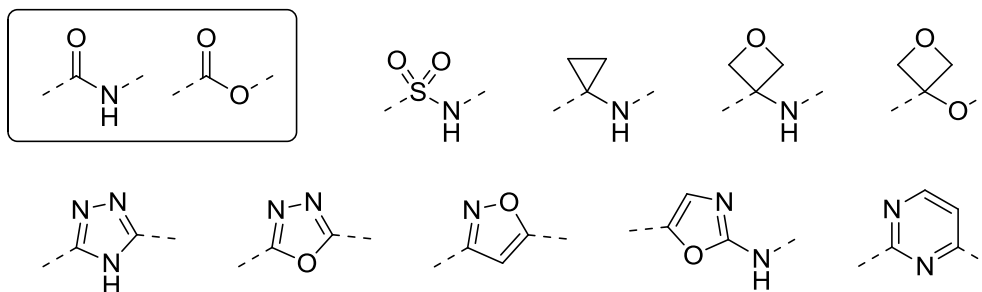


Figure 6.1: Common bioisosteres used to replace amide and ester moieties

Some key examples of commonly used bioisosteres are shown in (**Figure 6.2**). In addition to the use of bioisosteres in improving metabolic stability, they are also incorporated into therapeutic agents for various other reasons, including:

a) Target selectivity and cell membrane permeability:

Carboxylic acids are very common in early stage hits and often critical for enzymatic potency, however they are universally recognized in biology and can lead to off-target interactions. A tetrazole heterocycle is the quintessential bioisostere and often incorporated for its reduced polarity and concomitant improved cell membrane permeability. However, it often provides insufficient selectivity and therefore dozens of other acidic replacements have been developed over the years to better complement the binding site of the desired target.²

b) Conformational rigidity:

A methylene unit introduces high rotational freedom into a molecule which is often detrimental to binding with a biological target. Therefore it is often replaced by a moiety that can form intramolecular interactions and lock it in the bioactive conformation, which usually leads to significant improvement in binding affinity. For example replacing a benzylic CH₂ (which is also metabolically labile) by an atom with a free electron pair enforces a more planar conformation due to resonance with π -system of the aromatic ring.³

c) *Solubility:*

Incorporation of a nitrogen atom into an aliphatic or aromatic system can drastically improve the water solubility of a compound, by acting as a hydrogen bond acceptor or hydrogen bond donor (if protonated in biological media).⁴

d) *Toxicity:*

A number of chemical structures are prone to metabolically induced toxicities. For example, the metal chelating hydroxamic acid can be metabolized to toxic hydroxylamine. This moiety can be successfully replaced by more favourable metal-ligating structural motifs, such small heterocycles.^{5,6}

e) *Lipophilicity:*

An oxetane ring can serve as a less lipophilic alternative to introduce conformational constraint compared to a gem-dimethyl moiety or cycloalkanes and often also improves solubility.⁷

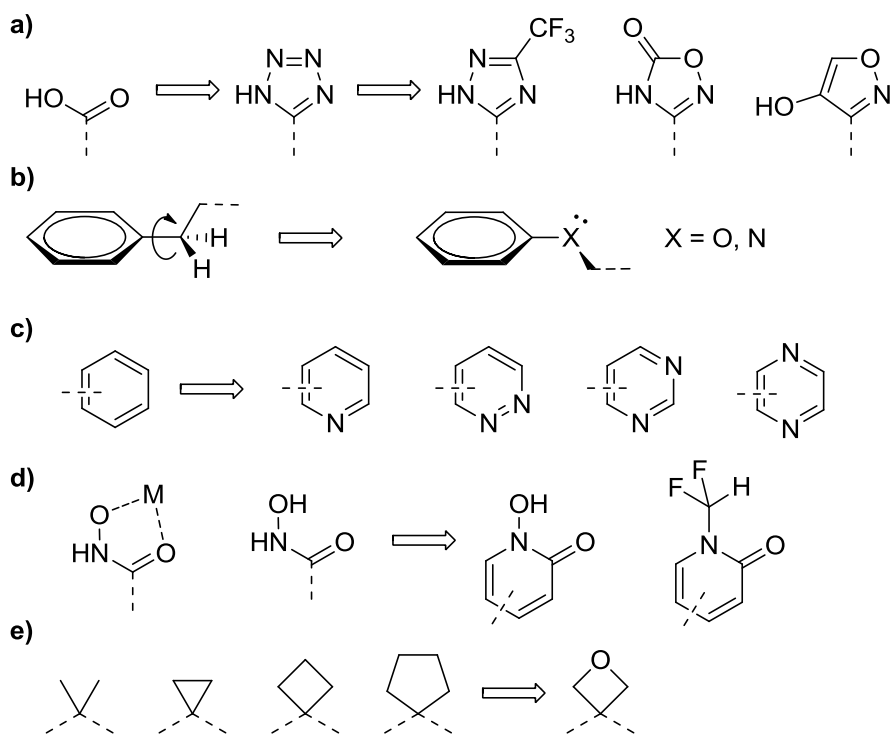


Figure 6.2: Common bioisostere replacements

The phosphate or pyrophosphate (also called diphosphate) functionalities are highly undesirable structural motifs in a therapeutic agent, as their polar/charged nature renders these agents incapable of penetrating cell membranes by passive diffusion. In general, compounds with a phosphate or pyrophosphate moiety exhibit very poor oral bioavailability and negligible distribution into soft tissues. These functional groups are also recognized to be the most challenging moieties to successfully mimic with a bioisostere.⁸ Nonetheless, phosphonic acids are often incorporated into exploratory molecules and biochemical tools due to their strong affinity for metal ions that are often associated with substrate binding of virally encoded enzymes, such as polymerase, helicase, integrase, and mammalian prenylase enzymes. Such moieties, which tightly bind a critical protein recognition motif, are often referred to as “warheads” in medicinal chemistry and almost always replaced during lead optimization in drug discovery programs. A number of phosphate/phosphonate bioisosteres have been developed in recent years including simple α -keto acids, sulfonyl and sulphonamide derivatives and various 5-member and 6-member heterocycles (**Figure 6.3**).⁸ However, few examples have been reported for the successful application of such moieties in the design of inhibitors targeting prenyl synthase enzymes (*i.e.* enzymes with similar substrate-recognition elements to hFPPS). These include derivatives of tetramic acids (**6.1**, **Figure 6.4**) for *S. pneumoniae* UPPS,⁹ α -phosphonosulphonic acids (**6.2**) for human SQS,¹⁰ and α,γ -diketo acids (**6.3**) for HCV RNA polymerase,¹¹ HIV integrase,¹² and human UPPS.¹³ To date, such modifications have not been reported for hFPPS. Clinically validated examples of phosphate bioisosteres include the drug raltegravir, which contains a modified dihydropyrimidine-4-carboxylate (**6.4**, **Figure 6.3**), an inhibitor of HIV integrase with good oral bioavailability.¹⁴ This drug binds to an aspartate-rich surface in the active site of the viral integrase *via* bifurcated metal-mediated interactions. It should be noted that the planar pyrimidinone moiety can more readily coordinate with 2 Mg^{2+} ions found in the HIV integrase active site (**Figure 6.5a**) than 3 Mg^{2+} ions in a triangular geometry as in the active site of hFPPS (**Figure 6.5b**).

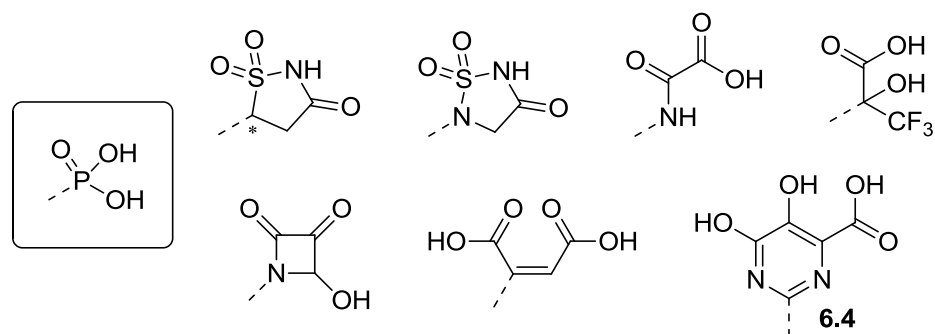


Figure 6.3: Examples of phosphonate/phosphate bioisosteres

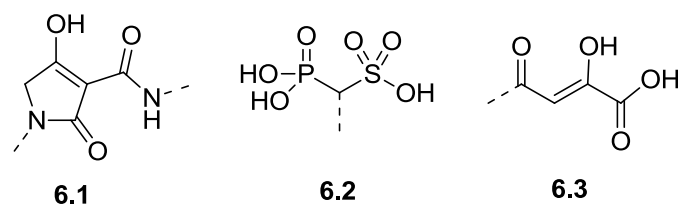


Figure 6.4: Example of bioisosteres successfully used to bind to a pyrophosphate recognition motif

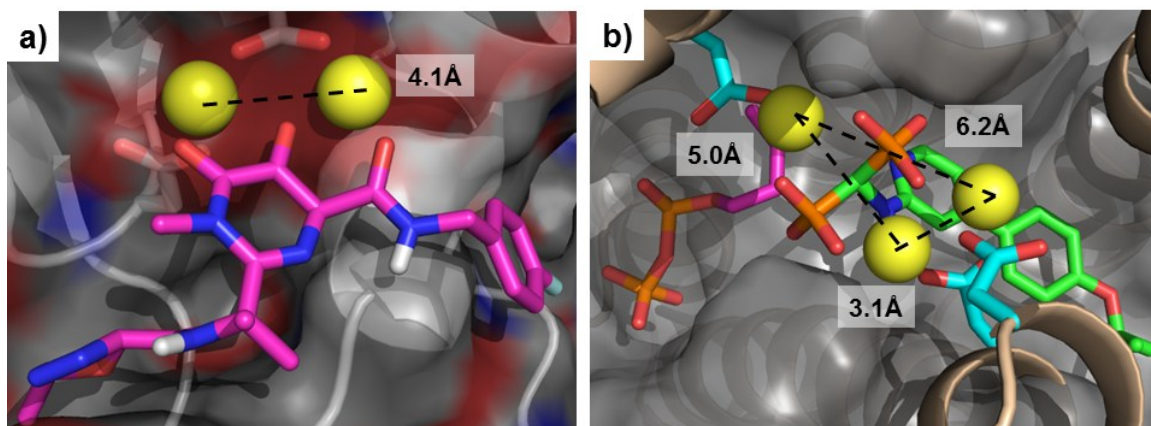


Figure 6.5: (a) HIV 1 integrase with raltegravir (PDB 3OYA); (b) hFPPS, with **4.5** and IPP (PDB 1ZW5 and 4DEM). Metals are depicted as yellow spheres and the distance between each are shown as dashed lines and indicated.

6.3 Synthesis of bioisosteric replacements of (bis)phosphonates

We have initiated the synthesis of several bioisostere derivatives of bisphosphonates, including the examples shown in **Figure 6.6**. The synthesis of analogs that were initiated, but not completed due to synthetic challenges are not included in this thesis. Furthermore, some analogs were prepared with an unoptimized side chain in order to simplify the synthesis and provide a rapid assessment of the synthetic challenges in making these compounds, as well as their potential to inhibit hFPPS.

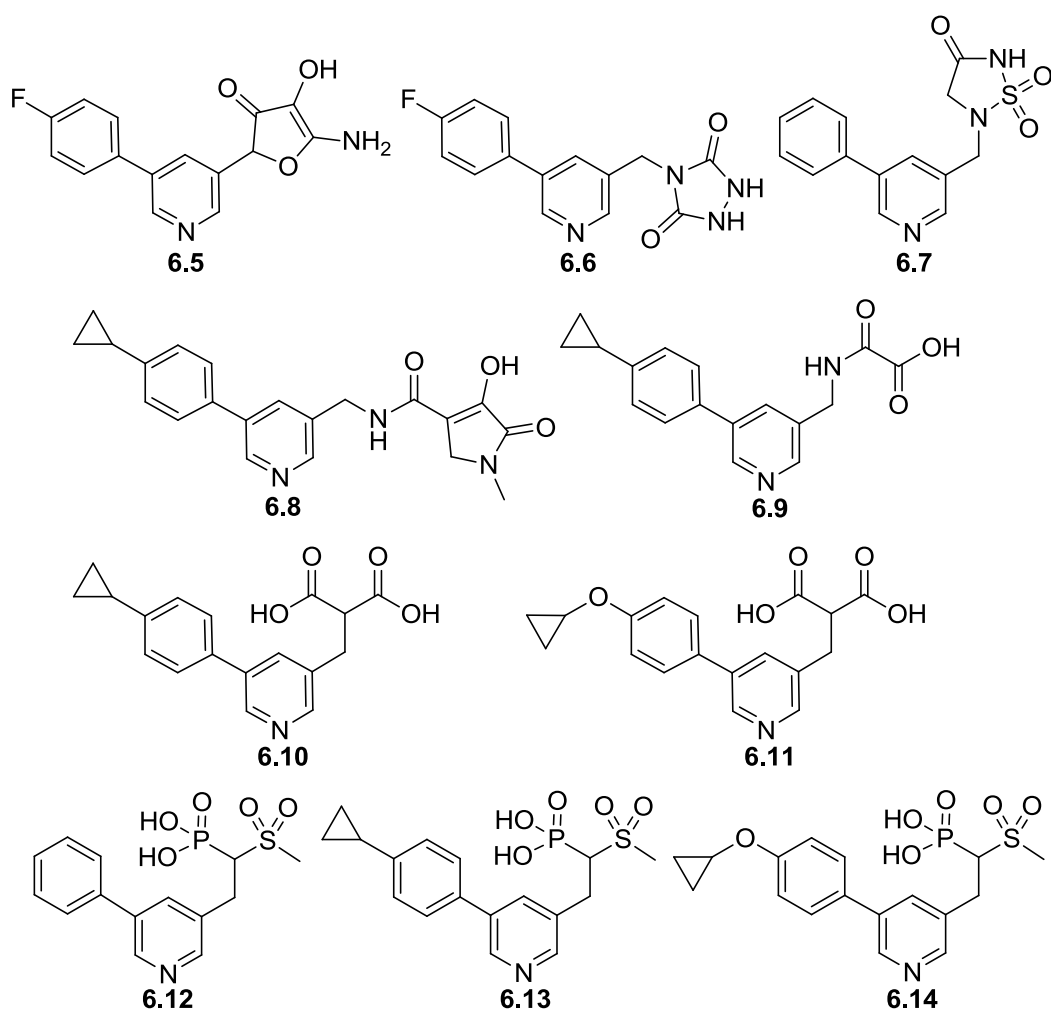
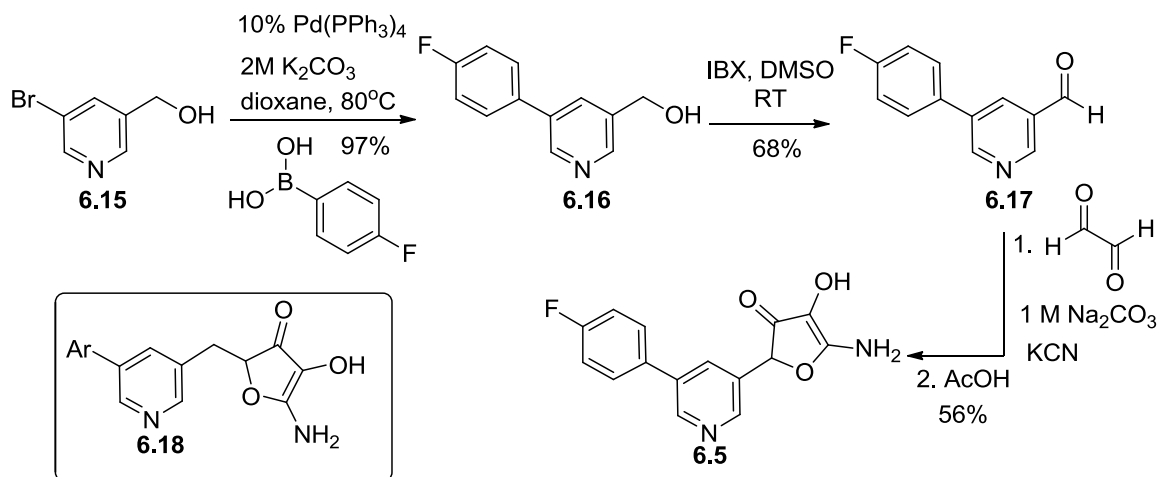


Figure 6.6: Bioisostere analogues of hFPPS inhibitors

Initially we focused on the synthesis of 5-membered heterocyclic analogs, such as compounds **6.5** to **6.7** (Figure 6.6). We hypothesized that these small, highly electronegative moieties would provide efficient replacements of the bisphosphonate moiety.

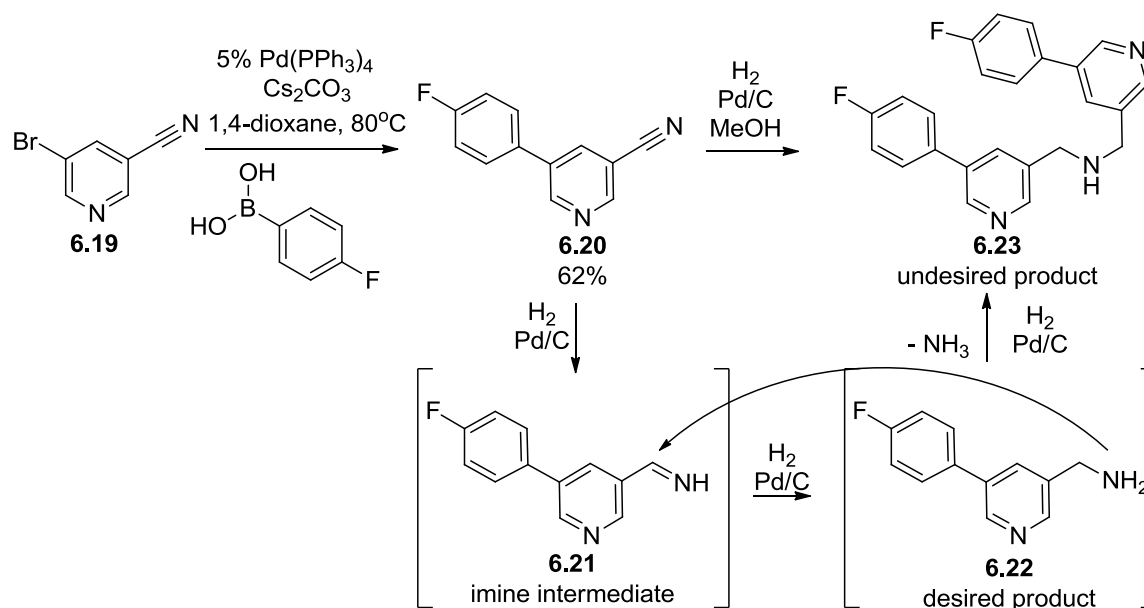
The synthesis of analog **6.5** was initiated by Suzuki cross-coupling of aryl bromide **6.15** (previously described in Chapter 2) with *p*-fluoroboronic acid, followed by oxidation of the benzylic alcohol with IBX, to give the aldehyde **6.17** (Scheme 6.1). This intermediate was readily transformed into the analog **6.5** by condensation with glyoxal and potassium cyanide, using literature protocols.¹⁵ However, this transformation proved incompatible with non-aromatic aldehydes, precluding access to inhibitors such as **6.18**.



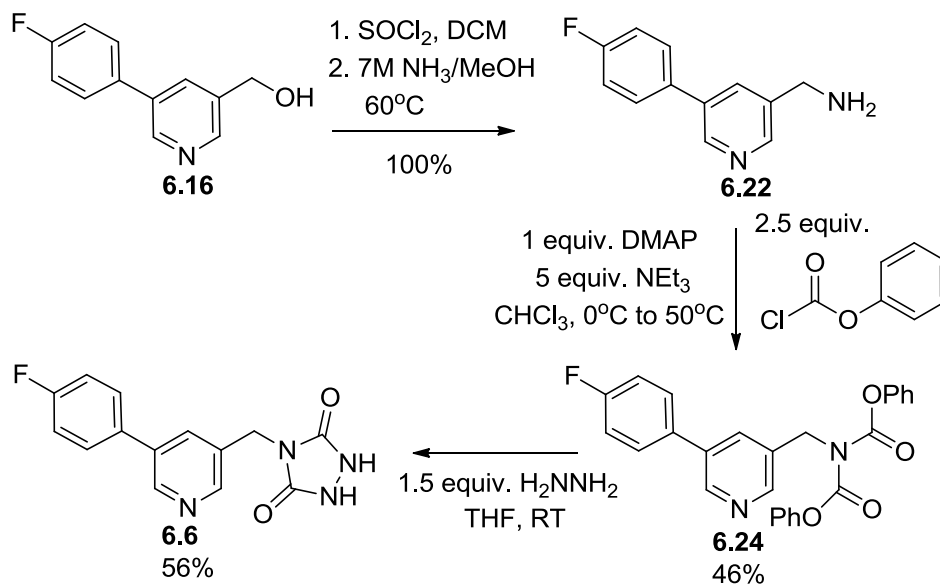
Scheme 6.1: Synthesis of analog **6.5**

The synthesis of analog **6.6** was initiated with the Suzuki cross-coupling reaction of commercially available 5-bromonicotinonitrile **6.19** with *p*-fluoroboronic acids to give the nitrile intermediate **6.20** (Scheme 6.2). However, the subsequent catalytic hydrogenation of this nitrile failed to give the desired benzylic amine **6.22** and instead produced the secondary amine **6.23**. Presumably the desired primary amine **6.22** is formed *in situ*, but immediately performs a nucleophilic attack on the imine intermediate **6.21**, which after elimination of ammonia and a second reduction results in the formation of secondary amine **6.23**. Efforts to reduce the nucleophilicity of amine **6.22** by the addition of various acids was explored, however, this led to numerous side-products. An alternative route was

successfully employed to obtain the desired amine **6.22** from the corresponding benzylic alcohol **6.16**, by converting it the corresponding benzylic chloride followed by treatment with excess ammonia at 60 °C (**Scheme 6.3**). The di-carbamate **6.10** was subsequently prepared by reacting the amine with phenylchloroformate and the desired urazole derivative **6.6** was formed upon cyclization with hydrazine.

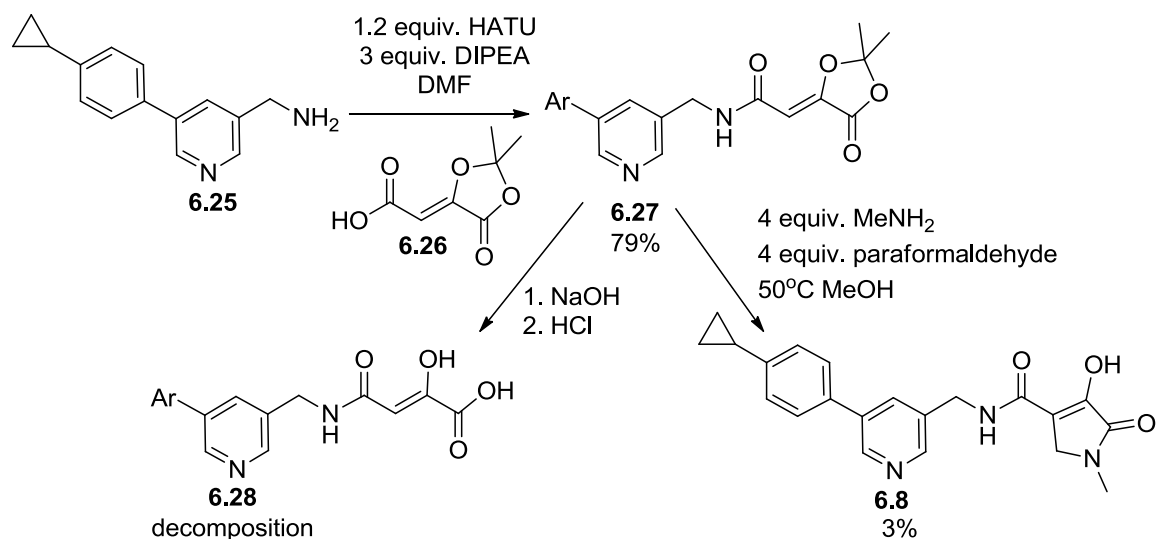


Scheme 6.2: Side reaction observed with catalytic hydrogenation



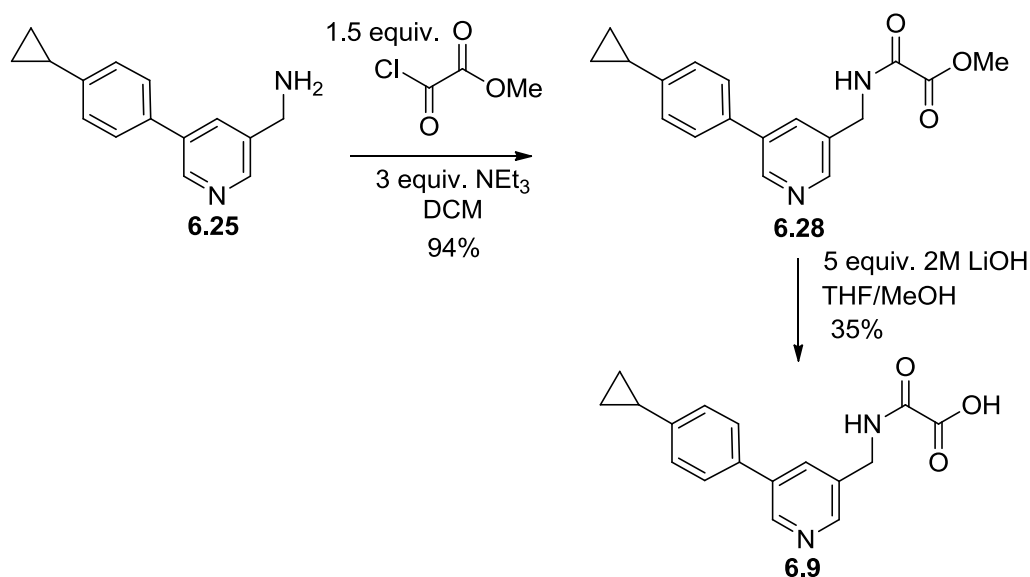
Scheme 6.3: Synthesis of analog **6.6**

Preparation of analog **6.8** required the α,γ -diketo acid synthon **6.26** which was made according to literature procedure (refer to experimental section for full details).¹⁶ This fragment was subsequently attached to the benzylic amine **6.25** (prepared using the same methodology as described in **Scheme 6.3**). The α -keto-acid functionality could be liberated using the published conditions (product detected by HPLC), but upon quenching the reaction with acid the mixture turned bright yellow and HPLC analysis showed complete decomposition to numerous side-products. Lower temperature and milder acidic conditions failed to suppress the decomposition, indicating that amide **6.28** may be chemically unstable. Finally, although we were able to successfully cyclize intermediate **6.27** to analog **6.8** using literature procedures, the yield for this reaction was extremely low (**Scheme 6.4**).



Scheme 6.4: Synthesis of analog **6.8**

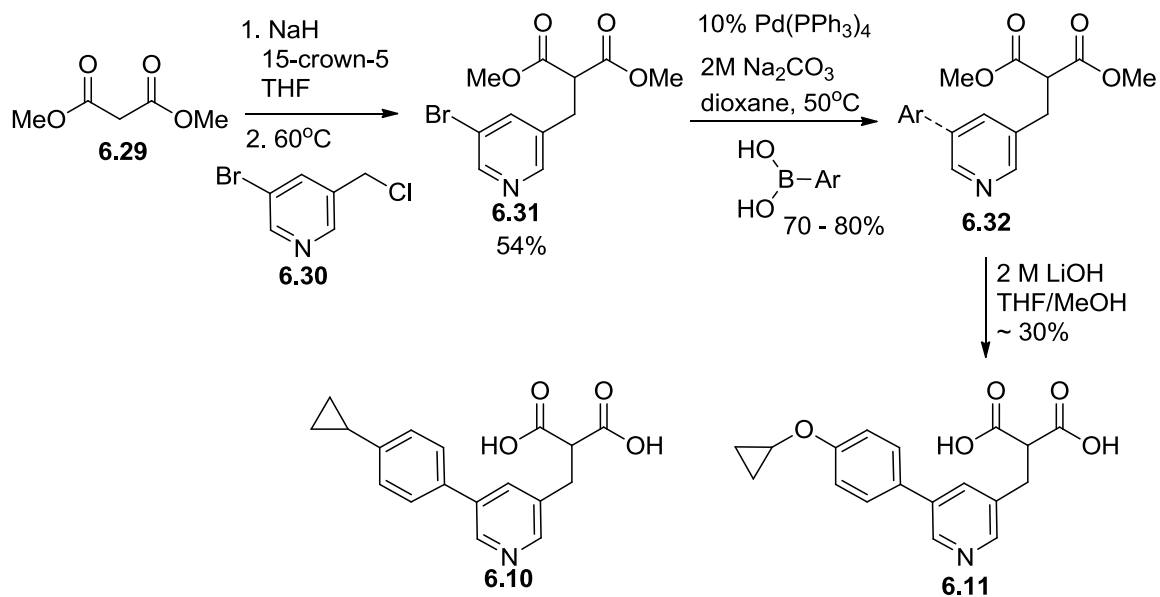
Acyclic (*potential*) bisphosphonate bioisosteres were also explored, including the 2-amino-2-oxoacetic acid derivative **6.9**, the malonate derivatives **6.10** and **6.11** and the methylsulfonylphosphonic acid derivatives **6.12-6.14** (**Figure 6.6**). The synthesis of analog **6.9** was achieved from coupling the amine **6.25** with chloro-methyloxalate, followed by saponification of the methyl ester with lithium hydroxide (**Scheme 6.5**).



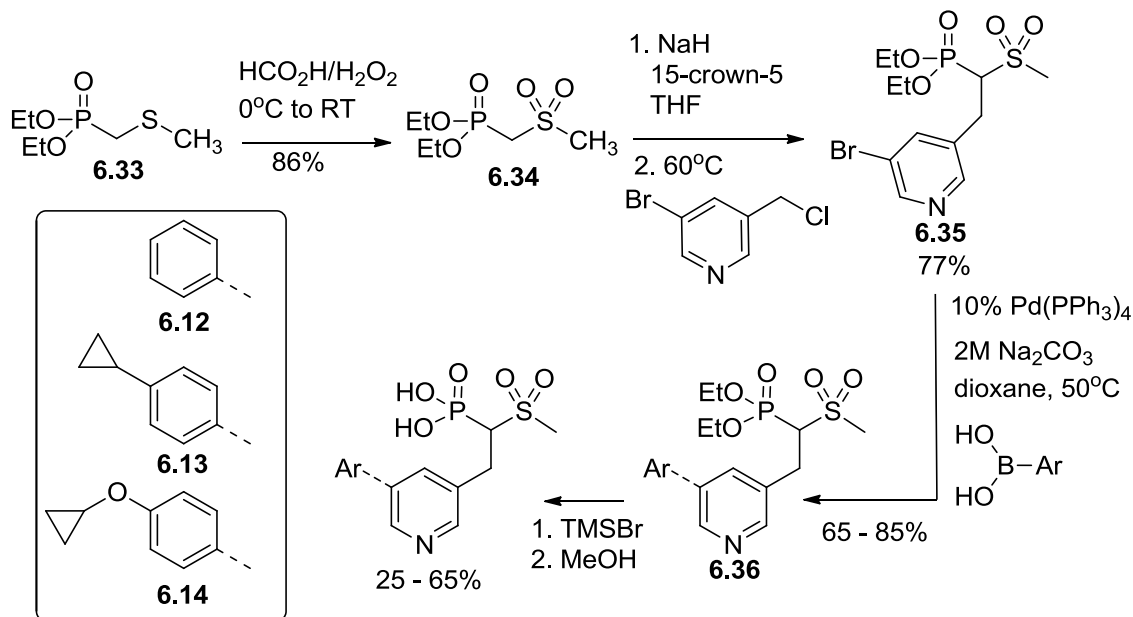
Scheme 6.5: Synthesis of analog **6.9**

Malonic acid derivatives could be readily prepared from the commercial dimethyl ester **6.29** after deprotonation with sodium hydride followed by alkylation with benzylic chloride **6.30** (described in Chapter 5) at 60°C to give intermediate **6.31** in good yield, without any observed bis-alkylation (**Scheme 6.6**). The cyclopropylbenzene and cyclopropoxybenzene side chains were attached to the pyridine core via standard Suzuki cross-coupling reactions and the methyl esters were saponified with lithium hydroxide. The final free acid compounds **6.10** and **6.11** were isolated after purification by C18 reversed phase chromatography.

Finally, the α -phosphonosulfones were synthesized in similar manner to the malonates (**Scheme 6.7**). The required sulfone **6.34** was prepared by oxidation of the corresponding thio-ether **6.33** in excellent yield. The subsequent alkylation proceeded smoothly to give the desired product **6.35** in good yields, without any bis-alkylation observed. Next, the Suzuki cross-couplings and phosphonate ester deprotections were performed using our standard procedures to furnish the α -phosphonosulfone analogs **6.12**, **6.13** and **6.14**.



Scheme 6.6: Synthesis of inhibitors **6.10** and **6.11**



Scheme 6.7: Synthesis of inhibitors **6.12** – **6.14**

6.4 In vitro enzymatic activity of bioisostere analogs

The enzymatic activity of our novel, bioisostere-bearing compounds **6.5** to **6.14** (Figure 6.6) were evaluated using the sensitized hFPPS inhibition assay conditions **M2** (described in detail in Chapter 7). Weak inhibition of hFPPS was observed with the malonic acid analogs **6.10** and **6.11**, and α -phosphonosulfones **6.12**, **6.13** and **6.14** at a concentration of 100 μ M. However, we did not observe any clear preference for a given type of bisphosphonate replacement or the substitution of the pyridine ring (*i.e.* all compounds appeared to have an IC₅₀ of approximately \sim 80-100 μ M) amongst these analogs. This may suggest that the SAR is different from the corresponding bisphosphonates, although it is precarious to draw conclusions when the potency is so weak.

No appreciable activity was observed against hGGPPS 100 μ M for any of the bioisosteres (data not shown).

Inhibitor	hFPPS inhibition			
concentration	10 μ M	20 μ M	50 μ M	100 μ M
RIS	100%	<i>nd</i>	<i>nd</i>	<i>nd</i>
6.5	0%	<i>nd</i>	<i>nd</i>	0%
6.6	0%	<i>nd</i>	<i>nd</i>	0%
6.7	0%	<i>nd</i>	<i>nd</i>	9%
6.8	0%	<i>nd</i>	<i>nd</i>	9%
6.9	0%	<i>nd</i>	<i>nd</i>	17%
6.10	<i>nd</i>	21%	33%	70%
6.11	12%	25%	45%	63%
6.12	6%	<i>nd</i>	<i>nd</i>	47%
6.13	5%	19%	34%	49%
6.14	8%	13%	22%	34%

Table 6.1: hFPPS enzymatic inhibition data for bioisosteres. The values of % inhibition shown are the average of three determinations. (<10% standard deviation)
(*nd* = not determined)

6.5 Conclusions and outlook

In summary, a number of bioisosteres have been investigated to replace the polar and promiscuous bisphosphonate moiety of current hFPPS inhibitors. The best bioisosteres identified so far are only weak inhibitors of hFPPS (IC_{50} ~80-100 μ M) and further optimization is currently ongoing.

An alternative strategy to mask the charge of the bisphosphonates is to modify them with metabolically labile moieties (pro-drugs). This line of research is currently being pursued by my colleagues in the Tsantrizos research group.

6.6 References

- (1) Meanwell, N. A.; Synopsis of Some Recent Tactical Application of Bioisosteres in Drug Design *J. Med. Chem.* **2011**, *54*, 2529.
- (2) Carini, D.; Christ, D.; Duncia, J.; Pierce, M.; Borchardt, R., Freidinger, R., Sawyer, T., Smith, P., Eds.; Springer US: 2002; Vol. 11, p 29.
- (3) Brameld, K. A.; Kuhn, B.; Reuter, D. C.; Stahl, M.; Small Molecule Conformational Preferences Derived from Crystal Structure Data. A Medicinal Chemistry Focused Analysis *J. Chem. Inf. Mod.* **2008**, *48*, 1.
- (4) Yu, K.-L.; Sin, N.; Civiello, R. L.; Wang, X. A.; Combrink, K. D.; Gulgeze, H. B.; Venables, B. L.; Wright, J. J. K.; Dalterio, R. A.; Zadjura, L.; Marino, A.; Dando, S.; D'Arienzo, C.; Kadow, K. F.; Cianci, C. W.; Li, Z.; Clarke, J.; Genovesi, E. V.; Medina, I.; Lamb, L.; Colonna, R. J.; Yang, Z.; Krystal, M.; Meanwell, N. A.; Respiratory syncytial virus fusion inhibitors. Part 4: Optimization for oral bioavailability *Bioorg. Med. Chem. Lett.* **2007**, *17*, 895.
- (5) Flipo, M.; Charton, J.; Hocine, A.; Dassonneville, S.; Deprez, B.; Deprez-Poulain, R.; Hydroxamates: Relationships between Structure and Plasma Stability *J. Med. Chem.* **2009**, *52*, 6790.
- (6) Chowdhury, M. A.; Abdellatif, K. R. A.; Dong, Y.; Das, D.; Suresh, M. R.; Knaus, E. E.; Synthesis of Celecoxib Analogues Possessing a N-Difluoromethyl-1,2-dihydropyrid-2-one 5-Lipoxygenase Pharmacophore: Biological Evaluation as Dual Inhibitors of Cyclooxygenases and 5-Lipoxygenase with Anti-Inflammatory Activity *J. Med. Chem.* **2009**, *52*, 1525.
- (7) Wuitschik, G.; Carreira, E. M.; Wagner, B. r.; Fischer, H.; Parrilla, I.; Schuler, F.; Rogers-Evans, M.; Muller, K.; Oxetanes in Drug Discovery: Structural and Synthetic Insights *J. Med. Chem.* **2010**, *53*, 3227.
- (8) Rye, C. S.; Baell, J. B. *Phosphate Isosteres in Medicinal Chemistry*, 2005; Vol. 12.
- (9) Peukert, S.; Sun, Y.; Zhang, R.; Hurley, B.; Sabio, M.; Shen, X.; Gray, C.; Dzink-Fox, J.; Tao, J.; Cebula, R.; Wattanasin, S.; Design and structure–activity relationships of potent and selective inhibitors of undecaprenyl pyrophosphate synthase (UPPS): Tetramic, tetronic acids and dihydropyridin-2-ones *Bioorg. Med. Chem. Lett.* **2008**, *18*, 1840.
- (10) Dickson, J. K.; Biller, S. A.; Magnin, D. R.; Petrillo, E. W.; Hillyer, J. W.; Hsieh, D. C.; Lan, S.-J.; Rinehart, J. K.; Gregg, R. E.; Harrity, T. W.; Jolibois, K. G.; Kalinowski, S. S.; Kunselman, L. K.; Mookhtiar, K. A.; Ciosek, C. P.; Orally Active Squalene Synthase Inhibitors: Bis((acyloxy)alkyl) Prodrugs of the α -Phosphonosulfonic Acid Moiety *J. Med. Chem.* **1996**, *39*, 661.
- (11) Summa, V.; Petrocchi, A.; Pace, P.; Matassa, V. G.; De Francesco, R.; Altamura, S.; Tomei, L.; Koch, U.; Neuner, P.; Discovery of α,γ -Diketo Acids as Potent Selective and Reversible Inhibitors of Hepatitis C Virus NS5b RNA-Dependent RNA Polymerase *J. Med. Chem.* **2003**, *47*, 14.
- (12) Hazuda, D. J.; Felock, P.; Witmer, M.; Wolfe, A.; Stillmock, K.; Grobler, J. A.; Espeseth, A.; Gabryelski, L.; Schleif, W.; Blau, C.; Miller, M. D.; Inhibitors of Strand

Transfer That Prevent Integration and Inhibit HIV-1 Replication in Cells *Science* **2000**, 287, 646.

(13) Zhang, Y.; Lin, F. Y.; Li, K.; Zhu, W.; Liu, Y. L.; Cao, R.; Pang, R.; Lee, E.; Axelson, J.; Hensler, M.; Wang, K.; Molohon, K. J.; Wang, Y.; Mitchell, D. A.; Nizet, V.; Oldfield, E.; HIV-1 integrase inhibitor-inspired antibacterials targeting isoprenoid biosynthesis *ACS Med. Chem. Lett.* **2012**, 3, 402.

(14) Summa, V.; Petrocchi, A.; Bonelli, F.; Crescenzi, B.; Donghi, M.; Ferrara, M.; Fiore, F.; Gardelli, C.; Gonzalez Paz, O.; Hazuda, D. J.; Jones, P.; Kinzel, O.; Laufer, R.; Monteagudo, E.; Muraglia, E.; Nizi, E.; Orvieto, F.; Pace, P.; Pescatore, G.; Scarpelli, R.; Stillmock, K.; Witmer, M. V.; Rowley, M.; Discovery of Raltegravir, a Potent, Selective Orally Bioavailable HIV-Integrase Inhibitor for the Treatment of HIV-AIDS Infection *J. Med. Chem.* **2008**, 51, 5843.

(15) Weitman, M.; Lerman, L.; Cohen, S.; Nudelman, A.; Major, D. T.; Gottlieb, H. E.; Facile structural elucidation of imidazoles and oxazoles based on NMR spectroscopy and quantum mechanical calculations *Tetrahedron* **2010**, 66, 1465.

(16) Banville, J.; Bouthillier, G.; Plamondon, S.; Remillard, R.; Meanwell, N. A.; Martel, A.; Walker, M. A.; (Z)-2,2-Dimethyl-5-carboxymethylene-1,3-dioxolan-4-one: a new synthon for the synthesis of α,γ -diketoacid derivatives *Tetrahedron Lett.* **2010**, 51, 3170.

6.7 Experimental

6.7.1 Synthesis

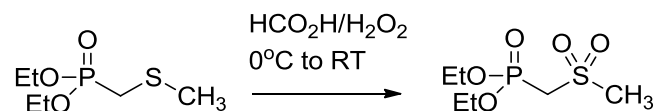
General Procedures for Characterization of Compounds

All intermediate compounds were purified by normal phase flash column chromatography on silica gel using a CombiFlash instrument and the solvent gradient indicated. The final compounds were purified by reverse-phase C18 chromatography (H₂O/ACN +0.01% formic acid gradient) and fully characterized by ¹H, ¹³C and ³¹P NMR, and MS. Chemical shifts (δ) are reported in ppm relative to the internal deuterated solvent (¹H, ¹³C) or external H₃PO₄ (δ 0.00 ³¹P), unless indicated otherwise. The homogeneity of the (>95%) was confirmed by C18 reversed phase HPLC. See Appendix III for HPLC traces of the final compounds.

6.30: 3-Bromo-5-(chloromethyl)pyridine:

See experimental of Chapter 4.

6.34 (JDS05-080): diethyl ((methylsulfonyl)methyl)phosphonate

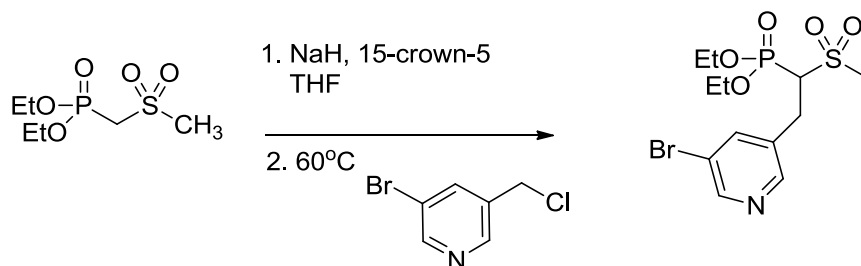


To an ice-cooled solution of diethyl ((methylthio)methyl)phosphonate (1.1 g, 5.5 mmol) in 4 mL formic acid is added hydrogen peroxide (30%, 1 mL) and the reaction is stirred 15 min at 0°C, followed by 12 h at RT. The solution is concentrated in vacuo (aqueous NaOH in receiving flask) and co-evaporated twice with toluene. The residue is dissolved in hot toluene and allowed to cool. Hexanes was added dropwise until a precipitate started to form, at which point the mixture was aged for 1h at -20°C. The desired product was collected filtration as clear colorless crystals (1.1 g, 86%). ¹H NMR (400 MHz, CDCl₃) δ 4.30 – 4.18 (m, 2H), 3.59 (d, *J* = 16.4 Hz, 2H), 3.21 (s, 1H), 1.38 (t, *J* = 7.1 Hz, 3H).

General protocol for alkylation with 3-bromo-5-(chloromethyl)pyridine at elevated temperature

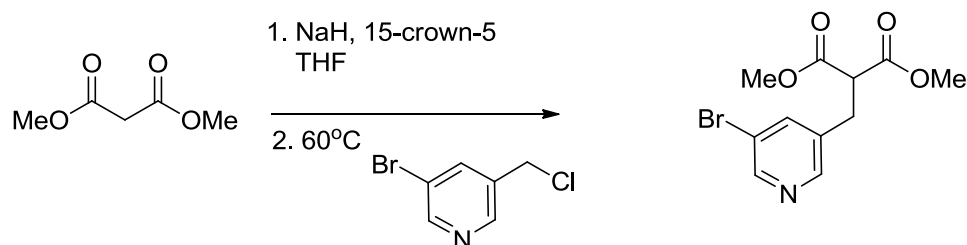
To an ice-cooled solution nucleophile (2 equivalents) and 15-crown-5 ether (0.1 equivalent) in anhydrous THF was added NaH (2 equivalents) in one portion. The suspension is stirred for 15 min at RT and 3-bromo-5-(chloromethyl)pyridine (1 equivalent) is added via syringe as a solution in THF. The reaction was stirred at 60°C until all starting material is consumed, as determined by HPLC analysis. The reaction was quenched with satd. NH₄Cl, concentrated in vacuo and redissolved in 100 mL EtOAc. The organic phase is washed with 10 mL satd. NH₄Cl, satd. NaHCO₃, water and brine; dried over anhydrous Na₂SO₄, filtered and concentrated in vacuo. The residue was purified by silica gel (silica was pre-washed with 0.1% NEt₃ in hexanes/EtOAc 3:1) chromatography on a CombiFlash instrument, using a solvent gradient from 1:10 EtOAc/Hexanes to 100% EtOAc and then to 10% MeOH in EtOAc. In cases where the desired product is contaminated the starting nucleophile, the mixture is dissolved in 100 mL toluene, washed 5 times with 10 mL water, followed by 10 mL brine; dried over anhydrous Na₂SO₄, filtered and concentrated in vacuo to furnish the desired compound in >95% purity.

6.35 (JDS10-034): diethyl (2-(5-bromopyridin-3-yl)-1-(methylsulfonyl)ethyl)phosphonate



Isolated 168 mg (after toluene extraction, 77%) as a pale yellow oil. ¹H NMR (500 MHz, CDCl₃) δ 8.50 (d, *J* = 2.0 Hz, 1H), 8.40 (d, *J* = 1.5 Hz, 1H), 7.76 (t, *J* = 2.1 Hz, 1H), 4.22 – 4.14 (m, 2H), 4.02 – 3.95 (m, 2H), 3.57 – 3.45 (m, 3H), 3.24 (s, 3H), 1.28 (td, *J* = 7.1, 0.7 Hz, 3H), 1.13 (td, *J* = 7.1, 0.5 Hz, 3H). ¹³C NMR (126 MHz, CDCl₃) δ 149.40, 148.63, 139.33, 135.01, 134.97, 134.99 (d, *J* = 3.9 Hz), 63.75 (dd, *J* = 219.5, 6.7 Hz), 63.06 (d, *J* = 138.6 Hz), 42.10 (d, *J* = 0.9 Hz), 26.53 (d, *J* = 4.1 Hz), 16.15 (dd, *J* = 32.7, 6.3 Hz). ³¹P NMR (81 MHz, CDCl₃) δ 15.06 (s). MS (ESI): calcd 399.998 and 401.996; found 400.50 and 402.49 [M+H]⁺

6.31 (JDS10-033): dimethyl 2-((5-bromopyridin-3-yl)methyl)malonate



Isolated 118 mg (54%) as a colorless oil. ^1H NMR (500 MHz, CDCl_3) δ 8.47 (d, $J = 2.1$ Hz, 1H), 8.32 (d, $J = 1.7$ Hz, 1H), 7.65 (t, $J = 2.1$ Hz, 1H), 3.65 (s, 6H), 3.60 (t, $J = 7.7$ Hz, 1H), 3.13 (d, $J = 7.7$ Hz, 2H). ^{13}C NMR (126 MHz, CDCl_3) δ 168.42, 149.37, 148.28, 138.99, 135.04, 120.53, 52.78, 52.67, 31.32. MS (ESI): calcd 302.003 and 304.001; found 302.48 and 304.50 $[\text{M}+\text{H}]^+$

General procedure of Suzuki cross coupling

Method A:

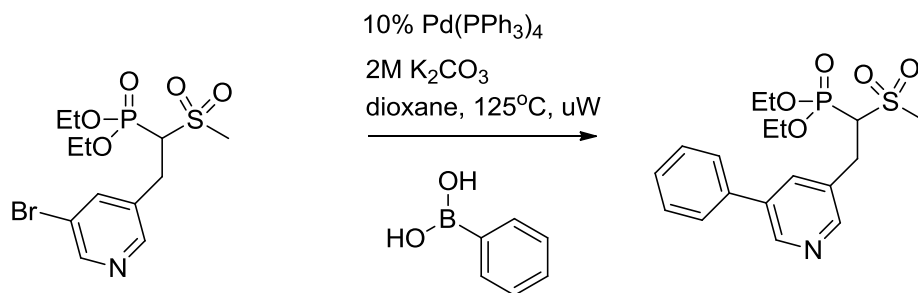
A 5 mL vial was charged with the aryl halide (1 equivalent), $\text{Pd}(\text{PPh}_3)_4$ (0.1 equivalent), a stir bar and the boron-coupling partner (1.25 equivalents) if a solid. The vial was capped with a rubber septum, evacuated and back-filled with Argon; anhydrous 1,4-dioxane was added via syringe to bring the final concentration of aryl halide to 0.1M and the solution was flushed with Argon. At this point the boron-coupling partner, if not at solid, was added as a solution in 1,4-dioxane. Na_2CO_3 or K_2CO_3 solution (2.5 equivalents) was added and the vial was flushed again with Argon. The reaction vessel was equipped with an Argon-filled balloon and stirred at 80°C until complete consumption of starting material. The reaction mixture was cooled down, diluted with EtOAc and filtered through a plug of Celite, rinsed three times with EtOAc/MeOH 1:1. The filtrate concentrated in vacuo and purified by normal phase column chromatography on silica gel (silica gel was pre-treated with 1% NEt_3 in hexanes/EtOAc in a 3:1 ratio) using a gradient from 100% hexanes to 100% EtOAc and then to 10% MeOH.

Method B:

A 0.5-2 mL microwave reaction vessel was charged with a magnetic stir bar, boronic acid or boronate ester (1.5 equivalent), $\text{Pd}(\text{PPh}_3)_4$ (0.1 equivalent) and aryl halide (if a solid, 1

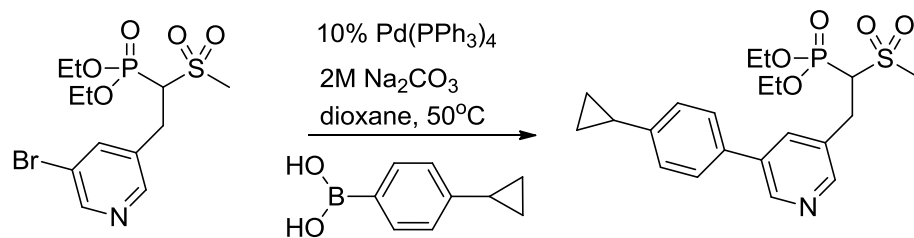
equivalent); if the aryl halide is an oil, it was added as a solution in 1,4-dioxane *via* syringe. The reaction vessel was capped with a septum, degassed and flushed with Argon. 1,4-Dioxane was added to bring the concentration of aryl halide to 0.1 M and the mixture was again degassed and flushed with Argon. A solution of 2M K₂CO₃ (2.5 equivalents) was added and the mixture was again degassed and flushed with Argon. The rubber septum was replaced by a Teflon lined seal, under a flow of Argon. The reaction was irradiated to 125 °C for 10 to 30min (~40W), reaction progress was followed by TLC and/or HPLC. The crude was filtered through a plug of Celite, rinsed with 10 mL 1:1 EtOAc/Acetone and concentrated under vacuum. The residue was purified by silica gel chromatography (silica was pre-washed with 0.1% Et₃N in hexanes/EtOAc, 3:1 ratio) using a CombiFlash instrument and a solvent gradient from 1:1 EtOAc/Hexanes to 100% EtOAc and then to 25% MeOH in EtOAc.

JDS05-089: diethyl (1-(methylsulfonyl)-2-(5-phenylpyridin-3-yl)ethyl)phosphonate



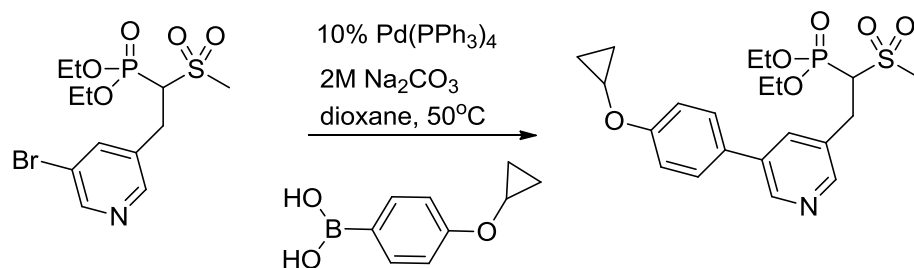
Method B; Isolated 42 mg (85%) as a clear oil. ¹H NMR (400 MHz, CDCl₃) δ 8.76 (bs, 1H), 8.54 (bs, 1H), 7.86 (s, 1H), 7.58 (d, *J* = 7.3 Hz, 2H), 7.49 (t, *J* = 7.5 Hz, 2H), 7.42 (t, *J* = 7.3 Hz, 1H), 4.25 (m, 2H), 4.10 – 3.97 (m, 2H), 3.69 (m, 1H), 3.56 (m, 1H), 3.38 – 3.27 (m, 4H), 1.33 (t, *J* = 7.1 Hz, 3H), 1.16 (t, *J* = 7.1 Hz, 3H). ¹³C NMR (75 MHz, CD₃OD) δ 148.26, 145.25, 136.95, 136.06, 128.90, 128.15, 126.74, 63.50 (dd, *J* = 93.2, 6.3 Hz), 61.42 (d, *J* = 139.4 Hz), 41.13, 26.60, 15.06 (dd, *J* = 17.8, 6.1 Hz). ³¹P NMR (81 MHz, CD₃OD) δ 16.60 (s). MS (ESI): calcd 398.119; found 398.24 [M+H]⁺

JDS10-037: diethyl (2-(5-(4-cyclopropylphenyl)pyridin-3-yl)-1-(methylsulfonyl)ethyl)phosphonate



Method A; Isolated 34.5 mg (63%) as a colorless oil. ^1H NMR (400 MHz, CDCl_3) δ 8.72 (s, 1H), 8.48 (s, 1H), 7.81 (s, 1H), 7.47 (d, $J = 8.3$ Hz, 2H), 7.18 (d, $J = 8.2$ Hz, 2H), 4.29 – 4.19 (m, 2H), 4.02 (dt, $J = 14.3, 7.2$ Hz, 2H), 3.73 – 3.61 (m, 1H), 3.59 – 3.49 (m, 2H), 3.30 (s, 3H), 1.99 – 1.90 (m, 1H), 1.33 (t, $J = 7.1$ Hz, 3H), 1.14 (t, $J = 7.1$ Hz, 3H), 1.05 – 0.99 (m, 2H), 0.78 – 0.70 (m, 2H). ^{13}C NMR (75 MHz, CDCl_3) δ 148.65, 146.60, 144.55, 134.88, 134.30, 126.91, 126.36, 115.31, 64.53 (d, $J = 7.9$ Hz), 63.56 (d, $J = 138.6$ Hz), 62.91 (d, $J = 6.8$ Hz), 42.17, 27.07 (d, $J = 4.0$ Hz), 16.28 (d, $J = 6.1$ Hz), 16.00 (d, $J = 6.7$ Hz), 15.15, 9.53. ^{31}P NMR (81 MHz, CDCl_3) δ 15.31 (s). MS (ESI): calcd 438.150; found 438.61 $[\text{M}+\text{H}]^+$

JDS10-038: diethyl (2-(5-(4-cyclopropoxyphenyl)pyridin-3-yl)-1-(methylsulfonyl)ethyl)phosphonate

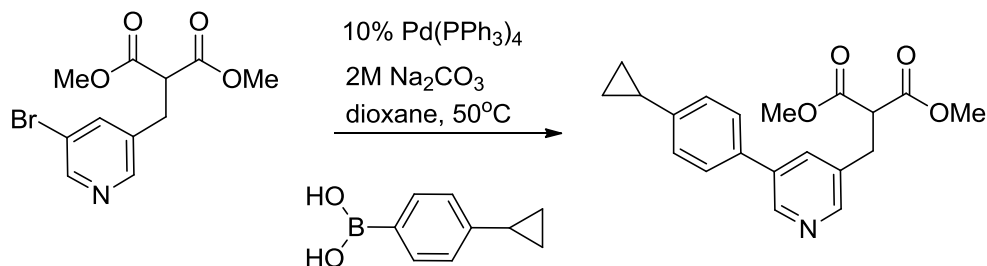


Method A; Isolated 38.2 mg (67%) as a colorless oil. ^1H NMR (400 MHz, CDCl_3) δ 8.71 (s, 1H), 8.47 (s, 1H), 7.80 (s, 1H), 7.51 (d, $J = 8.7$ Hz, 2H), 7.15 (d, $J = 8.7$ Hz, 2H), 4.24 (m, 2H), 4.08 – 3.99 (m, 2H), 3.81 – 3.75 (m, 1H), 3.67 (ddd, $J = 19.2, 14.7, 4.3$ Hz, 1H), 3.55 (m, 2H), 3.30 (s, 3H), 1.33 (t, $J = 7.1$ Hz, 3H), 1.16 (t, $J = 7.1$ Hz, 3H), 0.84 – 0.79 (m, 4H). ^{13}C NMR (75 MHz, CDCl_3) δ 159.28, 148.37, 146.45, 136.06, 134.71, 133.08, 129.99, 128.07, 115.67, 64.51 (d, $J = 6.6$ Hz), 63.55 (d, $J = 138.5$ Hz), 62.92 (d, $J = 6.9$ Hz), 50.95,

42.15, 27.07 (d, $J = 4.0$ Hz), 16.28 (d, $J = 6.1$ Hz), 16.01 (d, $J = 6.6$ Hz), 6.22. ^{31}P NMR (81 MHz, CDCl_3) δ 15.32 (s).

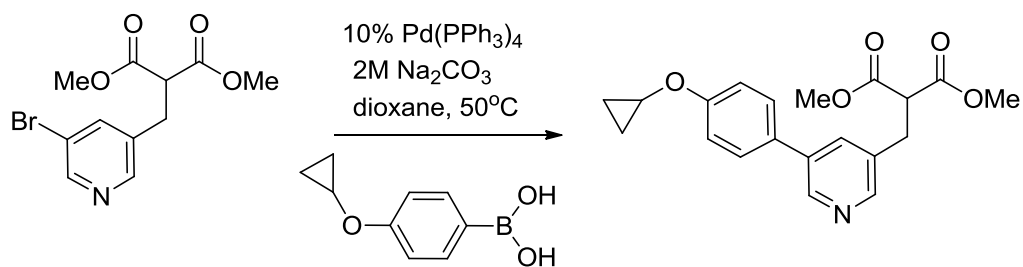
MS (ESI): calcd 454.145; found 454.61 $[\text{M}+\text{H}]^+$

JDS10-039: dimethyl 2-((5-(4-cyclopropylphenyl)pyridin-3-yl)methyl)malonate



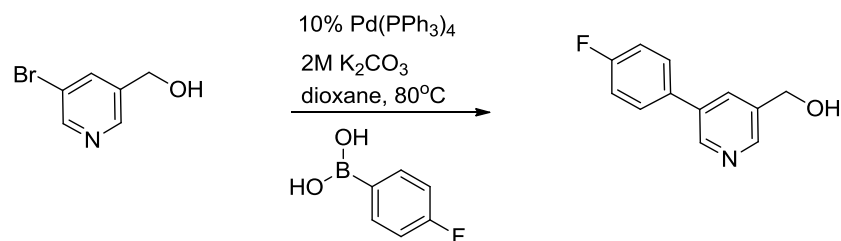
Method A; Isolated 36 mg (80%) as a colorless oil. ^1H NMR (300 MHz, CDCl_3) δ 8.99 (s, 1H), 8.70 (s, 1H), 7.96 (d, $J = 7.9$ Hz, 2H), 7.92 (s, 1H), 7.10 (d, $J = 8.0$ Hz, 2H), 3.68 (s, 6H), 3.34 (d, $J = 7.6$ Hz, 2H), 1.92 (m, 1H), 1.27 (t, $J = 7.1$ Hz, 1H), 0.96 (m, 2H), 0.78 – 0.70 (m, 2H). ^{13}C NMR (75 MHz, CDCl_3) δ 168.40, 145.55, 143.52, 133.80, 127.02, 126.89, 126.75, 126.58, 125.97, 124.75, 52.93, 52.61, 31.79, 15.55, 9.44. MS (ESI): calcd 340.155; found 340.58 $[\text{M}+\text{H}]^+$

JDS10-036: dimethyl 2-((5-(4-cyclopropoxyphenyl)pyridin-3-yl)methyl)malonate



Method A; Isolated 25.8 mg (73%) as a colorless oil. ^1H NMR (400 MHz, CDCl_3) δ 8.69 (s, 1H), 8.40 (s, 1H), 7.68 (s, 1H), 7.49 (d, $J = 8.6$ Hz, 2H), 7.15 (d, $J = 8.6$ Hz, 2H), 3.82 – 3.74 (m, 1H), 3.72 (s, 6H), 3.28 (d, $J = 7.8$ Hz, 2H), 1.33 (t, $J = 7.2$ Hz, 1H), 0.86 – 0.77 (m, 4H). ^{13}C NMR (75 MHz, CDCl_3) δ 168.76, 159.22, 148.08, 146.46, 136.07, 134.37, 133.15, 130.13, 128.10, 115.62, 53.09, 52.74, 50.94, 31.89, 6.22. MS (ESI): calcd 356.150; found 356.28 $[\text{M}+\text{H}]^+$

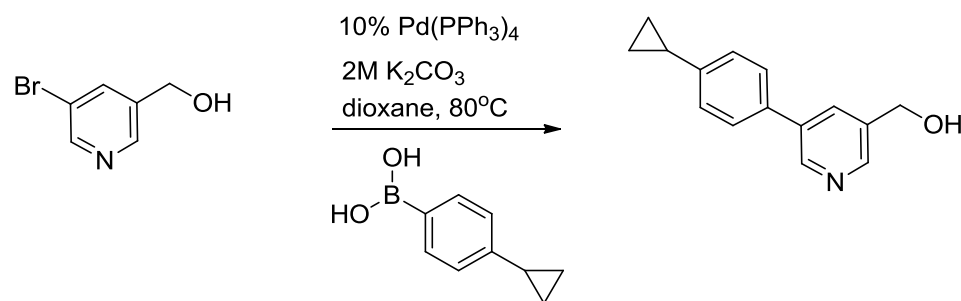
JDS08-002: (5-(4-fluorophenyl)pyridin-3-yl)methanol



Method A; Isolated 2610 mg (97%) as a pale yellow solid. ¹H NMR (300 MHz, CDCl₃) δ 8.55 (bs, 1H), 8.44 (bs, 1H), 7.85 (s, 1H), 7.45 (dd, *J* = 8.5, 5.4 Hz, 2H), 7.10 (m, 2H), 4.75 (s, 2H).

¹³C NMR (75 MHz, CDCl₃) δ 164.57, 161.28, 146.59 (d, *J* = 12.7 Hz), 137.09, 135.70, 135.06, 133.31, 128.75 (d, *J* = 8.2 Hz), 128.01, 62.02. MS (ESI): calcd 204.082; found 204.48 [M+H]⁺

JDS09-014: (5-(4-cyclopropylphenyl)pyridin-3-yl)methanol



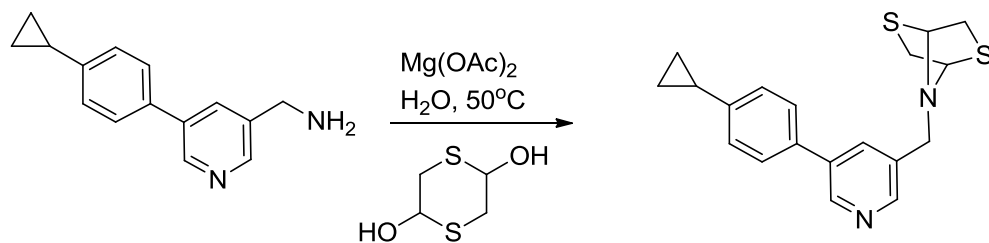
Method A; Isolated 212 mg (59%) as a pale yellow solid. ¹H NMR (400 MHz, CDCl₃) δ 8.76 (s, 1H), 8.55 (s, 1H), 7.91 (s, 1H), 7.49 (d, *J* = 8.4 Hz, 2H), 7.18 (d, *J* = 8.2 Hz, 2H), 4.81 (s, 2H), 1.95 (m, 1H), 1.02 (m, 2H), 0.75 (m, 2H). ¹³C NMR (75 MHz, CDCl₃) δ 147.17, 146.67, 144.45, 136.48, 136.13, 134.51, 132.95, 126.98, 126.32, 62.74, 15.16, 9.53. MS (ESI): calcd 226.123; found 226.86 [M+H]⁺

JDS09-015: (5-(4-cyclopropylphenyl)pyridin-3-yl)methanamine



To an ice-cooled solution of (5-(4-cyclopropylphenyl)pyridin-3-yl)methanol (200 mg, 0.888 mmol) in anhydrous DCM was added thionyl chloride (0.097 mL, 1.3 mmol) and the reaction was stirred at RT for 3 h. The reaction was carefully quenched with satd. NaHCO₃, separated and extracted 2 times with 30 mL DCM, the combined organic extracts were dried over anhydrous Na₂SO₄, filtered and concentrated in vacuo. The residue was transferred to a 75 mL pressure vessel and ammonia in MeOH (7 M, 32 mL, 222 mmol) was added. The vessel was tightly sealed with a Teflon cap and the reaction was stirred at 60°C for 12 h. The reaction was cooled down, concentrated in vacuo and redissolved in 100 mL EtOAc. Washed with 10 mL satd. NaHCO₃ and brine; dried over anhydrous Na₂SO₄, filtered and concentrated in vacuo to furnish the desired amine in quantitative yield and sufficient purity (~94% as determined by HPLC) for the following steps. ¹H NMR (400 MHz, CDCl₃) δ 8.71 (bs, 1H), 8.51 (bs, 1H), 7.84 (s, 1H), 7.49 (d, *J* = 8.2 Hz, 2H), 7.17 (d, *J* = 8.2 Hz, 2H), 3.98 (s, 2H), 1.94 (m, 1H), 1.05 – 0.99 (m, 2H), 0.77 – 0.71 (m, 2H). ¹³C NMR (75 MHz, CD₃OD) δ 146.34, 145.16, 144.60, 138.23, 136.71, 133.95, 133.81, 126.53, 125.94, 42.56, 14.59, 8.73. MS (ESI): calcd 225.139; found 225.53 [M+H]⁺

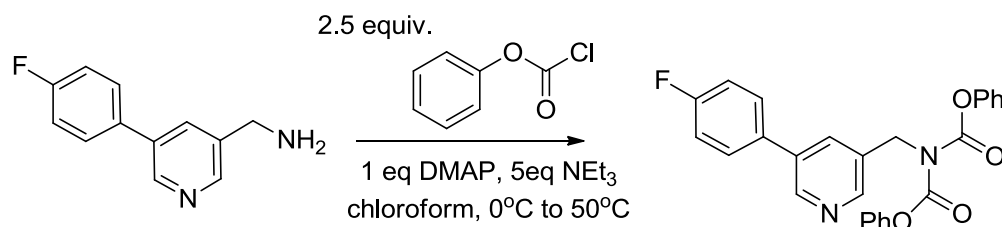
JDS09-019: 7-((5-(4-cyclopropylphenyl)pyridin-3-yl)methyl)-2,5-dithia-7-azabicyclo[2.2.1]heptanes



To a suspension of 1,4-dithiane-2,5-diol (37 mg, 0.24 mmol) in 3 mL distilled water was added magnesium acetate tetrahydrate (4.8 mg, 0.022 mmol) and the mixture was stirred at 50°C for 15 min. (5-(4-cyclopropylphenyl)pyridin-3-yl)methanamine (50 mg, 0.22 mmol) was added as a solution in 2 mL MeOH and the reaction was stirred 12 at 50°C. The reaction mixture was cooled down, extracted 3 times with 50 mL EtOAc and the combined organic extracts were dried over anhydrous Na₂SO₄, filtered and concentrated in vacuo. The residue was purified by silica gel chromatography on a CombiFlash instrument, using a solvent gradient from 1:10 EtOAc/Hexanes to 50% EtOAc (+0.1 NEt₃). The desired product was isolated as a white semi-solid (65 mg, 86%).

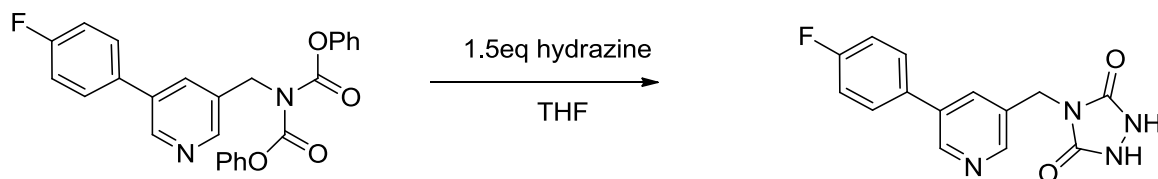
^1H NMR (500 MHz, CDCl_3) δ 8.79 (s, 1H), 8.57 (s, 1H), 7.96 (s, 1H), 7.49 (d, J = 8.3 Hz, 2H), 7.18 (d, J = 8.2 Hz, 2H), 4.80 (d, J = 3.0 Hz, 2H), 3.74 – 3.65 (m, 2H), 3.40 (dd, J = 9.6, 3.0 Hz, 2H), 3.26 (d, J = 9.5 Hz, 2H), 1.95 (m, 1H), 1.02 (m, 2H), 0.75 (m, 2H). ^{13}C NMR (126 MHz, CDCl_3) δ 147.54, 146.85, 144.77, 136.80, 134.91, 134.09, 133.26, 127.03, 126.40, 69.65, 50.33, 43.85, 15.19, 9.60. MS (ESI): calcd 341.11462; found 341.23 $[\text{M}+\text{H}]^+$

6.24 (JDS08-075): diphenylcarbamoyl-(5-(4-fluorophenyl)pyridin-3-yl)methanamine



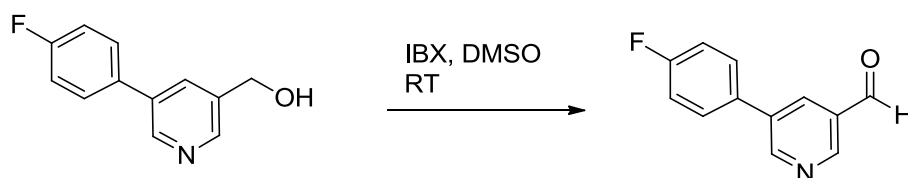
To an ice-cooled solution of (5-(4-fluorophenyl)pyridin-3-yl)methanamine (30.0 mg, 0.148 mmol) and *N,N*-dimethyl-4-aminopyridine (19.9 mg, 0.163 mmol) in 5 mL anhydrous chloroform was added triethylamine (0.10 mL, 0.74 mmol) and phenyl chloroformate (0.05 mL, 0.37 mmol) via syringe. The reaction was stirred at RT for 1 h and then heated to 50°C for 6 h. The reaction mixture was cooled down, diluted with 100 mL EtOAc and washed 2 times with 10 mL satd. NaHCO_3 , 10 mL water and washed with brine, dried over anhydrous Na_2SO_4 , filtered and concentrated in vacuo. The residue was purified by silica gel chromatography on a CombiFlash instrument, using a solvent gradient from 1:10 EtOAc/Hexanes to 100% EtOAc (+0.1% NEt_3). The desired product was isolated as white foam 30 mg (46%). ^1H NMR (400 MHz, CD_3OD) δ 8.77 (br. s, 1H), 8.67 (br. s, 1H), 8.16 (t, J = 1.9 Hz, 1H), 7.70 – 7.64 (m, 2H), 7.45 – 7.38 (m, 4H), 7.31 – 7.15 (m, 8H), 5.26 (s, 2H). ^{13}C NMR (75 MHz, CD_3OD) δ 164.81, 161.54, 152.07, 150.62, 147.15, 146.42, 134.79, 133.14, 129.26, 128.81 (d, J = 8.4 Hz), 126.09, 121.01, 115.71 (d, J = 22.0 Hz). MS (ESI): calcd 443.141; found 443.65 $[\text{M}+\text{H}]^+$

Bioisotere 6.6 (JDS08-080): 4-((5-(4-fluorophenyl)pyridin-3-yl)methyl)-1,2,4-triazolidine-3,5-dione



To an ice-cooled solution of di-carbamate precursor (25 mg, 0.057 mmol) in anhydrous THF was added hydrazine (1.0M in THF, 0.085 mL, 0.085 mmol) and the reaction was stirred at RT for 8h. The reaction mixture was concentrated in vacuo and the residue was purified by preparative HPLC (Water Atlantis C18 column) using a gradient from water to acetonitrile (+0.1% formic acid). Pure fractions were lyophilized to yield the desired compound as a white powder (9 mg, 56%). ¹H NMR (400 MHz, DMSO-d₆) δ 8.80 (d, *J* = 2.2 Hz, 1H), 8.49 (d, *J* = 1.8 Hz, 1H), 7.93 (t, *J* = 1.9 Hz, 1H), 7.73 (dd, *J* = 8.8, 5.4 Hz, 2H), 7.35 (t, *J* = 8.9 Hz, 2H), 7.17 – 7.12 (m, NH), 6.78 – 6.72 (m, NH), 4.65 (s, 2H). ¹³C NMR (75 MHz, DMSO-d₆) δ 164.42, 161.16, 154.99, 148.11, 147.24, 134.85, 133.93, 133.65 (d, *J* = 3.2 Hz), 133.17, 129.48 (d, *J* = 8.4 Hz), 116.53 (d, *J* = 21.6 Hz), 115.66. MS (ESI): calcd 285.07878; found 285.07967 [M-H]⁺

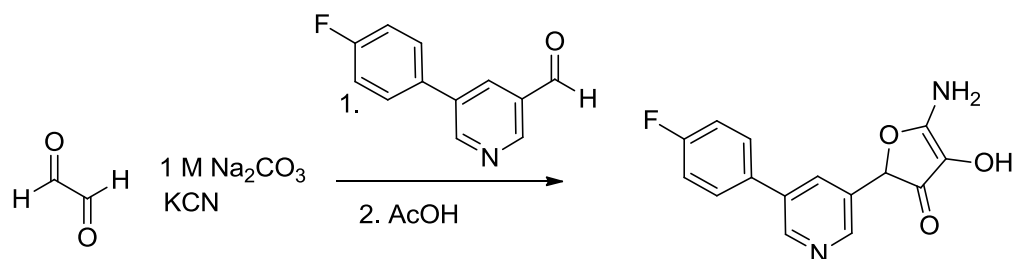
6.17 (JDS07-088): 5-(4-fluorophenyl)nicotinaldehyde



To a solution of (5-(4-fluorophenyl)pyridin-3-yl)methanol (550 mg, 2.71 mmol) in anhydrous DMSO was added IBX (1140 mg, 4.06 mmol) and the reaction was stirred at RT for 30 min. The reaction was quenched by the addition of 35 mL water and the aqueous phase was extracted 4 times with 50 mL EtOAc. The combined organic layers were washed with 10 mL satd. NaHCO₃ and brine; dried over anhydrous Na₂SO₄, filtered and concentrated in vacuo. The residue was purified by silica gel chromatography on a CombiFlash instrument, using a solvent gradient from 1:10 EtOAc/Hexanes to 100% EtOAc (+0.1 NEt₃). Isolated 370 mg (68%) as white waxy solid.

^1H NMR (400 MHz, acetone- d_6) δ 10.26 (s, 1H), 9.14 (d, J = 2.4 Hz, 1H), 9.08 (d, J = 1.9 Hz, 1H), 8.50 – 8.45 (m, 1H), 7.92 – 7.84 (m, 2H), 7.37 – 7.31 (m, 2H). ^{13}C NMR (75 MHz, CDCl_3) δ 190.67, 164.95, 153.06, 150.77, 136.35, 133.38, 132.45 (d, J = 3.3 Hz), 131.32, 128.99 (d, J = 8.3 Hz), 116.42 (d, J = 21.8 Hz). MS (ESI): calcd 202.067; found 202.42 $[\text{M}+\text{H}]^+$

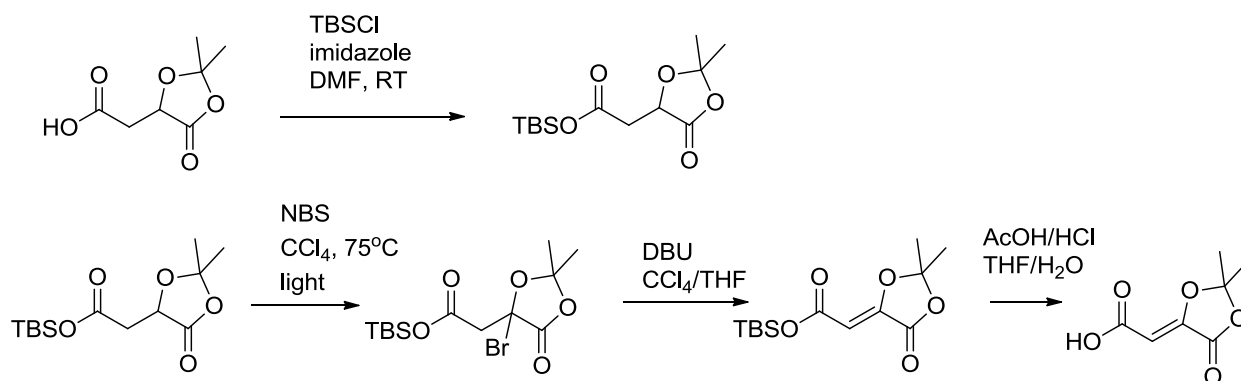
Bioisostere 6.5 (JDS08-083): 5-amino-2-(5-(4-fluorophenyl)pyridin-3-yl)-4-hydroxyfuran-3(2H)-one



To a solution of degassed Na_2CO_3 (1.0 M, 0.53 mL, 0.53 mmol) was added potassium cyanide (18 mg, 0.27 mmol) followed glyoxal sodium sulfite hydrate (43 mg, 0.16 mmol) to obtain a clear solution. 5-(4-fluorophenyl)nicotinaldehyde (25 mg, 0.12 mmol) was added as a solid, followed by 0.5 mL 1,4-dioxane and the reaction was stirred at RT for 30 min. To the resulting green/gray suspension was added acetic acid (0.071 mL, 1.2 mmol) and the resulting clear yellow solution was stirred at RT for 2 h. The reaction mixture was diluted with 100 mL EtOAc, washed 2 times with semi-satd. NaCl and once with brine; dried over anhydrous Na_2SO_4 , filtered and concentrated in vacuo. The residue was suspended in MeOH, filtered through a plug of cotton and purified by preparative HPLC (Water Atlantis C18 column) using a gradient from water to acetonitrile (+0.1% formic acid). Pure fractions were lyophilized to yield the desired compound as a white powder (9 mg, 56%) in 92.32% homogeneity as determined by HPLC-MS.

^1H NMR (400 MHz, CD_3OD) δ 8.79 (d, J = 2.0 Hz, 1H), 8.51 (d, J = 1.7 Hz, 1H), 7.99 (s, 1H), 7.70 (dd, J = 8.7, 5.2 Hz, 2H), 7.24 (t, J = 8.7 Hz, 2H), 5.68 (s, 1H). ^{13}C NMR (75 MHz, CD_3OD) δ 181.29, 175.05, 164.85, 161.57, 147.24, 145.69, 136.15, 133.18, 132.98 (d, J = 3.2 Hz), 132.00, 128.86 (d, J = 8.3 Hz), 115.69 (d, J = 22.0 Hz), 112.59, 81.64. MS (ESI): calcd 285.06755; found 285.06618 $[\text{M}-\text{H}]^-$

6.26 (JDS10-007): (Z)-2-(2,2-dimethyl-5-oxo-1,3-dioxolan-4-ylidene)acetic acid



This compound was synthesized according to literature procedure:

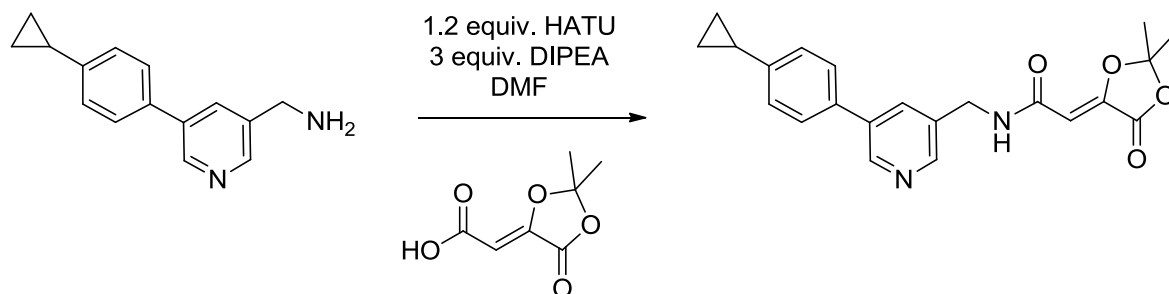
(Z)-2,2-Dimethyl-5-carboxymethylene-1,3-dioxolan-4-one: a new synthon for the synthesis of α , γ -diketo acid derivatives

Jacques Banville *, Gilles Bouthillier, Serge Plamondon, Roger Remillard, Nicholas A.

Meanwell, Alain Martel, Michael A. Walker, Tetrahedron Lett. (2010), 51 3170

¹H NMR (400 MHz, CDCl₃) δ 5.87 (s, 1H), 1.76 (s, 6H).

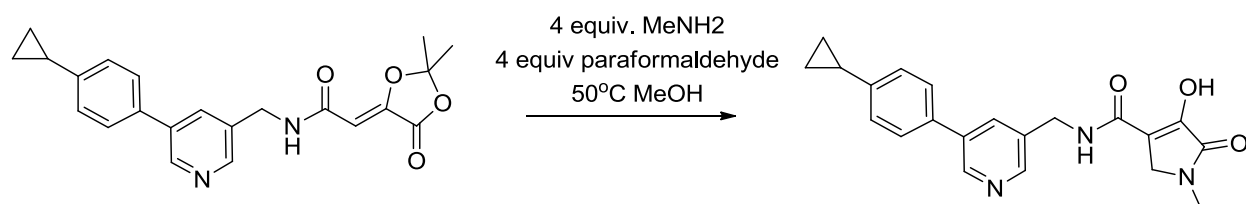
6.27 (JDS10-008): (Z)-N-((5-(4-cyclopropylphenyl)pyridin-3-yl)methyl)-2-(2,2-dimethyl-5-oxo-1,3-dioxolan-4-ylidene)acetamide



To a mixture of (Z)-2-(2,2-dimethyl-5-oxo-1,3-dioxolan-4-ylidene)acetic acid (42.2 mg, 0.245 mmol) and (5-(4-cyclopropylphenyl)pyridin-3-yl)methanamine (50.0 mg, 0.223 mmol) in 4 mL of anhydrous DMF was added in sequence: DIPEA (0.12 mL, 0.67 mmol) and HATU (102 mg, 0.267 mmol). The reaction was stirred at RT overnight. The reaction mixture was diluted with 100 mL EtOAc, washed with 10 mL saturated NaHCO₃ and 5 times 10 mL water and washed with brine, dried over anhydrous Na₂SO₄, filtered and concentrated in vacuo. The residue was purified by silica gel chromatography on a CombiFlash instrument, using a solvent gradient from 1:10 EtOAc/Hexanes to 100% EtOAc (+0.1% NEt₃). The desired product was isolated as a pale yellow semi-solid 66.7 mg

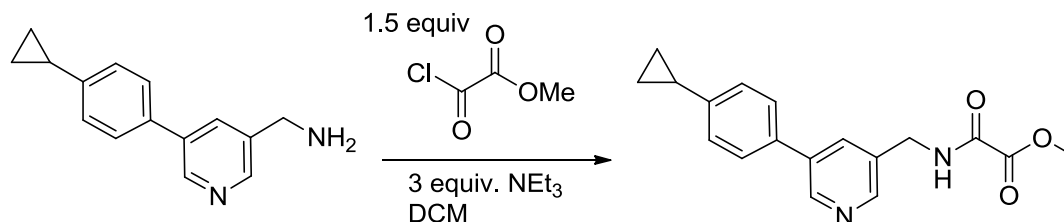
(79%). ^1H NMR (400 MHz, CDCl_3) δ 8.75 (d, $J = 1.9$ Hz, 1H), 8.51 (d, $J = 1.7$ Hz, 1H), 7.82 (t, $J = 1.9$ Hz, 1H), 7.47 (d, $J = 8.1$ Hz, 2H), 7.17 (d, $J = 8.3$ Hz, 2H), 6.68 (s, NH), 5.91 (s, 1H), 4.64 (d, $J = 6.0$ Hz, 2H), 1.74 – 1.72 (s, 6H). ^{13}C NMR (75 MHz, CDCl_3) δ 163.26, 161.68, 147.32, 147.16, 144.55, 143.37, 136.53, 134.27, 133.71, 126.97, 126.29, 114.08, 100.69, 40.95, 26.80, 15.16, 9.59. MS (ESI): calcd 379.166; found 379.55 $[\text{M}+\text{H}]^+$

Bioisostere 6.8 (JDS10-011): N-((5-(4-cyclopropylphenyl)pyridin-3-yl)methyl)-4-hydroxy-1-methyl-5-oxo-2,5-dihydro-1H-pyrrole-3-carboxamide



A pressure vessel was charged with (Z)-N-((5-(4-cyclopropylphenyl)pyridin-3-yl)methyl)-2-(2,2-dimethyl-5-oxo-1,3-dioxolan-4-ylidene)acetamide (32 mg, 0.085 mmol), paraformaldehyde (10.2 mg, 0.34 mmol), methylamine (2M in THF, 0.17 mL, 0.34 mmol) and acetic acid (0.02 mL, 0.34 mmol), dissolved in 4 mL anhydrous MeOH and tightly sealed with a Teflon cap. The reaction was stirred at 60°C for 2 h. The reaction was cooled down and concentrated in vacuo. The residue was purified by silica gel chromatography using a CombiFlash instrument and a solvent gradient from 10% EtOAc/Hexanes to 100% EtOAc and then to 40% MeOH in EtOAc (+0.1% NEt_3). The product was isolated as a purple oil in ~75% purity. The mixture was purified by reverse phase C18 chromatography using a CombiFlash instrument and a solvent gradient from 10% $\text{CH}_3\text{CN}/\text{H}_2\text{O}$ to 100% CH_3CN with 0.1% formic acid. Fractions of sufficient purity were pooled and lyophilized to dryness. Isolated ~1 mg (~3%) as a white powder. ^1H NMR (500 MHz, $\text{DMSO}-d_6$) δ 8.72 (s, 1H), 8.47 (s, 1H), 7.92 (s, 1H), 7.56 (d, $J = 8.2$ Hz, 2H), 7.20 (d, $J = 8.2$ Hz, 2H), 4.48 (d, $J = 5.9$ Hz, 2H), 3.88 (s, 2H), 2.92 (s, 3H), 2.00 – 1.93 (m, 1H), 1.01 – 0.96 (m, 2H), 0.74 – 0.69 (m, 2H). MS (ESI): calcd 362.15047; found 362.15159 $[\text{M}-\text{H}]^-$

6.28 (JDS10-018): methyl 2-(((5-(4-cyclopropylphenyl)pyridin-3-yl)methyl)amino)-2-oxoacetate

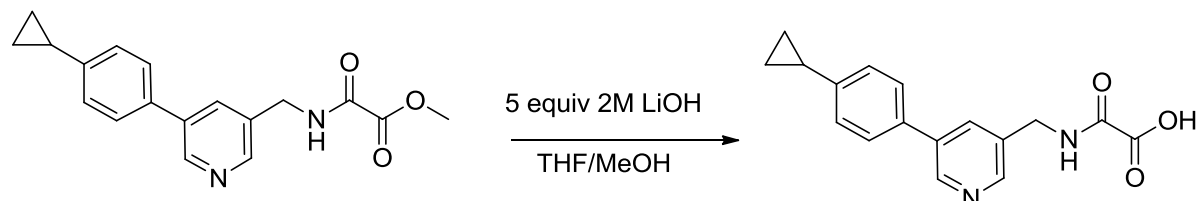


To an ice-cooled solution of (5-(4-cyclopropylphenyl)pyridin-3-yl)methanamine (40.0 mg, 0.178 mmol) and triethylamine (0.075 mL, 0.54 mmol) in 3 mL anhydrous DCM was added methyl 2-chloro-2-oxoacetate (0.025 mL, 0.27 mmol) via syringe and the solution is stirred at RT for 3 h. The reaction mixture was concentrated in vacuo and the residue was purified by silica gel chromatography using a CombiFlash instrument and a solvent gradient from 10% EtOAc/Hexanes to 100% EtOAc and then to 25% MeOH in EtOAc (+0.1% NEt₃). The desired product was isolated as a colorless oil (51.9 mg, 94%). ¹H NMR (300 MHz, CDCl₃) δ 8.72 (d, *J* = 2.0 Hz, 1H), 8.47 (d, *J* = 1.8 Hz, 1H), 7.78 (t, *J* = 2.1 Hz, 1H), 7.42 (d, *J* = 8.3 Hz, 2H), 7.14 (d, *J* = 8.3 Hz, 2H), 4.57 (d, *J* = 6.3 Hz, 2H), 3.87 (s, 3H), 1.92 (m, 1H), 1.00 (m, 2H), 0.72 (m, 2H). ¹³C NMR (75 MHz, CDCl₃) δ 160.86, 156.50, 147.62, 147.50, 144.62, 136.64, 134.11, 133.83, 132.43, 126.99, 126.32, 53.72, 41.34, 15.16, 9.57. MS (ESI): calcd 309.124; found 309.24 [M-H]⁺

General procedure for saponification of methyl esters:

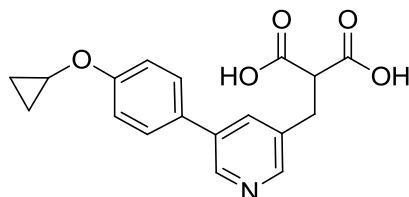
To an ice-cooled solution of the methyl ester in 1:1 THF/MeOH was added 2M LiOH (5 equivalents) and the reaction was stirred at RT until complete consumption of the starting material as determined by HPLC. The reaction is acidified to pH=2 with 5M HCl and concentrated to dryness. The residue was purified by reverse phase chromatography on C18 silica using a CombiFlash instrument and a solvent gradient from 10% CH₃CN/H₂O to 100% CH₃CN with 0.1% formic acid. Fractions of sufficient purity were pooled and lyophilized to dryness.

Bioisostere 6.9 (JDS10-019): 2-(((5-(4-cyclopropylphenyl)pyridin-3-yl)methyl)amino)-2-oxoacetic acid



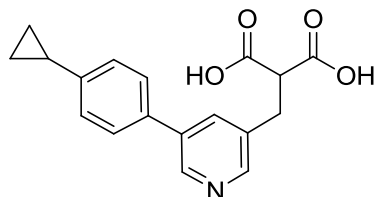
Isolated 8.4 mg (35%) as a white powder. ^1H NMR (500 MHz, DMSO- d_6) δ 9.42 (s, NH), 8.75 (s, 1H), 8.45 (s, 1H), 7.92 (s, 1H), 7.58 (d, $J = 8.2$ Hz, 2H), 7.21 (d, $J = 8.2$ Hz, 2H), 4.40 (d, $J = 6.1$ Hz, 2H), 2.00 – 1.92 (m, 1H), 1.03 – 0.95 (m, 2H), 0.75 – 0.68 (m, 2H). ^{13}C NMR (126 MHz, DMSO - d_6) δ 162.42, 159.33, 147.81, 146.51, 144.53, 135.54, 134.60, 134.24, 133.45, 127.10, 126.54, 104.99, 15.28, 10.13. MS (ESI): calcd 295.10827; found 295.10900 $[\text{M-H}]^-$

Bioisostere 6.11 (JDS10-042): 2-(((5-(4-cyclopropoxyphenyl)pyridin-3-yl)methyl)malonic acid



Isolated 7.5 mg (33%) as a white powder. ^1H NMR (500 MHz, D_2O) δ 8.57 (d, $J = 2.2$ Hz, 1H), 8.34 (d, $J = 2.0$ Hz, 1H), 7.93 (t, $J = 2.1$ Hz, 1H), 7.67 (d, $J = 8.9$ Hz, 2H), 7.26 (d, $J = 8.9$ Hz, 2H), 3.94 (tt, $J = 6.1, 3.0$ Hz, 1H), 3.43 (t, $J = 8.0$ Hz, 1H), 3.12 (d, $J = 7.9$ Hz, 2H), 0.86 (m, 2H), 0.79 – 0.75 (m, 2H). MS (ESI): calcd 326.10285; found 326.10357 $[\text{M-H}]^-$

Bioisostere 6.10 (JDS10-043): 2-(((5-(4-cyclopropylphenyl)pyridin-3-yl)methyl)malonic acid



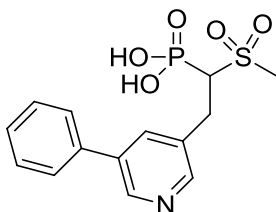
Isolated 8.0 mg (29%) as a white powder. ^1H NMR (500 MHz, D_2O) δ 8.59 (d, $J = 2.2$ Hz, 1H), 8.35 (d, $J = 2.0$ Hz, 1H), 7.95 (t, $J = 2.1$ Hz, 1H), 7.62 (d, $J = 8.4$ Hz, 2H), 7.27 (d, $J =$

8.3 Hz, 2H), 3.42 (t, $J = 8.0$ Hz, 1H), 3.12 (d, $J = 8.0$ Hz, 2H), 2.02 – 1.96 (m, 1H), 1.03 (m, 2H), 0.77 – 0.73 (m, 2H). ^{13}C NMR (126 MHz, D_2O) δ 178.20, 147.21, 144.85, 144.32, 136.59, 135.96, 135.36, 134.19, 127.06, 126.01, 104.99, 59.76, 33.29, 14.30, 9.15. MS (ESI): calcd 310.10793; found 310.10888 $[\text{M}-\text{H}]^-$

General procedure of deprotection of di-ethyl phosphonate esters:

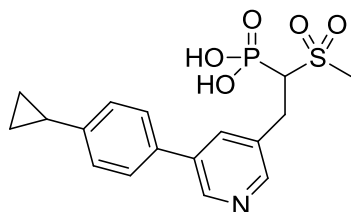
A 12 mL Teflon lined screw cap vial was charged with the tetra-ethyl bisphosphonate compound, dissolved in 5 mL distilled DCM and cooled in an ice bath. Bromotrimethyl silane (15 equivalents) was added via syringe and the reaction mixture was stirred at RT for 5-7 days. The reaction mixture was transferred to a 10 mL recovery flask and concentrated in vacuo (satd. NaHCO_3 in receiving flask). To the resulting oil was added 2 mL of HPLC-grade MeOH and concentrated in vacuo, this was repeated a total of five times. The crude thus obtained was purified by reverse phase chromatography on C18 silica using a Combiflash instrument and a gradient from 10% ACN/ H_2O to 100% ACN (+0.1% formic acid).

Bioisostere 6.12 (JDS05-093): (1-(methylsulfonyl)-2-(5-phenylpyridin-3-yl)ethyl)phosphonic acid



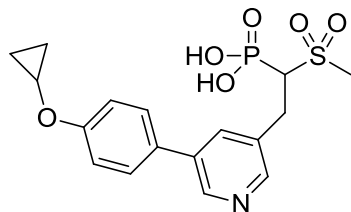
Isolated 22.5 mg (65%) as a white powder. ^1H NMR (500 MHz, D_2O) δ 8.50 (d, $J = 2.1$ Hz, 1H), 8.35 (d, $J = 2.0$ Hz, 1H), 8.01 (t, $J = 2.0$ Hz, 1H), 7.62 – 7.56 (m, 2H), 7.45 – 7.38 (m, 2H), 7.36 – 7.32 (m, 1H), 3.50 (m, 2H), 3.20 (m, 1H), 3.03 (s, 3H). ^{13}C NMR (126 MHz, D_2O) δ 147.68, 144.70, 137.03, δ 136.76 (d, $J = 9.6$ Hz), 136.24, 135.76, 129.14, 128.32, 127.04, 41.12, 29.05, 65.20 (d, $J = 108.8$ Hz). ^{31}P NMR (81 MHz, D_2O) δ 6.60 (s). MS (ESI): calcd 340.04085; found 340.04176 $[\text{M}-\text{H}]^-$

Bioisostere 6.13 (JDS10-040): (2-(5-(4-cyclopropylphenyl)pyridin-3-yl)-1-(methylsulfonyl)ethyl)phosphonic acid



Isolated 10.3 mg (37%) as a white, fluffy powder. ^1H NMR (500 MHz, D_2O) δ 8.61 (d, J = 2.1 Hz, 1H), 8.45 (d, J = 2.0 Hz, 1H), 8.11 (t, J = 2.0 Hz, 1H), 7.63 (d, J = 8.4 Hz, 2H), 7.27 (d, J = 8.2 Hz, 2H), 3.67 – 3.57 (m, 2H), 3.32 (ddd, J = 16.0, 10.3, 3.7 Hz, 1H), 3.16 (s, 3H), 1.99 (m, 1H), 1.02 (m, 2H), 0.77 – 0.73 (m, 2H). ^{13}C NMR (126 MHz, D_2O) δ 147.39, 144.92, 144.43, 136.72 (d, J = 9.6 Hz), 135.96, 135.40, 134.03, 127.03, 126.01, 65.20 (d, J = 108.6 Hz), 41.11, 29.03, 14.30, 9.16. ^{31}P NMR (81 MHz, D_2O) δ 6.60 (s). MS (ESI): calcd 380.07215; found 380.07316 $[\text{M-H}]^-$

Bioisostere 6.14 (JDS10-041): (2-(5-(4-cyclopropoxyphenyl)pyridin-3-yl)-1-(methylsulfonyl)ethyl)phosphonic acid



Isolated 8.3 mg (26%) as a white, fluffy powder. ^1H NMR (500 MHz, D_2O) δ 8.61 (d, J = 2.2 Hz, 1H), 8.45 (d, J = 2.0 Hz, 1H), 8.11 (t, J = 2.1 Hz, 1H), 7.70 (d, J = 8.9 Hz, 2H), 7.28 (d, J = 8.9 Hz, 2H), 3.95 (tt, J = 6.1, 3.0 Hz, 1H), 3.68 – 3.58 (m, 2H), 3.37 – 3.30 (m, 1H), 3.17 (s, 3H), 0.88 – 0.84 (m, 2H), 0.77 (m, 2H). ^{13}C NMR (126 MHz, D_2O) δ 158.35, 147.17, 144.34, 136.73 (d, J = 9.5 Hz), 135.74, 135.30, 130.28, 128.27, 115.66, 65.22 (d, J = 108.9 Hz), 51.28, 41.11, 29.04, 5.44. ^{31}P NMR (81 MHz, D_2O) δ 6.62 (s). MS (ESI): calcd 396.0607; found 396.06805 $[\text{M-H}]^-$

6.7.2 Enzymatic inhibition assays

The *sensitized M2* inhibition assay for hFPPS was performed as described in Chapter 7.

The inhibition assay for hGGPPS was performed as described in Chapter 3.

7 Modification of the hFPPS enzymatic assay

7.1 Preface

The work described in this chapter has not yet been published. I performed all the synthesis and enzymatic work.

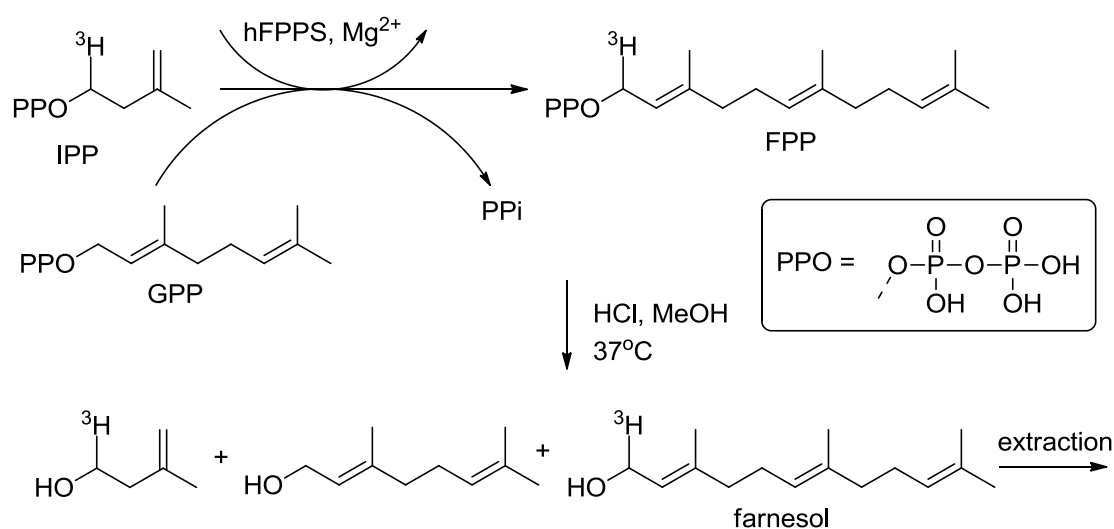
7.2 Introduction

The goal of the following enzymatic work was to identify *in vitro* assay conditions that would allow the accurate and reliable determination of inhibition activity against hFPPS of both bisphosphonate and *non*-bisphosphonate compounds synthesized in our group. A number of literature compounds were used to assess the validity of our assays, including risedronate and the Novartis allosteric inhibitors **1.5** and **1.6** (Figure 7.3, refer to experimental section for their synthesis).

To date, a number of different assays have been reported in the literature for evaluating the *in vitro* potency of hFPPS inhibitors. The sensitivity and reliability of these assays varies significantly; for example the reported IC₅₀ value of the drug zoledronate varies from ~4 nM to 475 nM, depending on the assay conditions.¹ It is common knowledge that all biological data obtained *in vitro* is only meaningful for SAR comparison of compounds, when tested under the same assay conditions. The relative *in vitro* activity of inhibitors does not necessarily translate to cell based potency due to unpredictable factors, including cell-membrane permeability, efflux and metabolic stability. Furthermore, cell-based potency does not guarantee good results *in vivo* due to issues such as poor oral bio-availability, tissue-distribution and biological redundancy/rescue mechanisms. Finally, even with extensive pre-clinical data, drug candidates often fail to perform well in clinical trials for a variety of reasons, including toxicity, lack of efficacy and dose-limiting side-effects. Nonetheless, a reliable assessment of *in vitro* potency is mandatory for

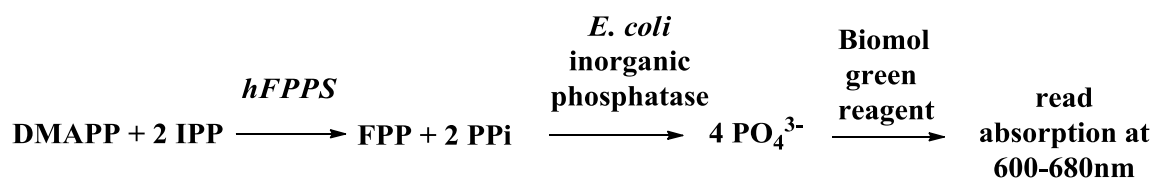
understanding and optimizing the SAR within a series of compounds at an early phase of every drug discovery program. Consequently, we considered a number of alternative methods for assessing the *in vitro* potency of our compounds, such as DSF (Chapter 8). Furthermore, we decided to investigate other reported hFPPS inhibition assays, in addition to exploring the conditions of the original enzymatic assay developed by Reed and Rilling in 1975.^{2,3}

The most commonly used type of hFPPS assay is summarised in **Scheme 7.1**;¹ we have used this assay with various modifications (methods **M1** and **M2**, **Table 7.1**; refer to the experimental section for details) to evaluate the compounds prepared in this thesis. Using this assay, GPP and tritium-labeled IPP are incubated with the enzyme, in the presence or absence of an inhibitor, and the relative catalytic turnover is estimated from the ratio of isolated tritium-labeled farnesol (**Scheme 7.1**), detected using a liquid scintillation counter. However, the standard (**M1**) assay conditions were originally developed for bisphosphonate inhibitors and were found to be insensitive or inaccurate in measuring hFPPS inhibition for compounds that were *non*-bisphosphonates, such as the Novartis allosteric inhibitors **1.5** and **1.6**.⁴ The reasons for this discrepancy is not completely clear, however, unofficial reports (personal communications) suggest that lipophilic compounds are prone to form aggregates in the assay medium used for original enzymatic assay leading to artefacts in the data.



Scheme 7.1: ³H-IPP dependant hFPPS assay

In their efforts to overcome the low-throughput and cost of the above radioactive assay, Wattanasin and co-workers (Novartis) used a robotized colorimetric enzymatic assay to determine the enzymatic activity of their novel inhibitors against *S. pneumoniae* UPPS and hFPPS (as a counterscreen).⁵ In this assay, the catalytic turnover of each enzyme was estimated from the formation of inorganic pyrophosphate (PPi) (**Scheme 7.2**). To maximize the signal strength the authors used DMAPP and IPP as substrates; *i.e.* 2 equivalents of PPi are produced per equivalent of the FPP product. Inorganic PPi was then converted to inorganic phosphate (PO_4^{3-}) by a second enzyme in the assay, *E. coli* inorganic pyrophosphatase. After the enzymatic reaction was stopped, a reagent called “Biomol green” was added, to form a green/blue complex with phosphate in a dose-dependent manner. Finally, the absorption between 600-680 nm was read and used as a measure to determine the level of FPP biosynthesis. This method has the advantage that it can be performed with a standard plate reader, which allows for high throughput analysis (96-384 well plates). However, the readout is indirect and depends on a separate enzyme and reagent, which can introduce variability and artefacts into the data. The major drawback of this type of assay is low sensitivity, as micromolar levels of phosphate must be produced in order to accurately be detected by the colorimetric reagent. Two other important differences from the radioactive enzymatic assay are the lower concentration of Mg^{2+} used and the addition of a detergent (**Table 7.1**).



Scheme 7.2: Colorimetric hFPPS assay

7.3 Exploring the effect of assay buffer components

7.3.1 Magnesium concentration

Three Mg^{2+} ions are required for the allylic substrates to bind to hFPPS active site and for the catalytic condensation to proceed.⁶ Many techniques have been employed to measure the cellular concentration of Mg^{2+} , such as selective Mg^{2+} electrodes and fluorescent indicators, all of which indicate a range between 17 and 20 mM for total cell content.⁷ However the majority of intracellular Mg^{2+} ions are not free in solution, but bound to proteins, polynucleotides and phosphonucleotides; particularly ATP, which has a high Mg^{2+} -affinity ($K_d \sim 78 \mu\text{M}$) and is present at a concentration of $\sim 5 \text{ mM}$. Thus the free, cytosolic Mg^{2+} concentrations lie between 0.5 and 1 mM. The concentration of Mg^{2+} in the original enzymatic assay (**M1**) was 2 mM, hence, we decided to lower the concentration to 1 mM in order to make the assay more biologically relevant. In addition, we assumed that at lower concentrations of Mg^{2+} the binding affinity of the allylic substrates may be reduced, allowing them to be more readily displaced by a non-bisphosphonate inhibitor. Interestingly, decreasing the amount of Mg^{2+} from 2 mM to 1 mM or 0.5 mM resulted in an increase of enzymatic turnover of approximately 50%, while the inhibition activity for the drug risedronate was unaffected (**Figure 7.1**); further decreasing the concentration of Mg^{2+} to 0.05 mM or lower (*i.e.* outside of the biological range), proved detrimental to enzyme activity.

7.3.2 Detergent

The colorimetric assay used by Wattanasin and co-workers also included the detergent Triton X-100; which we found had no effect on the enzyme catalytic function (data not shown). However, this may be of critical importance for *non*-bisphosphonate compounds, which are inherently more lipophilic and can form aggregates in solution.⁸ Aggregate formation can decrease the amount of free compound in solution, effectively lowering its concentration and resulting false negative results. In the other scenario, aggregates have been shown to indiscriminately bind to and inhibit proteins, resulting in false positive

results.⁹ Therefore, it was decided to include 0.01% Triton X-100 as part of the new assay conditions, in order to prevent potential aggregation of non-bisphosphonate compounds. It is worth noting that our hGGPPS assay already contains detergent, namely 0.2% Tween 20, in order to solubilize the GGPP product and prevent product-inhibition of the enzyme.

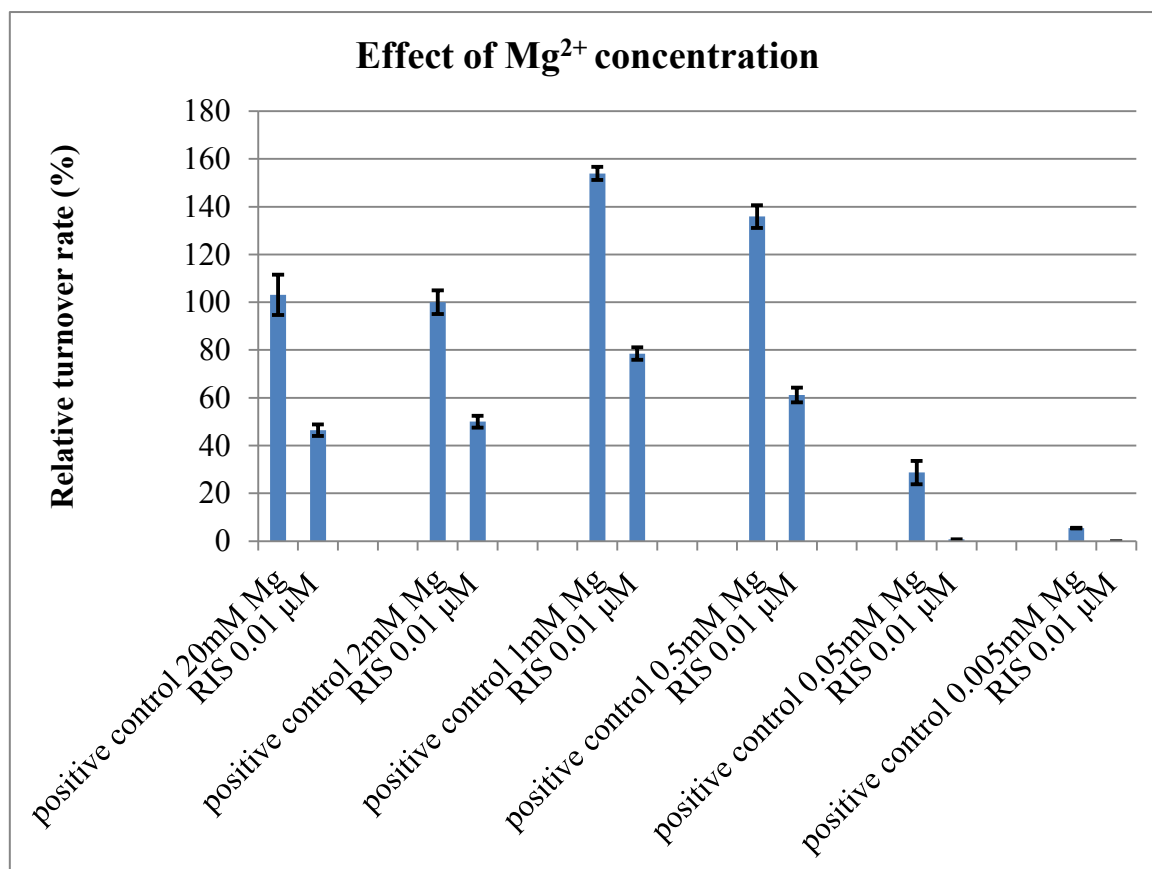


Figure 7.1: hFPPS enzymatic data at different Mg²⁺ concentrations

Readouts were normalized to the positive control at 2 mM MgCl₂. (**M1** assay conditions)

7.3.3 hFPPS and substrate concentrations

In the development of their allosteric hFPPS inhibitors, Jahnke and co-workers (Novartis) employed two different enzymatic assays, including a high throughput protein LC-MS/MS method.¹⁰ The second assay employed tritium labeled IPP, similar to the original **M1** assay. However, the procedure was fully automated and uses a lipid-coated FlashPlate[®] with an imbedded scintillation cocktail.¹¹ The more lipophilic FPP enzymatic product binds to the lipid coating and the proximity allows for the detection by a scintillation counter in real time, thus enabling real time readouts. A fascinating finding of these kinetics experiments, was that DMAPP acts as an inhibitor for the second condensation, with an IC₅₀ value of ~ 1 μM (i.e. for the conversion of ³H-GPP → ³H-FPP). The concentration of hFPPS enzyme and substrates were varied throughout this report, consequently, it was not clear to us which conditions were used to obtain the IC₅₀ values reported for allosteric inhibitors **1.5** and **1.6**. Therefore, we needed to investigate the effect of hFPPS/substrate ratio in our hands.

In our previous assay conditions (**M1**) the concentration of hFPPS used was 40 ng/100 μL (~10 nM). This means the lowest IC₅₀ that can be measured is 5 nM; as an IC₅₀ is the concentration of a compound that results in 50% inhibition of the target and the perfect inhibitor would theoretically exist only in the protein bound form and completely inhibit the enzyme. Lowering the substrate concentrations by 10-fold, from 10 μM to 1 μM for both GPP and IPP, had a negligible on effect enzymatic turnover (**Figure 7.2a**). In contrast, changing the allylic substrate from GPP to DMAPP resulted in slower catalytic turnover.

We also investigated the effects of lowering the amount of protein in the assay by 10-fold (hFPPS concentration from 10 nM to 1 nM), in an attempt to make the assay more sensitive. Since for the same concentration of inhibitor, lowering the enzyme concentration will shift the equilibrium in favour of the protein-bound state vs. the free-state for the inhibitors, this should theoretically increase the measured inhibition. Under these conditions, it was found that the turnover rate was significantly slower with DMAPP as the allylic substrate, not reaching the plateau even after 30 min incubation at 37 °C (**Figure 7.2b**). Based on these experiments, it was found that a combination of 1 nM hFPPS with 0.2 μM GPP and IPP gave reliable and reproducible results (as demonstrated by the error bars).

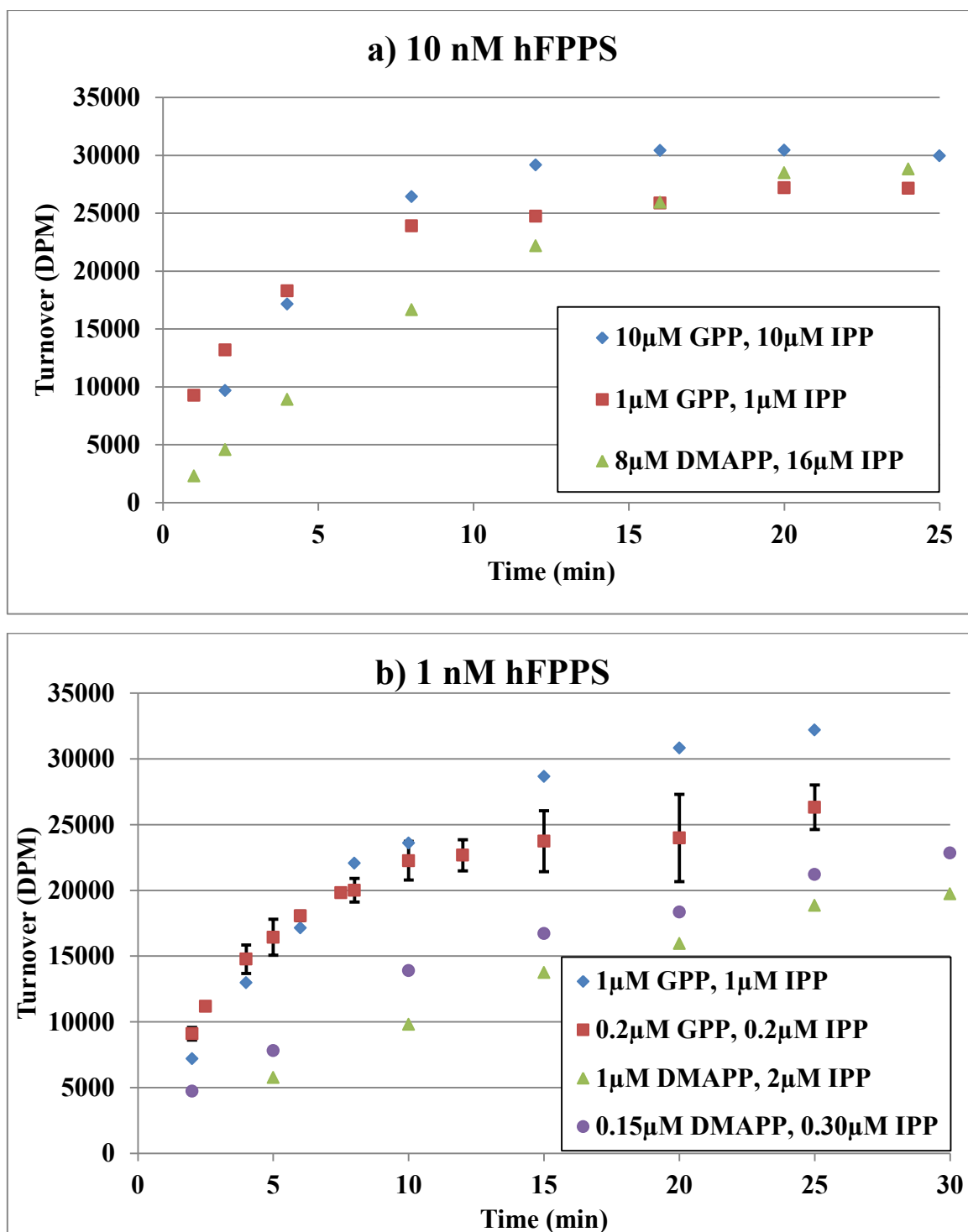


Figure 7.2: Catalytic turnover over time at 10 nM (a) and 1 nM hFPPS (b).

FPP production was estimated by the tritium radioactivity measured for ^3H -farnesol, in disintegrations per minute (DPM), on the vertical axis.

7.4 Sensitized hFPPS enzymatic assay

A combination of 1 nM hFPPS with 0.2 μ M GPP and IPP, combined with a Mg^{2+} concentration of 1 mM and the addition of 0.01% Triton X-100 detergent, led to a more sensitized assay which we refer to as method M2. A comparison of the key differences in assay conditions is summarized in **Table 7.1**. It should be noted that the full details of the conditions used by Novartis are not known.

In order to establish the effect of assay modifications the IC_{50} values of key inhibitors were determined under **M1** and **M2** conditions (**Figure 7.3**, **Table 7.2**). The bisphosphonates risedronate and cyclopropyl-bearing **5.15** proved to be essentially equipotent in both assays. This is somewhat surprising as we expected these inhibitors to have lower IC_{50} values when tested in the **M2** assay. This observation exemplifies that biological data cannot be predicted in advance with theoretical models. In contrast to the bisphosphonates, allosteric inhibitor **1.5** exhibited a ~ 20 -fold increase in measured enzymatic potency in the **M2** assay, from $\text{IC}_{50} \sim 20 \mu\text{M}$ to 920 nM (an IC_{50} value of 200 nM was reported by Jahnke and co-workers under their assay conditions)⁴. However, inhibitor **1.6** was found to be less active, $\text{IC}_{50} \sim 5.7 \mu\text{M}$, than **1.5**; a >70 -fold difference from the reported IC_{50} value of 80 nM. The reason for this large discrepancy is unknown, but a possible explanation may be the presence of BSA (bovine serum albumin) in our assay, which is not present in the Novartis FlashPlate[®] assay (**Table 7.1**); protein binding is known to affect lipophilic compounds and result in less inhibition of the intended therapeutic target. This can be detrimental if the off-target binding occurs to proteins with a much higher expression level, such as blood serum proteins. It is therefore routine practice in drug discovery to also test the enzymatic potency of promising compounds in the presence of human serum, generally resulting in a lower measured IC_{50} and this phenomenon is known as the serum shift.¹² Removal of BSA from the **M2** assay buffer resulted in poor enzymatic turnover (data not shown). This is not surprising; BSA is generally included in enzymatic assays to simulate a higher protein concentration, as proteins tend to unfold at low concentrations (and aggregate at high concentrations).

M1 Standard assay ¹	Novartis colorimetric assay ⁵	Novartis FlashPlate [®] assay ^{4,11}	M2 Sensitized assay
50 mM Tris pH 7.7	100 mM Tris pH 7.3	20 mM HEPES pH 7.4	50 mM Tris pH 7.7
2 mM MgCl ₂	1 mM MgCl ₂	5 mM MgCl ₂	1 mM MgCl ₂
20 µg/mL BSA	20 µg/mL BSA	-	20 µg/mL BSA
0.5 mM TCEP	-	-	0.5 mM TCEP
-	50 mM KCl	1 mM CaCl ₂	-
-	0.01% Triton X-100	-	0.01% Triton X-100
0.4 ng/µL hFPPS ~10 nM	?	0.04 ng/µL hFPPS ~1 nM	0.04 ng/µL hFPPS ~1 nM
10 µM GPP	8 µM DMAPP	0.15 µM GPP/DMAPP	0.2 µM GPP
10 µM IPP	16 µM IPP	0.19 µM IPP	0.2 µM IPP
10 min pre- incubation	?	10 min pre- incubation	10 min pre- incubation
8 min incubation	?	?	8 min incubation

Table 7.1: Summary of various hFPPS enzymatic assay conditions

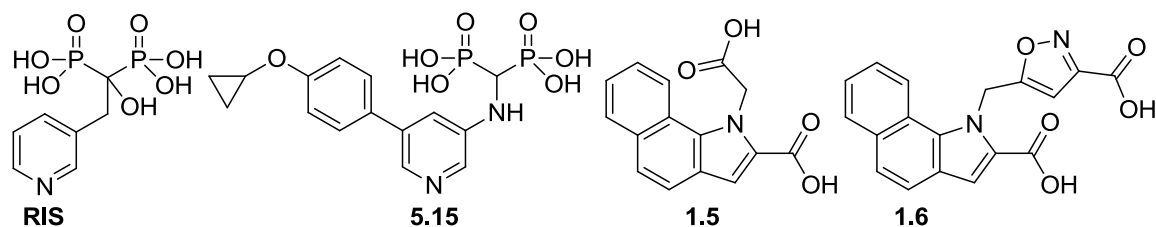


Figure 7.3: Inhibitors tested in **M1** and **M2** assays

Inhibitor	Reported hFPPS IC ₅₀	M1 hFPPS IC ₅₀	M2 hFPPS IC ₅₀
RIS	5.7 nM ¹³ 2.7 nM ¹¹	11 nM	5.2 nM
5.15	-	16 nM	18 nM
1.5	200 nM ⁴	~20 μM	920 nM
1.6	80 nM ⁴	>50 μM	5.7 μM

Table 7.2: Comparison of *in vitro* hFPPS inhibition observed under **M1** and **M2** assay conditions. The values are the average of triplicate determinations (a standard deviation of <10% was observed)

7.5 Conclusions and outlook

An investigation of the known enzymatic assays was undertaken in order to optimize our own *in vitro* assays. Interestingly, our sensitized assay (labeled as **M2**) results in only minor differences in the inhibition observed with bisphosphonates as compared to our original assay (**M1**), whereas a very significant difference (~20-fold) was observed for *non*-bisphosphonate inhibitors, highlighting the importance of these investigations.

7.6 References

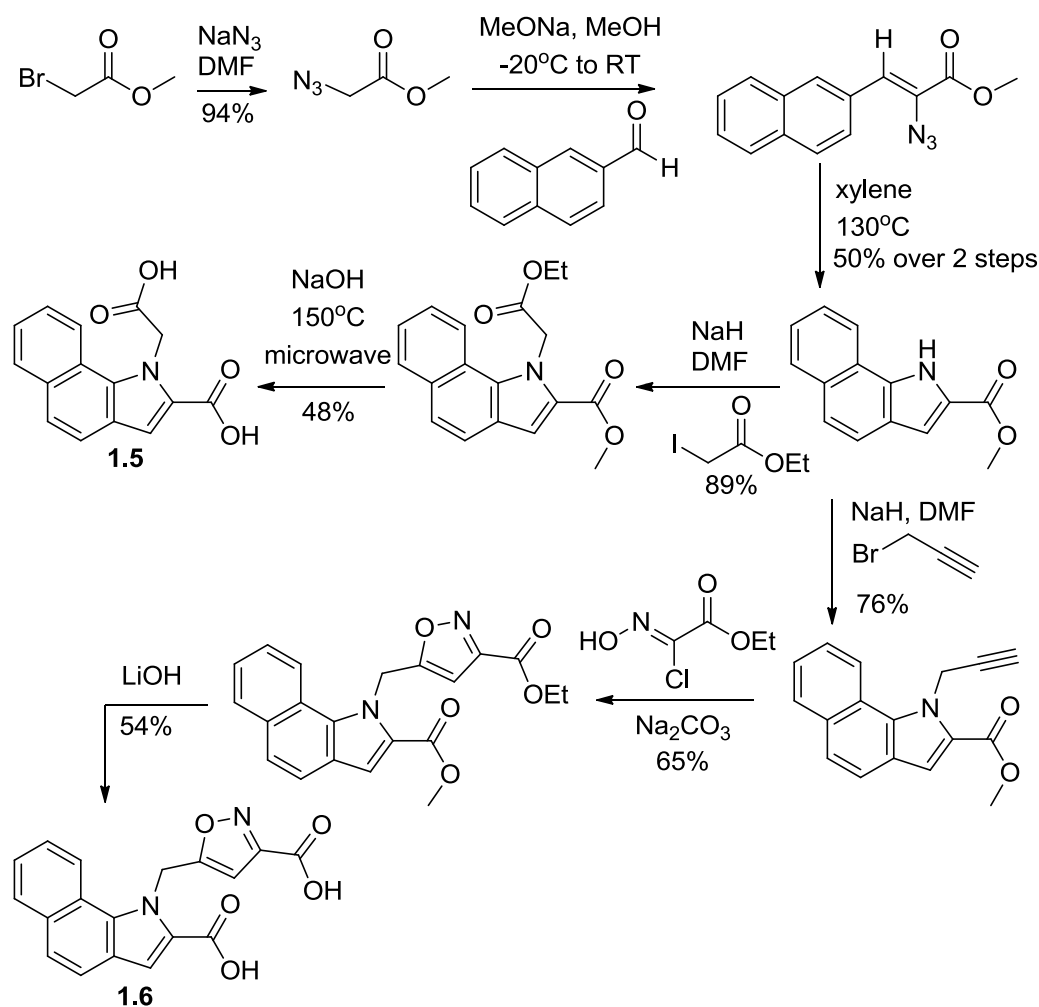
- (1) Dunford, J. E.; Kwaasi, A. A.; Rogers, M. J.; Barnett, B. L.; Ebetino, F. H.; Russell, R. G. G.; Oppermann, U.; Kavanagh, K. L.; Structure–Activity Relationships Among the Nitrogen Containing Bisphosphonates in Clinical Use and Other Analogues: Time-Dependent Inhibition of Human Farnesyl Pyrophosphate Synthase *J. Med. Chem.* **2008**, *51*, 2187.
- (2) Reed, B. C.; Rilling, H. C.; Crystallization and partial characterization of prenyltransferase from avian liver *Biochemistry* **1975**, *14*, 50.
- (3) Dunford, J. E.; Thompson, K.; Coxon, F. P.; Luckman, S. P.; Hahn, F. M.; Poulter, C. D.; Ebetino, F. H.; Rogers, M. J.; Structure-Activity Relationships for Inhibition of Farnesyl Diphosphate Synthase in Vitro and Inhibition of Bone Resorption in Vivo by Nitrogen-Containing Bisphosphonates *J. Pharmacol. Exp. Ther.* **2001**, *296*, 235.
- (4) Jahnke, W.; Rondeau, J.-M.; Cotesta, S.; Marzinzik, A.; Pellé, X.; Geiser, M.; Strauss, A.; Götte, M.; Bitsch, F.; Hemmig, R.; Henry, C.; Lehmann, S.; Glickman, J. F.; Roddy, T. P.; Stout, S. J.; Green, J. R.; Allosteric non-bisphosphonate FPPS inhibitors identified by fragment-based discovery *Nat. Chem. Biol.* **2010**, *6*, 660.
- (5) Peukert, S.; Sun, Y.; Zhang, R.; Hurley, B.; Sabio, M.; Shen, X.; Gray, C.; Dzink-Fox, J.; Tao, J.; Cebula, R.; Wattanasin, S.; Design and structure–activity relationships of potent and selective inhibitors of undecaprenyl pyrophosphate synthase (UPPS): Tetramic, tetronic acids and dihydropyridin-2-ones *Bioorg. Med. Chem. Lett.* **2008**, *18*, 1840.
- (6) Tarshis, L. C.; Proteau, P. J.; Kellogg, B. A.; Sacchettini, J. C.; Poulter, C. D.; Regulation of product chain length by isoprenyl diphosphate synthases *Proc. Natl. Acad. Sci. USA* **1996**, *93*, 15018.
- (7) Romani, A. M. P.; Cellular magnesium homeostasis *Arch. Biochem. Biophys.* **2011**, *512*, 1.
- (8) Owen, S. C.; Doak, A. K.; Wassam, P.; Shoichet, M. S.; Shoichet, B. K.; Colloidal Aggregation Affects the Efficacy of Anticancer Drugs in Cell Culture *ACS Chem. Bio.* **2012**, *7*, 1429.
- (9) Feng, B. Y.; Shoichet, B. K.; A detergent-based assay for the detection of promiscuous inhibitors *Nat. Protocols* **2006**, *1*, 550.
- (10) Roddy, T. P.; Horvath, C. R.; Stout, S. J.; Kenney, K. L.; Ho, P.-I.; Zhang, J.-H.; Vickers, C.; Kaushik, V.; Hubbard, B.; Wang, Y. K.; Mass Spectrometric Techniques for Label-free High-Throughput Screening in Drug Discovery *Analytical Chemistry* **2007**, *79*, 8207.
- (11) Glickman, J. F.; Schmid, A.; Farnesyl pyrophosphate synthase: Real-time kinetics and inhibition by nitrogen-containing bisphosphonates in a scintillation assay *Assay and Drug Development Technologies* **2007**, *5*, 205.
- (12) Rusnak, D. W.; Lai, Z.; Lansing, T. J.; Rhodes, N.; Gilmer, T. M.; Copeland, R. A.; A simple method for predicting serum protein binding of compounds from IC₅₀ shift analysis for in vitro assays *Bioorg. Med. Chem. Lett.* **2004**, *14*, 2309.
- (13) Kavanagh, K. L.; Guo, K.; Dunford, J. E.; Wu, X.; Knapp, S.; Ebetino, F. H.; Rogers, M. J.; Russell, R. G. G.; Oppermann, U.; The molecular mechanism of nitrogen-containing bisphosphonates as antiosteoporosis drugs *Proc. Natl. Acad. Sci. USA* **2006**, *103*, 7829.

7.7 Experimental

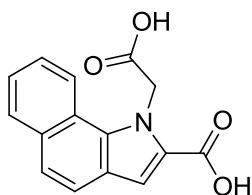
7.7.1 Synthesis

All intermediate compounds were purified by normal phase flash column chromatography on silica gel using a CombiFlash. Final products were purified by reverse phase C18 chromatography (H₂O/ACN +0.01% formic acid gradient) and characterized by ¹H, ¹³C NMR and LR-MS. Chemical shifts (δ) are reported in ppm relative to the internal deuterated solvent (¹H, ¹³C).. The homogeneity (>95%) of the final inhibitors was confirmed by HPLC. See Appendix III for HPLC traces of the final compounds.

Allosteric inhibitors **1.5** and **1.6** were synthesized as previously described.⁴

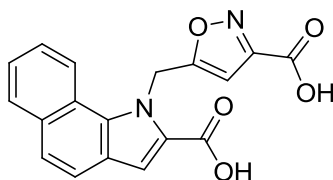


1.5 (JDS10-012): 1-(carboxymethyl)-1H-benzo[g]indole-2-carboxylic acid



^1H NMR (500 MHz, DMSO- d_6) δ 13.24 (br. s, 1H), 12.98 (br. s, 1H), 8.21 (d, J = 8.4 Hz, 1H), 8.03 (d, J = 8.0 Hz, 1H), 7.74 (d, J = 8.6 Hz, 1H), 7.63 – 7.57 (m, 2H), 7.55 (t, J = 7.5 Hz, 1H), 7.45 (s, 1H). ^{13}C NMR (126 MHz, DMSO- d_6) δ 170.57, 162.94, 133.48, 132.69, 129.42, 127.19, 126.03, 125.11, 123.05, 122.49, 122.36, 121.36, 121.02, 112.07, 49.00. MS (ESI): calcd 268.0610 for ($\text{C}_{15}\text{H}_{10}\text{NO}_4$); found 268.10 [$\text{M}-\text{H}$] $^-$

1.6 (JDS10-031): 5-((2-carboxy-1H-benzo[g]indol-1-yl)methyl)isoxazole-3-carboxylic acid



^1H NMR (500 MHz, DMSO- d_6) δ 13.11 (br. s, 1H), 8.35 (d, J = 8.1 Hz, 1H), 8.03 (d, J = 8.0, 1H), 7.78 (d, J = 8.6 Hz, 1H), 7.64 (d, J = 8.6 Hz, 1H), 7.59 – 7.52 (m, 3H), 6.63 (br. s, 2H), 6.47 (s, 1H). MS (ESI): calcd 337.0824 for ($\text{C}_{18}\text{H}_{13}\text{N}_2\text{O}_5$); found 337.16 [$\text{M}+\text{H}$] $^+$

7.7.2 Enzymatic inhibition assays

Note:

The third batch of expressed hFPPS protein, which was used for the results presented in this chapter, was found to be significantly more active than the previous two batches, which were used for Chapters 3,4 and 5. Therefore the incubation time was reduced to 8 min for the **M1** enzymatic assay, from 20 min for previous batches of hFPPS enzyme.

In vitro Sensitized Inhibition Assay for hFPPS (M2):

All assays were run in triplicate using 4 ng of the human recombinant FPPS and 0.2 μ M of each substrates, GPP and IPP (3 H-IPP, 3.33 mCi/ mmol) in a final volume of 100 μ L buffer containing 50 mM Tris pH 7.7, 1 mM MgCl_2 , 0.5 mM TCEP, 20 μ g/mL BSA and 0.01% Triton X-100. For assays run with a 10 min pre-incubation period, the enzyme and inhibitor were incubated in the assay buffer in a volume of 80 μ L at 37 °C for 10 min. After 10 min, the substrates were added to start the reaction and also bring the inhibitor and substrate to the desired final concentrations. For assays run without pre-incubation, the reaction was started with the addition of enzyme to the mixture of inhibitor and the two substrates. After addition of all substrates, all assays were incubated at 37 °C for 8 min. Assays were terminated by the addition of 200 μ L of HCl/methanol (1:4) and incubated for 10 min at 37 °C. The assay mixture was then extracted with 700 μ L of ligroin (in order to separate reaction products from unused substrate), dried through a plug of anhydrous MgSO_4 and 300 μ L of the ligroin phase was combined with 8 mL of scintillation cocktail. The radioactivity was then counted using a Beckman Coulter LS6500 liquid scintillation counter.

Reagents for Enzymatic assay:

Ligroin was purchased from Sigma Aldrich, liquid scintillation cocktail was purchased from MP Biomedicals: Ecolite (#882475), 3 H-IPP was purchased from American Radiolabeled Chemicals (ART 0377A: 1mCi/mL, 60Ci/mmol in 0.1M Tris pH 7.5), unlabeled IPP and GPP were purchased from Isoprenoids, Lc. as their ammonium salts.

hFPPS solution: The hFPPS enzyme was stored at -80 °C as a 2 μ g/ μ L solution in the eluent buffer (50 mM HEPES pH 7.5, 500 mM NaCl, 250 mM imidazole, 5% glycerol, 0.5 mM TCEP).

IPP-solution: 3 H-IPP was diluted with IPP to a specific activity of 33 mCi/ mmol and 2 μ M concentration in 200 mM Tris pH 7.7. It was stored at -10 °C, warmed to 0 °C and kept on ice during assay setup.

GPP-solution: GPP was dissolved and diluted to a 2 μ M concentration in 200 mM Tris pH 7.7. It was stored at -10 °C, warmed to 0 °C and kept on ice during assay setup.

8 Differential Scanning Fluorimetry and allosteric binding

8.1 Preface

Part of the material discussed in this chapter has been submitted for publication in the following manuscript:

“Ternary complex structures of human farnesyl pyrophosphate synthase bound with a novel inhibitor and secondary ligands provide insights into the molecular details of the enzyme’s active site closure”

Park, J.; Lin, Y.-S.; De Schutter, J.W.; Tsantrizos, Y.S.; Berghuis, A.M. *BMC Structural Biology* **2012**; *in press*

The work presented in this chapter played a key role for the invention described in a US provisional patent application (filed on November 20th, 2012; serial number 61/728,489):

“Thienopyrimidine Inhibitors of farnesyl and/or geranylgeranyl pyrophosphate synthase”

Y. S. Tsantrizos, A. M. Berghuis, J.W. De Schutter, C.-Y. Leung, J. Park, M. Sebag

I developed the Differential Scanning Fluorimetry (DSF) protocol for investigating differential binding of inhibitors to hFPPS. Zheping Hu, an undergraduate student in our group who performed approximately one third of the DSF experiments described in this chapter. The thienopyrimidine bisphosphonate inhibitors used for the DSF studies were synthesized by other members of the group (John Mancuso, Adrienne Langille and Chun-Yuen Leung), therefore their synthesis is not described in this thesis. I synthesized all the **non**-bisphosphonate compounds described in this chapter, **8.7 – 8.9**.

Protein expression and purification was carried out by Yih-Shyan Lin, Chun-Yuen Leung and Jaeok Park. All crystallographic and ITC studies were performed by Jaeok Park (PDF with Prof. Berghuis; Biochemistry Department, McGill University).

8.2 Introduction

Many biochemical techniques have been developed to probe the *in vitro* structure and conformation of proteins, in order to better understand their function, catalytic mechanism, biological significance and interactions with small molecules. Examples include, live cell imaging (often fluorescence coupled confocal microscopy), enzymatic assays, circular dichroism measurements, enzymatic digests, pull-down affinity assays and site-directed mutagenesis studies. These analytical tools span a large variety of detection methods, such as MS, NMR, UV absorbance, fluorescence measurement, X-ray diffraction, radioactive isotope labelling and electron microscopy. Each technique has inherent advantages and limitations. For example X-ray crystallography can provide detailed information at the atomic resolution level of the protein, but only in the solid state, which may not be representative of the biologically relevant form (e.g. protein conformation, protein clusters, trans-membrane or membrane associated proteins) and crystal packing artefacts are common. In contrast, the common protein-detected NMR experiments analyze the protein in solution, with the associated degrees of flexibility, but only detect correlations between labelled atoms and cannot resolve individual residues. The X-ray crystallography and NMR experiments complement each other and together more precise structural insight into the protein can be gained. Every biochemical experiment also has limitations when it comes to the amount and type of sample needed, the time it takes to run the experiment, the information that is desired and of course the associated costs. To date, no single technique exists that can resolve a single target biomolecule inside a living cell to determine its cellular location, structure, conformation, function and current state. It is only through the combination of many biochemical experiments that a clear picture of the biomolecule of interest can be gained.

In the past, many biophysical techniques have been successfully applied to hFPPS, including X-ray crystallography¹, ligand-detected NMR², ITC³, kinetic studies³, site directed mutagenesis (PDB 2QIS and 3CP6, unpublished) and DSC⁴. In the course of our own investigations, we have performed *in silico* docking studies, ligand line broadening ¹H NMR experiments, X-ray crystallography and ITC experiments using a number of our

novel inhibitors and the His-tagged hFPPS enzyme. The main limitations of our biophysical arsenal are cost and low throughput. Therefore we decided to explore the application of Differential Scanning Fluorimetry (DSF) as screening tool, in order to quickly acquire preliminary data on binding mode and affinity.⁵

8.2.1 Differential Scanning Fluorimetry (DSF):

DSF is a relatively new technique that uses an environment-sensitive fluorescent dye to detect the unfolding of proteins.⁶ These dyes fluoresce poorly in aqueous solution (due to solvent quenching) but become highly fluorescent in non-polar environments, such as hydrophobic sites on proteins. The various dyes differ with respect to their optical properties, particularly in the fluorescence quantum yield; the relative increase in fluorescence intensity upon changing from a polar to a hydrophobic environment.

Most non-membrane associated proteins have evolved to contain amino acids with polar sidechains on their outer surface (to increase aqueous solubility) and hydrophobic sidechains on the inside (to form lipophilic, intramolecular interactions).⁷ These stabilizing interactions greatly contribute to protein tertiary structure and there is little solvent-accessible hydrophobic surface area available for binding of the dye. Thus, upon addition of the DSF dye to a protein in its native state, low fluorescence is measured (in RFU, relative fluorescence unit, **Figure 8.1**). However, upon heating, the protein starts to unfold and more hydrophobic sites become solvent-exposed, resulting in an increase in fluorescence as the dye binds to available lipophilic areas. Finally, as most of the ternary structure is lost, the protein starts to aggregate, with concomitant loss of hydrophobic surface area and a decrease in fluorescence. Therefore, the fluorescence intensity can be plotted as a function of temperature to generate a sigmoidal melting curve that describes the two-state transition of the protein. At lower limits of fluorescence (LL) the protein exists in its native state and at the upper limit (UL) it become fully denatured; the difference in fluorescence between the LL and UL should be high in order to clearly resolve protein unfolding and is strongly dependant on the quantum yield of the employed dye. The inflection point of the transition curve denotes the largest change in unfolding and is arbitrarily set as the melting temperature (T_m) of the protein. Therefore, the simplest way to

calculate T_m values is to determine the minimum of the negative first derivative of the melt curve ($-d(RFU)/dT$, **Figure 8.2**).

In summary, DSF uses an environment-sensitive fluorescent dye that acts as a reporter for protein unfolding *in vitro* to measure the transition from native to denatured state.

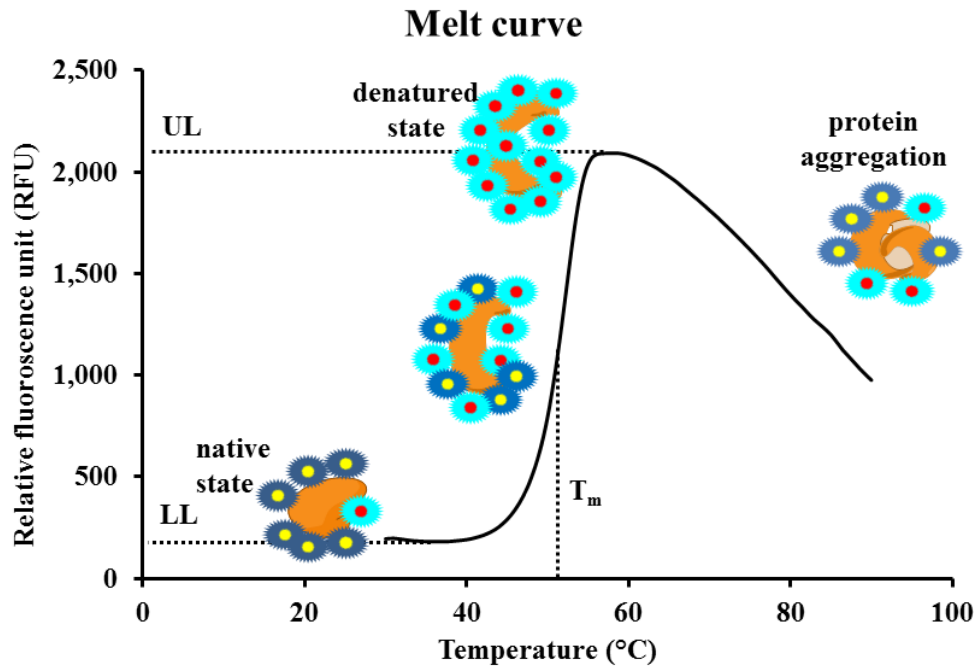


Figure 8.1: Typical DSF melt curve

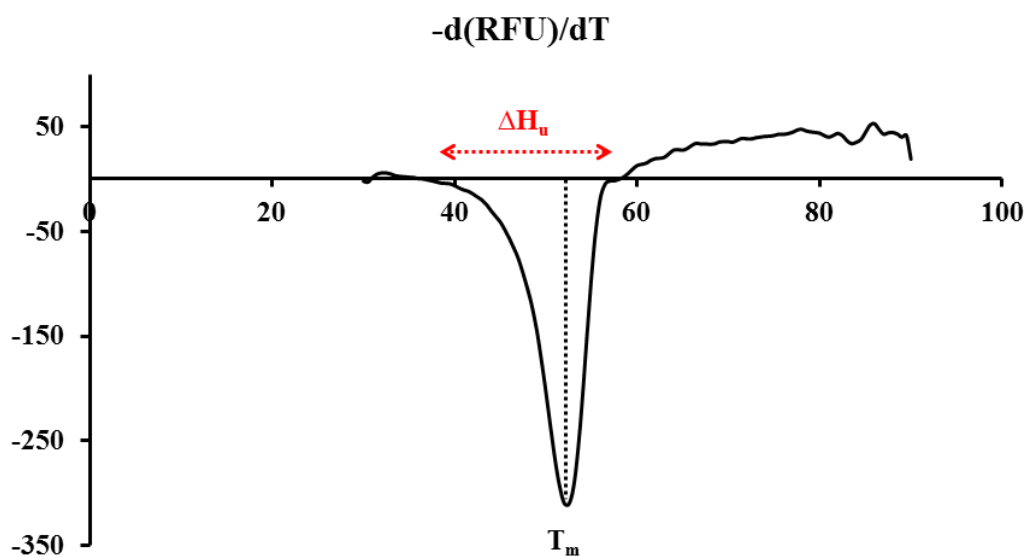
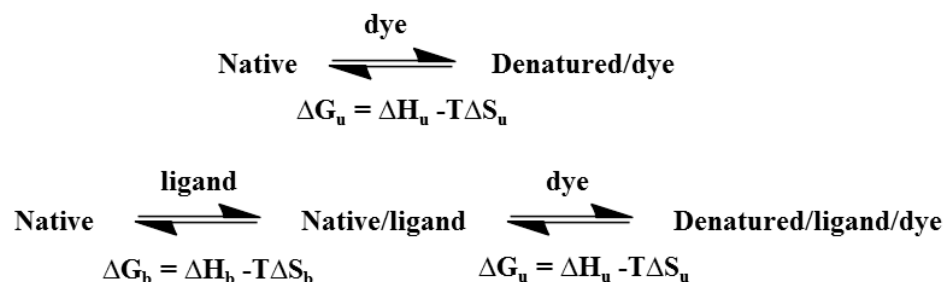


Figure 8.2: Negative first derivative of melt curve

The stability of a protein is related to its Gibbs free energy of unfolding (ΔG_u), which is temperature-dependent and in an idealistic model, the fluorescent dye would exclusively bind to the unfolded parts of the protein (**Scheme 8.1**). The stability of most proteins decreases with increasing temperature and so the ΔG_u will reach zero at the equilibrium where the concentration of folded and unfolded protein are equal. This temperature is considered as the melting temperature, T_m , and if the protein unfolds in a reversible two-state manner, the equilibrium thermodynamics model will apply. Therefore, a compound that binds to the protein, will contribute the free energy of binding (ΔG_b) and usually increase ΔG_u , which may cause an increase in the melting temperature (ΔT_m , **Figure 8.3**). It is well known that the stabilizing effect of ligands is proportional to their *in situ* concentration and affinity for the protein.⁸ Therefore, plotting ΔT_m against concentration (titration curve, **Figure 8.4**) provides information about the binding affinity of the compound.



Scheme 8.1: Two state thermodynamic equilibrium model

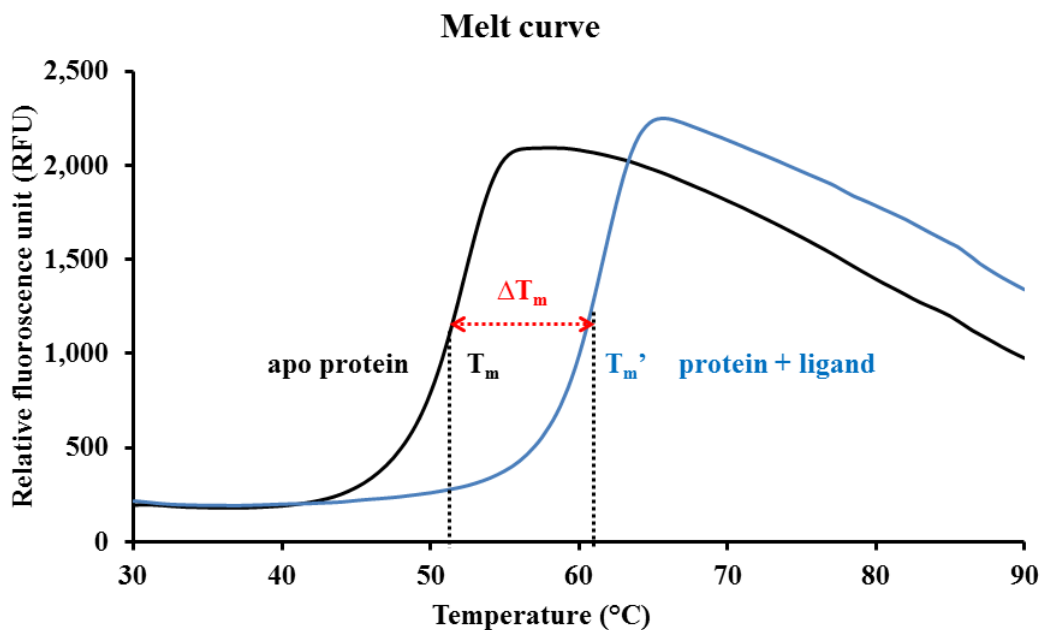


Figure 8.3: Increase in T_m due to ligand binding

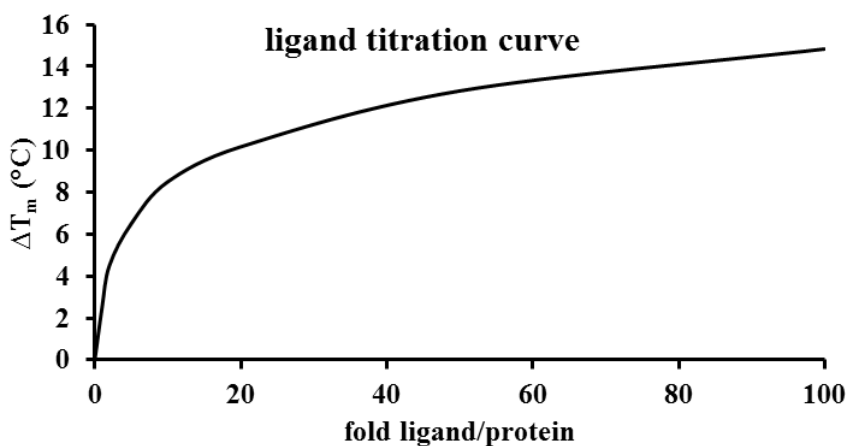


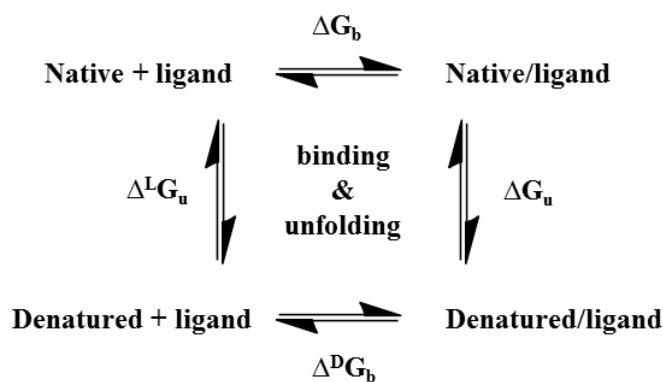
Figure 8.4: Example of DSF titration curve

8.2.2 Limitations of DSF:

In principal, we can assume that equilibrium conditions (**Scheme 8.1**) would allow the derivation of the enthalpy of protein unfolding (ΔH_u) from the $d(RFU)/dT$ plot (**Figure 8.2**) and the dissociation constant (K_D) from the ligand titration curve (**Figure 8.4**).⁹ Unfortunately, most DSF experiments cannot be represented by such a model, because the unfolding of many proteins is not a reversible (equilibrium) monomolecular two-state

reaction and the ligand does not exclusively bind to the native state. Instead, a mixed mechanism must be taken into account (**Scheme 8.2**) and the fluorescent dye can potentially bind to any of four distinct states. The proper equations to calculate ΔH_u and K_D from DSF data could be derived by performing extensive controls and validation by a secondary technique (such as ITC).⁹ However, this would have to be performed for every type of compound with distinct physicochemical properties; such investigations do not fit our objectives towards developing a rapid and general protocol for investigating the hFPPS binding interactions of various compounds with large structural diversity. Furthermore, care should be taken with ranking ligands according to their relative ΔT_m values or titration curves, as these values do not always reflect their relative affinities for the protein. The magnitude of the ΔT_m shift observed is dependent on the individual contributions of enthalpy and entropy to binding. Larger ΔT_m shifts are observed for more entropically driven binding, as the entropic term contributes more to the Gibbs free energy at higher temperatures ($\Delta G = \Delta H - T\Delta S$). Similarly, a given ΔT_m shift is not unique to a certain binding affinity; as ligands with a range of affinities, with different entropic and enthalpic components, might give rise to the same change in ΔT_m . Competing effects could also mask ligand binding; for example, a compound binding strongly and enthalpically to the native state could be masked by weaker, entropically driven binding to the denatured state. As a result, it is only possible to rank compounds with similar physicochemical properties based on their relative ΔT_m values.⁸

In other words, due to the elevated temperatures required for this technique (above 37 °C), DSF has an inherent bias for compounds with entropy-driven binding modes.



Scheme 8.2: Mixed mechanism of DSF equilibria

8.3 Development and validation of a DSF protocol for hFPPS

8.3.1 Development of a DSF protocol for hFPPS:

DSF monitors thermal unfolding of proteins in the presence of a fluorescent dye and is typically performed by using a real-time PCR instrument, which is equipped with the appropriate fluorescence detector and a precise temperature controller.

To date, the dye with the most favorable properties for DSF is SYPRO[®] Orange thanks to its high signal-to-noise ratio (good quantum yield from polar to hydrophobic environment).⁶ The relatively high wavelength for excitation for SYPRO[®] Orange, near 492 nm, also decreases the likelihood that any small molecule would interfere with the experiment by absorbing the excitation light, and decreasing the fluorescence, which is measured at 610 nm. Therefore, SYPRO[®] Orange was selected for our investigations. Two other dyes, Nile red and 1,8-ANS, were also evaluated, however, they produced poor melting curves, with slopes considerably less sharp compared to SYPRO[®] Orange and a small difference between UL and LL (data not shown); and were therefore abandoned.

In order to validate our experimental protocol for the DSF studies, we reproduced a literature experiment, where a titration curve was reported for the binding of oxaloacetic acid into porcine heart citrate synthase.⁶ We subsequently developed a protocol that is suitable for investigating the binding of inhibitors to hFPPS. Among the factors that were taken into consideration were the protein stability, the buffer, salts and detergents used; these additives may result in nonspecific interactions with the protein. Therefore, initial experiments were performed under conditions similar to those previously reported for ITC (10 mM HEPES pH 7.5, 100 mM NaCl) and DSC ([hFPPS] 30 μ M, 25 mM Tris pH 7.5, 25 mM NaCl, 5 mM MgCl₂). Since HEPES has a smaller temperature-dependence ($-0.015 \Delta\text{pH}/\Delta\text{T}$) than Tris ($-0.028 \Delta\text{pH}/\Delta\text{T}$), it was selected as the buffer, and used at 10 mM concentration at pH 7.5, along with 100 mM NaCl and 5 mM MgCl₂. To minimize the cost of the assay, the effect of protein concentration on the quality of data was also examined over a range from 1 to 30 μ M of hFPPS (data not shown). The signal over noise ratio of the melting curves remained similar down to a concentration of 4 μ M hFPPS, which was set as the standard protein concentration for all further DSF experiments (**Figure 8.5**).

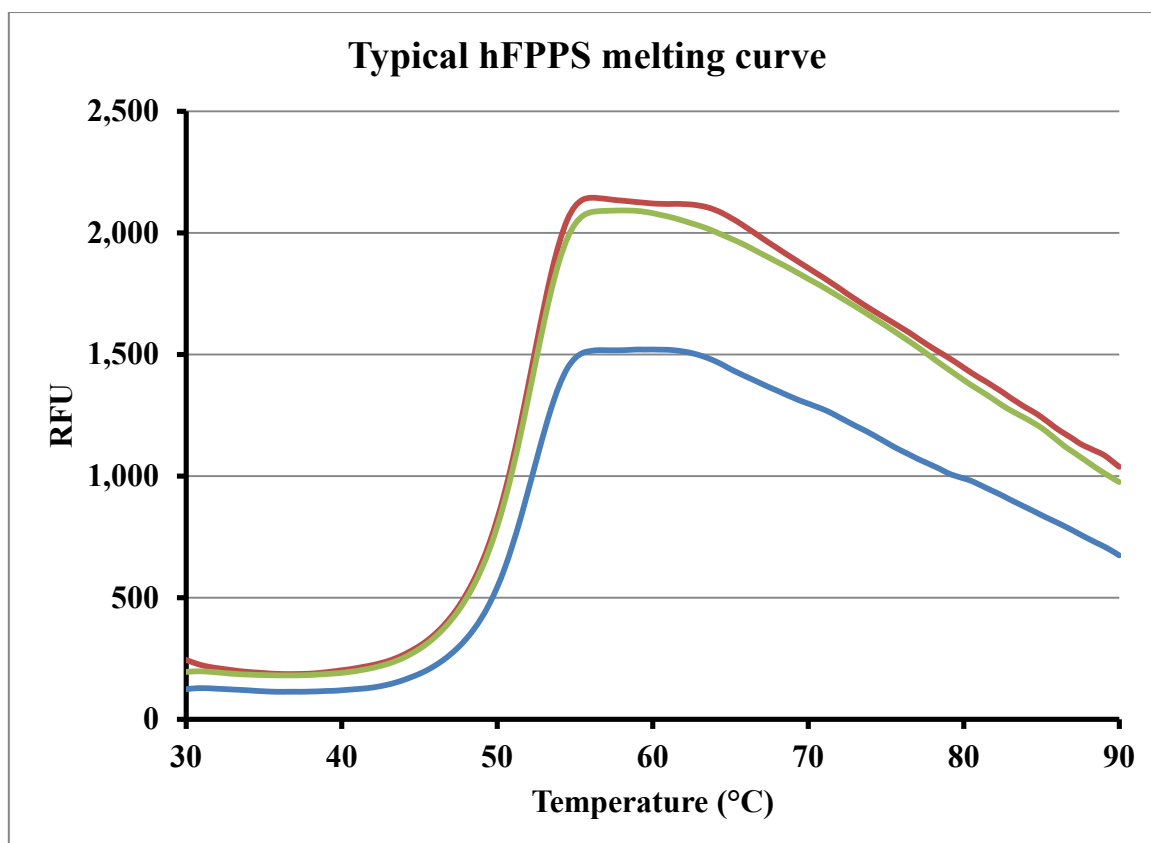


Figure 8.5: Triplicate of hFPPS melting curve, calculated T_m values are 52.5, 52.5 and 53 °C. Conditions: 4 ng/ μ L hFPPS (batch #3), 10 mM HEPES pH 7.5, 5x SYPRO[®] Orange, 5 mM MgCl₂, 10 mM NaCl.

8.3.2 Validation of hFPPS DSF protocol:

All biochemical assays exhibit inherent variability as a consequence of factors such as environment (humidity, room temperature), instrumentation (calibration, cross-talk between wells), reagents (quality, expiry date), experimenter (experience, manual technique) and most importantly the purity and quality of the protein. Consequently, the reported data points represent an average of triplicate determinations. The absolute fluorescence measured between individual wells containing the same sample mixture can be quite different. Fortunately, this does not affect the numerical results, as the T_m is determined at the inflection point of the melt curve, the sharpest increase in fluorescence, a relative value (Figure 8.5).

A titration with risedronate was also performed to assess the ability of our assay to detect the stabilization of hFPPS in the presence of this inhibitor. A significant increase was observed in melting temperature compared to the apo protein (**Figure 8.6**). This stabilization occurs in a dose dependant manner and reaches a maximum ΔT_m value of ~ 23 °C. In order to validate the DSF numerical results quantitatively, we compared our risedronate titration results to those reported for Differential Scanning Calorimetry (DSC), the most closely related technique, which measures heat instead of fluorescence. At a [RIS]/[hFPPS] ratio of 10:1 the average measured ΔT_m was 20 °C ([RIS] = 40 μ M, [hFPPS] = 4 μ M) by DSF, in close agreement with the 20.7 °C ΔT_m value reported for DSC ([RIS] = 300 μ M, [hFPPS] = 30 μ M).⁴ Furthermore, the additional stabilization of IPP ($\Delta\Delta T_m$) was reported to be 8.3 °C by DSC at a [RIS]/[hFPPS]/[IPP] ratio of 10:1:10; we obtained a similar $\Delta\Delta T_m$ value of 6 °C. It should be noted that the DSC experiments were performed using His-tag-free hFPPS and in Tris buffer; in contrast, to our DSF experiment was performed on protein with the His-tag attached in HEPES buffer.

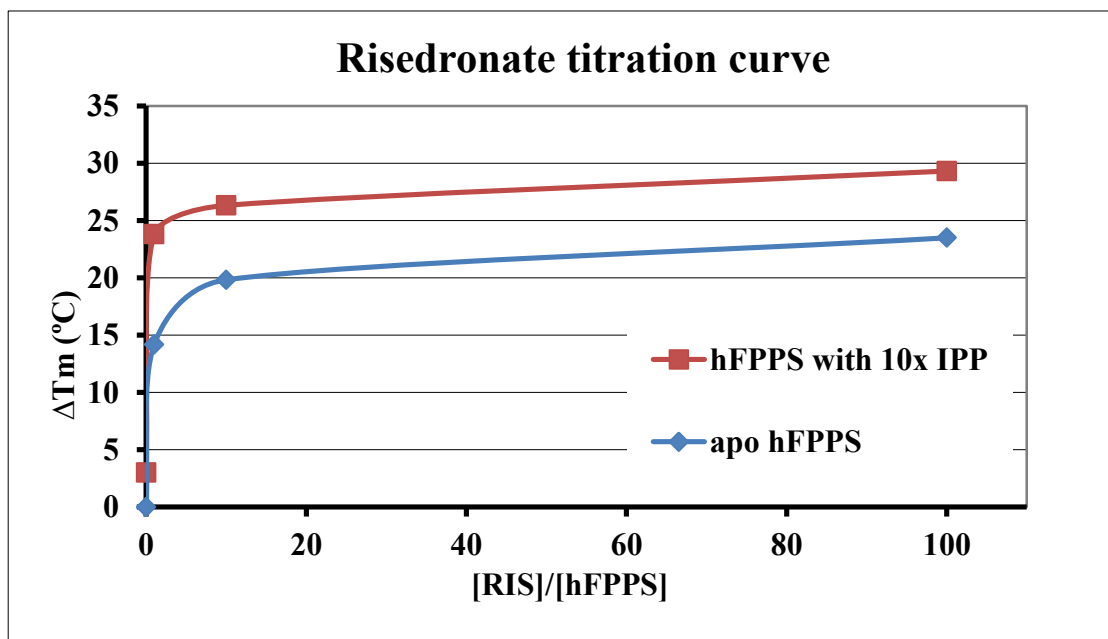


Figure 8.6: Risedronate titration curve in the absence and presence of IPP (hFPPS batch #1, [NaCl] 100 mM)

In order to assess the reproducibility of the DSF protocol the titration curve of risedronate was performed a total of 5 times over a time period of several months (**Figure 8.7**). The results are very consistent; with an RMSD value of 1.3 °C and an average standard deviation of 0.62 °C. We therefore assume an inherent variability in our DSF protocol of approximately ± 1 °C for all of our subsequent studies and include a risedronate control on every plate to ensure no significant errors have occurred.

It should be noted that the repeated titrations were performed using the same batch of protein. Over the course of the work described in this chapter, three different batches of hFPPS were used for DSF experiments. The first and second batch of expressed protein were semi-purified, with a Ni-NTA affinity column (to retain the His-tag on the protein), while the third batch of hFPPS was further purified by a Superdex 200 size-exclusion column. As a result, a small signal due to an impurity was observed in the melting curve of hFPPS batch #2 (**Figure 8.8**). Fortunately, this did not appear to have a deleterious effect on our DSF data and the T_m calculated was consistent with all previous runs. The data obtained from titration curves of risedronate was also consistent across all three batches of hFPPS protein (**Figure 8.9**).

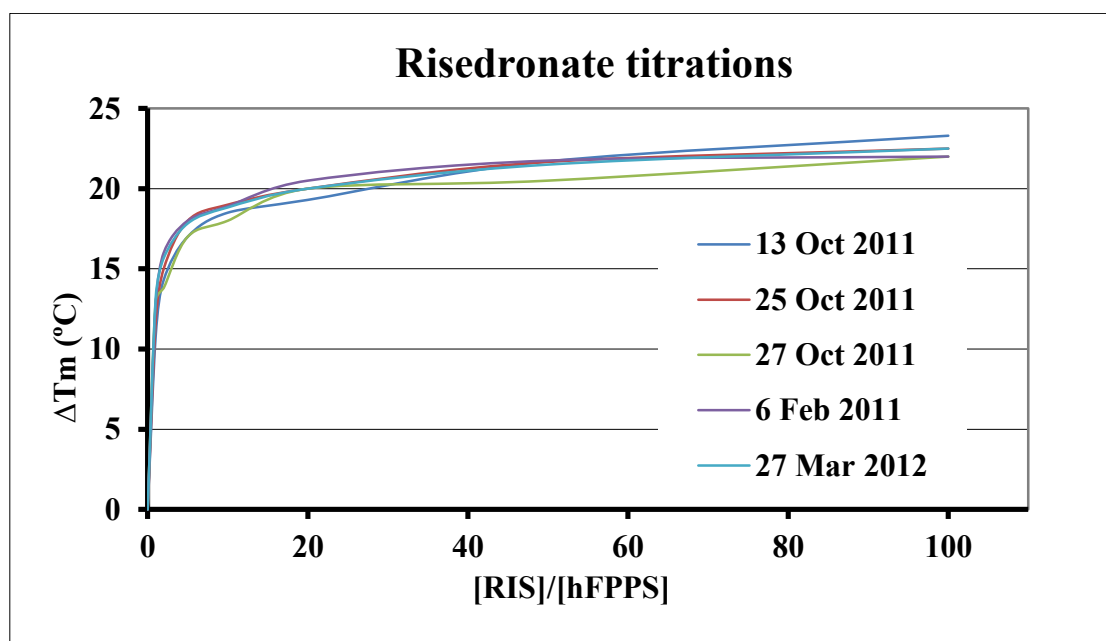


Figure 8.7: Combined titration curves for risedronate
(hFPPS batch #1, [NaCl] 100 mM)

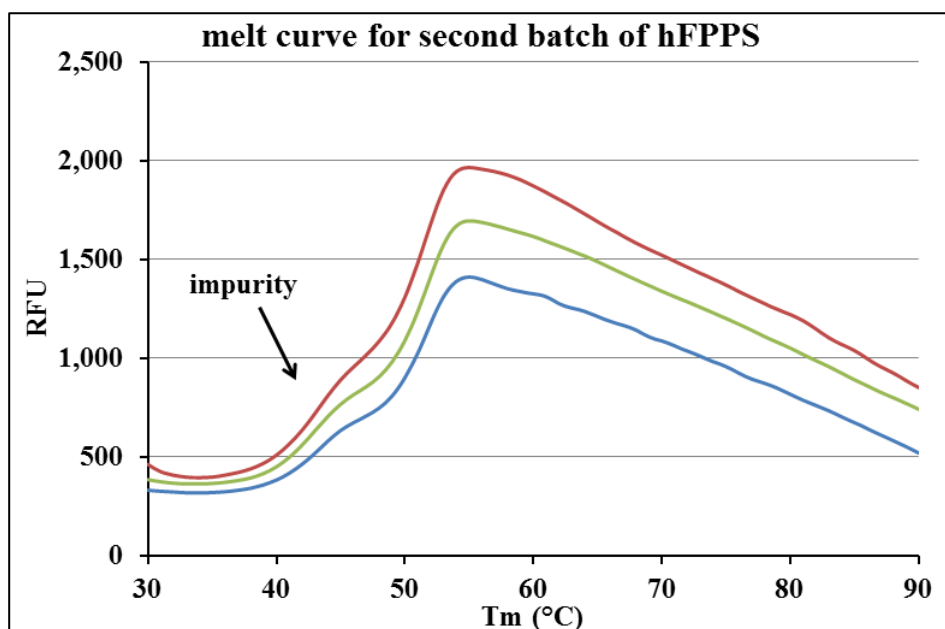


Figure 8.8: Triplicate melting curve for second batch of hFPPS ([NaCl] 100 mM)

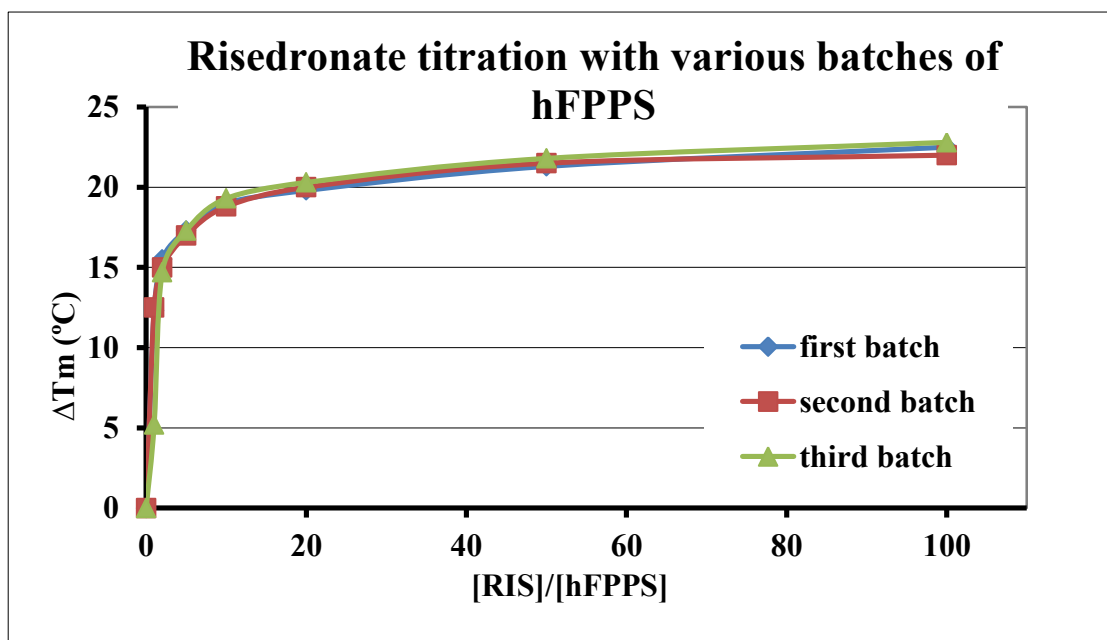


Figure 8.9: Comparison of risedronate titration curves across three batches of purified recombinant hFPPS protein ([NaCl] 100 mM)

8.4 Elucidation of ligand binding properties by DSF:

The DSF assay was then used as a rapid screening tool that would allow us to determine the affinity and binding characteristics of our novel inhibitors. The effects of buffer components were examined for several hFPPS inhibitors with a range of physicochemical properties, *in vitro* activity and *variable* binding modes (**Figure 8.10**). We selected a set of hFPPS inhibitors for which the enzyme-bound conformation has been established by X-ray crystallography (except for compound **1.6** which is assumed to be an allosteric inhibitor of hFPPS and bind similarly to **1.5**). Some ITC data is also available; it has been reported that the binding of risedronate is entropy driven;³ in contrast, allosteric inhibitor **1.5** has a larger enthalpic contribution to the free energy of binding.²

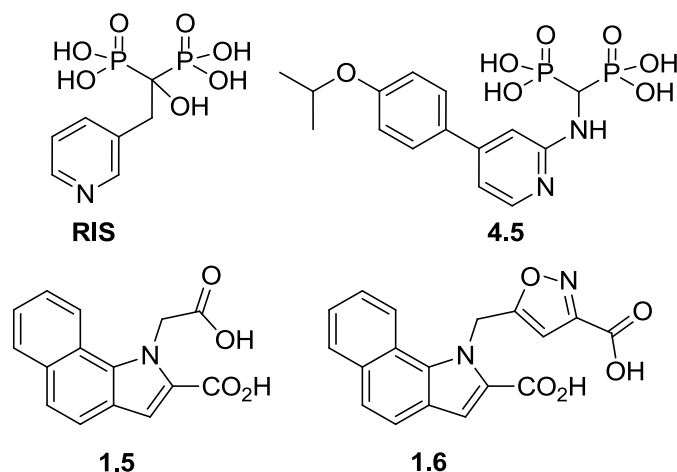


Figure 8.10: Inhibitors for DSF experiments

8.4.1 The effect of Mg^{2+} :

The presence of Mg^{2+} is critical for enzymatic catalysis and binding of bisphosphonate inhibitors to the active site of hFPPS.^{10,11} Consequently, we examined the effect of $[\text{MgCl}_2]$ on the thermal stability of the protein by DSF. Reducing the concentration of Mg^{2+} from 5 mM (used for the reported DSC experiments)⁴ clearly had a negative effect on the thermal stability (**Figure 8.11**). In the absence of any magnesium hFPPS melts approximately 5 °C lower; it may be that high magnesium concentrations promote the semi-closed conformation (which is reportedly more stable). However, binding of Mg^{2+} ions may also induce a conformation that exposes more hydrophobic surface area, resulting in increased fluorescence.¹² The precise conformational effects are unknown, as there is no structural data for hFPPS with bound Mg^{2+} , but in the absence of a ligand occupying the allylic sub-pocket. The magnesium-dependence of *N*-BP binding is also evident from this experiment; we observed that a minimum concentration of ~1 mM MgCl_2 is required to achieve the full stabilization benefit.

In contrast, it was previously reported that binding of the allosteric inhibitors **1.5** and **1.6** to hFPPS is not Mg^{2+} dependent.² We confirmed this observation by acquiring the titration curve of compound **1.5** with and without MgCl_2 in the buffer (**Figure 8.12**). The stabilization is identical (<0.5 °C) in both the absence or presence of 5mM MgCl_2 . Furthermore, inhibitor **1.6** induced a ΔT_m approximately 4 °C lower than **1.5**, consistent with their relative IC_{50} values of 5.7 μM and 920 nM, respectively (refer to section 7.4). However, not enough DSF data for allosteric inhibitors has yet been obtained to correlate ΔT_m to enzymatic activity.

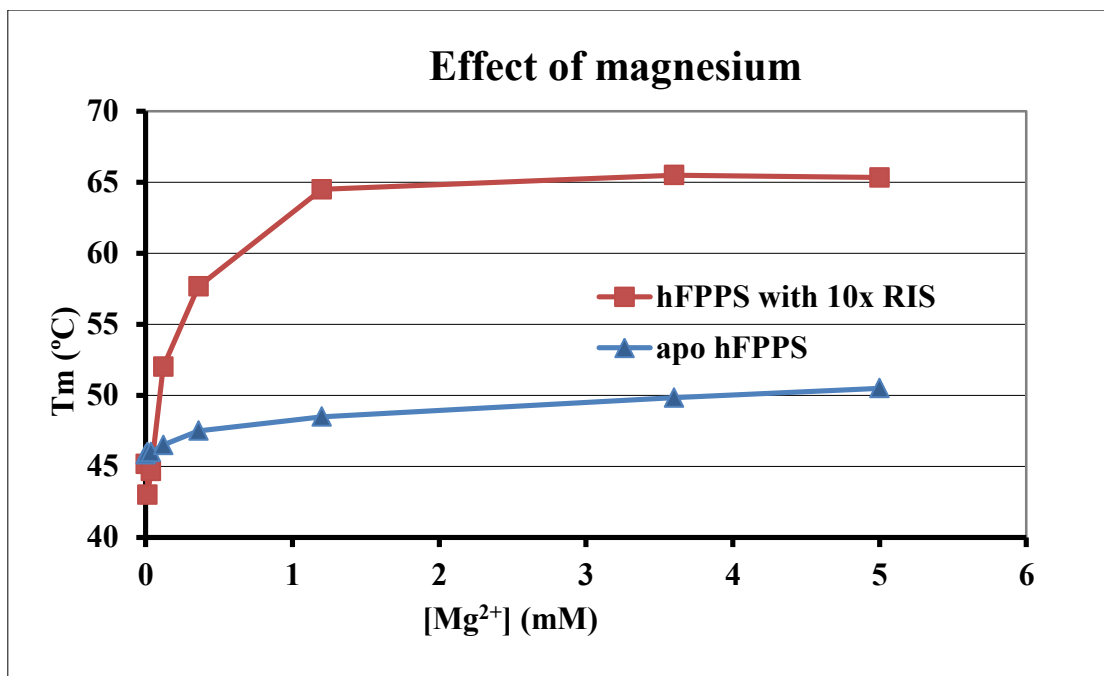


Figure 8.11: Stabilizing effect of $MgCl_2$ on hFPPS
(hFPPS batch #1, $[NaCl]$ 100 mM)

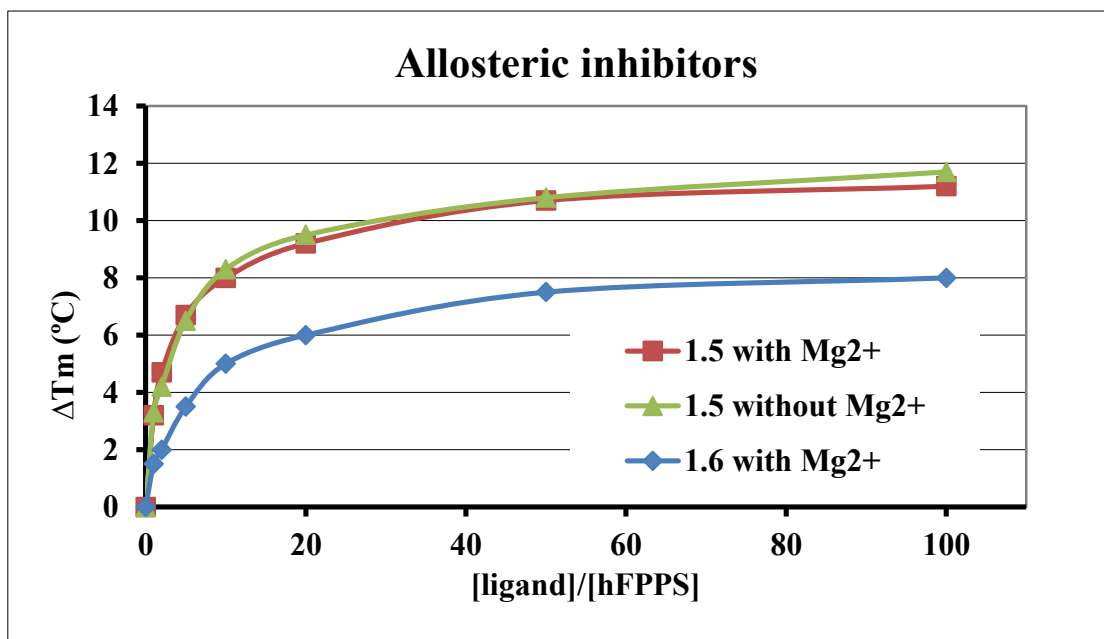


Figure 8.12: Titration curves for allosteric inhibitors 1.5 and 1.6
(hFPPS batch #3, $[NaCl]$ 10 mM, 0.01% Triton X-100)

8.4.2 The effect of DMSO, NaCl and detergent on hFPPS stability and ligand binding:

The effects of [DMSO], [NaCl] and detergent were analyzed, as these have a large impact on the solubility of small molecules in the assay buffer. In order to obtain titration curves, the compounds are added in increments from 1 to 100 equivalents with respect to [hFPPS], resulting in concentrations in a range from 4 to 400 μ M, which may give rise to solubility issues. Our novel bisphosphonate inhibitors have excellent aqueous solubility (>10 mM), but fragments and bioisosteres will undoubtedly require some organic solvent to fully dissolve.

DMSO is commonly preferred to dissolve compounds for biochemical assays, since at low concentrations it has minimal effect on protein structure compared to other organic water-miscible solvents such as methanol, ethanol, acetonitrile or acetone.^{13,14} The concentration of DMSO is kept as low as possible in biochemical assays, preferably below 2% v/v, but many proteins will tolerate up to 5% v/v, with minor, but measurable effects.¹⁵ Although we found that the addition of DMSO to the DSF buffer results in lower T_m values for hFPPS (in a concentration dependant manner, **Figure 8.13**); at 2% to 5% v/v concentration the ΔT_m values were within the expected variability of the assay (-0.5 $^{\circ}$ C to -1 $^{\circ}$ C). Fortunately, DMSO does not greatly interfere with the binding of risedronate and the stabilization observed remains unaffected (≤ 1 $^{\circ}$ C) at concentrations below 5% v/v DMSO.

It is common for a hydrophobic compound, stored in a stock solution containing DMSO, to precipitate when it is added to an assay buffer containing high concentrations of NaCl (e.g. 100 mM). Upon lowering the [NaCl] in the DSF buffer we acquired better quality thermal melt data with reduced variability (data not shown); a phenomenon that has previously been reported.¹⁶ Additionally, we observed a minor increase in hFPPS stability, ~ 2 $^{\circ}$ C (**Figure 8.14**); this may be due the “salting out” effect, as proteins have varying solubility and stability in aqueous media, largely depending on their surface charge, and are thus sensitive to the ionic strength of the solution.¹⁷ Concomitant with an increase in protein stability, the relative stabilizing effect induced by the binding of risedronate was decreased by approximately 4 $^{\circ}$ C when the NaCl concentration was reduced from 100 mM to 10 mM NaCl.

In order to analyze lipophilic compounds, the inclusion of a detergent would be necessary to prevent aggregation phenomena.¹⁸ Over the course of many high throughput screens so called “promiscuous inhibitors” have been identified; i.e. compounds that inhibit unrelated enzymes through non-specific interactions. The non-selective mechanism of action involves aggregate formation, which can be blocked by the inclusion of an appropriate detergent.¹⁹ Upon the addition of 0.01% Triton X-100 to the assay buffer hFPPS melted approximately ~5 °C lower, but the overall shape and quality of the hFPPS melting curves were preserved (data not shown); (partial) protein denaturation by detergents is commonly observed, for example in efforts to solubilise membrane proteins.²⁰

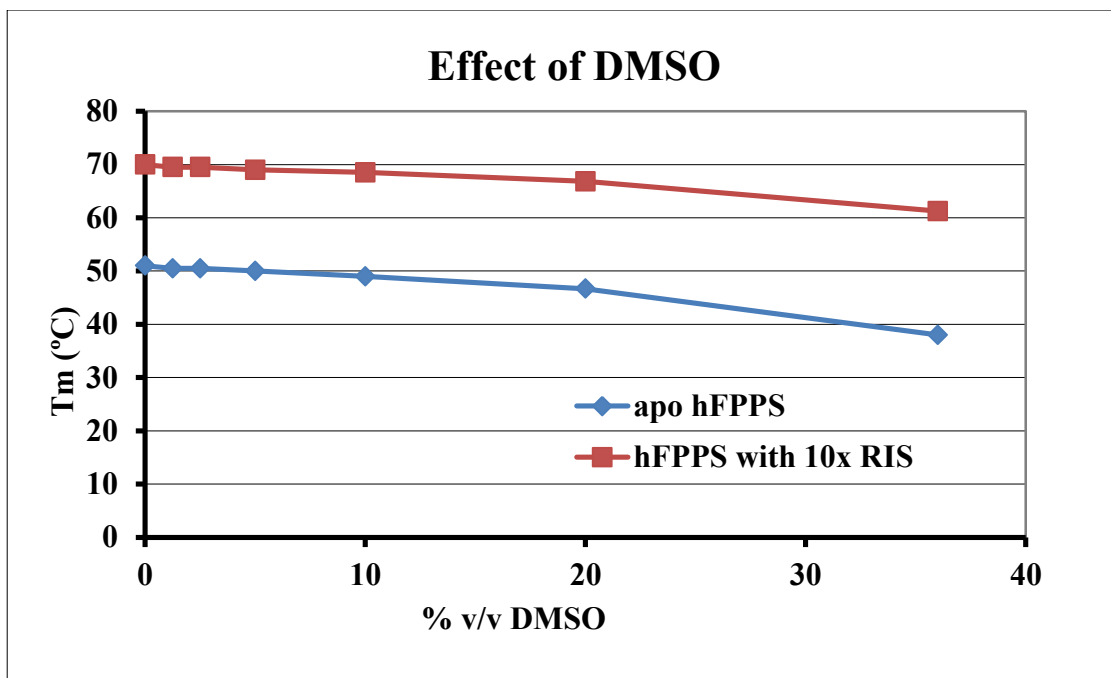


Figure 8.13: Destabilizing effect of DMSO on hFPPS
(hFPPS batch #1, [NaCl] 100 mM)

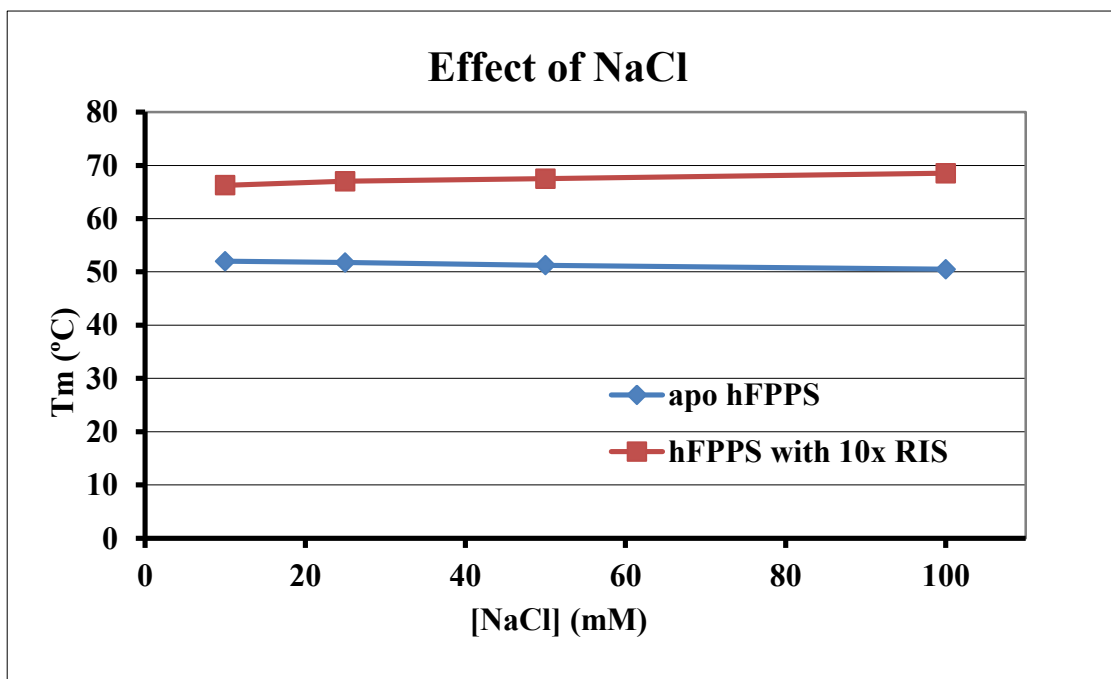


Figure 8.14: Destabilizing effect of NaCl on hFPPS
(hFPPS batch #1, [NaCl] 100 mM)

8.4.3 Elucidation of binding characteristics by DSF

With the observation that [NaCl] decreases the ΔT_m of risedronate, it was clearly necessary to more thoroughly examine the effect of buffer modifications. Therefore, the titration curve was determined under three conditions ([NaCl] 10 or 100 mM, +0.01% Triton X-100) for three structurally different hFPPS inhibitors (risedronate, **4.5** and **1.5**), in order to gain insight into the relationship between physicochemical characteristics, binding characteristics and buffer composition.

As previously observed (**Figure 8.14**), reducing the NaCl concentration resulted in decreased stabilization by risedronate, most notably at lower concentrations of the inhibitor (**Figure 8.15**). This decrease in ΔT_m may be due to a change in desolvation entropy, as at lower ionic strength of the solvent, charged molecules are less readily dehydrated.^{17,21} Thus, at lower [NaCl], risedronate has a higher dehydration entropy penalty which is transferred to the hFPPS/RIS complex, resulting in a lower T_m . An alternative explanation lies in the fact that the ionic strength of the solution affects the protonation state of risedronate, although the precise correlation is still a topic of debate in the literature.²² As the bisphosphonate moiety binds in the tetra-anionic state to the Mg^{2+} triad in the hFPPS active site, any change in the protonation equilibrium will also affect the binding to the enzyme.^{11,23}

Interestingly, the addition of 0.01% Triton X-100 had the inverse effect and increased the ΔT_m to within ~ 2 °C of the [NaCl] 100 mM titration curve (**Figure 8.15**). Whether this due to an entropic desolvation effect or the stabilization effect is simply amplified for protein that is inherently less stable in the buffer, is not clear.

The titration curves of inhibitor **4.5** were similarly affected by [NaCl] and detergent as observed for risedronate, consistent with the fact that both compounds are bisphosphonates and bind to the allylic sub-pocket of the enzyme with the assistance of Mg^{2+} ions (compare **Figure 8.15** and **Figure 8.16**). Furthermore, the lower ΔT_m values observed for **4.5** correlate with its 3-fold lower enzymatic potency as compared to risedronate. These findings indicate that compounds, within a structural class, exhibit similar characteristics by DSF and it may be possible to rank their binding affinity according to their ΔT_m values.

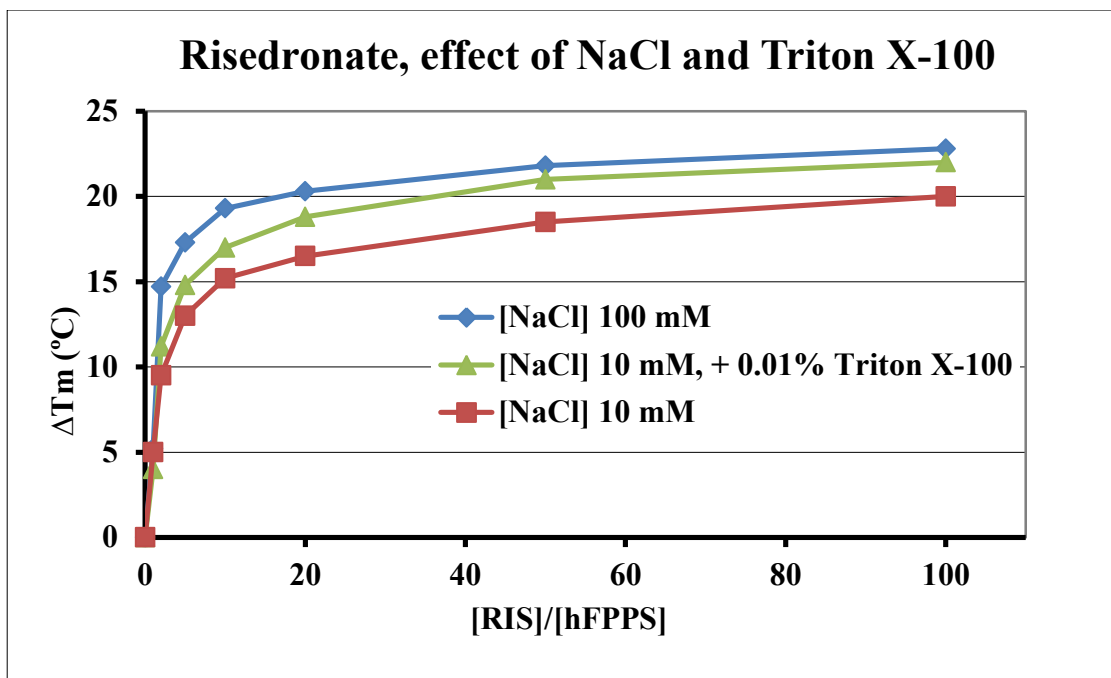


Figure 8.15: Effect of buffer composition on risedronate binding (hFPPS batch #3)

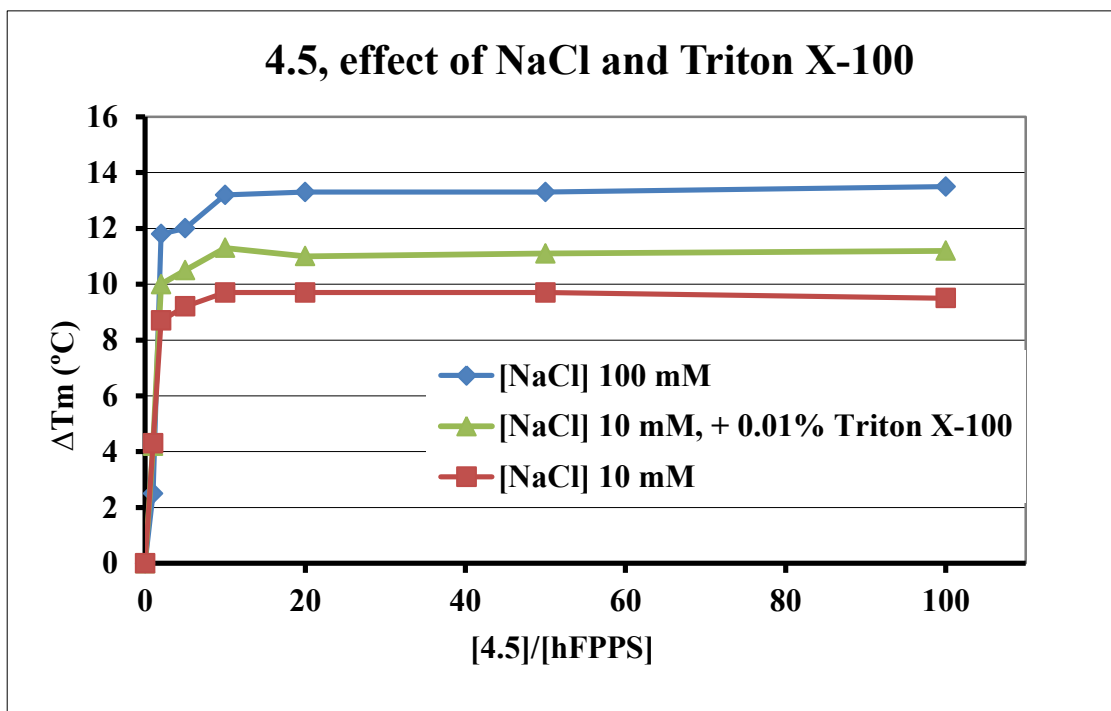


Figure 8.16: Effect of buffer composition on 4.5 binding (hFPPS batch #3)

In contrast to the bisphosphonate inhibitors, allosteric inhibitor **1.5** exhibits different characteristics by DSF. Lowering the NaCl concentration has no measurable effect on stabilization; the difference between the titration curves is under 1 °C (i.e. the expected variability of the technique, **Figure 8.17**). Addition of the Triton X-100 leads to a small increase in ΔT_m (~2 °C). It is not clear if this is due to the prevention of aggregate formation *in situ*, or an amplification of stabilization due to non-specific interactions between the detergent and the protein. It should be noted that risedronate and **4.5** induce the semi-closed conformation, while **1.5** binds to hFPPS in the open state and this may be the reason for the difference in binding characteristics, as observed in these DSF experiments.

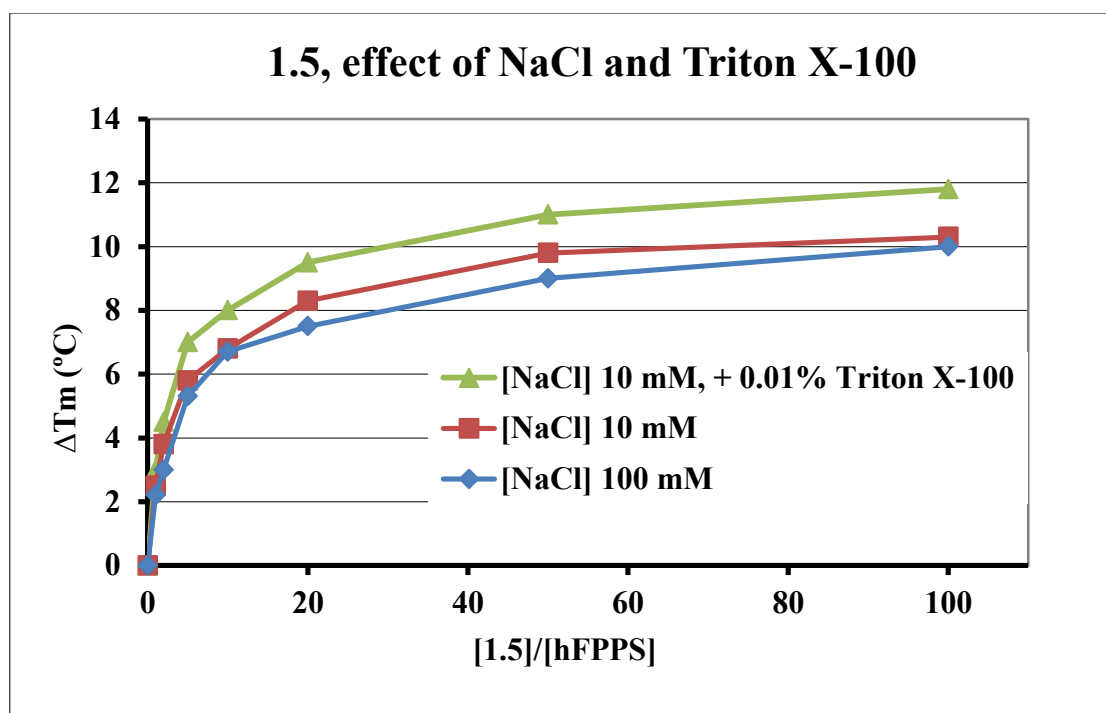


Figure 8.17: Effect of buffer composition on **1.5** binding (hFPPS batch #3)

In summary, these DSF experiments have demonstrated that modulating the buffer components can result in significant changes in the data and this can be exploited to elucidate preliminary information about the ligands. For example, analysis of the thermal stability of hFPPS-inhibitor complexes in the absence of Mg^{2+} ions in the assay buffer can be used to differentiate inhibitors that bind to the IPP sub-pocket or (*more likely*) an allosteric pocket of the enzyme, as opposed to the allylic sub-pocket. Secondly, changing

the NaCl concentration and the addition of a detergent can expose compounds with different binding behaviour. In addition, the similarities observed in the melting curves of hFPPS/RIS and hFPPS/**4.3** complexes suggest that there may be a correlation between enzymatic activity and the melting temperature of the inhibitor-enzyme complex (ΔT_m). Although DSF cannot distinguish between non-selective “sticking” of a compound to the protein surface vs binding of a true inhibitor to a catalytically relevant site of the enzyme, DSF can serve as an initial analytical tool to rapidly screen both active site and allosteric hFPPS inhibitors and reveal compounds that warrant more extensive characterization by other biophysical methods such as X-ray crystallography, NMR and ITC experiments.

8.5 Inhibitor and fragment screening by hFPPS

8.5.1 ΔT_m - IC_{50} correlation

A potentially promising application of DSF assays is screening compound libraries for the identification of new “hits” that inhibit hFPPS. If this technique can be successfully applied in high-throughput screening, it would be faster and far more economical than any functional assay. However, we first needed to establish the limit of detection with respect to binding affinity and the relationship (*if any*) between the *in vitro* potency of hFPPS inhibitors and the protein stabilization (ΔT_m) observed by DSF. Towards this end, several of our inhibitors with a range of enzymatic activity were analyzed by DSF. A clear correlation was observed between ΔT_m and IC_{50} values for our pyridine-based inhibitors described in Chapters 2, 4 and 5 (**Figure 8.18**). Since artefacts appear at higher concentrations of the inhibitors, a ratio of 10:1 [inhibitor]/[hFPPS] was selected for a second, larger screening in order to determine the variability of the correlation (**Figure 8.19**).

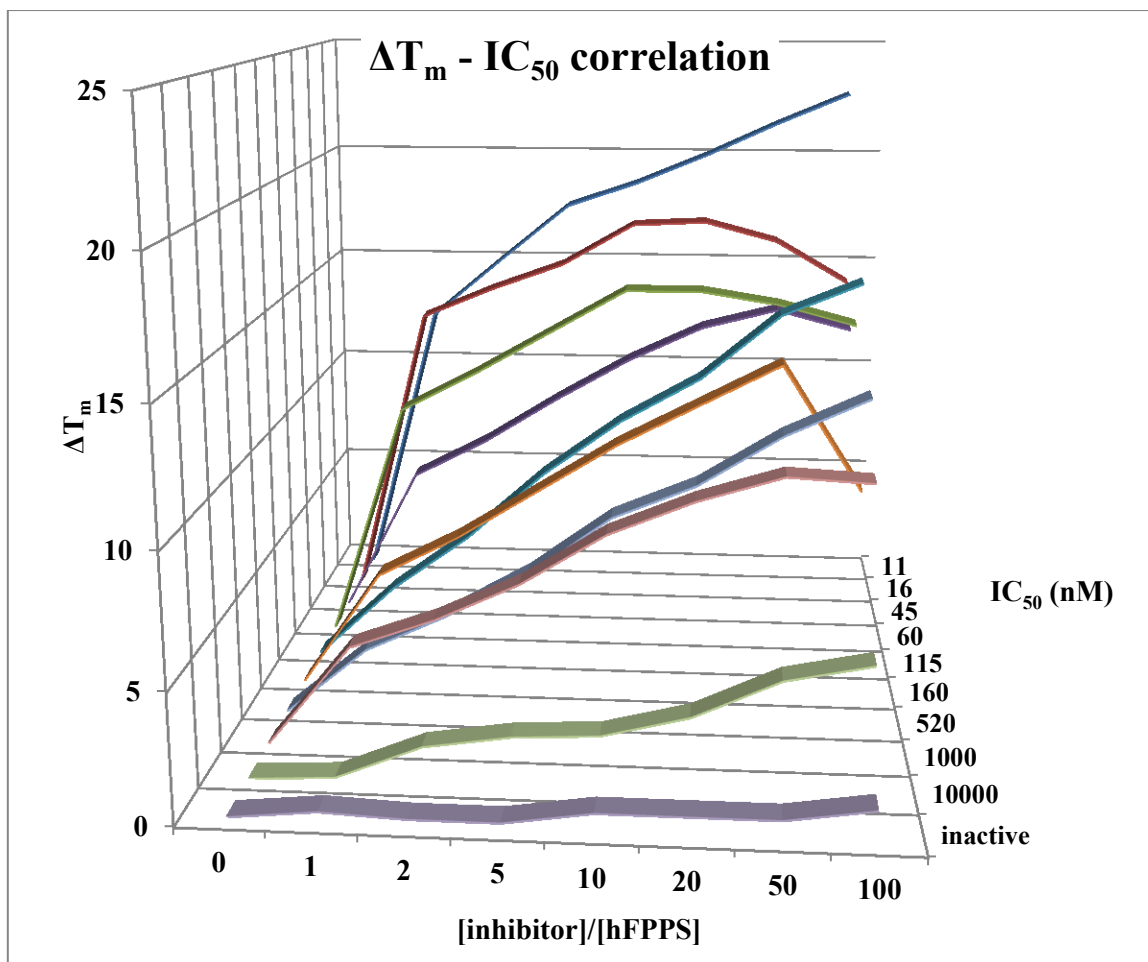


Figure 8.18: Overlay of DSF titration curves according to *in vitro* potency (hFPPS batch #1, [NaCl] 100 mM)

Inhibitors with a bisphosphonate moiety *meta* to the heterocyclic nitrogen of the pyridine core (including risedronate), generic structure **8.1** (blue data points, **Figure 8.20**) exhibit a positive, linear correlation between the stabilization and enzymatic potency, with an R^2 value of 0.86 for a least squares linear regression analysis of the data. Interestingly, the data points for 2-aminopyridine bisphosphonates, **8.2**, closely overlap and exhibit an almost identical correlation between ΔT_m and IC_{50} values (green data points, **Figure 8.19**). This can be rationalized by the fact that the inhibitors are structurally analogous and therefore have similar physicochemical properties. A regression analysis of the combined data of **8.1** and **8.2** type inhibitors results in an R^2 value of 0.84 (**Figure 8.30**) and similar results were obtained for the same correlation experiments with reduced ionic strength of the buffer ([NaCl] 10 mM; $R^2 = 0.81$) and in the presence of a detergent ([NaCl] 10mM, +0.01%

Triton X-100; $R^2 = 0.81$). These observations strongly suggest that the compounds have the same binding properties, such as thermodynamic behaviour and enzyme binding site. The combined DSF data implies that inhibitors **8.1** and **8.2** belong to the same class of inhibitors and their *in vitro* potency is proportional to the thermal stability of their corresponding complexes with hFPPS.

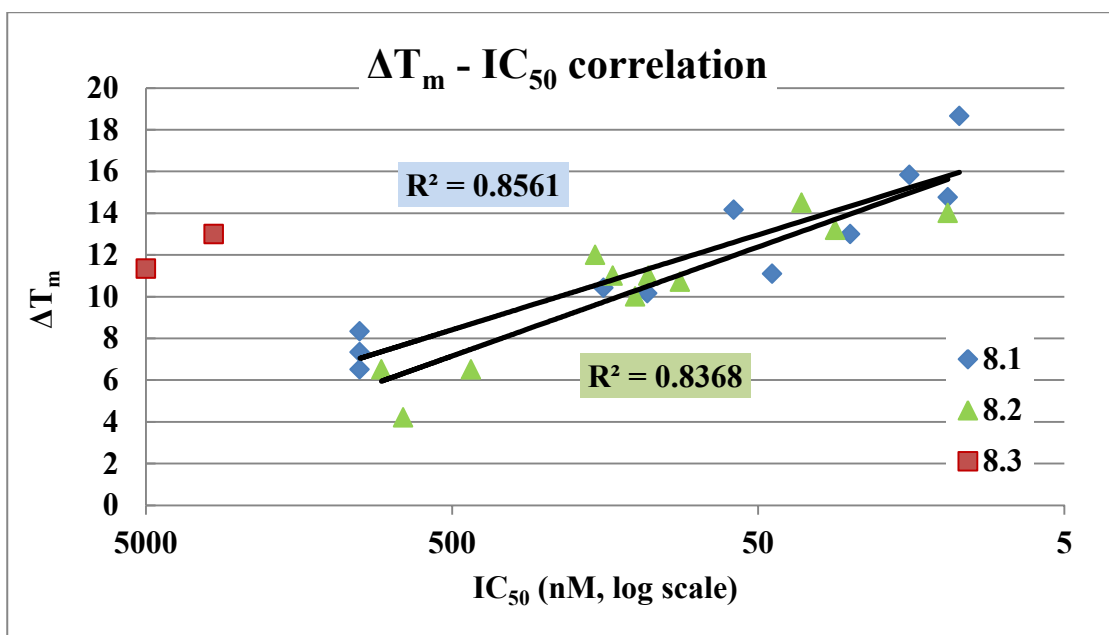


Figure 8.19: Correlation between stabilization (at 10x inhibitor) and enzymatic activity. Inhibitors of type **8.1**, **8.2** and **8.3** are depicted in blue, green and red respectively; linear least squares fits are depicted as black lines and R^2 values are indicated with the associated color. (hFPPS batch #1,2 and 3; [NaCl] 100 mM)

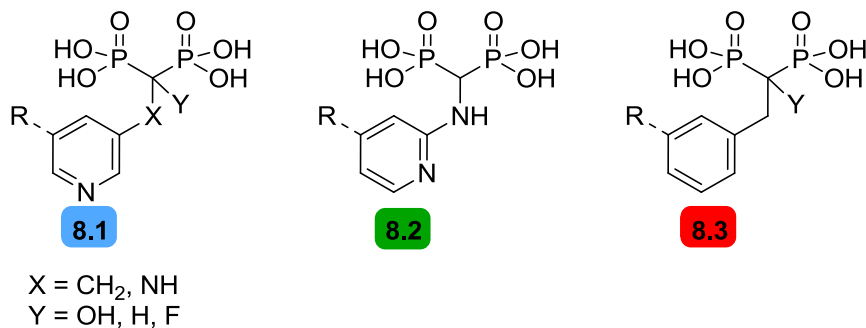


Figure 8.20: General structures of pyridine-3-bisphosphonates, **8.1**; 2-aminopyridine bisphosphonates, **8.2** and bisphosphonates with a phenyl core, **8.3**.

In a DSF screening scenario, where target affinity is ranked according to ΔT_m , bisphosphonates with a phenyl core (**8.3**, **Figure 8.20**) appear as outliers relative to the correlation for pyridine-based bisphosphonate inhibitors (red data points, **Figure 8.19**). However, they are not true false positives because they do inhibit hFPPS, with IC_{50} values in the 1-10 μM range. In order to better understand this observation the titration curves were determined for two compounds which differ only in the inclusion of a heterocyclic nitrogen (i.e. **8.1** and **8.3** with identical R- and Y- substituent, **Figure 8.20**). The DSF titration curves obtained were identical, ≤ 1 $^{\circ}C$ difference (**Figure 8.21**), and this exemplifies the inherent serendipity that is associated with medicinal chemistry; a difference in one atom can have a large impact on the biopharmaceutical properties of a compound, in this case *in vitro* enzymatic potency. These observations are not detrimental to the feasibility of compound screening by DSF, but show that a complementary assay is required to confirm hits. Furthermore, this demonstrates that DSF can potentially detect inhibitors with IC_{50} values in the 1-10 μM range, a common activity range for hits.

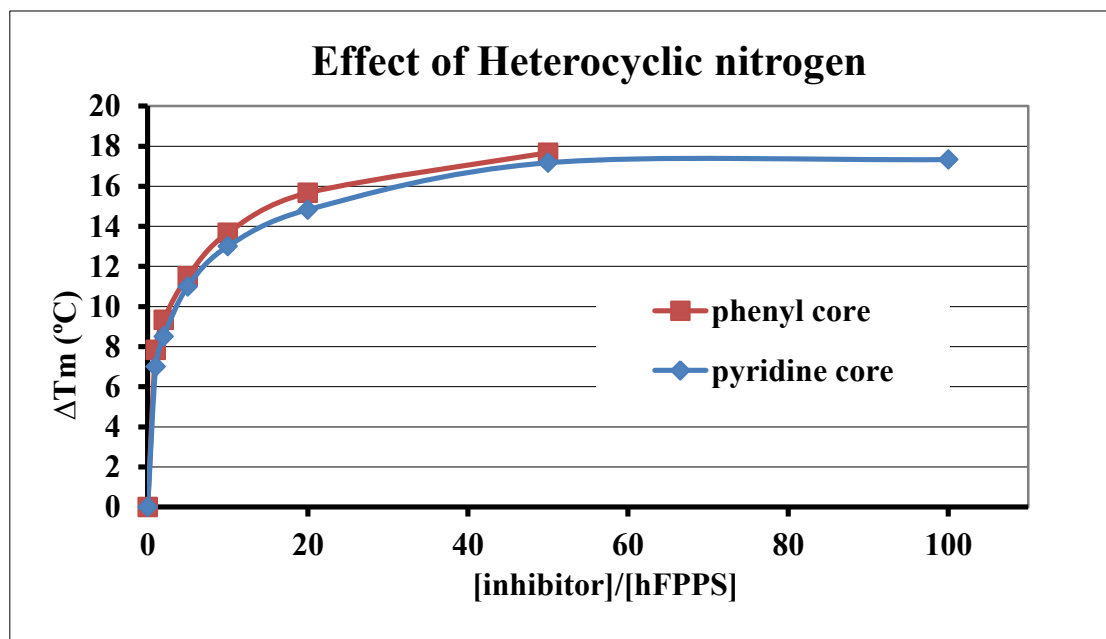


Figure 8.21: Titration curves for two inhibitors differing only in the presence of heterocyclic nitrogen. (hFPPS batch #1; [NaCl] 100 mM)

8.5.2 Fragment-based screening by DSF:

A small library of approximately 200 molecules, including synthesis intermediates and commercial compounds, was screened against hFPPS by DSF analysis (**Figure 8.22**). Special consideration was given to acidic moieties, potentially capable of interacting with Mg^{2+} triad of the allylic sub-pocket or basic residues of the IPP sub-pocket. The fragments were screened under various DSF conditions, including the presence of an *N*-BP in order to induce the semi-closed conformation of hFPPS and promote binding into the IPP sub-pocket. Unfortunately, to date only weak hits were identified, $\Delta T_m \sim 4^\circ\text{C}$, which proved to be statistical artefacts and could not be reproduced in a full titration curve. Further screenings are currently ongoing.

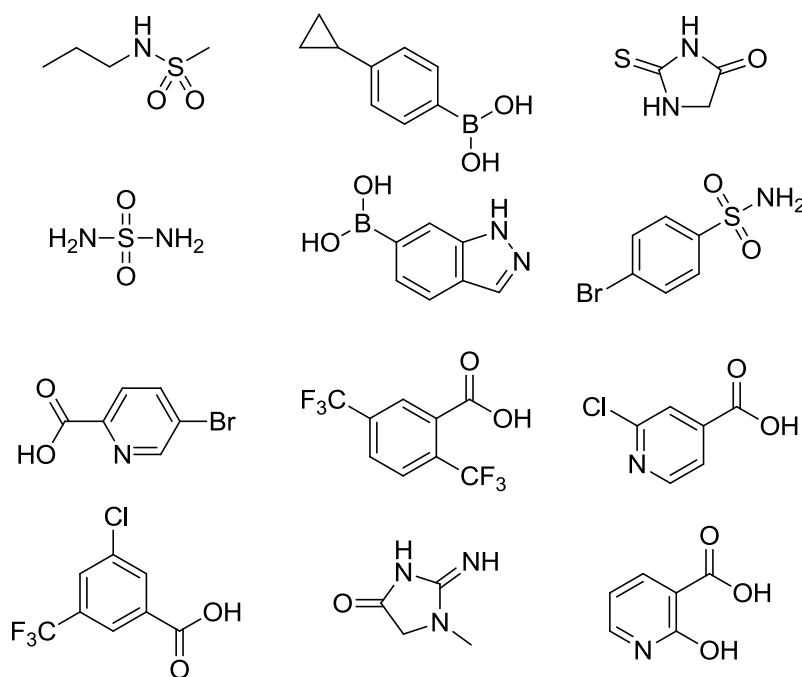


Figure 8.22: Selection of compounds included in DSF fragment screening

In summary, we have established a linear, positive correlation between the stabilizing effect of pyridine-based hFPPS inhibitors and their *in vitro* enzymatic potency. This demonstrates that it is possible to rank compounds according to their ΔT_m values *within a structural class* of inhibitors. Data outliers were discovered, indicating the technique is susceptible to artefacts, and identified to belong to bisphosphonates which lack a basic nitrogen in the aromatic core. This underscores the Achilles heel of DSF, namely that physicochemical properties and binding characteristics cannot be discriminated. The experiments described in this chapter demonstrate the viability of screening compounds against hFPPS by DSF.

8.6 DSF co-incubation studies, elucidation of binding mode

As previously described, the addition of IPP substrate to the hFPPS/RIS complex led to an additional increase in stabilization, so called additive stabilization $\Delta\Delta T_m$ (**Figure 8.6**). This observation is in complete agreement with previously reported DSC experiments,⁴ and also with the known binding mode of risedronate, which exclusively occupies the allylic sub-pocket of the hFPPS enzyme.¹¹ This observation led us to investigate the possibility of deriving more structural information about inhibitor binding modes by performing DSF co-binding experiments with ligands with known binding sites. Such DSF parallel titrations will be complementary to our previous NMR line broadening studies, which can only be performed with weakly binding ligands and reveal competition for binding to the protein. In contrast, DSF gives the highest signal (ΔT_m) with strongly binding ligands and reports cooperative binding by the ligands ($\Delta\Delta T_m$).

To this end the titration curves of the substrates and product of hFPPS (DMAPP, IPP, GPP and FPP) were determined (**Figure 8.23**). As the C₁₀ and C₁₅ compounds are quite amphiphilic, these experiments were performed in the presence of the Triton X-100 detergent in order to prevent micelle formation. Despite the decreased NaCl concentration, FPP still crashed out of solution above 40 μ M. The quantitative results are as expected; GPP induces the largest stabilization, presumably because it can form more lipophilic interactions due its longer C₁₀ alkenyl chain. IPP exhibits a slightly larger ΔT_m than

DMAPP, most likely due its ability to bind in both the allylic and IPP sub-pockets. In order to validate the experimental design, the first DSF co-binding experiment was performed with risedronate and the GPP and IPP substrates. Each parallel titration was performed on a single 96 well plate and the results are shown in surface representation in order to identify a general trend, rather than a numerical value (**Figure 8.24**). In accordance with the known binding mode, no additional stabilization was observed with GPP, which competes with risedronate for the allylic sub-pocket of hFPPS. As expected a clear co-operative binding trend was observed with IPP with a maximum additive stabilization $\Delta\Delta T_m$ value of 7 °C.

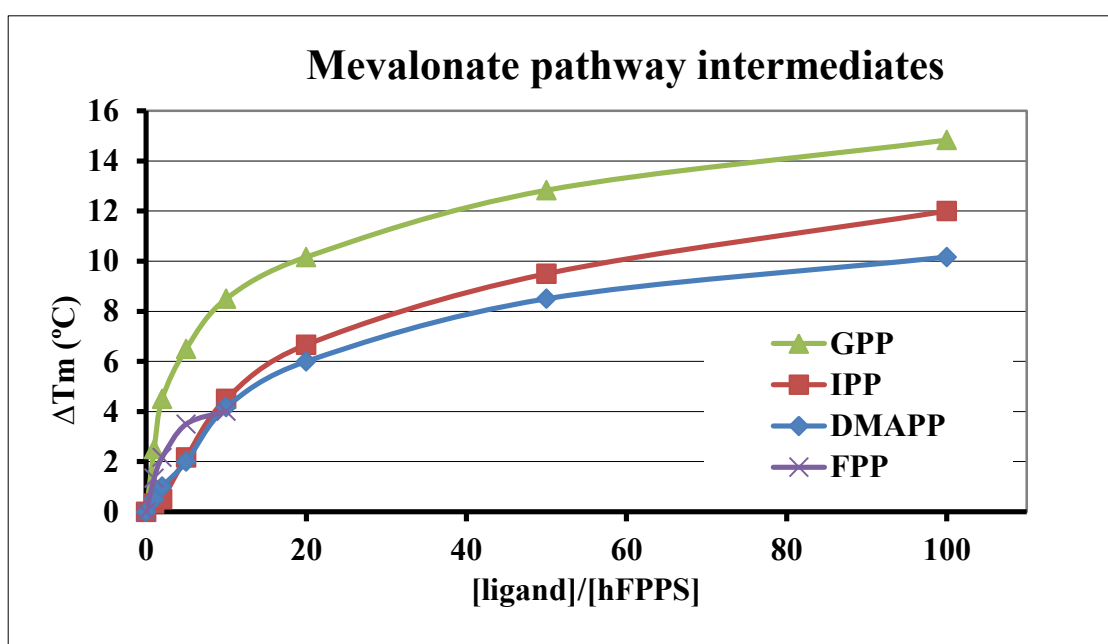


Figure 8.23: Titration curves of DMAPP, IPP, GPP and FPP
(hFPPS batch #3, [NaCl] 10 mM, 0.01% Triton X-100)

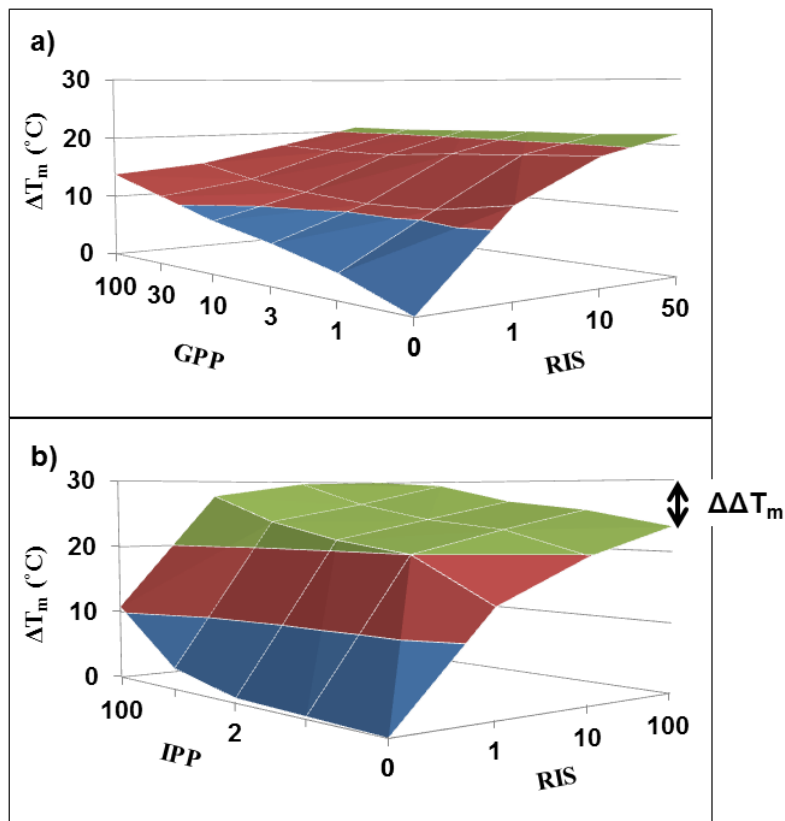


Figure 8.24: DSF parallel titrations of risedronate with GPP (panel a) and IPP (panel b) (hFPPS batch #1, [NaCl] 100 mM)

Next, the parallel titration with inhibitor **4.5** and IPP was performed. In agreement with the crystal structure obtained for the hFPPS/**4.5** complex (Chapter 4), a clear co-operative binding trend was observed with a maximum $\Delta\Delta T_m$ value of 15 °C (**Figure 8.25**). It should be noted that the total stabilization for the hFPPS/RIS/IPP and hFPPS/**4.5**/IPP ternary complexes is identical, ΔT_m value of ~30 °C. This suggests that the protein ternary structure may be the dominant factor for DSF data; as, so far, the fully closed conformation has melted at 81 °C, regardless of the ligands.

In order to further study this additive stabilization phenomenon we performed comparative titrations with IPP, pyrophosphate (PPi, $[P_2O_7]^{4-}$) and inorganic phosphate (Pi, $[PO_4]^{3-}$). The results clearly show that phosphate provides no benefit towards thermal stability (**Figure 8.26**), indicating that it is not capable of inducing the fully closed conformation. This was confirmed by resolving the hFPPS/**4.5**/Pi complex crystal structure (PDB 4H5C) in which hFPPS adopts a semi-closed conformation. Pyrophosphate, on the other hand, does provide

additional stabilization, but not as strong as IPP; suggesting it may induce an hFPPS conformation in between the semi-closed and fully closed conformation. However, the X-ray crystal structure of the hFPPS/**4.5**/PPi complex (PDB 4H5D) revealed that the KRRK C-terminal tail was fully resolved and closed the active site in an identical manner to the hFPPS/**4.5**/IPP complex (PDB 4H5E). This demonstrates that the melting temperature of the ternary complex can be lower than 81 °C as a result of ligand energetic factors. To understand these observations, the thermodynamic parameters of PPi and IPP co-binding **4.5** were measured by ITC (**Table 8.1**). This data indicated that PPi co-binding is stronger (more negative ΔG) than IPP, seemingly at odds with our DSF experiments. However, PPi binding comes from a more favorable (more negative) enthalpy change, ΔH , but has less favorable (more negative) entropic term, ΔS , compared to IPP. The entropic effects of course become more dominant with increasing temperature and, based on the thermodynamic data, IPP co-binding becomes more favorable at temperatures above 70 °C. This is in full agreement with the T_m values observed by DSF, 75 °C for the hFPPS/**4.5**/PPi complex and 81 °C for hFPPS/**4.5**/IPP. These thermodynamic studies expose the inherent bias that DSF experiments have for entropy driven binding.

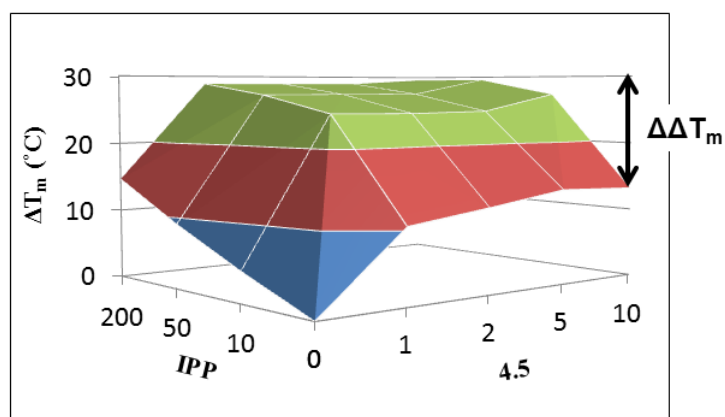


Figure 8.25: DSF parallel titration of **4.5** with IPP
(hFPPS batch #1, [NaCl] 100 mM)

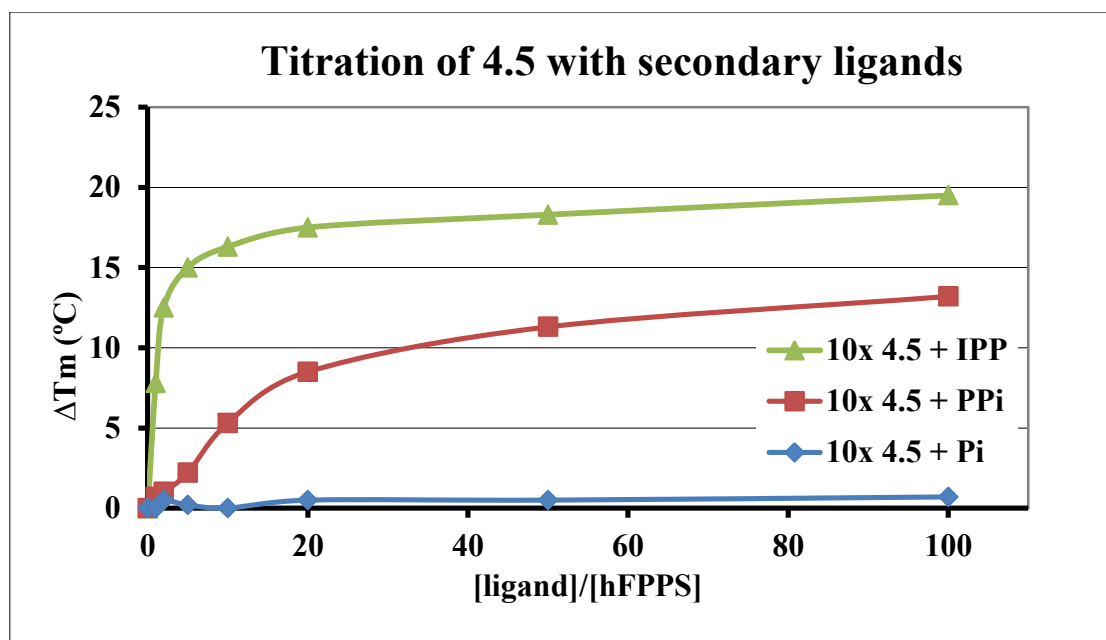


Figure 8.26: Titration curve of ten-fold **4.5** with IPP, PPi and Pi (hFPPS batch #3, [NaCl] 10 mM)

	ΔH kcal/mol	$T\Delta S$ kcal/mol	$\Delta G = \Delta H - T\Delta S$ kcal/mol
PPi	-13.5 ± 0.2	-4.9 ± 0.2	-8.6
IPP	$-10.7 \pm 0.0.5$	-2.4 ± 0.5	-8.3

Table 8.1: ITC thermodynamic data for hFPPS/**4.5** 1:3 at 30 °C

Our previous NMR line broadening studies showed competition between **2.22** and risedronate and IPP, leading us to hypothesize that the inhibitor bound in both sub-pocket simultaneously (Chapter 2). This was cast in doubt with the crystal structure of hFPPS/**4.5**, which showed binding in the allylic sub-pocket exclusively (Chapter 4). In order to resolve this discrepancy, the parallel titration with inhibitor **2.22** and IPP was performed (**Figure 8.27**). Although the data is not as good due to the poor affinity of **2.22** for hFPPS, in fact it binds less tightly than IPP, there is a clear co-operative binding trend with a maximum $\Delta\Delta T_m$ value of 17 °C. This data strongly suggests that the inhibitor does not occupy the IPP sub-pocket. A likely explanation for the competition observed by NMR, is that the weak

affinity that IPP has for the allylic sub-pocket is sufficient to displace the weakly binding **2.22** inhibitor and we conclude that it most likely does not bind in the IPP sub-pocket.

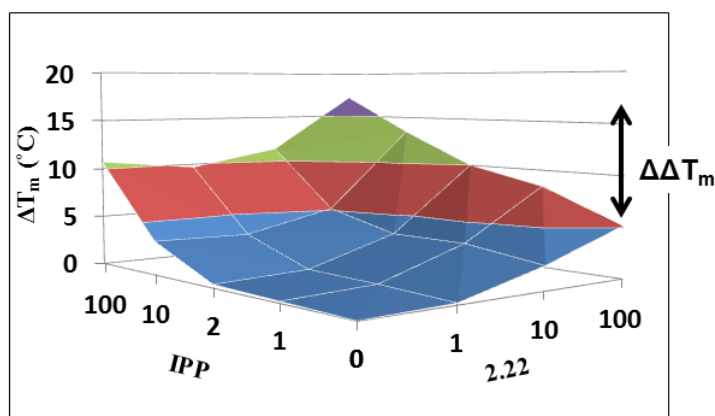


Figure 8.27: DSF parallel titration of **2.22** with IPP
(hFPPS batch #1, [NaCl] 100 mM)

Finally, the parallel titrations of inhibitor **1.5** with risedronate and IPP were performed in order to determine allosteric binding characteristics by DSF (**Figure 8.28**). There are two reported ternary structure of hFPPS with an allosteric inhibitor and zoledronate co-bound (PDB 3N45 and 3N46). However, although there is a co-operative binding trend, the effect is weak, with a maximum $\Delta\Delta T_m$ value of 4 °C; indicating that this type of DSF co-binding experiment is not well suited to detect allosteric binding. In contrast to risedronate (**Figure 8.24**), **4.5** (**Figure 8.25**) and **2.22** (**Figure 8.27**), the **1.5**-IPP parallel titration curve does not show cooperative binding; at no point does the ΔT_m go higher than for the **1.5** and IPP curves on the horizontal axes. This observation is in agreement with the proposed mechanism that the allosteric inhibitors prevent the binding of IPP by electrostatic repulsion and induce the open conformation of hFPPS.² Therefore this type of DSF experiment seems well suited to determine the possible allosteric binding mode of an inhibitor.

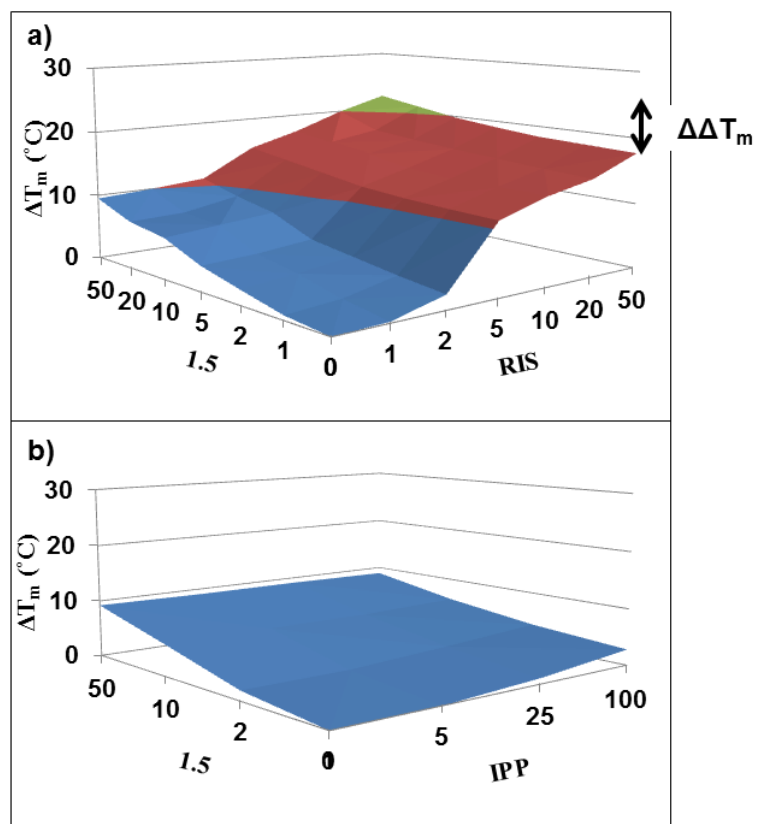


Figure 8.28: DSF parallel titrations of **1.5** with risedronate (panel a) and IPP (panel b, in the absence of Mg^{2+})
(hFPPS batch #3, [NaCl] 10 mM, 0.01% Triton X-100)

8.7 Discovery of the allosteric binding mode of thienopyrimidines

In our continuing efforts to develop inhibitors of hFPPS with improved biopharmaceutical properties, bisphosphonates with a thienopyrimidine core were explored. The thienopyrimidine moiety (**Figure 8.29**) has the advantage that it is more lipophilic and the heterocyclic nitrogens are less basic compared to pyridine. Although we only have preliminary enzymatic inhibition data for a limited number of thienopyrimidine bisphosphonates, it is clear from the ΔT_m - IC_{50} correlation plot (purple data points, **Figure 8.30**) that they exhibit different binding characteristics compared to our previous pyridine based inhibitors. This may be entirely attributed to their different physicochemical properties, but nonetheless the enzymatic potency of analog **8.4** (IC_{50} value of 250 nM) was surprising, given that the large naphthyl side chain was not expected to fit in the limited volume of the allylic sub-pocket within the hFPPS active site cavity. Therefore the parallel titration of inhibitor **8.4** with IPP was performed in order to determine if it exhibited allosteric binding characteristics by DSF (**Figure 8.31**). Indeed, we did not observe any additive stabilization (**Figure 8.31** vs **Figure 8.25**) strongly suggesting that this inhibitor does not bind in the usual way that *N*-BPs are known to bind. Analog **8.5** was subsequently selected for X-ray crystallography studies and, gratifyingly, the resolved hFPPS/**8.5** complex shows that the inhibitor occupies the same allosteric pocket as the previously reported Novartis inhibitors **1.5** (**Figure 8.32**). This discovery marks a milestone in our research project and the identification of a novel class of hFPPS allosteric inhibitors.

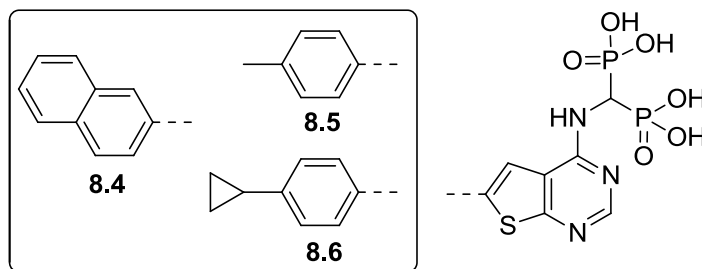


Figure 8.29: Examples of thienopyrimidine bisphosphonates

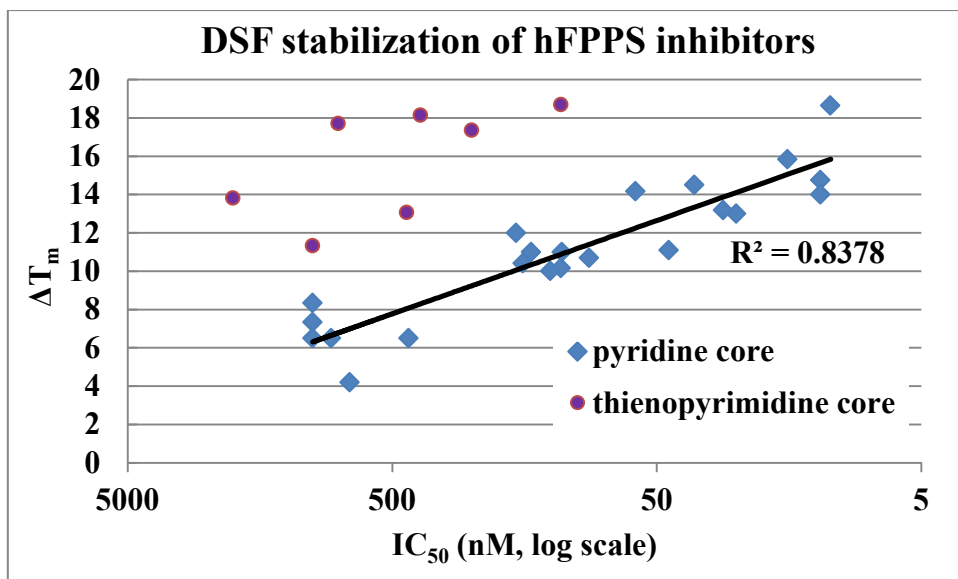


Figure 8.30: Correlation between stabilization (at 10x inhibitor) and enzymatic activity (hFPPS batch #1,2 and 3; [NaCl] 100 mM)

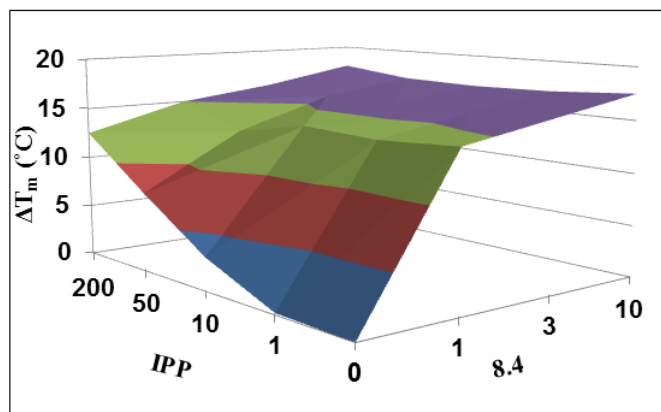


Figure 8.31: DSF parallel titration of **8.4** with IPP (hFPPS batch #1, [NaCl] 100 mM)

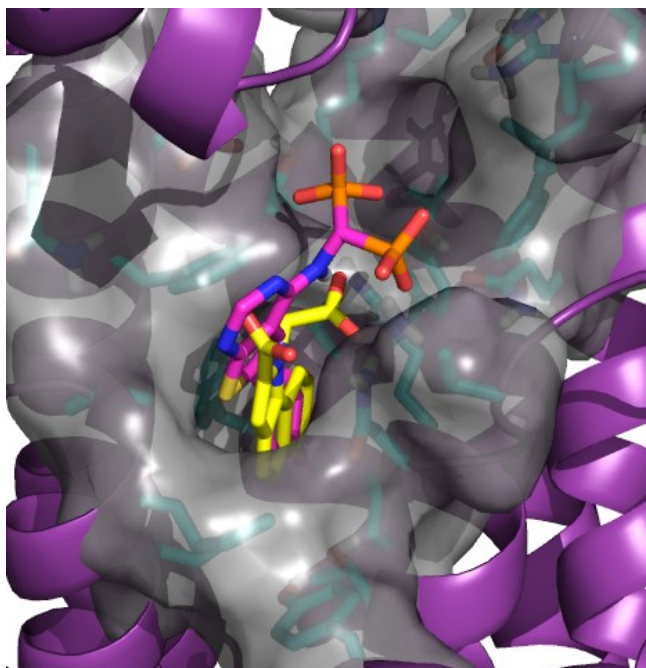


Figure 8.32: Composite picture of hFPPS/8.5 protein crystal structure (purple backbone, semi-transparent surface, unpublished) overlapped with hFPPS/1.5 (PDB 3N6K); analogs 1.5 and 8.5 are shown in stick representation, yellow and magenta respectively.

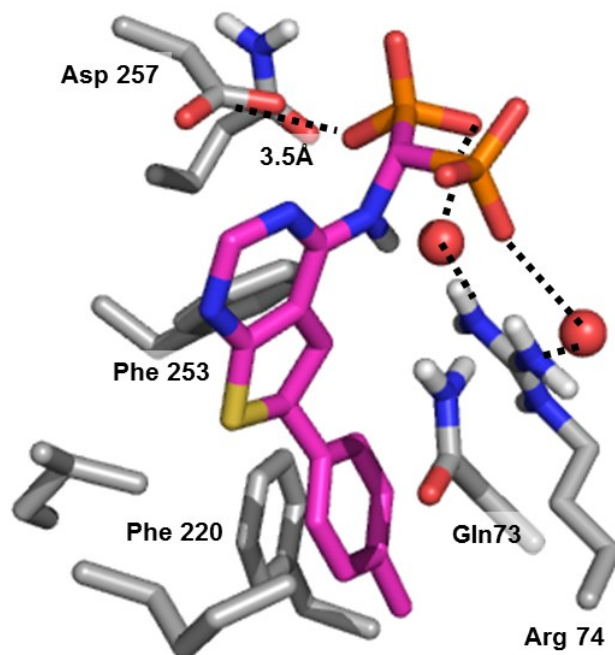


Figure 8.33: Expansion of hFPPS/8.5 crystal structure (unpublished)
Ionic interactions are depicted by dashed lines.

Closer inspection of the hFPPS/**8.5** co-crystal structure reveals that the *para*-tolyl moiety binds deeply into the allosteric pocket and engages in π -stacking interactions with Gln73 and Phe 220, similarly to **1.5** (**Figure 8.33**). An additional, an edge-to-face π -stacking interaction is formed between Phe 253 and the thienopyrimidine core. The bisphosphonate moiety engages in water-mediated ionic interactions with Arg74 at the bottom of the IPP sub-pocket. All these interactions are favorable and positively contribute to the binding affinity of **8.5**; however, one phosphonate is within Van der Waals contact of Asp 257, most likely resulting in electrostatic repulsion between the two acidic moieties. Based on these observations we envisioned that it would be beneficial to install a longer linker in order to form direct salt bridges with Arg 74 and also to remove one acidic moiety to prevent electrostatic repulsion with Asp 257. Surprisingly, the novel monophosphate analog **8.7** (**Figure 8.34**, refer to experimental section for details of the synthesis) was found to be significantly less potent in our hFPPS enzymatic assays as compared to the corresponding bisphosphonate compound **8.6** (**Table 8.2**). Additionally, the carboxylic acids **8.8** and **8.9** were found to be inactive against hFPPS at concentration up to 100 μ M. In retrospect, this loss of potency is not unprecedented; analogous observations were previously reported during optimization of a peptidomimetic inhibitors of HCV NS3/4A protease.^{24,25} In those investigations, a 270-fold loss in potency was observed when two negatively charged residues (P5 and P6 of a hexapeptide) were deleted,^{25,26} even though structural studies suggested that those residues were solvent-exposed and did not directly interact with the protease active site.^{24,26} Parallel studies on the same target showed that charged moieties on an inhibitor can provide *electrostatic pre-collision guidance*, that “draws” the molecule towards an area of the protein surface with opposite charge density.²⁷ Interestingly, in both cases, the active site cavity of the HCV NS3/4A protease,²⁸ as well as the IPP sub-pocket of the hFPPS active site are surrounded by positive residues.

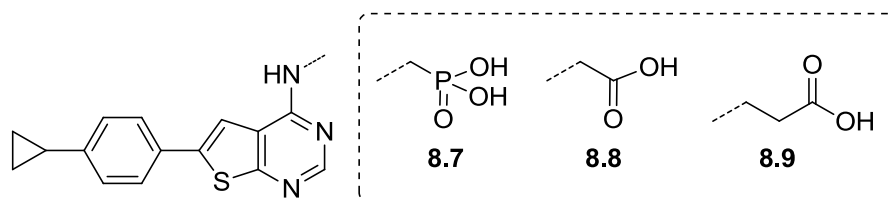


Figure 8.34: Non-bisphosphonate thienopyrimidine analogs

	hFPPS M1 assay	hFPPS M2 assay		
	IC ₅₀	IC ₅₀	10 μ M	100 μ M
8.4	250 nM	<i>nd</i>	<i>nd</i>	<i>nd</i>
8.5	400 nM	<i>nd</i>	<i>nd</i>	<i>nd</i>
8.6	115 nM	29 nM	<i>nd</i>	<i>nd</i>
8.7	<i>nd</i>	36 μ M	<i>nd</i>	<i>nd</i>
8.8	<i>nd</i>	<i>nd</i>	0%	11%
8.9	<i>nd</i>	<i>nd</i>	0%	4%

Table 8.2: Human FPPS inhibition data of thienopyrimidine based inhibitors The values of % inhibition shown are the average of three determinations. (<10% standard deviation)
(*nd* = not determined)

8.8 Conclusions and outlook

In summary, we have demonstrated a linear, positive correlation between the stabilizing effect of pyridine-based hFPPS inhibitors and their *in vitro* enzymatic potency. This demonstrates that it is possible to rank compounds according to their ΔT_m values with reasonable accuracy, as long as they belong to same structural class of inhibitors. Furthermore, by performing parallel titrations with an inhibitor and secondary ligands we have established a method to distinguish inhibitors that bind to the active site of hFPPS vs those that bind to an allosteric pocket. These studies led to the discovery of a novel class of thienopyrimidine-based hFPPS inhibitors and, *in principal*, it should be possible to optimize these compounds into potent ***non***-bisphosphonate inhibitors of hFPPS.

8.9 Acknowledgements

We wish to thank Dr. Robert Zamboni (Zamboni Chemical solutions) for access to their RT-PCR instrument and a kind donation of the SYPRO[®] Orange dye.

8.10 References

- (1) Hosfield, D. J.; Zhang, Y.; Dougan, D. R.; Broun, A.; Tari, L. W.; Swanson, R. V.; Finn, J.; Structural Basis for Bisphosphonate-mediated Inhibition of Isoprenoid Biosynthesis *J. Biol. Chem.* **2004**, *279*, 8526.
- (2) Jahnke, W.; Rondeau, J.-M.; Cotesta, S.; Marzinzik, A.; Pellé, X.; Geiser, M.; Strauss, A.; Götte, M.; Bitsch, F.; Hemmig, R.; Henry, C.; Lehmann, S.; Glickman, J. F.; Roddy, T. P.; Stout, S. J.; Green, J. R.; Allosteric non-bisphosphonate FPPS inhibitors identified by fragment-based discovery *Nat. Chem. Biol.* **2010**, *6*, 660.
- (3) Kavanagh, K. L.; Guo, K.; Dunford, J. E.; Wu, X.; Knapp, S.; Ebetino, F. H.; Rogers, M. J.; Russell, R. G. G.; Oppermann, U.; The molecular mechanism of nitrogen-containing bisphosphonates as antiosteoporosis drugs *Proc. Natl. Acad. Sci. USA* **2006**, *103*, 7829.
- (4) Rondeau, J.-M.; Bitsch, F.; Bourgier, E.; Geiser, M.; Hemmig, R.; Kroemer, M.; Lehmann, S.; Ramage, P.; Rieffel, S.; Strauss, A.; Green, J. R.; Jahnke, W.; Structural Basis for the Exceptional in vivo Efficacy of Bisphosphonate Drugs *ChemMedChem* **2006**, *1*, 267.
- (5) Hubbard, R. E.; Murray, J. B. 2011; Vol. 493, p 509.
- (6) Niesen, F. H.; Berglund, H.; Vedadi, M.; The use of differential scanning fluorimetry to detect ligand interactions that promote protein stability *Nat. Protocols* **2007**, *2*, 2212.
- (7) Baldwin, R. L.; How Hofmeister ion interactions affect protein stability *Biophysical Journal* **1996**, *71*, 2056.
- (8) Holdgate, G. A.; Ward, W. H. J.; Measurements of binding thermodynamics in drug discovery *Drug Discovery Today* **2005**, *10*, 1543.
- (9) Layton, C. J.; Hellinga, H. W.; Thermodynamic Analysis of Ligand-Induced Changes in Protein Thermal Unfolding Applied to High-Throughput Determination of Ligand Affinities with Extrinsic Fluorescent Dyes *Biochemistry* **2010**, *49*, 10831.
- (10) Bruenger, E.; Rilling, H. C.; Determination of isopentenyl diphosphate and farnesyl diphosphate in tissue samples with a comment on secondary regulation of polyisoprenoid biosynthesis *Analytical Biochemistry* **1988**, *173*, 321.
- (11) Dunford, J. E.; Thompson, K.; Coxon, F. P.; Luckman, S. P.; Hahn, F. M.; Poulter, C. D.; Ebetino, F. H.; Rogers, M. J.; Structure-Activity Relationships for Inhibition of Farnesyl Diphosphate Synthase in Vitro and Inhibition of Bone Resorption in Vivo by Nitrogen-Containing Bisphosphonates *J. Pharmacol. Exp. Ther.* **2001**, *296*, 235.
- (12) Xue, Y.; Wang, S.; Feng, X.; Effect of Metal Ion on the Structural Stability of Tumour Suppressor Protein p53 DNA-Binding Domain *J. Biochemistry* **2009**, *146*, 193.
- (13) Williams, E. T.; Ehsani, M. E.; Wang, X.; Wang, H.; Qian, Y.-W.; Wrighton, S. A.; Perkins, E. J.; Effect of buffer components and carrier solvents on in vitro activity of recombinant human carboxylesterases *J. Pharmacol. Tox. Met.* **2008**, *57*, 138.
- (14) Bhattacharjya, S.; Balaram, P.; Effects of organic solvents on protein structures: Observation of a structured helical core in hen egg-white lysozyme in aqueous dimethylsulfoxide *Proteins: Structure, Function, and Bioinformatics* **1997**, *29*, 492.
- (15) Tjernberg, A.; Markova, N.; Griffiths, W. J.; Hallén, D.; DMSO-Related Effects in Protein Characterization *J. Biomol. Scr.* **2006**, *11*, 131.

- (16) Crowther, G. J.; Napuli, A. J.; Thomas, A. P.; Chung, D. J.; Kovzun, K. V.; Leibly, D. J.; Castaneda, L. J.; Bhandari, J.; Damman, C. J.; Hui, R.; Hol, W. G. J.; Buckner, F. S.; Verlinde, C. L. M. J.; Zhang, Z.; Fan, E.; van Voorhis, W. C.; Buffer Optimization of Thermal Melt Assays of Plasmodium Proteins for Detection of Small-Molecule Ligands *J. Biomol. Scr.* **2009**, *14*, 700.
- (17) Collins, K. D.; Ions from the Hofmeister series and osmolytes: effects on proteins in solution and in the crystallization process *Methods* **2004**, *34*, 300.
- (18) Feng, B. Y.; Shoichet, B. K.; A detergent-based assay for the detection of promiscuous inhibitors *Nat. Protocols* **2006**, *1*, 550.
- (19) Ryan, A. J.; Gray, N. M.; Lowe, P. N.; Chung, C.-w.; Effect of Detergent on “Promiscuous” Inhibitors *J. Med. Chem.* **2003**, *46*, 3448.
- (20) Khao, J.; Arce-Lopera, J.; Sturgis, J.; Duneau, J.-P.; Structure of a protein-detergent complex: the balance between detergent cohesion and binding *Eur. Biophys.* **2011**, *40*, 1143.
- (21) Kiriukhin, M. Y.; Collins, K. D.; Dynamic hydration numbers for biologically important ions *Biophys. Chem.* **2002**, *99*, 155.
- (22) Meloun, M.; Ferenčíková, Z.; Netolická, L.; Pekárek, T.; Thermodynamic Dissociation Constants of Alendronate and Ibandronate by Regression Analysis of Potentiometric Data *J. Chem. Engin. Data* **2011**, *56*, 3848.
- (23) Hounslow, A. M.; Carran, J.; Brown, R. J.; Rejman, D.; Blackburn, G. M.; Watts, D. J.; Determination of the Microscopic Equilibrium Dissociation Constants for Risedronate and Its Analogues Reveals Two Distinct Roles for the Nitrogen Atom in Nitrogen-Containing Bisphosphonate Drugs *J. Med. Chem.* **2008**, *51*, 4170.
- (24) Tsantrizos, Y. S.; Bolger, G.; Bonneau, P.; Cameron, D. R.; Goudreau, N.; Kukolj, G.; LaPlante, S. R.; Llinàs-Brunet, M.; Nar, H.; Lamarre, D.; Macrocyclic Inhibitors of the NS3 Protease as Potential Therapeutic Agents of Hepatitis C Virus Infection *Angew. Chem. Int. Ed.* **2003**, *42*, 1356.
- (25) Llinàs-Brunet, M.; Bailey, M.; Fazal, G.; Ghio, E.; Gorys, V.; Goulet, S.; Halmos, T.; Maurice, R.; Poirier, M.; Poupart, M.-A.; Rancourt, J.; Thibeault, D.; Wernic, D.; Lamarre, D.; Highly potent and selective peptide-based inhibitors of the hepatitis C virus serine protease: towards smaller inhibitors *Bioorg. Med. Chem. Lett.* **2000**, *10*, 2267.
- (26) LaPlante, S. R.; Cameron, D. R.; Aubry, N.; Lefebvre, S.; Kukolj, G.; Maurice, R.; Thibeault, D.; Lamarre, D.; Llinàs-Brunet, M.; Solution Structure of Substrate-based Ligands When Bound to Hepatitis C Virus NS3 Protease Domain *J. Biol. Chem.* **1999**, *274*, 18618.
- (27) Koch, U.; Biasiol, G.; Brunetti, M.; Fattori, D.; Pallaoro, M.; Steinkühler, C.; Role of Charged Residues in the Catalytic Mechanism of Hepatitis C Virus NS3 Protease: Electrostatic Precollision Guidance and Transition-State Stabilization *Biochemistry* **2000**, *40*, 631.
- (28) Tsantrizos, Y. S.; The design of a potent inhibitor of the hepatitis C virus NS3 protease: BILN 2061—From the NMR tube to the clinic *Peptide Science* **2004**, *76*, 309.

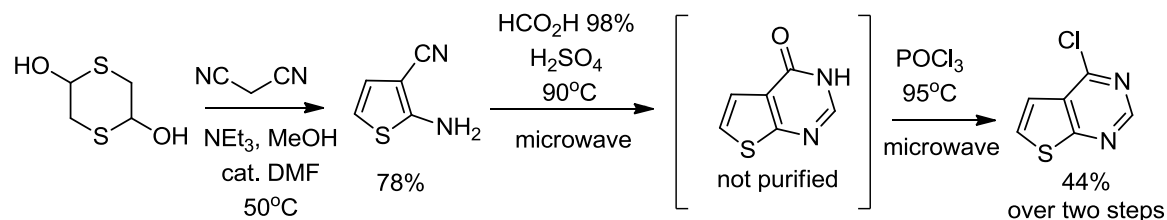
8.11 Experimental

8.11.1 Synthesis

JDS09-072: 4-chlorothieno[2,3-d]pyrimidine

This compound was synthesized according to literature procedure:

Hesse S. *et. al. Tet. Lett.* 2007, 48, 5261



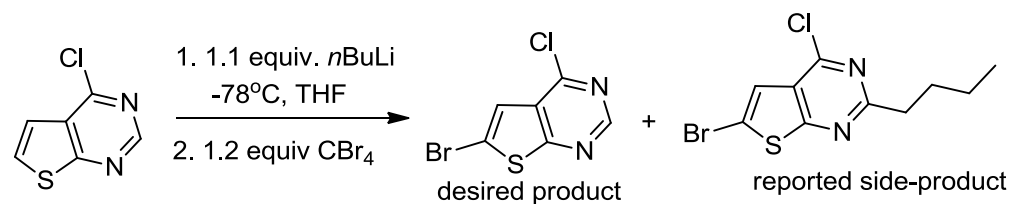
Isolated as a colorless oil.

^1H NMR (400 MHz, DMSO-d_6) δ 8.95 (s, 1H), 8.14 (d, $J = 6.0$ Hz, 1H), 7.59 (dd, $J = 6.0$, 1.8 Hz, 1H).

JDS09-088: 6-bromo-4-chlorothieno[2,3-d]pyrimidine

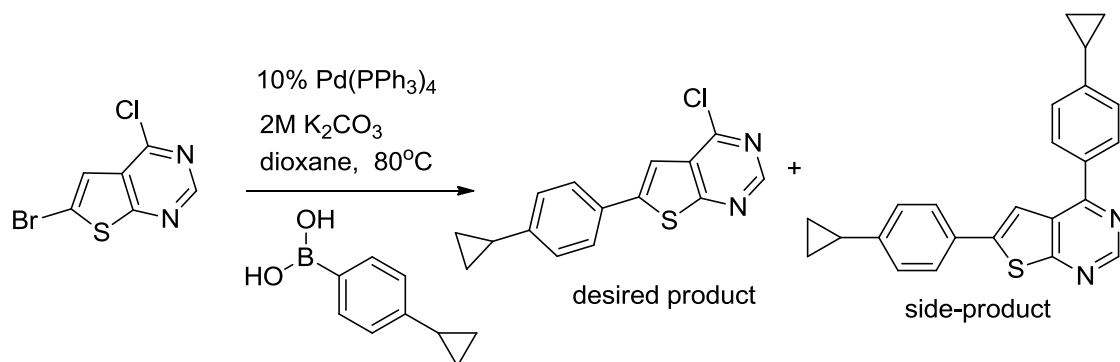
This compound was synthesized according to literature procedure:

Jang M.-J. *et. al. Bioorg. Med. Chem. Lett.* **2010**, 20, 844



Isolated 35mg (48%) as a pale blue powder

^1H NMR (400 MHz, CDCl_3) δ 8.83 (s, 1H), 7.50 (s, 1H).

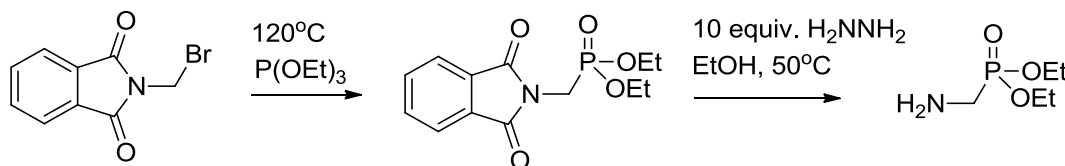
JDS09-102: 4-chloro-6-(4-cyclopropylphenyl)thieno[2,3-d]pyrimidine

A 100 mL RBF was charged with a magnetic stir bar, 6-bromo-4-chloro-2-thienylpyrimidine (755 mg, 3.03 mmol), (4-cyclopropylphenyl)boronic acid (588 mg, 3.63 mmol), $\text{Pd}(\text{PPh}_3)_4$ (350 mg, 0.303 mmol), capped with a rubber septum, evacuated and back-filled with Argon. 30 mL 1,4-dioxane was added to bring the concentration of aryl bromide to 0.1M and the solution was flushed again with Argon. 2M K_2CO_3 (3.78 mL, 7.56 mmol) was added via syringe and again the solution was flushed with Argon. The reaction was stirred at 80°C for 10 h. The crude was filtered through a plug of Celite, rinsed with 10 mL 1:1 EtOAc/Acetone and concentrated under vacuum. The residue was purified by silica gel chromatography using a CombiFlash instrument and a solvent gradient from hexanes to 10% EtOAc/hexanes. The desired product was isolated as a white powder (388 mg, 45%) along with 239 of impure bis-coupled side-product. ^1H NMR (500 MHz, CDCl_3) δ 8.77 (s, 1H), 7.58 (d, $J = 8.3$ Hz, 2H), 7.48 (s, 1H), 7.13 (d, $J = 8.3$ Hz, 2H), 1.93 (m, 1H), 1.04 (m, 2H), 0.76 (m, 2H). ^{13}C NMR (126 MHz, CDCl_3) δ 168.15, 153.75, 152.25, 146.60, 146.43, 131.28, 129.53, 126.68, 126.37, 113.35, 15.44, 9.92. MS (ESI): calcd 287.041; found 287.13 $[\text{M}+\text{H}]^+$

JDS09-105: diethyl (aminomethyl)phosphonate

This compound was synthesized according to literature procedure:

Meser A.M. *et. al. Chem. Eur. J.* **2008**, *14*, 7250

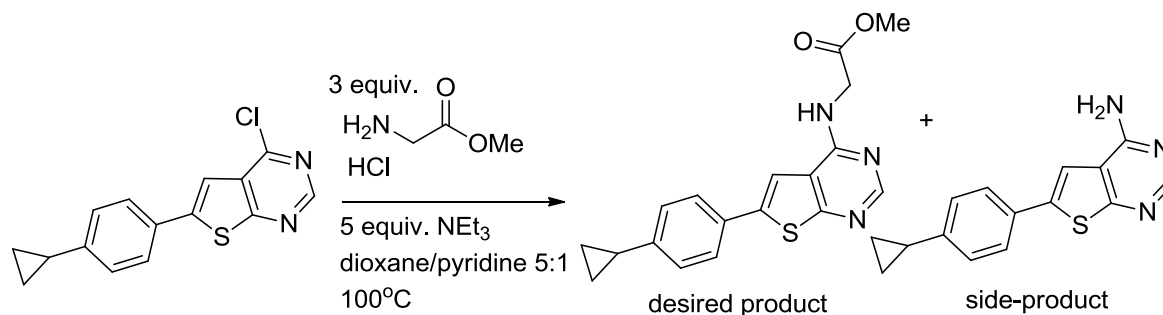


Isolated 616 mg (88% over two steps) as a colorless oil. ^1H NMR (500 MHz, CD_3CN) δ 4.11 – 3.98 (m, 4H), 2.90 (d, J = 10.6 Hz, 2H), 1.27 (t, J = 7.1 Hz, 6H).

General protocol for $\text{S}_{\text{N}}\text{Ar}$ reaction on 4-chloro-thienopyrimidine scaffold:

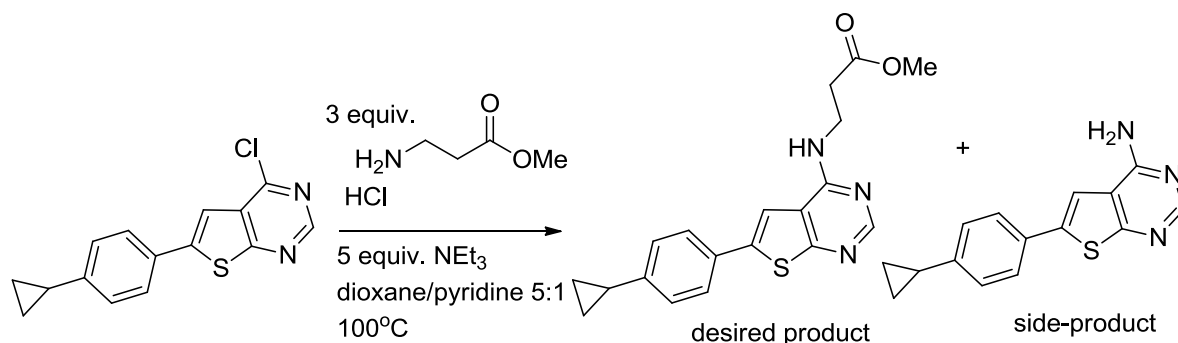
A solution of 4-chloro-6-(4-cyclopropylphenyl)thieno[2,3-d]pyrimidine (1 equivalent) and amine (1.5 equivalents) and triethylamine (2.5 equivalents) in anhydrous 1,4-dioxane was stirred at 75°C for 9 h, after which low conversion was observed by HPLC. An additional 2.5 equivalents was added and stirring was continued for 10 h at 100°C . Less than 50% conversion was observed by HPLC, therefore another 1.5 equivalents of amine and 1 mL of pyridine was added to the reaction and stirring was continued for an additional 22 h at 100°C . The reaction mixture was cooled down and concentrated under vacuum. The residue was purified by silica gel chromatography using a CombiFlash instrument and a solvent gradient from 1% EtOAc/hexanes to 100% EtOAc. The desired product was isolated along with the corresponding amine side-product.

JDS09-107: methyl 2-(((6-(4-cyclopropylphenyl)thieno[2,3-d]pyrimidin-4-yl)amino)acetate



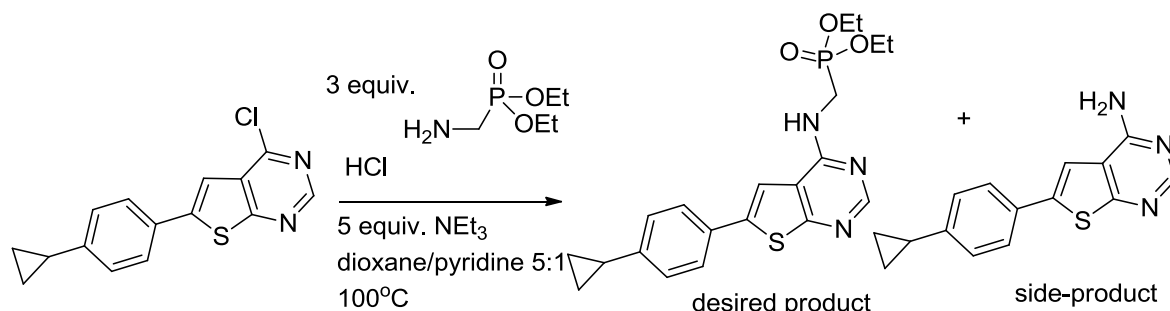
Isolated 13 mg (44%) as a colorless oil along with 15 mg of NH_2 -side-product. ^1H NMR (300 MHz, CDCl_3) δ 8.42 (s, 1H), 7.56 – 7.49 (m, 2H), 7.29 (s, 1H), 7.11 (d, J = 8.3 Hz, 2H), 5.92 (t, J = 4.8 Hz, NH), 4.40 (d, J = 5.2 Hz, 2H), 3.84 (s, 3H), 1.92 (m, 1H), 1.02 (m, 2H), 0.77 – 0.70 (m, 2H). ^{13}C NMR (75 MHz, CDCl_3) δ 171.20, 165.85, 155.75, 153.35, 145.13, 141.60, 130.53, 126.23 (2C), 117.92, 111.19, 52.58, 42.53, 15.32, 9.64. MS (ESI): calcd 340.112; found 340.01 $[\text{M}+\text{H}]^+$

JDS09-110: methyl 3-(((6-(4-cyclopropylphenyl)thieno[2,3-d]pyrimidin-4-yl)amino)propanoate



Isolated 13.2 mg (43%) as a colorless oil, along with 13 mg of NH₂-side-product. ¹H NMR (300 MHz, CDCl₃) δ 8.39 (s, 1H), 7.47 (d, *J* = 8.3 Hz, 2H), 7.17 (s, 1H), 7.04 (d, *J* = 8.3 Hz, 2H), 5.82 (t, *J* = 5.7 Hz, NH), 3.87 (m, 2H), 3.66 (s, 3H), 2.68 (t, *J* = 5.8 Hz, 2H), 1.92 – 1.76 (m, 1H), 0.99 – 0.89 (m, 2H), 0.72 – 0.61 (m, 2H). ¹³C NMR (75 MHz, CDCl₃) δ 173.45, 156.23, 153.59, 145.06, 141.21, 130.60, 126.22, 126.20, 111.21, 51.88, 36.24, 33.53, 15.31, 9.64. MS (ESI): calcd 354.128; found 354.26 [M+H]⁺

JDS09-111: diethyl (((6-(4-cyclopropylphenyl)thieno[2,3-d]pyrimidin-4-yl)amino)methyl)phosphonate

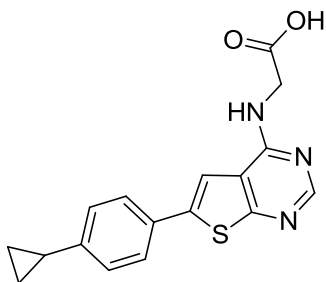


Isolated 21.6 mg (30%) as a colorless oil along with 5 mg of NH₂-side-product. ¹H NMR (300 MHz, CD₃OD) δ 8.06 (s, 1H), 7.37 (s, 1H), 7.25 (d, *J* = 8.3 Hz, 2H), 6.84 (d, *J* = 8.3 Hz, 2H), 3.97 – 3.82 (m, 6H), 1.70 – 1.59 (m, 1H), 1.03 (t, *J* = 7.1 Hz, 6H), 0.78 – 0.69 (m, 2H), 0.49 – 0.38 (m, 2H). ¹³C NMR (75 MHz, CD₃OD) δ 164.33, δ 156.28 (d, *J* = 2.3 Hz), 152.75, 145.22, 140.76, 130.28, 125.83, 125.58, 118.16, 112.58, 62.66 (d, *J* = 6.8 Hz), 35.29 (d, *J* = 158.0 Hz), 15.30 (d, *J* = 5.9 Hz), 14.65, 8.70. MS (ESI): calcd 418.135; found 418.29 [M+H]⁺

General procedure for saponification of methyl esters:

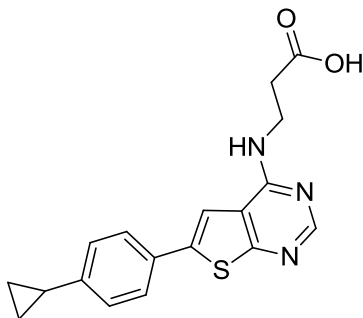
To an ice-cooled solution of methyl ester (1 equivalent) in 1:1 THF/MeOH was added 2M LiOH (5 equivalents) and the reaction was stirred at RT until complete consumption of the starting material as determined by HPLC. The reaction is acidified to pH=2 with 5M HCl and concentrated to dryness. The residue is suspended in an minimum of HPLC grade MeOH, carboxylic acid is precipitated with Milli-Q water and the suspension is aged 10 min on ice. The slurry is filtered and washed with 5mL cold Milli-Q water and twice with 5 mL distilled Et₂O; dried on high vacuum.

Inhibitor 8.8 (JDS09-119): 2-((6-(4-cyclopropylphenyl)thieno[2,3-d]pyrimidin-4-yl)amino)acetic acid



Isolated 3.4 mg (27%) as white powder. ¹H NMR (500 MHz, CD₃OD) δ 8.27 (s, 1H), 7.70 (s, 1H), 7.58 (d, *J* = 8.3 Hz, 2H), 7.15 (d, *J* = 8.3 Hz, 2H), 4.25 (s, 2H), 1.99 – 1.91 (m, 1H), 1.05 – 0.99 (m, 2H), 0.76 – 0.71 (m, 2H). ¹³C NMR (126 MHz, DMSO-d₆) δ 171.22, 164.48, 156.24, 153.78, 144.52, 138.09, 130.32, 126.18, 125.57, 117.60, 114.47, 104.57, 15.01, 9.79. MS (ESI): calcd 324.08067; found 324.08206 [M-H]⁻

Inhibitor 8.9 (JDS09-121): 3-((6-(4-cyclopropylphenyl)thieno[2,3-d]pyrimidin-4-yl)amino)propanoic acid

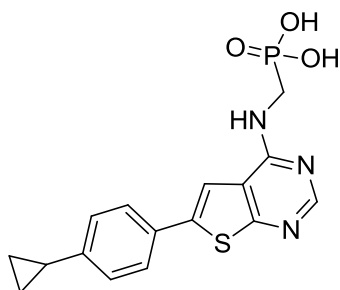


Isolated 9.7 mg (78%) as a white powder. ^1H NMR (500 MHz, DMSO- d_6) δ 9.09 (bs, NH), 8.54 (s, 1H), 8.16 (s, 1H), 7.59 – 7.51 (m, 2H), 7.21 (d, J = 8.3 Hz, 2H), 3.75 (dd, J = 12.3, 6.7 Hz, 2H), 2.69 (t, J = 6.9 Hz, 2H), 1.97 (m, 1H), 1.04 – 0.97 (m, 2H), 0.77 – 0.69 (m, 2H). ^{13}C NMR (126 MHz, DMSO- d_6) δ 173.08, 155.58, 150.72, 145.69, 140.56, 129.94, 126.76, 126.10, 124.63, 118.40, 115.28, 37.51, 33.50, 15.45, 10.33. MS (ESI): calcd 338.09632; found 338.09726 $[\text{M-H}]^-$

General procedure of deprotection of diethyl phosponate esters:

A 12 mL Teflon lined screw cap vial was charged with the tetra-ethyl bisphosphonate compound, dissolved in 5 mL distilled DCM and cooled in an ice bath. Bromotrimethyl silane (15 equivalents) was added via syringe and the reaction mixture was stirred at RT for 5-7 days. The reaction mixture was transferred to a 10 mL recovery flask and concentrated in vacuo (satd. NaHCO_3 in receiving flask). To the resulting oil was added 2 mL of HPLC-grade MeOH and concentrated in vacuo, this was repeated a total of five times. The crude thus obtained was suspended in a minimum amount of HPLC-grade MeOH, the mixture was sonicated and the desired compound was precipitated out of solution by the addition of Milli-Q water. The slurry was filtered and the cake washed twice with Milli-Q water, twice with ACS-grade isopropanol twice with distilled THF, twice with distilled DCM and twice with distilled Et_2O . The residue was then dried under high vacuum to obtain the desired product.

Inhibitor 8.7 (JDS09-123): (((6-(4-cyclopropylphenyl)thieno[2,3-d]pyrimidin-4-yl)amino)methyl)phosphonic acid



Isolated 12.5 mg (90%) as a white powder. ^1H NMR (500 MHz, D_2O) δ 8.09 (s, 1H), 7.47 (s, 1H), 7.33 (d, J = 8.2 Hz, 2H), 6.89 (d, J = 8.3 Hz, 2H), 3.47 (d, J = 13.3 Hz, 2H), 1.85 – 1.78 (m, 1H), 1.03 – 0.97 (m, 2H), 0.68 – 0.62 (m, 2H). ^{13}C NMR (126 MHz, D_2O) δ

162.33, δ 156.29 (d, $J = 9.4$ Hz), 152.27, 144.81, 139.91, 129.39, 125.25, 125.13, 118.20, 113.05, 40.36 (d, $J = 136.2$ Hz), 14.55, 9.49. ^{31}P NMR (81 MHz, D_2O) δ 13.67 (s). MS (ESI): calcd 360.05717; found 360.05840 $[\text{M-H}]^-$

8.11.2 Enzymatic inhibition assays:

The **M1** hFPPS enzymatic assay was performed as described in chapter 3, except the incubation time was reduced to 8 min.

The **M2** hFPPS enzymatic assay was performed as described in chapter 7.

8.11.3 DSF protocol for hFPPS:

Expression and purification of recombinant human FPPS was performed as previously described in chapters 1 and 4.

Triton X-100 was purchased from Sigma Aldrich (cat. # T8787). SYPRO[®] Orange (Invitrogen) was purchased as a 5000x solution in DMSO from Sigma Aldrich (cat. # S5692). Pyrophosphate (cat. # P8010) and inorganic phosphate (cat. # S7907) were purchased from Sigma Aldrich.

IPP was purchased as its tetra ammonium salt from Isoprenoids LC.

Experiments were performed with an iCycler RT-PCR instrument with an iQ5 detector (Bio-Rad). The samples were irradiated at 495 nm (excitation wavelength) and the fluorescence was measured at 610 nm, while heating in a gradient from 30°C to 90°C in 0.5°C increments with a 10 s dwelling time.

Samples were prepared in triplicate on standard, unskirted PCR plates (Axygen) in a final volume of 40 μL containing 4 μM hFPPS (4 ng/ μL His-tag hFPPS), 10 mM HEPES (pH 7.5), 5x SYPRO[®] Orange dye, 10-100 mM NaCl and 0-5 mM MgCl_2 , 0-0.01% Triton X-100. Inhibitors and ligands were included in a range from 4 to 400 μM .

9 Contributions to knowledge

9.1 Summary of accomplishments

The goal of the research project described in this thesis was to develop novel hFPPS inhibitors with improved biopharmaceutical properties, particularly decreased bone-affinity and improved cell-based potency.

Others in the field have attempted to make more lipophilic hFPPS inhibitors by attaching greasy *n*-alkyl chains on the pyridine core (i.e. **1.1**, **Figure 9.1**).¹ However, the concomitant increase in steric size severely comprised the selectivity of these bisphosphonates for hFPPS over hGGPPS (compare RIS vs. **1.1**, **Table 9.1**). Over the course of our SAR studies we have identified that the *p*-cyclopropoxyphenyl moiety to be a suitable substituent on the pyridine core, *meta* with respect to the bisphosphonate. Our biophysical studies suggest that this substituent engages in several specific interactions in the allylic subpocket of the enzyme and therefore selectivity for hFPPS is retained. Furthermore, it has been reported that removal of the C α -hydroxyl moiety results in a ~6-fold reduction in inhibition potency (compare RIS vs. **9.1**, **Table 9.1**).² We have found that an amine linker between the pyridine core and bisphosphonate is an appropriate replacement, resulting compounds, such as **5.15**, that are equipotent to risedronate. Lastly, replacement of a *single* phosphonate with a carboxylic acid on the risedronate scaffold almost completely nullifies its ability to inhibit hFPPS (44.000-fold loss in potency, RIS vs. **9.2**, **Table 9.1**).² In contrast, on our scaffold, replacement of *both* phosphonates results in a 15.000-fold reduction in enzymatic potency. Therefore our novel hFPPS inhibitors can serve as promising leads for further investigations towards the replacement of the bisphosphonate moiety with potential bioisosteres.

An ¹H NMR assay that measures affinity for the bone mineral hydroxyapatite was adopted from the scientific literature,³ and used to compare risedronate and **5.15** (**Figure 9.1**), which are equipotent in both our *in vitro* hFPPS inhibition assays (this work was performed

by Demetrios Gritzalis an MSc candidate in the Tsantrizos research group). The results are summarized in **Figure 9.2**; (a) The ratio of signals 1:1.7 corresponds to H₆ of RIS and 2H' of **5.15** in the absence of hydroxyapatite. (b) A decrease in signal intensity was observed upon addition of 0.2 mg of hydroxyapatite (indicating preferential binding of RIS to hydroxyapatite) to give signal ratio of 1:2.7 (H₆ of RIS: 2H' of **5.15**). (c) A further addition of 0.2 mg hydroxyapatite (a total of 0.4 mg) to the same sample, resulted in a ratio of 1:3.8 (H₆ of RIS: 2H' of **5.15**). The results of this study strongly suggest that we have successfully decreased the bone affinity for our inhibitor **5.15** while maintaining hFPPS inhibition activity, compared to the drug risedronate.

Preliminary anti-proliferation and cytotoxic effects of several hFPPS inhibitors were determined using three human MM cell lines, the data is summarized in **Table 9.1** (this work performed by X.F. Huang in the laboratory of Dr. M. Sebag, MUHC, Montreal). Cell viability was determined by MTT staining, and reductions in cell growth were noted with the commercial drugs zoledronate and risedronate. Gratifyingly, the median effective concentrations for 50% growth inhibition (EC₅₀) were consistently lower for compound **4.7** and **5.15**, as compared to those of zoledronate and risedronate. The improved cell-based potency is most likely due to the reduced polarity and hydrophilicity of these inhibitors. The allosteric inhibitor **1.5** developed by Novartis proved to be completely inactive against all three MM cell lines.

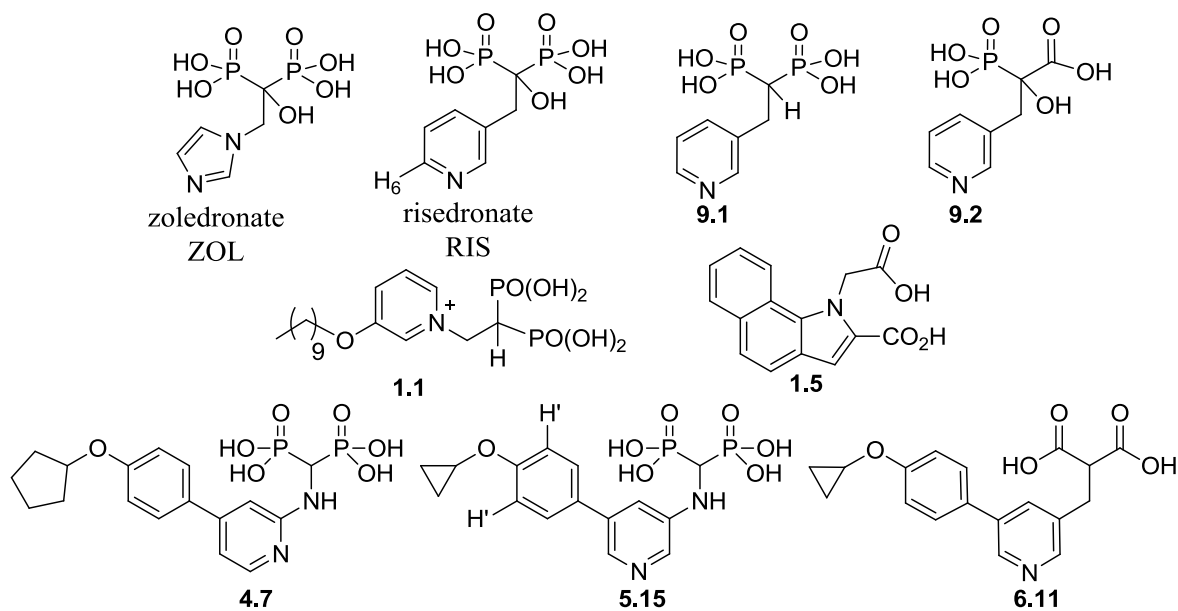


Figure 9.1: Selected inhibitors of hFPPS and hGGPPS.

Compound	hFPPS IC ₅₀ (nM)		hGGPPS IC ₅₀ (nM)	Multiple Myeloma cells EC ₅₀ (μM)		
	M1	M2		JJN3	RPMI- 8226	KMS 28PE
ZOL	4.1	<i>nd</i>	IN	9.4	10.5	6.4
RIS	11 (5.7)	5.2	IN	10.0	<i>nd</i>	10.6
9.1	35	-	-	-	-	-
9.2	253.000	-	-	-	-	-
1.1	100	-	280	-	-	-
1.5	~20.000	920	IN	IN	IN	IN
4.7	32	<i>nd</i>	IN	8.6	3.6	3.2
5.15	16	18	IN	<i>nd</i>	6.8	<i>nd</i>
6.11	<i>nd</i>	~80.000	IN	<i>nd</i>	<i>nd</i>	<i>nd</i>

Table 9.1: Enzymatic inhibition data and anti-proliferation activity data for key analogs.

Values in *italics* are reported data from the literature. The EC₅₀ values represent the average of $n \geq 8$ determinations with R^2 in the range of 0.97– 0.98. IN = inactive (IC₅₀ > 100 μM).

(*nd* = not determined)

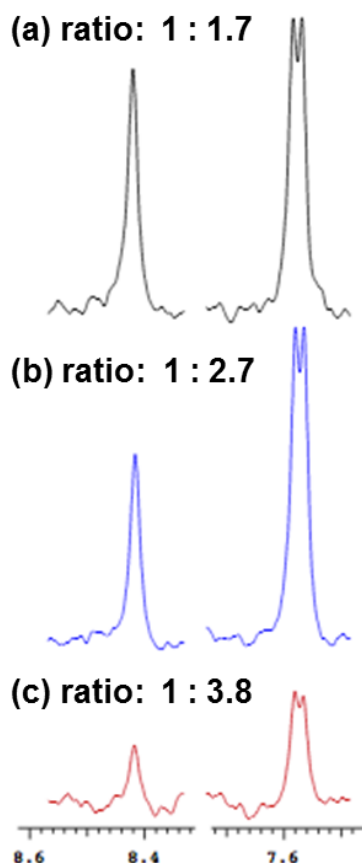


Figure 9.2: ^1H NMR bone-affinity assay for risedronate (signal at 8.41 ppm, H_6) and inhibitor **5.15** (signal at 7.59 ppm, $2\text{H}'$). (a) no additive; (b) with 0.2 mg hydroxyapatite; (c) with 0.4 mg hydroxyapatite.

References:

- (1) Zhang, Y.; Cao, R.; Yin, F.; Hudock, M. P.; Guo, R.-T.; Krysiak, K.; Mukherjee, S.; Gao, Y.-G.; Robinson, H.; Song, Y.; No, J. H.; Bergan, K.; Leon, A.; Cass, L.; Goddard, A.; Chang, T.-K.; Lin, F.-Y.; Beek, E. V.; Papapoulos, S.; Wang, A. H. J.; Kubo, T.; Ochi, M.; Mukkamala, D.; Oldfield, E.; Lipophilic Bisphosphonates as Dual Farnesyl/Geranylgeranyl Diphosphate Synthase Inhibitors: An X-ray and NMR Investigation *J. Am. Chem. Soc.* **2009**, *131*, 5153.
- (2) Marma, M. S.; Xia, Z.; Stewart, C.; Coxon, F.; Dunford, J. E.; Baron, R.; Kashemirov, B. A.; Ebetino, F. H.; Triffitt, J. T.; Russell, R. G. G.; McKenna, C. E.; Synthesis and Biological Evaluation of α -Halogenated Bisphosphonate and Phosphonocarboxylate Analogues of Risedronate *J. Med. Chem.* **2007**, *50*, 5967.
- (3) Jahnke, W.; Henry, C.; An in vitro assay to measure targeted drug delivery to bone mineral *ChemMedChem* **2010**, *5*, 770.

9.2 Claims to original knowledge

- a) An *in silico* screening was performed to select a small library of substituted bisphosphonates for synthesis. Biological evaluation identified hFPPS inhibitors with IC₅₀ values of approximately 0.5 μ M. Simultaneously, the SAR data showed that *meta* substitution between the bisphosphonate moiety, the heterocyclic side chain and the pyridine nitrogen is best suited to complement the hFPPS active site. Furthermore, ¹H NMR line broadening studies showed that our analogs are competitive with the drug risedronate for binding to the hFPPS.
- b) *Proof-of-concept* 2,5-disubstituted-pyridine-3-bisphosphonate derivatives were successfully synthesized. However, these model compounds exhibited very weak activity in inhibiting either hFPPS or hGGPPS.
- c) Lead optimization efforts and structural studies lead to the discovery that an amine linker between the pyridine core and the bisphosphonate is strongly preferred, most likely due to rotational constraint resulting in a favored planar conformation similar to the bio-active conformation. Furthermore, SAR data revealed that the pyridine nitrogen can be positioned either *ortho* or *meta* to the bisphosphonate moiety without affecting enzymatic potency, as hydrogen bonding opportunities are available at both sites.
- d) Further lead optimization efforts demonstrated that a direct aryl-aryl connection between the pyridine core and aromatic substituent is best suited for binding to the expanded allylic sub-pocket. Furthermore, the *in vitro* enzymatic potency of novel inhibitors was improved to IC₅₀ ~ 15 nM (i.e. equipotent to the drug risedronate in our assay), despite lacking a hydroxyl moiety at the bisphosphonate Ca. Computational docking results strongly suggest that the improved potency is due to a novel CH/ π -interaction with capping phenyl Phe 112. Two hits were discovered, analogs **5.19** and **5.20** that are active against hGGPPS with an enzymatic potency of IC₅₀ ~ 5 μ M.
- e) A number of bisphosphonate bioisosteres were investigated and resulted in weak inhibitors of hFPPS (IC₅₀ ~80-100 μ M).

- f) A custom hFPPS enzymatic inhibition assay (labeled as **M2**) was developed with significantly improved (~20-fold) sensitivity for *non*-bisphosphonate hFPPS inhibitors.
- g) A DSF protocol was developed and validated for hFPPS. The technique was applied to determine a linear, positive correlation between the stabilizing effect of pyridine-based hFPPS inhibitors and their *in vitro* enzymatic potency. Furthermore, parallel titration DSF experiments with an inhibitor and secondary ligands were established as a valid method to distinguish binding to the active site vs. an allosteric pocket of hFPPS. These studies led to the discovery of a novel class of thienopyrimidine-based hFPPS allosteric inhibitors.

9.3 Peer reviewed publications

Ternary complex structures of human farnesyl pyrophosphate synthase bound with a novel inhibitor and secondary ligands provide insights into the molecular details of the enzyme's active site closure

Park, J.; Lin, Y.-S.; De Schutter, J.W.; Tsantrizos, Y.S.; Berghuis, A.M.

BMC Structural Biology **2012**; *in press*

Design of Potent Bisphosphonate Inhibitors of the Human Farnesyl Pyrophosphate Synthase *via* Targeted Interactions with the Active Site “Capping” Phenyls

De Schutter, J.W.; Shaw, J.; Lin, Y.-S.; Tsantrizos Y.S.

Bioorg. Med. Chem. **2012**, 20, 5583-5591

Design and Synthesis of Active Site Inhibitors of the Human Farnesyl Pyrophosphate Synthase: Apoptosis and Inhibition of ERK Phosphorylation in Multiple Myeloma Cells
Lin, Y.-S.; Park, J.; De Schutter, J.W.; Huang, X.-F.; Berghuis, A.; Sebag, M.; Tsantrizos, Y.S.

J. Med. Chem. **2012**, 55, 3201-3215

Toward a Computational Tool Predicting the Stereochemical Outcome of Asymmetric Reactions. Development of the Molecular Mechanics-Based Program ACE and Application to Asymmetric Epoxidation Reactions

Weill, N.; Corbeil, C.; De Schutter, J.W.; Moitessier, N.

J. Comp. Chem. **2011**, 32, 2878-2889

Novel bisphosphonate inhibitors of the human farnesyl pyrophosphate synthase

De Schutter, J.W.; Zaretsky S.; Welbourn, S.; Pause, A.; Tsantrizos Y.S.

Bioorg. Med. Chem. Lett. **2010**, 20, 5781-5786

9.4 Patent applications

Thienopyrimidine Inhibitors of farnesyl and/or geranylgeranyl pyrophosphate synthase

Y. S. Tsantrizos, A. M. Berghuis, J.W. De Schutter, C.-Y. Leung, J. Park, M. Sebag

(filed on November 20th, **2012**; serial number 61/728,489):

Heterocyclyl-pyridinyl-based Bisphosphonic Acid, Pharmaceutically Acceptable Salt Thereof, Composition Thereof and Method of Use Thereof

Tsantrizos, Y.S.; De Schutter, J.W.; Lin, Y.-S.

PCT/CA2001/050322; filed May 18, **2011**

9.5 Conference proceedings

J.W. De Schutter, Y.-S. Lin, J. Park, A. Berghuis and Y.S. Tsantrizos

Human Farnesyl Pyrophosphate Synthase: New Opportunities for a Challenging Therapeutic Target (*poster presentation*)

243rd ACS national meeting and exposition, March **2012**, San Diego, California, USA

J.W. De Schutter, Z. Hu and Y.S. Tsantrizos

New Insights into Ligand Interactions with Human Farnesyl Pyrophosphate Synthase through Differential Scanning Fluorimetry (*poster presentation*)

Annual GRASP/MSBM Symposium, November **2011**, Montreal, QC, Canada

J.W. De Schutter and Y.S. Tsantrizos

Human Farnesyl Pyrophosphate Synthase – New Opportunities for a Challenging Therapeutic Target (*oral presentation*)

94th Canadian Chemistry Conference and Exhibition, June **2011**, Montreal, QC, Canada

J.W. De Schutter and Y.S. Tsantrizos

Novel Inhibitors of Human Farnesyl Pyrophosphate Synthase; *in Silico* Design, Synthesis, Biological Evaluation and NMR studies (*oral presentation*)

Congrès de l'ACFAS, May **2011**, Sherbrooke, QC, Canada

J.W. De Schutter and Y.S. Tsantrizos

Novel Inhibitors of Human Farnesyl Pyrophosphate Synthase; *in Silico* Design, Synthesis, Biological Evaluation and NMR studies (*oral presentation*)

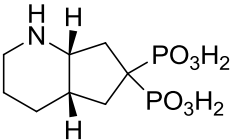
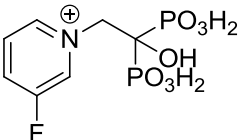
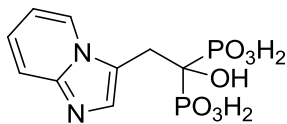
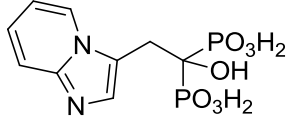
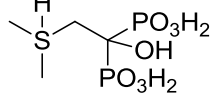
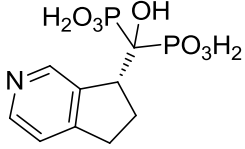
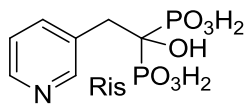
Annual GRASP/MSBM Symposium, November **2010**, Montreal, QC, Canada

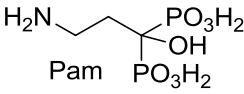
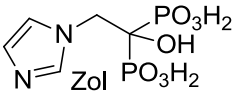
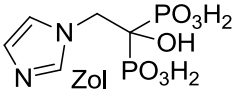
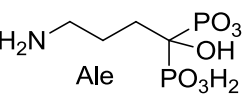
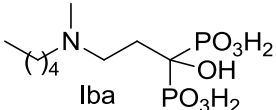
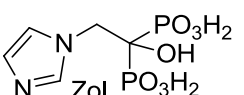
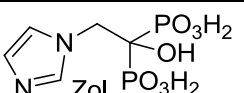
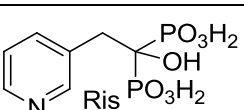
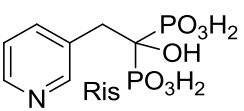
J.W. De Schutter and Y.S. Tsantrizos

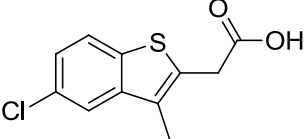
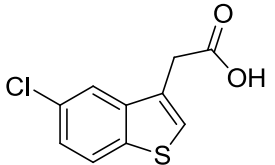
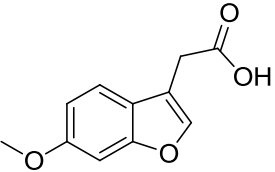
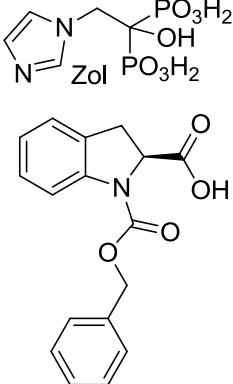
Novel Inhibitors of Human Farnesyl Pyrophosphate Synthase; *in Silico* Design, Synthesis, Biological Evaluation and NMR studies (*oral presentation*)

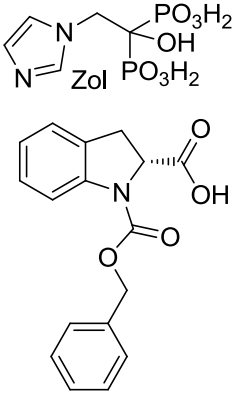
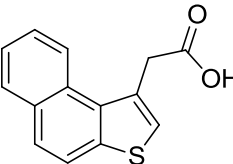
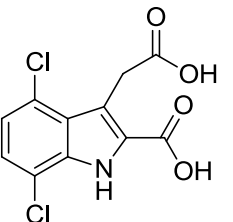
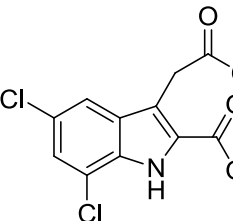
93rd Canadian Chemistry Conference and Exhibition, June **2010**, Toronto, ON, Canada

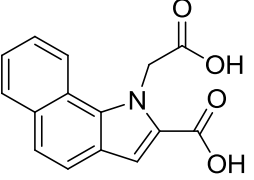
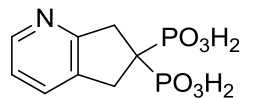
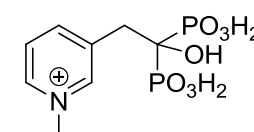
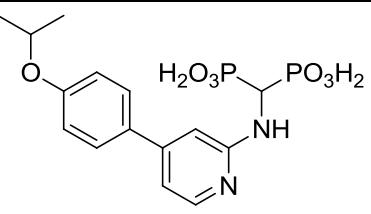
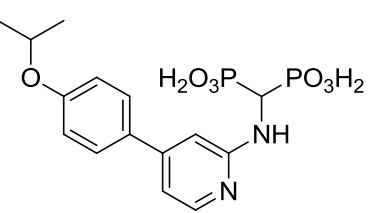
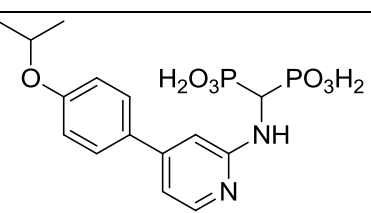
10 Appendices

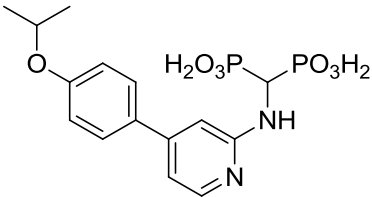
PDB code	protein	resolution (Å)	additives	ligand	reference	Principal author	Notes
3CP6	hFPPS (T201A)	1.95	Mg			U. Oppermann	
2OPM	hFPPS	2.40	Mg, PO4		<i>J. Am. Chem. Soc.</i> 2009 , p5153	E. Oldfield	ligand overlaps with 3RYE
3B7L	hFPPS	1.95	Mg			U. Oppermann	4 Mg in active site
2VF6	hFPPS	2.10	Mg			M. Pokross	
2OPN	hFPPS	2.70	Mg, PO4			E. Oldfield	invalid Lewis structure protein preparation failed
2RAH	hFPPS	2.00	Mg, SO4			M. Pokross	only 1 Mg in active site
2QIS	hFPPS (T210S)	1.80	Mg			U. Oppermann	
2F7M	hFPPS	2.30	PO4	apo	<i>ChemMedChem</i> 2006 , p273	W. Jahnke (Novartis)	

2F89	hFPPS	2.60	Mn, PO4	 Pam	<i>ChemMedChem</i> 2006 , p273	W. Jahnke (Novartis)	
2F8C	hFPPS	2.20	Mg, PO4	 Zol	<i>ChemMedChem</i> 2006 , p273	W. Jahnke (Novartis))	
2F8Z	hFPPS	2.60	Mg, IPP	 Zol	<i>ChemMedChem</i> 2006 , p273	W. Jahnke (Novartis)	
2F92	hFPPS	2.15	Zn, PO4	 Ale	<i>ChemMedChem</i> 2006 , p273	W. Jahnke (Novartis)	
2F94	hFPPS	1.94	Zn, PO4	 lba	<i>ChemMedChem</i> 2006 , p273	W. Jahnke (Novartis)	ligand pierces GPP pocket
2F9K	hFPPS	2.06	Zn, PO4	 Zol	<i>ChemMedChem</i> 2006 , p273	W. Jahnke (Novartis)	
1ZW5	hFPPS	2.30	Mg, IPP	 Zol		U. Oppermann	
1YV5	hFPPS	2.00	Mg, PO4	 Ris		U. Oppermann	
1YQ7	hFPPS	2.20	Mg, PO4	 Ris		U. Oppermann	

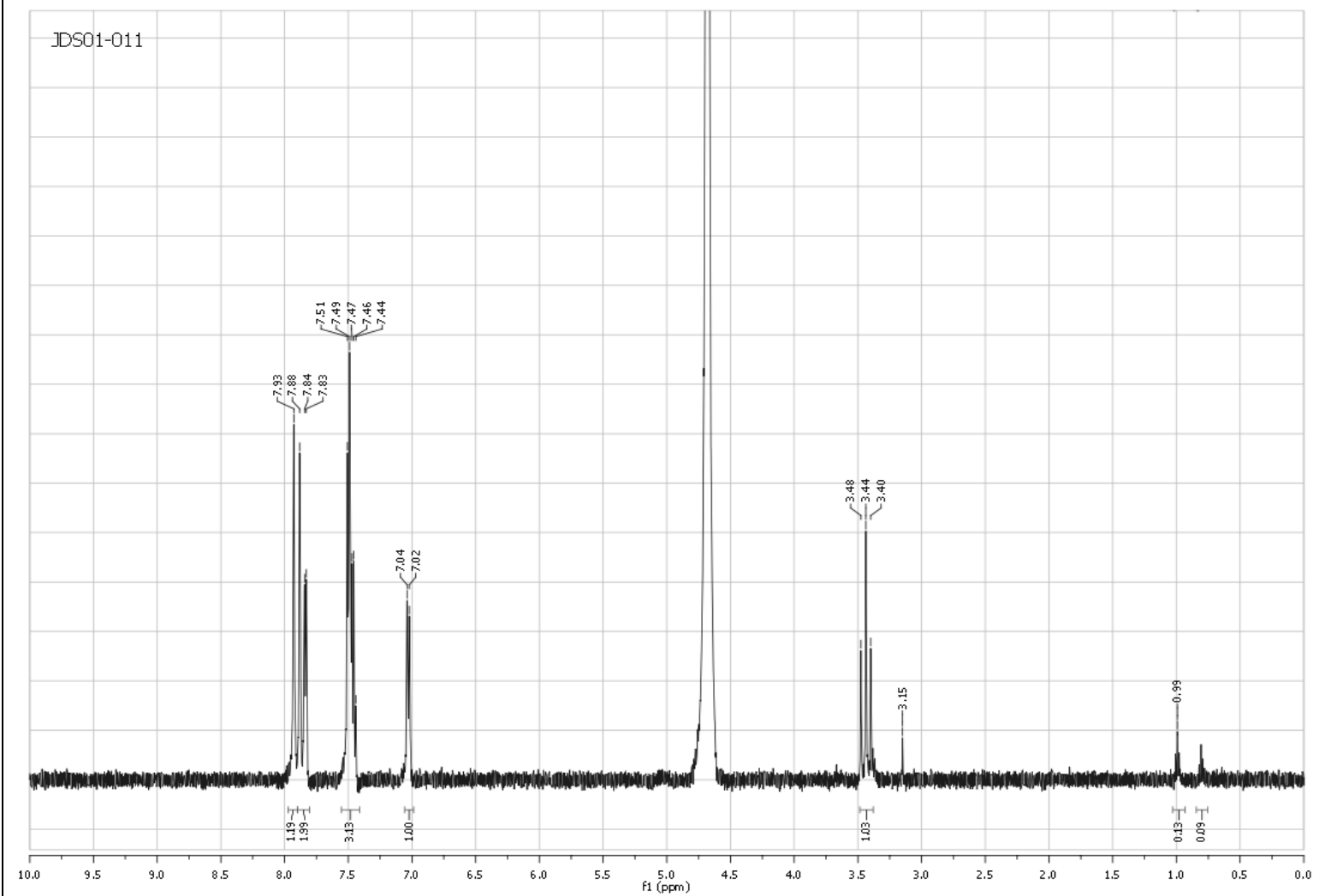
3N1V	hFPPS	2.18	PO4		<i>Nat. Chem. Bio.</i> 2010 , p660	W. Jahnke (Novartis)	ligand binds twice: allosteric site and protein surface
3N1W	hFPPS	2.56	PO4		<i>Nat. Chem. Bio.</i> 2010 , p660	W. Jahnke (Novartis)	
3N3L	hFPPS	2.74	PO4		<i>Nat. Chem. Bio.</i> 2010 , p660	W. Jahnke (Novartis)	ligand binds twice: allosteric site and protein surface
3N45	hFPPS	1.88	Mg, PO4		<i>Nat. Chem. Bio.</i> 2010 , p660	W. Jahnke (Novartis)	

3N46	hFPPS	2.35	Mg, PO4		<i>Nat. Chem. Bio.</i> 2010 , p660	W. Jahnke (Novartis)	
3N49	hFPPS	2.50	PO4		<i>Nat. Chem. Bio.</i> 2010 , p660	W. Jahnke (Novartis)	
3N5H	hFPPS	2.20	PO4		<i>Nat. Chem. Bio.</i> 2010 , p660	W. Jahnke (Novartis)	ligand binds twice: allosteric site and protein surface
3N5J	hFPPS	2.35	PO4		<i>Nat. Chem. Bio.</i> 2010 , p660	W. Jahnke (Novartis)	ligand binds twice: allosteric site and protein surface

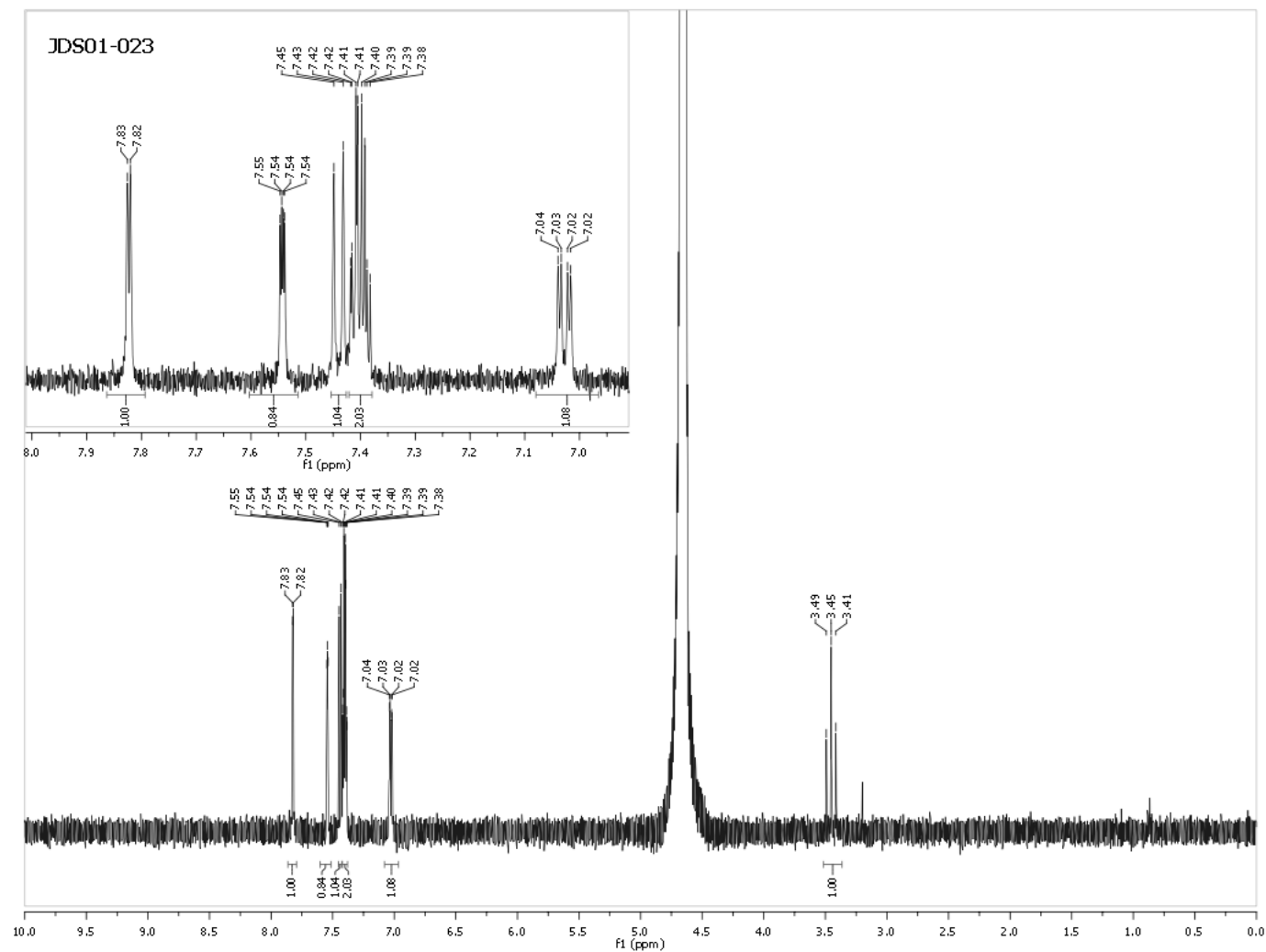
3N6K	hFPPS	2.25	PO4		<i>Nat Chem. Bio.</i> 2010 , p660	W. Jahnke (Novartis)	
3S4J	hFPPS	1.95	Mg, SO4			M. Pokross	
3RYE	hFPPS	2.1	Mg, SO4			M. Pokross	ligand overlaps with 2OPM
4DEM	hFPPS	1.80	Mg		<i>J. Med. Chem.</i> 2012 , p5583	Y.S. Tsantrizos	
4H5C	hFPPS	na	Mg, Pi			A.M. Berghuis	
4H5D	hFPPS	na	Mg, PPi			A.M. Berghuis	

4H5E	hFPPS	<i>na</i>	Mg, IPP			A.M. Berghuis	
------	-------	-----------	---------	--	--	------------------	--

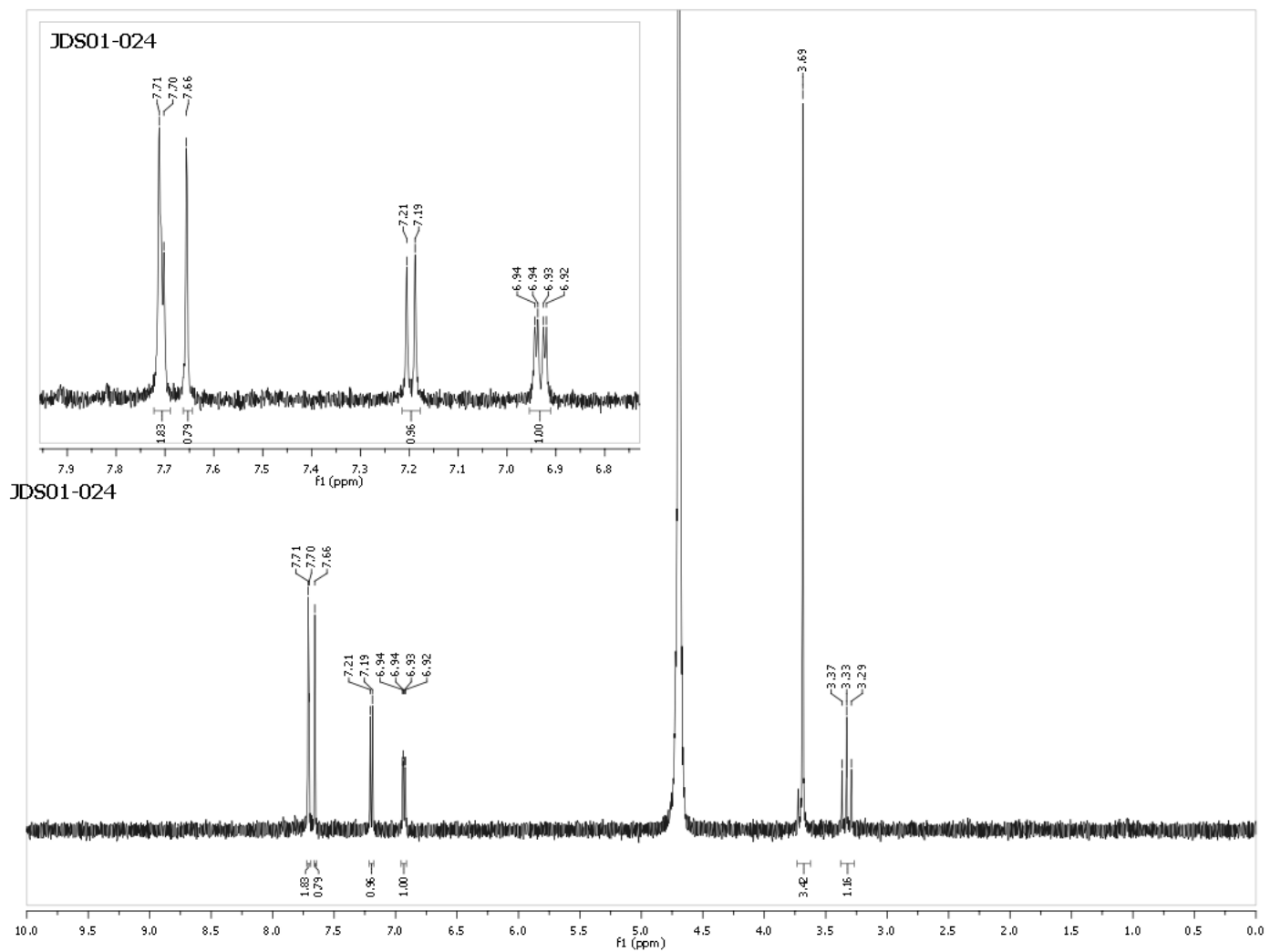
JDS01-011



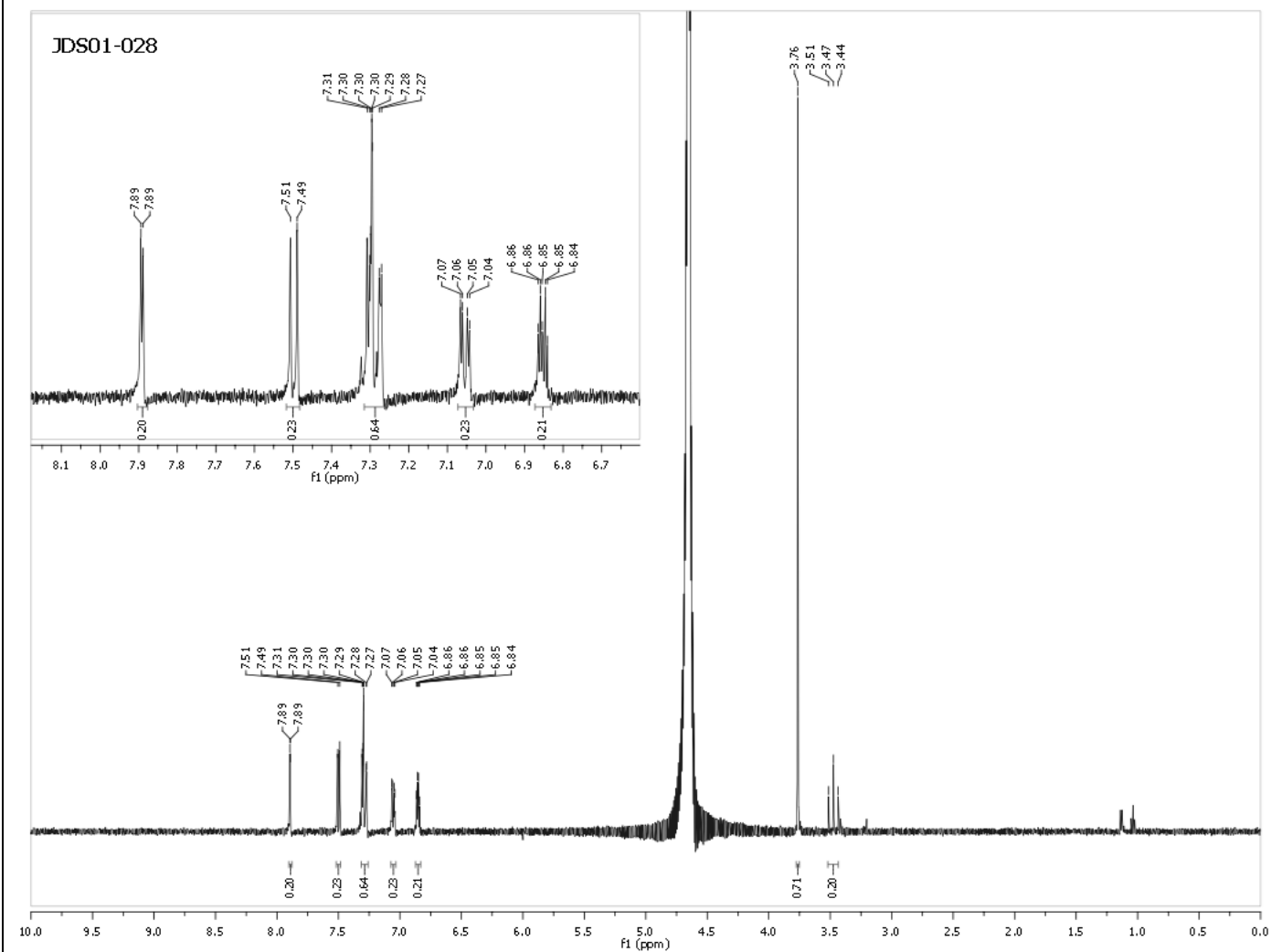
JDS01-023



JDS01-024

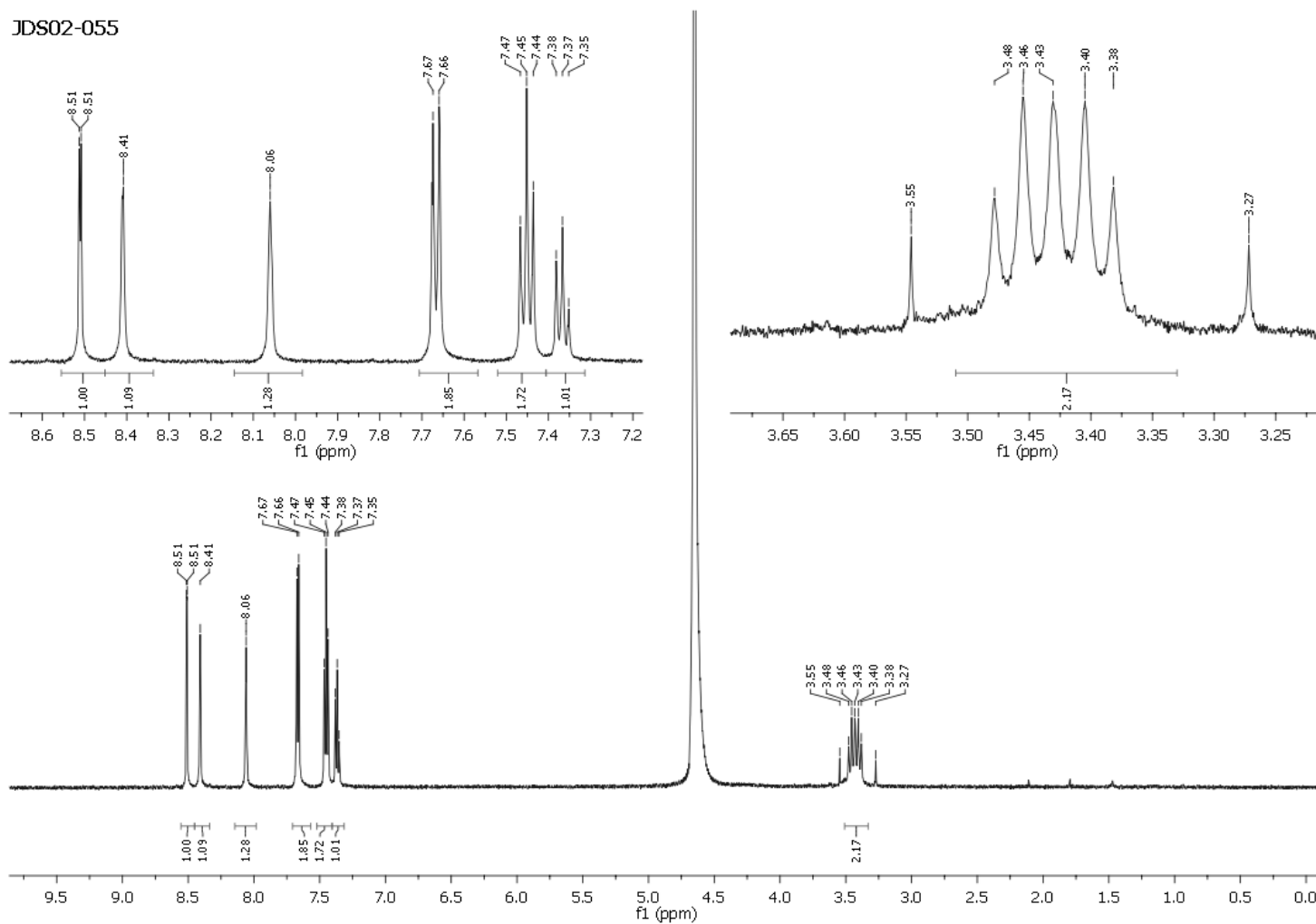


JDS01-028



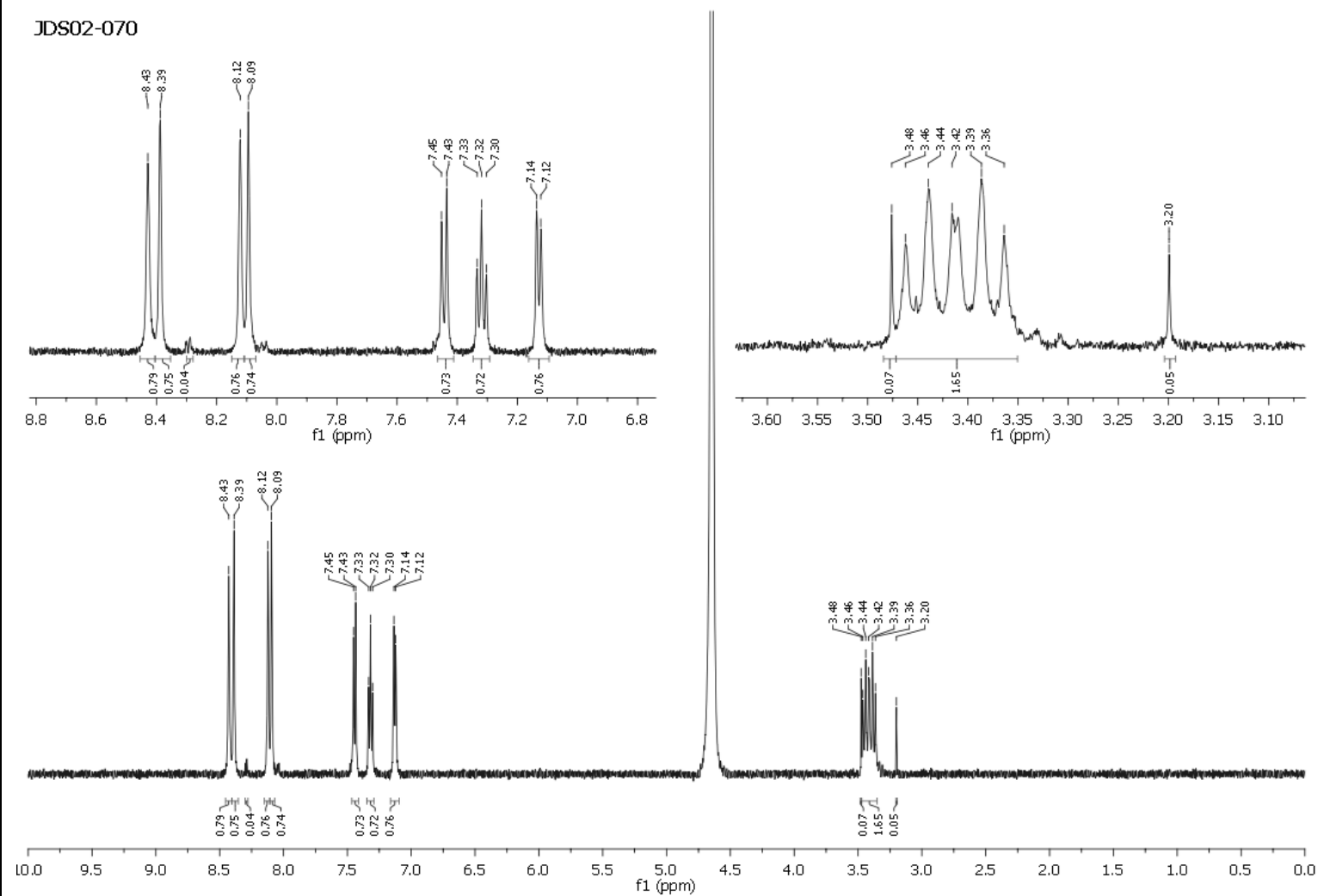
JDS02-055

JDS02-055

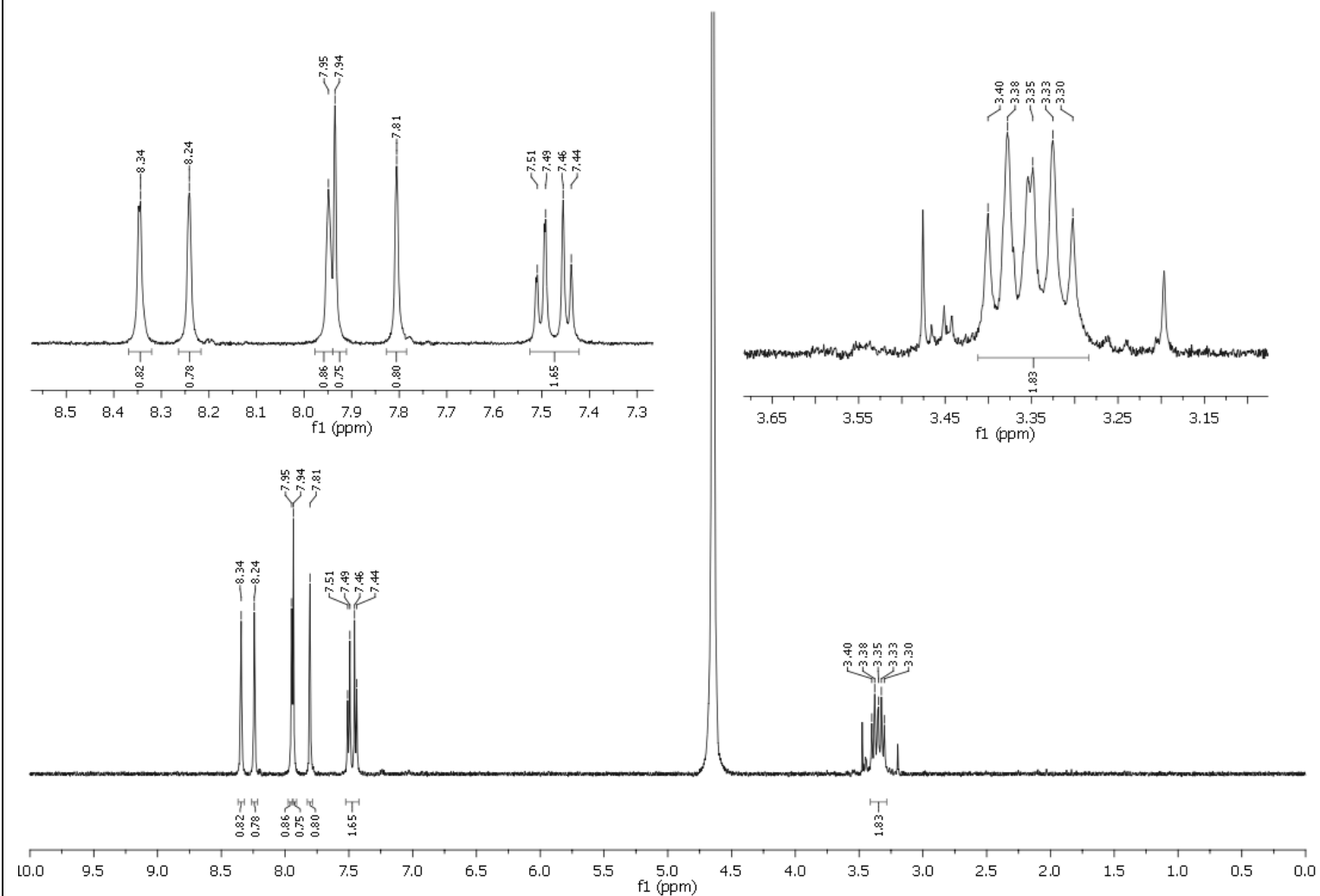


JDS02-070

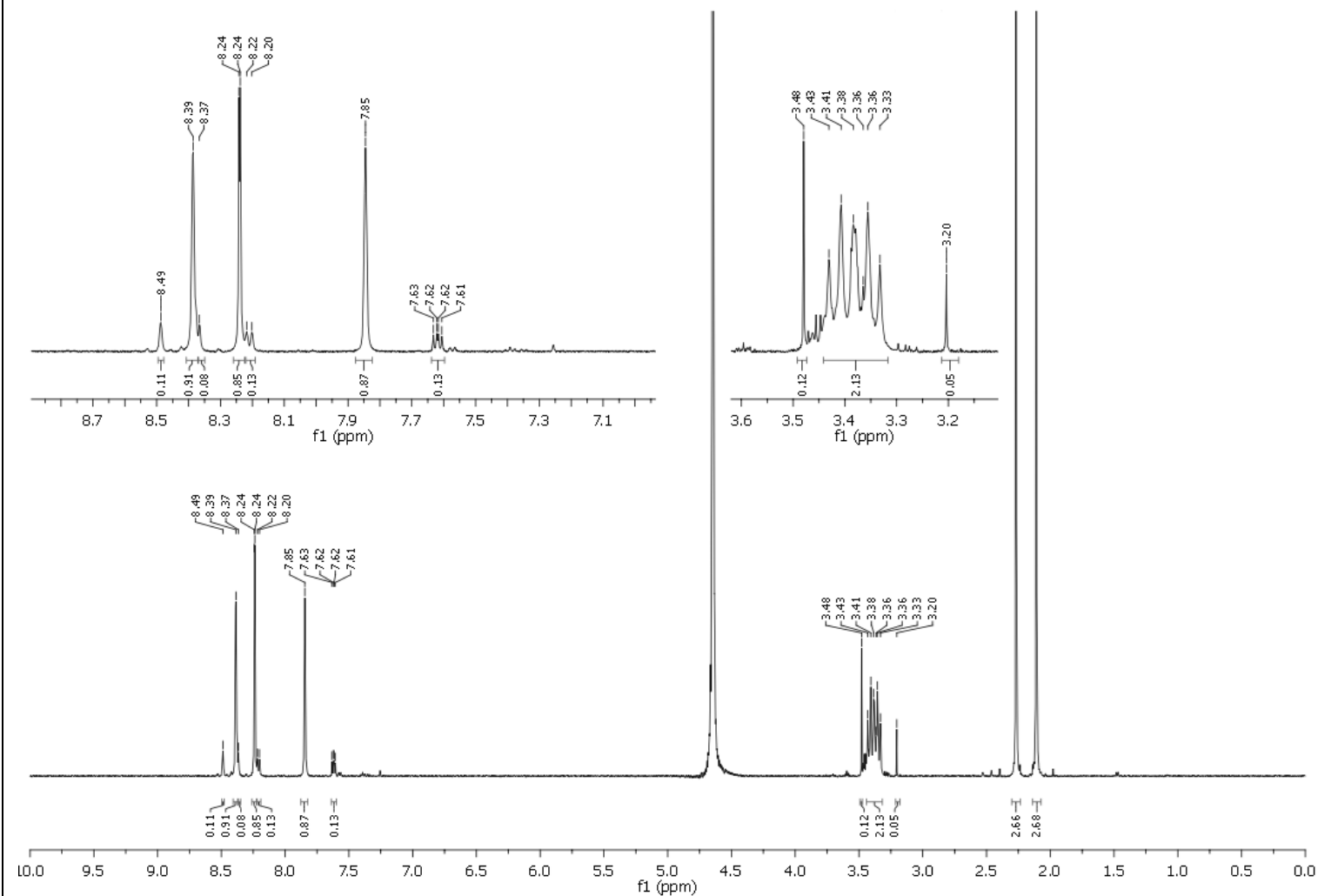
JDS02-070



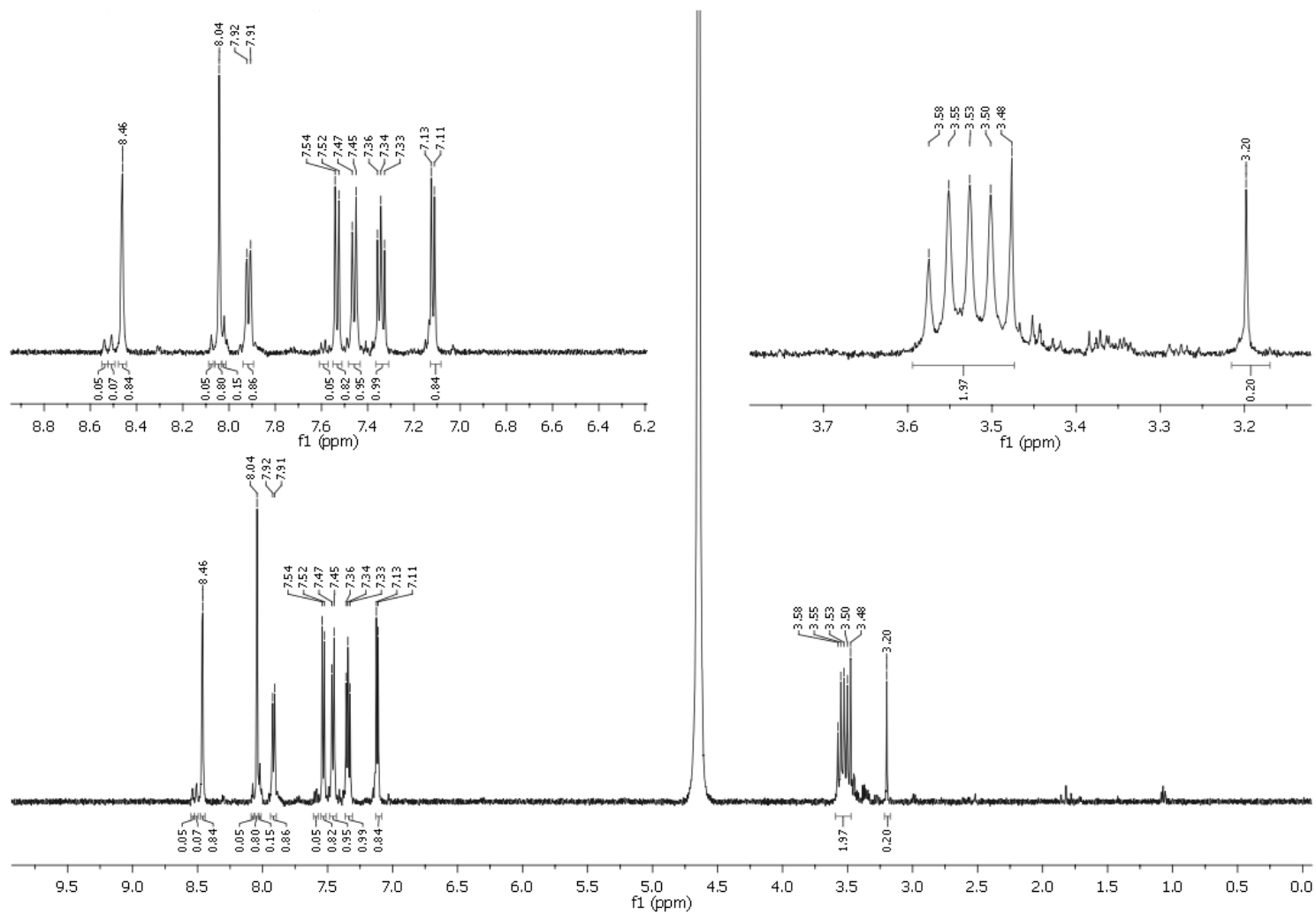
JDS02-071



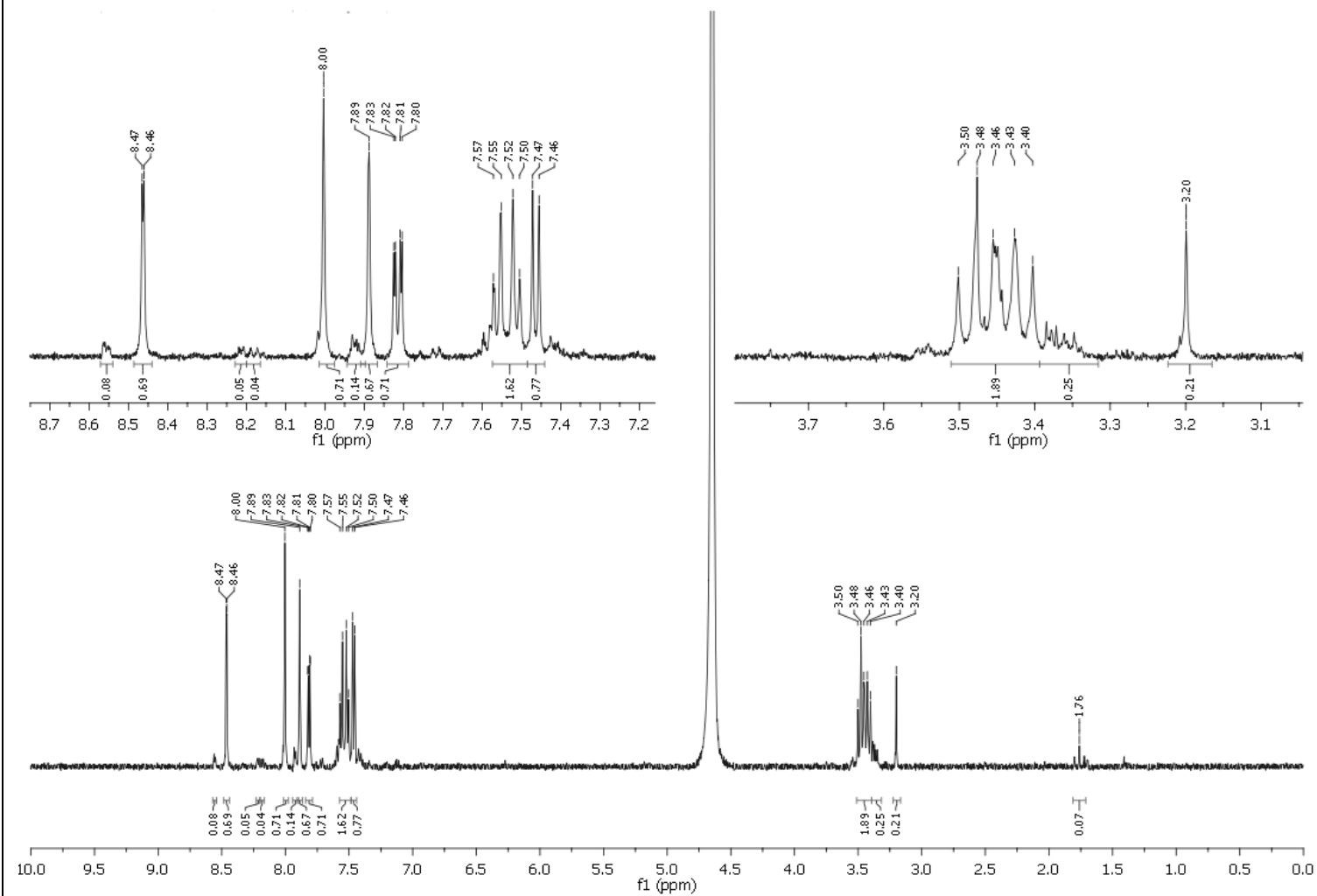
JDS02-072



JDS02-073

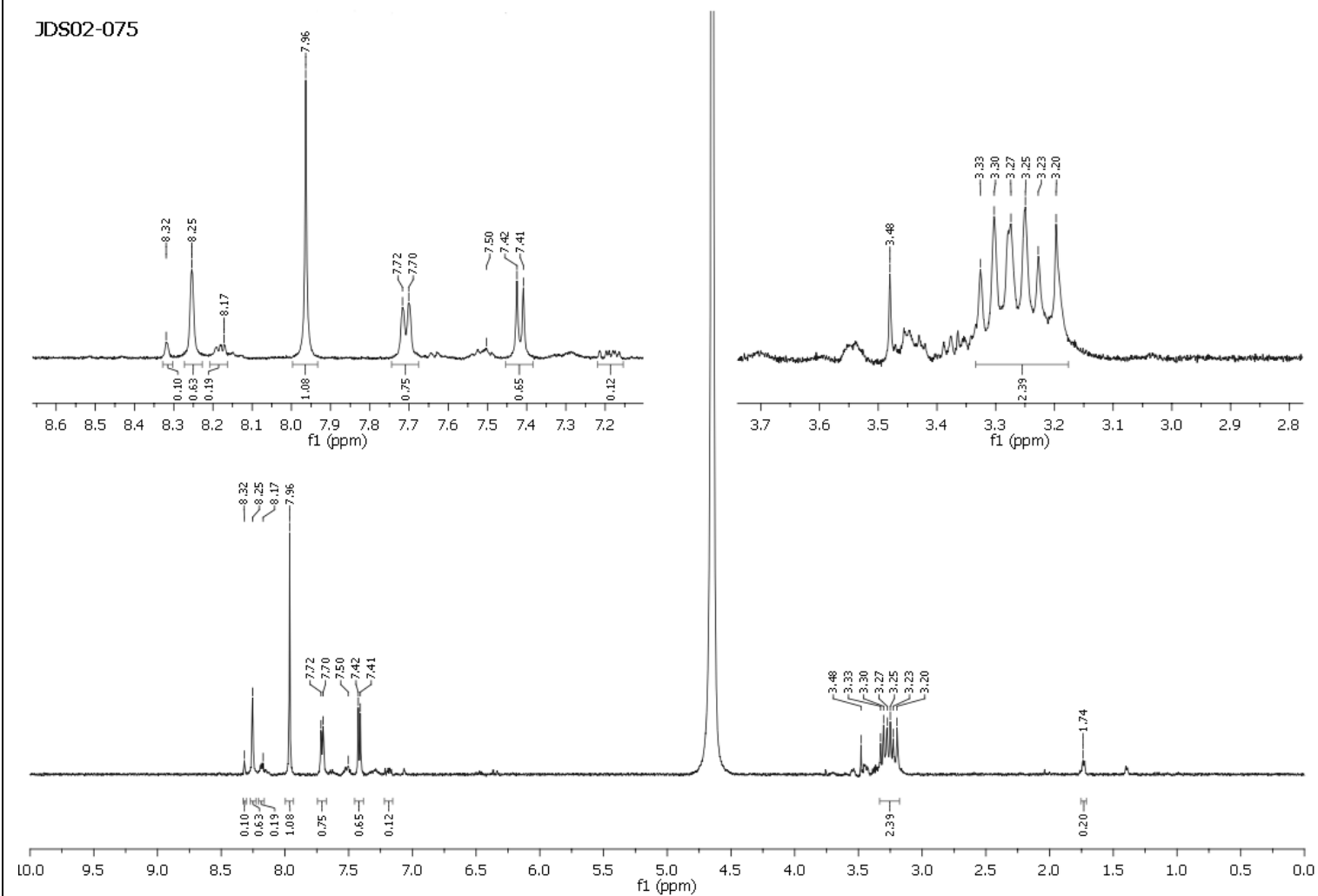


JDS02-074

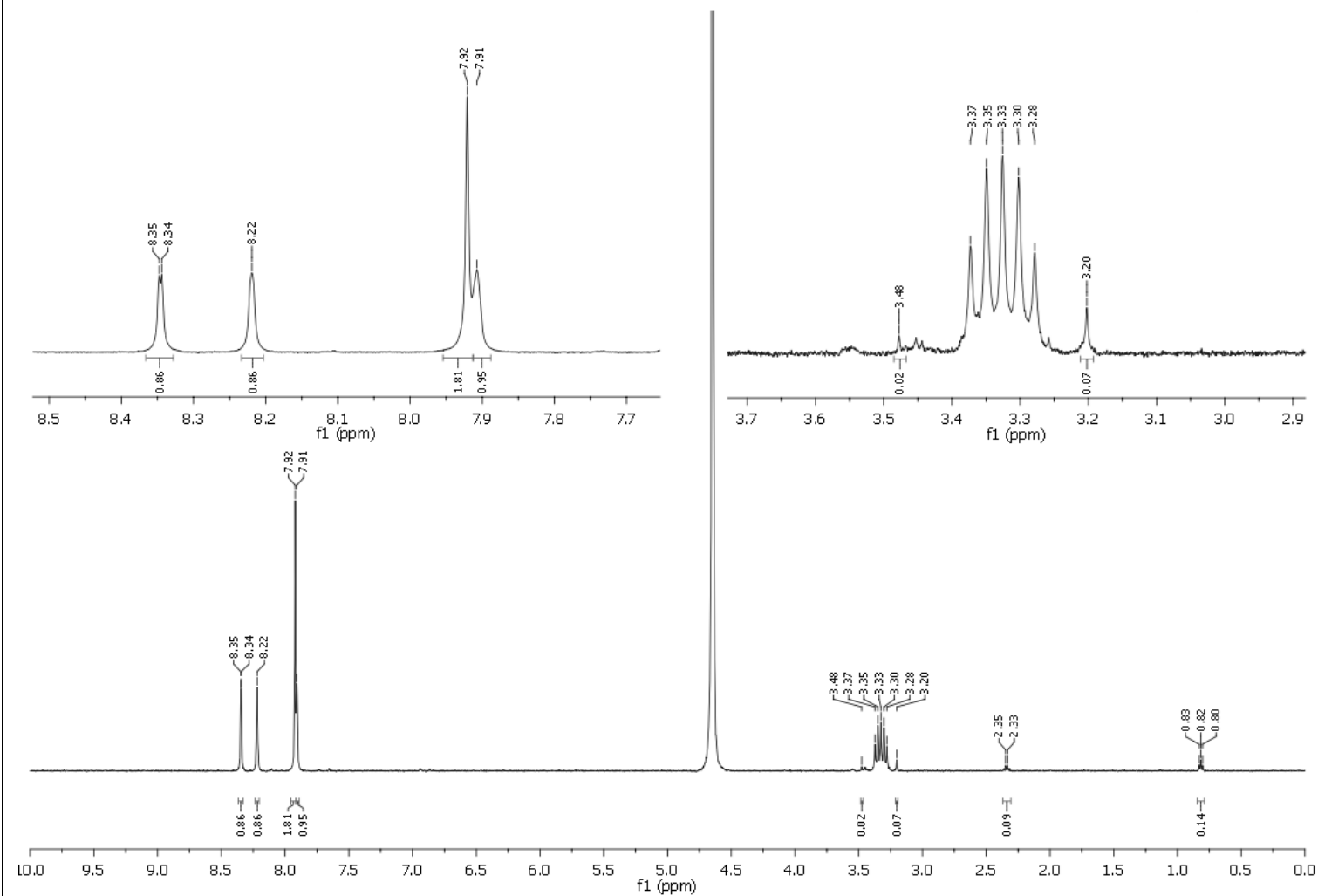


JDS02-075

JDS02-075

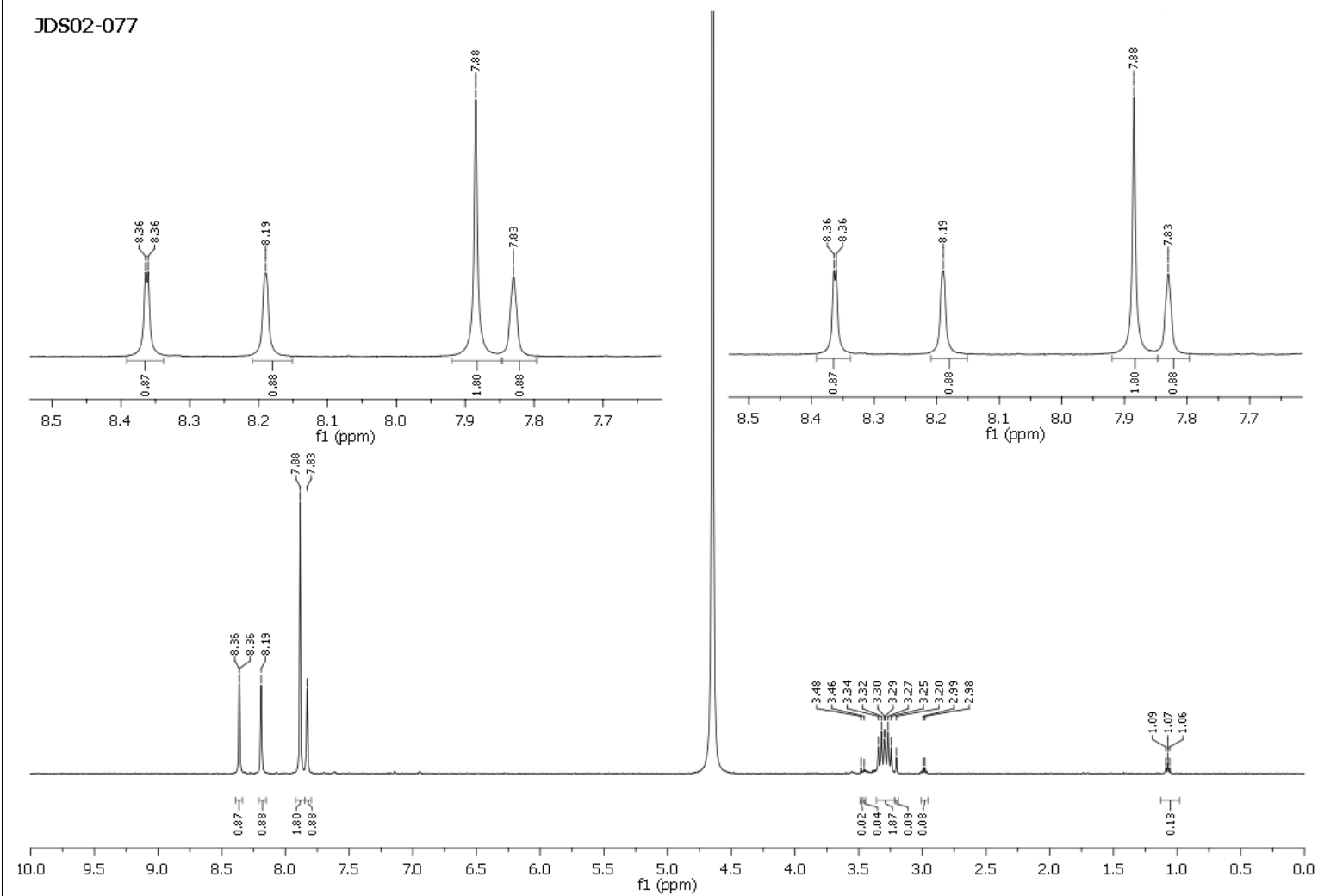


JDS02-076

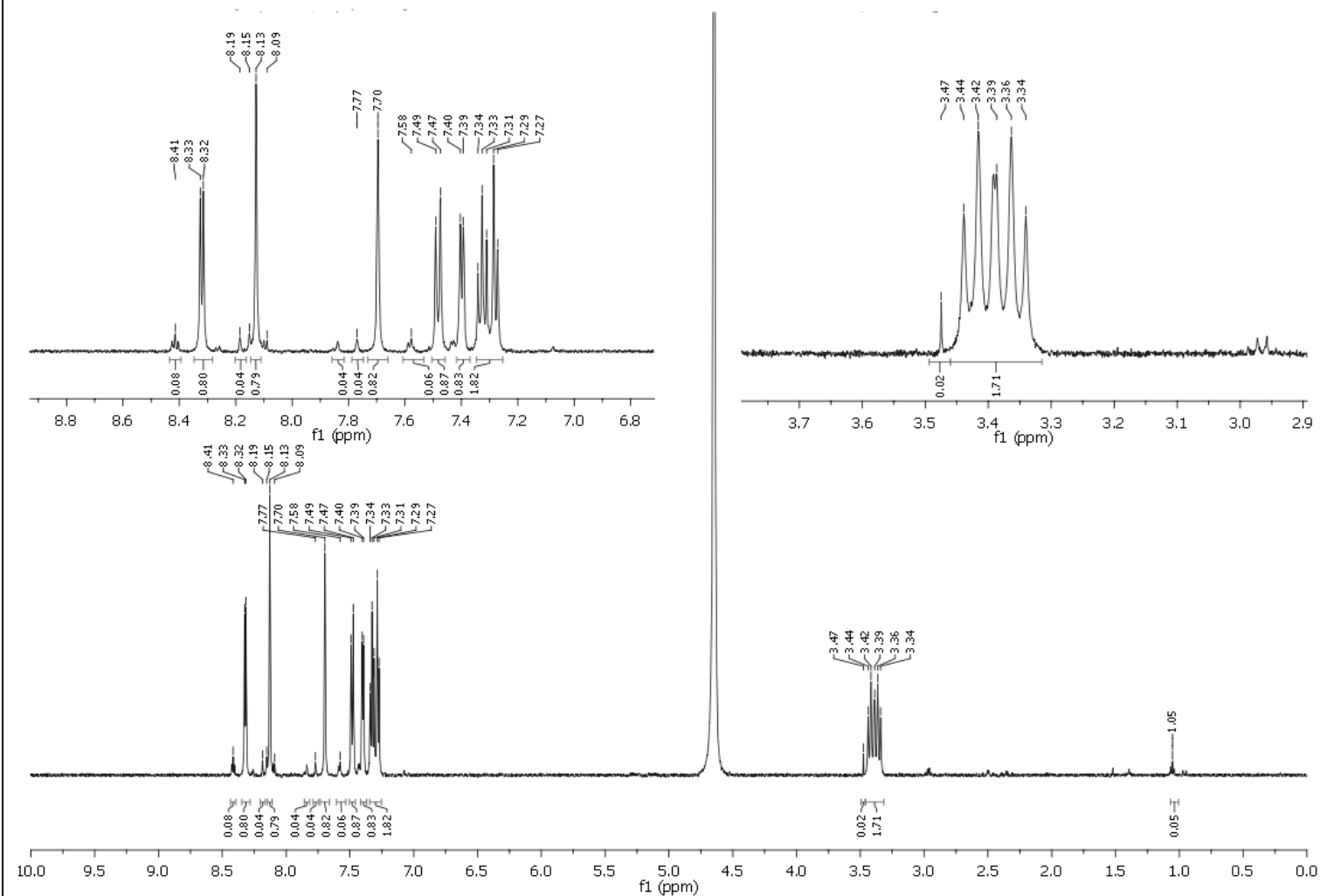


JDS02-077

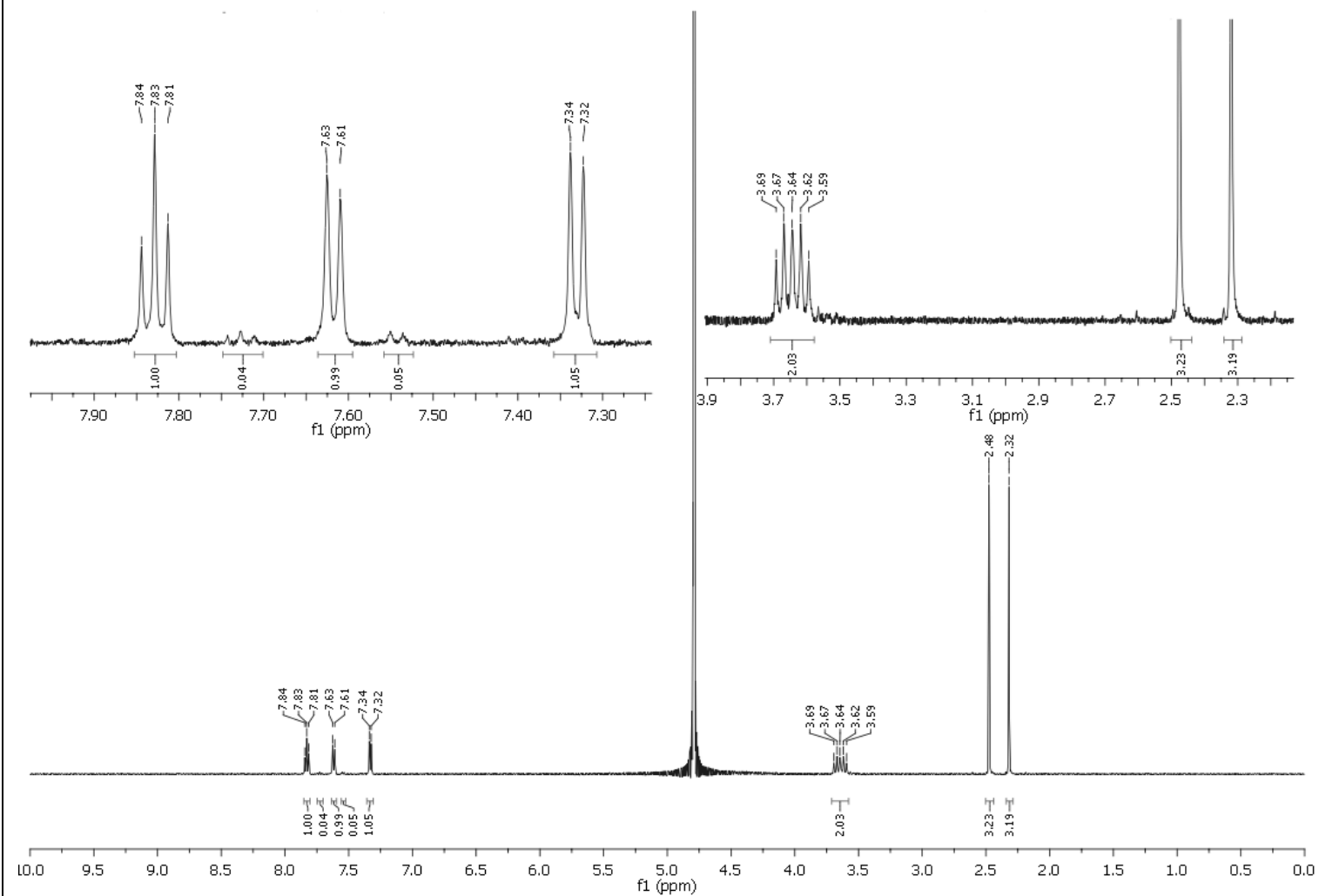
JDS02-077



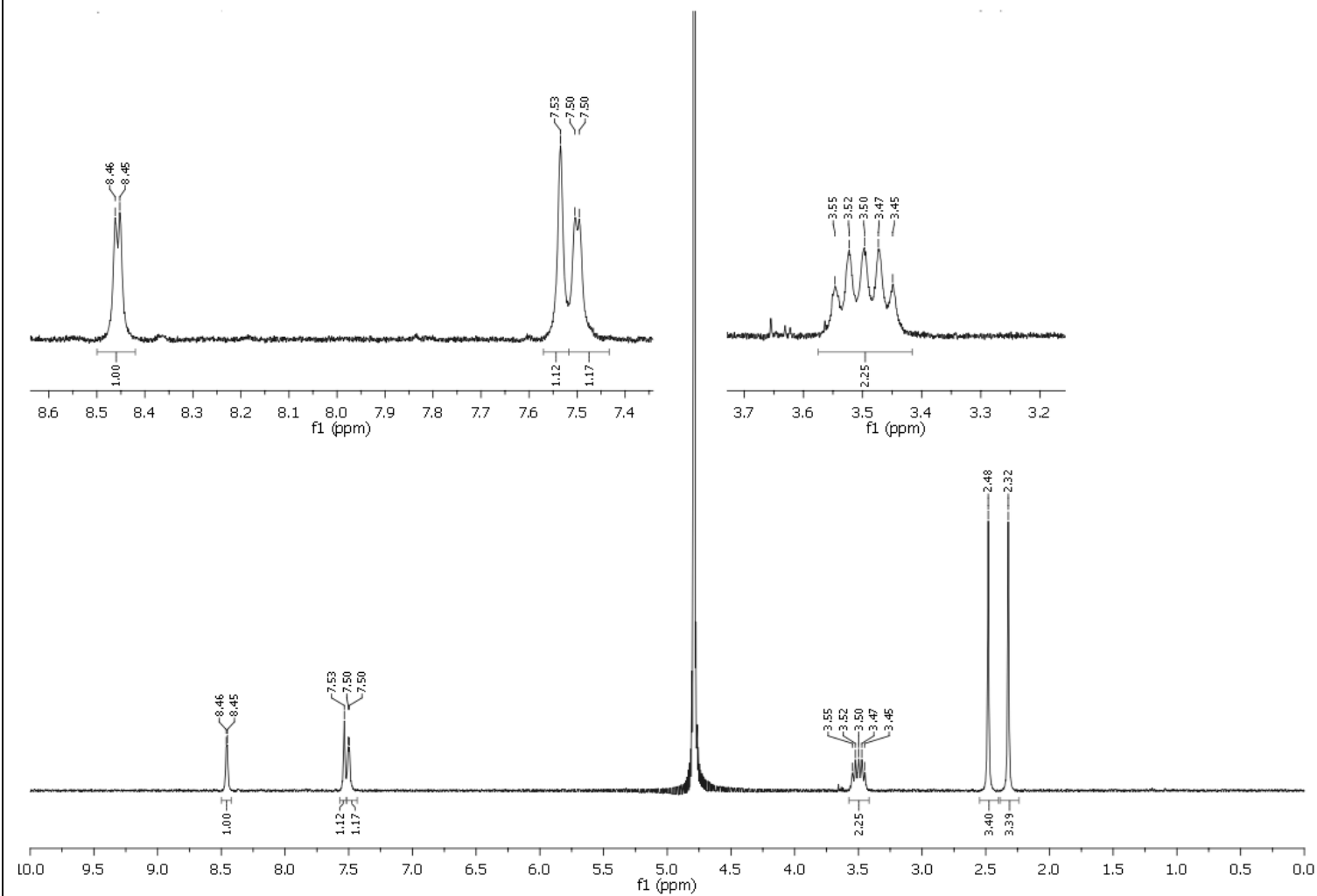
JDS02-078



JDS02-107

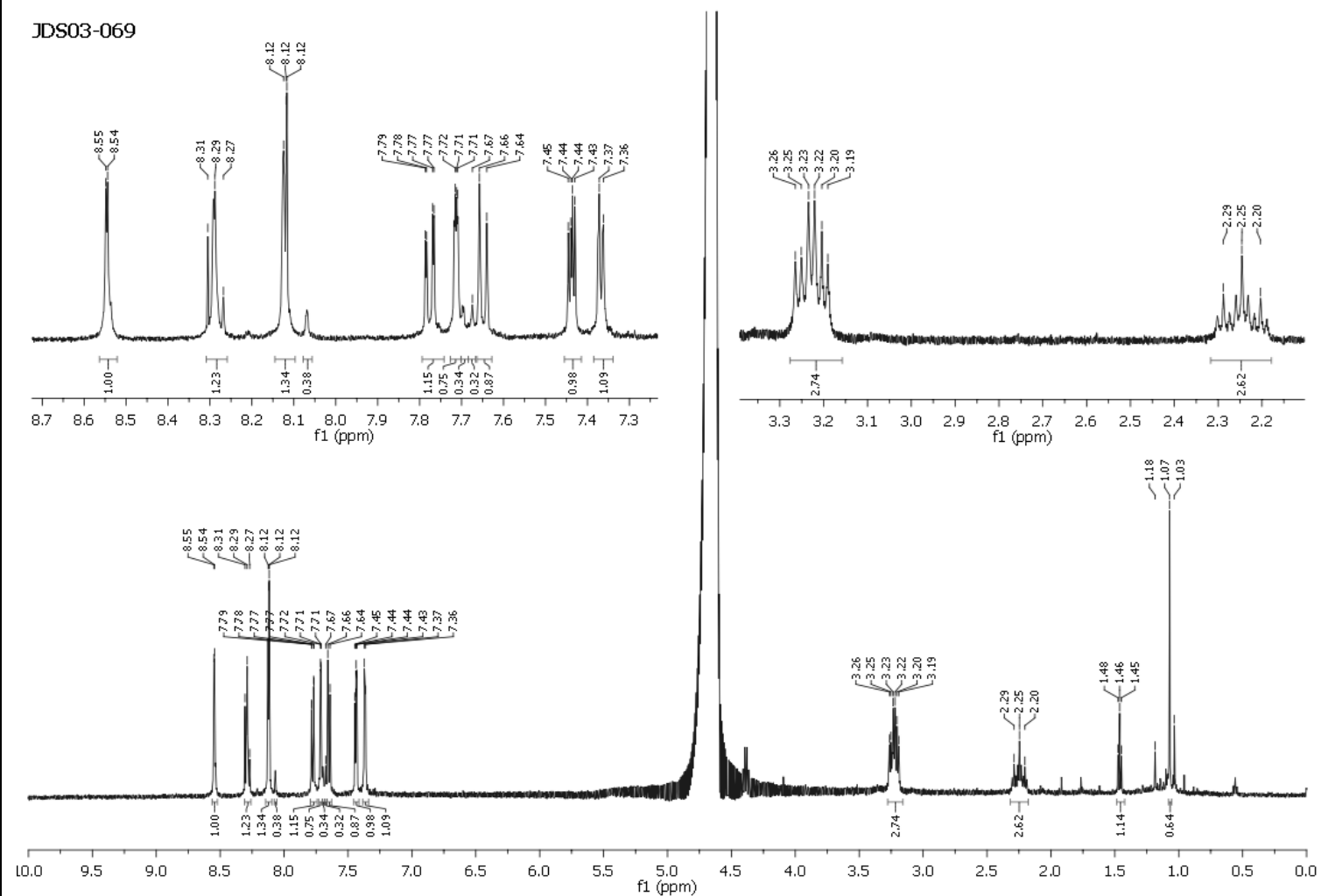


JDS02-108



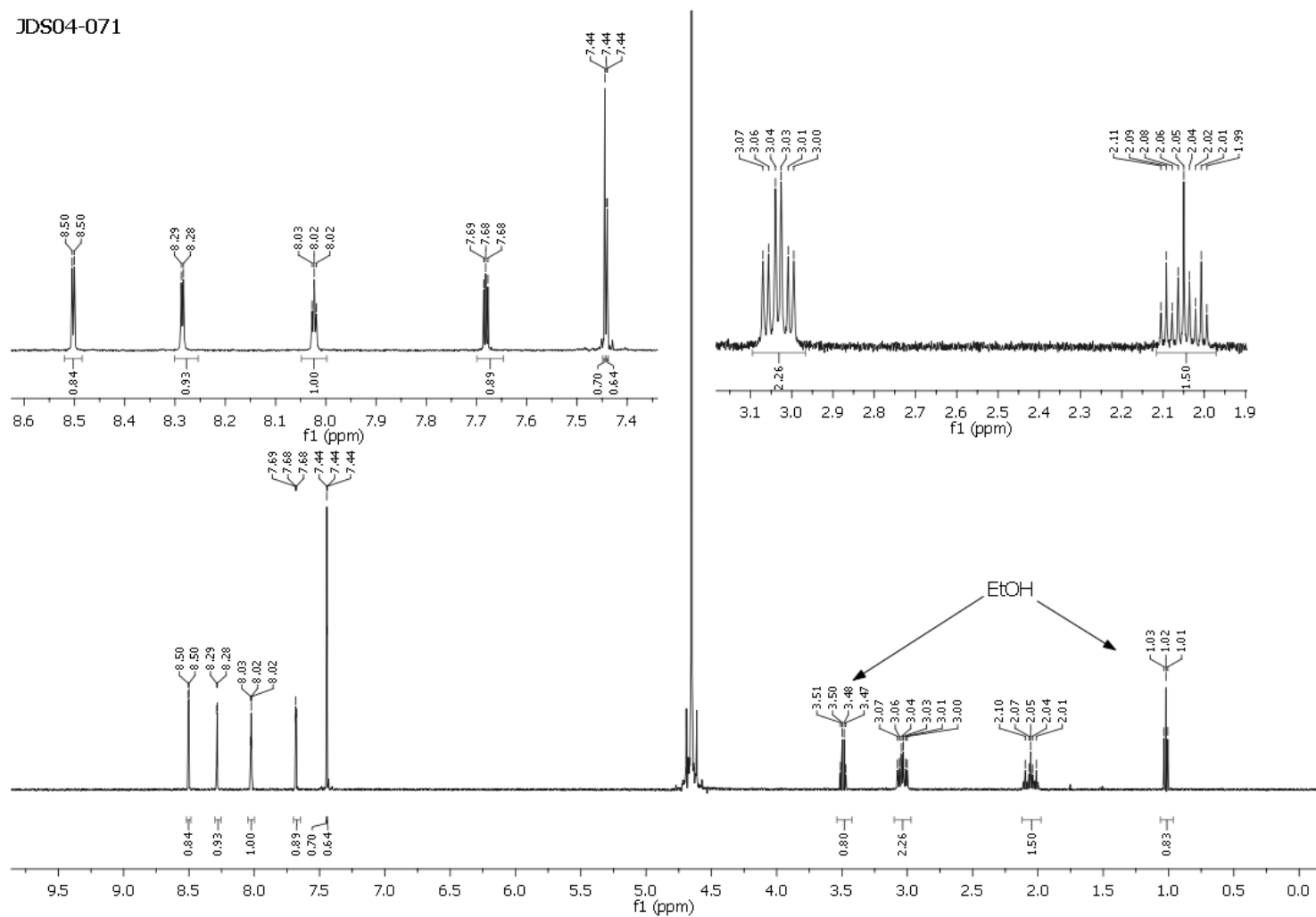
JDS03-069

JDS03-069



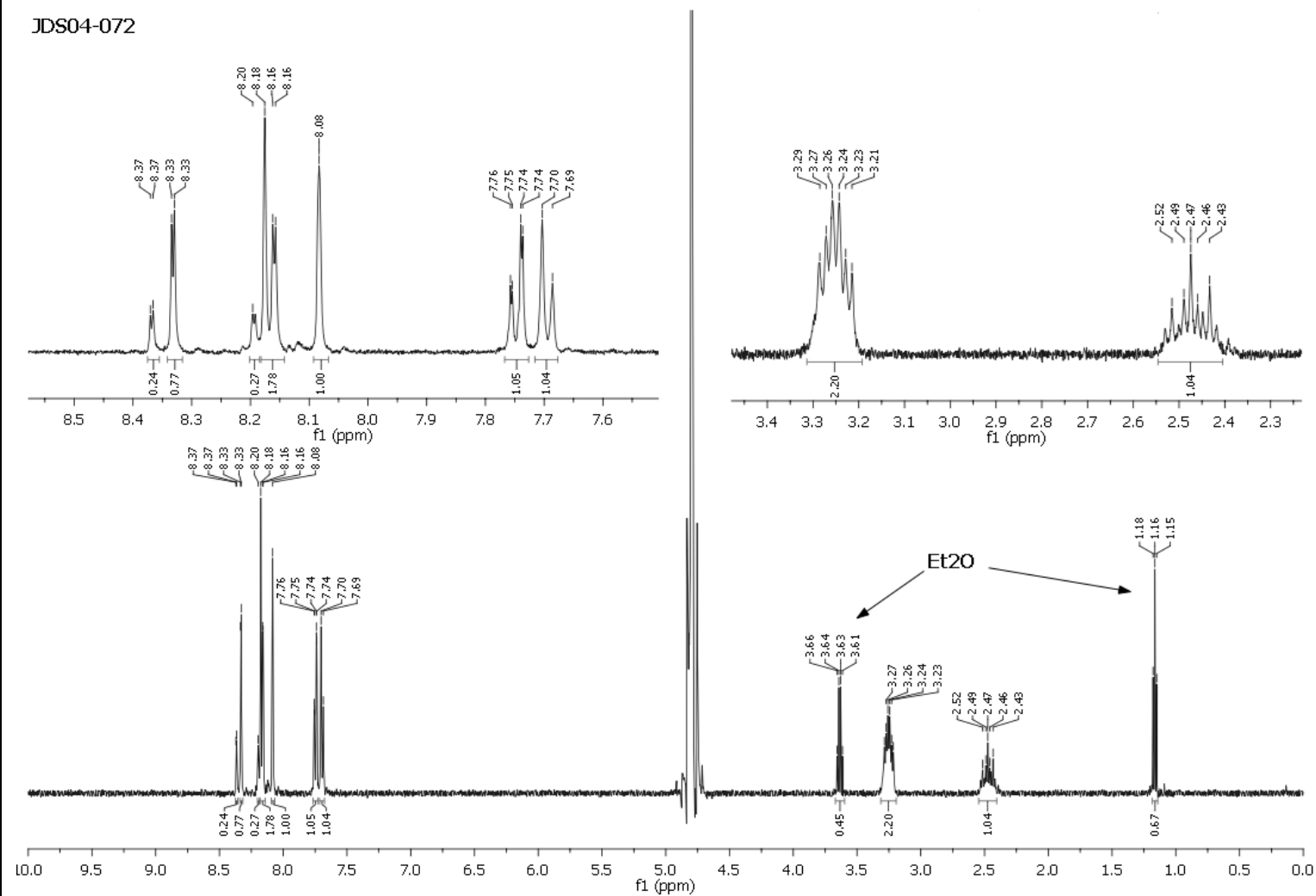
JDS04-071

JDS04-071

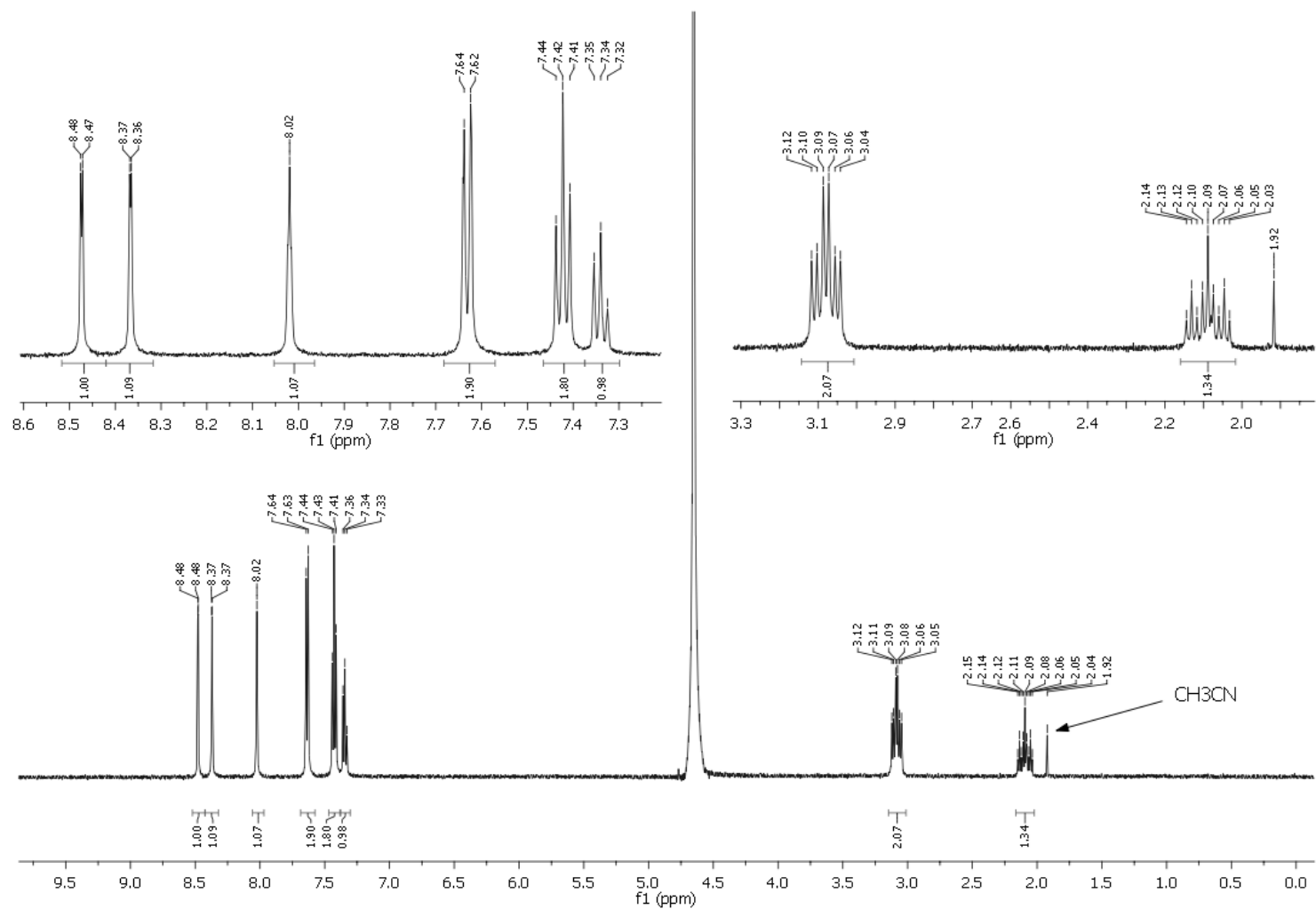


JDS04-072

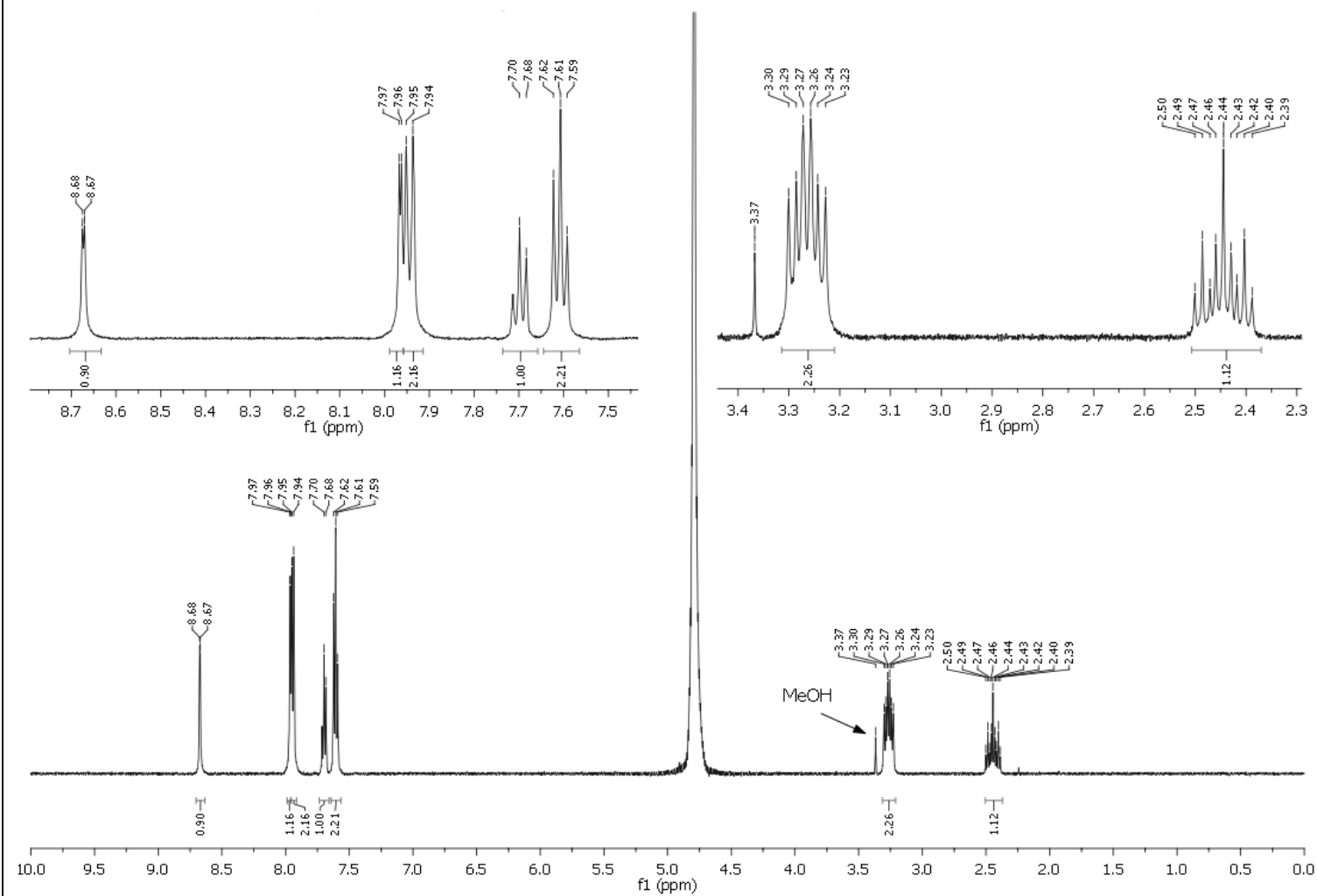
JDS04-072



JDS04-085

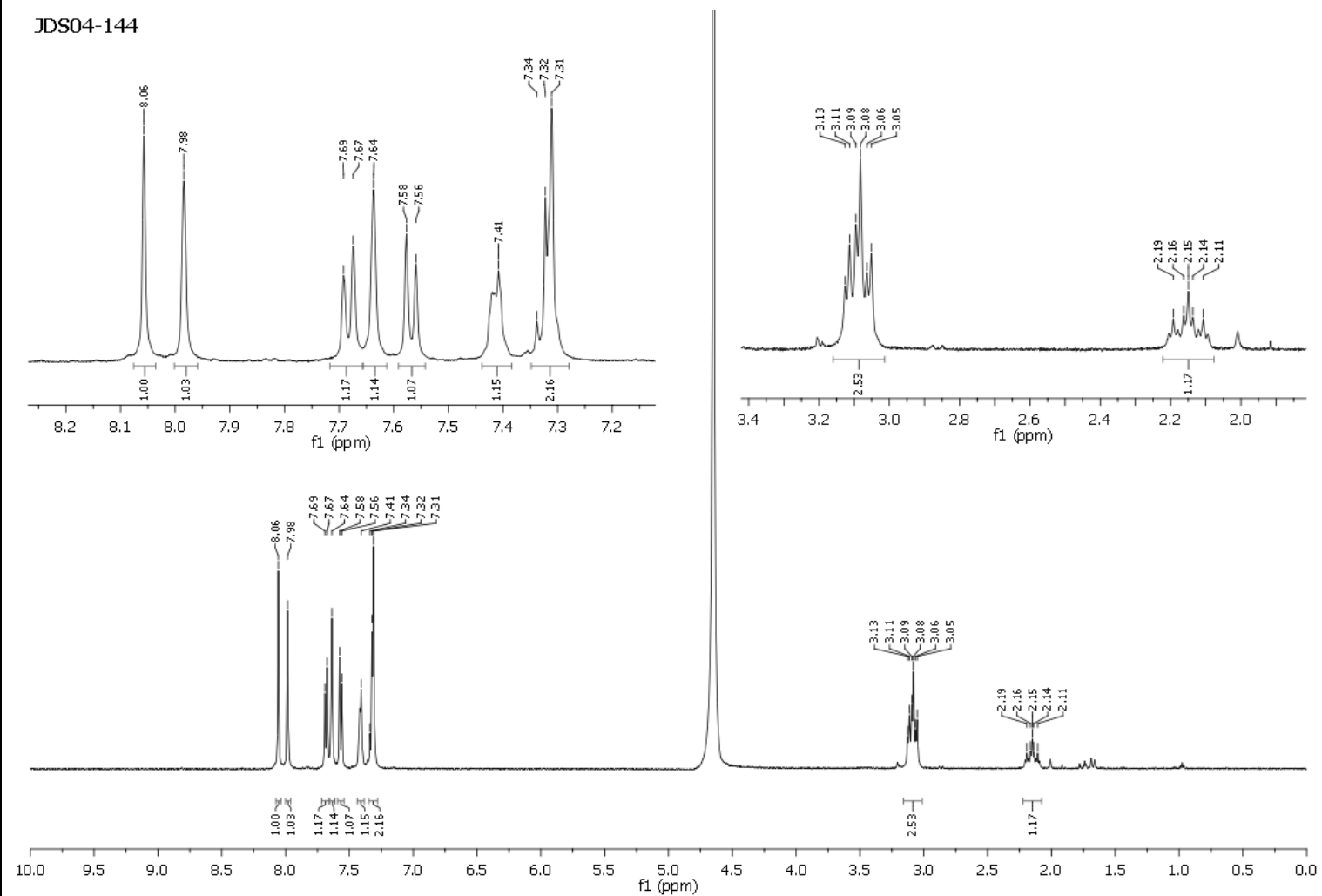


JDS04-131

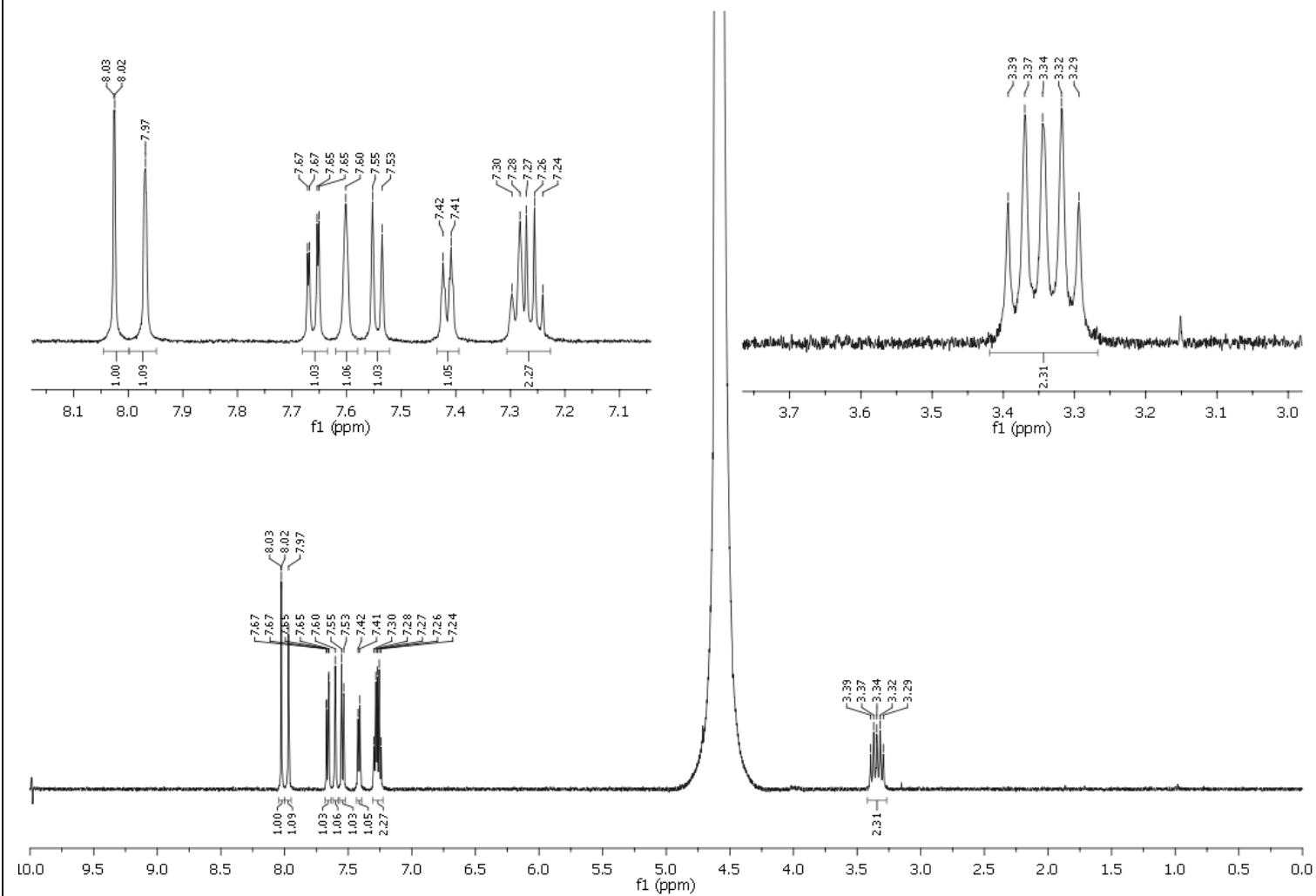


JDS04-144

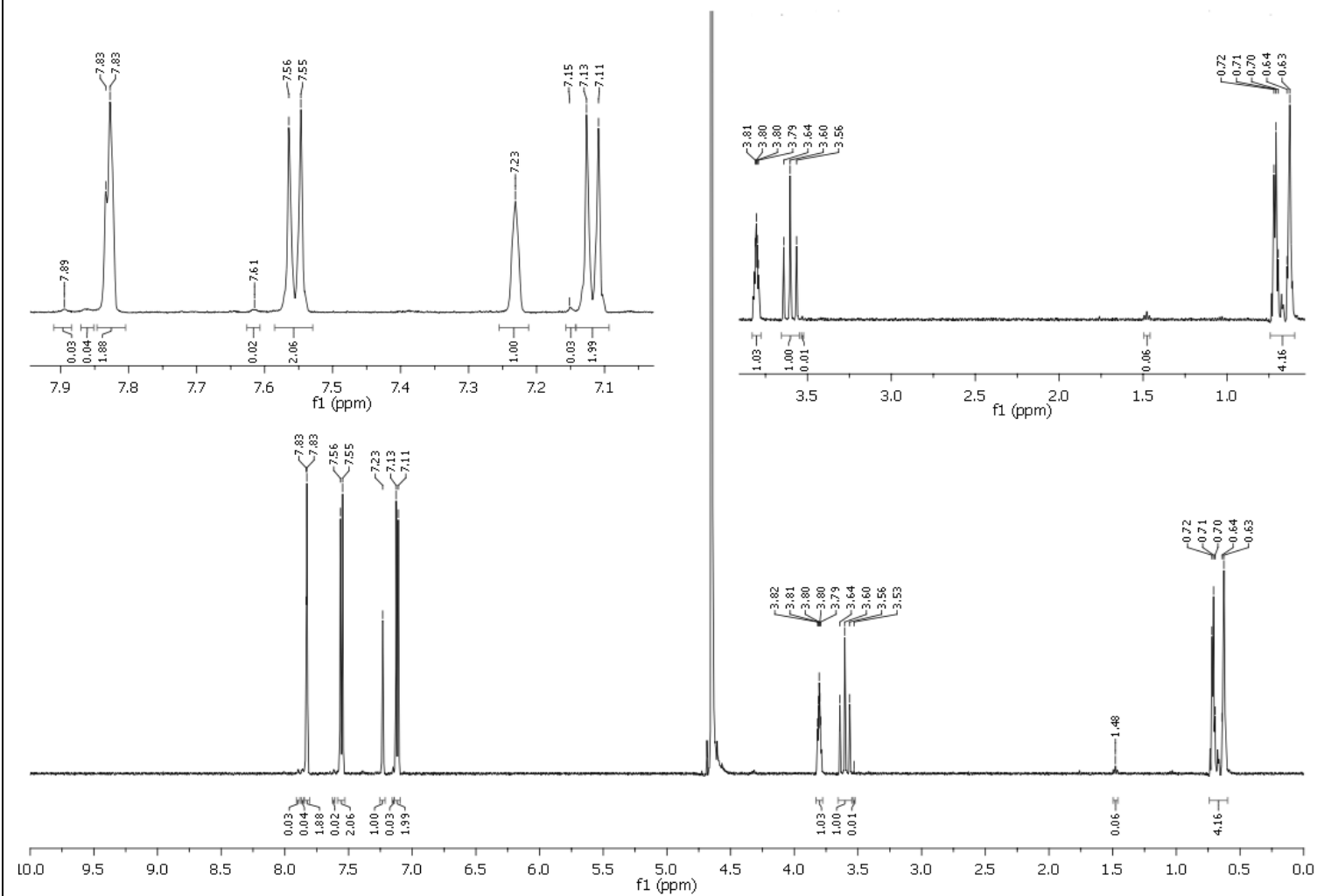
JDS04-144



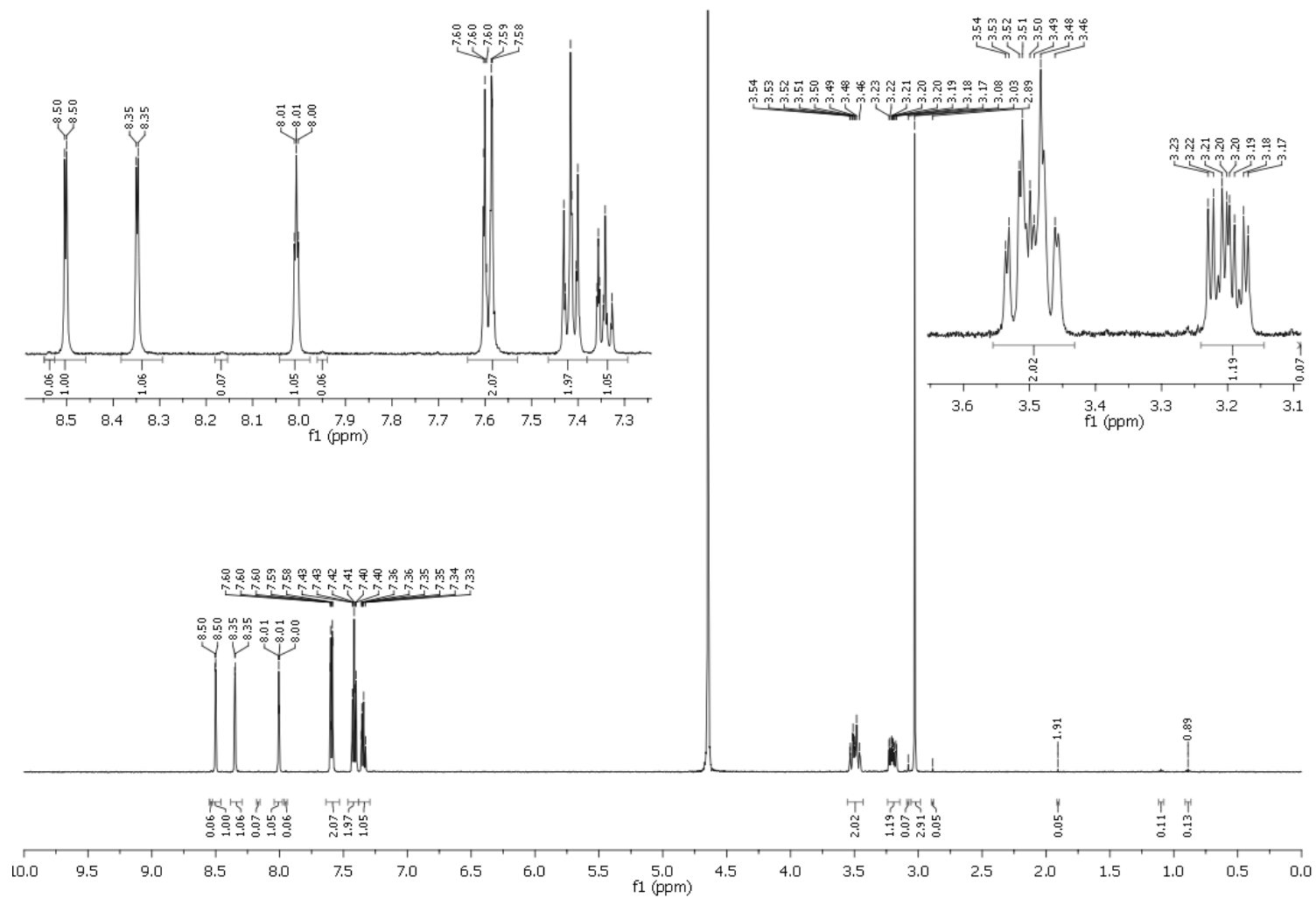
JDS04-145



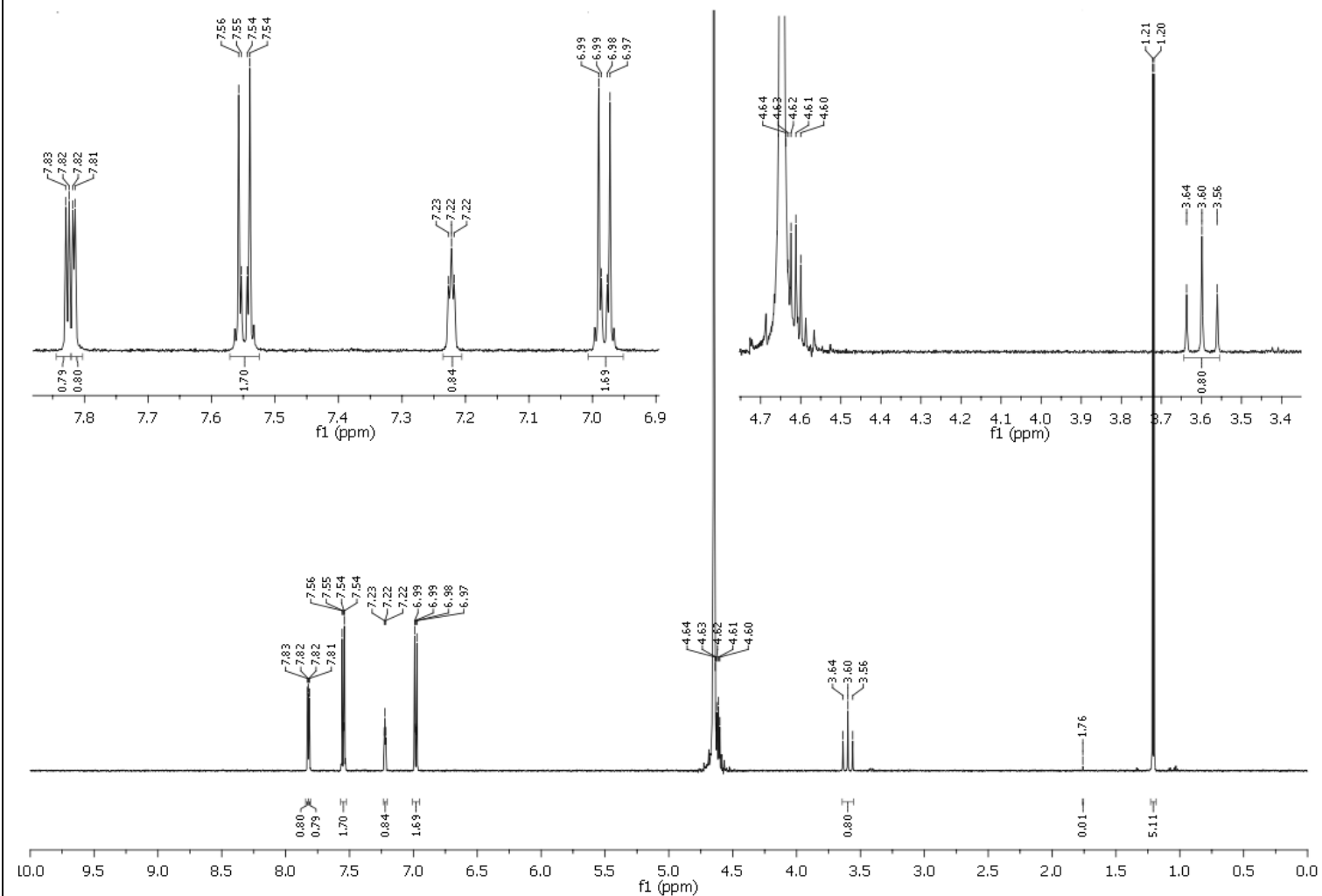
JDS05-020



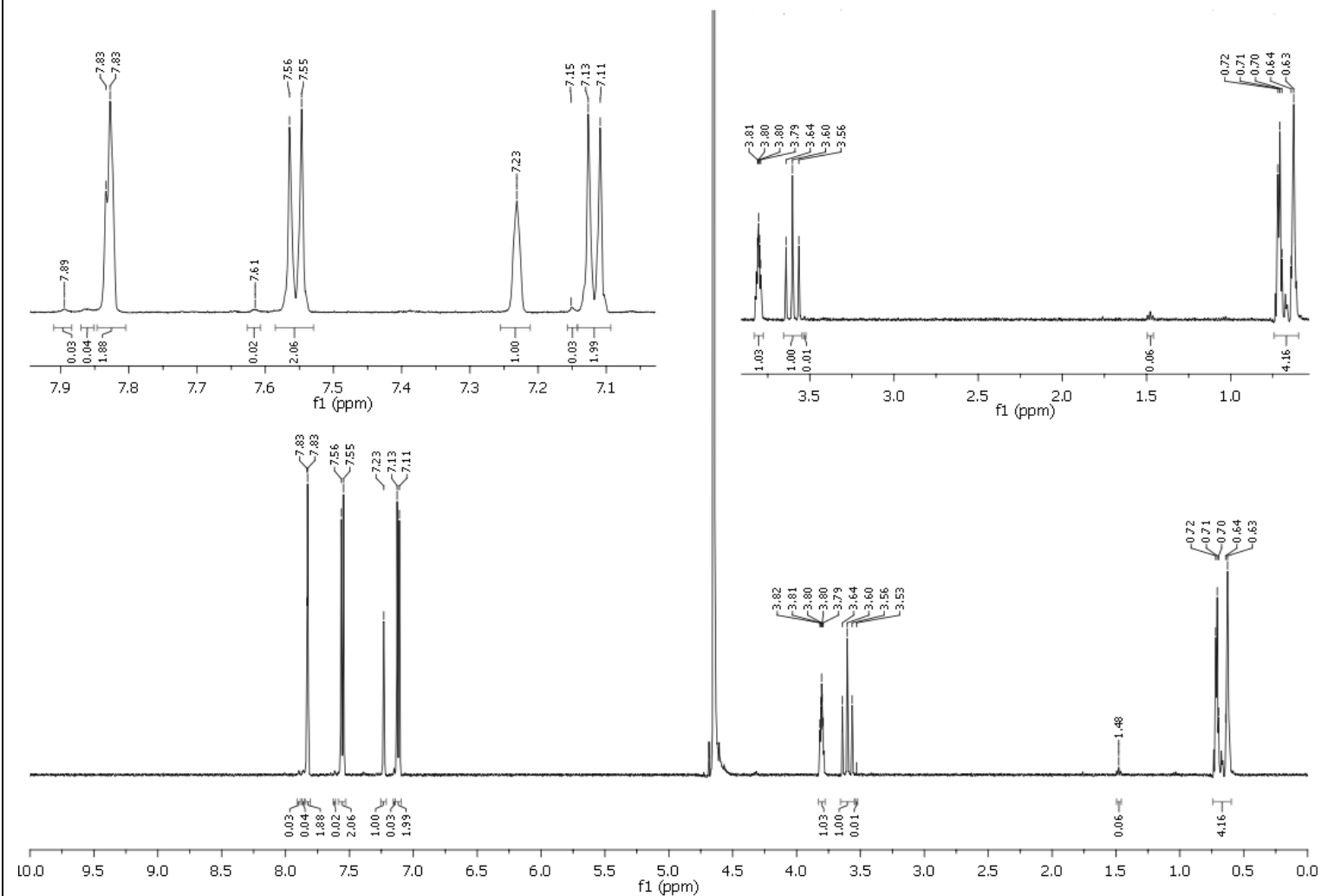
JDS05-093



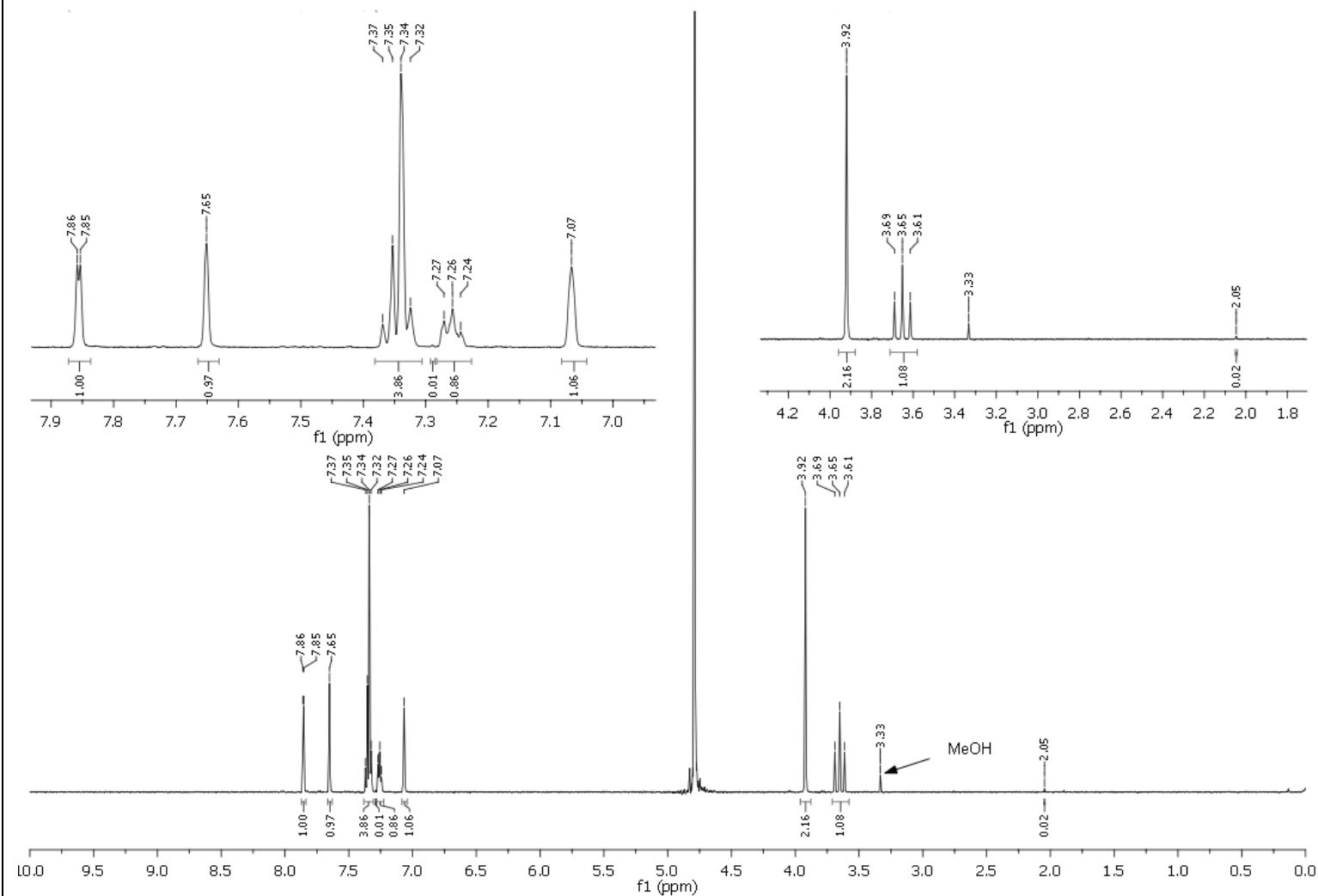
JDS05-119



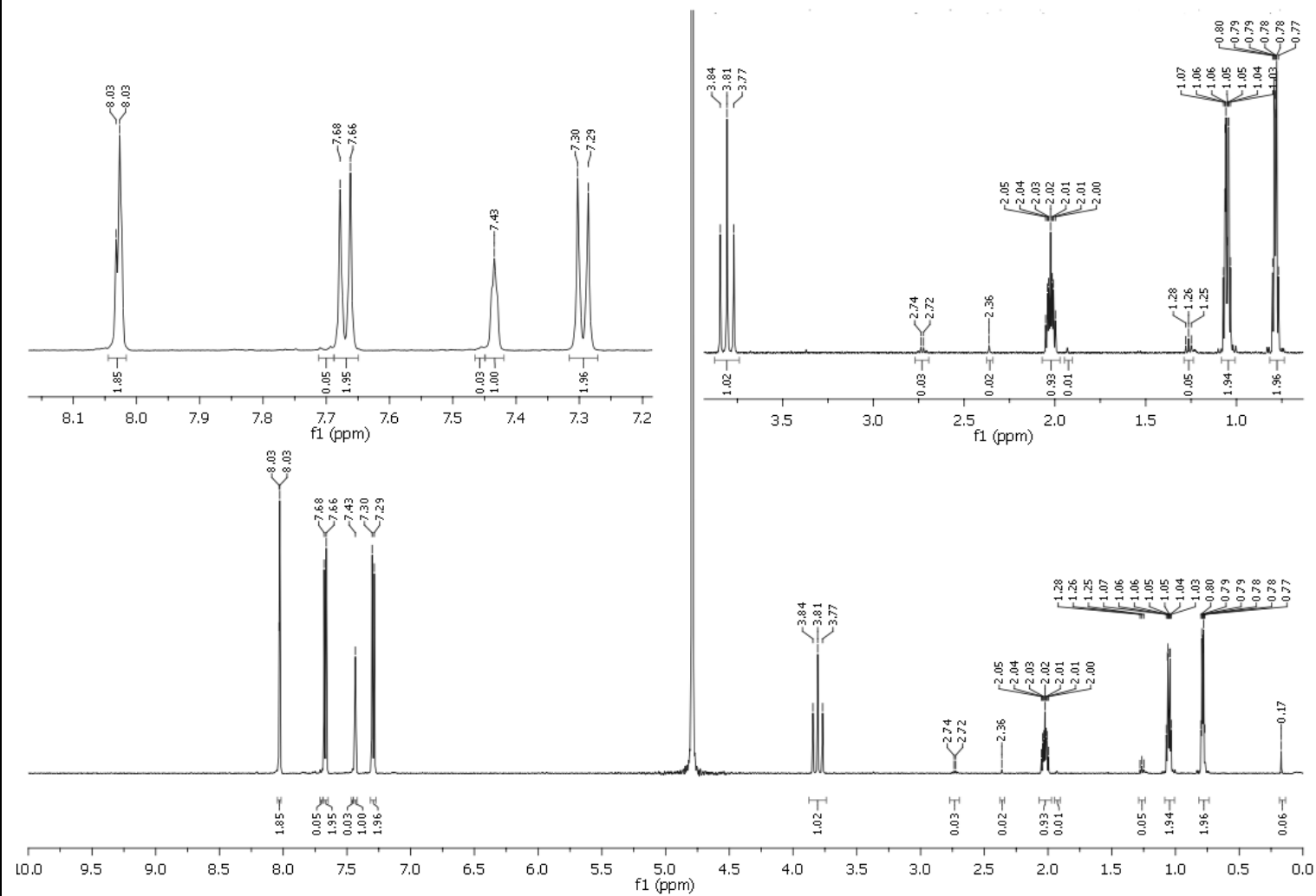
JDS05-120



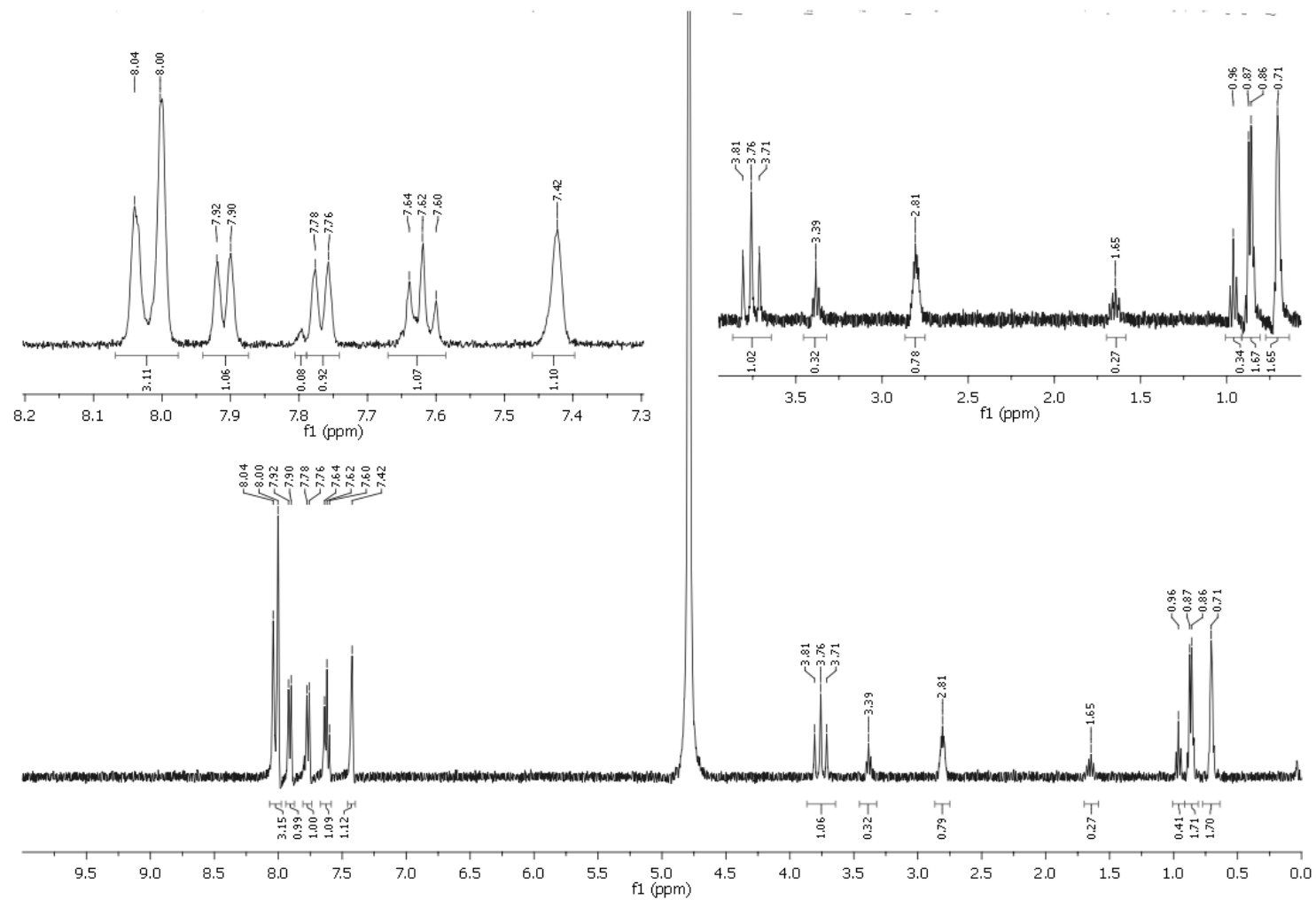
JDS05-126



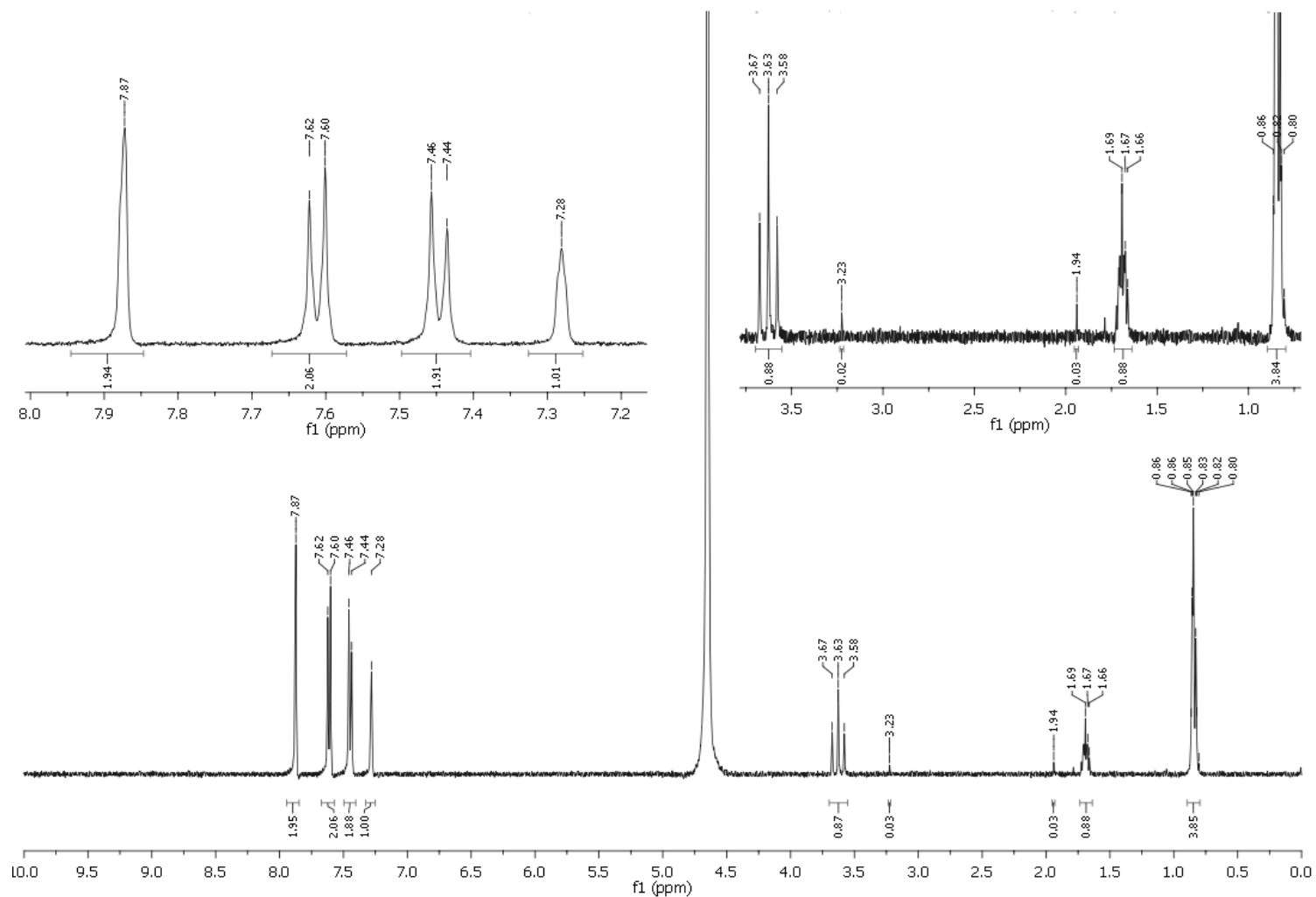
JDS05-137



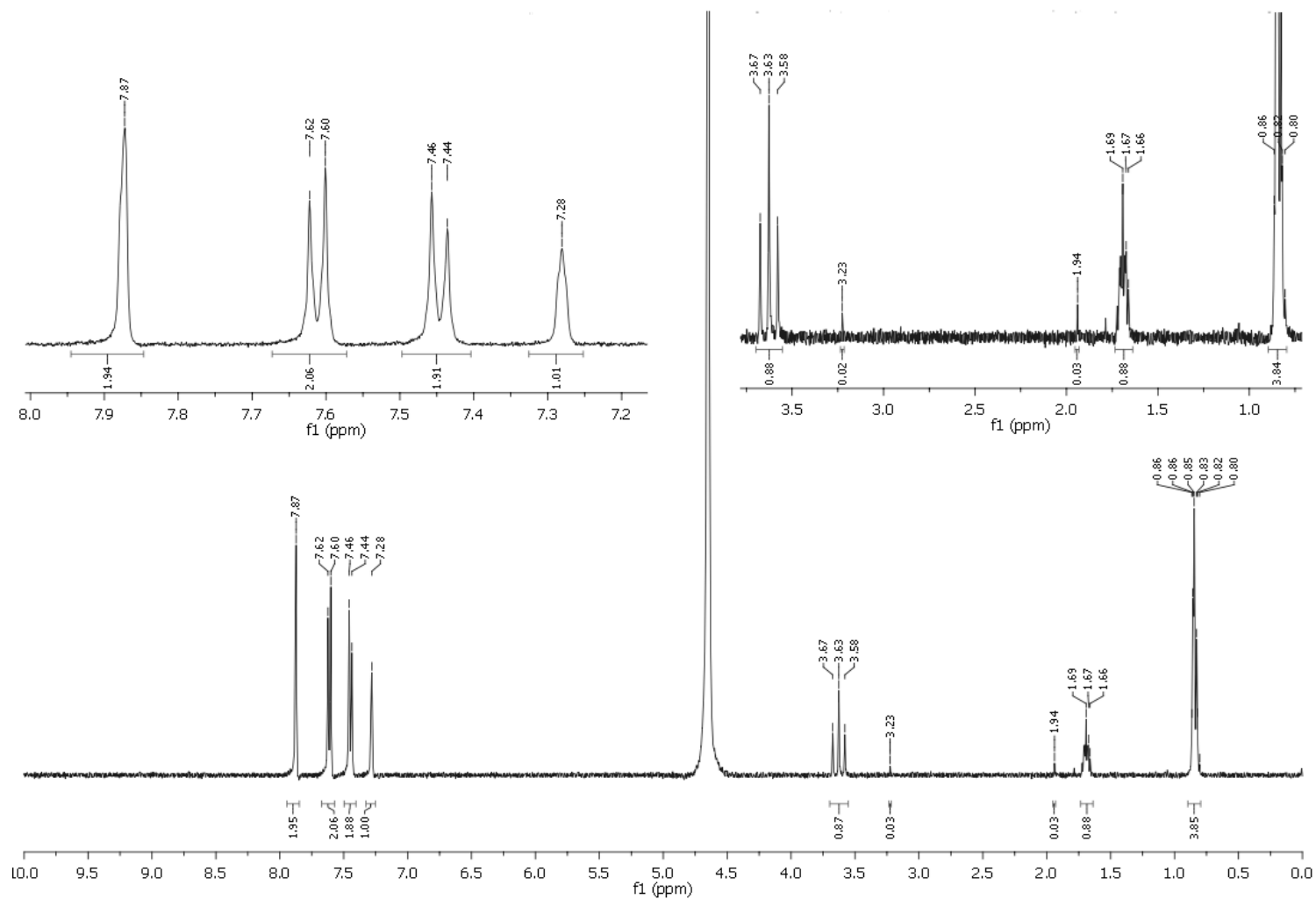
JDS07-022



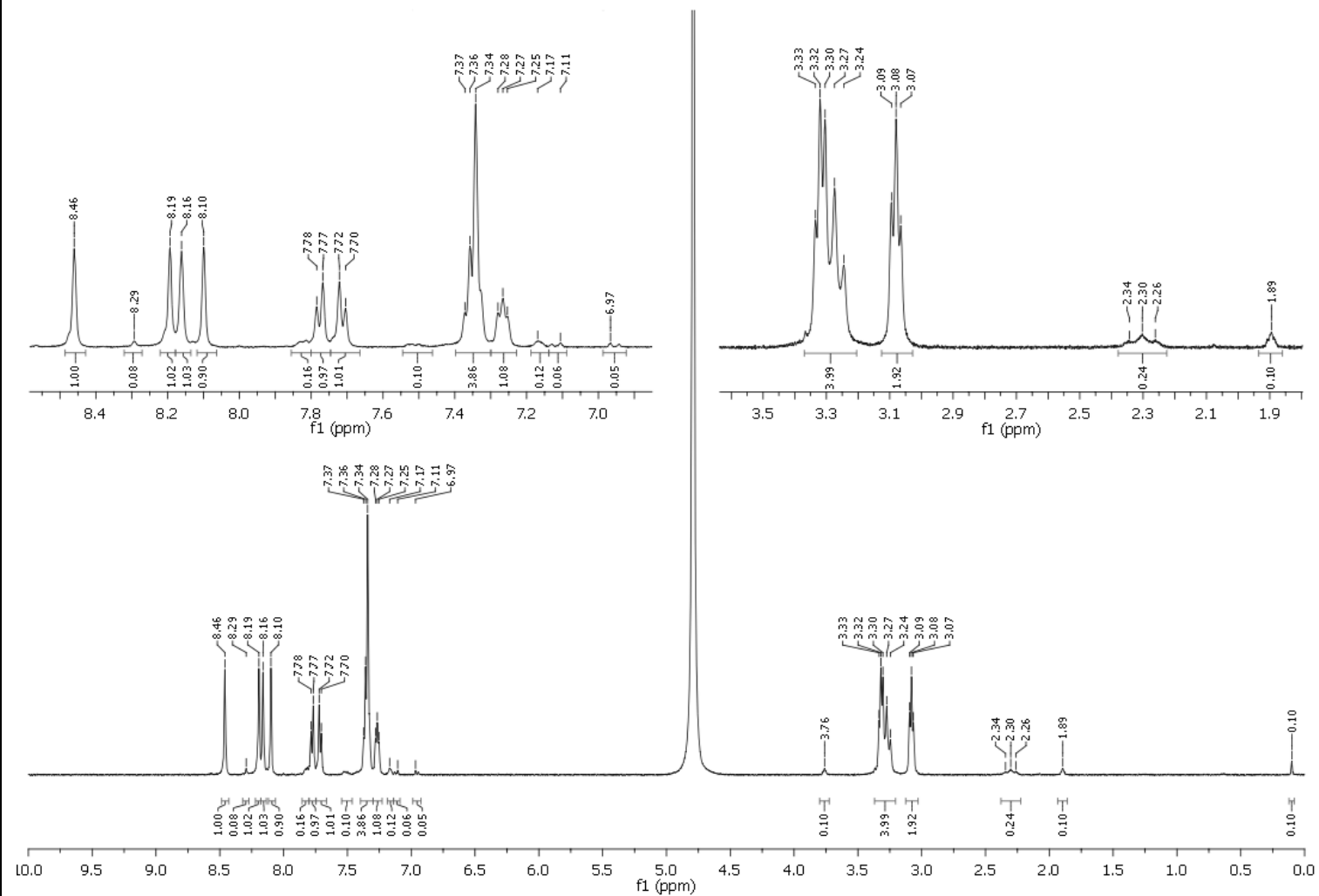
JDS07-023



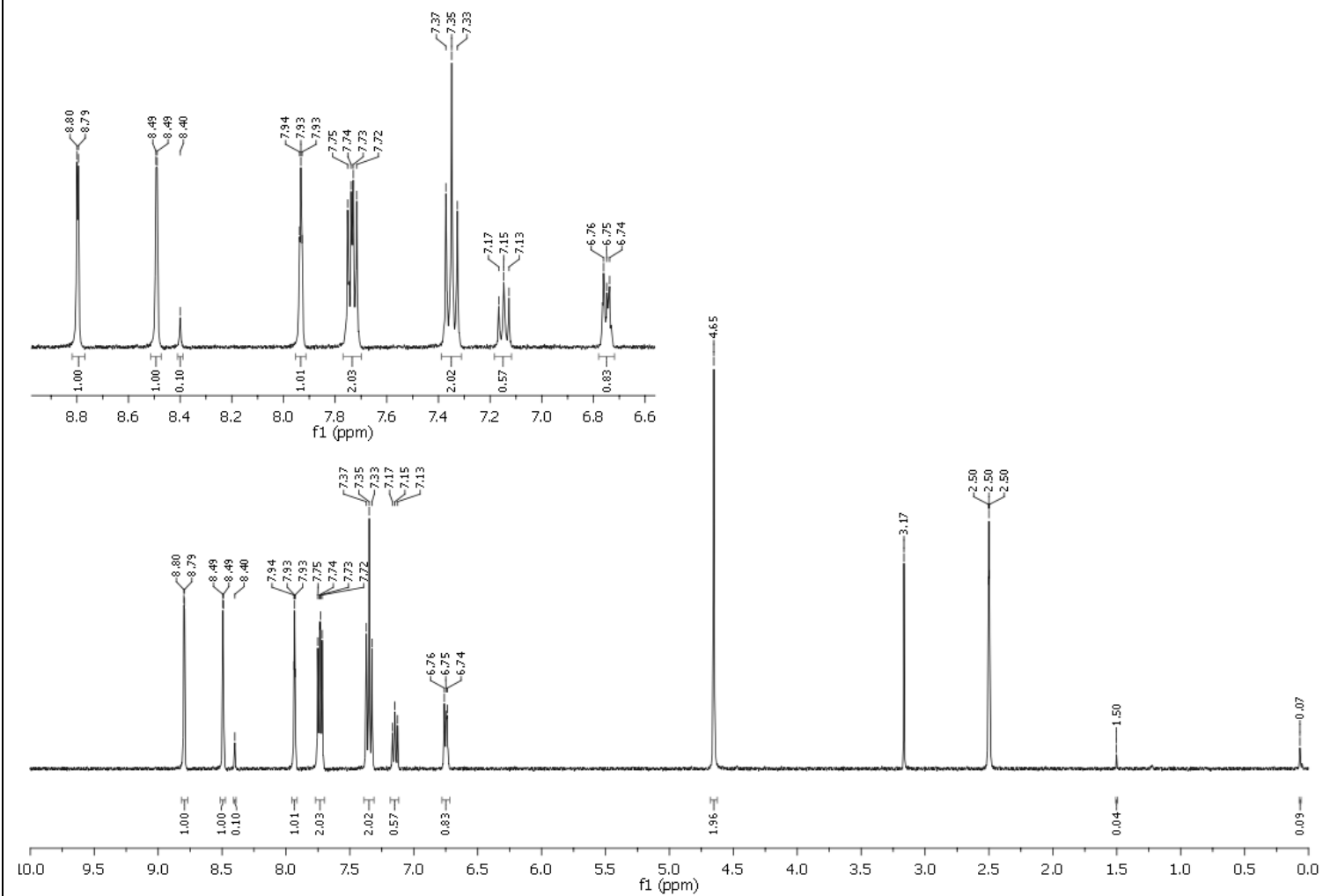
JDS07-024



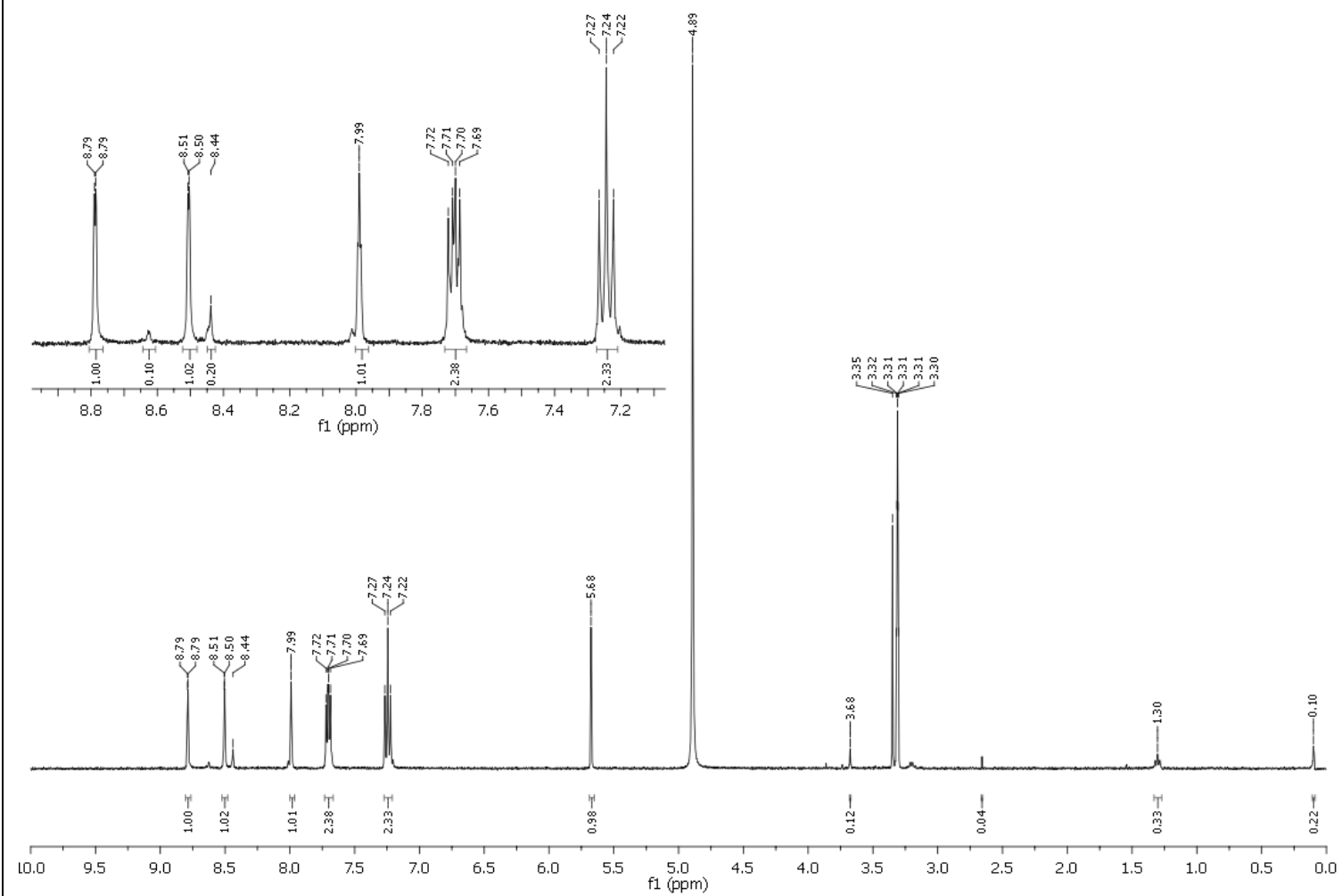
JDS07-067



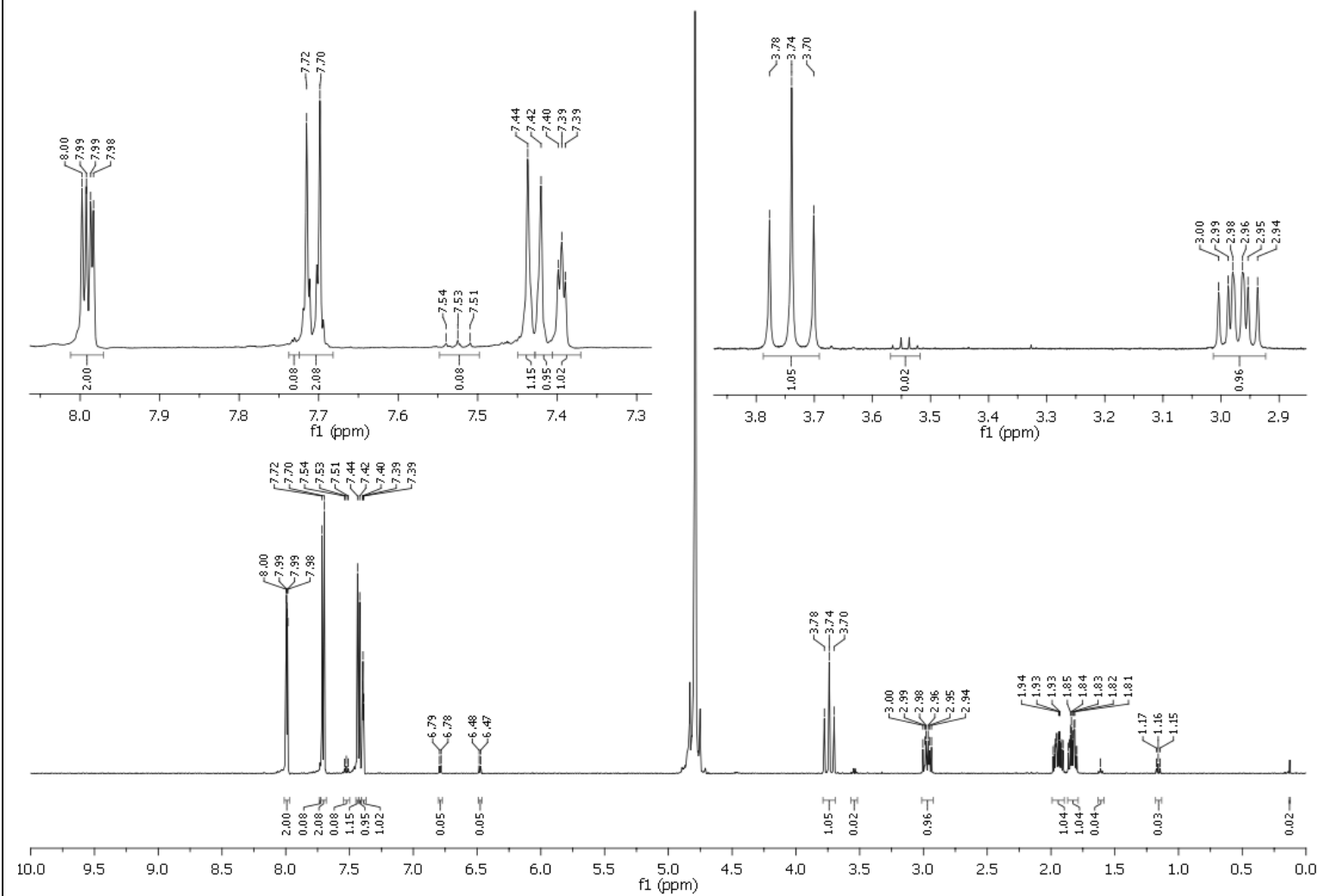
JDS08-080



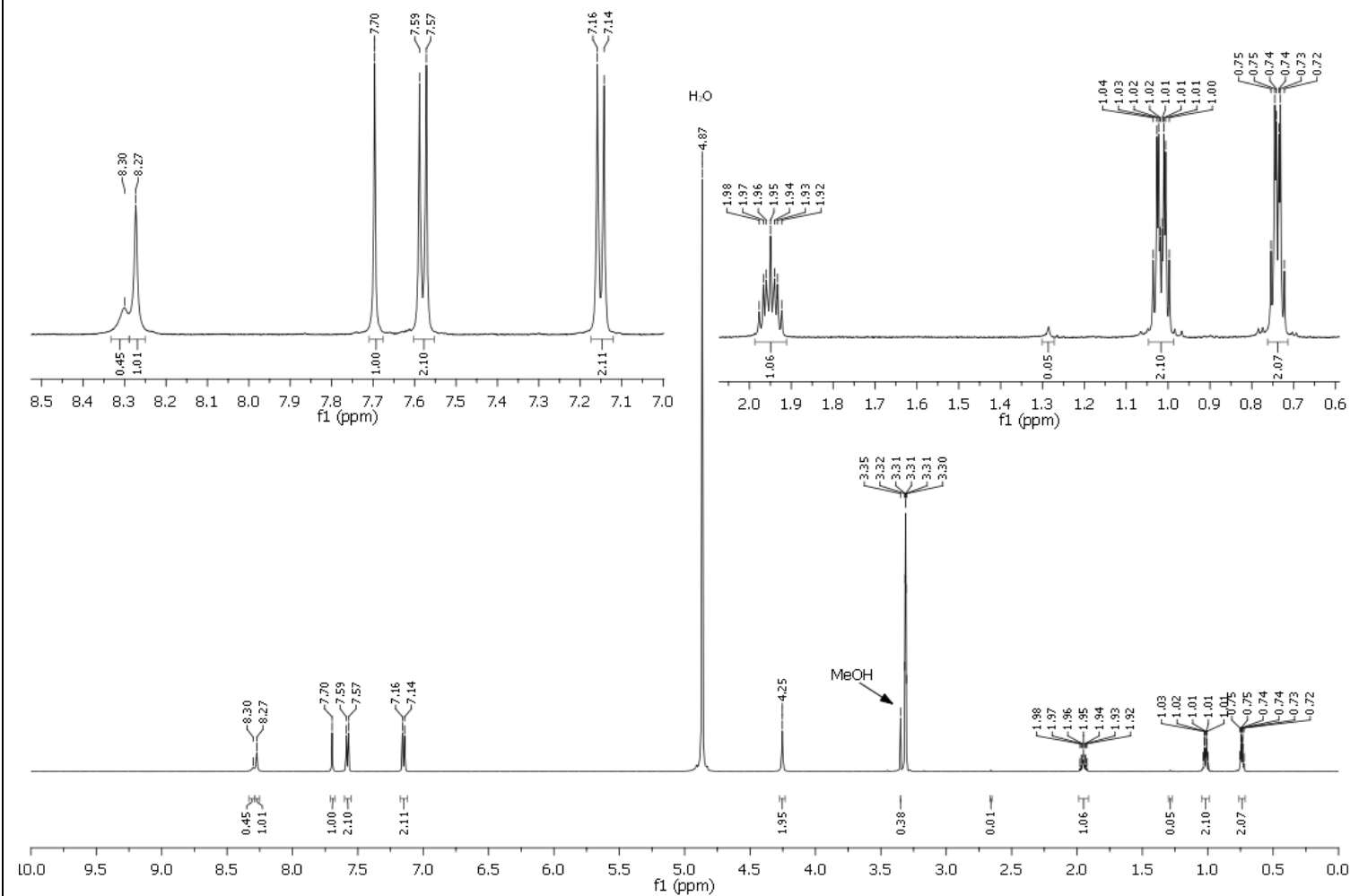
JDS08-083



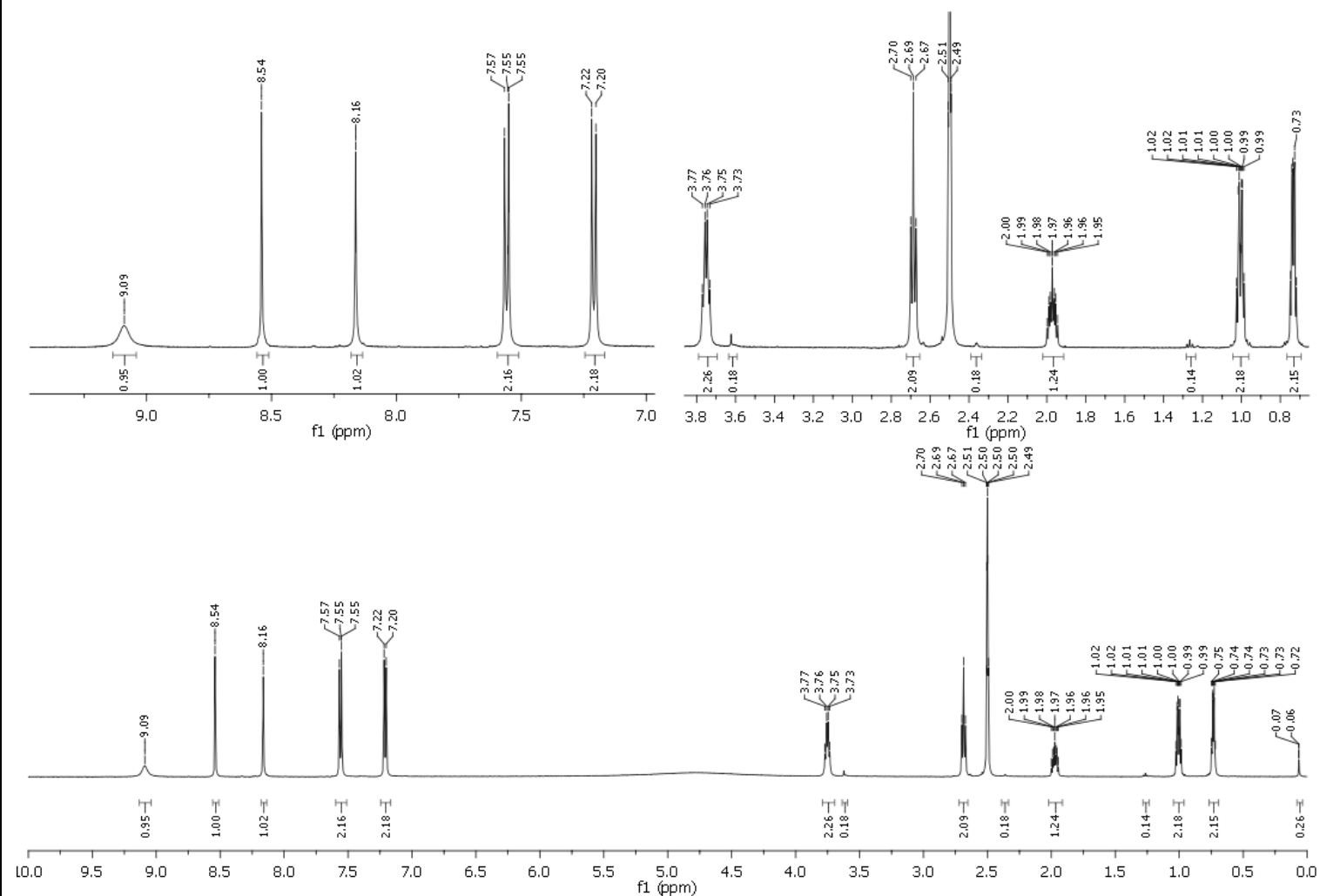
JDS09-083



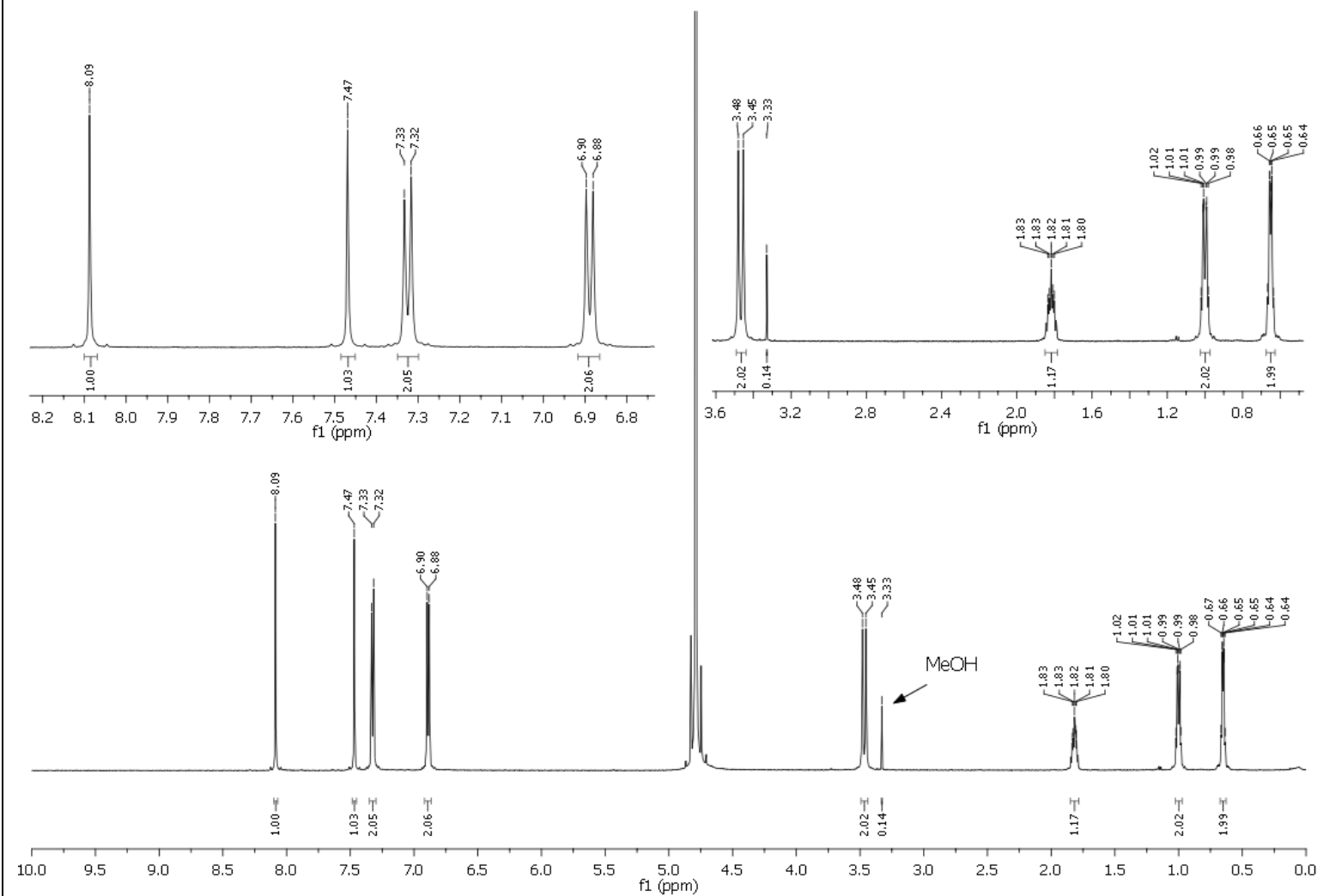
JDS09-119



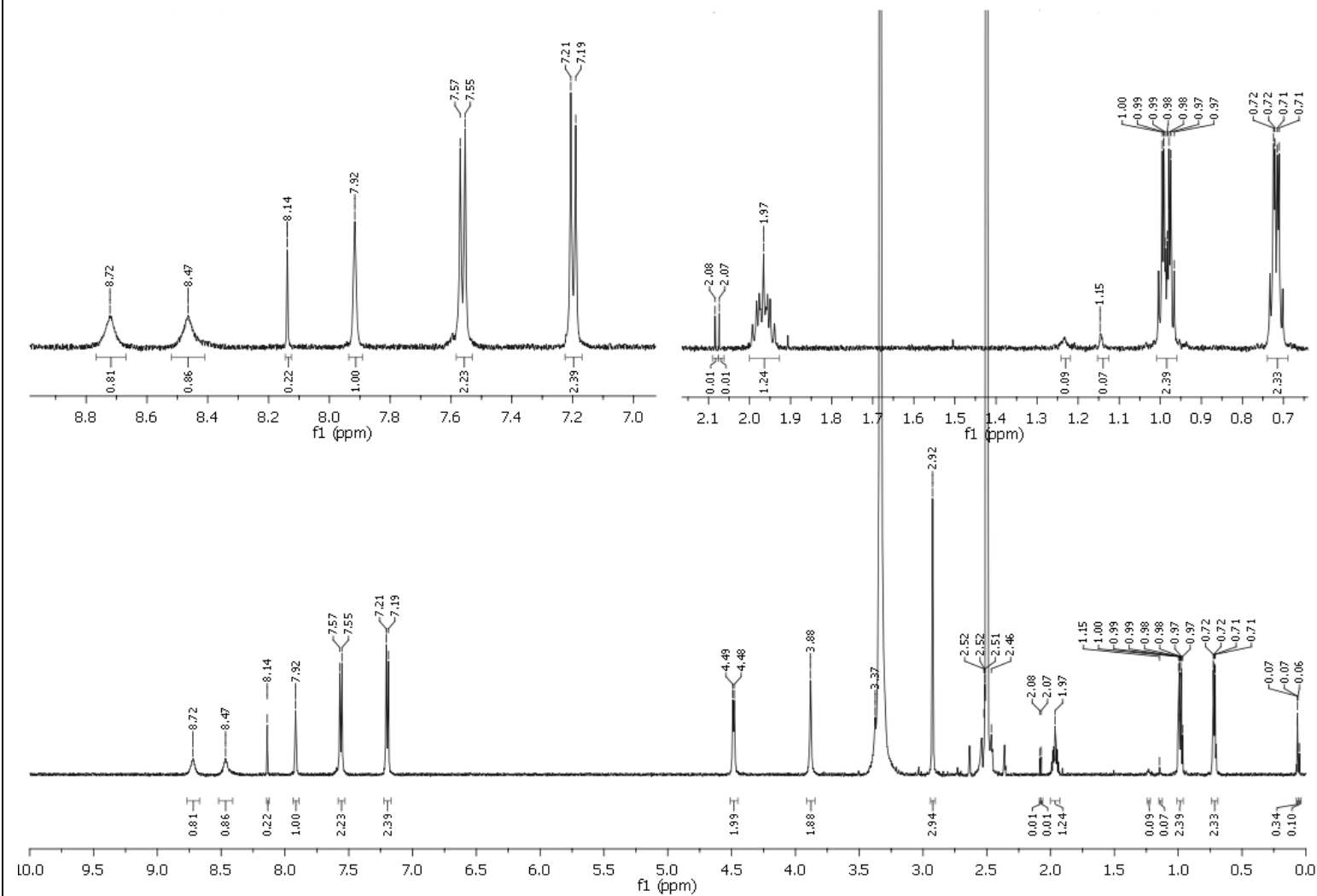
JDS09-121



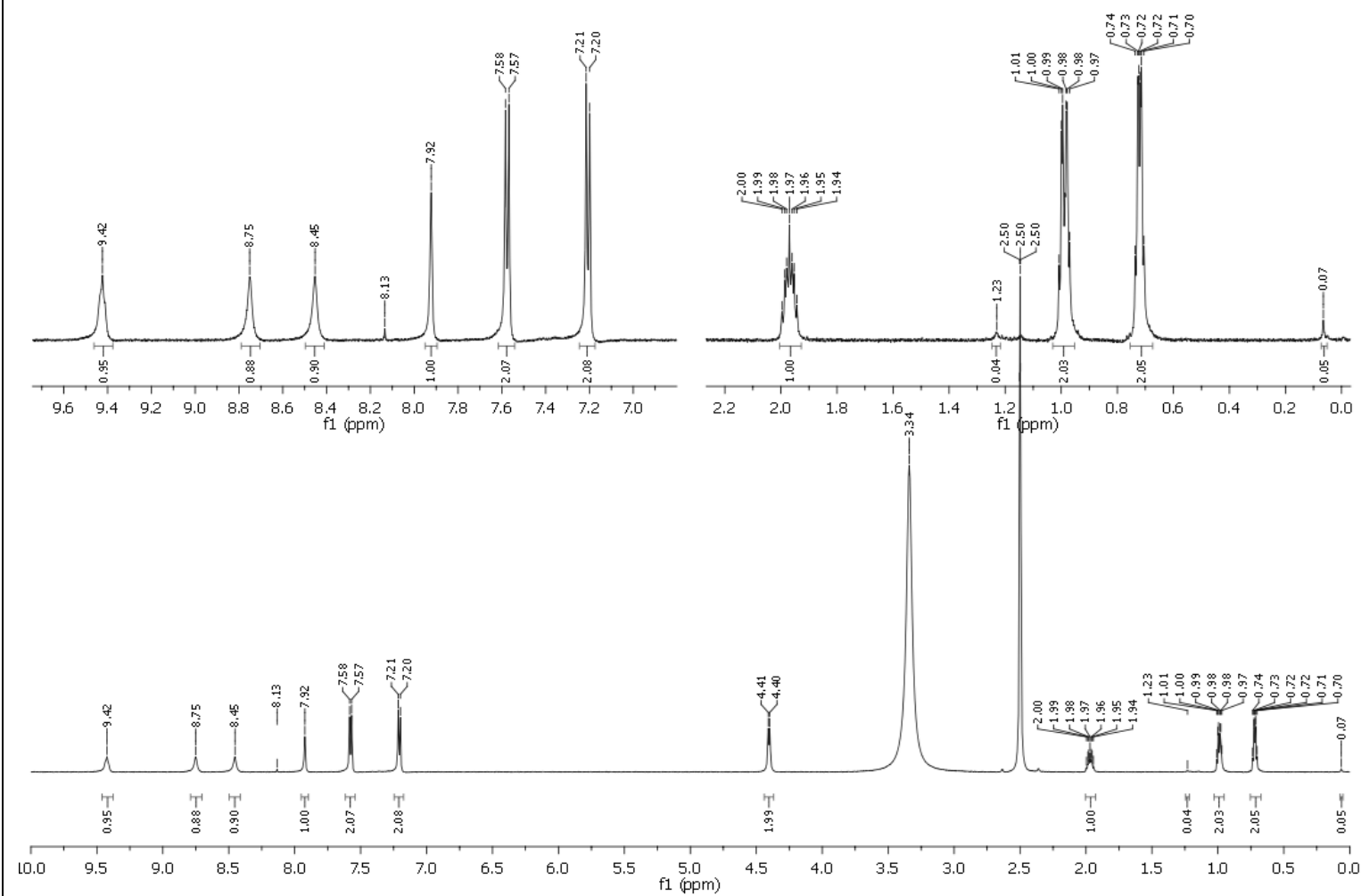
JDS09-123



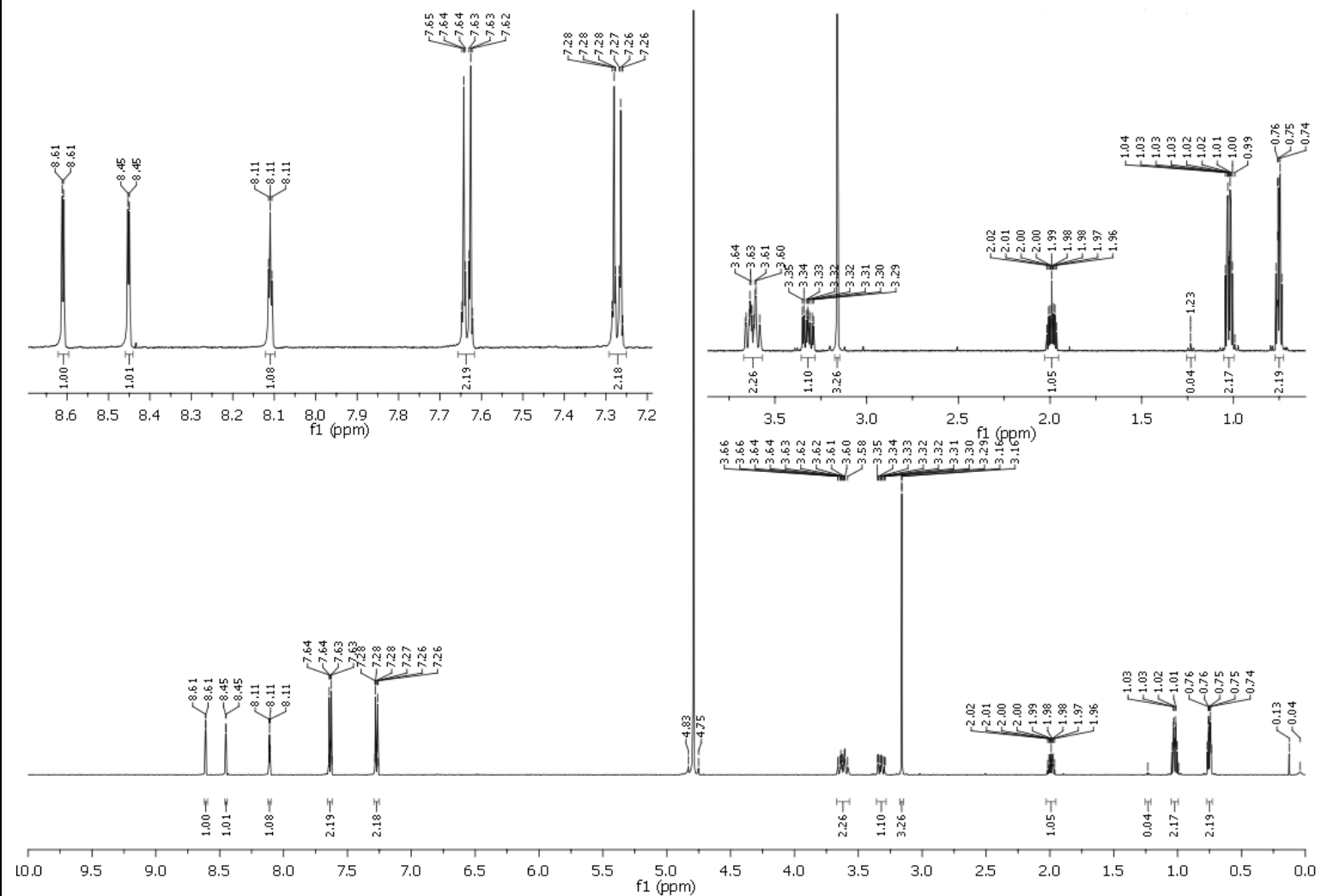
JDS10-011



JDS10-019

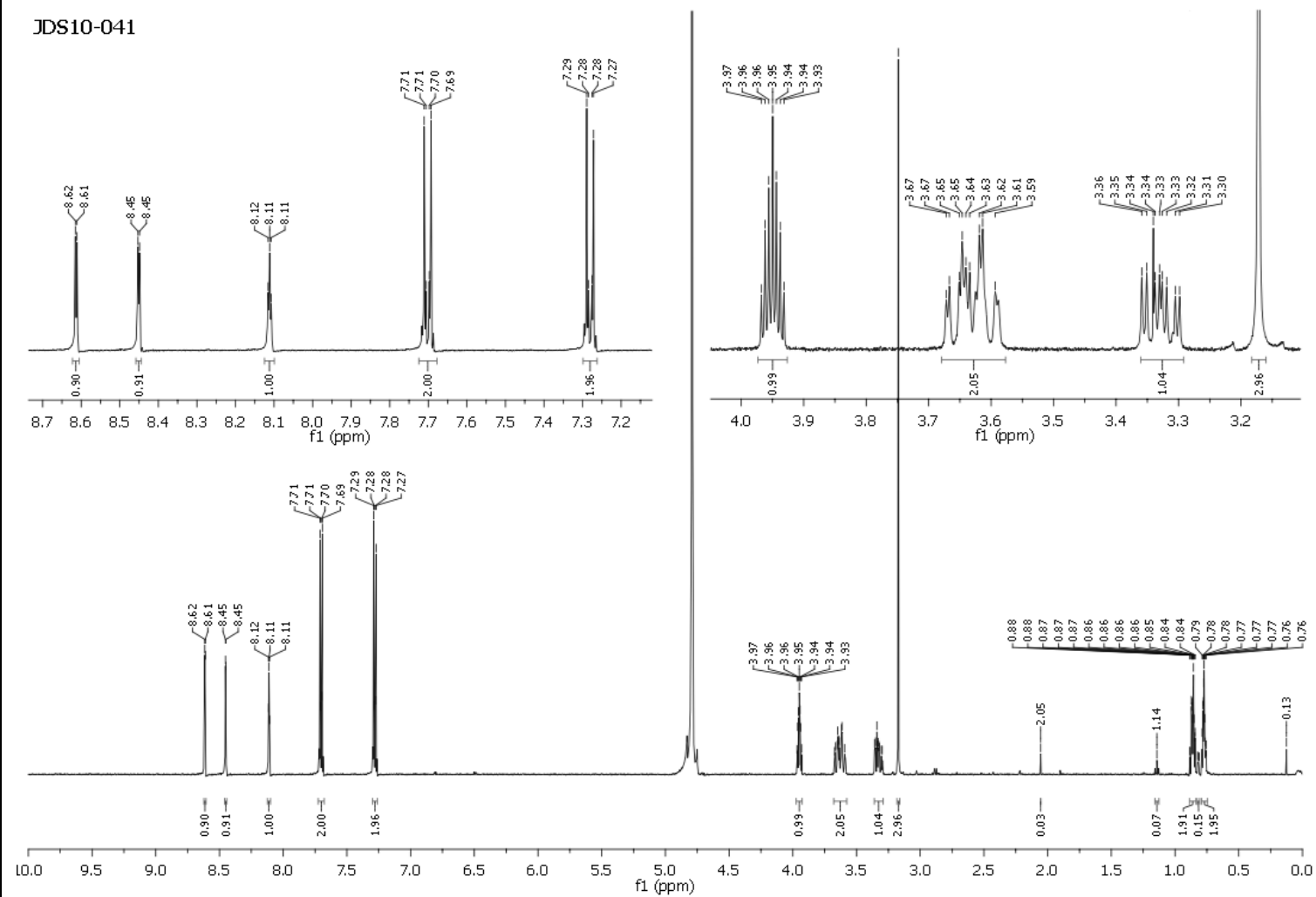


JDS10-040

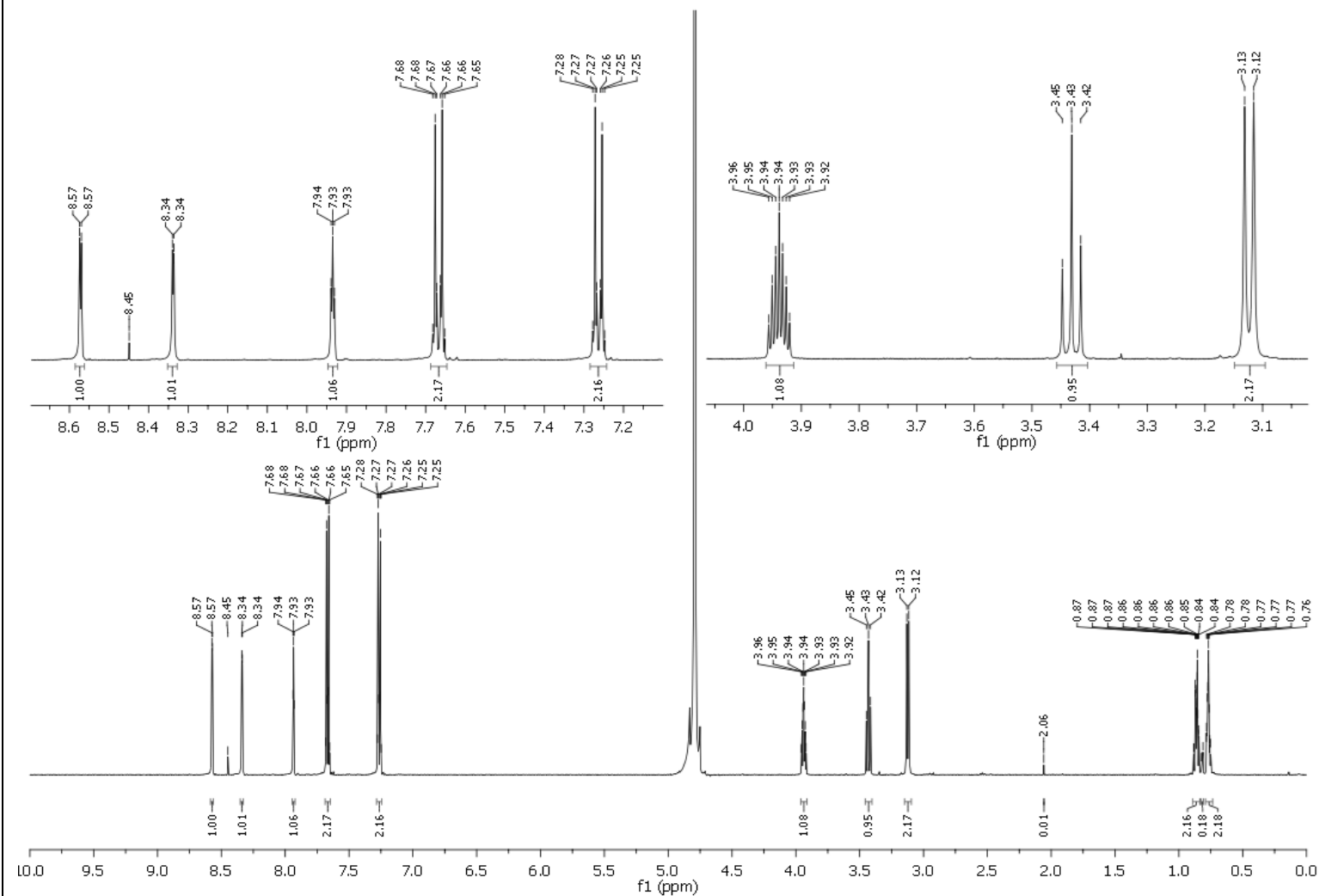


JDS10-041

JDS10-041

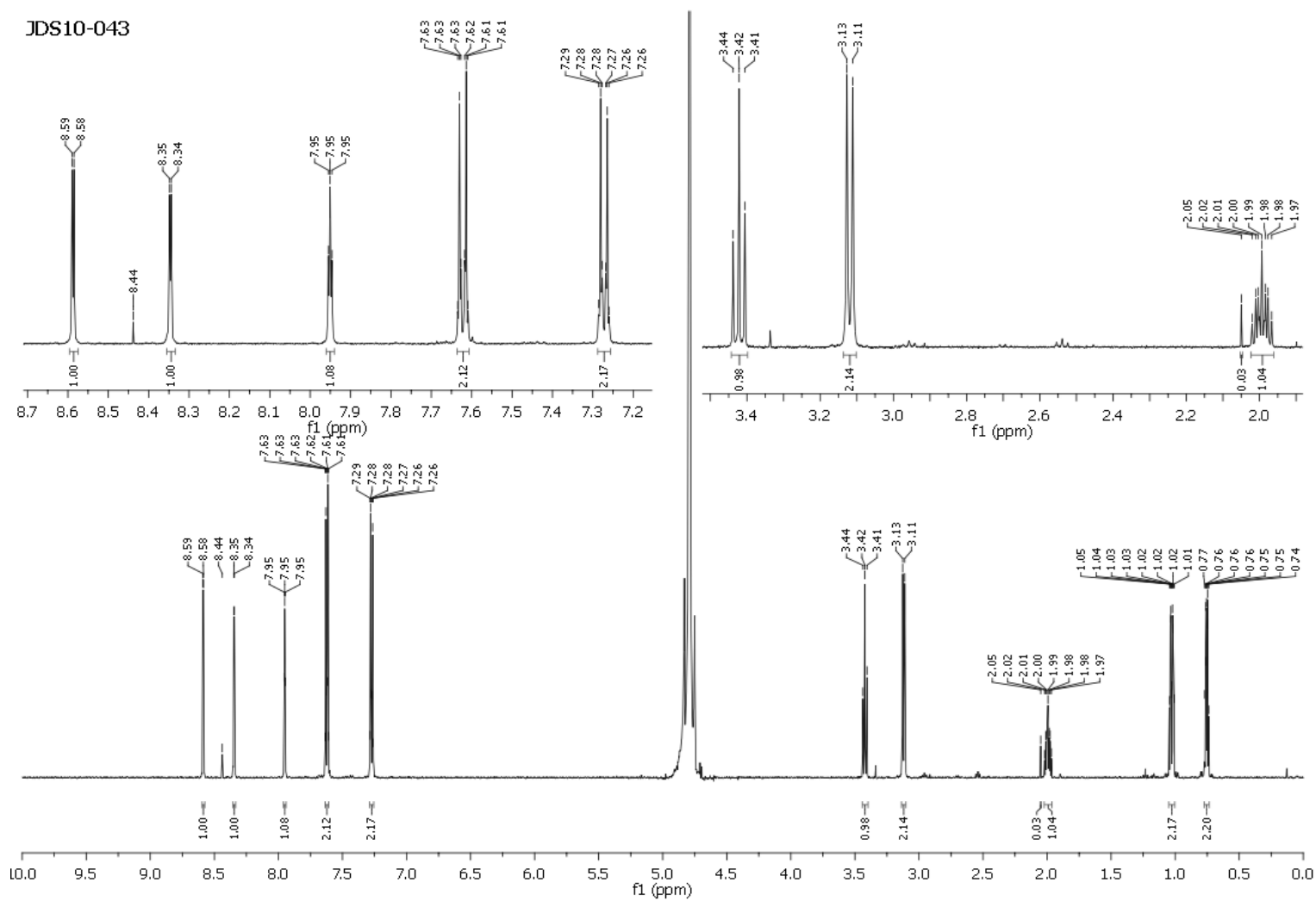


JDS10-042

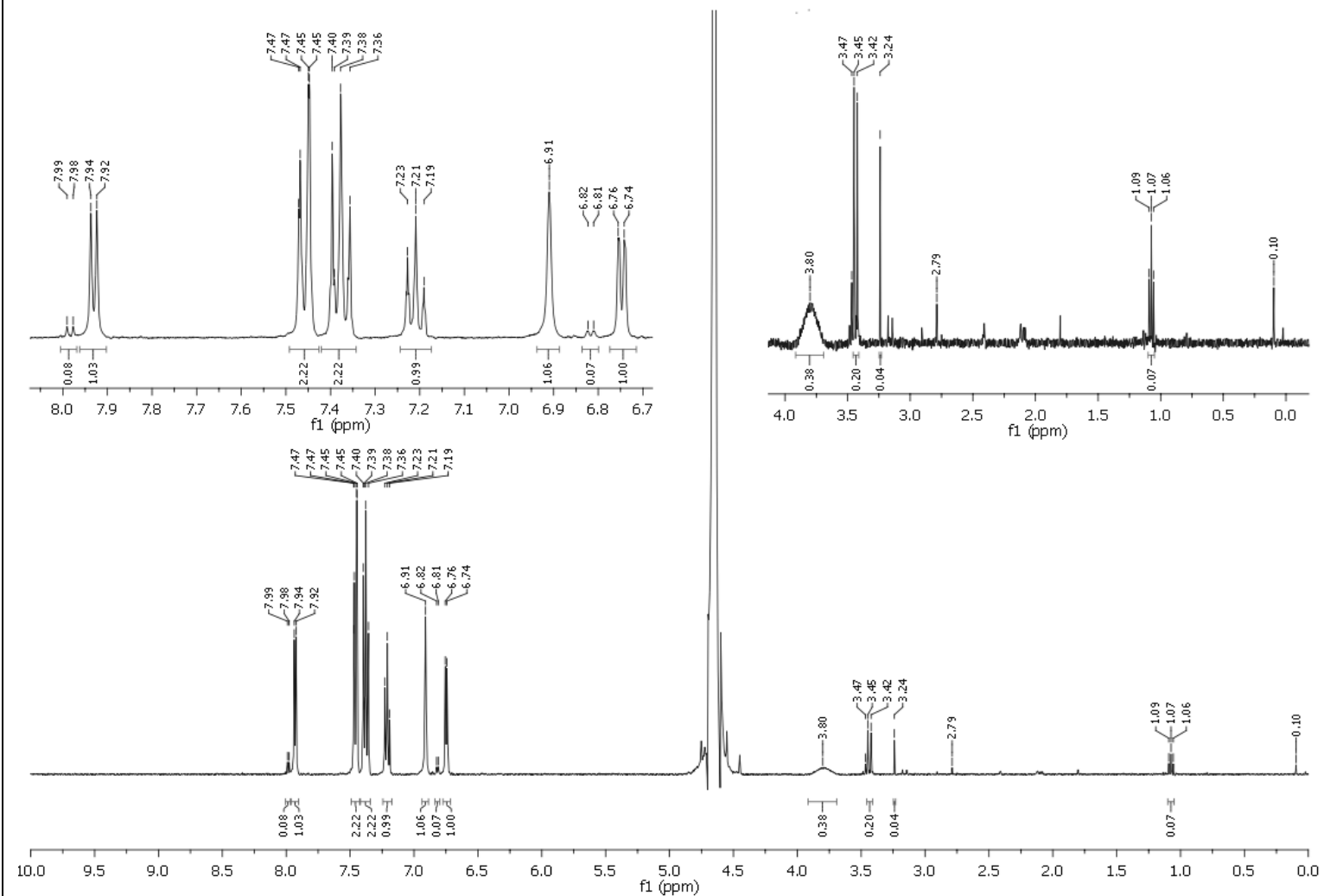


JDS10-043

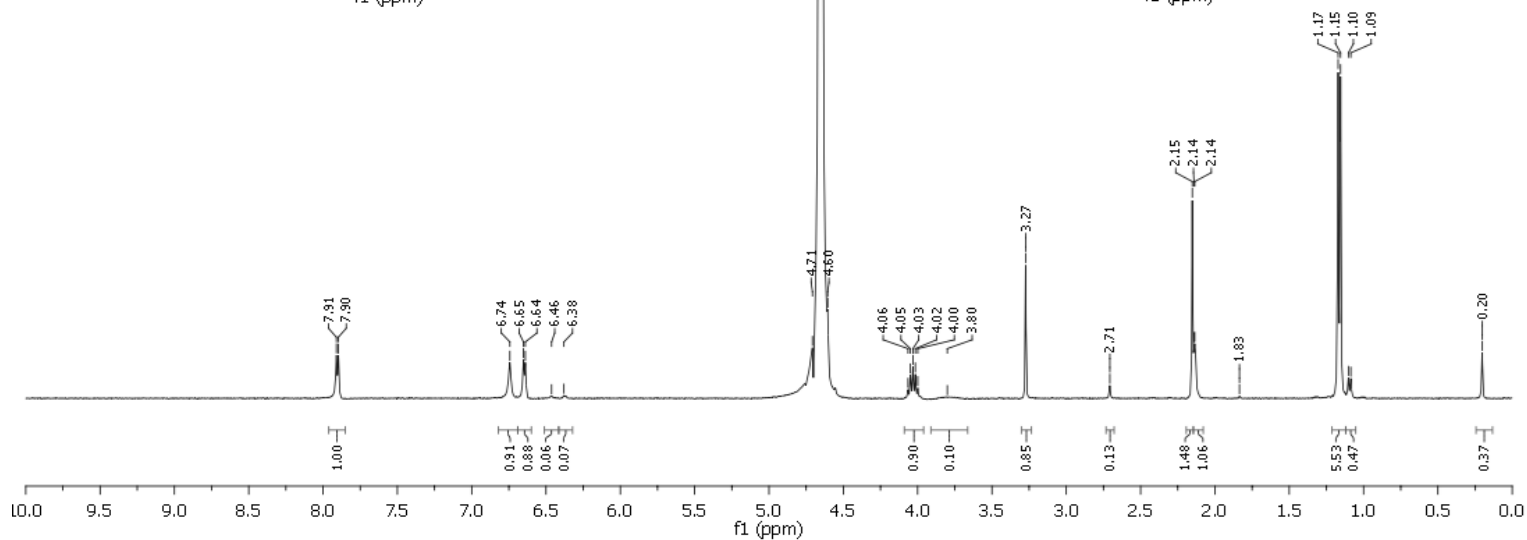
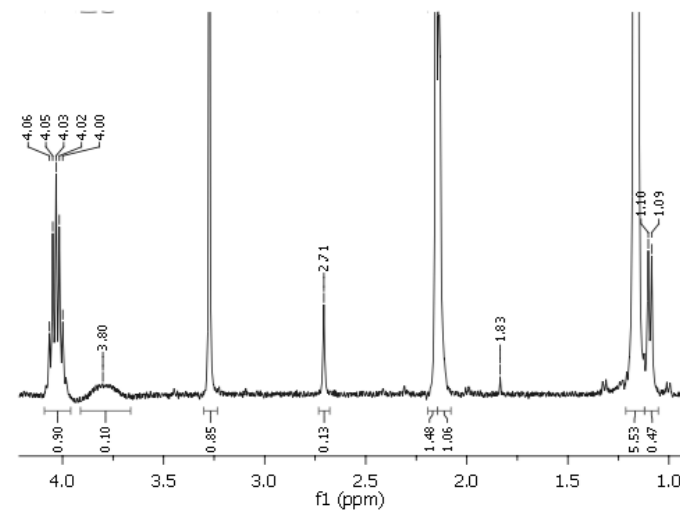
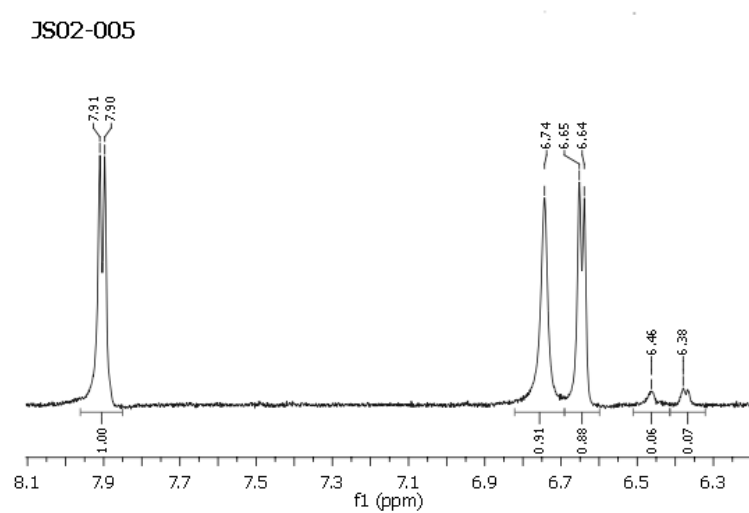
JDS10-043



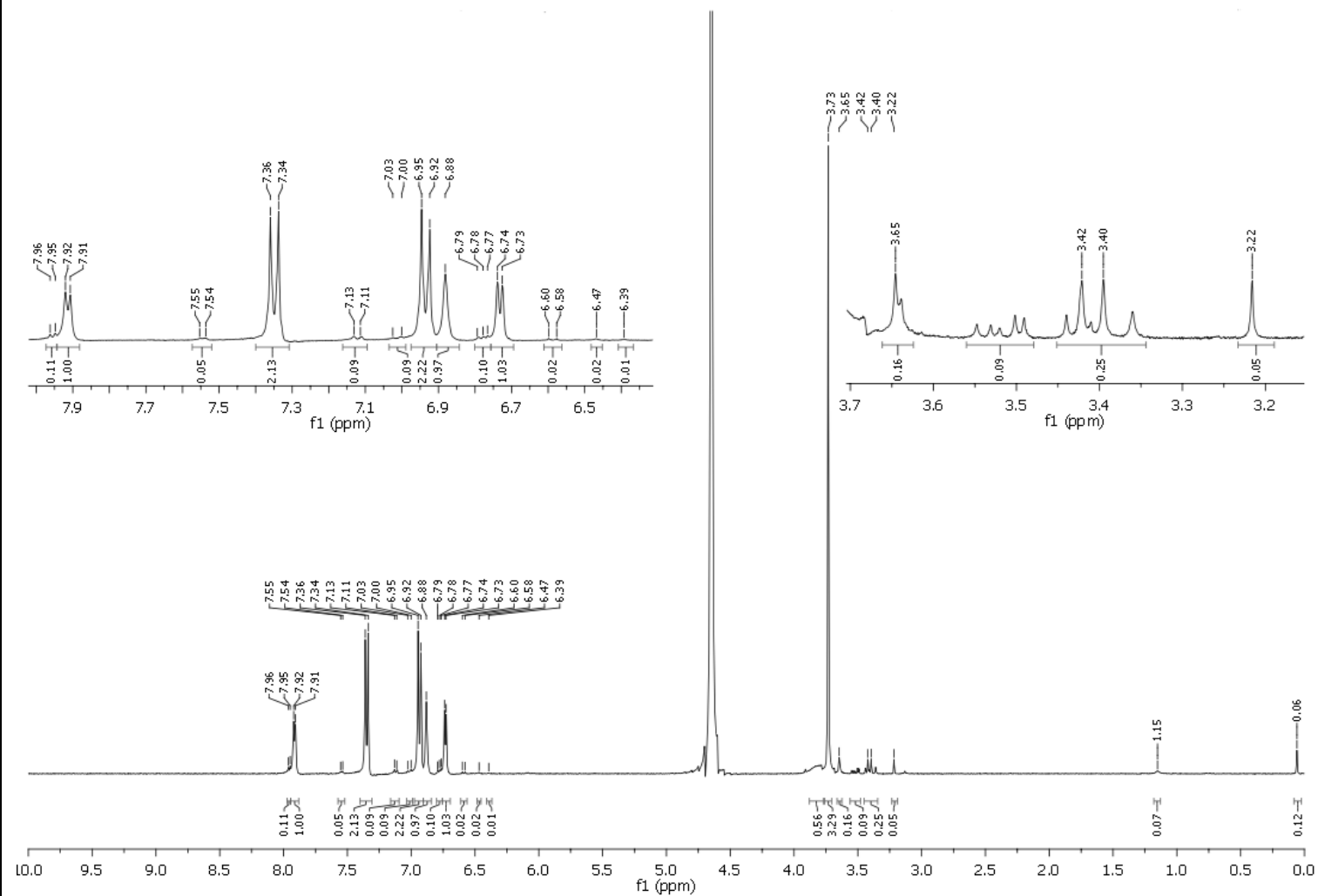
JS02-003



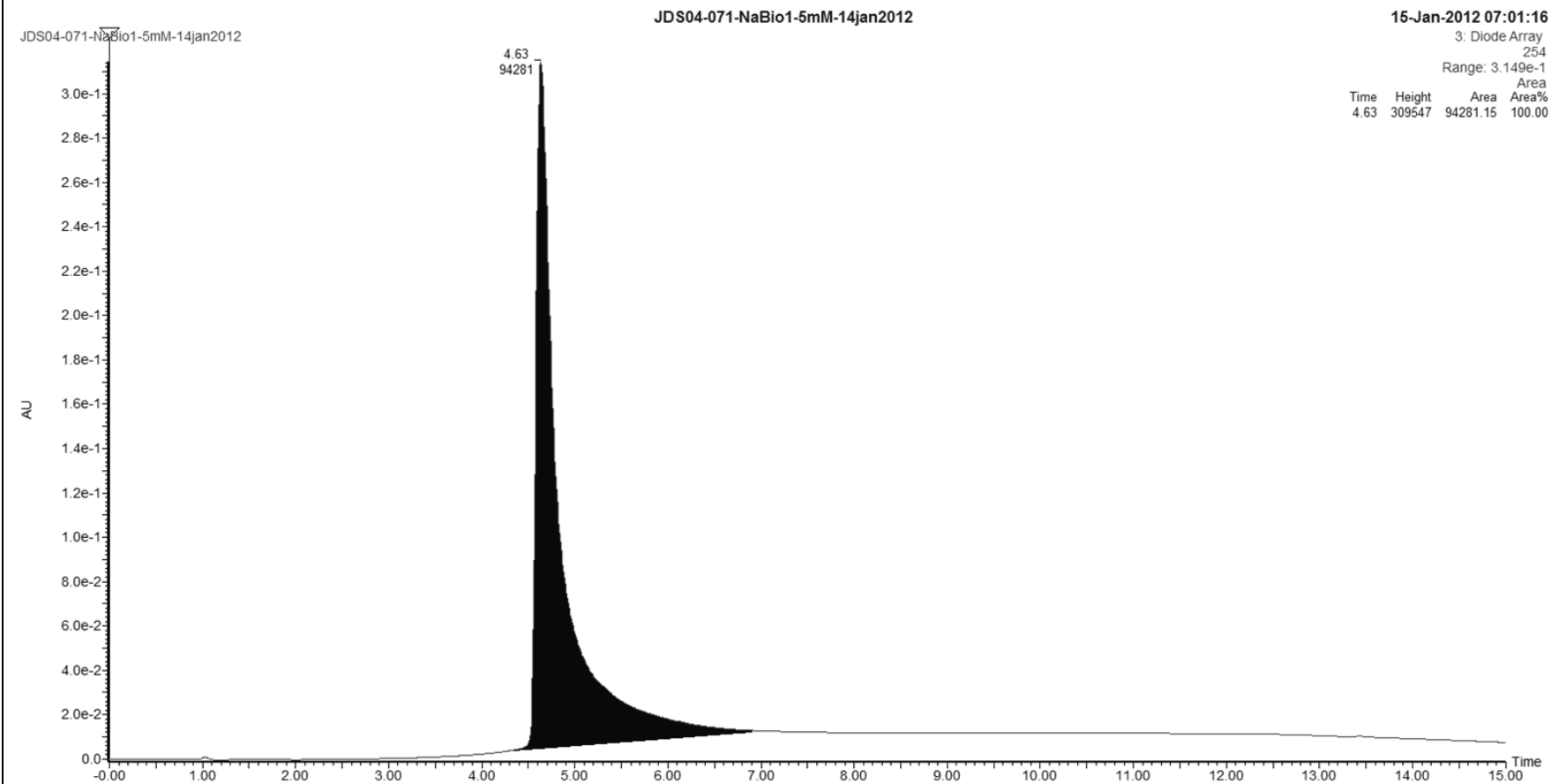
JS02-005



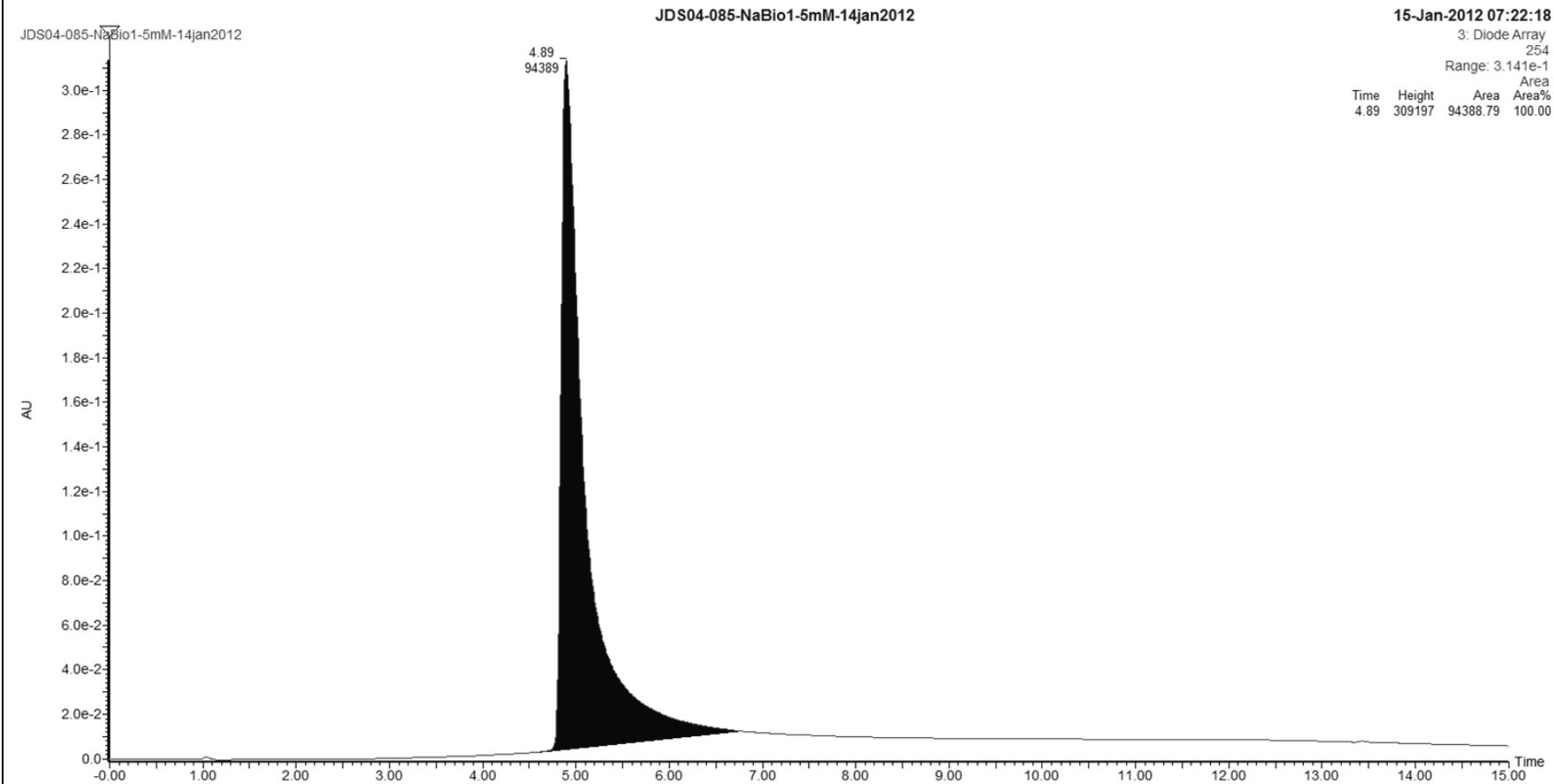
JS02-018



JDS04-071



JDS04-085



JDS05-020

JDS05-020-NaBio1mM-1to100-4dec11

05-Dec-2011 00:13:52

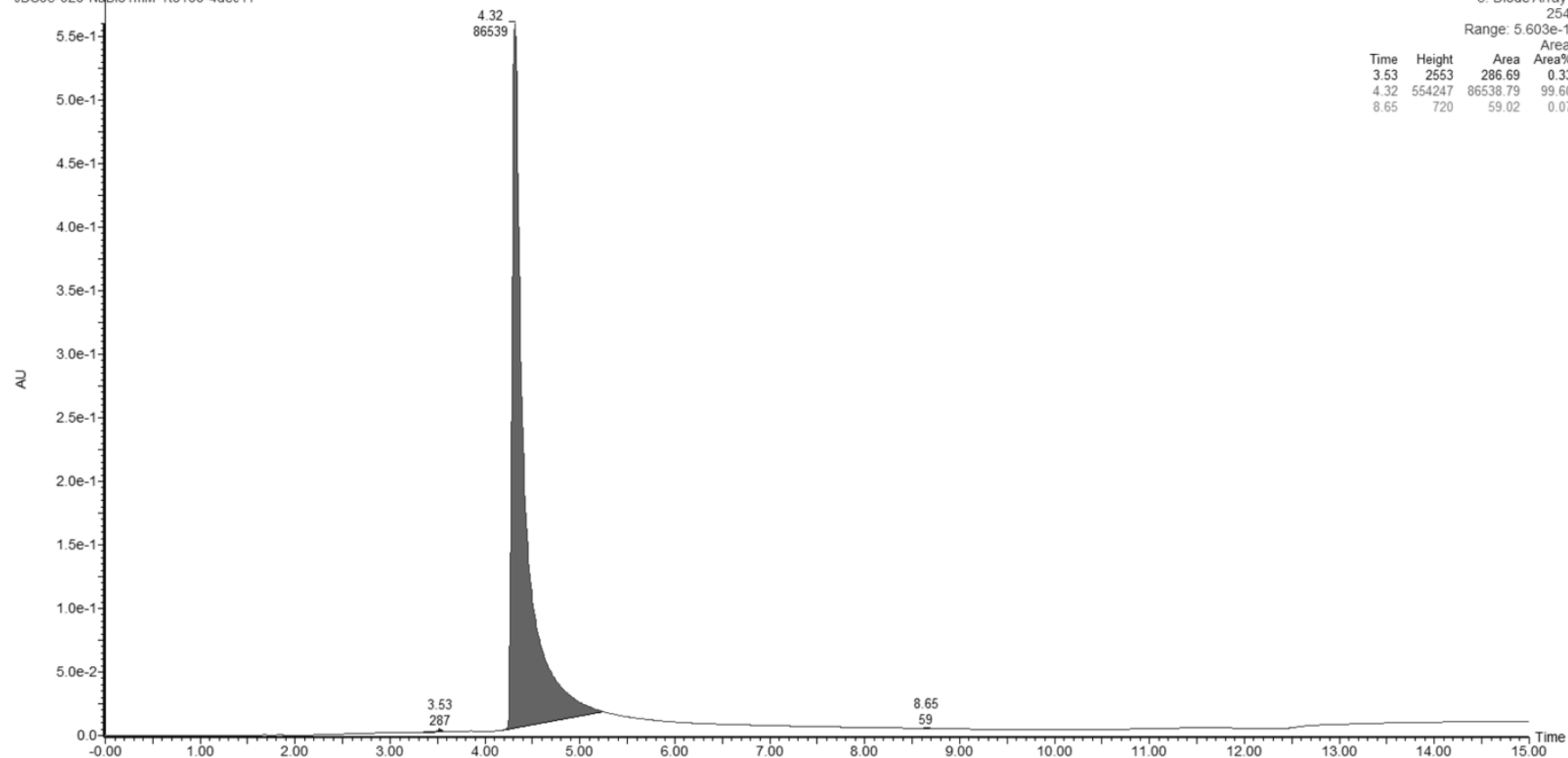
3: Diode Array

254

Range: 5.603e-1

Time	Height	Area	Area%
3.53	2553	286.69	0.33
4.32	554247	86538.79	99.60
8.65	720	59.02	0.07

JDS05-020-NaBio1mM-1to100-4dec11



JDS05-093

JDS05-093

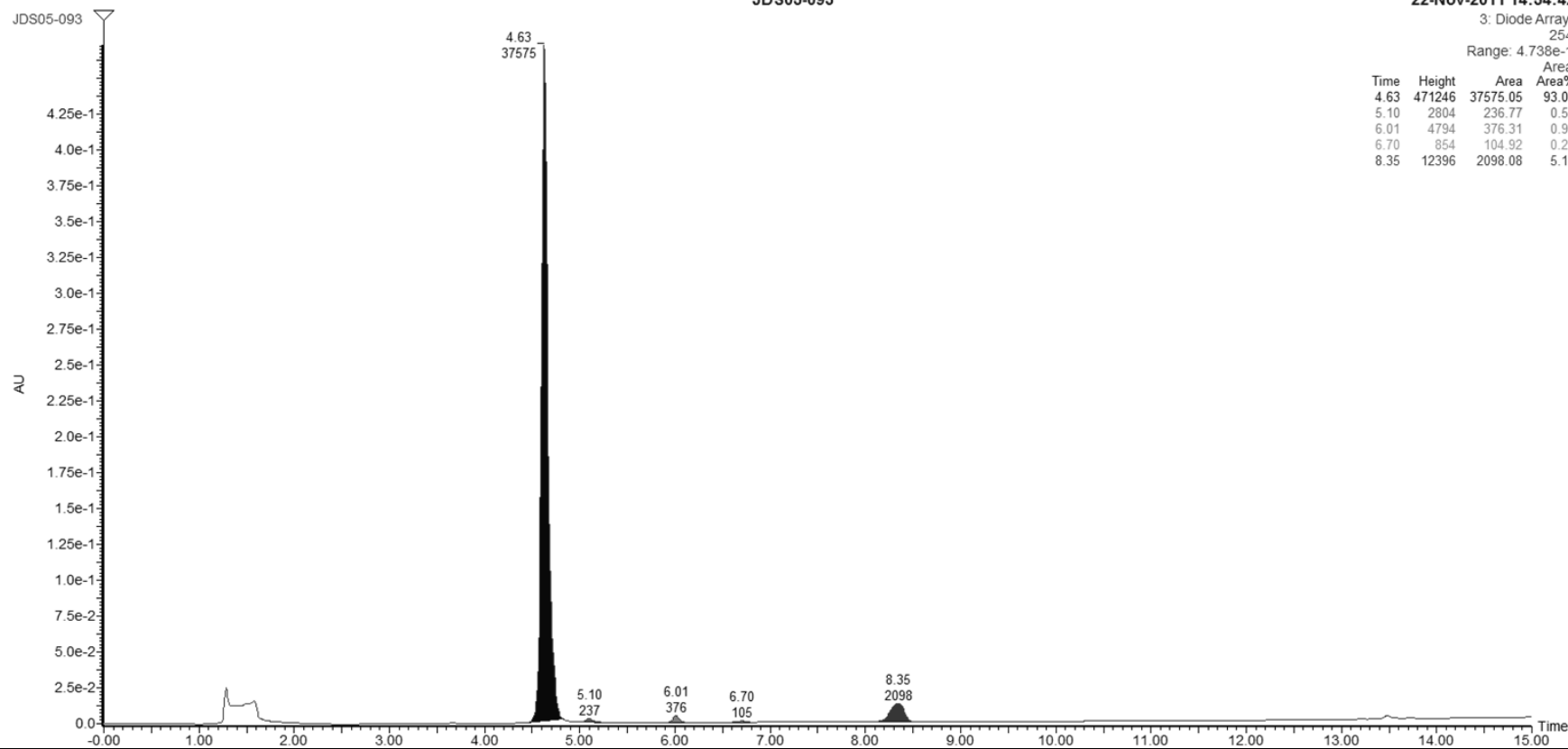
22-Nov-2011 14:54:42

3: Diode Array

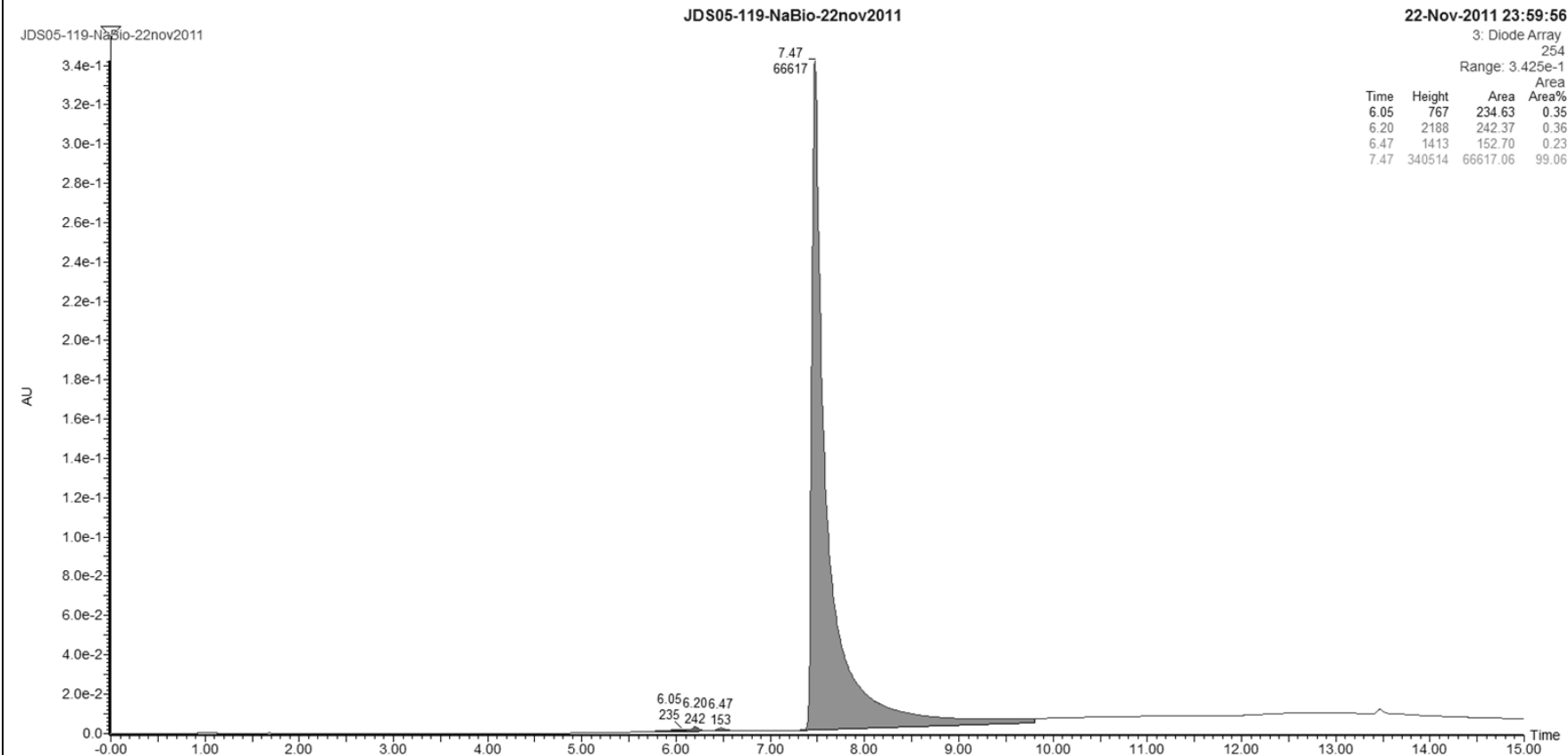
254

Range: 4.738e-1

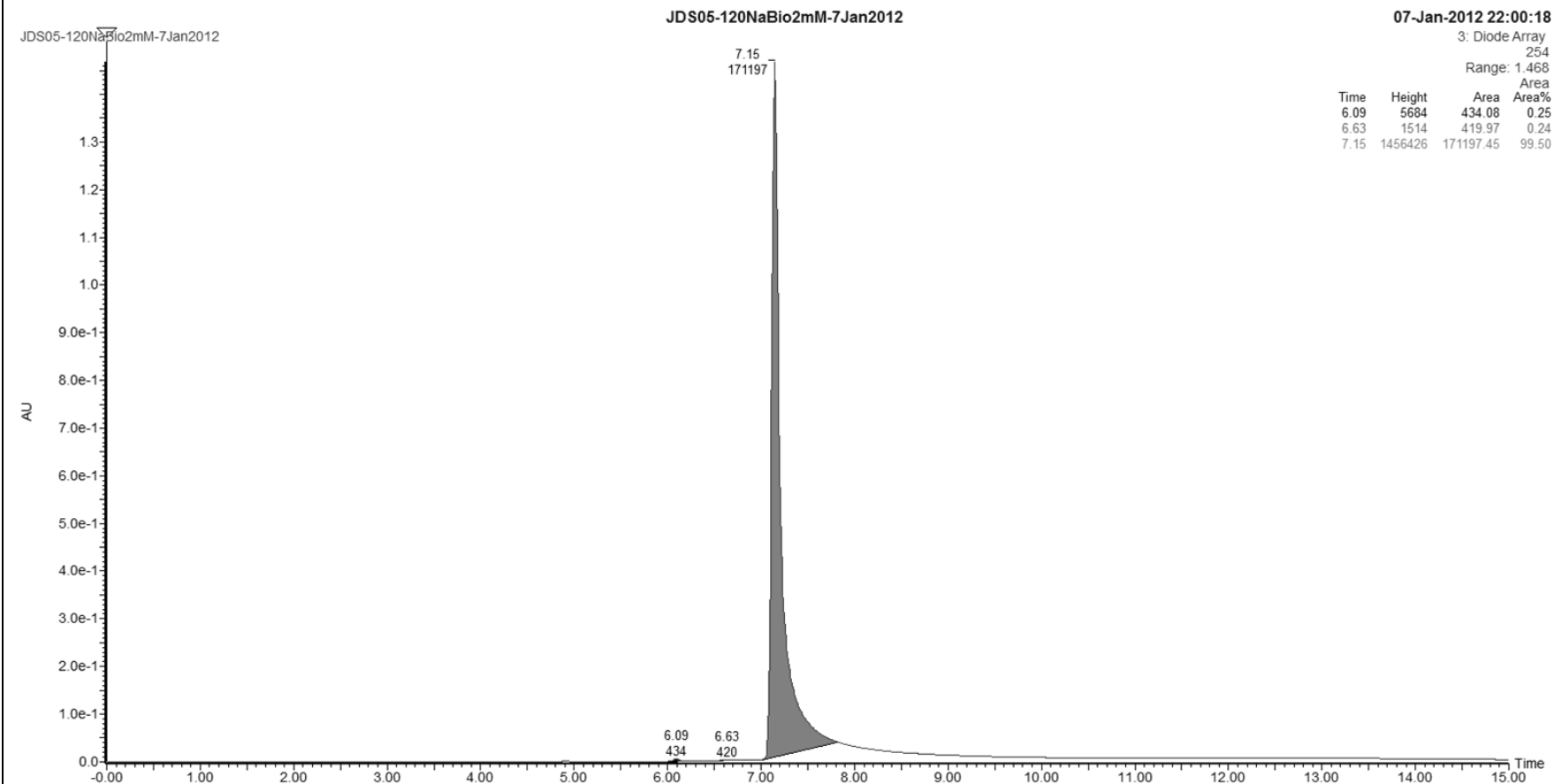
Time	Height	Area	Area%
4.63	471246	37575.05	93.03
5.10	2804	236.77	0.59
6.01	4794	376.31	0.93
6.70	854	104.92	0.26
8.35	12396	2098.08	5.19



JDS05-119



JDS05-120



JDS05-126

JDS05-126NaBio2mM-7Jan2012

JDS05-126NaBio2mM-7Jan2012

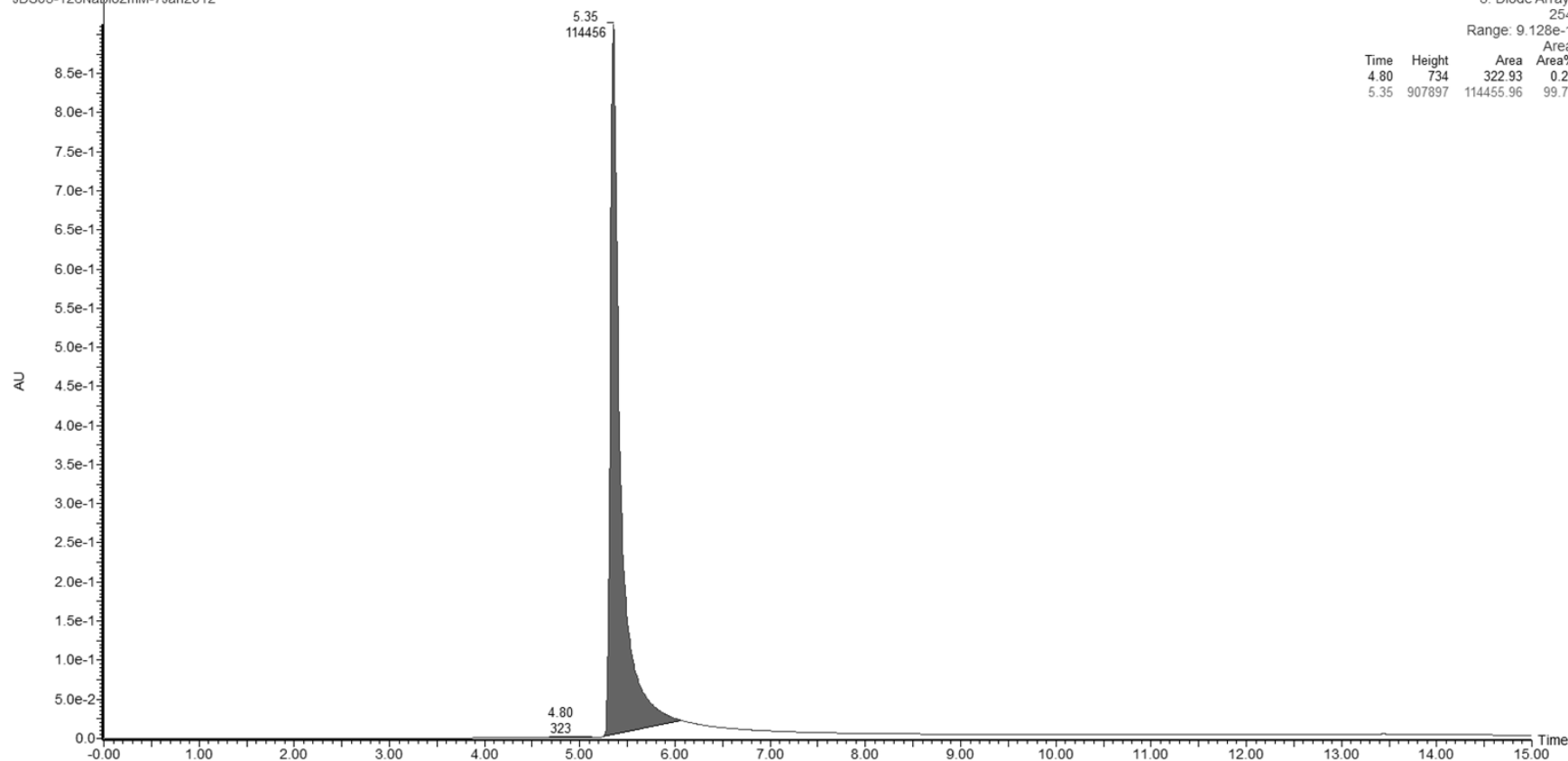
07-Jan-2012 22:42:23

3: Diode Array

254

Range: 9.128e-1

Time	Height	Area	Area%
4.80	734	322.93	0.28
5.35	907897	114455.96	99.72



JDS05-137

JDS05-137NaBio2mM-7Jan2012

JDS05-137NaBio2mM-7Jan2012

07-Jan-2012 23:24:28

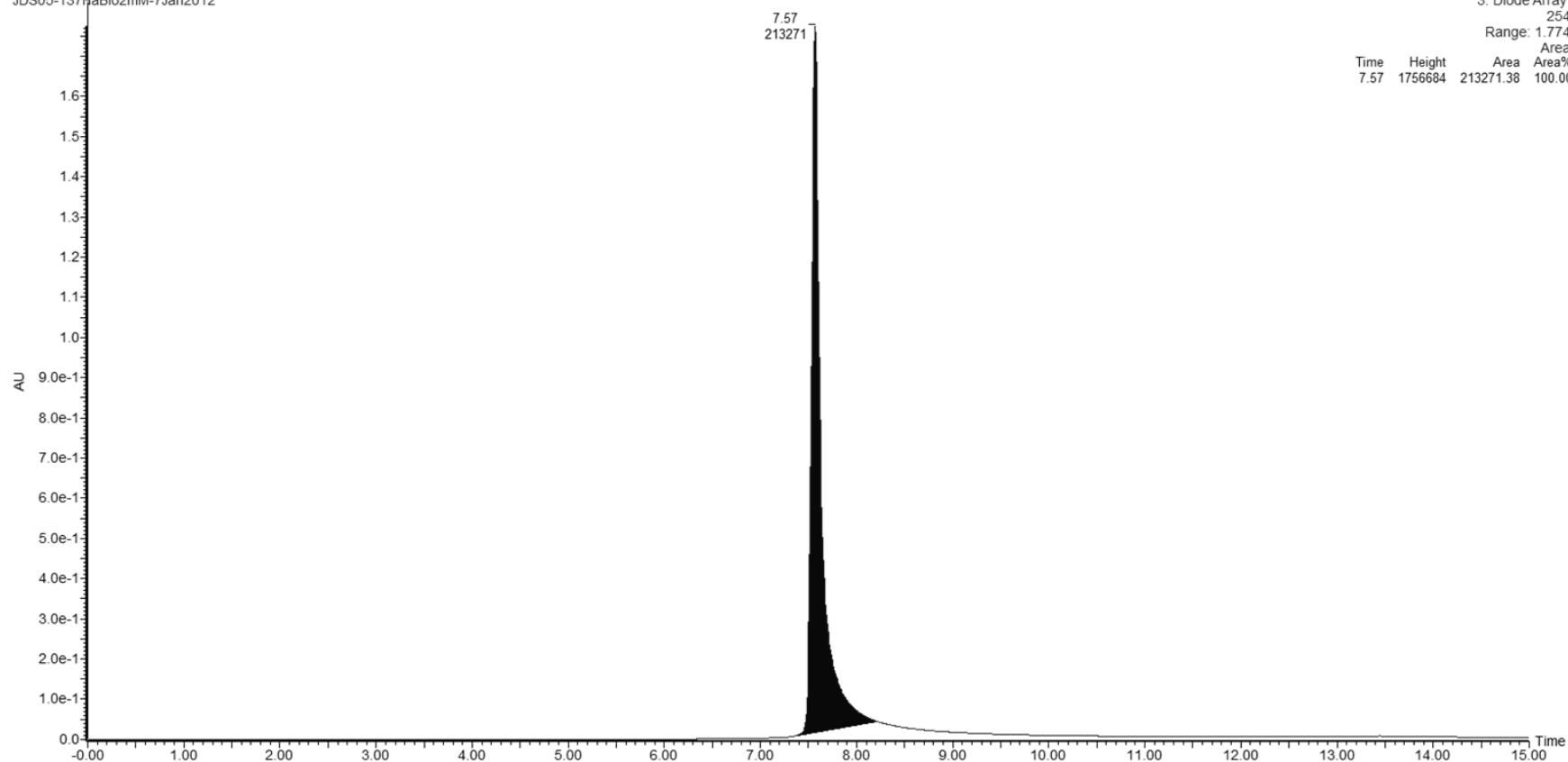
3: Diode Array

254

Range: 1.774

Area

Time	Height	Area	Area%
7.57	1756684	213271.38	100.00



JDS07-022

JDS07-022-NaBio1mM-1to100-4dec11

JDS07-022-NaBio1mM-1to100-4dec11

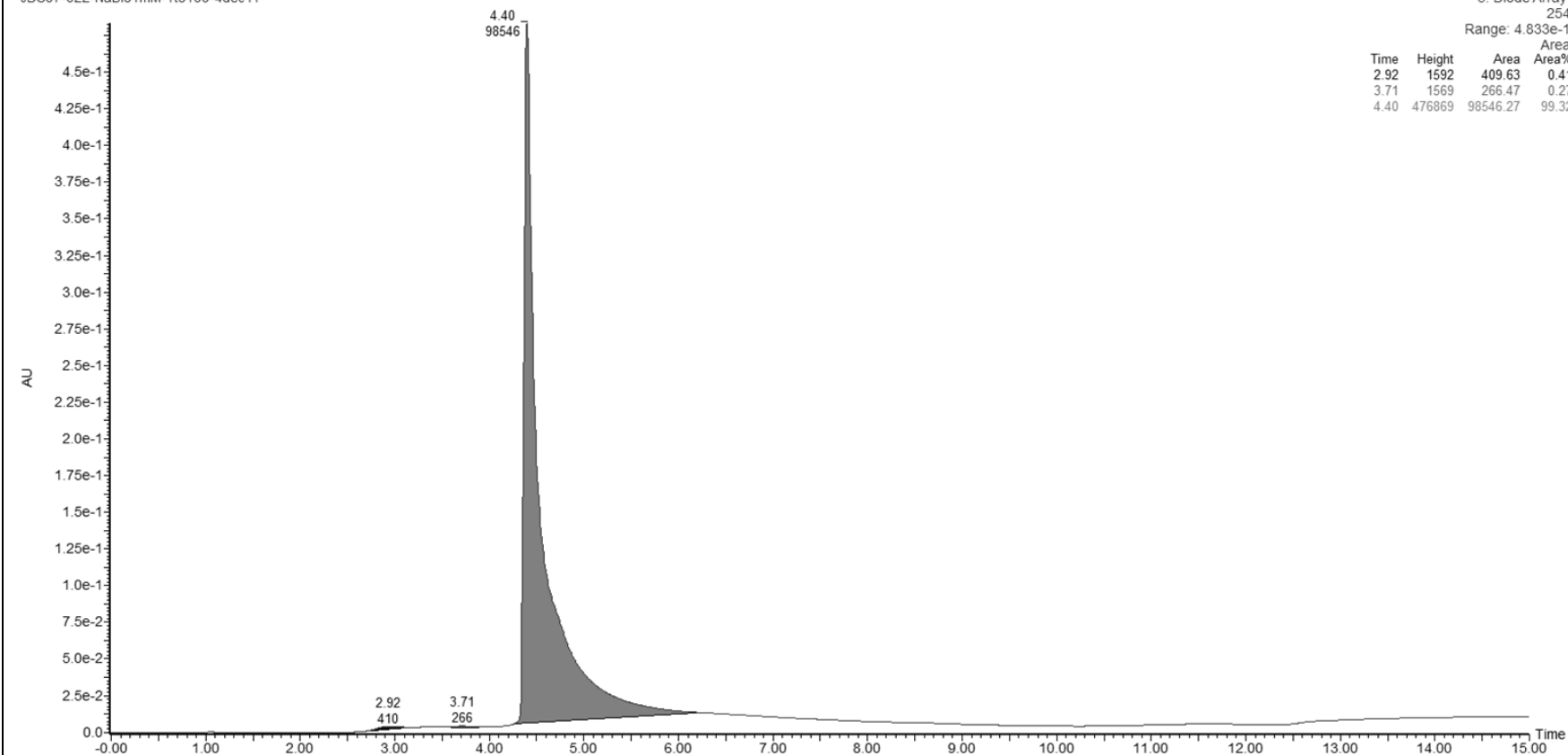
05-Dec-2011 03:02:12

3: Diode Array

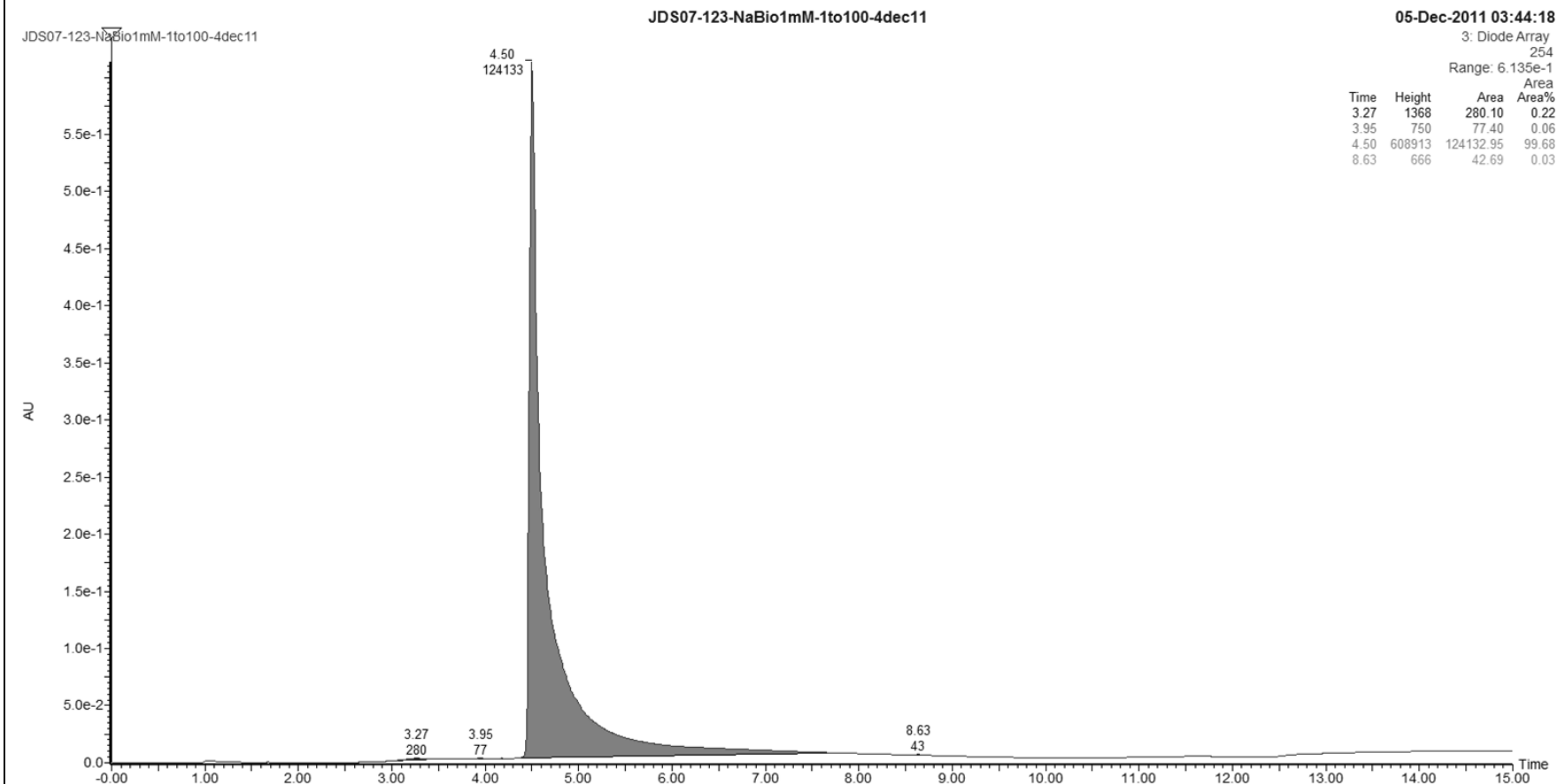
254

Range: 4.833e-1

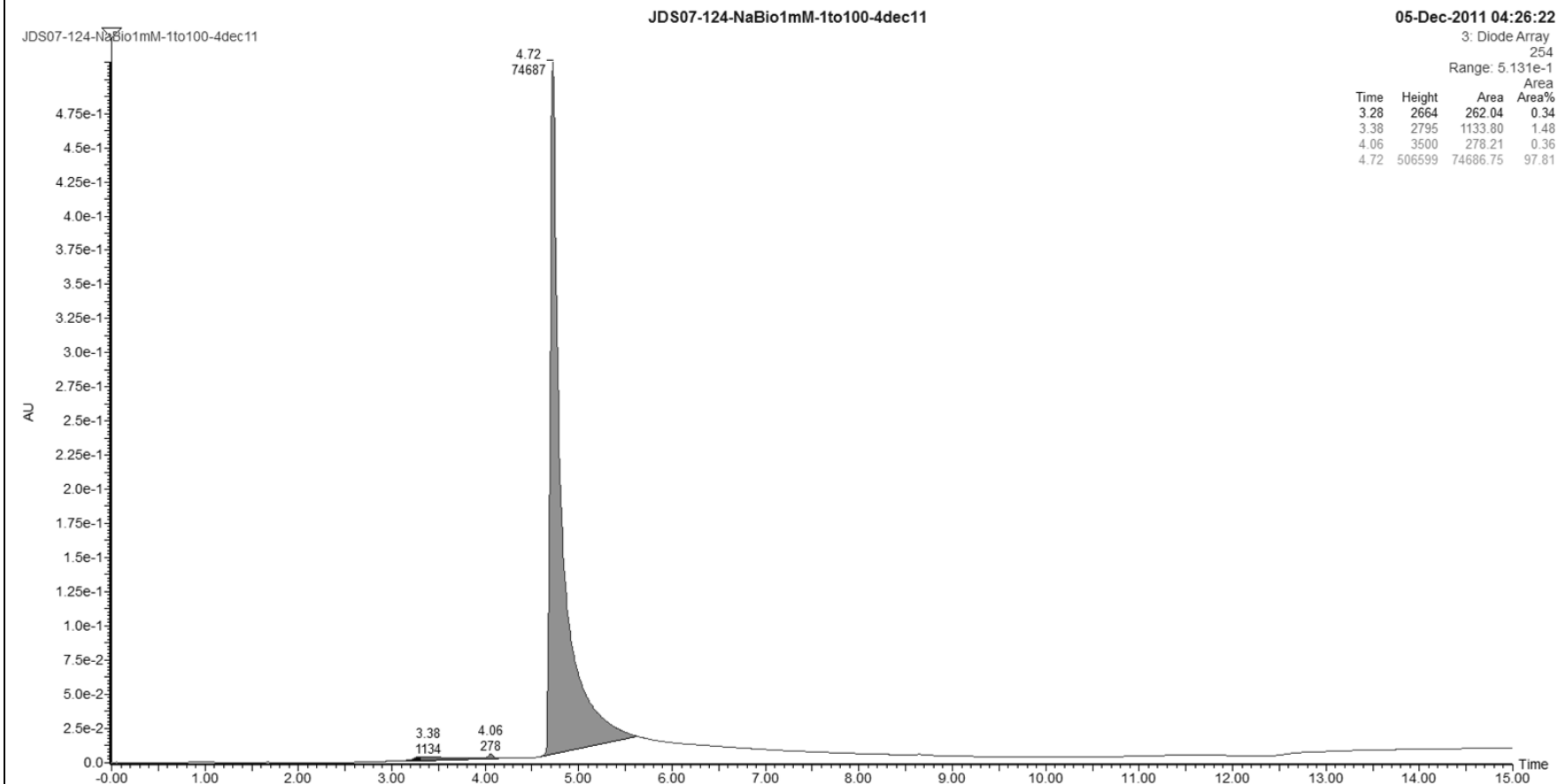
Time	Height	Area	Area%
2.92	1592	409.63	0.41
3.71	1569	266.47	0.27
4.40	476869	98546.27	99.32



JDS07-023



JDS07-024

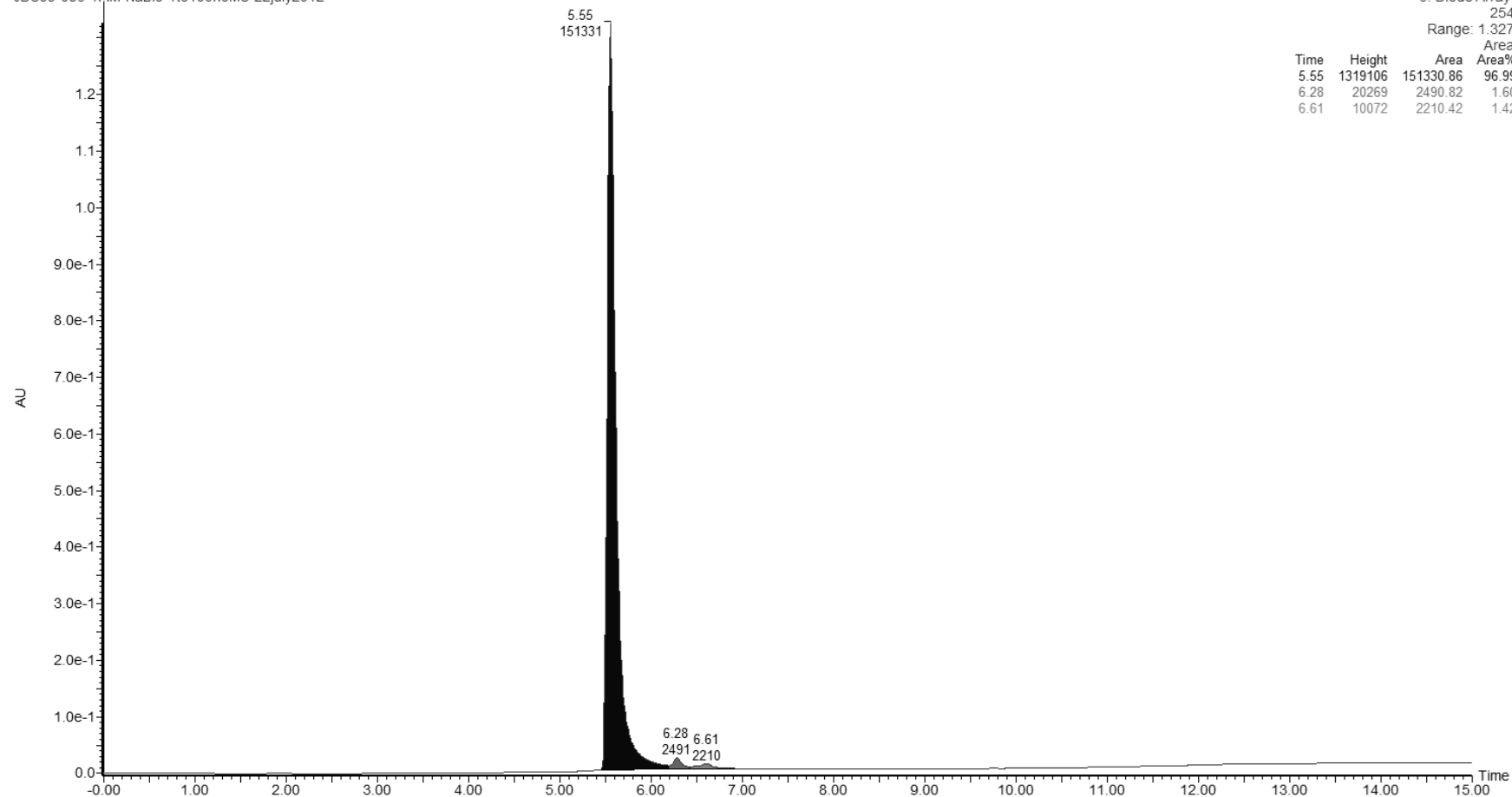


JDS09-083

JDS09-083-1mM-NaBio-1to100noMS-22july2012

22-Jul-2012 00:23:02

JDS09-083-1mM-NaBio-1to100noMS-22july2012



3: Diode Array
254
Range: 1.327

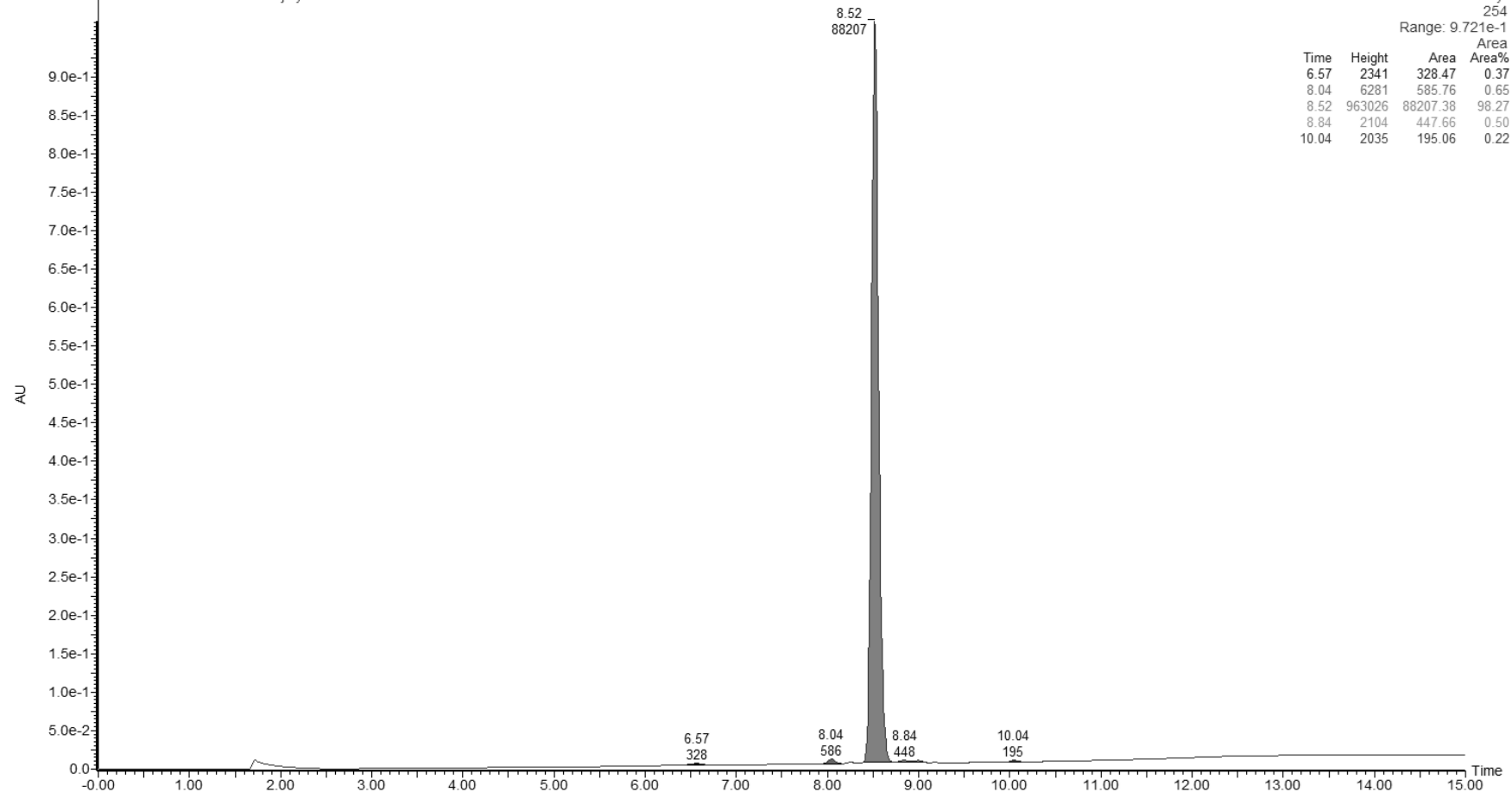
Time	Height	Area	Area%
5.55	1319106	151330.86	96.99
6.28	20269	2490.82	1.60
6.61	10072	2210.42	1.42

JDS09-119

JDS09-119-1mM-50dmso-1to100noMS-22july2012

22-Jul-2012 00:44:12

JDS09-119-1mM-50dmso-1to100noMS-22july2012

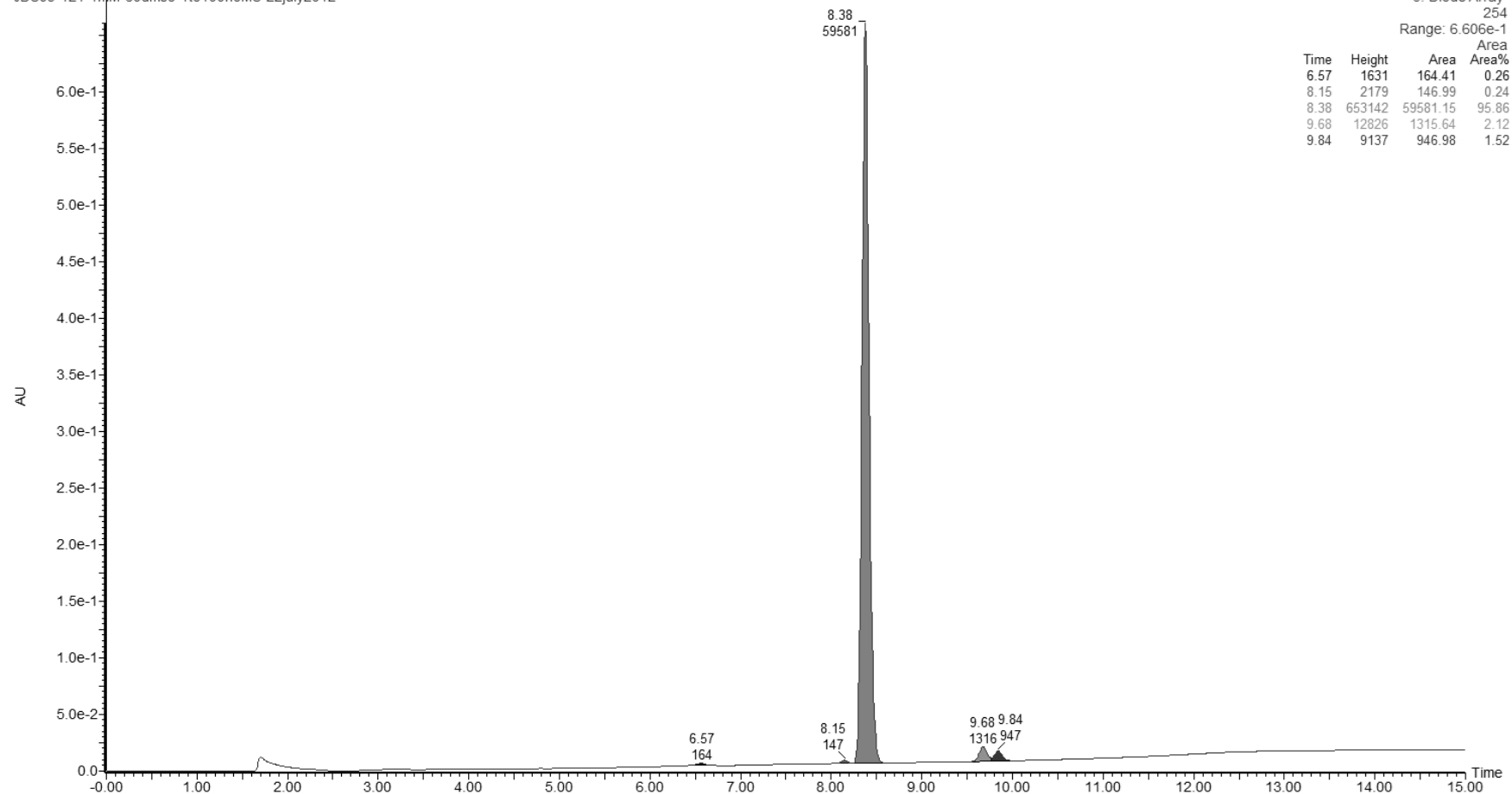


JDS09-121

JDS09-121-1mM-60dmso-1to100noMS-22july2012

22-Jul-2012 01:05:14

JDS09-121-1mM-60dmso-1to100noMS-22july2012



JDS09-123

JDS09-123-trit

25-Jul-2012 20:08:03

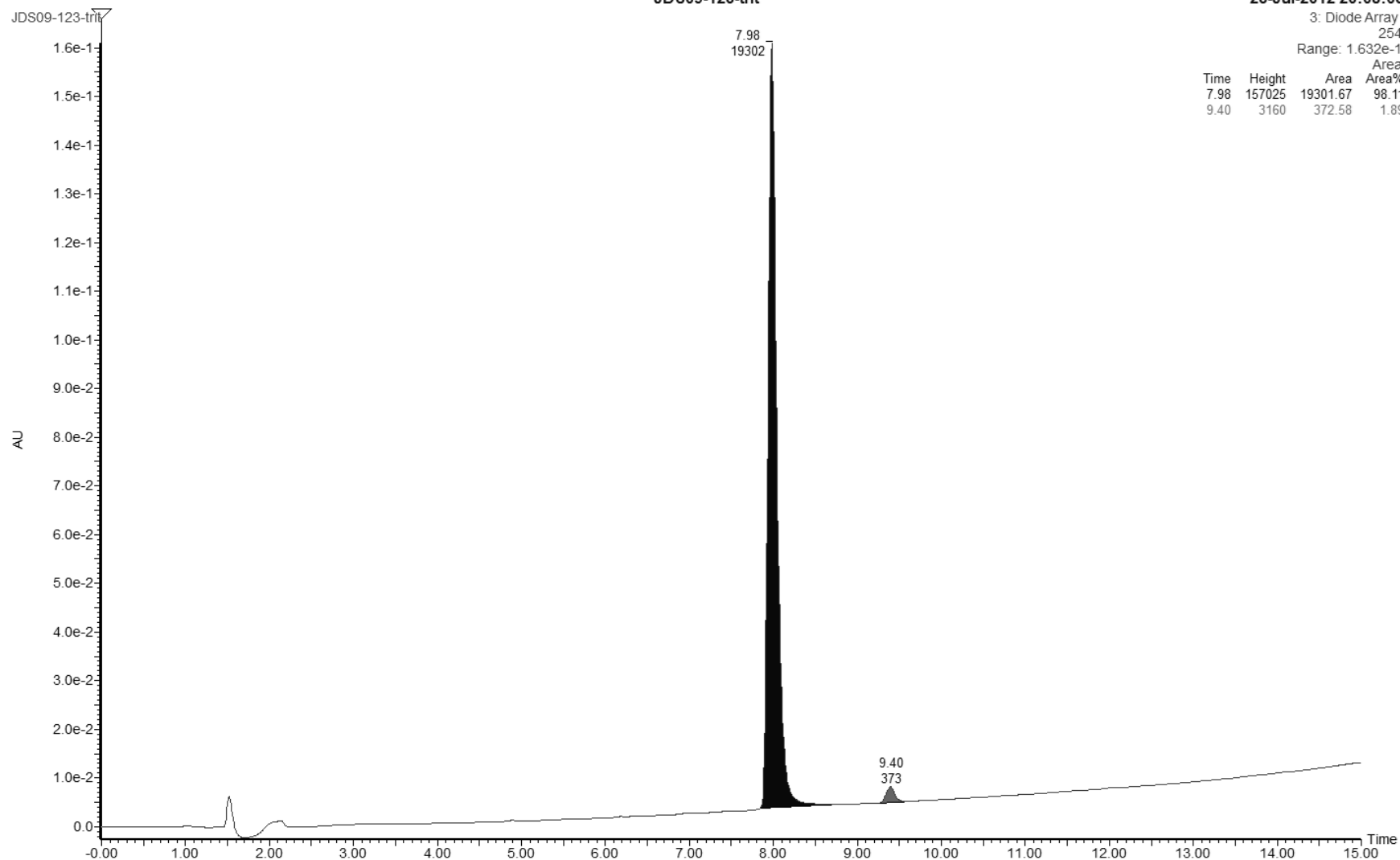
3: Diode Array

254

Range: 1.632e-1

Area

Time	Height	Area	Area%
7.98	157025	19301.67	98.11
9.40	3160	372.58	1.89



JDS10-011

JDS10-011-DMSOBio-1mM-95-5-AtIC18-20Sept2012

20-Sep-2012 13:54:10

JDS10-011-DMSOBio-1mM-95-5-AtIC18-20Sept2012

3: Diode Array

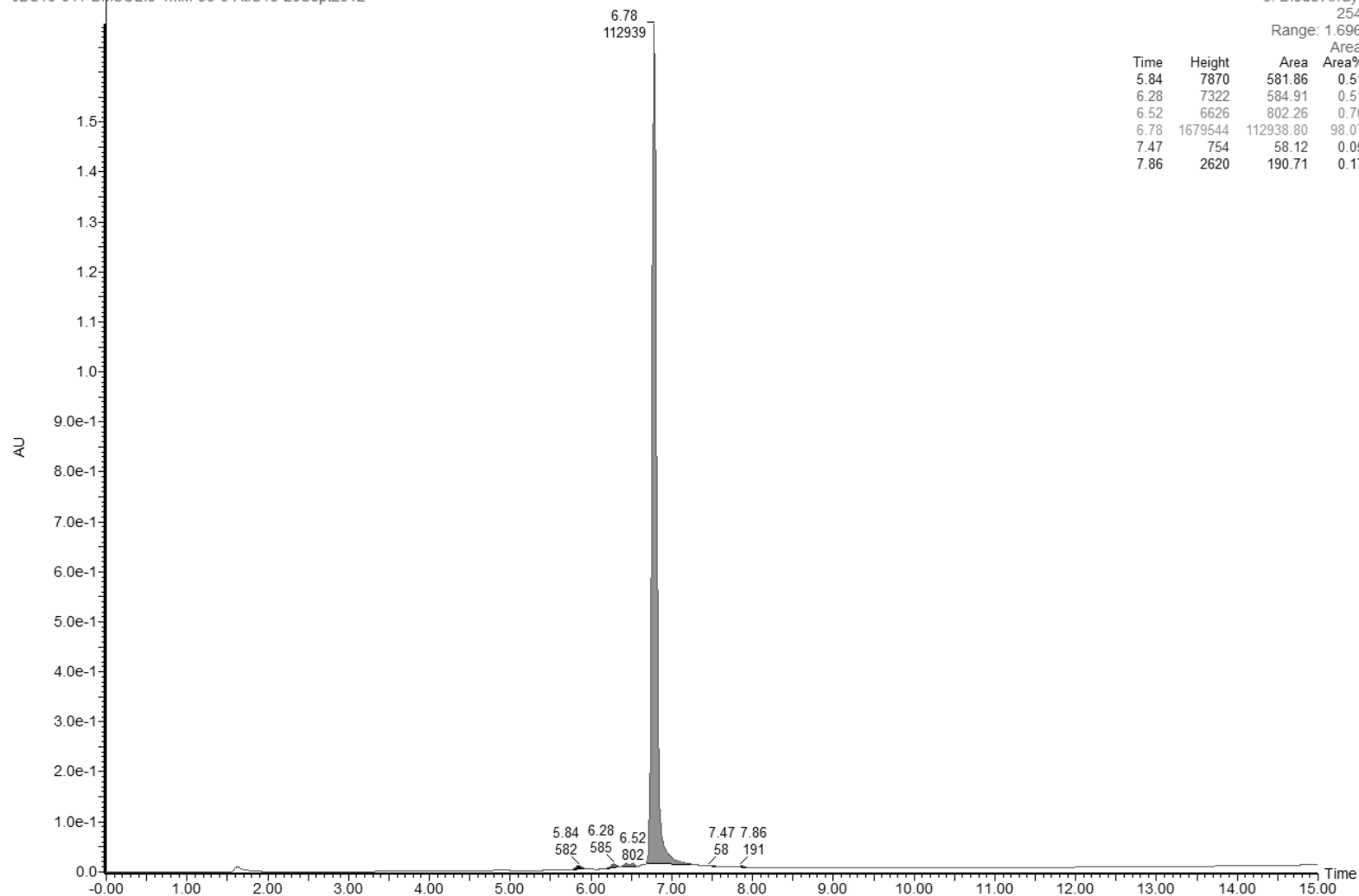
254

Range: 1.696

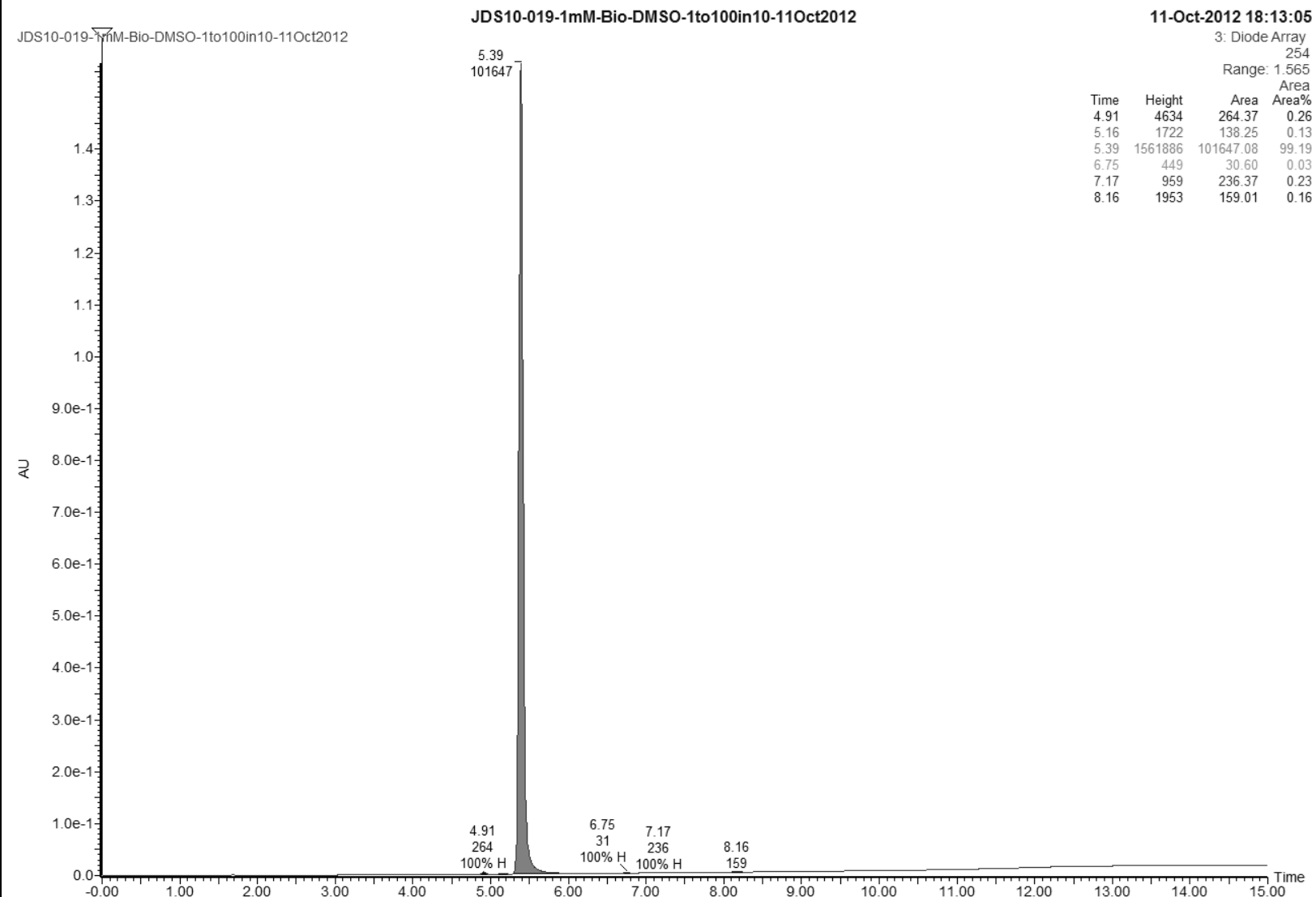
Area

Area%

Time	Height	Area	Area%
5.84	7870	581.86	0.51
6.28	7322	584.91	0.51
6.52	6626	802.26	0.70
6.78	1679544	112938.80	98.07
7.47	754	58.12	0.05
7.86	2620	190.71	0.17



JDS10-019



JS02-003

JS02-003-NaBio1mM-1to100-4dec11

05-Dec-2011 05:50:33

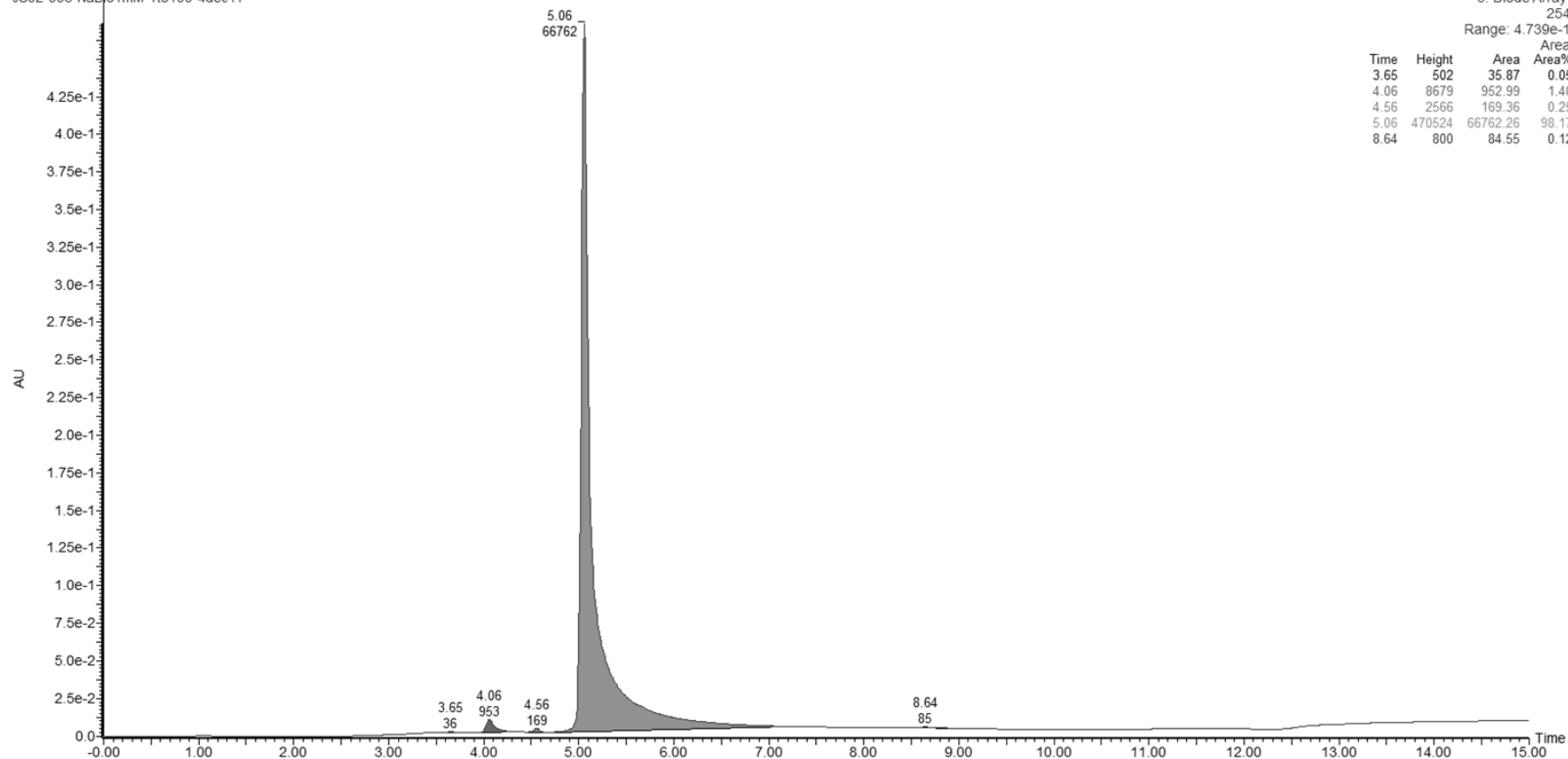
3: Diode Array

254

Range: 4.739e-1

Time	Height	Area	Area%
3.65	502	35.87	0.05
4.06	8679	952.99	1.40
4.56	2566	169.36	0.25
5.06	470524	66762.26	98.17
8.64	800	84.55	0.12

JS02-003-NaBio1mM-1to100-4dec11



JS02-005

JS02-005-NaBio1mM-1to100-4dec11

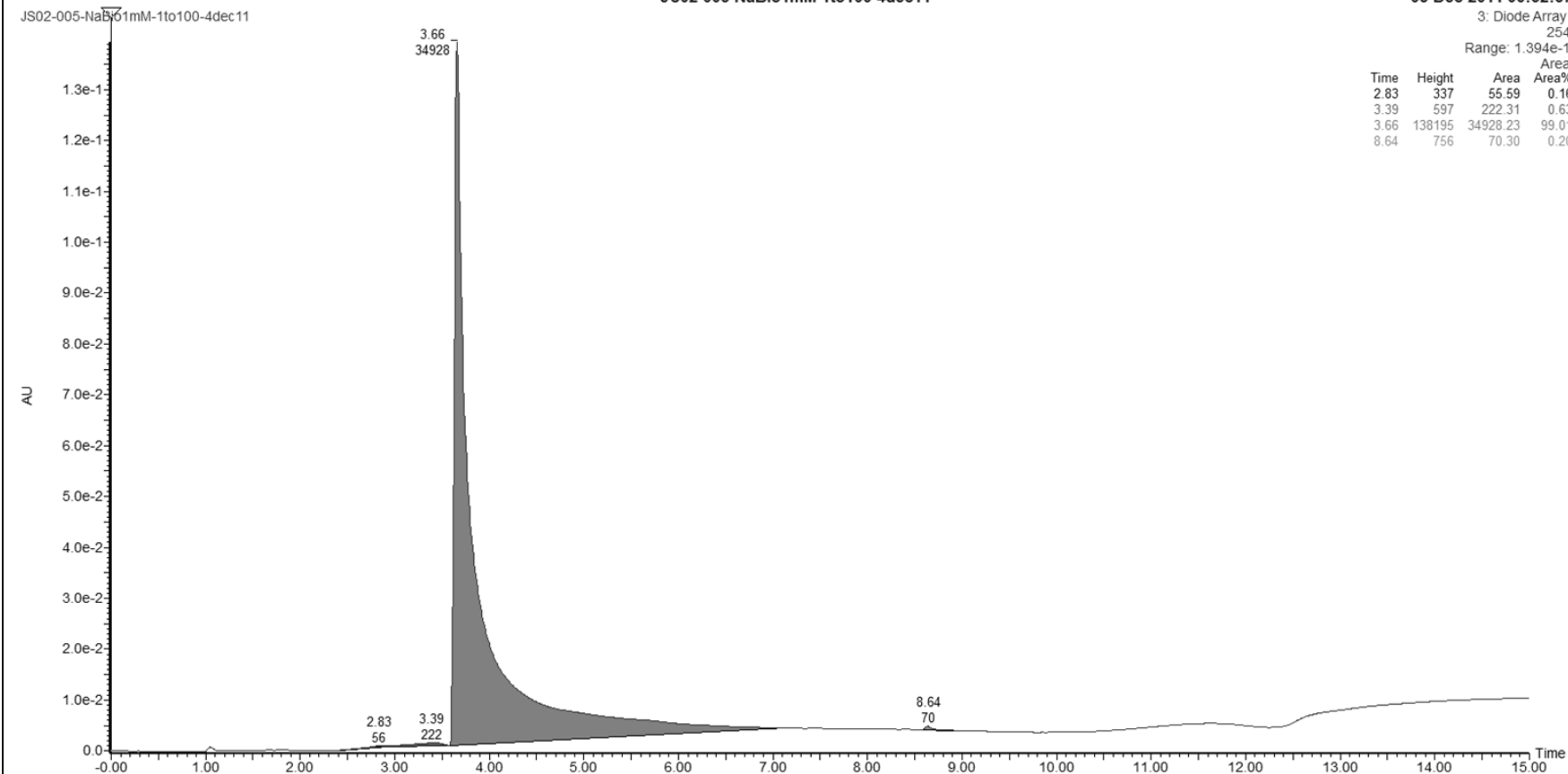
05-Dec-2011 06:32:37

3: Diode Array

254

Range: 1.394e-1

Time	Height	Area	Area%
2.83	337	55.59	0.16
3.39	597	222.31	0.63
3.66	138195	34928.23	99.01
8.64	756	70.30	0.20



JS02-018

JS02-018-NaBio1mM-1to100-4dec11

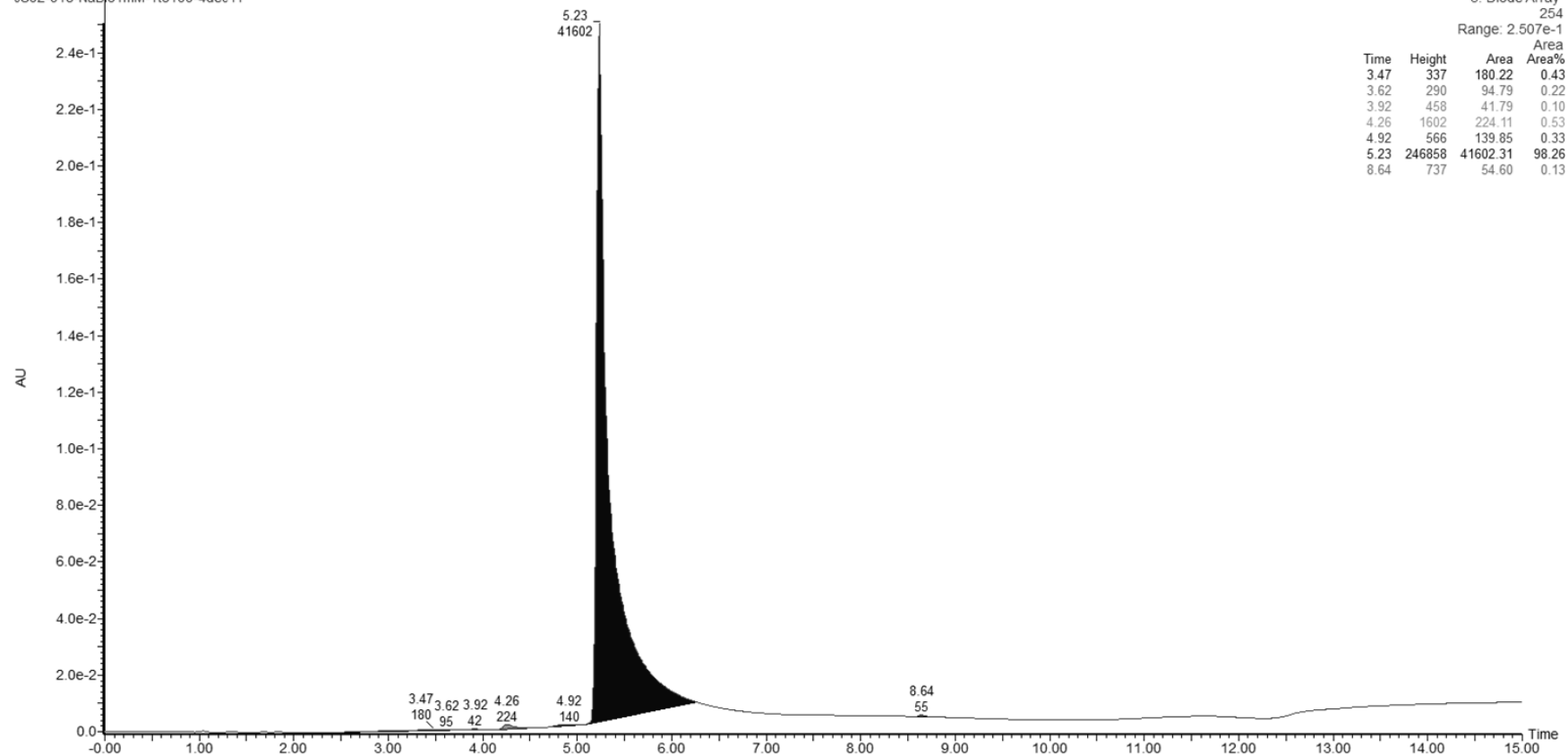
05-Dec-2011 07:56:59

3: Diode Array

254

Range: 2.507e-1

JS02-018-NaBio1mM-1to100-4dec11



YS05-035

